

NATIONAL ADVISORY COMMITTEE FOR AERONAUTICS

REPORT 1300

BASIC CONSIDERATIONS IN THE COMBUSTION OF HYDROCARBON FUELS WITH AIR

**By PROPULSION CHEMISTRY DIVISION
LEWIS FLIGHT PROPULSION LABORATORY**



1959

REPORT 1300

BASIC CONSIDERATIONS IN THE COMBUSTION OF HYDROCARBON FUELS WITH AIR

By PROPULSION CHEMISTRY DIVISION

**Lewis Flight Propulsion Laboratory
Cleveland, Ohio**

Edited by Henry C. Barnett and Robert R. Hibbard

National Advisory Committee for Aeronautics

Headquarters, 1512 H Street NW., Washington 25, D. C.

Created by Act of Congress approved March 3, 1915, for the supervision and direction of the scientific study of the problems of flight (U. S. Code, title 50, sec. 151). Its membership was increased from 12 to 15 by act approved March 2, 1929, and to 17 by act approved May 25, 1948. The members are appointed by the President and serve as such without compensation.

JAMES H. DOOLITTLE, Sc. D., Shell Oil Company, *Chairman*

LEONARD CARMICHAEL, Ph. D., Secretary, Smithsonian Institution, *Vice Chairman*

ALLEN V. ASTIN, Ph. D., Director, National Bureau of Standards.

PRESTON R. BASSETT, M. A., Vice President, Sperry Rand Corp.

DETLEV W. BRONK, Ph. D., President, Rockefeller Institute for Medical Research.

FREDERICK C. CRAWFORD, Sc. D., Chairman of the Board, Thompson Products, Inc.

WILLIAM V. DAVIS, JR., Vice Admiral, United States Navy, Deputy Chief of Naval Operations (Air).

JEROME C. HUNSAKER, Sc. D., Massachusetts Institute of Technology.

CHARLES J. MCCARTHY, S. B., Chairman of the Board, Chance Vought Aircraft, Inc.

CARL J. PFINGSTAG, Rear Admiral, United States Navy, Assistant Chief for Field Activities, Bureau of Aeronautics.

DONALD L. PUTT, Lieutenant General, United States Air Force, Deputy Chief of Staff, Development.

JAMES T. PYLE, A. B., Administrator of Civil Aeronautics.

FRANCIS W. REICHELDERFER, Sc. D., Chief, United States Weather Bureau.

EDWARD V. RICKENBACKER, Sc. D., Chairman of the Board, Eastern Air Lines, Inc.

LOUIS S. ROTHSCHILD, Ph. B., Under Secretary of Commerce for Transportation.

NATHAN F. TWINING, General, United States Air Force, Chief of Staff.

HUGH L. DRYDEN, Ph. D., *Director*

JOHN F. VICTORY, LL. D., *Executive Secretary*

JOHN W. CROWLEY, JR., B. S., *Associate Director for Research*

EDWARD H. CHAMBERLIN, *Executive Officer*

HENRY J. E. REID, D. Eng., Director, Langley Aeronautical Laboratory, Langley Field, Va.

SMITH J. DEFANCE, D. Eng., Director, Ames Aeronautical Laboratory, Moffett Field, Calif.

EDWARD R. SHARP, Sc. D., Director, Lewis Flight Propulsion Laboratory, Cleveland, Ohio

WALTER C. WILLIAMS, B. S., Chief, High-Speed Flight Station, Edwards, Calif.

FOREWORD

During the past ten years, investigations within the broad area of combustion research have been conducted by government, industry, and university. Much of this research has been sponsored and financed by the Federal Government, usually to further some application of combustion such as flight propulsion. As a result, extensive data have been published by a variety of sources. The greatest benefit can be derived by collecting, collating, and interpreting this information. Accordingly, the NACA Lewis laboratory has herein integrated and interpreted information on combustion with a view to its application to flight propulsion.

The principal problem of interest in this study is that of burning fuel continuously and efficiently in a small volume and at high rates. Heat-release rates must be large and combustion efficiency nearly perfect in order to obtain high thrust and low specific fuel consumption from a small, lightweight engine. Wide ranges of speed, altitude, and climate are generally encountered in flight, and these factors often change rapidly. Thus, the combustion system must perform over wide ranges of fuel flow, inlet airflow, pressure, and temperature.

In addition to burning fuel efficiently and at high rates, there are other factors that must be considered in jet-engine combustion. In general, the following conditions are desirable: Pressure loss through the combustion system should be kept to a minimum, since high pressure loss causes increased engine specific fuel consumption. Mixing of burned and unburned gases upstream of the combustor outlet must provide a preferred temperature distribution at the outlet. This requirement may result either from turbine stress-strength considerations or from the need of a nearly uniform jet velocity profile for high propulsive efficiency. Deposition of coke and formation of smoke are both undesirable in the operation of combustors. Of the two factors, coke deposition presents the more serious problem because of its adverse effect on combustor performance and life. The combustion system should be durable, yet lightweight. Reliable ignition is also necessary. Unfortunately, some of these requirements are conflicting with respect to design. Specifically, then, the combustion problem for a high-performance aircraft engine such as the jet or turbine type arises from two factors: (1) the extreme range and rapid variations of operating conditions encountered and (2) the many requirements of the combustor, some of which necessitate compromise in the design.

Many sources of basic and background information are available to the designer of high-speed combustion systems. The volume of literature concerning this subject, which was large before World War II, has since expanded tremendously with the expenditure of millions of dollars by the Federal Government. These funds have supported both fundamental and applied combustion research in laboratories throughout the nation.

A large number of recent research papers on the fundamentals of combustion are compiled in the Third and Fourth Symposia on Combustion published by the Williams & Wilkins Company; and there are a few very useful texts on basic aspects of combustion, such as *Explosion and Combustion Processes in Gases* by Jost, *Combustion, Flames, and Explosions of Gases* by Lewis and von Elbe, and *Flames* by Gaydon and Wolfhard. Much additional information exists in technical journals, symposia, and house organs such as progress reports on military projects.

Published information on the application of combustion research to flight propulsion is less comprehensive. Many individual papers on the subject appear in the classified literature; there are also a few summary papers. The Princeton University Press is preparing a twelve-volume treatise on *High-Speed Aerodynamics and Jet Propulsion* that will include a treatment of both basic and applied combustion, although it will be limited to the unclassified literature.

There is no single, completely adequate summary of the source material on combustion available to the flight-propulsion engineer. Such a summary should reduce design effort by organizing pertinent information on both basic and applied combustion and extracting those principles and ideas which are useful or significant in aircraft engine design. The NACA is now making such a study.

The chapters compiled here, which are the first part of such a study, cover unclassified material. They review such fundamental processes as fuel-air mixture preparation, gas flow and mixing, flammability and ignition, flame propagation in both homogeneous and heterogeneous mediums, flame stabilization, combustion oscillations, and smoke and carbon formation. The practical significance and the relation of these processes to theory are presented.

Certain limitations have been necessary. The references were selected from a complete review of the field in order to illustrate points that were pertinent to the subject at the date of writing. Thus, the references cited are a thorough bibliography, but not a complete one. Some important topics may have been omitted. Also, the study is directed toward air-breathing engines and hydrocarbon fuels; rocket engines and fuels other than hydrocarbons, such as the so-called high-energy fuels, are considered outside the scope of the study.

Because of continuing progress in the field, this report is not intended as a final summary of developments. Further, other reports in the NACA general study will deal separately with the applications of basic data to performance and design of combustion systems for engines.

WALTER T. OLSON

Chief, Propulsion Chemistry Division

CONTENTS

Chapter	Page
I—ATOMIZATION AND EVAPORATION OF LIQUID FUELS.....	1
II—FLOW AND MIXING PROCESSES IN COMBUSTION CHAMBERS...	32
III—IGNITION AND FLAMMABILITY OF HYDROCARBON FUELS.....	83
IV—LAMINAR FLAME PROPAGATION.....	127
V—TURBULENT FLAMES.....	163
VI—FLAME STABILIZATION.....	185
VII—DIFFUSION FLAMES.....	207
VIII—OSCILLATIONS IN COMBUSTORS.....	229
IX—SMOKE AND COKE FORMATION IN THE COMBUSTION OF HYDROCARBON-AIR MIXTURES.....	242
APPENDIX—PHYSICAL AND COMBUSTION PROPERTIES OF SELECTED FUELS.....	256

CONTENTS

Chapter	Page	Chapter	Page
I—ATOMIZATION AND EVAPORATION OF LIQUID FUELS, by Charles C. Graves and Donald W. Bahr	1	II—FLOW AND MIXING PROCESSES IN COMBUSTION CHAMBERS—Continued	
INTRODUCTION	1	AERODYNAMIC MIXING—Continued	
SYMBOLS	1	Fuel-Air Mixing	72
ATOMIZATION OF FUEL	2	Experiments on diffusion from simple point and line sources	72
Basic Relations for Fuel Atomization	2	Fuel droplet trajectories and impingement	73
Atomization theory	2	Turbulent spreading of evaporating liquid-fuel droplets from fuel injectors	74
Drop-size distribution in sprays	5	Combined spreading of liquid and vapor fuel in high-velocity airstreams	76
Dimensional analysis	7	Effect of solid boundaries and flow-area changes on fuel spreading	77
Air Atomization	7	Assumptions and procedure necessary for application to jet-engine design	77
Centrifugal Pressure-Atomizing Nozzles	11	Summary	77
Summary Comments on Utility of Fuel-Atomization Data	16	Jet Mixing	77
EVAPORATION OF FUEL	16	DESIGN SUMMARY	80
Equilibrium Flash Vaporization	16	REFERENCES	80
Steady-State Drop Evaporation into Static Surroundings	18	III—IGNITION AND FLAMMABILITY OF HYDROCARBON FUELS, by Frank E. Belles and Clyde C. Swett	83
Drop evaporation theory	18	INTRODUCTION	83
Evaporation into low-temperature surroundings	19	SYMBOLS	83
Evaporation into high-temperature surroundings	20	FLAME QUENCHING	84
Drop Evaporation under Forced Convection	21	Effects of Variables on Flame Quenching	84
Heat-transfer correlations	21	Geometry of quenching surface	84
Mass-transfer correlations	23	Hydrocarbon type	84
Unsteady-State Drop Evaporation	23	Inert diluents	84
Additional Considerations in Drop Evaporation	25	Temperature	86
Determination of Steady-State Drop Surface Temperature	26	Pressure	86
Summary of Drop Evaporation Relations	26	Oxygen concentration	87
EVAPORATION OF SPRAYS	26	Dead Space	87
Theory	26	Homogeneous Quenching	88
Experiment	27	Interpretations of Wall Quenching	89
SIGNIFICANCE OF ATOMIZATION AND EVAPORATION RESEARCH IN APPLICATION TO JET-ENGINE DESIGN	28	Quenching in Flammability and Spark-Ignition Measurements	91
REFERENCES	29	Flammability measurements	91
II—FLOW AND MIXING PROCESSES IN COMBUSTION CHAMBERS, by Wilfred E. Seull and William R. Mickelsen	32	Spark-ignition-energy measurements	92
INTRODUCTION	32	FLAMMABILITY LIMITS	93
SYMBOLS	32	Effects of Variables on Flammability Limits at Atmospheric Pressure	93
AERODYNAMIC FLOW	34	Hydrocarbon type	94
Combustor Approach-Stream Parameters	34	Petroleum fuels	95
Turbojet combustion chambers	34	Mists and sprays	96
Ramjet combustion chambers; generalized parameters	36	Diluents	97
Combustor Pressure Losses	37	Temperature	98
Effect on over-all cycle performance	37	Velocity and turbulence	99
Causes	38	Effects of Variables on Flammability Limits at Nonatmospheric Pressures	99
Estimation and correlation	42	Hydrocarbon type	100
Gas Jets	45	Petroleum fuels	100
Theoretical background	45	Significance of Flammability Limits	100
Experimental data	49	Limits of flame propagation	100
AERODYNAMIC MIXING	59	True flammability limits	101
Diffusion	59	IGNITION	102
Fundamental equations	59	Ignition by Heated Surfaces	103
Homogeneous, isotropic, turbulent fields	60	Mixture composition	103
Nonisotropic turbulent-flow fields	67	Ignition lag	104
Turbulent-flow fields containing periodic flow fluctuations	70	Heated spheres and rods	105
Concentration fluctuations	72	Turbulence	105
Summary	72	Surface condition and composition	105
		Surface area	106
		Fuel composition	106
		Pressure	107
		Diluents	107

Chapter	Page	Chapter	Page
III—IGNITION AND FLAMMABILITY OF HYDRO-CARBON FUELS—Continued		IV—LAMINAR FLAME PROPAGATION—Continued	
IGNITION—Continued		THEORIES OF LAMINAR FLAME PROPAGATION—Con.	
Ignition by Flames.....	107	Approximate Equations.....	149
Pilot flames.....	108	Thermal mechanism.....	149
Propagating flames through constrictions.....	108	Diffusional mechanism.....	151
Ignition by Hot Gases.....	108	Miscellaneous approximate equations.....	155
Heated air.....	109	Evaluation of thermal and diffusional mechanisms.....	155
Vitiated air.....	110	APPLICATION OF LAMINAR FLAME RESEARCH TO PRACTICAL COMBUSTION PROBLEMS.....	157
Ignition by Shock Waves.....	111	REFERENCES.....	159
Ignition by Capacitance Sparks.....	112	V—TURBULENT FLAMES, by Melvin Gerstein and Gordon L. Dugger.....	163
Mixture composition.....	114	INTRODUCTION.....	163
Fuel type.....	115	SYMBOLS.....	163
Electrode spacing.....	115	CHARACTERISTICS OF TURBULENT FLAMES.....	164
Electrode type.....	115	Bunsen Flames.....	164
Condenser voltage.....	116	Flame height.....	164
Spark duration.....	116	Brush width.....	165
Oscillation frequency.....	116	Flame radiation.....	165
Sparking rate.....	117	Flames in Tubes.....	166
Mixture velocity.....	117	Flames Supported on Rods (V-Flames).....	166
Turbulence.....	117	TURBULENT FLAME VELOCITY.....	166
Pressure.....	119	Measurement.....	166
Temperature.....	120	Open burner flames.....	166
Diluents.....	121	Flames in tubes.....	167
Ignition by Inductance Sparks.....	121	Spherical flames.....	167
Mixture composition, pressure, and temperature.....	121	Flames supported on rods (V-flames).....	168
Electrode spacing.....	122	Dependence of flame velocity on location of measurement.....	168
Electrode material.....	122	Effects of Chemical Variables.....	168
Circuit inductance and voltage.....	122	Fuel concentration.....	168
Current type.....	123	Fuel type.....	171
SIGNIFICANCE OF BASIC QUENCHING, FLAMMABILITY, AND IGNITION DATA IN RELATION TO AIRCRAFT PROPULSION PROBLEMS.....	123	Effects of Physical Variables.....	171
Quenching.....	123	Pressure.....	171
Flammability.....	123	Temperature.....	171
Ignition.....	123	Velocity and turbulence promotion.....	172
REFERENCES.....	124	THEORIES OF TURBULENT FLAME VELOCITY.....	175
IV—LAMINAR FLAME PROPAGATION, by Gordon L. Dugger, Dorothy M. Simon, and Melvin Gerstein.....	127	Turbulent Flames.....	175
INTRODUCTION.....	127	Damköhler theory.....	175
SYMBOLS.....	127	Shelkin theory.....	176
CHARACTERISTICS OF LAMINAR FLAMES.....	128	Delbourg theory.....	176
Temperature Profile.....	128	Karlovitz theory.....	177
Relation of Various Images to Temperature Profile.....	129	Leason theory.....	178
Luminous zone.....	129	Scurlock and Grover theory.....	178
Schlieren image.....	130	Flame-Induced Turbulence.....	180
Shadow image.....	130	SPACE HEATING RATES.....	182
FLAME VELOCITY.....	131	Turbulent Bunsen Flames.....	182
Methods of Measuring.....	131	Spherical Reactor.....	182
Stationary flame or burner.....	131	Comparison of Space Heat-Release Rates.....	183
Transparent tube.....	133	APPLICABILITY OF TURBULENT FLAME STUDIES TO JET-ENGINE COMBUSTION.....	184
Soap-bubble or constant-pressure bomb.....	133	REFERENCES.....	184
Constant-volume bomb.....	134	VI—FLAME STABILIZATION, by Gordon L. Dugger and Melvin Gerstein.....	185
Evaluation of methods.....	135	INTRODUCTION.....	185
Effects of Chemical Variables.....	136	SYMBOLS.....	185
Fuel-oxidant ratio.....	136	STABILITY DIAGRAMS: VELOCITY-CONCENTRATION LIMITS.....	185
Molecular structure of hydrocarbon.....	138	Open Flames with Secondary Air.....	185
Additives, antiknocks, and fuel blending.....	139	Flames Deprived of Secondary Air.....	186
Effects of Physical Variables.....	142	MECHANISMS OF FLAME STABILIZATION.....	187
Pressure.....	142	Critical Boundary Velocity Gradient.....	187
Temperature.....	145	Flames stabilized on burner.....	187
Electric fields.....	146	Flames supported on wires or rods.....	190
Acoustical and mechanical disturbances.....	146	Penetration distance.....	190
THEORIES OF LAMINAR FLAME PROPAGATION.....	148	Stabilization by Eddies.....	191
Comprehensive Equations.....	149		

CONTENTS

Chapter	Page
VI—FLAME STABILIZATION—Continued	
EFFECT OF VARIABLES ON STABILITY LIMITS.....	191
Flow Variables at Constant Pressure and Temperature.....	191
Characteristic dimension of burner or flameholder.....	191
Turbulence.....	193
Boundary-layer thickness.....	194
Electric fields.....	194
Acoustical disturbances.....	194
Pressure and Temperature Variation.....	195
Pressure.....	195
Mixture temperature.....	196
Liquid fuel.....	197
Flameholder temperature.....	197
Chemical Variables.....	197
Fuel type.....	197
Additives and fuel blending.....	197
Water vapor.....	198
Diluent concentration.....	198
THERMAL THEORIES OF FLAME STABILIZATION.....	198
Burner Flames—Critical Boundary Velocity Gradients.....	198
Flames Supported on Flameholders—Eddy Stabilization.....	199
NONISOTROPIC FLAMES.....	201
Cell Formation and Surface Breakup of Open Flames.....	201
Cellular Flames in Tubes.....	203
SIGNIFICANCE OF FLAME STABILIZATION IN JET-ENGINE COMBUSTION.....	204
REFERENCES.....	205
VII—DIFFUSION FLAMES, by Richard S. Brokaw and Melvin Gerstein.....	207
INTRODUCTION.....	207
SYMBOLS.....	207
GASEOUS DIFFUSION FLAMES.....	208
Appearance.....	208
Structure.....	209
Laminar flames.....	210
Turbulent flames.....	211
Theory.....	212
Laminar flames.....	212
Turbulent flames.....	214
Effect of Variables on Flame Height.....	215
Laminar flames.....	215
Turbulent flames.....	217
Stability.....	218
LIQUID DIFFUSION FLAMES.....	220
Single-Drop Combustion.....	220
Theory.....	220
Combustion in quiescent air.....	223
Combustion in airstreams.....	224
Fuel Sprays and Mists.....	226
Theory of combustion.....	226
Experimental observation.....	226
APPLICABILITY OF RESEARCH DATA ON DIFFUSION FLAMES TO JET-ENGINE COMBUSTOR DESIGN.....	227
REFERENCES.....	228
VIII—OSCILLATIONS IN COMBUSTORS, by Perry L. Blackshear, Jr., and Warren D. Rayle.....	229
INTRODUCTION.....	229
SYMBOLS.....	229

Chapter	Page
VIII—OSCILLATIONS IN COMBUSTORS—Continued	
MODES OF OSCILLATION.....	230
The Burner As a Resonant Room.....	230
The Burner As a Helmholtz Resonator.....	233
Systems of Oscillation with Nonacoustic Elements.....	234
INTERACTIONS.....	235
Elements Disturbed by Velocity and Pressure Oscillations.....	235
Effects of Feedback Loops on Pressure and Velocity.....	237
SIGNIFICANCE OF RESONANCE STUDIES IN DESIGN OF JET-ENGINE COMBUSTORS.....	239
Design Criteria Based on Mode of Resonance.....	239
Design Criteria Based on Sensitivity of Disturbed Elements.....	239
The Future for Combustion Oscillation.....	240
REFERENCES.....	240
IX—SMOKE AND COKE FORMATION IN THE COMBUSTION OF HYDROCARBON-AIR MIXTURES, by Rose L. Schalla and Robert R. Hibbard.....	242
INTRODUCTION.....	242
PHYSICAL AND CHEMICAL NATURE OF SMOKE AND COKE.....	242
Smoke.....	242
Coke.....	243
EFFECT OF OPERATING VARIABLES ON SMOKING TENDENCY.....	243
Burner Geometry.....	243
Diffusion flames.....	243
Bunsen flames.....	244
Fuel-Air Ratio.....	245
Diffusion flames.....	245
Bunsen flames.....	245
Temperature.....	246
Diffusion flames.....	246
Bunsen flames.....	246
Pressure.....	246
Diffusion flames.....	246
Bunsen flames.....	247
EFFECT OF FUEL VARIABLES ON SMOKING TENDENCY.....	247
Effect of Hydrocarbon Type on Diffusion Flames.....	247
Aromatics.....	247
Alkynes.....	248
Monoolefins.....	248
Diolefins.....	248
Cycloolefins.....	248
Paraffins.....	248
Cycloparaffins.....	248
Summary.....	248
Hydrocarbon blends and refinery streams.....	249
Effect of Hydrocarbon Type on Bunsen Flames.....	249
Methods of Correlating Smoking Tendency with Hydrocarbon Structure in Diffusion Flames.....	250
Effect of Nonhydrocarbon Components.....	250
Diffusion flames.....	250
Bunsen flames.....	251
Effect of Additives.....	251
Diffusion flames.....	251
Bunsen flames.....	251
THEORIES OF SMOKE AND COKE FORMATION.....	251
Smoke.....	251
Coke.....	253
EFFECT OF SOLIDS ON RADIANT HEAT TRANSFER.....	254
SIGNIFICANCE OF BASIC SMOKE AND COKE STUDIES IN DESIGN OF JET-ENGINE COMBUSTORS.....	254
REFERENCES.....	255
APPENDIX—PHYSICAL AND COMBUSTION PROPERTIES OF SELECTED FUELS.....	256
APPENDIX REFERENCES.....	259

TABLES

	Page
I—MATHEMATICAL EXPRESSIONS FOR DROP-SIZE DISTRIBUTION.....	6
II—COMPARISON OF EXPERIMENTAL AND CALCULATED VAPORIZATION TIMES FOR UNSTEADY-STATE VAPORIZATION OF SINGLE FUEL DROPS SUDDENLY EXPOSED TO CONSTANT-VELOCITY AIRSTREAM.....	25
III—EQUATIONS FOR CONCENTRATION OF HEAT OR MASS DOWNSTREAM OF VARIOUS SOURCES.....	68-9
IV—ARRANGEMENTS FOR MIXING OF GAS STREAMS.....	79
V—FLAMMABILITY LIMITS IN AIR AT ATMOSPHERIC PRESSURE AND ROOM TEMPERATURE.....	93
VI—TYPICAL DISTILLATION DATA FOR AIRCRAFT FUELS.....	95
VII—FLAMMABILITY LIMITS OF AIRCRAFT FUELS AT 300° F.....	95
VIII—LIMITS OF FLAMMABILITY OF OIL MISTS.....	96
IX—SPRAY FLAMMABILITY LIMITS COMPARED WITH MINIMUM OXYGEN CONCENTRATIONS FOR COMBUSTION OF HYDROCARBON VAPORS IN OXYGEN-NITROGEN MIXTURES.....	97
X—COMPARISON OF MAXIMUM FLAME VELOCITIES DETERMINED BY VARIOUS METHODS.....	134
XI—BOND DISSOCIATION ENERGIES FOR C ₄ AND C ₆ HYDROCARBONS AT CONCENTRATION FOR MAXIMUM FLAME VELOCITY.....	136
XII—EMPIRICAL COEFFICIENTS FOR CALCULATING MAXIMUM FLAME VELOCITY FROM HYDROCARBON STRUCTURE.....	139
XIII—VALUES OF EMPIRICAL EQUATIONS FOR EFFECT OF O ₂ /(O ₂ +N ₂) ON RELATIVE MAXIMUM FLAME VELOCITY.....	142
XIV—SUMMARY OF BURNING-VELOCITY CORRELATIONS.....	143
XV—MAXIMUM FLAME VELOCITIES.....	144
XVI—FLAME-VELOCITY MEASUREMENTS OF STOICHIOMETRIC HYDROCARBON-AIR MIXTURES.....	144
XVII—EFFECT OF PRESSURE ON FLAME VELOCITY.....	145
XVIII—EFFECT OF INITIAL MIXTURE TEMPERATURE ON LAMINAR FLAME VELOCITY.....	147
XIX—PERCENT AVERAGE DEVIATION IN RATIO OF PREDICTED TO MEASURED FLAME VELOCITY.....	153
XX—HYDROGEN ATOM CONCENTRATION IN COMBUSTION ZONE OF MOIST CARBON MONOXIDE—OXYGEN FLAMES.....	153
XXI—COMPARISONS FOR FLAMES WITH ARGON AND HELIUM AS INERT.....	157
XXII—EXPERIMENTAL RELATIONS BETWEEN TURBULENT FLAME VELOCITY AND REYNOLDS NUMBER.....	171
XXIII—EXPERIMENTAL RELATIONS BETWEEN TURBULENT FLAME VELOCITY AND TURBULENCE INTENSITY.....	174
XXIV—SPACE HEATING RATES OF TURBULENT BUNSEN FLAMES.....	182
XXV—HEATING VALUES FOR VARIOUS TYPES OF COMBUSTION.....	183
XXVI—CORRELATING PARAMETERS FOR CONCENTRATION LIMITS OF BLOWOFF FROM FLAMEHOLDERS.....	192
XXVII—EVAPORATION CONSTANTS FOR VARIOUS FUELS BURNING IN AIR.....	223
XXVIII—EVAPORATION CONSTANTS FOR ISOCTANE IN VARIOUS OXYGEN-NITROGEN ATMOSPHERES.....	223
XXIX—SPATIAL FLAME SPEEDS OF MIST AND VAPOR.....	227
XXX—VALUES OF $\alpha_{r,n}$ FOR THE LOWER RADIAL, TRANSVERSE, AND COMPOUND MODES.....	230
XXXI—SUGGESTED METHODS FOR CONTROLLING VARIOUS TYPES OF OSCILLATION.....	240
XXXII—PHYSICAL AND COMBUSTION PROPERTIES OF FUELS.....	257-8
XXXIII—EXPERIMENTAL BURNING VELOCITIES OF PROPANE-AIR MIXTURES.....	256

REPORT 1300

BASIC CONSIDERATIONS IN THE COMBUSTION OF HYDROCARBON FUELS WITH AIR¹

CHAPTER I

ATOMIZATION AND EVAPORATION OF LIQUID FUELS

By CHARLES C. GRAVES and DONALD W. BAHR

INTRODUCTION

In both turbojet and ramjet engines, the fuel is usually fed into the combustion chamber either as a well-atomized liquid spray or as a vapor (prevaporizing combustor). Accordingly, the formation of liquid sprays, the evaporation of both single drops and entire sprays, and the conditions required for various degrees of fuel flash vaporization are of interest to the combustion-chamber designer. Theoretical and experimental work on most of these factors is not sufficiently complete to permit much direct application to particular combustion chambers. However, even if used only in a qualitative sense, knowledge of the principles and trends involved is required for good combustion-chamber design.

The factors involved in the atomization and evaporation of liquid fuel are discussed herein primarily in their own light and not in relation to their effect on other processes contributing to over-all combustion-chamber performance. A detailed discussion of the mixing of the liquid and vapor fuel with the combustion air is presented in chapter II.

SYMBOLS

The following symbols are used in this chapter:

a	constant
\mathcal{B}	constant
b	constant
c	constant
\bar{c}	root mean square molecular velocity of surrounding fluid
c_p	specific heat at constant pressure
$D_{g,M}$	mass diffusion coefficient
$D_{v,g}$	diffusion coefficient of vapor in surrounding fluid
\mathcal{D}	distribution constant
d_{dr}	drop diameter
$d_{dr,M}$	mass- or volume-median drop diameter
$d_{dr,m}$	mean drop diameter
$d_{dr,max}$	maximum stable drop diameter
$d_{dr,o}$	initial drop diameter
$d_{dr,32}$	Sauter mean drop diameter
d_h	orifice diameter
d_j	diameter of undisturbed jet

d_{th}	air-atomizer throat diameter
F_{vent}	ventilation factor
\mathcal{F}	function
f	fuel-air ratio
g	acceleration due to gravity
H_v	latent heat of vaporization
h	specific enthalpy
i	constant
j	constant
K	constant
\mathcal{K}	evaporation constant
k	constant
l	mean free molecular path of surrounding fluid
M	molecular weight
m	mass
dm/dt	evaporation rate of drop
N_{dr}	number of drops
N_{fl}	flow number
Nu_H	Nusselt number for heat transfer
Nu_M	Nusselt number for mass transfer
Pr	Prandtl number
p	ambient pressure
p_{BM}	log mean pressure of nondiffusing gas over stagnant film
Δp_n	nozzle pressure drop
q	constant
R	universal gas constant
Re	Reynolds number
$ReSc'$	$dU_{rel} \rho_g / D_{g,M}$
$\mathcal{R}_1, \mathcal{R}_2, \mathcal{R}_3$	ratios of various atomizer dimensions to orifice diameter
r	radius
r_h	orifice radius
Sc	Schmidt number
s	constant
T	static temperature
$T_{a,w}$	air temperature at which water has same difference between air temperature and drop surface temperature as given liquid
T_{bp}	normal boiling point of evaporating liquid
\mathcal{T}	film thickness
t	time
t_b	breakup time of liquid jet

¹ Technical information herein has been compiled from data of the NACA and other organizations. Data originating outside the NACA cannot be reproduced for further dissemination without the permission of the originating organization.

U	velocity
$U_{l,h}$	velocity of liquid at orifice
U_{rel}	relative velocity between drop and air or liquid film and air
$U_{rel,b}$	relative velocity between drop and air at instant of breakup
V_{fl}	volume flow rate
We	Weber number
w	weight-flow rate
x	distance between liquid surface and surface where diffusion starts
y	variable in logarithmic-normal distribution function
Z	$\mu_l/\sqrt{\rho_l \sigma d_j}$
z	axial distance downstream of fuel injector
α	accommodation coefficient
β	spray-cone angle, deg
Γ	gamma function
ι_{dr}	weight fraction of fuel spray containing drops of diameter larger than d_{dr}
ι_v	fraction of fuel vaporized
κ	thermal conductivity
Λ	size constant in drop-distribution functions
λ	wavelength of surface disturbance
λ_{max}	wavelength of surface disturbance producing maximum film or jet instability
μ	absolute viscosity
ν	kinematic viscosity
ρ	density
σ	surface tension
Φ	fraction of heat entering film around evaporating drop that arrives at drop surface
Subscripts:	
a	air
av	average
f	fuel
g	surrounding fluid
H	heating; heat transfer
j	jet
l	liquid
mx	vapor-air mixture
o	initial
S	drop surface
t	total
v	vapor
1	condition prior to vaporization
2	condition at end of vaporization
∞	infinite distance from drop

ATOMIZATION OF FUEL

A number of excellent papers on the general subject of atomization are available in the literature (e. g., refs. 1 to 4). For a more detailed study of atomization, the reader is referred particularly to the survey by Giffen and Muraszew (ref. 4) and the bibliography of reference 3 on work in atomization up to 1952.

BASIC RELATIONS FOR FUEL ATOMIZATION

Atomization theory.—In order to provide the rapid liquid-fuel evaporation rates required in jet-engine combustors, the

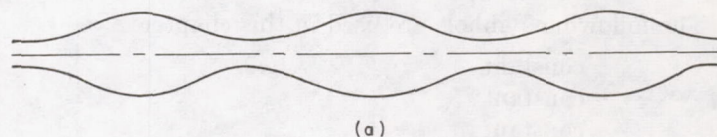
fuel must be finely atomized and well-distributed. The mechanism of atomization is not well understood; and no general theory has been evolved to predict the degree of atomization for particular nozzle designs, fuel properties, and operating conditions. However, a general picture of the atomization process can be drawn from considerable experimental work and some limited theoretical work performed in previous years.

The atomization of liquid fuel can be considered to occur in six steps:

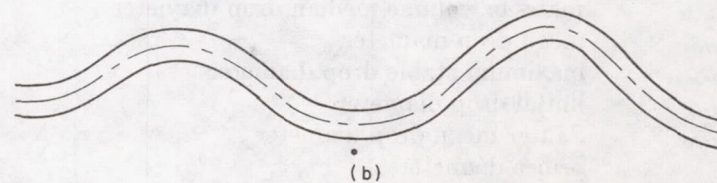
- (1) Stretching of fuel into sheets or streams as a result of accelerating the liquid through the nozzle orifice
- (2) Appearance of small local ripples and protuberances at the liquid surface as a result of initial liquid turbulence and the action of the air on the liquid stream
- (3) Formation of ligaments as a result of air pressure and shearing forces
- (4) Collapse of ligaments into drops as a result of surface tension
- (5) Further breakup of these drops
- (6) Agglomeration of drops

Combinations of part or of all these steps would appear to occur whether atomization is effected by injecting fuel at high velocity into relatively quiescent air (pressure atomization) or by the action of a high-velocity airstream on a relatively low-velocity fuel stream (air atomization). The relative importance of each step varies with application, depending upon such factors as relative velocity between fuel and air and fuel-air ratio. The various factors involved in the atomization process might be best considered by following the changes occurring in atomization as the relative velocity between the fuel and the air is increased from low to high values.

Rayleigh (ref. 5) treated the effect of rotationally symmetric disturbances (fig. 1(a)) on the breakup of a liquid jet.



(a)



(b)

- (a) Rotationally symmetric oscillations.
(b) Wave formation.

FIGURE 1.—Disturbance of low-velocity liquid jet.

He showed that a liquid jet subject to surface disturbances becomes unstable when the wavelength of the surface disturbance λ divided by the diameter of the undisturbed jet d_j is greater than π . Under such conditions the surface disturbances increase and finally result in the breakup of the jet into drops. When λ/d_j is equal to 4.51, the surface disturbances increase at the maximum rate and result in the maximum degree of jet instability. In experiments on a free-falling jet, Tyler (ref. 6) obtained a value for λ/d_j equal to 4.65. On the basis of these tests, Tyler concluded that the breakup of such jets occurs under the condition of maximum degree of instability as given by the Rayleigh theory.

Weber (ref. 7) extended the Rayleigh analysis to viscous liquids moving at low velocities. When the air and fuel have the same velocity, the breakup time t_b of a liquid jet caused by rotationally symmetric disturbances (fig. 1(a)) can be expressed by the equation

$$t_b = K \left[\left(\frac{\rho_l}{\sigma} \right)^{0.5} d_j^{1.5} + 3 \left(\frac{\mu_l}{\sigma} \right) d_j \right] \quad (1)$$

The value of λ/d_j for the maximum degree of jet instability is given by the equation

$$\frac{\lambda_{max}}{d_j} = \pi \sqrt{2} \left[1 + 3 \left(\frac{\mu_l^2}{\sigma \rho_l d_j} \right)^{1/2} \right]^{1/2} = \pi \sqrt{2} (1 + 3Z)^{1/2} \quad (2)$$

where

$$Z = \frac{\sqrt{2 \left(\frac{\rho_l}{\rho_g} \right) We_j}}{Re_j}$$

$$Re_j = \frac{\rho_l U_{rel} d_j}{\mu_l}$$

$$We_j = \frac{\rho_g U_{rel}^2 d_j}{2\sigma}$$

When the three preceding terms are combined,

$$Z = \frac{\mu_l}{\sqrt{\rho_l \sigma} d_j}$$

From these equations, it can be seen that both breakup time and the optimum value of λ/d_j for breakup increase with increasing viscosity and decrease with increasing surface tension. The trends predicted by the Weber analysis (ref. 7) are in agreement with the experiments of Haenlein (ref. 8).

In an analysis of the effect of viscosity on jet instability (ref. 9), the wavelength of the surface disturbance resulting in maximum instability was found to be a function of the ratio μ_l/μ_g .

At higher relative velocities, wave formation (fig. 1(b)) is encountered as a result of air effects. Weber showed that a minimum relative velocity must exist for the onset of wave formation. As this velocity is exceeded, the required distance for breakup decreases.

The various stages of atomization for simple jets were separated by Ohnesorge (ref. 10) into three groups, as shown in figure 2. Here, the dimensionless parameter Z of equation (2) is plotted against the jet Reynolds number. In region I,

the jet broke up in accordance with the Rayleigh-type disturbances (fig. 1(a)). In region II, the jet breakup occurred in the form of helicoidal waves. In region III, complete disruption of the jet occurred at the orifice.

Jet breakup resulting from wave formation has also been considered for swirl-type pressure-atomizing nozzles. For swirl-type nozzles operating under a moderate pressure differential, the liquid emerges from the orifice in the form of a conical film. Waves and holes appear in the film, which eventually disintegrates to form the spray. Two theoretical investigations (refs. 11 and 12) have been made in an attempt to explain the breakup of the film as the result of wave formation. The analyses follow the classical treatments given by Lamb (ref. 13). The relative velocity between the film and the surrounding medium is assumed constant, and the film is treated as two-dimensional. If the film is flat (fig. 3(a)), it is not subject to disturbing or restoring forces. However, if there is a slight surface bulge,

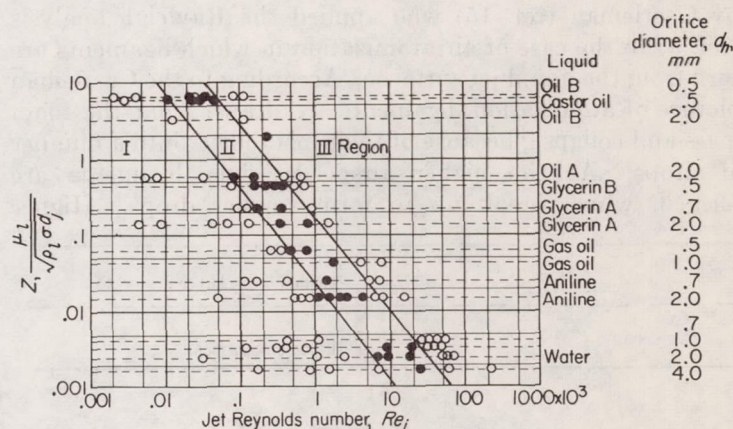


FIGURE 2.—Stages of atomization with simple orifice (ref. 10).

the film is subject to both aerodynamic and surface-tension forces. At the bulge, a local decrease in pressure occurs that tends to increase the surface disturbance. This force is opposed by restoring forces resulting from surface tension. Under certain conditions, where aerodynamic forces predominate, the film becomes unstable and eventually breaks up.

The analysis in reference 11 is concerned with film breakup resulting from asymmetric oscillations. For this type of oscillation, the cross section of the film is as shown in figure 3(b). The thickness of the disturbed film is considered to be constant. It was found that the film is unstable for

$$We \left(\frac{\rho_l}{\rho_g} \right) = \left(\frac{\rho_g U_{rel}^2 \mathcal{F}}{Z\sigma} \right) \left(\frac{\rho_l}{\rho_g} \right) > 1 \quad (3)$$

For $We(\rho_l/\rho_g) \gg 1$, the wavelength λ of the surface disturbance resulting in maximum instability of the film is

$$\lambda_{max} = \frac{4\pi\sigma}{\rho_g U_{rel}^2} \quad (4)$$

Equation (4) can be expressed as

$$\frac{\lambda_{max}}{\mathcal{F}} = \frac{2\pi}{We} \quad (5)$$

Fair agreement was found between predicted and calculated values of λ_{max} obtained from photographs of swirl atomizer sprays (ref. 14). Symmetrical oscillations, in which the mean surface of the film remains flat, would also result in an unstable film. However, the degree of instability was stated to be much less than for the asymmetric oscillation considered in reference 11.

In reference 12, a similar type of analysis was made independently. In this treatment, the film cross section was considered to have the form shown in figure 3(c). The case of exponential increase in wave amplitude was considered in detail.

At high relative velocities between liquid and air, complete disruption of the liquid jet occurs close to the fuel orifice and results in the formation of large numbers of drops. This type of atomization occurs particularly in the case of air atomization and is also found with pressure-atomizing nozzles operating under high injection-pressure differentials. An analytical study of this type of atomization was made by Castleman (ref. 15) who applied the Rayleigh analysis (ref. 5) to the case of air atomization in which ligaments are torn from the liquid jet surface. According to the Castleman picture of atomization, ligaments are drawn from the main mass and collapse, because of their instability, into a number of drops. At the higher airspeeds, finer ligaments are formed, which break up to form smaller drops. Higher

surface tension would cause quicker collapse of the ligaments before they are drawn too finely and would result in larger drops. These trends are verified by experiment.

At high relative velocities between fuel and air, the drops formed from the breakup of the ligaments may, in turn, be broken up as a result of air effects. This mechanism was studied by Hinze (ref. 16) and Lane (ref. 17). Hinze showed that the criterion for drop breakup is the appropriate value of the Weber number We as given by

$$We = \frac{\rho_g U_{rel}^2 d_{dr}}{2\sigma} \quad (6)$$

The predicted value of We for breakup varied between 6 for low-viscosity liquids and 10 for high-viscosity liquids for a liquid drop exposed suddenly to a constant-velocity airstream. Under most atomization conditions, however, the relative velocity between drop and airstream decreases rapidly. If the viscosity appreciably decreases the rate of drop deformation, the relative velocity may be reduced below the critical value before the drop is substantially deformed. Consequently, the critical initial value of velocity for drop breakup under actual atomizing conditions may be much higher than the steady-state critical velocity obtained from equation (6). In addition, the actual effect of drop viscosity on drop breakup may be much higher than that predicted from theory.

Lane (ref. 17) investigated the breakup of individual drops exposed to steady and transient airstreams. In one set of experiments, water drops having initial diameters ranging from 0.5 to 5.0 millimeters were dropped into a constant-velocity airstream. At a critical relative velocity between drop and air, the freely falling drops assumed the form of hollow bags, which subsequently burst and produced a shower of drops. The relation between drop velocity and diameter at breakup could be expressed by the equation

$$U_{rel,b}^2 d_{dr} = 612 \quad (7)$$

where the drop diameter is in millimeters and $U_{rel,b}$ is in meters per second. Additional tests using liquids having surface tensions σ varying from approximately 28 to 475 dynes per centimeter established the relation

$$U_{rel,b} \propto \sqrt{\frac{\sigma}{d_{dr}}} \quad (8)$$

These results are in agreement with the prediction of Hinze that drop breakup is associated with a critical value of Weber number. Experiments conducted with high-velocity transient air blasts showed that under these conditions thin layers were stripped from the drop surface before it was appreciably deformed. Drop-size measurements indicated that equation (7) would predict too great a rate of decrease in drop size at the very high-velocity conditions. On the basis of the Hinze and Lane results, average spray drop size as affected by drop breakup would be expected to be larger for fuels having higher surface tensions and viscosities. Calculations based on the breakup of single drops have been found to give a close estimate of the maximum drop size found in isooctane sprays atomized by high-velocity airstreams (ref. 18).

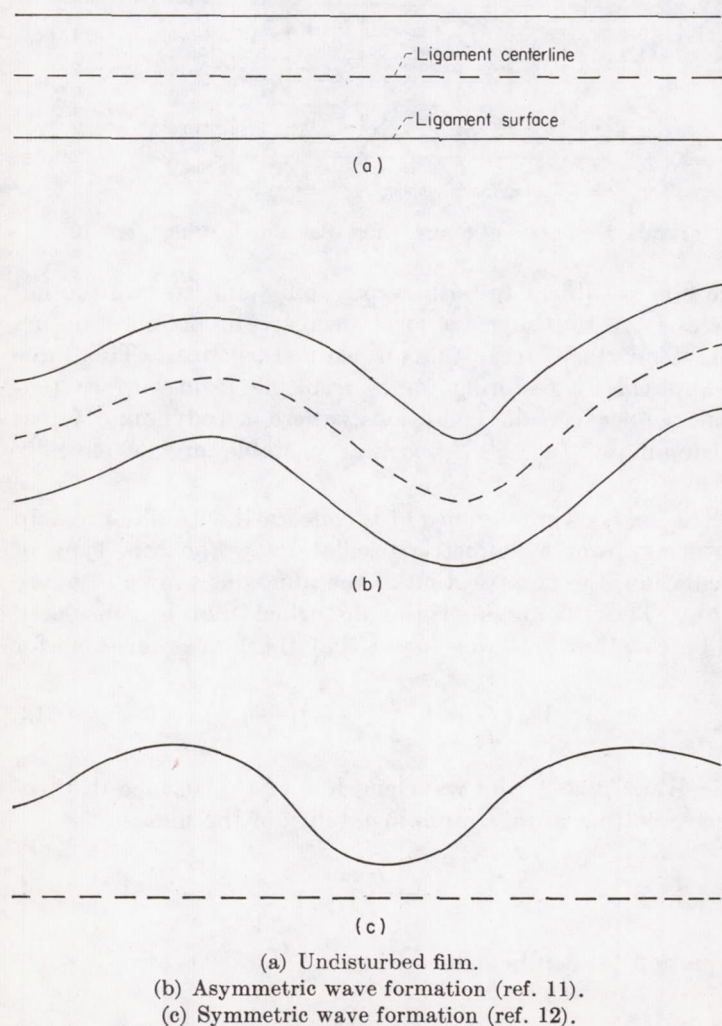


FIGURE 3.—Wave formation for liquid sheets.

Collision of drops with resulting agglomeration may cause a sizable increase in average drop size. Under the high turbulence levels in jet-engine combustors, the collision rate might be expected to be large, particularly where there is a large number of drops per unit volume of combustion space. Where pressure-atomizing nozzles are used, collisions also occur as a result of the difference in velocities of the various sized drops. Under conditions of high nozzle pressure drop, atomization occurs close to the nozzle orifice. Small drops decrease rapidly in velocity and tend to collect near the nozzle. The larger drops, which retain their velocity over longer distances, overtake and collide with smaller drops in their flight path.

The effect of agglomeration is indicated for pressure-atomizing nozzles from determination of mean drop sizes at various distances from the nozzle orifice in reference 19. Agglomeration was believed to have caused the observed increase in mean drop size with increase in distance from the nozzle. In tests using the molten-wax method (ref. 20), agglomeration was found to be quite pronounced for low-cone-angle swirl nozzles operating at high pressure drops.

Drop-size distribution in sprays.—One of the liquid-fuel spray characteristics of direct interest to the combustion-chamber designer is the fractional weight of the spray distributed among the various drop sizes. Drop-size distribution relations have been used in the calculation of theoretical evaporation rates of liquid-fuel sprays (ref. 21). Eventually, when the process of fuel spray evaporation is better understood, knowledge of drop-size distribution will be of use to the designer in the determination of fuel spray evaporation rates for particular designs and operating conditions.

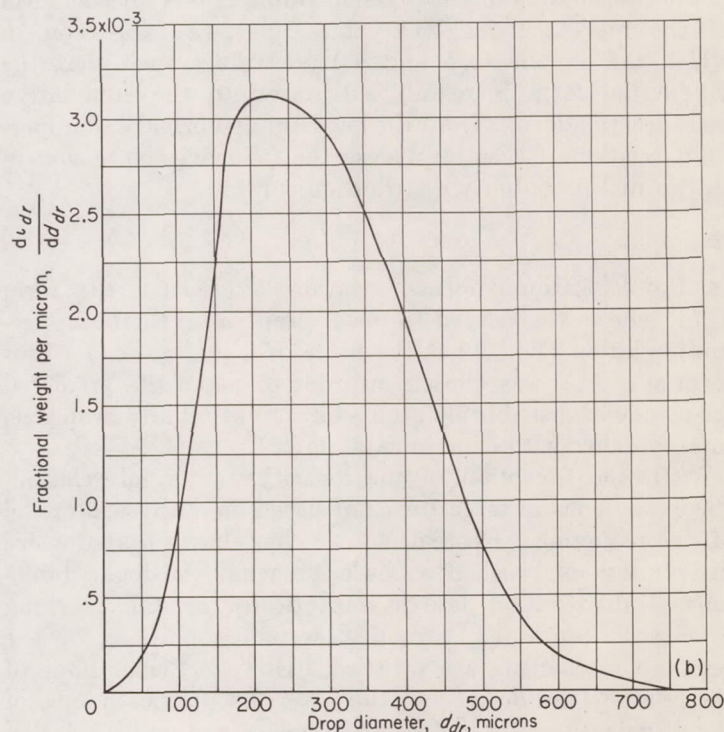
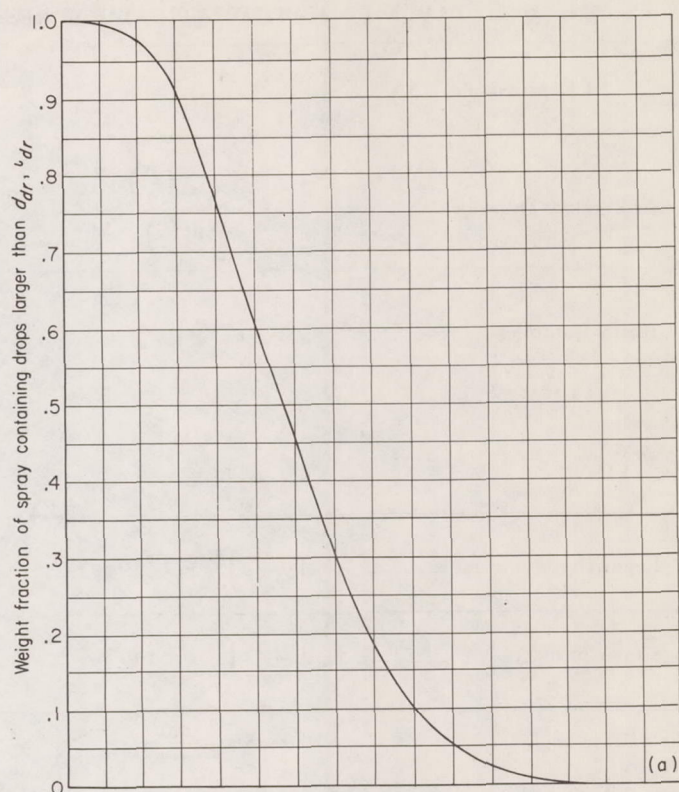
A typical example of the drop-size distribution for a liquid-fuel spray is shown in figure 4(a), where the distribution is given in the cumulative mass-fraction form; that is, the weight fraction ι_{dr} of the total spray containing drops of diameter larger than d_{dr} . In figure 4(b), the same distribution is given in the differential form; here, the area under the curve between two values of d_{dr} represents the weight fraction of the total spray containing that particular range of drop diameters.

Since the theory of atomization is still not completely understood, recourse has been made to empirically fitted mathematical expressions for drop-size distributions, such as presented in table I. Four of the more well-known relations, Nukiyama-Tanasawa (ref. 22), Rosin-Rammler (ref. 23), logarithmic-normal (ref. 24), and upper-limit (ref. 25), are presented in table I. The relations are given in both the cumulative mass-fraction and differential forms. In addition, expressions are given for the mean drop diameter $d_{dr,m}$.

The general expression for $d_{dr,m}$ is given by

$$d_{dr,m} = \left[\frac{\int_0^{N_{dr}} d_{dr}^c d(N_{dr})}{\int_0^{N_{dr}} d_{dr}^s d(N_{dr})} \right]^{\frac{1}{c-s}} = \left[\frac{\int_0^1 d_{dr}^{c-3} d(\iota_{dr})}{\int_0^1 d_{dr}^{s-3} d(\iota_{dr})} \right]^{\frac{1}{c-s}} \quad (9)$$

For example, the Sauter mean diameter $d_{dr,32}$, which involves a ratio of volume d_{dr}^3 and surface d_{dr}^2 , is obtained by setting



(a) Cumulative form.
(b) Differential form.

FIGURE 4.—Fuel spray drop-size distribution.

$c=3$ and $s=2$. Relations for the Sauter mean diameter are also presented in table I.

The median drop diameter $d_{dr,M}$ may also be used. Median drop diameters are defined as diameters dividing the spray into two equal parts, in terms of such properties as volume, surface area, or number. A commonly used median diameter is the mass- or volume-median diameter.

TABLE I.—MATHEMATICAL EXPRESSIONS FOR DROP-SIZE DISTRIBUTION (Ref. 25)

Expression	d_r	$\frac{d d_r}{d d_r}$	$d_{dr,m}^{c-s}$	$d_{dr,32}$
Nukiyama-Tanasawa -----	$1 - \frac{\Gamma(b d_{dr}^q (\frac{6}{q}))}{\Gamma(\frac{6}{q})}$	$\frac{-b^{6/q}}{\Gamma(\frac{6}{q})} d_{dr}^5 e^{-b d_{dr}^q}$	$b^{-(\frac{c-s}{d})} \frac{\Gamma(\frac{c+3}{q})}{\Gamma(\frac{s+3}{q})}$	$\frac{b^{-1/q} \Gamma(\frac{6}{q})}{\Gamma(\frac{5}{q})^5}$
Rosin-Rammler -----	$e^{-b d_{dr}^q}$ or $e^{-(d_{dr}/\Lambda)^{\mathcal{D}}}$	$-b q d_{dr}^{q-1} e^{-b d_{dr}^q}$ or $-\frac{\mathcal{D}}{\Lambda} d_{dr}^{\mathcal{D}-1} e^{-(d_{dr}/\Lambda)^{\mathcal{D}}}$	$\Lambda^{c-s} \frac{\Gamma(\frac{c-3}{\mathcal{D}} + 1)}{\Gamma(\frac{s-3}{\mathcal{D}} + 1)}$	$\frac{b^{-1/q}}{\Gamma(1 - \frac{1}{q})}$ or $\frac{\Lambda}{\Gamma(1 - \frac{1}{\mathcal{D}})}$
Logarithmic-normal ^a -----	$1 - \frac{1}{\sqrt{\pi}} \int_{-\infty}^{qy} e^{-q^2 y^2} d(qy)$	$\frac{-q}{d_{dr} \sqrt{\pi}} e^{-q^2 y^2}$	$\Lambda e^{\frac{c+s-6}{4q^2}}$	$\frac{\Lambda}{e^{1/4q^2}}$
Upper-limit ^b -----	$1 - \frac{1}{\sqrt{\pi}} \int_{-\infty}^{qy} e^{-q^2 y^2} d(qy)$	$\frac{-q d_{dr,max}}{d_{dr}(d_{dr,max} - d_{dr}) \sqrt{\pi}} e^{-q^2 y^2}$		$\frac{d_{dr,max}}{1 + K e^{1/4q^2}}$

^a Where $y = \ln \frac{d_{dr}}{\Lambda}$.^b Where $y = \ln \frac{K d_{dr}}{d_{dr,max} - d_{dr}}$.

The Rosin-Rammler expression (table I) is a special form of the more general Nukiyama-Tanasawa expression in which the exponents b and q have values such that the differential form is readily integrated to the cumulative mass-fraction form. Both the logarithmic-normal and upper-limit relations (see table I) use the following expression in the normal-probability distribution curve:

$$y = \ln[\mathcal{F}(d_{dr})] \quad (10)$$

In the logarithmic-normal relation, $\mathcal{F}(d_{dr})$ has the form d_{dr}/Λ , where Λ is related to mean drop size. In the upper-limit relation $\mathcal{F}(d_{dr})$ has the form $K d_{dr}/(d_{dr,max} - d_{dr})$. This form of $\mathcal{F}(d_{dr})$ was chosen in order to make the predicted frequency of distribution approach zero at a finite drop size, in accordance with experimental data.

With the exception of the logarithmic-normal relation, the expressions in table I are not based on a physical model of size reduction. Epstein (ref. 24) has shown that the size distribution of crushed solids approaches the logarithmic-normal distribution law asymptotically as the crushing process is continued, provided certain conditions of the breakup mechanism are satisfied. However, since none of the relations are derived on the basis of a physical model of the atomization of a fuel spray, the choice of which relation to use must depend upon the ability of the relation to represent accurately the experimental drop-size distribution data. In some cases, the choice based on accuracy of representation may be tempered by ease of use of the relation in application to such processes as fuel spray evaporation and combustion.

The expressions in table I require evaluation of two constants, one a measure of mean drop size and the other a measure of spray uniformity. The upper-limit equation requires evaluation of an additional constant, the maximum

stable drop diameter $d_{dr,max}$. Determination of the constants in the relations of table I, as required for the best fitting of the relations to experimentally determined drop-size distributions, is readily accomplished by graphical methods. Functional scales are employed (e. g., probability paper) so that the data approximate a straight line when plotted. Values of the constants are obtained from the slopes and the intercepts of best straight lines through the data. However, the use of such graphical procedures may result in appreciable error (ref. 26).

Of the four relations in table I, the Rosin-Rammler expression is the easiest to use in the cumulative mass-fraction form. In this form, it is a simple exponential function, whereas the other relations require use of tables of the incomplete gamma function Γ of probability integral. The upper-limit and logarithmic-probability relations have the simplest form in terms of the Sauter mean diameter. The upper-limit relation follows the trends of experimentally determined drop-size distribution data more closely, in that it is based on the existence of a maximum stable drop diameter. While the other relations predict existence of drops of infinite diameter, the predicted frequency of occurrence of the larger-diameter drops becomes quite small. Accordingly, errors associated with the predicted occurrence of infinite-diameter drops may be small where such relations are used in theoretical analyses of fuel spray evaporation or combustion rates, particularly finely atomized sprays. Under these conditions, the Rosin-Rammler relation appears to be the most convenient to use. It should be noted, however, that appreciable differences between calculated and actual mean drop sizes may be encountered in the application of the first three relations of table I, particularly the Nukiyama-Tanasawa relation, to experimental drop-size distribution data (ref. 25). For

example, the Nukiyama-Tanasawa relation may give a Sauter mean diameter larger than that of the largest drop found in the sample. References 25 to 27 give a more complete discussion of the application, advantages, and disadvantages of the relations of table I.

Several other methods of treating experimental drop-size distribution data have been reported in the recent literature. Since these methods have not had much use up to the present time, only a brief description will be given. In reference 28 an adjustment factor (a function of drop diameter) was applied to the logarithmic-normal relation to correct for deviation of the experimental data from the probability curve. The primary purpose of this adjustment factor appears to be correction for the deviation between the experimental and logarithmic-probability distribution in the larger drop-size ranges. Reference 29 found that, for data from a pressure-atomizing nozzle, a plot of the square root of drop diameter gave a better straight-line plot on probability paper than a plot of the diameter to the first power. In reference 30, for data from an air-atomizing nozzle, the following distribution function gave satisfactory representation of the experimental data:

$$\frac{d(N_{dr})}{d(d_{dr})} = KN_{dr}e^{-Kd_{dr}} \quad (11)$$

Dimensional analysis.—Dimensional analyses have been used by a number of investigators in studies of atomization (see, e. g., refs. 4, 20, 31, and 32). Theoretical and experimental investigations of atomization indicate that the following flow and geometric variables should be considered in a dimensional analysis of the atomization process:

Variable	Dimensions (M, L, T system)
Average drop diameter, $d_{dr,av}$	L
Atomizer orifice diameter, d_h	L
Surface tension, σ	M/T ²
Density of atomized liquid, ρ_l	M/L ³
Viscosity of atomized liquid, μ_l	M/LT
Velocity of liquid at orifice, $U_{l,h}$	L/T
Velocity of surrounding fluid, U_g	L/T
Density of surrounding fluid, ρ_g	M/L ³
Viscosity of surrounding fluid, μ_g	M/LT
Ratios of various atomizer dimensions to orifice diameter (dimensionless), R_1, R_2, R_3	

From dimensional analysis, the relation among these variables can be reduced to the following dimensionless equation:

$$\frac{d_{dr,av}}{d_h} = \mathcal{F}(Re_j, We_j, \frac{\rho_g}{\rho_l}, \frac{\mu_g}{\mu_l}, \frac{U_g}{U_{l,h}}, R_1, R_2, R_3 \dots) \quad (12)$$

As previously noted, the jet Weber and Reynolds numbers and the viscosity and density ratios of equation (12) have been encountered in fundamental studies of the breakup of liquid jets and drops. The velocity ratio $U_g/U_{l,h}$ of equation (12) would be important in air atomization.

AIR ATOMIZATION

One of the most extensive series of experiments on air atomization was conducted by Nukiyama and Tanasawa

(refs. 22 and 33 to 35). Drop-size distribution and average drop size were determined for a range of liquid properties, flow conditions, and atomizer sizes and configurations. With the exception of a few scattered tests, all data were obtained at subsonic air velocities. All tests were conducted with the atomizer exhausting into the room air. Drop sizes were determined by collecting samples of the spray on small oil-coated glass slides. The experimental results were expressed in terms of the Sauter mean diameter $d_{dr,32}$ calculated directly from the data by the equation

$$d_{dr,32} = \frac{\sum d_{dr}^3 \Delta N_{dr}}{\sum d_{dr}^2 \Delta N_{dr}} \quad (13)$$

where ΔN_{dr} is the number of droplets having diameters between $d_{dr} - (\Delta d_{dr}/2)$ and $d_{dr} + (\Delta d_{dr}/2)$. The degree of accuracy of drop-size measurements was estimated to be on the order of ± 15 percent.

In reference 33, experiments were conducted using water and a converging air nozzle as shown in figure 5(a). The Sauter mean diameter was essentially independent of the size of the air and water nozzles for water-nozzle diameters from 0.2 to 1.0 millimeter and air-nozzle diameters from 2 to 5 millimeters. Transition from laminar to turbulent flow conditions in the water jet appeared to have little effect on drop size. The Sauter mean diameter was found to be a function of (1) the relative velocity U_{rel} between water and air and (2) the ratio of volume flow rates of air and water $V_{fl,a}/V_{fl,w}$. The volume flow rate of air was computed on the basis of the density at the throat of the air nozzle. The relative velocity U_{rel} was calculated from the volume flow rates and the cross-sectional areas at the throats of the water and air nozzles. Drop size decreased with increasing $V_{fl,a}/V_{fl,w}$. However, for $V_{fl,a}/V_{fl,w} > 5000$, the effect of the ratio became negligible, and $d_{dr,32}$ was inversely proportional to the relative velocity.

In reference 34, similar experiments were conducted with water and the two atomizers shown in figures 5(b) and (c). The data covered a range of nozzle sizes and flow conditions. It was concluded that, if the air velocity is based on the cross-sectional area of the vena contracta, there is no effect of atomizer configuration on average drop size. Relative position of the water and air nozzles had a negligible effect on average drop size, even when the water nozzle was well into the vena contracta region of the air jet. However, at greater

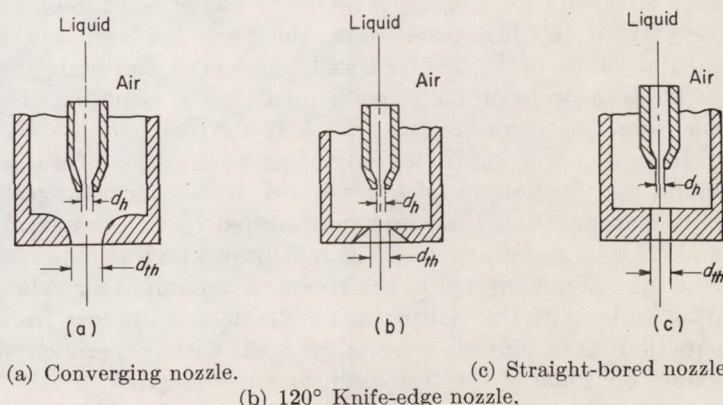


FIGURE 5.—Air-atomizing nozzles (refs. 22 and 33 to 35).

distances downstream of the air jet where lower air velocities would exist, an increase in average drop size was obtained. The sizes of air and water nozzles were again found to have little effect on average drop sizes.

In reference 22, the Nukiyama-Tanasawa distribution function (table I) was developed and applied to data from references 33 and 34. For high values of $V_{f,l,a}/V_{f,l,i}$ and U_{rel} , the values of b and q in this relation were found to be 2 and 1, respectively, for all nozzles. At low values of either $V_{f,l,a}/V_{f,l,i}$ or U_{rel} , $b=2$ and $q<1$.

In reference 35, drop-size distributions and average drop sizes were determined for the nozzle type of figure 5(c) over a range of atomizer sizes, flow conditions, and liquid properties. Ranges of liquid surface tensions σ from 30 to 73 dynes per centimeter, densities ρ_l from 0.8 to 1.2 grams per cubic centimeter, and viscosities μ_l from 0.01 to 0.3 poise were obtained by varying the proportions of an alcohol-glycerin-water solution. The effects of flow conditions and liquid properties on average drop size were correlated by the expression

$$d_{dr,32} = 585 \frac{\sqrt{\sigma}}{U_{rel} \sqrt{\rho_l}} + 597 \left(\frac{\mu_l}{\sqrt{\sigma \rho_l}} \right)^{0.45} \left(1000 \frac{V_{f,l,i}}{V_{f,l,a}} \right)^{1.5} \text{ microns} \quad (14)$$

where the fuel properties have the units given previously and U_{rel} is in meters per second. From this relation, it is seen that, for large values of $V_{f,l,a}/V_{f,l,i}$, atomization is a function only of relative velocity, surface tension, and liquid density. At lower values of $V_{f,l,a}/V_{f,l,i}$, drop size increases and liquid viscosity influences atomization. [Equation (14) is not dimensionally consistent.]

Ingebo (ref. 18) made a photographic investigation of isooctane sprays produced by contraststream injection from a simple orifice into high-velocity airstreams. The air pressure, air temperature, and fuel-orifice pressure drop were held constant during the tests. The mean drop diameter $d_{dr,20}$ (diam. of drop having area equal to total spray area divided by total number of drops in spray) was determined at several stations downstream of the fuel injector for air velocities of 140 and 180 feet per second. In order to compare experimental values of $d_{dr,20}$ with values predicted by equation (14), use was made of the following relation, obtained from the Nukiyama-Tanasawa distribution function (ref. 22) for q equal to 1 (see table I):

$$d_{dr,20} = 0.693 d_{dr,32} \quad (15)$$

At a distance 1 inch downstream of the fuel orifice and an air velocity of 180 feet per second, the predicted and experimental values of $d_{dr,20}$ agreed well. However, the change in mean drop size with air velocity predicted by equation (14) was somewhat greater than that found experimentally.

Hrubecky (ref. 36), in a study of air atomization of water, found that (1) liquid injection parallel to the airstream gave better atomization than injection normal to the airstream, and (2) best atomization with parallel injection was obtained when the liquid entered in the region of maximum air velocity. Values of the Sauter mean diameter obtained from equation (14) agreed reasonably well with experimental values for some of the test conditions investigated.

The experiments of Nukiyama and Tanasawa did not cover the effects of gas properties on atomization. However, in reference 37, some limited experimental results are presented which indicate the general effect of gas temperature, viscosity, and density on median drop size for Venturi atomizers. Comparison of data obtained with nitrogen and ethene as the atomizing gases indicated that, at constant gas velocity, density, and ratio of liquid-to-gas volume flow rates, a 60-percent decrease in gas viscosity resulted in approximately the same percentage increase in median diameter. The effect of gas density on atomization was indicated from comparison of data obtained with nitrogen and helium as the atomizing gases. At constant gas viscosity and ratio of liquid-to-gas volume flow rates, a decrease in gas density at the atomizer throat from 1.18 to 0.169 gram per liter resulted in an approximately twofold increase in median drop diameter despite an increase in velocity.

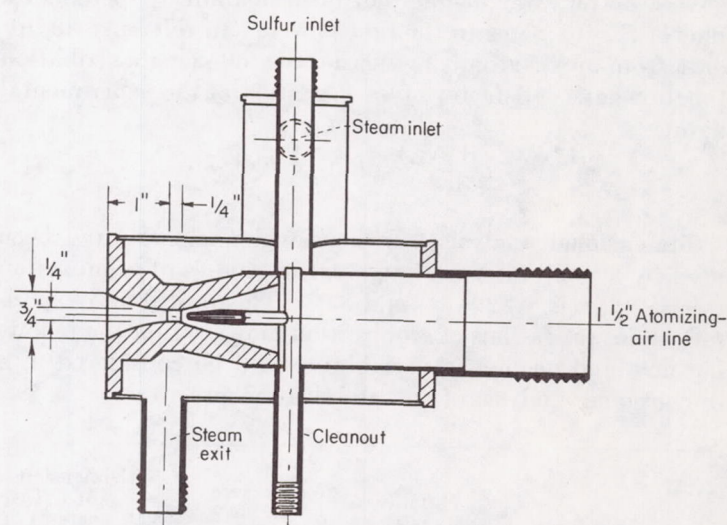
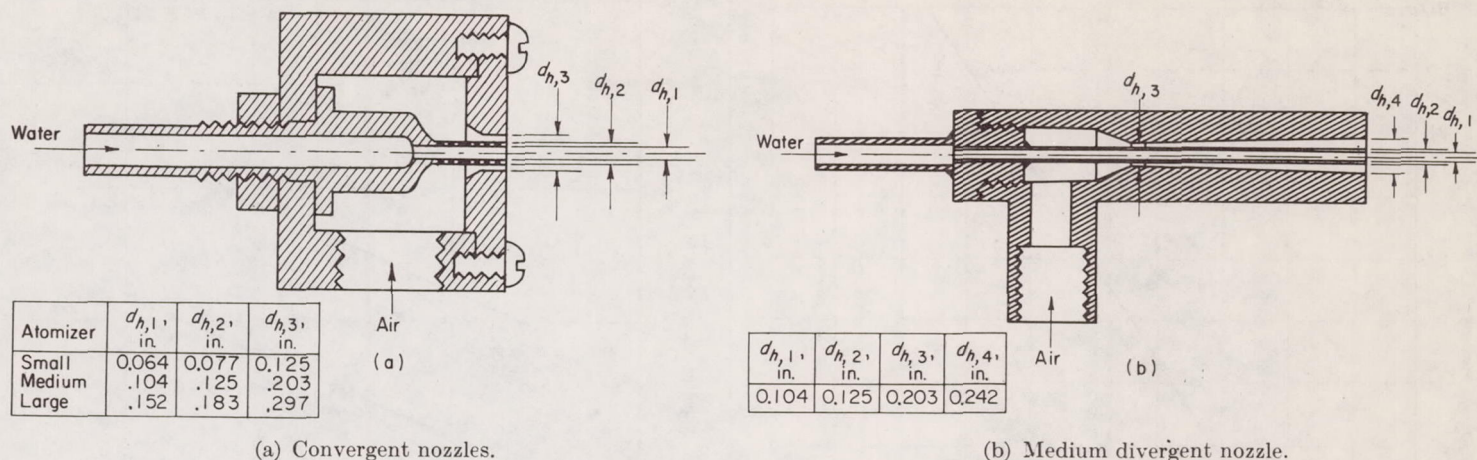


FIGURE 6.—Venturi-type sulfur atomizer (reprinted by permission from ref. 38).

Results obtained with an exhaust-gas Venturi atomizer indicated that, at high liquid-to-gas volume flow ratios, improved atomization would be expected with the use of high atomizing-gas temperatures. At low ratios of liquid-to-gas volume flow rates, the improvement would be small. This result is consistent with trends suggested by consideration of the Nukiyama-Tanasawa drop-size correlation (eq. (14)) and effects of increased temperature on fuel viscosity. Heating the fuel by the high-temperature atomizing gas would result in lowered fuel viscosity. As indicated by equation (14), this reduced viscosity would appreciably affect drop size only at the large ratios of liquid-to-gas volume flow rates. The effect would be expected to be greater for liquids having high viscosity indices.

Drop-size measurements were made in reference 38 for the atomization of molten sulfur in a Venturi-type atomizer. A sketch of the atomizer is presented in figure 6. The throat had a diameter of 1/4 inch. A flared diverging section was provided to reduce wall wetting. The air temperature for all experiments was held at approximately 293° F.



(a) Convergent nozzles.

(b) Medium divergent nozzle.

FIGURE 7.—Sonic air-atomizing nozzles (ref. 39).

For subsonic throat velocities, the Sauter mean diameter $d_{dr,32}$ in microns was given in reference 38 by

$$d_{dr,32} = \frac{26,100}{U_{rel}} + 75 \left(1000 \frac{V_{fl,l}}{V_{fl,a}} \right)^{1.5} \quad (16)$$

where the volume flow rate of air was based on conditions at the Venturi throat. The Sauter mean diameter was given in terms of weight flow by

$$d_{dr,32} = 687 \frac{\left(1.5 + \frac{w_l}{w_a} \right)}{w_a^{0.9}} \quad (17)$$

where U_{rel} is in feet per second and w_a and w_l are the weight-flow rates of air and sulfur, respectively, in pounds per hour. It was noted that the data at subsonic air velocities were in approximate agreement with the predictions of the Nukiyama-Tanasawa equation if approximate corrections were made for the effect of air temperature on atomization as found in reference 37.

For a limited set of data at sonic throat velocities,

$$d_{dr,32} = 29,900 \frac{\left(1.5 + \frac{w_l}{w_a} \right)}{w_a^{1.63}} \quad (18)$$

It was suggested that equations (17) and (18) could be applied to other atomizers by multiplying w_a and w_l for the new atomizer by $(0.25/d_{th})^2$, where d_{th} is the new throat diameter in inches.

Air atomization at sonic air velocities was also studied in reference 39. All tests were conducted for the atomizers exhausting to room air. Drop samples were collected by swinging a transparent, oil-coated plastic slide across the spray. The drop samples were analyzed by photomicrographing the slides and counting the number of drops contained within 5-micron intervals of drop diameter. Results were expressed in terms of the volume-median drop diameter—that is, the drop diameter that divides the spray into two groups of equal volume. Three convergent nozzles and one divergent nozzle were tested. The three convergent nozzles

were scaled in proportion, as indicated in figure 7(a). A sketch of the divergent nozzle is shown in figure 7(b).

The results of the tests for water atomization are presented in figure 8, where the volume-median diameter is plotted against the water-to-air weight-flow ratio. The atomization was independent of either air pressure or water-flow rate for a constant value of water-to-air weight-flow ratio. The volume-median diameter increased with increase in nozzle size and water-to-air weight-flow ratio. The nozzle-size effects were considered to be mainly a function of the air-orifice size. As indicated in figure 8, the divergent nozzle produced larger median drop diameters than the convergent nozzle having the same throat diameter. This result might be

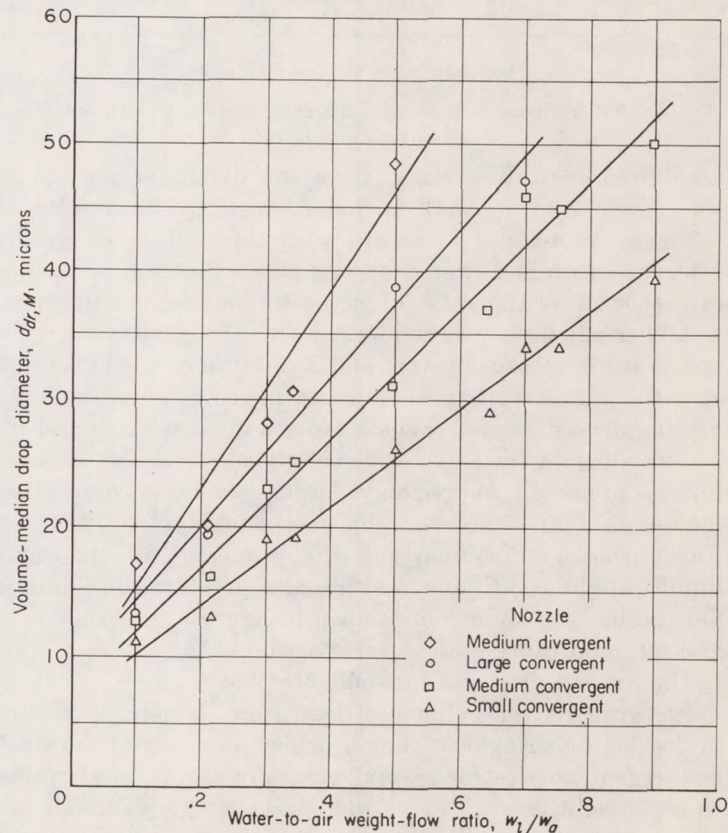


FIGURE 8.—Effect of water-to-air weight-flow ratio on volume-median drop diameter (ref. 39).

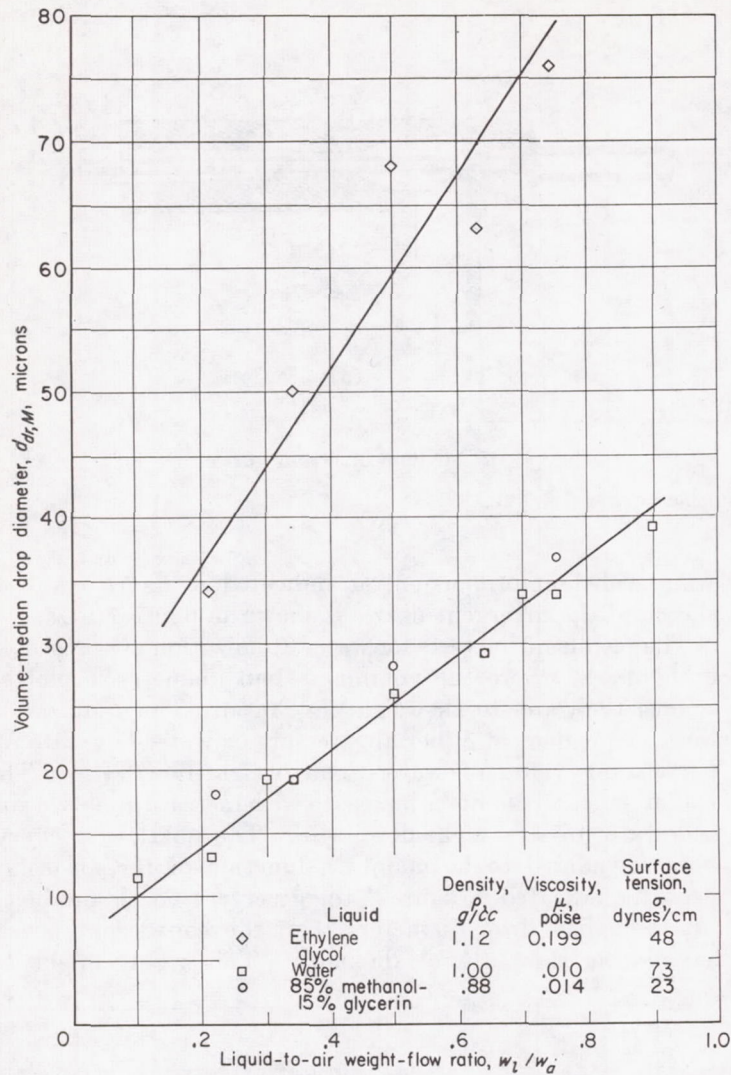


FIGURE 9.—Volume-median drop diameter obtained with sonic air atomization (ref. 39).

attributed to wall wetting, since the divergent portion of the nozzle had a small included angle. The results of reference 39 are not in accord with those of reference 38, where it was found that drop size was a function of airflow rate as well as the ratio of liquid-to-air weight-flow rates.

Additional tests were conducted with the small convergent nozzle using ethylene glycol and a mixture of methanol and glycerin. The results are shown in figure 9, where volume-median drop diameter is again plotted against the liquid-to-air weight-flow ratio. Ethylene glycol, a dense, viscous liquid, produced appreciably larger volume-median drop diameters than water or the methanol-glycerin mixture. For purposes of comparison, the properties of the three liquids at the conditions used are also presented in figure 9. On the basis of the results shown in figure 9, viscosity is of greater importance than surface tension in the determination of the median drop size for sonic atomizers.

In figure 10, the volume-median drop diameter is plotted on log-log paper against the air-orifice diameter of the three convergent nozzles for several values of the ratio of water-to-air weight-flow rate. From the average value of the slopes of best straight lines through the data, the volume-

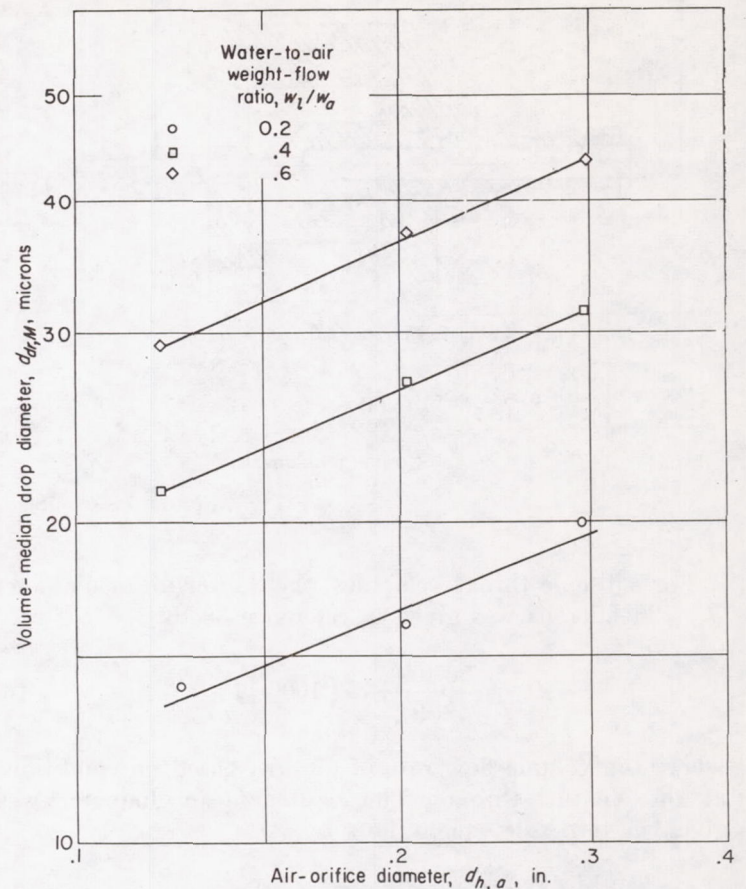
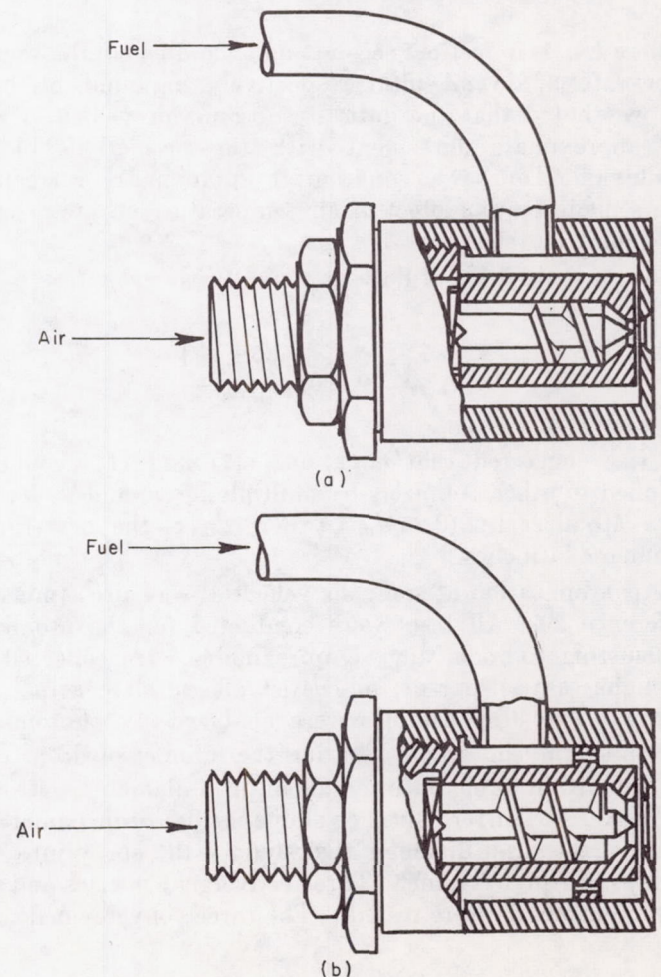


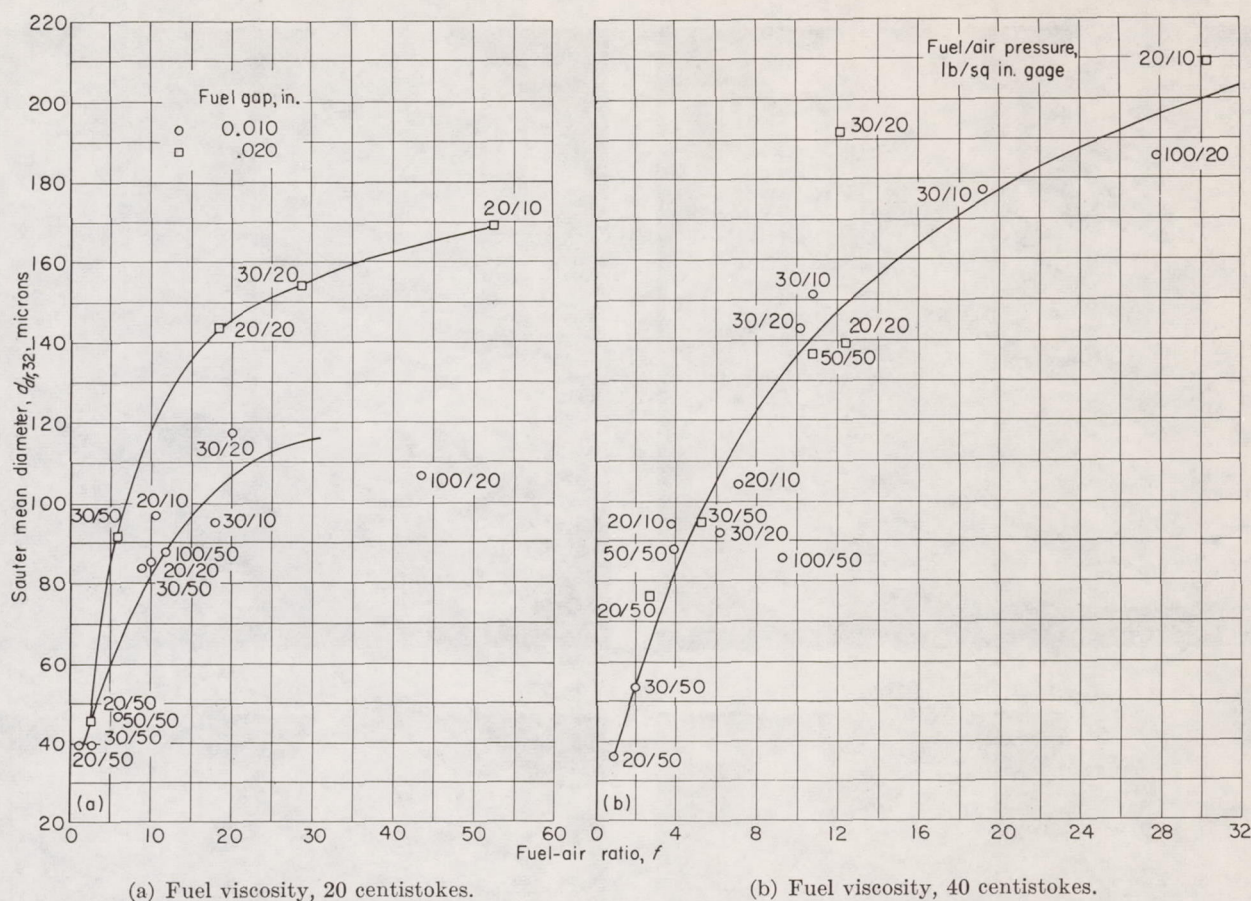
FIGURE 10.—Effect of air-orifice diameter of sonic air atomizer on volume-median drop diameter (ref. 39).



(a) $\frac{1}{8}$ -Inch orifice.

(b) $\frac{1}{4}$ -Inch orifice.

FIGURE 11.—High-pressure air atomizers (refs. 30 and 40).



(a) Fuel viscosity, 20 centistokes.

(b) Fuel viscosity, 40 centistokes.

FIGURE 12.—Sauter mean diameter against fuel-air ratio for $\frac{1}{4}$ -inch atomizer (ref. 40).

median drop diameter is approximately proportional to the 0.4 power of the air-orifice diameter.

Tests were conducted in reference 30 to determine flow characteristics and drop-size distribution for a particular high-pressure air atomizer designed to be used with highly viscous fuels in gas-turbine combustors. The general features of the atomizer are presented in figure 11(a). A high rotational speed was imparted to the air by means of the helical swirler in the innerbody. Fuel entered the atomizing section in a radial direction through a narrow gap formed between the end of the innerbody and the outer casing. This type of design presented the fuel as a thin film to a high-speed, swirling airstream. Tests were made for two fuel-gap widths (0.005 and 0.010 in.), air pressures from 20 to 100 pounds per square inch gage, and fuel pressures from 10 to 50 pounds per square inch gage. All data were obtained with the atomizer exhausting to room air. Drop sizes were determined by the molten-wax method, with the wax preheated to simulate fuels having kinematic viscosities of 10 and 20 centistokes, respectively. In order to minimize effects of changes in viscosity with cooling on the initial phase of atomization, the supply temperatures of the atomizing air and wax were held at the same value. The experimental drop-size data were satisfactorily represented by equation (11). Although the information obtained was insufficient to determine definite correlations, the data indicated that average drop size increased with (1) increase in fuel flow, (2) decrease in airflow, (3) increase in fuel gap, and (4) increase in fuel viscosity. The range of ratios of fuel- to air-mass-flow rates was appreciably larger (0.8

to 400) than that investigated in reference 39 (0.1 to 0.9).

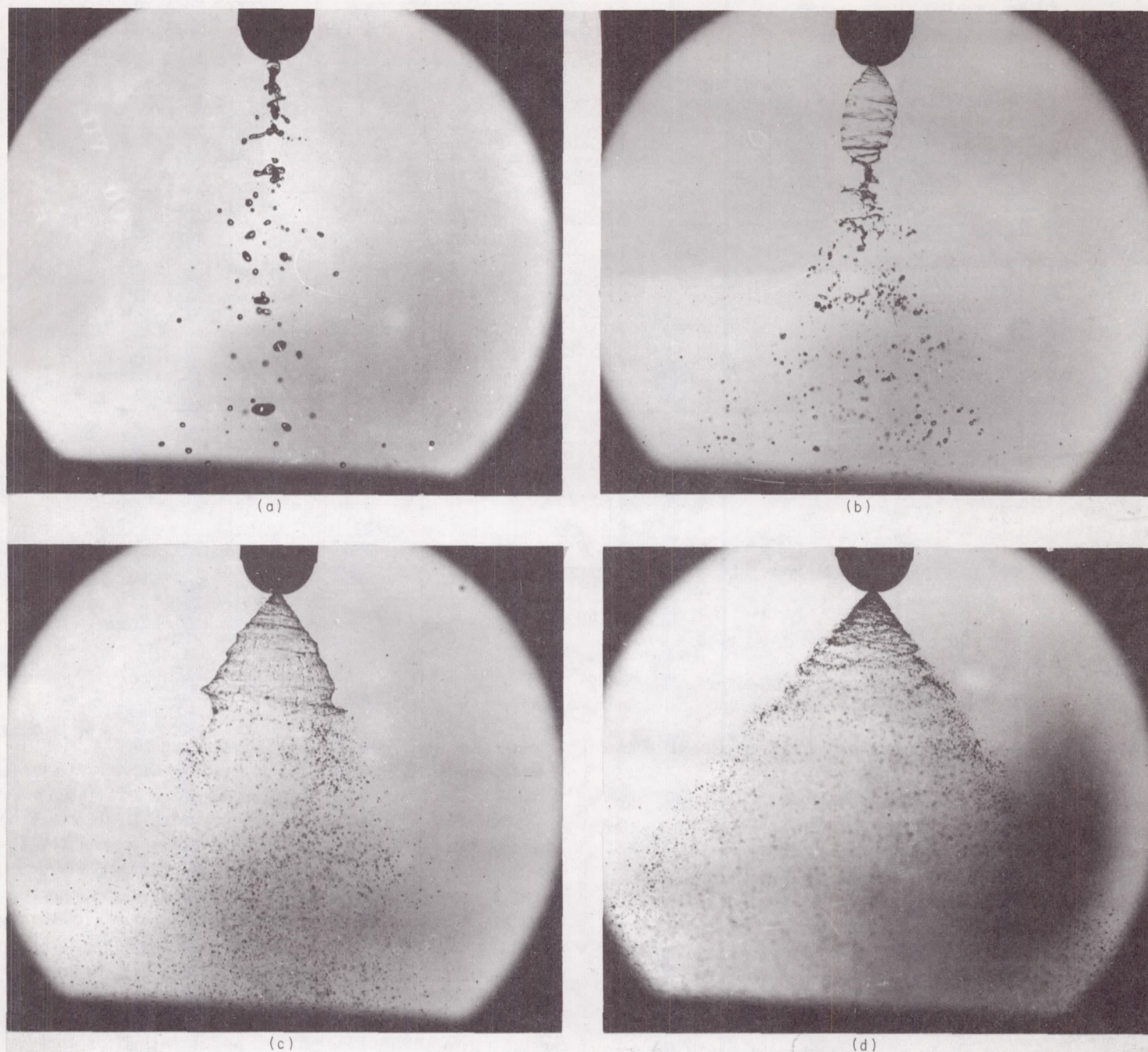
In reference 40, additional tests were conducted on a larger version of the N. G. T. E. air-blast atomizer of reference 30. A sketch of the larger atomizer is presented in figure 11(b). There is some difference in the general features of the two atomizers of figure 11. However, the actual atomizing sections were considered to have sufficient geometric similarity to permit some confidence to be placed in conclusions as to the effect of atomizer size on mean drop size. The experimental drop-size data were again found to be satisfactorily represented by equation (11).

The data of reference 40 are plotted in figure 12 as the Sauter mean diameter against fuel-air ratios for fuel viscosities of 20 and 40 centistokes. An approximate correlation is indicated. However, it was noted in reference 40 that, at a given fuel-air ratio, smaller mean drop sizes were obtained at the higher fuel-flow (or airflow) rates. This trend is in agreement with the results obtained in reference 38.

From comparison of the drop-size data obtained with the atomizers of references 30 and 40 it was concluded that mean drop size was approximately proportional to the square root of the air-orifice diameter. This is in reasonable agreement with the data obtained in reference 39 (see fig. 10).

CENTRIFUGAL PRESSURE-ATOMIZING NOZZLES

The centrifugal pressure-atomizing nozzle, which is widely used in gas-turbine combustors, can produce well-atomized sprays without the high efflux velocities, and hence long penetration distances, of the simple orifice nozzles such as used in diesel engines. In addition, its wide dispersion of fuel is conducive to better mixing of fuel and air.



(a) Pressure drop, 0.8 pound per square inch.
 (c) Pressure drop, 4.5 pounds per square inch.

(b) Pressure drop, 2 pounds per square inch.
 (d) Pressure drop, 34 pounds per square inch.

FIGURE 13.—Variation of fuel spray configuration with fuel-nozzle pressure drop.

The general characteristics of the spray produced by a fixed-configuration centrifugal pressure-atomizing (simplex) nozzle at various nozzle pressure drops are illustrated in figure 13. The pictures were obtained with the nozzle spraying JP-1 fuel into quiescent room air. Four steps in spray formation are evident. At a very low pressure drop (fig. 13(a)) the rotational energy imparted to the fuel by the nozzle is so low that the fuel simply dribbles from the orifice. With an increase in pressure drop (fig. 13(b)) a "bubble" form of the spray appears. The turbulent, high-temperature gas streams in the combustor would probably

break up this "bubble" to form a coarse spray. The surface disturbances considered in the analyses of spray formation (see section on atomization theory) are indicated by the corrugations in the liquid film. With further increase in pressure drop (fig. 13(c)) the "bubble" opens. However, the corrugated film persists for some distance from the nozzle orifice, and the spray-cone angle is not well defined. Finally, at a high pressure drop (fig. 13(d)) the corrugated film breaks up close to the nozzle orifice, and a relatively fine spray having a well-defined cone angle is produced.

Much work has been devoted to the simplex nozzle as a

result of the impetus given by its use in the earlier models of aircraft gas-turbine combustors and for such industrial purposes as spray-drying. The two general types of the simplex nozzle used might be classified as the grooved-core and the whirl-chamber types. In the grooved-core nozzle, the swirl required for the hollow-cone spray is obtained by using spiral grooves in the nozzle insert. In the whirl-chamber nozzle, this swirl is imparted by injecting the liquid tangentially into a whirl chamber. The major portion of data reported on drop-size distribution has been obtained with the whirl-type nozzle. With the exception of some limited data in references 2 and 41, no published data are available for wide-flow-range nozzles such as the duplex that are generally used in current turbojet-engine combustors. The various types of simplex and wide-flow-range nozzles are described in references 42 to 44.

It is emphasized that only a few of the investigations have been of such scope as to offer hope of predicting reasonably accurate atomization characteristics for nozzles, fuels, or operating conditions other than the particular ones tested. Appreciably different variation in trends and sometimes opposite trends have been obtained or suggested by different investigators. In addition, values for average drop size and spray uniformity have usually been obtained for the nozzles spraying into quiescent air at room temperature and pressure. Under actual combustor conditions, the fuel spray is generally subjected to a blast of highly turbulent hot gases covering a range of pressures, temperatures, and velocities. Quantitative knowledge of the effect of such variables on fuel sprays from swirl-type nozzles is lacking. However, some trends may be assumed from results of several of the investigations reported in the literature. In general, data available in the literature on fuel sprays are sufficient to give the combustor designer a rough idea of the spray-atomization characteristics required for calculations of fuel spray burning and evaporation rates.

An extensive study of atomization for centrifugal pressure nozzles operating with fuel oil was made by Longwell (ref. 45). Drop-size distribution was determined by freezing part of the spray and sieving drops into various size groups. The drop-size distribution data were correlated by the following equations:

$$d_{dr,M} = \frac{0.72 \times 10^4 r_h e^{0.70v}}{\sin \frac{\beta}{2} \Delta p_n^{0.37}} \quad (19)$$

$$\iota_{dr} = e^{-0.693 \left(\frac{d_{dr}}{d_{dr,M}} \right)^{\mathcal{D}}} \quad (20)$$

where

- \mathcal{D} distribution constant
- d_{dr} drop diameter, microns
- $d_{dr,M}$ mass-median drop diameter, microns
- Δp_n nozzle pressure drop (50 to 300 lb/sq in.)
- r_h nozzle-orifice radius (0.04 to 1.4 cm)
- β spray-cone angle (60° to 120°)
- ι_{dr} fractional weight of spray containing drops of diameter larger than d_{dr}
- v kinematic viscosity (0.08 to 0.8 cm²/sec)

The distribution constant, which is a measure of the weight fraction of spray contained within a given range of drop diameters about the most probable drop diameter, is plotted in figure 14. Larger values of \mathcal{D} are associated with large fractions of the spray contained within the given drop-size range and consequently with a more uniform spray.

Correlations of drop-size data with operating parameters are given by Bowen and Joyce (ref. 46) and by Watson (ref. 47). As an example of such correlations, Watson reports that

$$d_{dr,32} = a(N_{fl})^i (v)^j (\Delta p_n)^{-k} \quad (21)$$

where the flow number N_{fl} is defined as

$$N_{fl} = \frac{\text{Flow rate (gal/hr)}}{\sqrt{\Delta p_n}} \quad (22)$$

Watson reports that Joseph Lucas and Company data show the exponents to have the following values:

$$\left. \begin{aligned} i &= 0.209 \\ j &= 0.215 \\ k &= 0.348 \end{aligned} \right\} \quad (23)$$

With these values equation (21) can be rearranged into log form as

$$\log d_{dr,32} = \log \mathcal{B} + 0.209 \log N_{fl} + 0.215 \log v - 0.348 \log \Delta p_n \quad (24)$$

In reference 48, the drop-size data for two Monarch nozzles having rated capacities of 3.0 and 17.5 gallons per hour

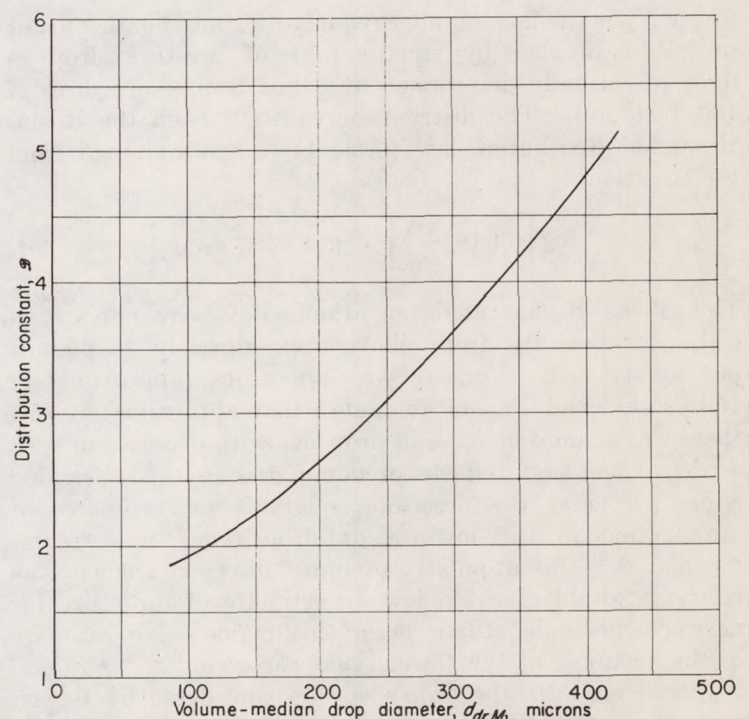


FIGURE 14.—Distribution constant for a fuel-oil spray (ref. 45).

were correlated in terms of the Rosin-Rammler distribution function. Molten wax, simulating kerosene, was sprayed into room air. Nozzle pressure drops ranged from 25 to 150 pounds per square inch. Drop sizes were determined by measuring photographs of representative samples of the solidified droplets. The final results were expressed by the following equations:

For the 3.0-gallon-per-hour nozzle:

$$\Lambda = 494 \Delta p_n^{-0.368} \text{ microns} \quad (25)$$

$$d_{dr,32} = 392 \Delta p_n^{-0.368} \text{ microns} \quad (26)$$

For the 17.5-gallon-per-hour nozzle:

$$\Lambda = 342 \Delta p_n^{-0.17} \text{ microns} \quad (27)$$

$$d_{dr,32} = 251 \Delta p_n^{-0.17} \text{ microns} \quad (28)$$

The spray-cone angles of the nozzles were not reported.

Bowen and Joyce (ref. 46) obtained correlations based on the complete set of molten-wax data up to that time. All the data were obtained with molten wax having a viscosity simulating that of kerosene (approximately 2.0 centistokes). The major portion of the data was obtained with Joseph Lucas and Company whirl-type centrifugal atomizers. The general features of the swirl chambers of these atomizers are given in reference 49. The following correlations were given:

$$\log d_{dr,32} = 2.6164 - (0.3712 - 0.0258 N_{fi}) \log \Delta p_n \quad (29)$$

$$\log \Lambda = (2.7008 + 0.02162 N_{fi}) - (0.3358 - 0.02427 N_{fi}) \log \Delta p_n \quad (30)$$

where N_{fi} is the flow number (equals 1.2 times nozzle output in gal/hr divided by square root of pressure drop in lb/sq in.; usually determined at a nozzle pressure drop of 100 lb/sq in.). The distribution constant \mathcal{D} in the Rosin-Rammler distribution law (table I) can be obtained from the equation

$$\log \left[\Gamma \left(1 - \frac{1}{\mathcal{D}} \right) \right] = \log \Lambda - \log d_{dr,32} \quad (31)$$

The effects of cone angle on atomization were not appreciable for pressure drops above approximately 30 pounds per square inch. For low pressure drops (approximately 10 lb/sq in.) and for cone angles less than approximately 75°, there was a rapid increase in drop size with decrease in cone angle. Cone-angle effects predominated in this operating region. Use of the preceding relations for estimates of atomization in the low-pressure-drop range was recommended only for atomizers of optimum cone angle. The relations would give too low an estimate of drop size for narrow-cone-angle atomizers in this region. No estimate of the accuracy of the correlations was given.

In reference 50, the drop-size data considered by Bowen and Joyce (ref. 46) were reanalyzed using the multiple-regression technique. An equation for the Sauter mean diameter of the form used by Bowen and Joyce was obtained and is given by

$\log d_{dr,32} = 2.6447 - (0.3970 - 0.03153 N_{fi}) \log \Delta p_n \quad (32)$
This equation gave an accuracy of ± 22.9 percent. The data were also correlated in terms of an equation of simpler form given by

$$\log d_{dr,32} = 2.6219 - 0.3395 \log \Delta p_n + 0.1979 \log N_{fi} \quad (33)$$

This equation gave an accuracy of ± 23.3 percent. An additional correlation including the effects of cone angle β was given by

$$\begin{aligned} \log d_{dr,32} = & 3.5060 - 0.5853 \log \Delta p_n + 0.08171 \log N_{fi} + \\ & 0.02331 N_{fi} \log \Delta p_n - 0.01743 \beta + 0.00008236 \beta^2 + \\ & 0.002467 \beta \log \Delta p_n \end{aligned} \quad (34)$$

This equation gave an accuracy of ± 18.1 percent. Use of this complicated equation was not considered warranted except under exceptional circumstances.

All the data of Bowen and Joyce considered in the foregoing correlations were obtained for a molten-wax viscosity of approximately 2.0 centistokes. However, Joyce (ref. 44) has presented a graph giving the results of some preliminary tests on the effect of viscosity on Sauter mean diameter. At a nozzle pressure drop of 100 pounds per square inch, an increase in kinematic viscosity from 2 to 18.5 centistokes increased the Sauter mean diameter from approximately 97 to 140 microns. The results of reference 44 indicate that the Sauter mean diameter is approximately proportional to viscosity to the 0.25 power.

A study of spatial spray distribution, drop-size distribution, and capacity of centrifugal pressure-atomizing nozzles is reported by Tate and Marshall (ref. 29). The drop-size distribution data were obtained with grooved-core commercial nozzles and dyed water. Spray samples were collected in glass-bottom collecting cells filled with a solution immiscible with water. Drop sizes were determined from a visual count of photomicrographs of the samples. Mean drop size and spray uniformity are expressed in terms of orifice diameter and calculated tangential and vertical velocities of the sprayed liquid. These velocity components are "superficial average" velocities, the tangential component being based on conditions just upstream of the orifice, and the vertical component on the assumption of a full-flowing orifice. Graphs and equations are presented that permit the calculation of drop-size distribution for the particular nozzles and operating conditions investigated. A method is suggested that might permit use of the correlation for whirl-chamber centrifugal nozzles. However, no confirmation of this method is given. No data were obtained to permit estimation of drop-size distribution for liquids other than water. However, a limited set of data was obtained giving the effect of viscosity on mean drop size for one grooved-core nozzle operating at constant pressure. When kinematic viscosity was increased from 1 to 7 centistokes, mean drop size increased from approximately 54 to 78 microns. The relation of Longwell (ref. 45) for the effect of pressure drop, orifice diameter, cone angle, and viscosity on mean drop size did not fit the data obtained in this investigation.

Shafer and Bovey (ref. 32) correlated the drop-size data of Rupe (ref. 19) in terms of the dimensionless group

$d_j \Delta p_n / \sigma$. The correlation indicates that, for the range of experimental conditions investigated by Rupe, surface tension was the major liquid property affecting drop size.

Turner and Moulton (ref. 28) obtained drop-size distribution data for several commercial grooved-core and whirl-chamber centrifugal pressure nozzles. Organic materials that solidified well above room temperature were sprayed into room air. The solidified droplets from the entire spray were collected, and a representative sample was analyzed by visual count under high magnification. Graphs and equations that permit calculation of drop-size distribution for the particular nozzles and operating conditions investigated are presented in reference 28. Data were obtained over a limited range of surface tensions and viscosities. The data indicated that mean drop size was proportional to (1) surface tension to powers from approximately 0.6 to 1.0, (2) viscosity to the 0.25 power or less, (3) weight-flow rate to the -0.38 to -0.58 power, and (4) orifice diameter to approximately the 1.5 power. The effect of liquid density on atomization was not determined. If the correlation is expressed in terms of injection pressure differential as a variable, the mean drop size will be approximately proportional to the square root of the orifice diameter, a result in agreement with reference 43.

The correlations of reference 28 predict surface-tension effects that are appreciably greater than expected (e. g., ref. 44). However, in reference 51, tests on a swirl-type pressure atomizer indicated that the changes in surface tension to be found among the various hydrocarbon-type fuels would have a negligible effect on average drop size. Viscosity was considered to be the dominant fuel property in the determination of fineness of atomization.

In reference 52 some drop-size measurements are reported for hollow-cone and solid-cone commercial nozzles spraying into room air. Water was used for all tests. With one exception, the nozzle pressure drop was 50 pounds per square inch. Spray samples were collected on greased glass slides and were photographed and measured under magnification. Reasonable agreement was found between the observed drop-size distribution and values obtained by other investigators (ref. 53) with the same type nozzles. The results indicated no significant difference in mean drop sizes produced by the hollow-cone and solid-cone nozzles. On the basis of the combined data for both type nozzles, it was concluded that the mass-median diameter was approximately proportional to the orifice diameter. This would be in agreement with the conclusion of Longwell (ref. 45). However, it is noted that, if the data were restricted to those obtained with the hollow-cone nozzles, the mass-median diameter would be approximately proportional to the 0.6 power of the orifice diameter, a result similar to that reported in references 28 and 46.

The drop-size correlations presented were based on data obtained with the nozzle spraying into quiescent room air. In turbojet combustors, however, the fuel is sprayed into highly turbulent gas streams covering a range of pressures, temperatures, and velocities. Investigations of the effect of these factors on atomization are sufficient to give only an indication of the trends involved.

The data of Lewis et al. (ref. 37) and Garner and Henny (ref. 54) indicate that drop size increases with a decrease in the pressure of the surrounding gas. The results of reference 37 also indicate that drop size increases with a decrease in the temperature of the surrounding gas.

Kruse, Hess, and Ludvik (ref. 55) have investigated the effect of air velocity and direction on the Sauter mean diameter. The results are illustrated in figure 15. With contra-stream injection, there was a steady decrease in drop size with increase in air velocity. With injection in the direction of the airstream, the drop size increased with increase in air velocity up to a point where the air and liquid velocities were approximately equal. Further increase in air velocity then resulted in a decrease in the drop size which approached that obtained with contrastream injection. Additional tests with the nozzle spraying normal to the airstream indicated drop sizes between those obtained with contrastream injection and injection in the direction of the airstream. These results are consistent with the theory that atomization is caused by interaction of the liquid with the airstream and, hence, is a function of the relative liquid-air velocity.

The major portion of the drop-size distribution data for centrifugal pressure-atomizing nozzles was obtained by some version of the molten-wax method. In this method, a wax or other material that melts well above room temperature is sprayed into room air. By appropriate choice of material and preheat temperature, the initial viscosity of the sprayed liquid at the nozzle can be set at the desired value. The droplets freeze in flight and are collected. Drop-size distribution is determined by the filtration or sedimentation method or by microscopic measurement of a representative sample (ref. 56). There is some question as to the validity of data obtained by the molten-wax method. A limited set of data by Longwell (ref. 45) suggests that this method may give a higher mean drop size than would be obtained by using the actual liquid the molten wax is intended to simulate. In these tests, two oils were sprayed into still air. One oil was preheated in order to reduce its viscosity to that of the less viscous oil. The tests indicated that the preheated oil gave a higher mean drop size. This was attributed by Longwell to the increase in viscosity of the preheated oil as it was cooled during atomization. A similar effect would be expected for the molten-wax method.

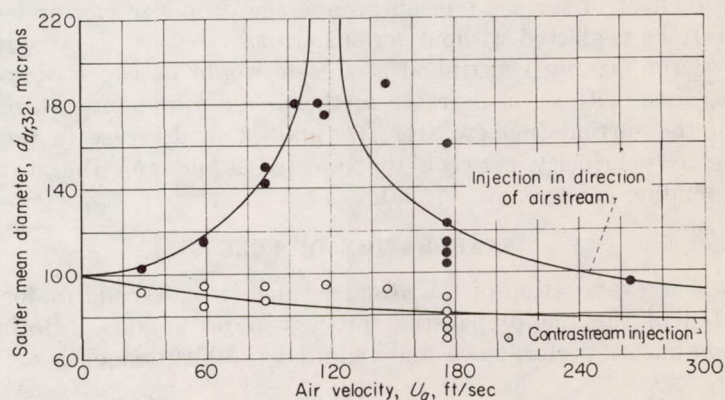


FIGURE 15.—Effect of airstream velocity and direction on Sauter mean diameter for commercial centrifugal pressure-atomizing nozzle (ref. 55).

SUMMARY COMMENTS ON UTILITY OF FUEL-ATOMIZATION DATA

For estimates of drop size to be expected with air atomizers operating at subsonic velocities, equation (14) is recommended. It is noted, however, that this relation is limited to air at 77° F and atmospheric pressure in the atomizing section. Rough corrections for changes in temperature, density, and viscosity of the atomizing gas may be made on the basis of the data of reference 37.

For air atomizers operating at sonic velocities, the results of references 39 and 40 indicate that average drop size may be approximately correlated in terms of the ratio of liquid-to-air weight-flow rate w_l/w_a , average drop size decreasing with decrease in w_l/w_a . The data of references 39 and 40 indicate that average drop size is approximately proportional to the square root of the air-orifice diameter for atomizers of similar shape. The data of reference 39 suggest that fuel viscosity has a greater effect than surface tension for sonic air atomizers. Air atomizers appear to be a particularly effective means for obtaining fine sprays with highly viscous fuels (20 to 40 centistokes).

The major portion of the drop-size data obtained with swirl-type pressure atomizers indicates that average drop size is roughly proportional to the square root of the orifice diameter and to the pressure drop to the -0.4 power. At constant atomizer size, the average drop size increases with decrease in spray-cone angle from the optimum value (80° to 100°). This increase in drop size becomes more pronounced at the lower nozzle pressure drops. The accuracy and limitations of the available correlations for drop size do not appear to warrant their use for more than rough estimates of atomization for atomizers and liquids other than the ones investigated.

The available data on centrifugal atomizers indicate that average drop size is approximately proportional to the fourth root of the fuel viscosity. Insufficient data are available to indicate quantitative effects of surface tension on atomization. In reference 28, the average drop size was found to be proportional to fuel surface tension to the 0.6 to 0.7 power. In reference 32, a dimensionless parameter corresponding to the Weber number was found to correlate drop size, thus indicating the surface tension to be the major fuel-property effect. However, in reference 50, the surface-tension effects appear to be minor. Since the surface-tension range for most hydrocarbon fuels is quite narrow, the effect of surface tension on average drop size can probably be neglected without serious error.

Drop size for centrifugal atomizers would be expected to increase with (1) a decrease in the pressure or temperature of the surrounding gas (ref. 37) and (2) a decrease in the relative velocity between the injected liquid and the surrounding gas stream (ref. 55).

EVAPORATION OF FUEL

The evaporation of the atomized fuel is the second major step of the fuel-preparation process in jet engines. Both combustor performance and required combustor length are

influenced by the rate of vapor formation. A knowledge of how the spray-evaporation process is affected by the air-flow conditions, fuel-injection conditions, and fuel type is therefore important. In this section, the steady-state evaporation of single drops and sprays into static and dynamic surroundings and into both low- and high-temperature surroundings is considered. The unsteady-state process existing during the initial period of drop evaporation is also discussed.

In addition to rate consideration, the vapor-liquid-phase equilibrium conditions must be included in an analysis of spray evaporation. Although the fuel injected into jet engines seldom attains phase equilibrium, the maximum amount of spray evaporation is represented by such conditions. For low-temperature operating conditions and for fuels of low volatility, the phase equilibrium conditions are important factors to be considered in an evaluation of the fuel spray-evaporation process in jet engines.

EQUILIBRIUM FLASH VAPORIZATION

Under some operating conditions and for the lower-volatility fuels, the fraction of fuel evaporated in an air-stream may be limited to a low value regardless of the time allowed for evaporation (ref. 57). Such conditions are reached when the vapor concentration of the fuel-air mixture reaches its saturation value. For multicomponent fuels, the calculation of this limiting value of percentage evaporated is based on the equilibrium flash-vaporization curve.

For fuels having known constituents, the equilibrium flash-vaporization curve at a given pressure and temperature may be calculated by simultaneous solution of material balance equations and equilibrium relations for the individual constituents. Such a calculation procedure might be applied to petroleum fractions by assuming the fuel to be composed of a finite number of individual constituents. However, such methods are generally impractical for petroleum fractions, and recourse has been made to empirical correlations that permit estimation of the equilibrium flash-vaporization curve from distillation curves. Graphs are presented in references 58 and 59 that relate the atmospheric equilibrium flash-vaporization curve to the true boiling point and the ASTM analytical distillation curves. Two methods are available for correcting the atmospheric equilibrium flash-vaporization curve to other pressures. For vapor pressures below and slightly above atmospheric pressure, the flash-vaporization curve is assumed to shift parallel to itself. The shift is based on a particular point on the atmospheric flash-vaporization curves, which is treated as a pure compound on a vapor-pressure chart. In reference 58 the base point is taken as the 40-percent-vaporized point on the atmospheric flash-vaporization curve. For correction of the atmospheric flash-vaporization curve to higher pressures, the recommended procedure is based on the construction of a phase diagram on a Cox vapor-pressure chart (refs. 58 and 60).

In order to relate initial and final conditions for

evaporation with or without the presence of air, the energy equation is applied, assuming an adiabatic mixing process. If kinetic energy is neglected, the energy equation is given by

$$h_{1,f,i} + \frac{h_{1,a}}{f} = (1 - \iota_v)h_{2,f,i} + \iota_v h_{2,f,v} + \frac{h_{2,a}}{f} \quad (35)$$

For petroleum fractions, the enthalpies required in the use of the energy equations may be estimated from empirical relations available in reference 58.

From Dalton's law, the fuel vapor pressure $p_{f,v}$, ambient pressure p , and fraction of fuel vaporized ι_v may be related by

$$\frac{p_{f,v}}{p} = \frac{\iota_v f \frac{M_a}{M_f}}{1 + \iota_v f \frac{M_a}{M_f}} \quad (36)$$

From equations (35) and (36) and the equilibrium flash-vaporization curves, the final temperature and percentage of fuel vaporized may be related to the fuel-air ratio, the total pressure, and the inlet temperatures of the fuel and air.

Within the specification limits of jet fuels, there may be rather wide variations in the ASTM distillation curve. These variations are reflected in the equilibrium flash-vaporization curves and, consequently, may result in appreciable changes in the conditions required to obtain various degrees of flash vaporization in the combustor or heat exchanger. In order to illustrate the effect of fuel variations on flash vaporization, the preceding calculation procedures were applied to the ASTM distillation curves for JP-4 fuels presented in figure 6(c) of reference 61. This figure is reproduced in figure 16. The atmospheric equilibrium flash-vaporization curves corresponding to the three ASTM distillation curves of figure 16 were calculated by the method of reference 58. The fuel vapor pressures and the temperature-enthalpy curves corresponding to the three fuels were also calculated by the method of reference 58.

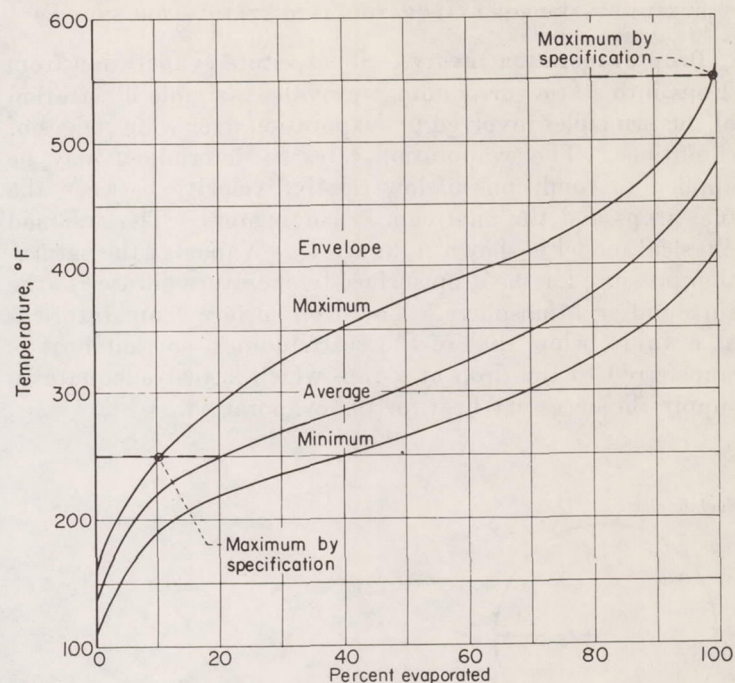
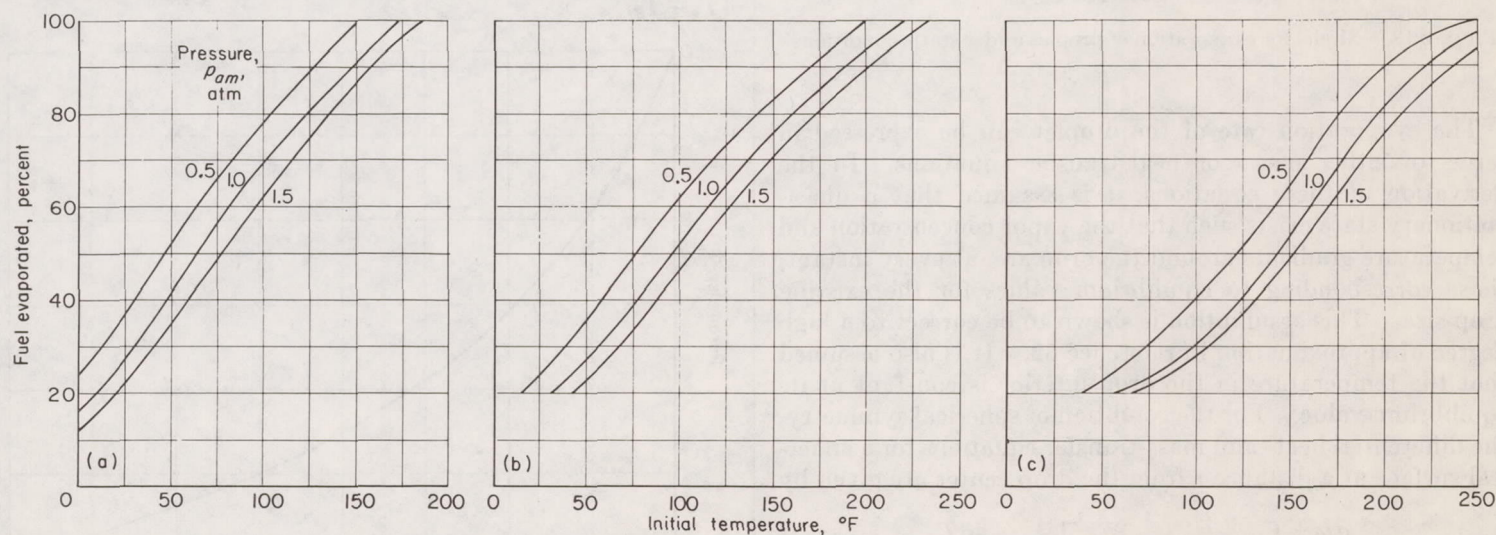


FIGURE 16.—Variation of ASTM distillation temperatures for MIL-F-5624A grade JP-4 fuel (ref. 61).

In figure 17, the percent of fuel evaporated is plotted against the inlet-air temperature for several values of ambient pressure and a fuel-air ratio of 0.06. The curves were calculated from equation (35), assuming the inlet temperatures of fuel and air to be equal. Inlet-air temperatures on the order of 250° F are required to achieve complete vaporization of the fuel. At lower air temperatures, the limitations imposed by equilibrium considerations would have a pronounced effect on the vaporization rate. The limitations could result in appreciable differences between actual evaporation rates and those calculated on the basis of the common assumption of zero fuel vapor pressure in the atmosphere surrounding individual drops.



(a) Minimum envelope of figure 16.

(b) Average curve of figure 16.

(c) Maximum envelope of figure 16.

FIGURE 17.—Equilibrium vaporization of grade JP-4 fuels. Fuel-air ratio, 0.06.

STEADY-STATE DROP EVAPORATION INTO STATIC SURROUNDINGS

Drop evaporation theory.—Steady-state evaporation from drops into static surroundings provides a simple illustration of the principles involved in evaporation over wide ranges of conditions. The evaporation rates so determined may be applied to conditions of low relative velocity between the fuel drops and the airstream in combustors. The assumed physical model is shown in figure 18. Vapor at the saturation pressure for the drop surface temperature diffuses to the surrounding atmosphere. The drop surface temperature is at a value below that of the surroundings, so that heat is transferred to the drop at a rate which is just adequate to supply the necessary heat for the evaporation.

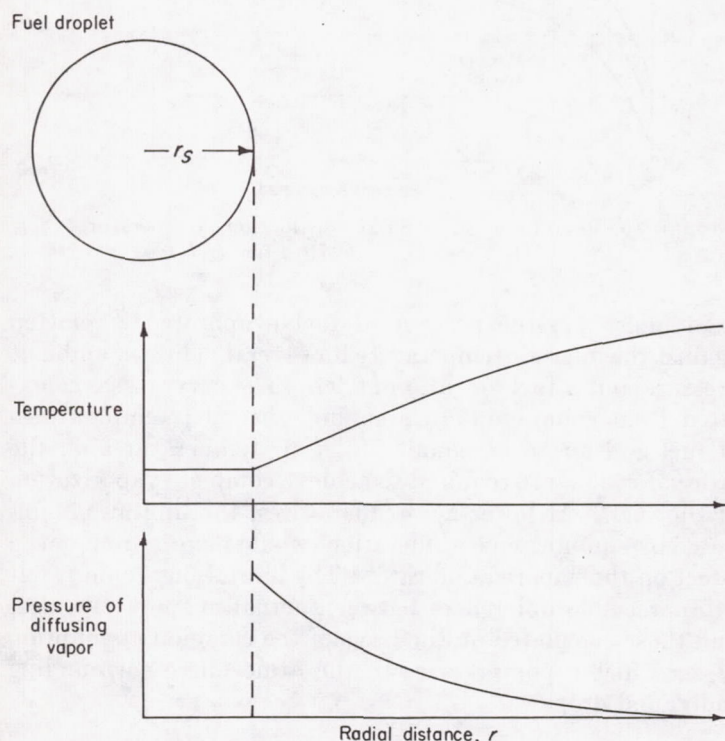


FIGURE 18.—Model for evaporation of droplet under static conditions.

The evaporation rate of the droplet can be expressed in terms of either mass- or heat-transfer equations. In the derivation of these equations, it is assumed that a quasi-stationary state exists such that the vapor concentration and temperature gradients around the drop are, at every instant, those corresponding to equilibrium values for the existing drop size. This assumption is shown to be correct to a high degree of approximation in reference 62. It is also assumed that the temperature in the drop interior is constant at its equilibrium value. For the condition of spherical symmetry, the differential heat- and mass-transfer equations for a spherical surface at a distance r from the drop center are given by

$$\frac{dm}{dt} = \left[\frac{1}{H_v + c_{p,v}(T - T_s)} \right] \kappa_{mz} 4\pi r^2 \frac{dT}{dr} \quad (37)$$

$$\frac{dm}{dt} = \frac{D_{v,g} p M_v 4\pi r^2}{RT} \frac{d}{dr} \left[\ln \left(1 - \frac{p_{f,v}}{p} \right) \right] \quad (38)$$

where

$c_{p,v}$	specific heat of diffusing vapor
$D_{v,g}$	diffusivity of diffusing vapor in air
H_v	latent heat of vaporization at drop surface temperature
M_v	molecular weight of diffusing vapor
$p_{f,v}$	vapor pressure of diffusing vapor
r	radial distance from drop center

In equation (37), the term $c_{p,v}(T - T_s)$ represents the enthalpy change of the fuel vapor between the drop surface and the surface considered. This relation equates the heat transferred by mass movement of the vapor to that transferred by thermal conductivity. Equation (38) is the application of the Stefan diffusion equation (ref. 63, p. 601) to drop evaporation.

For evaporation in quiescent surroundings these equations are integrated between the drop surface and infinity to obtain the following equations:

$$\frac{dm}{dt} = \frac{2\pi \kappa_{mz} d}{H_v} (T_g - T_s) \Phi \quad (39)$$

$$\frac{dm}{dt} = \frac{2\pi D_{v,g} M_v d}{RT} (p_{v,s} - p_{v,\infty}) \left(\frac{p}{p_{BM}} \right) \quad (40)$$

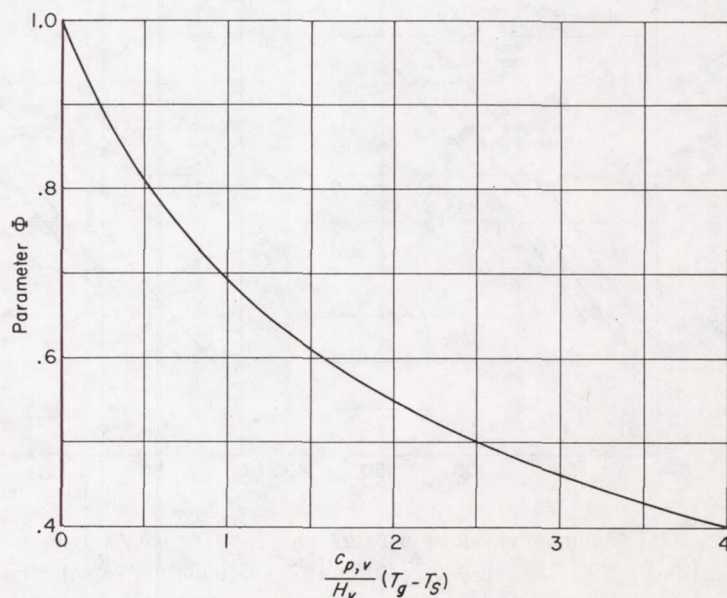
where

$$\Phi = \frac{\ln \left[1 + \frac{c_{p,v}(T_g - T_s)}{H_v} \right]}{\frac{c_{p,v}}{H_v} (T_g - T_s)}$$

$$p_{BM} = \frac{p_{v,s} - p_{v,\infty}}{\ln \left(\frac{p - p_{v,s}}{p - p_{v,\infty}} \right)}$$

For these integrations, $c_{p,v}$, κ_{mz} , and $D_{v,g}/T$ were assumed to be constant and to represent mean values between the drop surface and the surroundings.

The parameter Φ corrects for the effect of mass movement of the fuel vapor on the heat transferred to the drop surface (e. g., ref. 64). In figure 19, Φ is plotted against $(c_{p,v}/H_v)(T_g - T_s)$.

FIGURE 19.—Variation of Φ with $(c_{p,v}/H_v)(T_g - T_s)$.

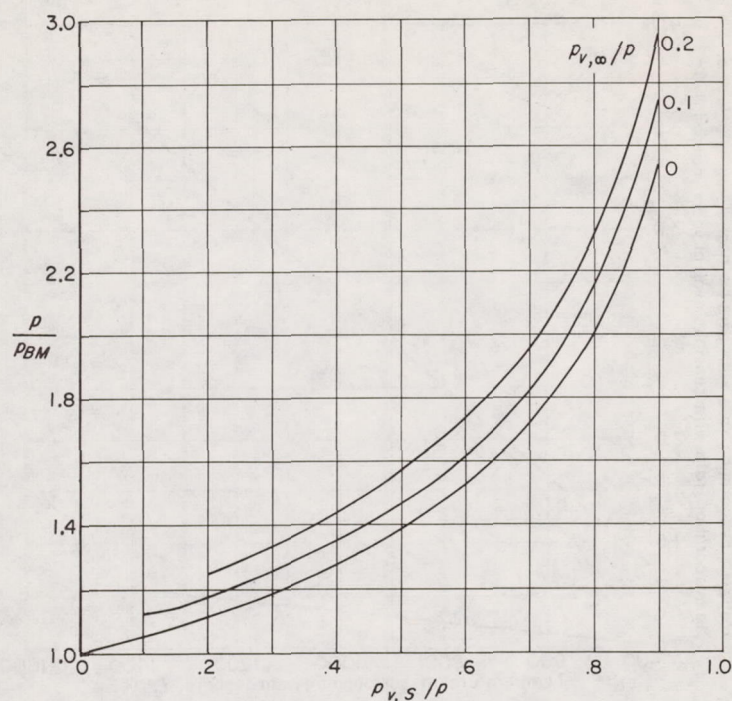


FIGURE 20.—Variation of p/p_{BM} with $p_{v,s}/p$ for several values of $p_{v,\infty}/p$.

The parameter p/p_{BM} can be considered to be a correction for the difference in the calculated values of diffusion rates based on diffusion of one gas through a second stagnant gas and equimolar counterdiffusion. In figure 20, p/p_{BM} is plotted against $p_{v,s}/p$ for several values of $p_{v,\infty}/p$.

In most studies of drop evaporation, the experimental conditions have been such that the correction factors Φ and p/p_{BM} of equations (39) and (40) could be assumed equal to unity without appreciable error. However, the work of Priem (ref. 65) indicates that inclusion of Φ gives close agreement between predicted and experimental values for evaporation in high-temperature airstreams where Φ is well below unity. Although it has no significant effect on the calculations, the use of the correction factor p/p_{BM} was considered warranted subject to additional information on drop evaporation.

Evaporation into low-temperature surroundings.—For evaporation into low-temperature surroundings where the sensible heat change of the vapor between the drop surface and surroundings is small compared with the latent heat of vaporization, Φ approaches unity and equation (39) reduces to the following relation:

$$\frac{dm}{dt} = \frac{2\pi\kappa_{mx}d_{dr}}{H_v}(T_g - T_s) \quad (41)$$

This equation is similar in form to that of simple heat transfer to a sphere in quiescent surroundings. Similarly, for evaporation where the vapor pressure at the drop surface is small compared with the total pressure, p/p_{BM} approaches unity and equation (40) reduces to

$$\frac{dm}{dt} = \frac{2\pi D_{v,g}M_v d_{dr}}{RT}(p_{v,s} - p_{v,\infty}) \quad (42)$$

This relation is the Langmuir equation (ref. 66). Equations

(41) and (42) are of similar form, illustrating the analogy between heat and mass transfer. Equation (42) has been experimentally verified with drops of several relatively low-volatility liquids evaporating into low-temperature surroundings (refs. 67 to 71). The equation was found to be valid at total pressures near atmospheric.

Replacing m in equation (41) by $\rho_l \pi d_{dr}^3/6$, rearranging, and integrating give the following relation between the initial drop diameter $d_{dr,o}$ and the drop diameter d_{dr} after an evaporation time t :

$$d_{dr}^2 = d_{dr,o}^2 - \mathcal{K}t \quad (43)$$

where

$$\mathcal{K} = \frac{8\kappa_{mx}(T_g - T_s)}{\rho_l H_v} \quad (44)$$

is known as the evaporation constant. Equation (43) shows that there is a linear relation between the square of the drop diameter and the evaporation time for drops evaporating in quiescent surroundings.

From equation (42), the drop evaporation rate per unit drop surface area is inversely proportional to the drop diameter. In addition, this rate is inversely proportional to pressure as determined by the pressure dependence of the diffusion coefficient. Therefore, for sufficiently small drops or low total pressures, the evaporation rate per unit area as obtained from equation (42) becomes greater than the theoretical maximum evaporation rate in a vacuum, as determined by gas kinetics (ref. 72). The maximum evaporation rate for a drop evaporating isothermally in a vacuum is given by the following equation:

$$\frac{dm}{dt} = \frac{\pi M_v d_{dr}^2 \bar{c}_v \alpha}{RT} p_{f,v,s} \quad (45)$$

The accommodation coefficient α represents the fraction of vapor molecules that condense as they strike the liquid surface.

The evaporation of very small drops was treated theoretically by Fuchs (ref. 73). In this analysis, diffusion was considered to start at a distance approximately 1 mean free path from the drop surface. For $p_{v,\infty}$ equal to zero, the drop evaporation rate according to this model is described in the following equation:

$$\frac{dm}{dt} = \frac{2\pi D_{v,g}M_v d_{dr} p_{v,s}}{RT} \frac{1}{\frac{2D_{v,g}}{d_{dr}\bar{c}_v\alpha} + \frac{d_{dr}}{d_{dr}+2x}} \quad (46)$$

where x is the distance between the drop surface and the surface where diffusion is assumed to start.

For drop diameters large compared with x , this equation reduces to the Langmuir equation for $p_{v,\infty}$ equal to zero. For very small drops, the second term in the denominator approaches zero, and the evaporation rate approaches that of a drop evaporating in a vacuum as given by equation (45). Similarly, for the larger drops, this theoretical maximum evaporation rate is approached at sufficiently low pressures where x again is large compared with the drop diameter.

This theory has been verified experimentally at low pressures (refs. 74 to 76). Evaporation rates of dibutyl phthalate, butyl stearate, and straight-chain paraffin hydrocarbon drops approximately 500 microns in diameter were determined over a range of temperature from 60° to 105° F and at pressures down to 0.1 millimeter of mercury absolute. However, for most applications, the use of equation (46) is not necessary. At atmospheric pressure, the effect predicted by Fuchs would be negligible for drops larger than 1 micron.

Other factors that affect predicted values of drop evaporation rate are the drop surface tension and free convection. The correction for the effect of surface tension on the saturation vapor pressure of the drop is insignificant for drops larger than 1 micron (ref. 77). For evaporation in low-temperature surroundings, the influence of free convection on the experimental results is also minor, if the drop diameters and containing vessel are small (ref. 70).

Evaporation into high-temperature surroundings.—If free-convection effects can be neglected, equations (39), (40), and (43) should apply to the steady-state evaporation of single drops in quiescent high-temperature surroundings. For this case the evaporation constant is given by

$$\mathcal{K} = \frac{8k_{mx}\Phi}{\rho_l H_v} (T_g - T_s) = \frac{8k_{mx}}{\rho_l c_{p,v}} \ln \left[1 + \frac{c_{p,v}}{H_v} (T_g - T_s) \right] \quad (47)$$

The sensible heat change of the diffusing vapor may be large compared with the latent heat of vaporization for evaporation in high-temperature surroundings. Consequently, the effect of Φ on the calculated evaporation rate may be appreciable. In figure 21 the reciprocal of Φ is presented for isooctane and water drops evaporating into various temperature surroundings. The reciprocal of Φ is approximately equal to the ratio of the evaporation rate predicted by the simple heat-transfer equation to that predicted by the heat-transfer equation accounting for the enthalpy change of the fuel vapor. A large difference between the two calculated evaporation rates is evident for the isooctane drops and higher air temperatures. The effect is much less for the water drops, since water has a high latent heat of vaporization.

Drop evaporation into high-temperature quiescent surroundings has not been studied extensively. Some data are presented in reference 78 for single drops of cetane, *n*-heptane, benzene, and ethyl alcohol evaporating in high-temperature air suspended from a silica filament. The drops were placed in an electric furnace and photographed while evaporating. The data indicated that equation (43) is valid over most of the evaporation period. However, the experimental values of the evaporation constant are over twice those calculated from equation (47), even for Φ taken equal to unity. Part of this discrepancy might be attributed to free-convection air currents in the furnace.

Most of the available experimental and analytical work in this region has been done with single drops burning in quiescent atmospheres. The burning drop has been considered theoretically as a special case of evaporation, where the heat for vaporization is supplied from a burning zone surrounding the drop. The drop surface temperature is

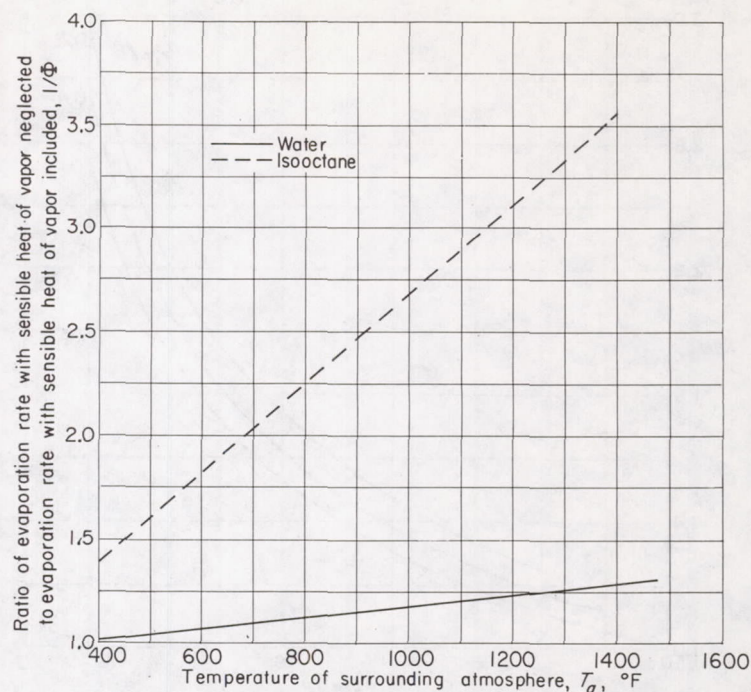


FIGURE 21.—Effect of enthalpy change of diffusing vapor on calculated evaporation rates of water and isooctane drops.

assumed to be at the fuel boiling point for the given ambient pressure. Because of the large temperature differences involved, the error introduced by this assumption is minor. The burning-zone temperature and the distance between the burning zone and the drop surface may be calculated from a simultaneous solution of the heat- and mass-transfer equations (e. g., refs. 79 and 80).

A typical plot of the square of the drop diameter against time after ignition for a drop burning in quiescent air is shown in figure 22. During the first time interval after ig-

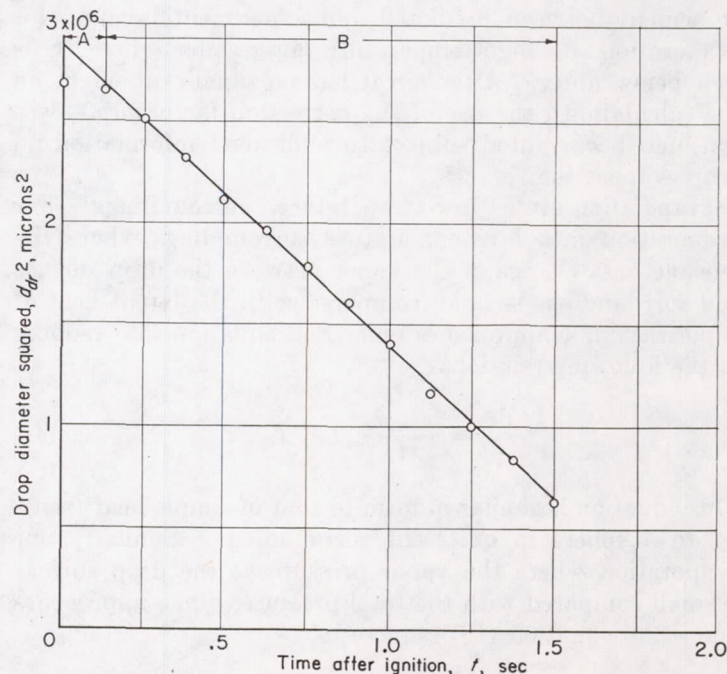


FIGURE 22.—Time variation in diameter of drop burning in quiescent oxygen-nitrogen atmosphere. Oxygen concentration, 34.9 percent by volume; evaporation constant, 1.5×10^6 microns squared per second (ref. 80).

niton (A), there is but a small change in drop diameter with time. In this interval the major portion of heat passing the drop surface is probably used to heat the drop interior rather than to supply the latent heat of vaporization (e. g., ref. 65). In the second time interval (B), the data follow fairly closely the linear relation given by equation (43). Values of the evaporation constant obtained from the slope of this straight-line portion of the curve are generally in good agreement with predicted values for steady-state burning.

Experimental values of the evaporation constant for typical hydrocarbon fuel drops burning in quiescent air range from approximately 8×10^{-6} to 10×10^{-6} square foot per second. A detailed discussion of analytical treatments of the burning of single drops, together with available experimental data, is presented in chapter VII.

DROP EVAPORATION UNDER FORCED CONVECTION

Drop evaporation under forced-convection conditions differs from evaporation into quiescent surroundings in two important respects: The assumptions of infinite film thickness and spherical symmetry are not applicable to drop evaporation into moving fluids.

As is shown in figure 23, the local heat-transfer rates change over the drop surface. In this figure, local heat-transfer rate, expressed as a fraction of the transfer rate at the forward stagnation point, is plotted against the angle from the forward stagnation point. These data were obtained by Frössling (ref. 81) for the sublimation of a naphthalene bead. From boundary-layer considerations, the local transfer rate would be expected to be maximum at the forward stagnation point and decrease gradually to a minimum at the separation point. The data of figure 23 apparently follow this type of change. Ranz and Marshall (ref. 82) determined the temperature profile around an evaporating water drop.

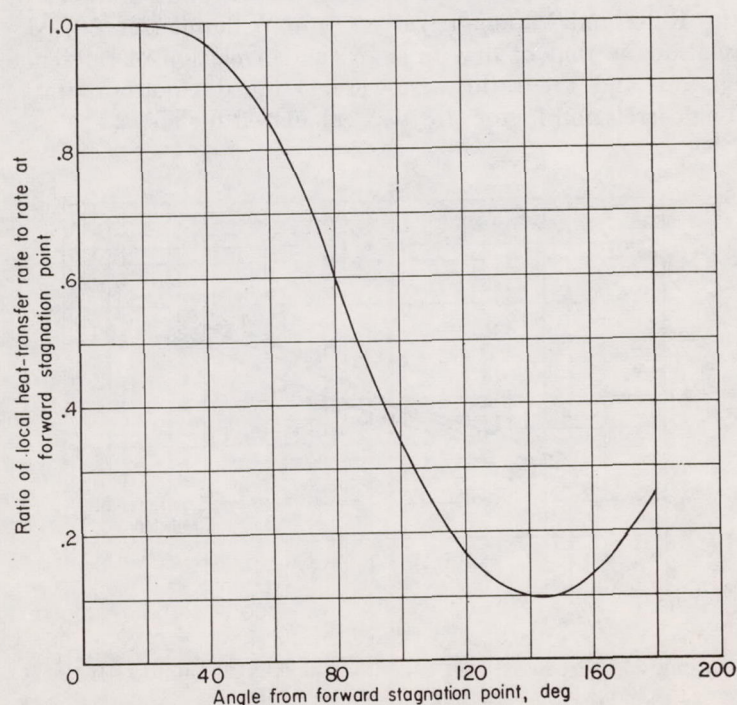


FIGURE 23 — Change in local heat-transfer rate over surface of sphere in airstream. Reynolds number, 136 (ref. 81).

These measurements also indicate a gradual decrease in the local transfer rate from the maximum value at the forward stagnation point.

Correlations of the drop evaporation rate under forced-convection conditions neglect the changes in the local transfer rate and use an average value for the entire sphere. The total drop in either temperature or partial pressure of diffusing vapor is assumed to take place across a stagnant film. These correlations are based on heat-transfer as well as mass-transfer relations. When the drop temperature is at its equilibrium value, the heat- and mass-transfer equations are, respectively, as follows:

$$\frac{dm}{dt} = \frac{\pi \kappa_{mz} d_{dr} (T_g - T_s)}{H_v} \Phi Nu_H \quad (48)$$

$$\frac{dm}{dt} = \frac{\pi D_{v,g} M_v d_{dr} (p_{f,v,s} - p_{f,v,g})}{RT} \left(\frac{p}{p_{BM}} \right) Nu_M \quad (49)$$

where

$$p_{BM} = \frac{p_{f,v,s} - p_{f,v,g}}{\ln \left[\frac{1 - \frac{p_{f,v,g}}{p}}{1 - \frac{p_{f,v,s}}{p}} \right]}$$

$$\Phi = \frac{\ln \left[1 + \frac{c_{p,v}}{H_v} (T_g - T_s) \right]}{\frac{c_{p,v}}{H_v} (T_g - T_s)}$$

As in equations (39) and (40), the terms κ_{mz} , $D_{v,g}$, and T of equations (48) and (49) are mean values over the stagnant film. Methods for calculating $D_{v,g}$ and κ_{mz} are presented in reference 65.

Heat-transfer correlations.—Several theoretical treatments of the heat transfer to spheres in fluid streams have been reported. Johnstone, Pigford, and Chapin (ref. 83) assumed that the velocity of the fluid around the sphere is tangential to the surface and equal to the approach velocity. For Reynolds numbers greater than 200, the resulting equation is

$$Nu_H = 0.714 Re^{1/2} Pr^{1/2} \quad (50)$$

where

$$Re = \frac{d U_{rel} \rho_g}{\mu_g}$$

$$Pr = \frac{c_{p,g} \mu_g}{\kappa_g}$$

and d is sphere diameter.

Drake, Sauer, and Schaaf (ref. 84) followed the assumptions described in reference 83 but used a different method for obtaining the solution. For Reynolds numbers below 1000, the two solutions differ. Kudryashev (ref. 85) also obtained an analytical solution based on the thermal boundary layer. The values of Nusselt number predicted by the various theoretical treatments are compared in figure 24 over a range of Reynolds numbers from 30 to 2000.

An extensive survey of published data on heat and mass transfer to spheres is described by Williams (ref. 86). The suggested empirical correlation of the heat-transfer

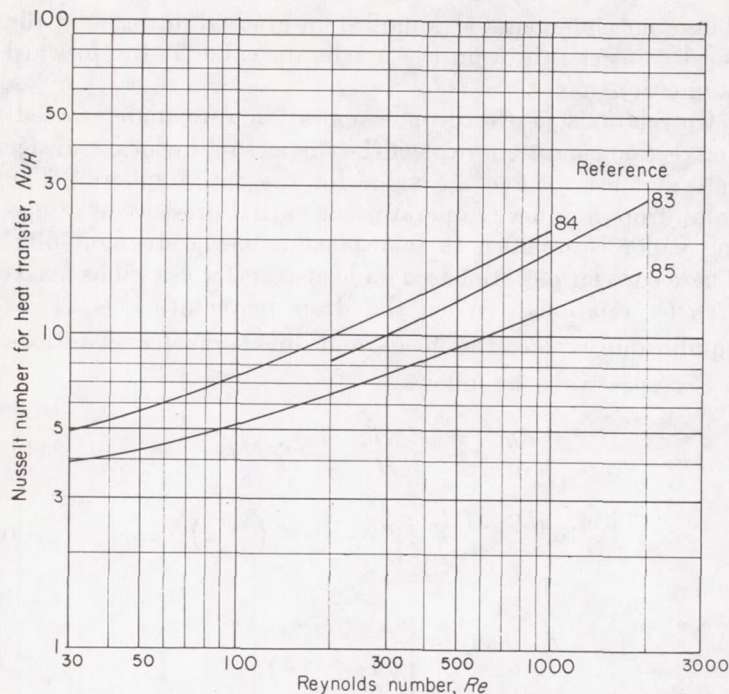


FIGURE 24.—Predicted Nusselt numbers for heat transfer for spheres in air.

data is given by the following equation:

$$Nu_H = 0.37 Re^{0.6} Pr^{1/3} \quad (51)$$

In the range of Reynolds numbers less than 1000, the data showed considerable scatter. This range was recently investigated by Tang, Duncan, and Schwyer (ref. 87). In this study, heat-transfer rates for steel spheres in airstreams were determined. The resulting correlation is as follows:

$$Nu_H = 2.1 + 0.37 Re^{1/2} \quad (52)$$

A similar investigation has been described by Kramers (ref. 88).

Ranz and Marshall (ref. 82) determined the evaporation rates of suspended water and benzene drops over a range of Reynolds numbers from 0 to 200 and at air temperatures from 80° to 400° F. For evaporating water drops, the data were correlated by the following relation:

$$Nu_H = 2.0 + 0.6 Re^{1/2} Pr^{1/3} \quad (53)$$

Ingebo (ref. 89) determined evaporation rates of nine pure liquids in airstreams having temperatures ranging from approximately 80° to 1000° F. A liquid drop was simulated by means of a wetted cork sphere having an average diameter of 0.69 centimeter. Reynolds numbers ranged from 1600 to 5700. Nusselt number was correlated in terms of Reynolds number, Schmidt number, and ratio of thermal conductivity of the air and the diffusing vapor. In a later report (ref. 90), data were obtained in air at approximately room temperature and for static pressures from approximately 1/2 to 2 atmospheres. The data indicated no effect of ambient pressure on evaporation rate as given by the Reynolds number. An

additional limited set of data was obtained for evaporation into streams of helium, argon, and carbon dioxide. The final correlation (ref. 90) is given by

$$Nu_H = 2.0 + 2.58 (10)^6 \left[Re Sc' \left(\frac{gl}{\bar{c}^2} \right) \right]^{0.6} \left(\frac{\kappa_g}{\kappa_v} \right)^{1/2} \quad (54)$$

where

$$Re Sc' = \frac{d_{dr} U_{rel} \rho_g}{D_{g,M}}$$

$$D_{g,M} = \frac{\rho M_v D_{v,g}}{RT}$$

In this case the Schmidt number Sc' is the molecular momentum-transfer coefficient divided by the molecular mass-transfer coefficient.

The dimensionless group gl/\bar{c}^2 in equation (54) is inversely proportional to ambient pressure and accordingly cancels the ambient-pressure term in the Reynolds number. The thermal-conductivity terms and $D_{g,M}$ are evaluated at the average temperature between the drop surface temperature and the fluid bulk temperature. The terms l and \bar{c} are evaluated at the drop surface temperature. It is noted that equation (54) is to be used with equation (48) for Φ equal to unity. Apparently, the temperature variation of the thermal-conductivity ratio κ_g/κ_v compensates for the effect of Φ on the calculated evaporation rate.

Another investigation of drop evaporation in high-temperature airstreams is reported by Gohrbandt (ref. 91). The evaporation rate of camphor spheres was determined over a range of Reynolds numbers from 100 to 2000 and air temperatures from about 85° to 930° F. The evaporation rate was found to be proportional to the drop diameter and the square root of the Reynolds number. The various predicted and experimental data for heat transfer to spheres in air are compared in figure 25. The Prandtl number of the Ranz and Marshall (ref. 82) and Williams (ref. 86) correlations is that of dry air. In the correlation of reference 89, Sc' and the ratio κ_g/κ_v were assumed equal to unity. The correlation factor gl/\bar{c}^2 was calculated for air.

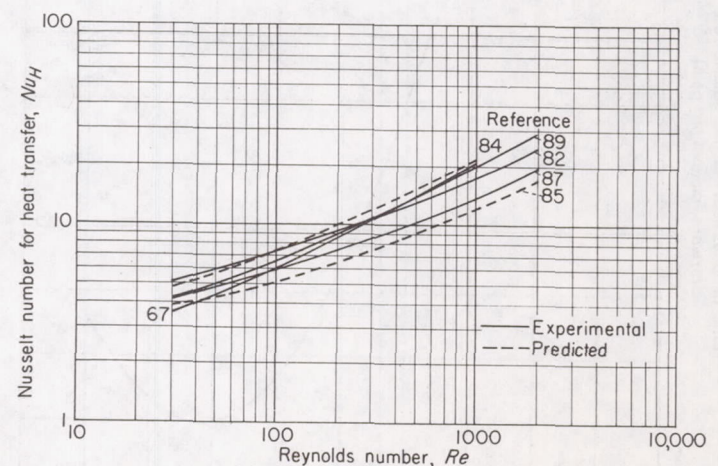


FIGURE 25.—Predicted and experimental Nusselt numbers for heat transfer for spheres in air.

Mass-transfer correlations.—A theoretical approach to mass transfer for spheres in moving fluids is described by Johnstone and Kleinschmidt (ref. 92). In this analysis, it is assumed that the sphere contacts a cylindrical tube having an inner diameter equal to that of the sphere and a thickness equal to the distance a diffusing molecule could travel in the time the sphere moves 1 diameter. Increasing the relative velocity between the sphere and surrounding gas decreases the available diffusion time and, therefore, the thickness of the imaginary tube. All molecules contained within the tube are considered to be absorbed. The Nusselt number for mass transfer obtained from this approach is

$$Nu_M = \left(\frac{p_{BM}}{p} \right)^{1/2} Re^{1/2} Sc^{1/2} \quad (55)$$

where

$$Sc = \frac{\mu_g}{\rho_g D_{v,g}}$$

Use of the diffusion equation in correlations of drop evaporation data is limited to evaporation in relatively low-temperature surroundings, since this equation is very sensitive to experimental errors in the drop surface temperature at the higher surface vapor pressures. However, several mass-transfer correlations for the evaporation rate of droplets in room-temperature air have been reported.

Williams (ref. 86) correlated the mass-transfer data of Frössling (ref. 81), Johnstone and Williams (ref. 93), Powell (ref. 94), and McInness (see ref. 86). The recommended equations for the mass-transfer Nusselt number are as follows:

$$\left. \begin{aligned} Nu_M &= 1.5 Re^{0.35} Sc^{1/3} & 5 < Re < 400 \\ Nu_M &= 0.43 Re^{0.56} Sc^{1/3} & 400 < Re < 10^5 \end{aligned} \right\} \quad (56)$$

Maisel and Sherwood (ref. 95) reported data on the evaporation of water and of benzene from porous spheres. The data for water are in good agreement with equation (56). Deviation of the data for benzene is attributed to incomplete wetting of the sphere.

Frössling (ref. 81) correlated data for evaporation of water, aniline, naphthalene, and nitrobenzene into airstreams at room temperature. The data were obtained over a range of Reynolds numbers from approximately 2 to 750. This correlation may be written in the following form:

$$Nu_M = 2 + 0.55 Re^{1/2} Sc^{1/3} \quad (57)$$

The mass-transfer correlation suggested by Ranz and Marshall (ref. 82) is as follows:

$$Nu_M = 2 + 0.60 Re^{1/2} Sc^{1/3} \quad (58)$$

This correlation is of the same form as their heat-transfer correlation, but with the Prandtl number replaced by the Schmidt number. Reference 82 shows that the data of Frössling (ref. 81) and of Maisel and Sherwood (ref. 95) agree closely with this correlation.

Another correlation of drop evaporation has been described by Kinzer and Gunn (ref. 96):

$$Nu_M = 2 + 0.564 F_{vent} Re^{1/2} Sc^{1/2} \quad (59)$$

This equation was used to express evaporation-rate data obtained for water drops falling freely at their terminal velocities through air at room temperature. Drops with diameters from 20 to 4200 microns were studied. Application of the experimental data to equation (59) indicated that the ventilation factor F_{vent} ranged from 0 to a value greater than 2 in the range of Reynolds numbers smaller than 100. For Reynolds numbers greater than 100, F_{vent} was approximately equal to 1. As noted in reference 96, the water drop evaporation data for the higher Reynolds number range would be adequately correlated by equation (57) if the constant were reduced from 0.55 to 0.505. This represents a difference in the calculated Nusselt number of approximately 7 percent for Reynolds numbers from 100 to 750.

UNSTEADY-STATE DROP EVAPORATION

The final case of single-drop evaporation to be considered is that of unsteady-state evaporation. Here, the initial drop temperature is above or below its equilibrium value and consequently changes with time. Both theoretical and experimental work has been reported for this case.

Topps (ref. 97) studied evaporation rates of small drops falling through a high-temperature atmosphere. Initial drop diameters ranged from approximately 300 to 550 microns. The results for this range of drop diameters indicated that the evaporation rate varied approximately as the 4.5 power of the initial drop diameter. This large reduction in evaporation rate with decrease in initial drop diameter was attributed by Topps to the conduction of heat to the drop interior, which reduced the heat available for evaporation of the smaller drops.

Kinzer and Gunn describe an investigation of the time rate of change in the average temperature of falling water drops in reference 96. A simplified theoretical expression was obtained for the time required for the drops to reach 63 percent of the equilibrium temperature difference. Thermal conductivity of the drop interior was assumed to be infinite. Satisfactory agreement was found between the predicted and experimental values.

El Wakil, Uyehara, and Myers (ref. 98) describe an analytical study of the unsteady-state evaporation of pure liquid drops for conditions similar to those existing in jet-engine combustors. In this analysis, the thermal conductivity of the drop interior is also assumed to be infinite. Motion pictures of the circulation of metallic powders within the evaporating drops disclose appreciable internal circulation currents and indicate that the assumption of infinite thermal conductivity is substantially correct (ref. 99). Temperature-time, mass-time, and penetration-time histories were calculated for drops evaporating in air. This type of calculation involves the simultaneous solution of the heat-transfer, mass-transfer, and drop-motion equations.

A typical set of results is presented in figure 26. In this figure, percent evaporated, relative velocity, and drop temperature are plotted against time in milliseconds. The calculations are for an isooctane drop having an initial diameter of 50 microns, initial temperature of 50° F, and initial velocity relative to air of 100 feet per second. The air was assumed to be at a pressure of ½ atmosphere and at a temperature of 1000° F. For this fuel, the amount of heat going to the drop interior far exceeded that supplying latent heat of vaporization during the major portion of the unsteady-state period.

A detailed analytical and experimental study has been conducted (ref. 65) to determine the validity of the theory of reference 98. Single drops were suspended from a fine thermocouple, exposed to a constant-velocity airstream, and photographed while evaporating. The drop diameter and temperature-time histories were determined for normal-paraffin fuels ranging from hexane to octadecane and for a range of air temperatures, air velocities, and initial drop diameters. All tests were made at room pressure. Close agreement between experiment and theory was found in the majority of tests. Examples of the agreement between predicted and experimental values are presented in figure 27. Figure 27(a) illustrates the condition giving the poorest agreement found, while figure 27(b) illustrates the best agreement.

Priem (ref. 65) also compared the experimental results with values obtained from two simplified calculations neglecting the unsteady-state period. In method 1 the drop was assumed to evaporate at its steady-state temperature. In method 2 the drop temperature was assumed to remain constant at the value existing prior to the start of vaporization (zero thermal conductivity inside drop). For high-volatility fuels and large drop sizes, values calculated from methods 1 and 2 were in close agreement with experiment. For low-volatility fuels and small drop sizes, there was an appreciable difference between the calculated and experi-

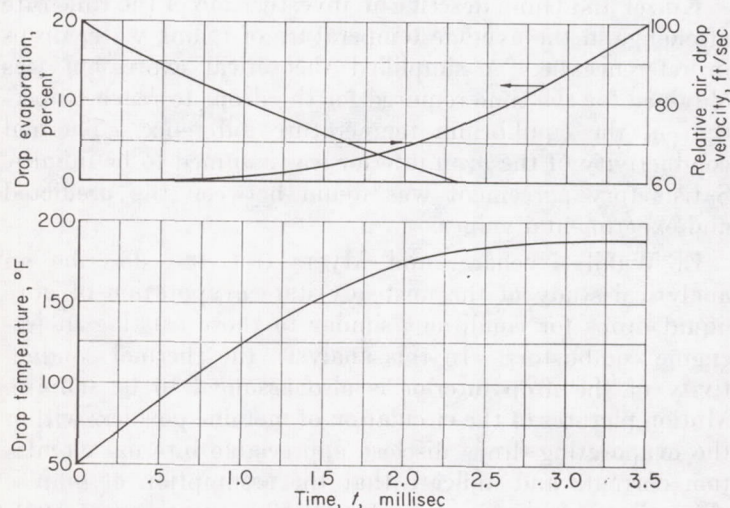
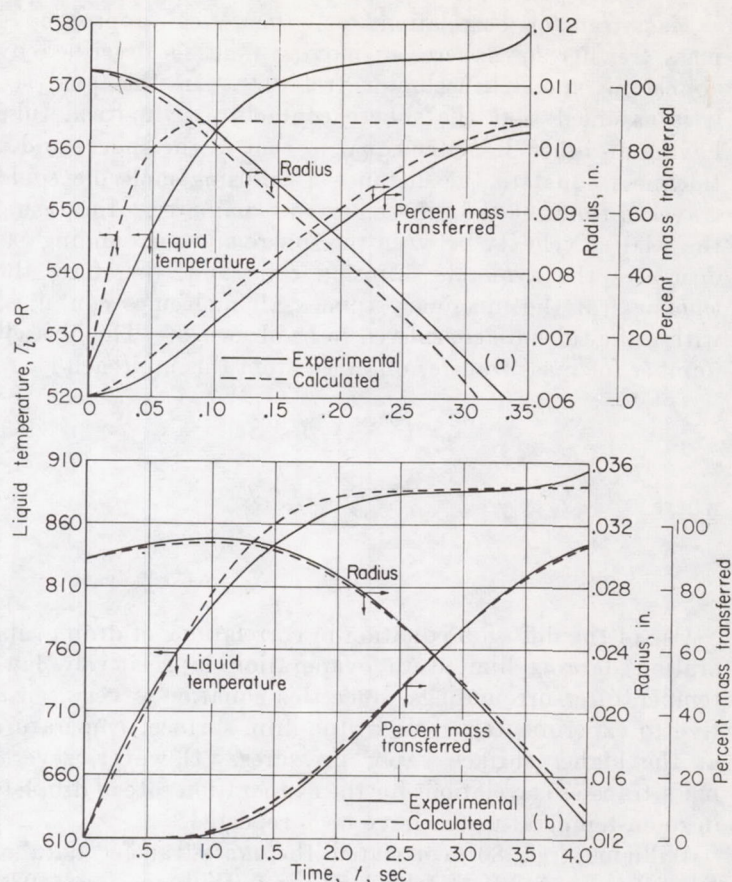


FIGURE 26.—Unsteady-state evaporation of isooctane drop into air at 1000° F and 0.5 atmosphere. Drop diameter, 50 microns; initial drop temperature, 50° F; initial drop velocity, 100 feet per second (ref. 98).



(a) Hexane droplet. Air temperature, 1280° R; air velocity, 120 inches per second; initial diameter, 560 microns.
(b) Hexadecane droplet. Air temperature, 1230° R; air velocity, 80 inches per second; initial diameter, 1520 microns.

FIGURE 27.—Comparison of experimental and calculated histories of droplets (ref. 65).

mental values, particularly during the initial period of vaporization. Of the two simplified methods, method 2 gave better agreement with experiment.

Another approach to the problem of obtaining a simplified calculation procedure for unsteady-state evaporation involves the division of the total evaporation time into two parts. In the first part the heat transferred to the drop surface is assumed to heat the drop from its initial temperature $T_{s,0}$ to the steady-state temperature T_s without vaporization. In the second part the drop is assumed to vaporize at its steady-state temperature.

Equating the heat transferred to the drop to the increase in sensible heat and assuming infinite thermal conductivity inside the drop,

$$\rho_l \frac{\pi}{6} d_{dr,s}^3 c_{p,l} \frac{dT_l}{dt} = Nu_H \kappa_g \pi d_{dr,s} (T_g - T_l) \quad (60)$$

where $c_{p,l}$ and T_l are the specific heat and temperature, respectively, of the drop. Equation (60) may be integrated to obtain the time Δt_H required for the drop temperature to increase from $T_{s,0}$ to T_s . Assuming constant ρ_l , $c_{p,l}$, Nu_H , κ_g , and T_g , the heating time Δt_H is given by

$$\Delta t_H = \left[\frac{\rho_l c_{p,l}}{6 N u_{H\kappa_g}} \ln \left(\frac{T_g - T_{s,o}}{T_g - T_s} \right) \right] d_{dr,s}^2 \quad (61)$$

For a variable gas velocity, such as occurs when a drop is injected into a gas stream, a mean value of the Nusselt number in equation (61) would be required. The vaporization time is obtained by adding the time Δt_H from equation (61) to the vaporization time obtained from the steady-state evaporation equations (48) and (49). For evaporation in a quiescent atmosphere, the time Δt_i for complete evaporation is given by

$$\Delta t_i = \left[\frac{1}{\mathcal{K}} + \frac{\rho_l c_{p,l}}{12 \kappa_g} \ln \left(\frac{T_g - T_{s,o}}{T_g - T_s} \right) \right] d_{dr,s}^2 \quad (62)$$

where the evaporation constant \mathcal{K} may be obtained from equation (44) or (47).

Values of Δt_H obtained from equation (61) for the conditions of figures 27(a) and (b) are 0.021 and 1.61 seconds, respectively. These values agree well with the time during which there is but a small change in drop size.

The times for 20-, 50-, and 80-percent evaporation as calculated by the various methods are compared in table II. The evaporation conditions are those of figure 27. For these cases, at least, the results using the simplified method, in which the heating time is added to the steady-state temperature vaporization time, are in reasonably good agreement with experiment and the times obtained from the step-by-step calculations of reference 65.

ADDITIONAL CONSIDERATIONS IN DROP EVAPORATION

Ranz and Marshall (ref. 82) have investigated the evaporation rate of water drops containing dissolved and suspended solids. For drops containing solids in solution, the initial evaporation rates were those to be expected for saturated solutions even though the average concentrations in the drops were below the saturation value. For drops contain-

ing solids in suspension, the initial drop evaporation rates were those corresponding to pure water.

The contribution of radiant energy in the evaporation of liquid drops is analytically investigated in reference 100. The results of this study demonstrate that, under the conditions normally encountered in jet-engine combustors, the transfer of radiant energy to the fuel drops is negligible unless solid particles are added to the fuel to increase its emissivity.

In calculations of evaporation rates for drops of wide-boiling-range jet-engine fuels (e. g., see fig. 16), the question arises whether the composition of the drops changes during the evaporation process. If the composition remains unchanged, the drops might be treated as a pure fuel. If the composition changes, a more complex treatment might be required. Lamb and coworkers (refs. 101 and 102) have investigated the evaporation in air of multicomponent sprays. The data indicate that the concentration of the higher-boiling component in the remaining drops increases as the spray evaporates. At higher air temperatures, this trend towards increased concentration of the higher-boiling component was more pronounced. From these experiments one would expect a continuous change in the composition of the remaining drops during the evaporation of a wide-boiling-range fuel.

An investigation of the effect of turbulence on the evaporation of water from spheres is reported by Maisel and Sherwood (ref. 103). The influences of both scale and intensity of turbulence were studied. The results indicate that increased turbulence intensity influences the buffer and laminar layers where most of the resistance to diffusion is located and therefore increases the evaporation rate. The scale of turbulence affects only the eddy diffusivity in the fully turbulent region, which represents a small fraction of the total resistance to diffusion. Thus, increasing the scale of turbulence does not appreciably influence the evaporation rate.

TABLE II.—COMPARISON OF EXPERIMENTAL AND CALCULATED VAPORIZATION TIMES FOR UNSTEADY-STATE VAPORIZATION OF SINGLE FUEL DROPS SUDDENLY EXPOSED TO CONSTANT-VELOCITY AIRSTREAM

Drop	Percent vaporized	Ratio of experimental to calculated vaporization times			
		Simplified calculations			Stepwise unsteady-state calculations (ref. 65, figs. 41 and 42)
		Drop temperature constant at steady-state value (ref. 65, figs. 41 and 42)	Drop temperature constant at initial value. Zero thermal conductivity of drop interior (ref. 65, figs. 47 and 48)	Heating period plus evaporation with drop temperature constant at steady-state value	
Hexane (fig. 27(a)) -----	20	1. 63	1. 45	1. 18	1. 20.
	50	1. 30	1. 25	1. 13	1. 15
	80	1. 25	1. 10	1. 14	1. 12
Hexadecane (fig. 27(b)) -----	20	2. 53	2. 37	0. 77	0. 98
	50	1. 65	1. 15	. 82	. 87
	80	1. 28	. 83	. 86	. 79

DETERMINATION OF STEADY-STATE DROP SURFACE TEMPERATURE

Drop evaporation rates are treated in terms of either heat-transfer or mass-transfer relations. The use of either type of equation generally requires an accurate knowledge of the drop surface temperature. For steady-state evaporation, this temperature is the wet-bulb temperature. Psychrometric data for some vapors, in addition to water, are available in reference 77.

Steady-state drop surface temperature data for drops evaporating in high-temperature airstreams are correlated in reference 89. The equation may be written as follows:

$$T_{a,w} = T_a - 0.80 T_{bp} + 75 \quad (63)$$

where $T_{a,w}$ is the air temperature at which water has the same difference between the air temperature and the drop surface temperature as the given liquid ($^{\circ}\text{C}$), T_a is the temperature of the air into which the liquid is evaporating ($^{\circ}\text{C}$), and T_{bp} is the normal boiling point of the evaporating liquid ($^{\circ}\text{C}$). The term $T_{a,w}$ is computed from equation (63), and the wet-bulb temperature for water corresponding to $T_{a,w}$ is determined from a psychrometric chart; $T_{a,w}$ minus this wet-bulb temperature is equal to T_a minus the drop surface temperature of the evaporating liquid. The data for this correlation were obtained with nine pure liquids for atmospheric ambient pressure and for air temperatures from 80° to 675°F .

The drop surface temperature may also be determined from a simultaneous solution of the appropriate heat- and mass-transfer equations. This approach has been employed, for example, in references 65 and 104 for drop evaporation under forced-convection conditions. In these treatments, Nusselt number correlations for heat and mass transfer are used to express the influence of the forced convection on the drop evaporation rate. Combining equations (48) and (49), the steady-state drop surface temperature T_s is given by the following equation, which may be solved by trial-and-error methods:

$$T_s = T_g - \left(\frac{H_v D_{v,g} M_v}{RT_{kmz}} \right) \left(\frac{p}{p_{BM}} \right) (p_{v,s} - p_{v,g}) \frac{Nu_M}{Nu_H} \quad (64)$$

From equations (53) and (58), the ratio Nu_M/Nu_H approaches unity at low Reynolds numbers and $(Sc/Pr)^{1/3}$ at high Reynolds numbers. Accordingly, if radiation effects can be neglected, the drop steady-state temperature is independent of gas velocity and drop diameter at very low or very high Reynolds numbers. Since $(Sc/Pr)^{1/3}$ generally does not differ appreciably from unity, the steady-state temperature would be a weak function of gas velocity and drop diameter at intermediate Reynolds numbers. Priem (ref. 65) has shown that the values of T_s obtained from equation (64) are in close agreement with experiment.

SUMMARY OF DROP EVAPORATION RELATIONS

Either heat-transfer or mass-transfer equations may be used to predict drop evaporation rates. For evaporation in high-temperature surroundings, however, the heat-transfer equation is preferred when using experimentally

determined drop temperatures. For evaporation in very high temperature surroundings, drop evaporation rates may be predicted by using the heat-transfer equation and assuming the drop surface temperature to be at the liquid boiling point for the given ambient pressure.

Drop evaporation rates in quiescent surroundings may be obtained by use of equations (39) and (40). Equation (39) may be used in the simplified form of equation (41) for evaporation in moderate-temperature surroundings. Also, equation (40) may be used in the simplified form of equation (42) when the vapor pressure at the drop surface is small compared with ambient pressure.

For evaporation under forced-convection conditions and low-temperature surroundings, equations (48) and (49) are used in conjunction with the Nusselt number correlations.

EVAPORATION OF SPRAYS

THEORY

Extension of single-drop data to sprays is difficult, since both drop-size distribution of the spray and relative velocities between the air and drops must be known. In addition, there are such complicating factors as drop distortion, unsteady-state evaporation, and interaction between drops.

Several theoretical analyses of spray evaporation have been made by using single-drop evaporation relations in conjunction with assumed drop-size distributions. One such analysis is that described by Probert (ref. 21). In this treatment, all drops are assumed to have zero relative velocity with respect to the air. The spray is assumed to follow the Rosin-Rammler distribution equation (ref. 23). The predicted evaporation as obtained from the Probert analysis is presented in figure 28. Here the percent of the spray evaporated is plotted against the parameter $x t / \Delta^2$. Curves are presented for several values of the distribution constant \mathcal{D} of the Rosin-Rammler distribution function.

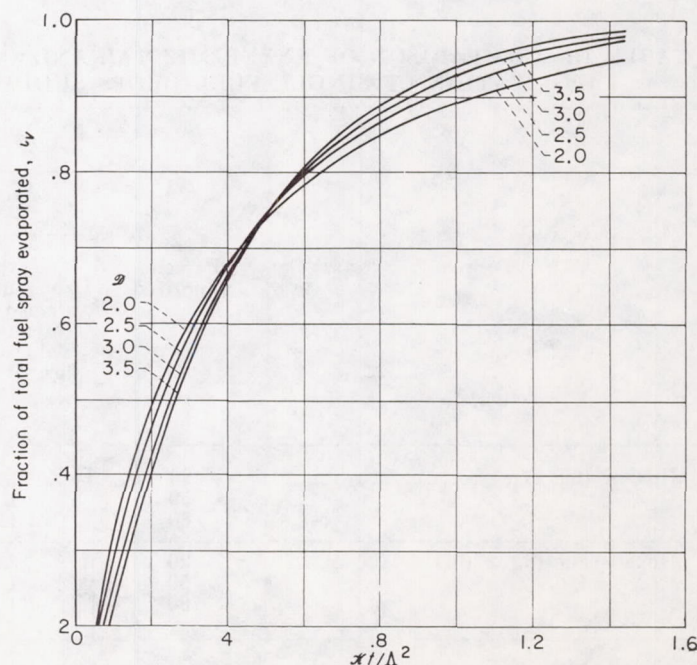


FIGURE 28.—Theoretical evaporation of liquid spray (ref. 80).

Another theoretical treatment of spray vaporization is presented by Tribus, Klein, and Rembowski in reference 105. Zero relative velocity between the air and droplets is assumed. The spray evaporation rate in this analysis is expressed in terms of the wet-bulb depression of the injected liquid. It is shown that, given an initial drop-size spectrum, successive spectra may be deduced by calculating the variation in drop size of the largest drop and relating all other drop sizes to this maximum.

EXPERIMENT

Because of the lack of experimental data on both drop-size distribution and relative velocity between drops and air, it is generally impractical to apply evaporation-rate relations for single drops to spray evaporation. Some attempts to measure directly the spray vaporization rate in airstreams have been made. An investigation of this type is described by Fledderman and Hanson (ref. 106). The influence of turbulence and air velocity on the spray vaporization rate is studied. A theoretical analysis of spray vaporization is also included in this study. Frössling's equation for single-drop evaporation (ref. 81) is combined with the drop-size distribution equation of Nukiyama and Tanasawa (ref. 22). The resulting expression, however, is very complex.

The experimental measurements were obtained by sampling hexane sprays at various distances downstream of a hollow-cone spray nozzle. The percentage of evaporated spray was determined over a limited range of air velocities. The results indicate a strong dependence of evaporation rate on the relative velocity between the drops and the airstream. Increased turbulence intensity was also found to increase the spray vaporization rate. The test results, however, do not provide conclusive information on the effect of scale of turbulence on the evaporation rate.

The results of a few measurements of the evaporation rate of kerosene sprays in essentially still air are reported by Sacks (ref. 107). In this program, kerosene was injected from a swirl-chamber fuel nozzle at pressures of 50 and 80 pounds per square inch. Over this range of conditions, 0.2 to 0.3 percent of the spray was found to evaporate per second, compared with a value of approximately 50 percent per second as calculated by using the Langmuir equation (ref. 66) and the relation of Probert (ref. 21). This large difference between predicted and experimental values was attributed primarily to the inability of the Langmuir equation to predict evaporation rates for single drops in a cloud of drops.

The evaporation of fuel sprays in high-velocity airstreams is also discussed in reference 108. In this investigation, the fuel was injected contrastream from a simple orifice, and the evaporation rates were determined by sampling the sprays. The influences of air temperature, air velocity, ambient air pressure, fuel temperature, and axial distance from the fuel orifice on the percentage of spray evaporation were investigated. In most of these measurements, a hydrocarbon fuel with a narrow boiling range of 317° to 346° F was used.

Ingebo (ref. 18) conducted an experimental and analytical investigation of the evaporation of isooctane sprays in airstreams at approximately room temperature and pressure

and velocities of 140 and 180 feet per second. The fuel was injected contrastream from a simple orifice. Evaporation rates and relative drop-air velocities were determined from high-speed photographs of the spray at various stations downstream of the fuel injector. The evaporation rates based on a mean drop diameter $d_{dr,20}$ (diameter of drop having an area equal to the total spray area divided by the total number of drops in the spray) correlated well with single-drop evaporation rates (ref. 89). Although the data of reference 18 were obtained for a limited range of conditions and for but one fuel, the results offer hope that a general relation for the evaporation rate of sprays in high-velocity airstreams may be obtained. Such a relation would require generalized expressions for predicting both the drag coefficients of evaporating drops and the spray drop-size distribution.

A study of the effect of the airflow and fuel-injection parameters on the evaporation of gasoline-type fuel sprays is reported in reference 109. This program was conducted by injecting isooctane contrastream from a simple orifice into air flowing through a duct 8 inches in diameter. Both the total-fuel and liquid-fuel distributions across the test duct were determined by sampling measurements. The measurements were made over ranges of air temperature, air velocity, air pressure, fuel-injection pressure, fuel-orifice size, and axial distance from the fuel orifice. These ranges and the resulting correlation of the measurements are illustrated in figure 29. The measurements were correlated by the following expression:

$$\frac{\epsilon_v}{1-\epsilon_v} = 9.35 \left[\left(\frac{T_a}{1000} \right)^{4.4} \left(\frac{U_a}{100} \right)^{0.80} p_a^{-1.2} \Delta p_n^{0.42} z^{0.84} \right] \quad (65)$$

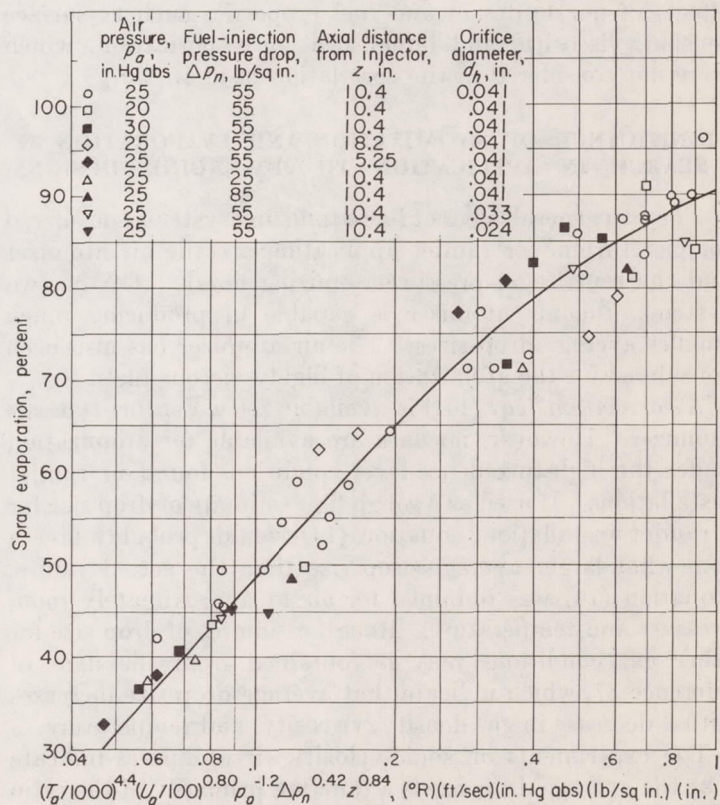


FIGURE 29.—Correlation of percentage fuel spray evaporated for contrastream injection of isooctane from a simple orifice. Air velocity 100 to 350 feet per second; air temperature, 80° to 390° F (ref. 108)

The relative effects of the variables on the spray evaporation rate are indicated by the exponents. The large influence of air temperature is evident. In comparison, the effects of the other variables are minor. The evaporation rate was essentially unaffected by changes in the diameter of the fuel orifice.

The driving force for evaporation is the temperature difference ΔT between the airstream temperature and the corresponding wet-bulb temperature of the drops. Examination of the data of reference 109 indicates that the term $\epsilon_v/(1-\epsilon_v)$ of equation (65) is roughly proportional to ΔT to a power somewhat less than unity. Over the range of airstream temperatures investigated, there was roughly a tenfold increase in ΔT for a 40-percent increase in T_a . However, the change in ΔT with T_a decreases rapidly at the higher airstream temperatures. Accordingly, the exponent of T_a in equation (65) would be expected to be appreciably lower for airstream temperatures much greater than those investigated in reference 109.

Foster and Ingebo (ref. 110) have recently investigated the evaporation of JP-5 fuel sprays in high-velocity airstreams. The fuel was injected contrastream from a multiple-orifice nozzle. The percent fuel evaporated was determined at various stations downstream of the fuel injector by means of the spillover sampling-tube technique. Figure 30 presents a correlation of the data in terms of the parameter $z^{0.33} \Delta T^{0.28} \left(\frac{U_g + U_f}{100 + U_g} \right)^2$, where U_f is the fuel velocity at the nozzle orifice in feet per second. An approximate correlation of the isooctane-spray evaporation data of reference 109 is also presented in figure 30. The difference in slopes of the correlating lines for the two fuels may be associated with effects of nozzle design and fuel properties such as surface tension, viscosity, and latent heat of vaporization, which were not considered in the correlation of figure 30.

SIGNIFICANCE OF ATOMIZATION AND EVAPORATION RESEARCH IN APPLICATION TO JET-ENGINE DESIGN

The two general types of fuel-atomizing systems considered for gas-turbine or ramjet application are the air atomizer and the centrifugal pressure-atomizing nozzle. Of the two systems, the air atomizer is capable of producing much smaller average drop sizes. The air atomizer has also been considered for the atomization of highly viscous fuels.

A correlation (eq. (14)) is available for a Venturi-type air atomizer. However, no data are available for atomization under the high-turbulence-level conditions found in ramjet installations. If used as a rough first estimate of drop size for a ramjet installation, equation (14) would probably give a somewhat larger average drop size than the actual values. Equation (14) was obtained for air at approximately room pressure and temperature. Rough estimates of drop size for other gas conditions may be obtained from the data of reference 37, which indicate that average drop size increases with a decrease in gas density, viscosity, and temperature.

The experiments on sonic-velocity air atomizers indicate that the average drop size is a function primarily of the ratio of liquid-to-air mass-flow rates w_l/w_a , the average drop size

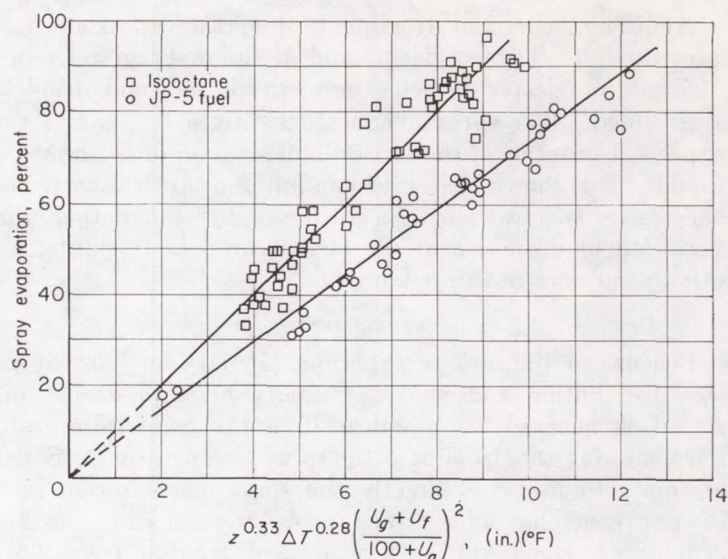


FIGURE 30.—Relation between percentage of JP-5 fuel and isooctane evaporated and distance downstream of injector, heat-transfer driving potential, air velocity, and fuel-injection velocity (ref. 110).

decreasing with decrease in w_l/w_a . Sauter mean diameters below 100 microns were obtained, even for an initial liquid viscosity of 40 centistokes (see ref. 40 and fig. 12(b)). The data of references 39 and 40 indicate that the average drop size is approximately proportional to the square root of the orifice diameter for atomizers of similar geometry.

The major portion of drop-size data for centrifugal pressure-atomizing nozzles has been obtained for fixed-configuration nozzles by use of some version of the molten-wax method. Correlations have been obtained (eqs. (29) to (34)) that permit rough estimates of atomization for fixed-configuration whirl-chamber nozzles spraying into quiescent room air. However, these correlations were for molten wax simulating kerosene and having a kinematic viscosity of approximately 2.0 centistokes. Data of references 29, 44, and 45 indicate that average drop size generally increases rather slowly with increase in viscosity. Average drop size is approximately proportional to viscosity to the 0.25 power or less. In reference 28 mean drop size was proportional to surface tension to powers from approximately 0.6 to unity. In reference 32, a correlation of drop-size data indicated that surface tension had a significant effect on atomization. However, data of reference 51 for liquids covering a wide range of surface tension indicate that the effect of surface tension on average drop size is minor. Since the range of surface tension covered by hydrocarbon fuels is quite narrow, it would appear that the effects of surface tension on the atomization of such fuels can be neglected.

Data of reference 46 show that there is an optimum cone angle that gives the smallest average drop size for a given nozzle size, operating pressure, and fuel. This optimum cone angle is generally between 80° and 90°. At low nozzle operating pressures, the cone angle exerts a predominant influence on average drop size. In this operating range, there is a large increase in average drop size as the cone angle is decreased from its optimum value.

The drop-size correlations were obtained from data for the nozzles spraying into quiescent room air. Accordingly, estimates of average drop size obtained from these investigations would probably be higher than the actual values for a turbo-jet installation where fuel is sprayed into high-temperature turbulent gases. The results of references 37 and 44 indicate that drop size should decrease with an increase in the temperature or pressure of the surrounding gas. Data in reference 55 indicate that a decrease in the relative velocity between the spray and the surrounding gas stream should result in an increase in drop size.

The effect of various ambient conditions on the steady-state evaporation of pure liquid drops may be readily predicted. Work on the evaporation of multicomponent liquid drops indicates that the concentration of the higher-boiling component in the drops increases as the spray evaporates. The unsteady-state period of drop evaporation has also been investigated. The data of reference 65 indicate that, at high air temperatures and with low-volatility fuels, the unsteady-state period represents a significant part of the evaporation time.

Either heat- or mass-transfer equations may be used for the prediction of single-drop evaporation rates under steady-state conditions. For evaporation in high-temperature surroundings, however, the heat-transfer equation is preferred in view of the sensitivity of the vapor-pressure term in the diffusion equation at the higher surface vapor pressures. For evaporation into very high temperature surroundings, the drop surface temperature may be assumed equal to the liquid boiling point for the given total pressure.

Single-drop evaporation rates in static surroundings may be obtained by use of equations (39) and (40). Equation (39) may be used in the simplified form of equation (41) for evaporation in low-temperature surroundings. Also, equation (40) may be used in the simplified form of equation (42) for low-volatility liquids.

For evaporation under forced-convection conditions at atmospheric surroundings, equations (48) and (49), in conjunction with the Nusselt number correlations of equations (53) and (58), give accurate prediction of drop evaporation rates. The Nusselt number correlation of equation (54) was obtained over a range of ambient pressures.

The evaporation of fuel sprays has been investigated both theoretically and experimentally. The theoretical analyses are generally not applicable, since they assume zero relative velocity between drops and air. Experimental results for spray evaporation in airstreams are quite limited. The most complete studies are for contraststream injection of isooctane or a JP-5 fuel from simple orifices into high-velocity airstreams. For these cases, the weight percent of the spray evaporated may be obtained from figure 30.

REFERENCES

1. Roesch, W. C., and Rose, R. F.: A Survey of the Literature on the Subject of Atomization. Prog. Rep. No. 1-46, Jet Prop. Lab., C. I. T., Feb. 28, 1946.
2. Dodge, R. A., Hagerty, W. W., and York, J. Louis: Continuous Fuel Sprays. AF Tech. Rep. No. 6067, U. S. Air Force, Air Materiel Command, Wright-Patterson Air Force Base, July 1950. (Univ. Mich. Contract No. W33-038-ac-21230.)
3. Anon.: The Penn State Bibliography on Sprays. Second ed., The Texas Co. (N. Y.), Dec. 1953.
4. Giffen, E., and Muraszew, A.: The Atomisation of Liquid Fuels. John Wiley & Sons, Inc., 1953.
5. Rayleigh: On the Instability of Jets. Proc. London Math. Soc., vol. X, Nov. 14, 1878, pp. 4-13.
6. Tyler, E.: Instability of Jets. Phil. Mag., ser. 7, vol. XVI, no. CV, Aug. 1933, pp. 504-518.
7. Weber, Constantin: Zum Zerfall eines Flüssigkeitsstrahles. Z.a.M.M., Bd. 11, Heft 2, Apr. 1931, pp. 136-145.
8. Haenlein, A.: Disintegration of a Liquid Jet. NACA TM 659, 1932.
9. Timotika, S.: On the Instability of a Cylindrical Thread of a Viscous Liquid Surrounded by Another Viscous Fluid. Proc. Roy. Soc. (London), vol. CL, no. A 870, June 1, 1935, pp. 322-337.
10. Ohnesorge, Wolfgang: Die Bildung von Tropfen Düsen und die Auflösung flüssiger Strahlen. Z.a.M.M., Bd. 16, Heft 6, Dec. 1936, pp. 355-358.
11. Squire, H. B.: Investigation of the Instability of a Moving Liquid Film. Combustion and Fuels Sub-committee, British A.R.C., Jan. 25, 1952.
12. York, J. L., and Stubbs, H. E.: The Mechanism of Disintegration of Liquid Sheets. Trans. ASME, vol. 75, no. 7, July 1953, pp. 1279-1286.
13. Lamb, Horace: Hydrodynamics. Sixth ed., Dover Pub., 1932.
14. Colburn, A. J., and Heath, H. H.: Swirl Atomiser Sprays in Partial Vacuum. Memo. No. M.86, British N.G.T.E., May 1950.
15. Castleman, R. A., Jr.: The Mechanism of the Atomization of Liquids. Jour. Res. Nat. Bur. Standards, vol. 6, no. 3, Mar. 1931, pp. 369-376.
16. Hinze, J. O.: Critical Speeds and Sizes of Liquid Globules. Appl. Sci. Res., vol. AI, 1949, pp. 273-288.
17. Lane, W. R.: Shatter of Drops in Streams of Air. Ind. and Eng. Chem., vol. 43, no. 6, June 1951, pp. 1312-1317.
18. Ingebo, Robert D.: Vaporization Rates and Drag Coefficients for Isooctane Sprays in Turbulent Air Streams. NACA TN 3265, 1954.
19. Rupe, Jack H.: A Technique for the Investigation of Spray Characteristics of Constant Flow Nozzles. Third Symposium on Combustion and Flame and Explosion Phenomena, The Williams & Wilkins Co. (Baltimore), 1949, pp. 680-694.
20. Hopkins, John L.: The Effect of Spray Cone Angle on Atomization. Tech. Rep. No. I.C.T./4, The Shell Petroleum Co. (London), Apr. 26, 1946.
21. Probert, R. P.: The Influence of Spray Particle Size and Distribution in the Combustion of Oil Droplets. Phil. Mag., ser. 7, vol. 37, no. 265, Feb. 1946, pp. 94-105.
22. Nukiyama, Shirô, and Tanasawa, Yasushi (E. Hope, trans.): Experiments on the Atomization of Liquids in an Air Stream. Rep. No. 3, On the Droplet-Size Distribution in an Atomized Jet, Defence Res. Board, Dept. Nat. Defence, Ottawa (Canada), Mar. 18, 1950. (Trans. from Trans. Soc. Mech. Eng. (Japan), vol. 5, no. 18, Feb. 1939, pp. 62-67.)
23. Rosin, P., and Rammler, E.: The Laws Governing the Fineness of Powdered Coal. Jour. Inst. Fuel, vol. 7, no. 31, Oct. 1933, pp. 29-36.
24. Epstein, Benjamin: Logarithmico-Normal Distribution in Breakage of Solids. Ind. and Eng. Chem., vol. 40, no. 12, Dec. 1948, pp. 2289-2291.
25. Mugele, R. A., and Evans, H. D.: Droplet Size Distribution in Sprays. Ind. and Eng. Chem., vol. 43, no. 6, June 1951, p. 1317.
26. Bowen, I. G., and Davies, G. P.: Particle Size Distribution and Estimation of Sauter Mean Diameter. Rep. No. I.C.T./28, The Shell Petroleum Co. (London), Oct. 1951.

27. Bevens, Rowland S.: Mathematical Expressions for Drop Size Distribution in Sprays. Conf. on Fuel Sprays, Univ. of Mich., Mar. 30-31, 1949.
28. Turner, G. M., and Moulton, R. W.: Drop Size Distribution from Spray Nozzles. Chem. Eng. Prog., vol. 49, no. 4, Apr. 1953, pp. 185-190.
29. Tate, R. W., and Marshall, W. R.: Atomization by Centrifugal Pressure Nozzles. Chem. Eng. Prog., vol. 49, no. 4, Apr. 1953, pp. 169-174.
30. Heath, H., and Radcliffe, A.: The Performance of an Air Blast Atomiser. Rep. No. R.71, British N.G.T.E., June 1950.
31. Holroyd, H. B.: On the Atomization of Liquid Jets. Jour. Franklin Inst., vol. 215, no. 1, Jan. 1933, pp. 93-97.
32. Shafer, M. R., and Bovey, H. L.: Applications of Dimensional Analysis to Spray-Nozzle Performance Data. Jour. Res. Nat. Bur. Standards, vol. 52, no. 3, Mar. 1954, pp. 141-147.
33. Nukiyama, Shirō, and Tanasawa, Yasushi (E. Hope, trans.): Experiments on the Atomization of Liquids in an Air Stream. Rep. No. 1, Defence Res. Board, Dept. Nat. Defence, Ottawa (Canada), Mar. 18, 1950. (Trans. from Soc. Mech. Eng. (Japan), vol. 4, no. 14, Feb. 1938, pp. 86-93.)
34. Nukiyama, Shirō, and Tanasawa, Yasushi (E. Hope, trans.): Experiments on the Atomization of Liquids in an Air Stream. Rep. No. 2, Defence Res. Board, Dept. Nat. Defence, Ottawa (Canada), Mar. 18, 1950. (Trans. from Trans. Soc. Mech. Eng. (Japan), vol. 4, no. 15, Feb. 1938, pp. 138-143.)
35. Nukiyama, Shirō, and Tanasawa, Yasushi (E. Hope, trans.): Experiments on the Atomization of Liquids in an Air Stream. Rep. No. 4, The Influence of the Characteristics of the Liquid on the Diameter of the Atomized Droplets. Defence Res. Board, Dept. Nat. Defence, Ottawa (Canada), Mar. 18, 1950. (Trans. from Trans. Soc. Mech. Eng. (Japan), vol. 5, no. 18, Feb. 1939, pp. 68-75.)
36. Hrubecky, Henry F.: Experiments in the Air-Stream Atomization Phenomena. Preprints of Papers, Heat Transfer and Fluid Mech. Inst., Univ. Calif. (Berkeley), June 30, July 1-2, 1954, pp. 263-274.
37. Lewis, H. C., et al.: Atomization of Liquids in High Velocity Gas Streams. Ind. and Eng. Chem., vol. 40, no. 1, Jan. 1948, pp. 67-74.
38. Conroy, E. H., and Johnstone, H. F.: Combustion of Sulfur in a Venturi Spray Burner. Ind. and Eng. Chem., vol. 41, no. 12, 1949, pp. 2741-2748.
39. Golitzine, N., Sharp, C. R., and Badham, L. G.: Spray Nozzles for the Simulation of Cloud Conditions in Icing Tests of Jet Engines. Rep. No. 14, Nat. Aero. Est. (Canada), 1951.
40. Radcliffe, A., and Clare, H.: A Correlation of the Performance of Two Air Blast Atomizers with Mixing Sections of Different Size. Rep. No. R.144, British N.G.T.E., Oct. 1953.
41. Radcliffe, A.: On the Performance of a Type of Swirl Atomizer. Rep. No. R.83, British N.G.T.E., Jan. 1951.
42. Joyce, J. R.: Fuel Atomisers for Gas Turbines. Rep. No. I.C.T./15, The Shell Petroleum Co. (London).
43. Ganger, Dean R.: Practical Observations on Gas Turbine Spray Nozzles. Conf. on Fuel Sprays, Univ. of Mich., Mar. 30-31, 1949.
44. Joyce, J. R.: The Atomisation of Liquid Fuels for Combustion. Jour. Inst. Fuel, vol. 22, no. 124, Feb. 1949, pp. 150-156.
45. Longwell, J. P.: Fuel Oil Atomization. D.Sc. Thesis, M. I. T., 1943.
46. Bowen, I. G., and Joyce, J. R.: The Effect of Cone Angle, Pressure, and Flow Number on the Particle Size of a Pressure Jet Atomiser. Tech. Rep. No. I.C.T./17, The Shell Petroleum Co. (London), Mar. 15, 1948.
47. Watson, E. A.: Fuel Control and Burning in Aero-Gas-Turbine Engines. The Chartered Mech. Eng. (London), vol. 3, no. 2, Feb. 1946, pp. 91-127.
48. Needham, H. C., and Starmer, R.: Particle Size Measurement. Special Rep. No. S.1, British N.G.T.E., July 1946.
49. Bowen, I. G., and Joyce, J. R.: Swirl Pressure Jet Atomisers. Tech. Rep. No. I.C.T./16, The Shell Petroleum Co. (London), Dec. 1947.
50. Davies, G. P.: Correlation Between Sauter Mean Diameter and the Pressure, Flow Number, and Cone Angle from Pressure Jet Atomizers. Tech. Rep. No. I.C.T./29, The Shell Petroleum Co. (London), Nov. 1951.
51. Giffen, E.: Atomisation of Fuel Sprays. Engineering, vol. 174, no. 4510, July 4, 1952, pp. 6-9.
52. Pigford, Robert L., and Pyle, Cyrus: Performance Characteristics of Spray-Type Absorption Equipment. Ind. and Eng. Chem., vol. 43, no. 7, 1951, pp. 1649-1662.
53. Houghton, H. G.: Spray Nozzles. Chemical Engineers' Handbook, John H. Perry, ed. Third ed., McGraw-Hill Book Co., Inc., 1950, pp. 1170-1175.
54. Garner, F. H., and Henny, V. E.: Behavior of Sprays under High Altitude Conditions. Fuel, vol. XXXII, 1953, pp. 151-156.
55. Kruse, C. W., Hess, A. D., and Ludvik, G. F.: The Performance of Liquid Spray Nozzles for Aircraft Insecticide Application. Jour. Nat. Malaria Soc., vol. 8, no. 4, Dec. 1949, pp. 312-334.
56. Tipler, W.: The Application of Optical and Sedimentation Methods to Particle Size Analysis of Wax Sprays. Tech. Rep. No. I.C.T./12, The Shell Petroleum Co. (London), May 27, 1947.
57. Gilbert, Mitchell, Howard, John N., and Hicks, Bruce L.: An Analysis of the Factors Affecting the State of Fuel and Air Mixtures. NACA TN 1078, 1946.
58. Maxwell, J. B.: Data Book on Hydrocarbons. D. Van Nostrand Co., Inc., 1950.
59. Edmister, Wayne C.: Application of Thermodynamics to Hydrocarbon Processing. Pt. XXIII—Equilibrium Flash Vaporization Correlations for Petroleum Fractions. Petroleum Refiner, vol. 28, no. 10, Oct. 1949, pp. 143-150.
60. Edmister, Wayne C.: Application of Thermodynamics to Hydrocarbon Processing. Pt. XXIV—Effect of Pressure on Phase Relationship for Petroleum Fractions. Petroleum Eng., vol. 28, no. 11, Nov. 1949, pp. 149-155.
61. Barnett, Henry C., and Hibbard, R. R.: Fuel Characteristics Pertinent to the Design of Aircraft Fuel Systems. NACA RM E53A21, 1953.
62. Luchak, G., and Langstroth, G. O.: Applications of Diffusion Theory to Evaporation from Droplets and Flat Surfaces. Suffield Rep. 171, Defence Res. Board (Canada), July 21, 1950.
63. Jakob, Max: Heat Transfer. Vol. I. John Wiley & Sons, Inc., 1949.
64. Colburn, A. P., and Drew, T. B.: The Condensation of Mixed Vapors. Trans. Am. Inst. Chem. Eng., vol. 33, 1937, pp. 197-212; discussion, pp. 212-215, 448.
65. Priem, Richard Jerome: Vaporization of Fuel Drops Including the Heating-Up Period. Ph.D. Thesis, Univ. Wis., 1955.
66. Langmuir, Irving: The Evaporation of Small Spheres. Phys. Rev., ser. 2, vol. XII, no. 5, Nov. 1918, pp. 368-370.
67. Topley, Bryan, and Whytlaw-Gray, Robert: Experiments on the Rate of Evaporation of Small Spheres As a Method of Determining Diffusion Coefficients—The Diffusion Coefficients of Iodine. Phil. Mag. and Jour. Sci., ser. 7, vol. 4, no. 24, Nov. 1927, pp. 873-888.
68. Houghton, H. G.: A Study of the Evaporation of Small Water Drops. Physics, vol. 4, no. 12, Dec. 1933, pp. 419-424.
69. Whytlaw-Gray, R. W., and Patterson, H. S.: Smoke. Edward Arnold & Co. (London), 1932.

70. Woodland, Dorothy J., and Mack, Edward, Jr.: The Effect of Curvature of Surface on Surface Energy. Rate of Evaporation of Liquid Droplets. Thickness of Saturated Vapor Films. *Jour. Am. Chem. Soc.*, vol. 55, no. 8, Aug. 1933, pp. 3149-3161.
71. Langstroth, G. O., Diehl, C. H. H., and Winhold, E. J.: The Evaporation of Droplets in Still Air. *Canadian Jour. Res.*, sec. A, vol. 8, Nov. 1950, pp. 580-595.
72. Kennard, E. H.: *Kinetic Theory of Gases*. McGraw-Hill Book Co., Inc., 1938, pp. 68-71.
73. Fuchs, N.: Concerning the Velocity of Evaporation of Small Droplets in a Gas Atmosphere. NACA TM 1160, 1947.
74. Bradley, R. S., Evans, M. G., and Whytlaw-Gray, R. W.: The Rate of Evaporation of Droplets. I—Evaporation and Diffusion Coefficients, and Vapour Pressures of Dibutyl Phthalate and Butyl Stearate. *Proc. Roy. Soc. (London)*, ser. A, vol. 186, no. A 1006, Sept. 1946, pp. 368-390.
75. Birks, J., and Bradley, R. S.: The Rate of Evaporation of Droplets. II—The Influence of Changes of Temperature and of the Surrounding Gas on the Rate of Evaporation of Drops of Di-*n*-butyl Phthalate. *Proc. Roy. Soc. (London)*, ser. A, vol. 198, no. A 1053, Aug. 1949, pp. 226-239.
76. Bradley, R. S., and Shellard, A. D.: The Rate of Evaporation of Droplets. III—Vapour Pressures and Rates of Evaporation of Straight-Chain Paraffin Hydrocarbons. *Proc. Roy. Soc. (London)*, ser. A, vol. 198, no. A 1053, Aug. 1949, pp. 239-251.
77. Perry, J. H., ed.: *Chemical Engineers' Handbook*. Third ed., McGraw-Hill Book Co., Inc., 1950.
78. Kumagai, S., and Isoda, H.: Experimental Study of Evaporation and Combustion of Fuel Droplets. *Sci. of Machine (Japan)*, vol. 4, no. 6, pp. 337-342, July 1952.
79. Spalding, D. B.: Combustion of Fuel Particles. *Fuel*, vol. XXX, no. 6, June 1951, pp. 121-130.
80. Graves, C. C.: Burning Rates of Single Fuel Drops and Their Application to Turbojet Combustion Process. NACA RM E53E22, 1953.
81. Frössling, Nils: On the Evaporation of Falling Droplets. *Beitrage zur Geophysik*, vol. 52, 1938, pp. 170-216.
82. Ranz, W. E., and Marshall, W. R., Jr.: Evaporation from Drops. Pt. I, *Chem. Eng. Prog.*, vol. 48, no. 3, Mar. 1952, pp. 141-146; pt. II, vol. 48, no. 4, Apr. 1952, pp. 173-180.
83. Johnstone, H. Fraser, Pigford, Robert L., and Chapin, John H.: Heat Transfer to Clouds of Falling Particles. *Bull. No. 330*, vol. 38, no. 43, Eng. Exp. Station, Univ. Ill., June 17, 1941.
84. Drake, R. M., Jr., Sauer, F. M., Jr., and Schaaf, S. A.: Forced Convection Heat Transfer from Cylinders and Spheres in a Rarefied Gas. Rep. No. He-150-74, *Inst. Eng. Res.*, Univ. Calif., Nov. 15, 1950. (Contract No. N7-onr-295-Task 3.)
85. Kudryashev, L. I. (M. Gayer, trans.): A Refinement of the Calculation of the Heat Transfer Coefficient Between Gas and Suspended Particles by Application of the Thermal Boundary Layer Method. *Trans. No. 368*, British R.A.E., Mar. 1951.
86. Williams, Glenn Carber: Heat Transfer, Mass Transfer and Friction for Spheres. D.Sc. Thesis, M. I. T., 1942.
87. Tang, Y. S., Duncan, J. M., and Schweyer, H. E.: Heat and Momentum Transfer Between a Spherical Particle and Air Streams. NACA TN 2867, 1953.
88. Kramers, H.: Heat Transfer from Spheres to Flowing Media. *Physica*, vol. 12, nos. 2-3, June 1946, pp. 61-80.
89. Ingebo, Robert D.: Vaporization Rates and Heat Transfer Coefficients for Pure Liquid Drops. NACA TN 2368, 1951.
90. Ingebo, Robert D.: Study of Pressure Effects on Vaporization Rate of Drops in Gas Streams. NACA TN 2850, 1953.
91. Gohrbandt, W.: The Evaporation of Spheres in a Hot Air Stream. Memo. No. M.110, British N.G.T.E., Apr. 1951.
92. Johnstone, H. F., and Kleinschmidt, R. V.: The Absorption of Gases in Wet Cyclone Scrubbers. *Trans. Am. Inst. Chem. Eng.*, ser. A, vol. 34, no. 2, Apr. 25, 1938, pp. 181-198.
93. Johnstone, H. F., and Williams, G. C.: Absorption of Gases by Liquid Droplets. *Ind. and Eng. Chem.*, vol. 31, no. 8, Aug. 1939, pp. 993-1001.
94. Powell, R. W.: Further Experiments on the Evaporation of Water from Saturated Surfaces. *Trans. Inst. Chem. Eng.*, vol. 18, 1940, pp. 36-50; discussion, pp. 51-55.
95. Maisel, D. S., and Sherwood, T. K.: Evaporation of Liquids into Turbulent Gas Streams. *Chem. Eng. Prog.*, vol. 46, no. 3, Mar. 1950, pp. 131-138.
96. Kinzer, Gilbert D., and Gunn, Ross: The Evaporation, Temperature and Thermal Relaxation-Time of Freely Falling Waterdrops. *Jour. Meteorology*, vol. 8, no. 2, Apr. 1951, pp. 71-83.
97. Topps, J. E. C.: An Experimental Study of the Evaporation and Combustion of Falling Droplets. N.G.T.E. Memo. M.105, British M.O.S., Feb. 1951.
98. El Wakil, M. M., Uyehara, O. A., and Myers, P. S.: A Theoretical Investigation of the Heating-Up Period of Injected Fuel Droplets Vaporizing in Air. NACA TN 3179, 1954.
99. El Wakil, M. M., Priem, R. J., Brikowski, H. J., Myers, P. S., and Uyehara, O. A.: Experimental and Calculated Temperature and Mass Histories of Vaporizing Fuel Drops. NACA TN 3490, 1956.
100. Berlad, A. L., and Hibbard, R. R.: Effect of Radiant Energy on Vaporization and Combustion of Liquid Fuels. NACA RM E52I09, 1952.
101. Anon.: Evaporation of Spray Droplets in the Absence of Flame. Semi-Annual Prog. Rep., Proj. Squid, Apr. 1, 1952.
102. Lamb, G. G.: Vaporization and Combustion of Multi-Component Fuel Droplets. Semi-Annual Prog. Rep., Proj. Squid, Apr. 1, 1953.
103. Maisel, D. S., and Sherwood, T. K.: Effect of Air Turbulence on Rate of Evaporation of Water. *Chem. Eng. Prog.*, vol. 46, no. 4, Apr. 1950, pp. 172-175.
104. Johnstone, H. F., and Eads, David K.: Vaporization of Small Sulfur Droplets. *Ind. and Eng. Chem.*, vol. 42, no. 11, Nov. 1950, pp. 2293-2298.
105. Tribus, M., Klein, J. S., and Rembowski, J.: A Method for Calculating the Rate of Evaporation and the Change in Drop Size Distribution for Pure Sprays Injected into Unsaturated Air. Proj. M992-C, *Eng. Res. Inst.*, Univ. of Mich., May 1952. (Wright Air Dev. Center, USAF Contract AF 18 (600)-51, E. O. No. 462 Br-1.)
106. Fledderman, R. G., and Hanson, A. R.: The Effects of Turbulence and Wing Speed on the Rate of Evaporation of a Fuel Spray. Rep. No. CM667, *Eng. Res. Inst.*, Univ. of Mich., June 20, 1951. (Contract NOrd 7924, Task UMH-3D, Proj. M604-3, U. S. Navy Dept., Bur. Ord.)
107. Sacks, W.: The Rate of Evaporation of a Kerosine Spray. Note 7, Nat. Aero. Establishment (Canada), 1951.
108. Longwell, John P., and Weiss, Malcolm A.: Mixing and Distribution of Liquids in High-Velocity Air Streams. *Ind. and Eng. Chem.*, vol. 45, no. 3, Mar. 1953, pp. 667-677.
109. Bahr, Donald W.: Evaporation and Spreading of Isooctane Sprays in High-Velocity Air Streams. NACA RM E53I14, 1953.
110. Foster, Hampton H., and Ingebo, Robert D.: Evaporation of JP-5 Fuel Sprays in Air Streams. NACA RM E55K02, 1956.

CHAPTER II

FLOW AND MIXING PROCESSES IN COMBUSTION CHAMBERS

By WILFRED E. SCULL and WILLIAM R. MICKELSEN

INTRODUCTION

The principal purpose of the combustion chamber in a jet engine is the efficient conversion of chemical energy contained in a fuel into the heat and kinetic energy of the exhaust gases. The energy conversion must occur efficiently not only in terms of the completeness of the combustion reaction, but also in an aerodynamic sense. Aerodynamic efficiency implies an efficient introduction and distribution of air in a combustion chamber for the purposes of burning a fuel-air mixture, and a dilution of the combustion products to the desired temperature level and proper temperature profile. In many instances, combustion efficiency may be sacrificed for aerodynamic efficiency, and vice versa.

According to various authors, the combustion problem may be quite largely aerodynamic in character. This was recognized in some of the earliest research on turbojet engines for aircraft propulsion (ref. 1), in which it was found that differences in combustor performance in engine tests and single-combustor tests could be traced directly to differences in the manner in which air flowed into the combustion chamber.

The importance of aerodynamics in the problem of combustion is further emphasized in the burning of a finely dispersed spray of liquid fuel or a portion of combustible gas well mixed with stoichiometric proportions of air. Such mixtures will not ignite and form a stable flame front at velocities greater than the velocity of laminar flame propagation (approximately 1 to 2 ft/sec for most hydrocarbon fuels), unless the aerodynamic flow pattern is such that localized vortices, zones of flow reversal, or a slowly moving boundary layer exists in the combustion zone. To stabilize the flame at the high velocities encountered in jet engines, it is therefore necessary to create low-velocity regions in which the flame can originate or else establish an aerodynamic flow pattern such that localized vortices or zones of flow reversal are created. Such vortices or zones of reverse flow allow the combustible mixture to attain local velocities necessary for high mass flow without exceeding translational velocities that could cause instability of the flame front.

The object of this discussion is the consideration of aerodynamic relations applicable to the design of combustion chambers of jet engines. Experimental and theoretical data relating combustor approach-stream parameters, combustor pressure losses, gas jets of many types, and orifice coefficients are included. Aerodynamic mixing is discussed in terms of fundamental turbulent diffusion theories relating heat, mass, and momentum transfer from different sources in various types of flow fields. The effect of periodic flow

fluctuations on diffusion is discussed. Fuel-air mixing is presented in terms of spreading of liquid and vapor fuel from several different sources.

SYMBOLS

The following symbols are used in this chapter:

A	cross-sectional area
\mathcal{A}	ratio of one of two parallel-jet areas to total mixed-jet area
a	distance between vortices in single row
B, B'	dimensionless quantities
B^*	function of flow rates, velocities, areas, and angles between two mixing jets
b_d	depth of rectangular duct
C^*	function of flow rates, areas, and total temperatures of two mixing jets
C_D	drag coefficient
C_{fr}	dimensionless friction coefficient (Fanning)
C_h	orifice discharge coefficient
C_{temp}	temperature coefficient in jet
\mathcal{C}	concentration
c	mixing-length parameter
c_p	specific heat at constant pressure
D_M	molecular diffusion coefficient (mass)
D_T	turbulent diffusion coefficient
$D_{T,H}$	coefficient of turbulent diffusion of heat
$D_{T,M}$	coefficient of turbulent diffusion of mass
$D_{T,mom}$	coefficient of turbulent diffusion of momentum
\mathcal{D}	drag
d	diameter
E, E', E''	functions of ϵ
$F(f_{per})$	spectrum density function of periodic flow fluctuation of finite band width
$F(f_T)$	spectrum density function of turbulent kinetic energy
$F(\sigma)$	function of y/y_o
$\mathcal{F}(\sigma)$	function of r/r_o
f	fuel-air ratio
f_T	frequency of turbulent fluctuations
f_v	frequency of vortex shedding
G	weight-flow rate per unit area
g	acceleration due to gravity, 32.17 ft/sec ²
h	enthalpy per unit volume
I	combustion intensity
J_1, J_2	modified Bessel functions of first and second kind, zero order
j	penetration of jet

K_{ps}	strength of point source	$\sqrt{u_x^2}$	turbulent intensity in x -direction
K_V	strength of individual vortex	$\overline{u_y}$	time-average of u_y
k_1, k_2, \dots	constants	$\sqrt{u_y^2}$	turbulent intensity in y -direction
L_{Eu}	Eulerian scale of turbulence	$\overline{u_z}$	time-average of u_z
L_{La}	Lagrangian scale of turbulence	$\sqrt{u_z^2}$	turbulent intensity in z -direction
l	length	V	volume
l^*	length of duct between station where Mach number is taken and station where choking would occur	W_{dt}	duct width
l_{mix}	mixing length, or mean free path of fluid particle in turbulent flow	W_{fh}	flameholder width
M	Mach number	w	weight-flow rate
m	momentum of jet at any cross section	w_d	weight-flow rate of diffusing quantity
N	number	w'_d	weight-flow rate of diffusing quantity as function of time t'
\mathcal{N}	engine rotational speed	X	distance normal to A , or rectangular coordinate
P	absolute pressure	x	longitudinal distance
P^*	absolute pressure with choked flow	x_j	longitudinal distance from jet centerline
ΔP	pressure loss	\overline{Y}	mean displacement
$\Delta P_t/P_t$	total-pressure-loss ratio	y	distance from centerline of plane-parallel jet
$P_{t,2}/P_{t,\infty}$	diffuser total-pressure-recovery factor	z	coordinate
$P_{t,3}/P_{t,2}$	compressor total-pressure ratio	α	angle between gas streams
$\Delta P_t/q_{ref}$	total-pressure-loss coefficient	β	dimensionless quantity
Pr	Prandtl number	γ	ratio of specific heats
\mathcal{P}	combustor total-pressure-loss factor	δ	ratio of absolute pressure to NACA standard sea-level pressure of 2116.2 lb/sq ft abs
Q	total quantity of heat transferred	$\delta(f_T - f_{per})$	Dirac delta function
q	incompressible dynamic pressure	ϵ	r/x
R	universal gas constant	ζ	approximate mean vorticity
Re	Reynolds number	η	efficiency
R_{Eu}	Eulerian double velocity correlation coefficient	θ	ratio of absolute temperature to NACA standard sea-level temperature of 518.7° R
R_{La}	Lagrangian double velocity correlation coefficient	ι_v	fraction of fuel evaporated before reaching point at which f_i is measured
r	radial distance	κ	thermal conductivity
$r_{cs}, r_{ds}, r_{ts}, r_{ss}$	cylinder-, disk-, ring-, and sphere-source radii	Λ	range of droplet
r_{hy}	hydraulic radius	λ_{La}	Lagrangian microscale of turbulence
$r_{1/2}$	half-radius of axisymmetric jet at longitudinal distance x	μ	absolute viscosity of fluid
r'	radial distance in disk source of radius r_{ds}	ν	kinematic viscosity of fluid
S	total fuel-spreading parameter	ξ	function of m, r, x, ν , and ρ in laminar free jet
Sc	Schmidt number	Π	compressor total-pressure ratio, $P_{t,3}/P_{t,2}$
s	lateral spacing between vortex rows	ρ	weight per unit volume
T	absolute temperature	$\sqrt{\rho U_z^2 / \rho}$	momentum-flux velocity
\overline{T}	mean absolute temperature	σ	y/y_o or r/r_o
\tilde{T}	fluctuating value of absolute temperature	τ	fluid shearing stress
t	time	ν	angle between orifice centerline and flow direction of gas stream
t_{La}	characteristic time related to Lagrangian scale	Φ	function of $P_{t,j}$ and P_j
t'	time controlling rate of fuel injection	φ	function of $P_{t,j}$ and P_j
U	velocity	Ψ	stream function
U_r	velocity component in r -direction	ψ	function of $U_x, D_T x, r$, and r'
U_x	velocity component in x -direction	Ω	function of B^*, C^*, γ_3 , and M_3
U_y	velocity component in y -direction	ω	standard square deviation
u_x	turbulent velocity in x -direction	ω'	standard square deviation evaluated at time $t-t'$
u_y	turbulent velocity in y -direction		
u_z	turbulent velocity in z -direction		
$\overline{u_x}$	time-average of u_x		

Subscripts:

<i>A</i>	known combustor-inlet conditions
<i>a</i>	air
<i>ad</i>	adiabatic
<i>B</i>	new combustor-inlet conditions
<i>C</i>	compressor
<i>corr</i>	corrected
<i>cy</i>	cycle
<i>cyl</i>	cylinder
<i>D</i>	first
<i>dr</i>	droplet
<i>dt</i>	duct
<i>E</i>	second
<i>e</i>	external
<i>f</i>	fuel
<i>fr</i>	friction
<i>H</i>	heat
<i>i</i>	rectangular coordinates
<i>j</i>	jet
<i>La</i>	Lagrangian characteristic
<i>l</i>	liquid
<i>M</i>	mass
<i>max</i>	maximum, on axis of jet
<i>mol</i>	molecular motion
<i>mom</i>	momentum
<i>mixg</i>	mixing
<i>n</i>	normal
<i>o</i>	outer boundary of jet
<i>ob</i>	oblique
<i>ov</i>	over-all
<i>pc</i>	potential core
<i>per</i>	periodic
<i>r</i>	radial direction
<i>ref</i>	reference
<i>rel</i>	relative to free stream
<i>S</i>	Stokes' law
<i>T</i>	turbulent
<i>t</i>	total
<i>tb</i>	turbine
<i>W</i>	finite band width
<i>x</i>	pertaining to <i>x</i> -direction
<i>y</i>	pertaining to <i>y</i> -direction
<i>z</i>	pertaining to <i>z</i> -direction
<i>0</i>	time zero
<i>1</i>	in space surrounding jet
<i>2</i>	compressor inlet
<i>3</i>	combustor inlet
<i>3a</i>	longitudinal position in combustor upstream of which all friction losses occur and downstream of which only combustion losses occur
<i>3b</i>	longitudinal position between combustor inlet and combustor outlet
<i>4</i>	combustor outlet
<i>∞</i>	free stream or ambient

AERODYNAMIC FLOW

COMBUSTOR APPROACH-STREAM PARAMETERS

Turbojet combustion chambers.—The more important combustor approach-stream parameters for a turbojet engine are inlet-air velocity, temperature, and pres-

sure. A less important parameter is the combustor-inlet velocity profile. Each of these parameters may vary over a wide range, depending upon the operational variables engine speed, flight Mach number, and flight altitude. The following table indicates the range of the combustor operating variables encountered during operation of a turbojet engine with a sea-level static compression ratio of 11 at a flight Mach number of 0.8 at various engine speeds and altitudes:

Altitude, ft	Engine speed	Inlet pressure, in. Hg abs	Inlet temperature, °F	Air-flow, lb/sec
Sea level---	Rated-----	376.5	708	197.9
	Idle-----	64.1	215	54.7
	Windmill-----	42.5	120	44.0
60,000-----	Rated-----	40.3	625	18.1
	Idle-----	6.1	113	4.7
	Windmill-----	2.2	30	2.7

In addition, supersonic flight speeds tend to increase the range of operating variables still further. For example, a supersonic turbojet engine which has a sea-level static compression ratio of 7.0 would have a combustor-inlet total temperature of 964° F during rated-engine-speed operation at a flight Mach number of 2.8 in the stratosphere.

Generalized parameters: Sanders (ref. 2) developed performance parameters for jet engines from concepts of flow similarity, inertia, elastic and viscous forces, and thermal expansions of the working fluid. Dimensionless and corrected dimensional generalizing parameters were employed to relate engine performance to the geometry of the engine boundaries, the Mach number, the Reynolds number, and the total-temperature ratio of the engine. For turbojet engines, it was shown that

$$\frac{w_a \sqrt{\theta_t}}{\delta_t} = F \left(\frac{P_t}{\delta_t}, \frac{T_t}{\theta_t}, \frac{\mathcal{A}}{\sqrt{\theta_t}} \right) \quad (1)$$

where

$$\theta_t = \frac{T_t}{518.7} \quad (2)$$

and

$$\delta_t = \frac{P_t}{2116.2} \quad (3)$$

with T_t in °R, P_t in pounds per square foot absolute, and θ_t and δ_t usually evaluated in terms of the total temperature and pressure at the compressor inlet.

From equation (1), it is apparent that the corrected weight-flow rate of air $w_a \sqrt{\theta_t} / \delta_t$, the corrected absolute total pressure P_t / δ_t , and the corrected absolute total temperature T_t / θ_t at any position in the engine are substantially constant for a constant corrected engine speed $\mathcal{A} / \sqrt{\theta_t}$. These generalizations are valid at altitudes to approximately 40,000 feet. At higher altitudes, the effect of Reynolds number becomes apparent in the performance of the compressor. As a result, the corrected airflow $w_a \sqrt{\theta_t} / \delta_t$ and compressor adiabatic efficiency $\eta_{ad, c}$ do not remain constant for a constant corrected engine speed, but begin to diminish slightly

with increasing altitudes (decreasing Reynolds numbers) (ref. 3). In addition, the decreasing Reynolds numbers may result in small changes in compressor total-pressure ratio $P_{t,3}/P_{t,2}$ at extreme altitudes if the corrected engine speed remains constant. The direction and magnitude of the change in compressor total-pressure ratio and the magnitude of the decrease in corrected airflow and compressor efficiency are functions of the particular engine under consideration (ref. 4).

New combustor-inlet conditions can be calculated as follows: Let subscripts A and B indicate the known and new inlet conditions, respectively, while subscripts 2 and 3 denote the compressor inlet and the combustor inlet, respectively. Then

$$\mathcal{N}_B = \mathcal{N}_A \left(\sqrt{\frac{\theta_{t,B}}{\theta_{t,A}}} \right)_2 \quad (4)$$

$$w_{a,B} = w_{a,A} \left(\frac{\delta_{t,B}}{\delta_{t,A}} \sqrt{\frac{\theta_{t,A}}{\theta_{t,B}}} \right)_2 \quad (5)$$

$$P_{t,B,3} = P_{t,A,3} \left(\frac{\delta_{t,B}}{\delta_{t,A}} \right)_2 \quad (6)$$

where θ_t and δ_t are evaluated at the stations indicated by the subscripts. The value of the compressor-inlet absolute total temperature $T_{t,2}$ used in the determination of θ_t in equation (2) can be obtained from the expression

$$T_{t,2} = T_\infty \left(1 + \frac{\gamma-1}{2} M_\infty^2 \right) \quad (7)$$

where M_∞ is the flight Mach number and T_∞ is ambient absolute temperature. Determination of the compressor-inlet absolute total pressure $P_{t,2}$ used in determination of δ_t in equation (3) requires a knowledge of the diffuser total-pressure-recovery factor. Losses in total pressure in the engine-inlet diffuser can occur as the result of friction, inefficient diffusion, or possible shock formation. Typical total-pressure-recovery factors that can be used for current

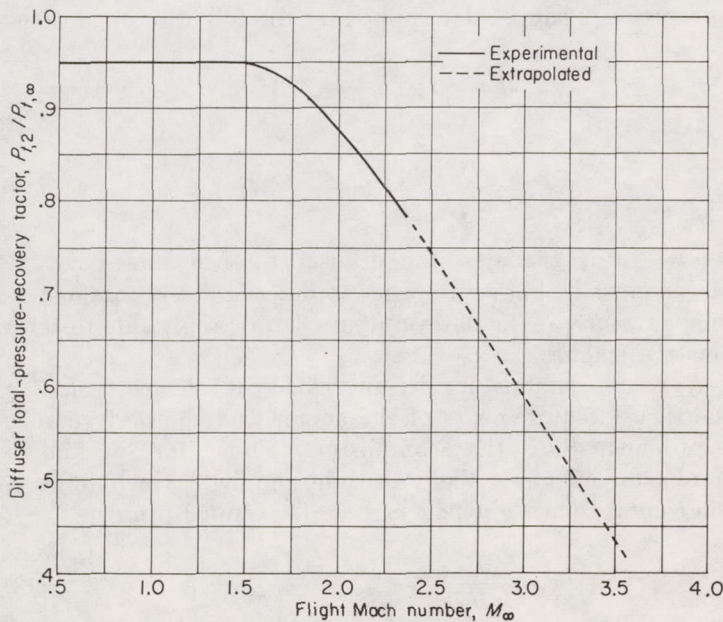


FIGURE 31.—Typical diffuser total-pressure-recovery factors.

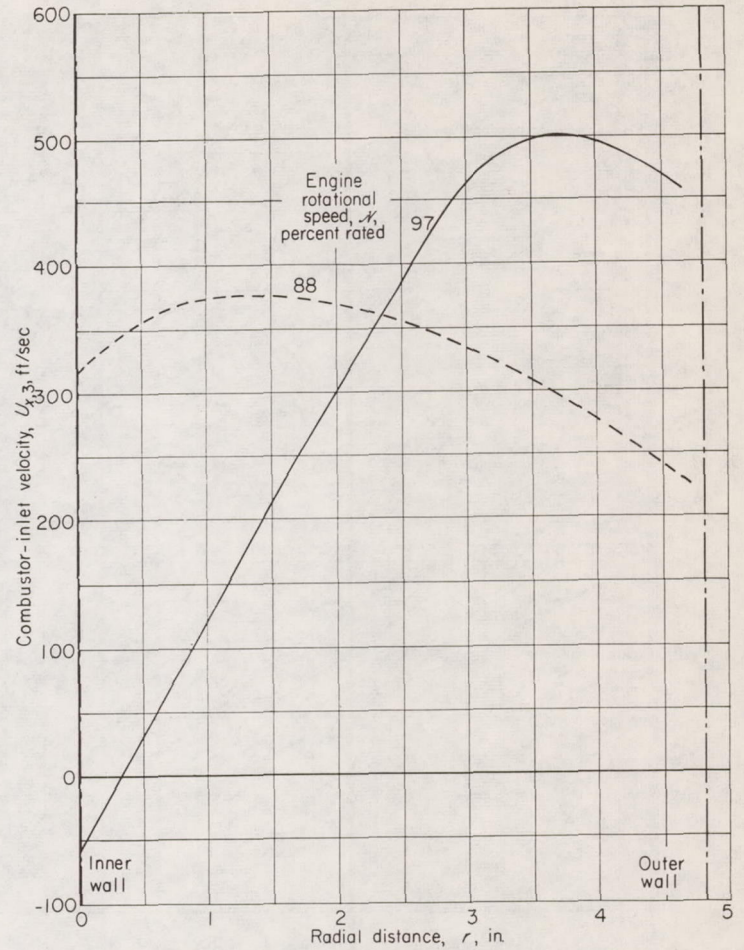


FIGURE 32.—Variation of combustor-inlet velocity profile with engine speed in axial-flow turbojet engine.

engine diffusers are presented in figure 31. The sharp decrease in recovery factors at high Mach numbers is due to shock formation at the diffuser inlet. The value of $P_{t,2}$ can be calculated from

$$P_{t,2} = \frac{P_{t,2}}{P_{t,\infty}} P_\infty \left(1 + \frac{\gamma-1}{2} M_\infty^2 \right)^{\frac{\gamma}{\gamma-1}} \quad (8)$$

where P_∞ is the ambient absolute pressure and $P_{t,2}/P_{t,\infty}$ is the diffuser total-pressure-recovery factor. As mentioned previously, the combustor-inlet total temperature can be determined from the constancy of T_t/θ_t with a constant $\mathcal{N}/\sqrt{\theta_t}$. However, if the compressor total-pressure ratio and adiabatic efficiency are known as a function of corrected engine speed and altitude, a better determination is

$$T_{t,3} = T_{t,2} \left[1 + \frac{(\Pi)^{\frac{\gamma-1}{\gamma}} - 1}{\eta_{ad,C}} \right] \quad (9)$$

The combustor-inlet absolute total pressure can be determined from the relation

$$P_{t,3} = P_{t,2} \frac{P_{t,3}}{P_{t,2}} = P_{t,2} \Pi \quad (10)$$

Compressor wake effects: The aerodynamic design of the turbojet combustor is closely related to the airflow pattern at the compressor exit. Ideally, the optimum combustor-

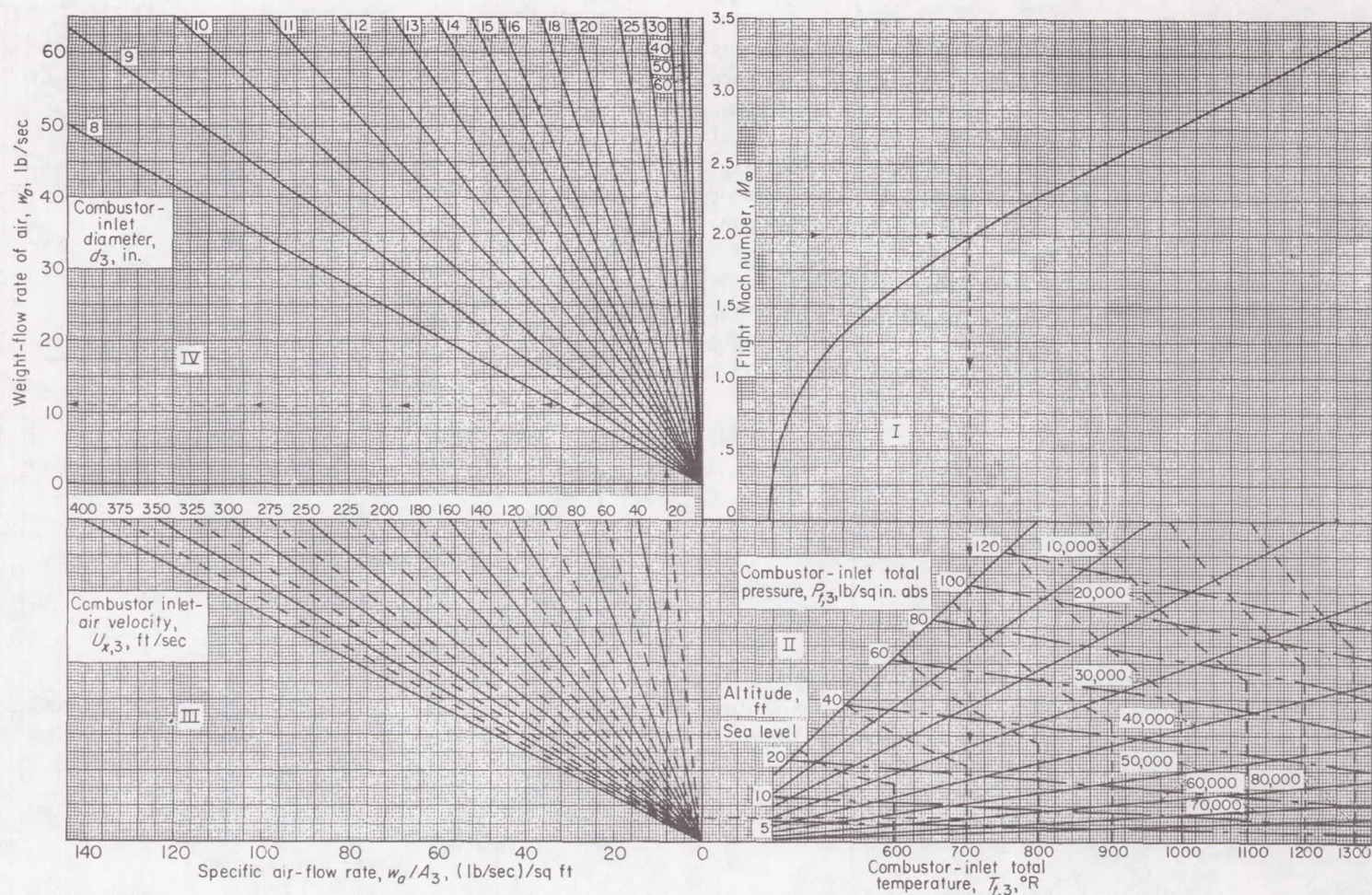


FIGURE 33.—Ramjet combustor-inlet conditions. (A large working copy of this fig. may be obtained on request from NACA Headquarters, Washington, D. C.)

inlet airflow pattern might have a uniform velocity profile with an average velocity determined by the preceding equations. However, especially in engines with centrifugal compressors, the velocity profile at the inlet may be nonuniform. Two combustor-inlet velocity profiles for an axial-flow turbojet engine are presented in figure 32. These particular profiles show wider variations with engine operating speed than are usually found in current engines.

Uneven velocity profiles can be significant in terms of combustor total-pressure losses and operating problems. Lloyd (ref. 5) indicates that one of the major sources of combustor total-pressure loss is the entry loss associated with the diffusing and evening of the high-velocity airstream from the compressor. In addition to total-pressure losses, uneven inlet velocity profiles with accompanying uneven secondary-air distribution and unequal liner cooling might result in distortion and cracking of the combustor liner (ref. 6). Maldistribution of the airflow at the combustor inlet might also be responsible for asymmetric fuel sprays and uncentralized burning.

Ramjet combustion chambers; generalized parameters.—Combustor approach-stream parameters (inlet-air velocity, temperature, and pressure) for a ramjet combustor are the same as for a turbojet combustor. As with a turbojet combustor, these parameters may vary over a wide range; however, the range depends only upon flight Mach number and

flight altitude for the ramjet. Determination of the approach-stream parameters is, in general, simpler for the ramjet combustor than for the turbojet. Since there is no compressor in a ramjet engine, all the compression occurs in the diffuser. Combustor-inlet absolute total temperature and pressure can be determined by the following equations:

$$T_{t,3} = T_{\infty} \left(1 + \frac{\gamma-1}{2} M_{\infty}^2 \right) \quad (11)$$

$$P_{t,3} = \frac{P_{t,2}}{P_{t,\infty}} \left(1 + \frac{\gamma-1}{2} M_{\infty}^2 \right)^{\frac{\gamma}{\gamma-1}} \quad (12)$$

As with the turbojet, the diffuser total-pressure-recovery factor must be known in order to determine the combustor-inlet pressure. The data in figure 31 are applicable to both types of engines.

As a rule, combustor inlet-air velocity is selected to satisfy the thrust requirements of the engine and the performance requirements of the combustor. Thus, for a known combustor-inlet area, flight altitude, and flight Mach number, the combustor weight flow can be determined from

$$w_a = \frac{A_3 U_{x,3}}{R_a} \frac{P_{t,3}}{T_{t,3} \left(1 + \frac{\gamma-1}{2} M_{\infty}^2 \right)^{\frac{1}{\gamma-1}}} \quad (13)$$

where

$$M_3 = \frac{U_{x,3}}{\sqrt{\gamma g R_a T_{t,3} - \frac{(\gamma-1)U_{x,3}^2}{2}}} \quad (14)$$

Data that can be used for rapid determination of the inlet conditions in a ramjet engine are presented in figure 33. This figure is based on the diffuser total-pressure recoveries of figure 31. Figure 33 can be adapted to diffuser total-pressure-recovery factors differing from those of figure 31 as follows:

- (1) As indicated by the arrows, determine $P_{t,3}$ and $T_{t,3}$ in quadrant II for the required flight conditions.
 - (2) Correct $P_{t,3}$ by the ratio of the new diffuser recovery factor to the recovery factor of figure 31.
 - (3) Locate the new $P_{t,3}$ in quadrant II on the same isothermal line as the $P_{t,3}$ of step (1).
- Further use of figure 33 is shown on the figure.

COMBUSTOR PRESSURE LOSSES

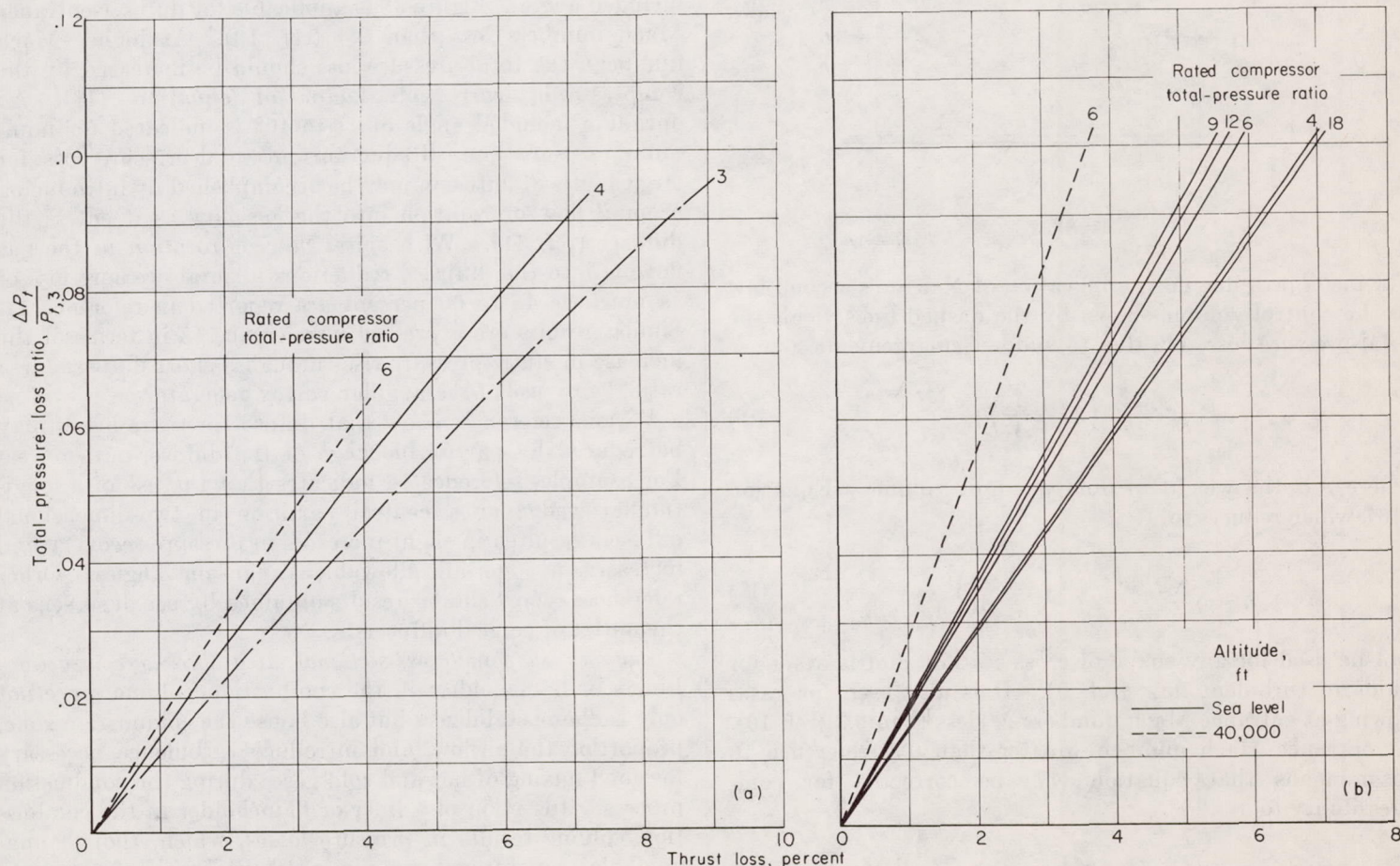
In any type of combustion chamber, regions of low gas velocity must be present if stable combustion is to be maintained. Liners and flameholders are used in turbojet and ramjet combustors, respectively, to provide stabilizing regions of low velocity. Advantages gained by use of such

stabilizing mechanisms may be balanced by combustor pressure losses, which result in losses in over-all cycle efficiency.

Effect on over-all cycle performance.—The effect of combustor pressure loss on cycle efficiency is expressed in reference 7 as

$$\frac{d\eta_{cy}}{d\left(\frac{\Delta P_t}{P_{t,3}}\right)} = - \frac{\eta_{ad,c} \eta_{ad,tb} \left(\frac{\gamma-1}{\gamma}\right) \left(1 - \frac{\Delta P_t}{P_{t,3}}\right)^{\frac{1-2\gamma}{\gamma}} \Pi^{\frac{1-\gamma}{\gamma}}}{\eta_{ad,c} \left(1 - \frac{T_{t,2}}{T_{t,4}}\right) - \frac{T_{t,2}}{T_{t,4}} \left(\Pi^{\frac{\gamma-1}{\gamma}} - 1\right)} \quad (15)$$

where ΔP_t is the combustor total-pressure loss, $T_{t,4}$ is the combustor-outlet total temperature, and η_{cy} is the over-all cycle efficiency. The denominator of the right side of equation (15) is always positive and proportional to the heat added in the combustor. As shown by figure 34, total-pressure losses in turbojet engines are important, especially when operating at very low or very high over-all pressure ratios. For compressor total-pressure ratios less than 9, increases in compressor total-pressure ratios resulted in decreased effects of combustor total-pressure losses. With higher pressure ratios, combustor pressure losses caused greater thrust losses. These increases in thrust loss are caused by the greatly increased power required to operate the compressor at the high pressure ratios. Increasing pres-



(a) Sea-level static conditions (ref. 5).

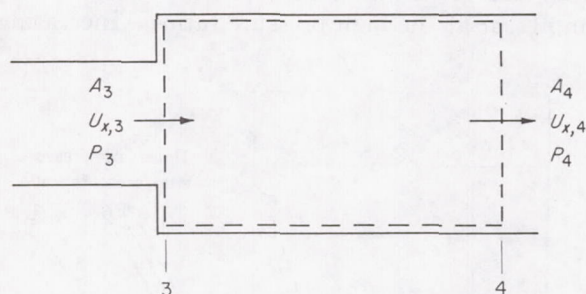
(b) Flight Mach number, 0.6; nozzle coefficient, 0.96; lower heating value of fuel, 18,700 Btu per pound; combustor-outlet total temperature, 1960° R; compressor efficiency, 0.85; turbine efficiency, 0.90; combustion efficiency, 97 percent.

FIGURE 34.—Calculated thrust loss of turbojet engine as function of combustor total-pressure loss.

sure losses with accompanying decreases in cycle efficiency result in increases in fuel consumption. Likewise, increases in unit size become necessary, since higher rotative speeds and accompanying higher turbine stresses are required to obtain the higher compression ratios needed to maintain maximum cycle efficiencies with increasing pressure losses (ref. 8).

Causes.—Pressure losses in combustors occur as the result of several factors: (1) abrupt changes in flow cross-sectional areas, (2) bluff bodies or flame-stabilizing devices in the combustion zone causing partial blockage of the open cross-sectional area, (3) frictional forces exerted upon the gas stream by flame-stabilizing devices and the walls of the combustion chamber, (4) increases in momentum imparted to the gas stream as it flows through the combustor, and (5) the high degree of turbulence necessary to mix gases in a restricted combustion volume.

Changes in flow cross-sectional area due to expansion: Pressure losses in the combustor-inlet diffuser, which partially slows the high-velocity airstream from the compressor, may be attributed to the combustor. For the case of sudden enlargements, which is the condition approached by some very short combustor-inlet diffusers, the following diagram is considered:



Sketch (a)

For incompressible flow, application of Newton's second law to the control volume shown by the dashed lines yields the total-pressure loss ΔP_t due to sudden enlargements as

$$\Delta P_t = \frac{\rho_3 U_{x,3}^2}{2g} \left(1 - 2 \frac{A_3}{A_4} \right) + \frac{\rho_4 U_{x,4}^2}{2g} \quad (16)$$

where ρ is the weight of fluid per unit volume. Equation (16), which reduces to

$$\Delta P_t = \frac{\rho_3 U_{x,3}^2}{2g} \left(1 - \frac{A_3}{A_4} \right)^2 \quad (17)$$

can be used for any shape of cross section, and is exact for fluids in turbulent flow (ref. 9). It is also used for gases flowing at entrance Mach numbers M_3 less than 0.3 (ref. 10). At entrance Mach numbers greater than 0.3, reference 10 recommends that equation (17) be corrected for compressibility to

$$\Delta P_t = \frac{\rho_3 U_{x,3}^2}{2g} \left(1 + \frac{M_3^2}{4} + \dots \right) \left(1 - \frac{A_3}{A_4} \right)^2 \quad (18)$$

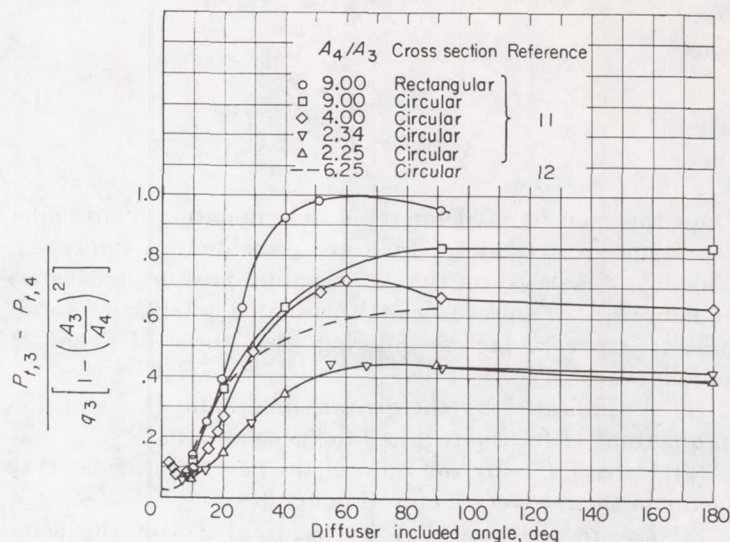


FIGURE 35.—Effect of diffuser included angle on diffuser total-pressure losses.

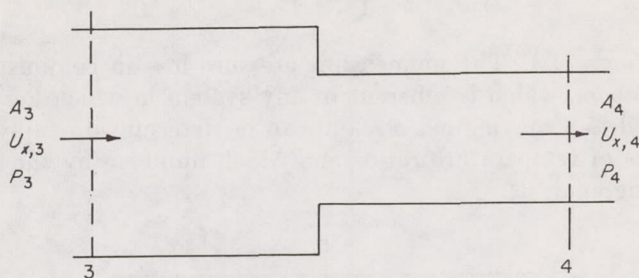
where M_3 is the Mach number at the entrance to a sudden expansion.

Obviously, a sudden enlargement is undesirable. However, length limitations in ramjet or turbojet engines generally necessitate short diffusers. As a result, diffuser included angles are usually large. Figure 35 (refs. 11 and 12) presents the pressure loss of diffusers as a function of the included angle. Figure 35 is applicable for diffuser-entrance Mach numbers less than 0.3 (ref. 10). At higher Mach numbers, the total-pressure loss should be increased by the compressibility-correction factor of equation (18). An optimum included angle of 7° to 10° is indicated for minimum pressure loss. Reductions in total-pressure loss for large angles of diffusion may be accomplished by introducing a spiral flow or rotation into the gas flow as it enters the diffuser (ref. 11). With spiral flow or rotation in the gas flowing into the diffuser, reductions in total-pressure loss of as much as 45 to 60 percent are reported in reference 11. Similar results are expressed in reference 13 in terms of the increase in static-pressure rise through a short diffuser (area ratio, 2) by use of rectangular vortex generators.

Various references show that diffuser pressure losses may be reduced by partial blockage of the diffuser-outlet area. For example, reference 14 indicates that the use of a longitudinal wedge or a central partition in two-dimensional diffusers resulted in slight increases in pressure recovery and increases in over-all allowable expansion angles. Other references report similar results obtained by use of screens at the outlet of conical diffusers.

Changes in flow cross-sectional area due to contraction: Liners or flameholders in the combustion volume serve not only as flame stabilizers but also house the combustion zone, proportion the airflow, and introduce turbulence necessary for good mixing of hot and cold gases during the combustion process. Insertion of a liner or flameholder in the combustion volume results in pressure losses, which, though unavoidable, can often be minimized. Blockage of the open cross-sectional area of a combustor may be considered some-

what similar to a sudden contraction in the flow area in a pipe. For sudden contractions, the following diagram is considered:



Sketch (b)

Assuming incompressibility, reference 15 indicates the total-pressure loss in this case to be

$$\Delta P_t = k_1 \frac{\rho_4 U_{x,4}^2}{2g} \quad (19)$$

where k_1 depends on the ratio of areas at stations 3 and 4 and is defined by

$$k_1 = 0.4 \left(1.25 - \frac{A_4}{A_3} \right) \text{ for } \frac{A_4}{A_3} < 0.715 \quad (20a)$$

and

$$k_1 = 0.75 \left(1 - \frac{A_4}{A_3} \right) \text{ for } \frac{A_4}{A_3} > 0.715 \quad (20b)$$

Total-pressure losses due to sudden contractions may be greatly reduced by using a conical or well-rounded transition section between areas 3 and 4. The value of k_1 for conical or well-rounded transition sections is reduced to approximately 0.05. This value of k_1 is applicable for all values of A_4/A_3 , provided the flow in the smaller area is turbulent.

Body shape and blocked area: Ramjet combustion chambers and afterburners utilize a flameholding mechanism consisting of gutters or similar devices to provide a recirculatory zone of low velocity for flame stabilization. Usually, such devices in the combustion chamber provide more turbulence and better mixing, with resultant increases in combustion efficiency. However, such devices create an unavoidable pressure loss with an accompanying adverse effect on over-all cycle efficiency. The effect of flameholder area blockage on the total-pressure-loss coefficient $\Delta P_t/q_{ref}$ (where q_{ref} is the reference velocity pressure based on the combustor inlet-air stagnation density and maximum cross-sectional area of the combustor) is shown in figure 36 (ref. 16) for an inlet Mach number of 0.162. Total-pressure losses increase with increases in blocked area.

Fluid friction: Frictional total-pressure losses in combustors are generally small enough to be neglected in comparison with other factors causing pressure losses. However, in ramjet engines and afterburners in which high-velocity gases scrub relatively long walls of the combustion chamber, frictional total-pressure losses may not be negli-

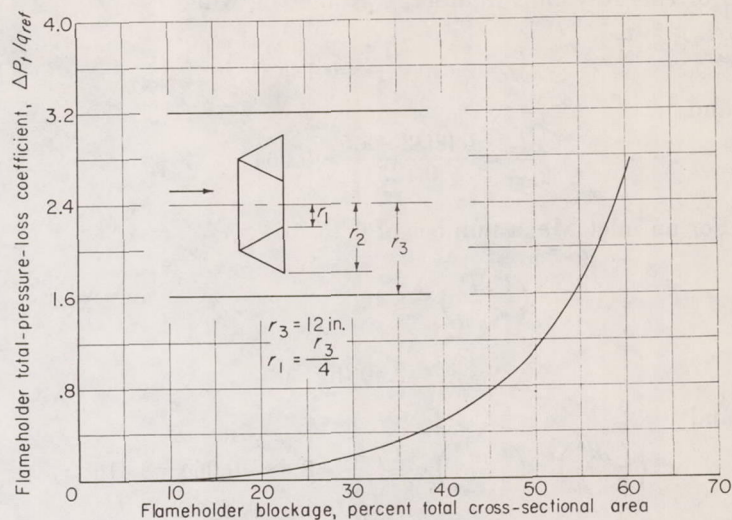


FIGURE 36.—Effect of area blockage on combustor isothermal total-pressure losses. Combustor-inlet Mach number, 0.162; annular V-gutter flameholder (ref. 16).

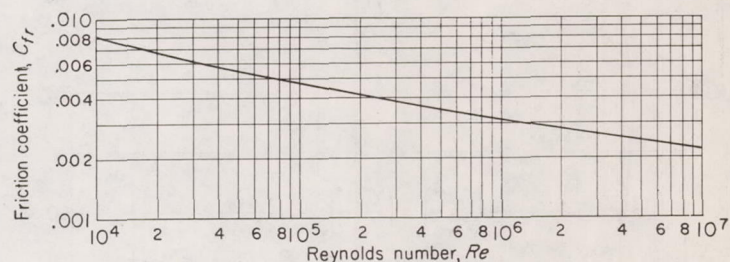


FIGURE 37.—Friction coefficients for sheet-metal surfaces as function of Reynolds number (ref. 18).

gible. The total-pressure loss due to friction $\Delta P_{t,fr}$ of a fluid flowing in a duct can be expressed by the Fanning friction equation (ref. 17):

$$\Delta P_{t,fr} = \frac{\rho U_x^2}{2g} C_{fr} \frac{l_{dt}}{r_{hy,dt}} \quad (21)$$

where ρ and U_x are average values. In figure 37 (ref. 18), values of C_{fr} are presented for a range of Reynolds numbers from 10^4 to 10^7 . The value of C_{fr} varies from 0.004 to 0.0035 for Reynolds numbers from 2.5×10^5 to 5.0×10^5 . Reference 19 includes data from which the effect of wall friction alone upon a fluid flowing in a cylindrical duct can be estimated if the Mach number at the entrance and the friction coefficient of the chamber are known. Figure 38 presents data showing the total-pressure loss in terms of these variables. Use of the figure can be demonstrated best by an example. Consider air flowing in a 6-inch-diameter duct at an inlet Mach number of 0.25 at sea level. The duct is 30 inches long and the total-pressure loss is required.

Average air velocity in duct = $0.25 \times 1120 = 280$ ft/sec

Air density = 0.0766 lb/cu ft

Air viscosity = 3.723×10^{-7} slugs/(ft)(sec)

$$\text{Reynolds number} = \frac{0.0766}{32.17} \times 280 \times 0.5 \div \frac{3.723 \times 10^{-7}}{32.17} = 8.95 \times 10^5$$

For this Reynolds number, $C_{fr}=0.0032$, while

$$r_{hy,dt} = \frac{1}{4} d_{dt} = \frac{0.5}{4} = 0.125 \text{ ft}$$

and

$$\frac{C_{fr} l_{dt}}{r_{hy,dt}} = \frac{0.0032 \times 2.5}{0.125} = 0.064$$

For an inlet Mach number of 0.25,

$$\left(\frac{C_{fr} l^*}{r_{hy,dt}} \right)_3 = 8.48$$

$$\frac{P_{t,3}}{P_t^*} = 2.40 \text{ (fig. 38)}$$

and

$$\left(\frac{C_{fr} l^*}{r_{hy,dt}} \right)_4 = \left(\frac{C_{fr} l^*}{r_{hy,dt}} \right)_3 - \frac{C_{fr} l_{dt}}{r_{hy,dt}} = 8.48 - 0.064 = 8.416$$

For $\left(\frac{C_{fr} l^*}{r_{hy,dt}} \right)_4 = 8.416$,

$$M_4 = 0.251$$

$$\frac{P_{t,4}}{P_t^*} = 2.39$$

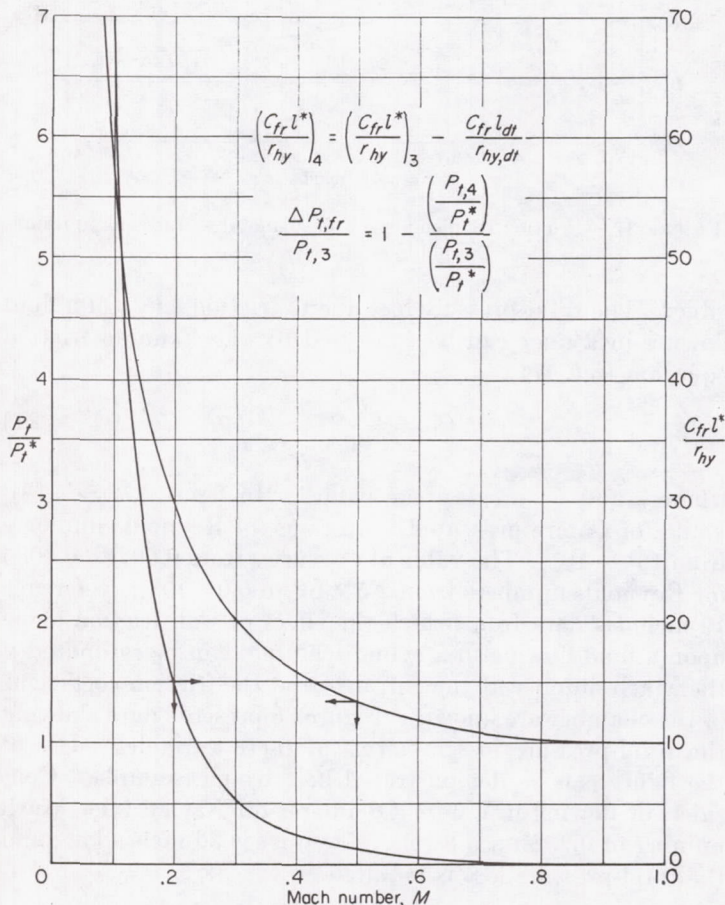
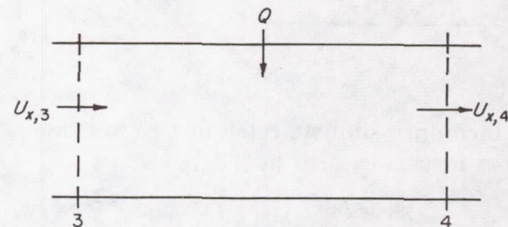


FIGURE 38.—Data for estimation of frictional total-pressure losses in cylindrical ducts (where P_t^* is total pressure with choked flow and l^* is length of duct between station where Mach number is taken and station where choking would occur, ref. 19).

and

$$\frac{\Delta P_{t,fr}}{P_{t,3}} = 1 - \left(\frac{P_{t,4}}{P_t^*} \right) = 1 - \frac{2.39}{2.40} = 0.004$$

Momentum: The momentum pressure loss in combustion chambers, which is inherent in any system in which heat is added to a moving gas stream, can be determined simply in terms of temperature ratios and Mach numbers by the following analysis:



Sketch (c)

It is assumed that the gases are evenly mixed with respect to temperature and pressure at the entrance and exit of the combustor, that the gases are perfect and nonviscous, and that one-dimensional flow applies. Application of Newton's second law and the continuity equation leads to

$$\frac{\Delta P_{t,mom}}{P_{t,3}} = 1 - \frac{(1 + \gamma_3 M_3^2) \left(1 + \frac{\gamma_4 - 1}{2} M_4^2 \right)^{\frac{\gamma_4}{\gamma_4 - 1}}}{(1 + \gamma_4 M_4^2) \left(1 + \frac{\gamma_3 - 1}{2} M_3^2 \right)^{\frac{\gamma_3}{\gamma_3 - 1}}} \quad (22)$$

and

$$\frac{T_{t,4}}{T_{t,3}} = \left(\frac{\gamma_4 R_3}{\gamma_3 R_4} \right) \left[\frac{M_4 (1 + \gamma_3 M_3^2)}{M_3 (1 + \gamma_4 M_4^2)} \right]^2 \left[\frac{1 + \frac{\gamma_4 - 1}{2} M_4^2}{1 + \frac{\gamma_3 - 1}{2} M_3^2} \right] \quad (23)$$

For critical or choked flow through an opening, the Mach number at the opening equals 1.0. For the condition of choking at the combustor exit, since M_4 equals 1.0,

$$\frac{\Delta P_{t,mom}}{P_{t,3}} = 1 - \left(\frac{1 + \gamma_3 M_3^2}{1 + \gamma_4} \right) \left(\frac{1 + \gamma_4}{2} \right)^{\frac{\gamma_4}{\gamma_4 - 1}} \left(1 + \frac{\gamma_3 - 1}{2} M_3^2 \right)^{\frac{\gamma_3}{\gamma_3 - 1}} \quad (24)$$

and

$$\frac{T_{t,4}}{T_{t,3}} = \left(\frac{\gamma_4 R_3}{\gamma_3 R_4} \right) \left[\frac{1 + \gamma_3 M_3^2}{M_3 (1 + \gamma_4)} \right]^2 \left[\frac{1 + \gamma_4}{2} \right] \left(1 + \frac{\gamma_3 - 1}{2} M_3^2 \right) \quad (25)$$

According to equation (23), the addition of heat or the increase of total temperature of any fluid in frictionless flow in a duct will result in an increase in M_4 if M_3 is subsonic, and a

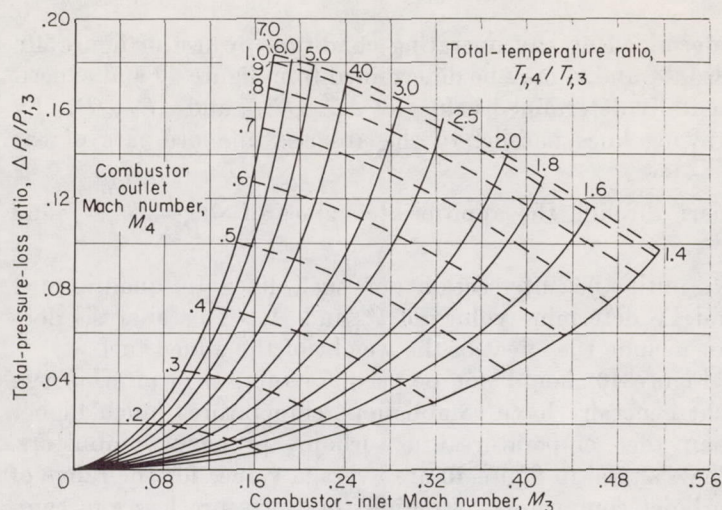


FIGURE 39.—Total-pressure loss due to heat addition in flowing fuel-air mixtures in constant-area duct. Hydrogen-carbon ratio of fuel, 0.167; initial mixture temperature, 500° R; lower heating value of fuel, 18,700 Btu per pound; efficiency of heat addition, 100 percent.

decrease in M_4 if M_3 is supersonic. Only the subsonic case is considered here. Choking at the combustor exit does not mean that more fuel cannot be burned, provided sufficient air is present. It does mean, however, that if more fuel is burned, the combustor-inlet conditions will adjust to compensate for the increase in total-temperature ratio. The preceding equations are expressed in figure 39 in terms of the effect of inlet and outlet conditions upon the total-pressure loss in a constant-area duct due to combustion of a mixture of air and fuel having a hydrogen-carbon ratio of 0.167 from an initial temperature of 500° R. Total-pressure loss due to combustion decreases with decreases in combustor-inlet Mach number for a given temperature ratio.

Isothermal flow behind bluff bodies: The flow behind bluff bodies such as flameholders in ramjet combustion chambers may have noticeable effects on the combustor performance. Introduction of a cylindrical rod or a V-gutter flameholder into a moving gas stream results in the formation of vortices in the region immediately downstream. These vortices can be explained as follows: At extremely low Reynolds numbers (using the width of the bluff body as the length dimension), the streamlines of the flow broaden out behind the obstacle. As the Reynolds number is increased, the streamlines widen more and more, forming a closed region behind the object, within which there is an inflow along the axis of the wake and a flow in the general direction of motion in the outer portions. These motions form a pair of vortices and exist at low Reynolds numbers but become more prominent as the Reynolds number increases. With further increases in Reynolds number, the vortices become more elongated and asymmetrical, break off, and move downstream. This vortex shedding occurs at some critical Reynolds number which depends upon flameholder shape, turbulence of the gas stream, and any wall effects from the combustion chamber. Reference 20 reports visual observation of the forma-

tion and shedding of vortices by the use of balsa dust injected upstream of various flameholders.

The asymmetric arrangement of vortex pairs behind the bluff object alters the pressure distribution around the body, and vortices are discharged alternately from the two sides. In this way, a definite frequency of eddy motion, which depends upon the Reynolds number, is begun. Downstream of the bluff object, the vortices arrange themselves in a double row in which each vortex is midway between the vortices in an opposite row; this arrangement is known as the Kármán vortex street. According to reference 21 (vol. II, pp. 556–562), regular vortex shedding occurs until Reynolds numbers approach 4 to 5×10^5 . Above these values, flow is turbulent.

Flow behind bluff bodies with heat addition: During combustion stabilized behind a flameholder in a flowing homogeneous fuel-air mixture, unburned mixture diffuses into the eddy region behind the flameholder and is burned, with accompanying diffusion of the combustion products and heat into the main stream to ignite the mixture flowing past. With a liquid fuel spray, heat from the burning mixture in the eddy region is transferred to the liquid fuel accumulated on the flameholder directly by radiation and convection, and indirectly by conduction through the flameholder itself. The amount of heat transferred controls the evaporation rate of the fuel. It is believed that the fuel vaporized by this heat mixes with air diffusing from the main stream and maintains the pilot flame in the eddy region. One of the differences noted in flow behind bluff bodies with and without heat addition is that no eddies are shed during combustion (ref. 22). One explanation of this fact is that the static pressure downstream of the bluff body is lower with combustion occurring. As a result of the reduced pressure, the eddy region becomes smaller and seems to attach itself to the bluff body.

Eddy formation: Small pressure losses induced by eddies downstream of flameholders may be estimated if data showing the strength, frequency of shedding, and longitudinal spacing between vortices in a row are known. Goldstein (ref. 21, vol. II) states that the average drag per unit length \mathcal{D} of a cylindrical obstacle perpendicular to a flowing fluid can be expressed by

$$\mathcal{D} = \frac{K_v^2 \rho}{2\pi a g} + \frac{K_v \rho s}{a g} (U_\infty - 2U_{rel}) \quad (26)$$

where U_{rel} is the velocity of the vortex system relative to the free stream. According to reference 23, the strength of vortices of stable rows can be expressed as

$$K_v = 2\sqrt{2} a U_{rel} \quad (27a)$$

and

$$\sinh \frac{\pi s}{a} = 1 \quad (27b)$$

$$\frac{s}{a} = 0.281 \quad (27c)$$

Use of these data allows reduction of equation (26) to

$$\mathcal{D} = \frac{\rho U_\infty^2}{2g} a \left[1.587 \frac{U_{rel}}{U_\infty} - 0.628 \left(\frac{U_{rel}}{U_\infty} \right)^2 \right] \quad (28)$$

This equation does not include wall effects of the combustor. A similar equation that includes wall effects is derived in reference 21 (vol. II). Reference 20 presents data for the shedding frequency and strength of vortices from 14 different flameholders, including a cylinder and a flat plate. From data such as these, necessary values for equation (28) can be determined, since a can be determined from equation (27a), and

$$\frac{U_{rel}}{U_\infty} = 1 - \frac{a f_v}{U_\infty} = 1 - \frac{2 \sqrt{2} U_{rel}}{U_\infty} \quad (29)$$

or

$$U_{rel} = \frac{U_\infty}{2} - \frac{\sqrt{U_\infty^2 - \sqrt{2} K_v f_v}}{2} \quad (30)$$

(The negative sign must be used in eq. (30), since a vortex of zero strength would not exist and U_{rel} would equal zero.) The magnitude of the eddy drag is quite small, as shown by the fact that a U-shaped flameholder $\frac{3}{4}$ inch wide would cause a drag of approximately 0.12 pound per foot of length of flameholder in an airstream flowing at 55 feet per second at sea level.

The isothermal total-pressure-loss coefficient for a flameholder due to vortex formation can be expressed essentially as

$$\frac{\Delta P_t}{q_{ref}} = \frac{a \left[1.587 \frac{U_{rel}}{U_\infty} - 0.628 \left(\frac{U_{rel}}{U_\infty} \right)^2 \right]}{W_{fn}} \quad (31)$$

This total-pressure loss would be additive to the theoretical pressure loss obtained in reference 16.

Estimation and correlation.—Data for estimation of the total-pressure losses in a combustor for known isothermal pressure loss are presented in reference 24. This method is based on the assumption that the over-all combustor total-pressure losses can be expressed as

$$\frac{\Delta P_{t,ov}}{P_{t,3}} = \frac{\Delta P_{t,fr}}{P_{t,3}} + \frac{\Delta P_{t,mom}}{P_{t,3a}} \quad (32)$$

where the subscript $3a$ denotes a fictitious longitudinal station in the combustor, upstream of which all friction losses occur and downstream of which only combustion total-pressure losses occur; and $\Delta P_{t,fr}$ includes not only skin-friction losses, but also losses due to sudden expansions and contractions and the presence of bluff bodies in the flow. General friction laws indicate that this can be expressed as

$$\frac{\Delta P_{t,fr}}{P_{t,3}} = \frac{\gamma_3 g \mathcal{D} A^2 M_3^2}{\left(1 + \frac{\gamma_3 - 1}{2} M_3^2 \right)^{\frac{\gamma_3 + 1}{\gamma_3 - 1}}} \quad (33)$$

where A is the cross-sectional area of an equivalent constant-area combustor, and \mathcal{D} and A are known or are determined from experimental tests of the combustor. With \mathcal{D} and A known, the over-all combustor total-pressure losses can be

determined at any operating condition by use of figure 40. Also, \mathcal{P} and A may be determined from figure 40 and experimentally determined values of $\Delta P_{t,ov}/P_{t,3}$ and $\Delta P_{t,fr}/P_{t,3}$ by drawing lines parallel to the abscissa and ordinate of the

chart through the appropriate values of $\frac{w_a \sqrt{T_{t,3}}}{P_{t,3}}$, $\frac{T_{t,4}}{T_{t,3}}$, and

M_3 until the intersections of such lines in quadrants I and IV determine values of \mathcal{P} and A . This analysis does not include the effect of the weight of the added fuel.

Figure 40 should not be used for ramjets or afterburners that generally have combustion temperatures much higher than the temperatures in turbojet primary combustors. The γ 's used in figure 40 are average values for the range of turbojet combustors. Friction total-pressure losses in ramjets and afterburners may be found as indicated in the preceding sections on sudden expansions and contractions and the presence of bluff bodies in the flow. Momentum total-pressure losses are calculated by use of equations (22) to (25). Values of the various factors in these equations can be determined from figure 41 for the appropriate γ 's corresponding to the temperatures and fuel-air ratios involved.

A correlation has been developed (ref. 25) for various combustors and experimental configurations in which

$$\frac{\Delta P_t}{P_{t,3}} \propto I^{1.5} \quad (34)$$

where I is the combustion intensity (Btu/(hr) (cu ft) (atm)). The value of I is preferably assessed on the size of the primary combustion zone only. This correlation was for use in combustion-chamber design. Using a design $\Delta P_t/P_{t,3}$, an intensity could be found from which primary-zone size could be determined. Values of the ratio l/d for cylindrical combustors were taken as 1.25 to 2.0. According to reference 25, the degree of combustion intensity is determined by the air-mixing pattern, the degree of turbulence, and the combustion properties of the fuel-air mixture, all of which contribute to pressure losses. Use of this correlation involves an arbitrary assumption as to the size of the primary zone.

A better correlation, and one which is generally used, is

$$\frac{\Delta P_t}{q_{ref}} = k_2 + k_3 \left(\frac{\rho_3}{\rho_4} \right) \quad (35)$$

where

$$q_{ref} = \frac{R_3 T_{t,3}}{P_{t,3}} \left(\frac{1}{2g} \right) \left(\frac{w_a}{A_{ref}} \right)^2 \quad (36)$$

A_{ref} is the reference area of the combustor, equal to the maximum open cross-sectional area of the combustor housing, and ρ is the gas density. This correlation (ref. 26) indicates that the total-pressure losses in a combustor are a function of the previously mentioned factors, friction and pressure losses associated with the introduction of a flame-stabilizing device in a gas stream ($k_2 + k_3$) q_{ref} , and pressure losses due to heat absorption (or density changes) and mixing of high-velocity gases

$$k_3 \left(\frac{\rho_3}{\rho_4} - 1 \right) q_{ref}$$

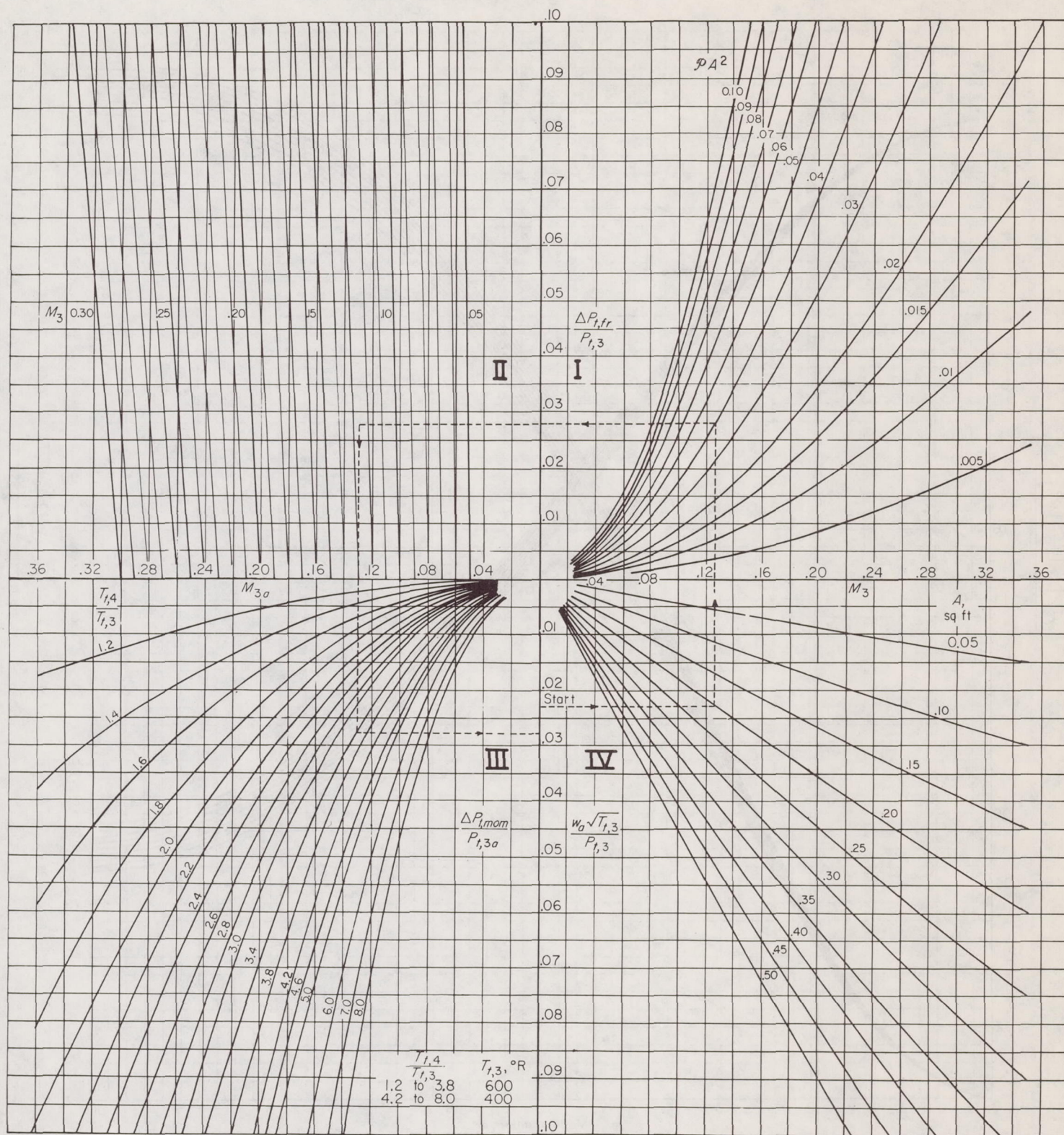


FIGURE 40.—Combustion-chamber pressure-loss chart (ref. 24); $\frac{\Delta P_{t,ov}}{P_{t,3}} \approx \frac{\Delta P_{t,fr}}{P_{t,3}} + \frac{\Delta P_{t,mom}}{P_{t,3a}}$. (A large working copy of this fig. may be obtained on request from NACA Headquarters, Washington, D. C.)

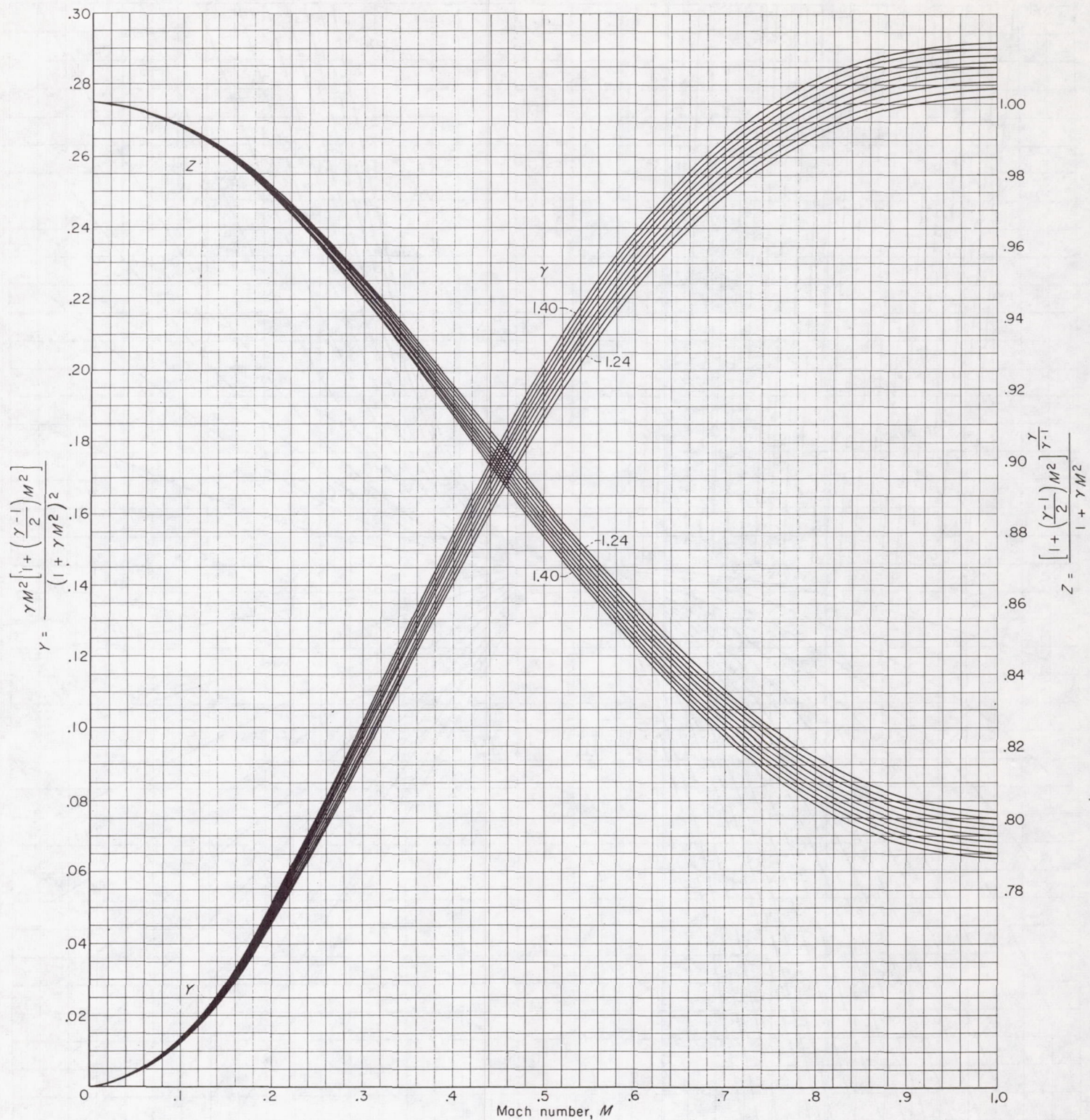


FIGURE 41.—Chart for estimating momentum pressure losses in constant-area duct. Method of application: (1) At combustor-inlet Mach number M_3 read Y_3 and Z_3 ; (2) multiply Y_3 by $T_{t,4}/T_{t,3}$ to obtain Y_4 ; (3) from Y_4 , read Z_4 and M_4 ; (4) then $\Delta P_{t,mom}/P_{t,3} = 1 - (Z_4/Z_3)$. (A large working copy of this fig. may be obtained on request from NACA Headquarters, Washington, D. C.)

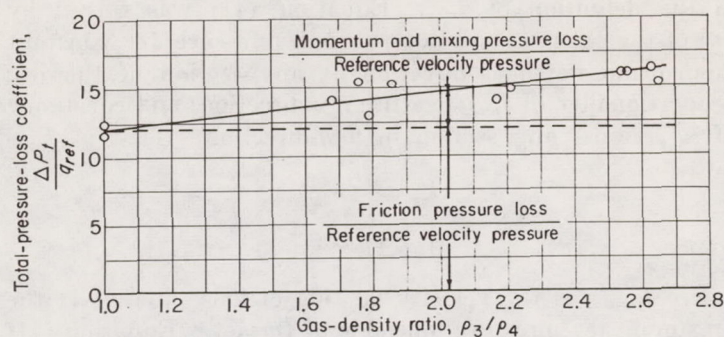


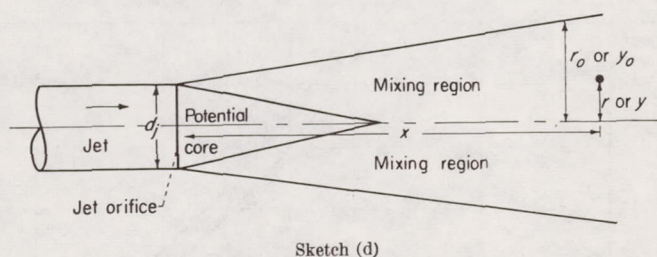
FIGURE 42.—Total-pressure losses as function of reference velocity pressures of typical turbojet combustor.

Pressure losses of a typical turbojet combustor are presented in figure 42. As indicated by equation (35), total-pressure losses increase linearly with increases in gas-density ratios. Friction pressure losses, the losses that would be found essentially by an isothermal test, are indicated at a density ratio of 1.0. Momentum and mixing pressure losses at any density ratio are the difference between the total-pressure losses and the friction pressure loss.

GAS JETS

Mixing of gas streams or jets is an important problem in the design and operation of combustion chambers. For example, air needed to create the turbulence required for rapid mixing and burning in the primary zone of a turbojet combustor usually enters in the form of air jets through small openings in the combustor liner. Also, adequate penetration of the dilution or secondary air must occur in order to attain the degree of mixing and temperature uniformity required by turbojet combustors, in which exhaust temperature profiles suitable for entry of the exhaust gases into the turbine are necessary. Such penetration is usually obtained by introduction of the secondary air through various openings in the downstream portion of the combustor. Similar problems also exist in the design and operation of ramjet combustors and afterburners. Adequate mixing of gases of different temperatures, which exist downstream of flameholders, may result in higher propulsive efficiencies (ref. 16).

As shown in the following sketch, a jet consists essentially of a uniform stream of fluid emanating from an orifice:



Within a certain region (the potential core) outside the orifice, the jet velocity and temperature are maintained. Outside and downstream of the potential core, a mixing region exists, in which the jet expands and interaction may

occur between the jet fluid and any surrounding atmosphere. Jet parameters of interest are usually the velocity and the temperature at any position within the jet, the width and penetration of the jet, and any interaction of the jet with adjacent jets. Gas jets and mixing problems can be classified into two general categories: free jets and jets issuing into fluids that are not at rest. Each of these categories can be further subdivided into laminar and turbulent flow.

Theoretical background.—*Free jets:* Unless specifically stated otherwise, all jets discussed as free jets have a single fluid composition.

Laminar flow: The study of a jet in laminar flow is usually only of academic interest. However, the results of such studies may be of value in fundamental-combustion investigations. An analysis of the spread of a free, laminar, two-dimensional jet and a circular jet is given in reference 21 (vol. I, pp. 145–148). For a laminar jet issuing from a small circular hole in a wall, the equation of motion can be written as

$$U_x \frac{\partial U_x}{\partial x} + U_r \frac{\partial U_x}{\partial r} = \frac{\nu}{r} \frac{\partial}{\partial r} \left(r \frac{\partial U_x}{\partial r} \right) \quad (37)$$

The following assumptions are made:

(1) $\partial^2 U_x / \partial x^2$ is small compared with $\partial^2 U_x / \partial r^2$ and can be neglected.

(2) No pressure gradients or lateral fluid limitations exist across the jet.

(3) Flow is steady.

(4) The momentum at any section of the jet is assumed constant, since no pressure gradients exist and motion is steady.

(5) $U_x = \frac{1}{r} \frac{\partial \Psi}{\partial r}$ and $U_r = -\frac{1}{r} \frac{\partial \Psi}{\partial x}$, where Ψ is a stream function such that U_x and U_r satisfy the continuity equation.

A solution of equation (37) for values of U_x and U_r is

$$U_x = \frac{3m}{8\pi\mu} \left(\frac{1}{x} \right) \frac{1}{\left(1 + \frac{1}{4} \xi^2 \right)^2} \quad (38a)$$

and

$$U_r = \frac{1}{4} \left(\frac{3mg}{\pi\rho} \right)^{1/2} \left(\frac{1}{x} \right) \left[\frac{\xi \left(1 - \frac{1}{4} \xi^2 \right)}{\left(1 + \frac{1}{4} \xi^2 \right)^2} \right] \quad (38b)$$

where

$$m = \text{a constant} = \frac{2\pi\rho}{g} \int_0^\infty U_x^2 r \, dr$$

and

$$\xi = \frac{1}{4\nu} \left(\frac{3mg}{\pi\rho} \right)^{1/2} \left(\frac{r}{x} \right)$$

This solution is applicable for large values of $mg/\rho\nu^2$.

Turbulent-flow velocity profiles: In practice, the motion in jets is usually turbulent in nature. One of the simplest cases of turbulent mixing is the plane-parallel mixing of a jet with gases at rest, with the mixing occurring along a single boundary between the gases. Reference 27 reports an early analysis of this type of mixing, with a free-turbulence or momentum-transfer theory based on the semiempirical general turbulence theory of Prandtl. The momentum-transfer theory indicated the temperature and velocity profiles to be similar in a free jet. Good experimental verification of the theoretical velocity profiles of reference 27 has been obtained by various investigators. However, experimental measurements of temperature profiles downstream of free jets indicate discrepancies between theory and experiment and no similarity of velocity and temperature profiles. Thus, the momentum-transfer theory is suitable for solution of mechanical flow problems of velocity profiles or fluid friction but is ineffective for solution of problems involving temperature profiles or heat transfer.

Reference 28 presents a theory in which the tangential turbulent stresses in flow are a function of the transverse transfer of vorticity. That is, the stresses are a function of the correlation between vorticity fluctuations and transverse velocity components. Conservation of the vorticity of a fluid element until mixing occurs is assumed. It is also noted that the Prandtl theory does not account for local pressure gradients, which appreciably affect momentum interchange but not vorticity transport. The vorticity-transfer theory of reference 28 gave velocity profiles almost as accurately as the momentum-transfer theory and, in addition, gave better agreement of theoretical and experimental temperature profiles. The vorticity-transfer theory is extended to plane-parallel free jets in references 29 and 30.

For two-dimensional compressible flow, Abramovich (ref. 29) indicates the equation of motion to be

$$\rho \frac{\partial U_x}{\partial t} + \rho U_x \frac{\partial U_x}{\partial x} + \rho U_y \frac{\partial U_x}{\partial y} = \mu \frac{\partial^2 U_x}{\partial y^2} - \frac{\partial P}{\partial x} \quad (39)$$

where all values are instantaneous. By using an approximate mean vorticity ζ , where

$$\zeta = \frac{1}{2} \left(\frac{\partial \bar{U}_x}{\partial y} \right)$$

and a defined value l_{mxg} , which is a mixing length or mean free path of a fluid particle in turbulent flow, and neglecting friction due to viscous force, equation (39) reduces to

$$\bar{\rho} \bar{U}_x \frac{\partial \bar{U}_x}{\partial x} + \bar{\rho} \bar{U}_y \frac{\partial \bar{U}_x}{\partial y} = \bar{l}_{mxg}^2 \frac{\partial \bar{U}_x}{\partial y} \frac{\partial}{\partial y} \left(\bar{\rho} \frac{\partial \bar{U}_x}{\partial y} \right) \quad (40)$$

where the bars indicate mean values. For incompressible flow, equation (40) reduces to

$$\bar{U}_x \frac{\partial \bar{U}_x}{\partial x} + \bar{U}_y \frac{\partial \bar{U}_x}{\partial y} = \bar{l}_{mxg}^2 \frac{\partial \bar{U}_x}{\partial y} \frac{\partial^2 \bar{U}_x}{\partial y^2} \quad (41)$$

Equation (41) is similar to the equation found in reference 27 by use of the momentum-transfer theory, differing only

in the definition of l_{mxg} . Equation (41) was solved by use of the same assumptions used in reference 27: constant momentum in the x -direction at any section of the jet; proportionality of l_{mxg} to x in an x -direction; and constancy of l_{mxg} across any section in a y -direction. That is,

$$U_{x,max} \propto x^{-1/2}$$

$$l_{mxg} \propto y_0 \propto x$$

where $U_{x,max}$ is the velocity on the jet axis, and y_0 is the maximum jet spread on one side of the jet. Equation (41) yields the same distribution for velocity as the momentum-transfer theory of reference 27:

$$U_x = 1.31 \frac{k_4 F(\sigma)}{(y_0)^{1/2}} \quad (42a)$$

$$y_0 = 3.02 k_5^{1/2} x \quad (42b)$$

This solution is expressed in figure 43 in terms of dimensionless ratios of $U_x/U_{x,max}$ for any cross section. Good agreement of experimental and theoretical profiles has been found.

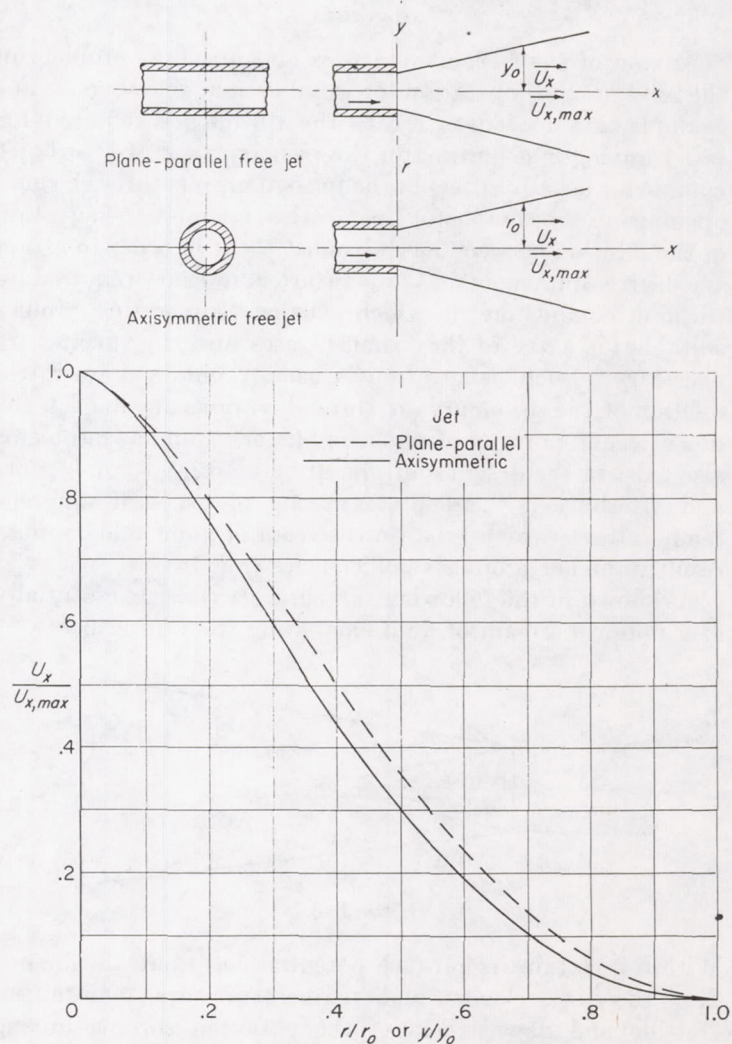


FIGURE 43.—Theoretical velocity distributions based on momentum-transfer theory in plane-parallel and axisymmetric free jets (ref. 30).

The theory of plane-parallel jet mixing was extended by Howarth (ref. 30) to axisymmetric free jets. For these jets, the equations of motion for each of two theories are as follows:

Momentum-transfer theory:

$$U_x \frac{\partial U_x}{\partial x} + U_r \frac{\partial U_x}{\partial r} = \frac{1}{r} \frac{\partial}{\partial r} \left(l_{mix}^2 \frac{\partial U_x}{\partial r} r \frac{\partial U_x}{\partial r} \right) \quad (43)$$

Modified vorticity-transfer theory:

$$U_x \frac{\partial U_x}{\partial x} + U_r \frac{\partial U_x}{\partial r} = l_{mix}^2 \frac{\partial U_x}{\partial r} \left(\frac{\partial^2 U_x}{\partial r^2} + \frac{1}{r} \frac{\partial U_x}{\partial r} \right) \quad (44)$$

These equations were solved by use of assumptions similar to those used in equation (41). Although the two different theories yield approximately the same result, slightly better agreement with experiment was obtained with the momentum-transfer theory. The solution of equation (43) involved use of the stream function Ψ , defined in assumption (5) of equation (37). The value of U_x at any radius r was determined as

$$U_x = 4.65 \frac{k_6}{r_0} \mathcal{F}(\sigma) \quad (45a)$$

$$r_0 = 3.4 k_7^{1/3} x \quad (45b)$$

where r_0 is the maximum spread of the jet at any cross section. This solution is expressed in figure 43 in terms of dimensionless ratios for any cross section. According to Howarth, these results are fairly accurate, at least over the central portion of the jet, at distances downstream of the nozzle greater than 8 jet-nozzle diameters.

Turbulent-flow temperature profiles: Abramovich (ref. 29) indicates the differential equation of heat balance for plane-parallel free jets emanating into fluids of different temperatures to be

$$\rho \frac{\partial T}{\partial t} + \rho U_x \frac{\partial T}{\partial x} + \rho U_y \frac{\partial T}{\partial y} = 0 \quad (46)$$

where all values are instantaneous. Equation (46) neglects molecular heat conduction and conversion of the energy of viscous forces into heat with respect to turbulent heat transfer in the same manner as friction due to viscosity was disregarded in equation (40) relative to turbulent friction. By use of instantaneous and fluctuating values of variables and by assuming

$$\frac{\rho \partial \bar{T}}{\partial t} = 0 \text{ (steady flow)}$$

and

$$\bar{T} = l_{mix} \frac{\partial \bar{T}}{\partial y}$$

equation (46) becomes

$$\bar{\rho} \bar{U}_x \frac{\partial \bar{T}}{\partial x} + \bar{\rho} \bar{U}_y \frac{\partial \bar{T}}{\partial y} = \bar{l}_{mix}^2 \left[\frac{\partial \bar{\rho}}{\partial y} \frac{\partial \bar{U}_x}{\partial y} \frac{\partial \bar{T}}{\partial y} + \frac{\partial}{\partial y} \left(\bar{\rho} \frac{\partial \bar{U}_x}{\partial y} \frac{\partial \bar{T}}{\partial y} \right) \right] \quad (47)$$

which, for incompressible flow, reduces to

$$\bar{U}_x \frac{\partial \bar{T}}{\partial x} + \bar{U}_y \frac{\partial \bar{T}}{\partial y} = \bar{l}_{mix}^2 \frac{\partial}{\partial y} \left(\frac{\partial \bar{U}_x}{\partial y} \frac{\partial \bar{T}}{\partial y} \right) \quad (48)$$

where the bars indicate mean values. Reference 29 presents a correlation of the solution of equation (48) in terms of a dimensionless parameter

$$C_{temp} = \frac{T - T_1}{T_j - T_1}$$

where

T temperature at any point in jet mixing region

T_1 temperature of fluid at rest in space surrounding jet

T_j temperature at any point in region of undisturbed flow in jet, or in potential core

This temperature coefficient has been used by other authors. Howarth (ref. 30), however, presents a solution of equation (48) as

$$\frac{C_{temp}}{C_{temp,max}} = [F(\sigma)]^{1/2}$$

where $C_{temp,max}$ and $U_{x,max} \propto (1/x)^{1/2}$. This solution is presented in figure 44.

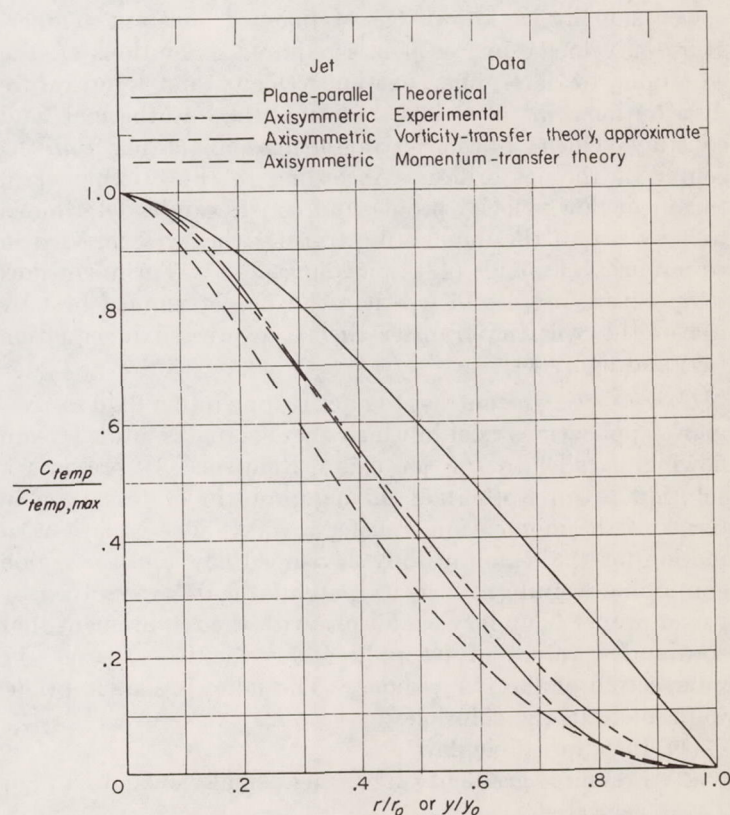
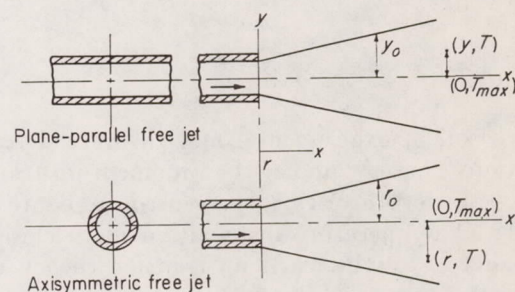


FIGURE 44.—Theoretical and experimental temperature distributions in plane-parallel and axisymmetric free jets (ref. 30).

For axisymmetric free jets, the differential equation of heat transfer becomes (ref. 30)

$$U_x \frac{\partial T}{\partial x} + U_r \frac{\partial T}{\partial r} = \frac{1}{r} \frac{\partial}{\partial r} \left(l_{mix}^2 \frac{\partial U_x}{\partial r} r \frac{\partial T}{\partial r} \right) \quad (49)$$

Similar boundary conditions apply for velocity and temperature distributions based on the momentum-transfer theory. Also, equation (49) differs from equation (43) only in a change of variable. Therefore, the solution of equation (49) based upon the momentum-transfer theory yields a temperature profile similar to that of the velocity. The boundary conditions used for temperature distribution with the vorticity-transfer theory are unequal to those used for velocity distribution. Howarth (ref. 30) presents a solution of equation (49) as

$$\frac{C_{temp}}{C_{temp,max}} = e^{\int_0^{r/xk_s^{1/2}} \frac{E}{E' - E'} d\epsilon} \quad (50)$$

where

$$\epsilon = \frac{r}{x}$$

A comparison of experimental and theoretical temperature distributions based upon the momentum-transfer and vorticity-transfer theories is presented in figure 44. The experimental temperature distribution more closely follows that predicted by the vorticity-transfer theory over most of the range.

Occasionally, a knowledge of lines of constant temperature or velocity in free jets is required. Solutions of the equations to determine constant velocity and temperature distributions in free jets indicate that isothermal and constant-velocity lines are straight lines emanating from the center of the jet orifice. According to the existing data, turbulent-flow velocity profiles in free jets can be determined best by use of the momentum-transfer theory, expressed in equations (41) and (43) and figure 43. Turbulent-flow temperature profiles in free jets can be determined best by use of the vorticity-transfer theory, expressed in equation (49) and figure 44.

Coaxial jets: In contrast to a jet issuing into a fluid at rest, many applications exist in which a jet emanates into a stream flowing parallel to the jet axis. Reference 31 presents a solution to an isothermal mixing problem of this type in terms of the momentum-transfer theory. The equations of motion for the region of fully developed flow and the region containing a uniform velocity potential core were solved by use of proper boundary conditions with the requirement that continuous values of jet radii and velocities exist at the intersection of the two regions. The following assumptions were made in the solution:

- (1) Incompressible flow
- (2) Pressure gradients near jet small enough to be neglected
- (3) Constant velocity throughout potential core
- (4) Constant momentum in x -direction at any jet section

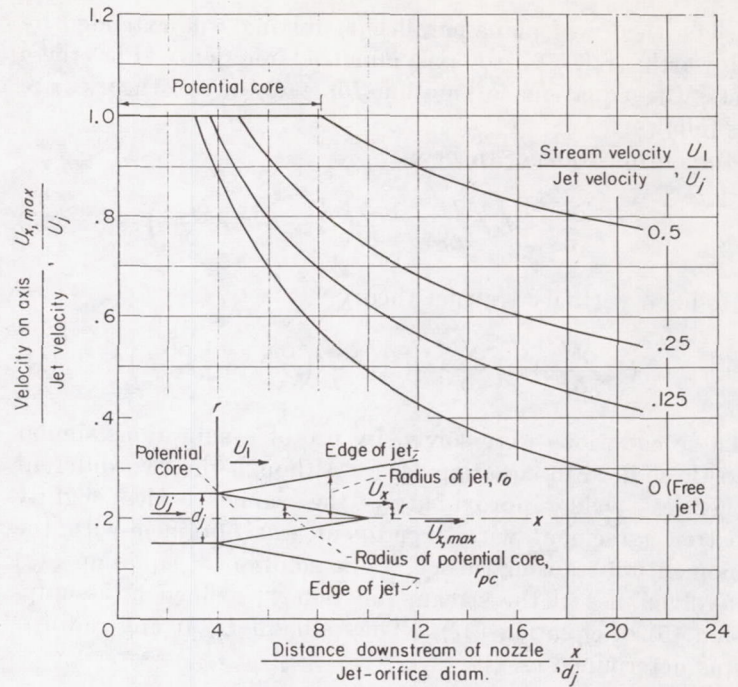


FIGURE 45.—Axial distribution of velocity on axis in circular coaxial jets (ref. 31).

- (5) Mixing length l_{mix} proportional to width of mixing region
- (6) Lateral distribution of velocity in region containing potential core equal to

$$U_x = U_1 + \frac{U_j - U_1}{2} \left[1 - \cos \pi \left(\frac{r_o - r}{r_o - r_{pc}} \right) \right] \quad (51)$$

- (7) Lateral velocity distribution in fully developed jet equal to

$$U_x = U_1 + \frac{U_{x,max} - U_1}{2} \left(1 + \cos \pi \frac{r}{r_o} \right) \quad (52)$$

where all velocities are in the x -direction, and

- U_x velocity at any position in jet
- U_1 velocity of coaxial stream
- U_j velocity of jet
- r_o outer radius of fully developed jet
- r radial distance from jet axis to point where U_x is measured
- r_{pc} radius of potential core
- $U_{x,max}$ velocity on jet axis

- (8) Mixing-length parameter c equal to $(0.0067)^{1/2}$ (differs slightly, approximately 14 percent, from a value found in another reference)

A diagram of the jet and the results of the analysis are presented in figures 45 and 46. Results of the analysis indicated that (1) length of the potential core decreases with decreasing ratios of stream-to-jet velocity to approximately 3.1 jet diameters for a free jet, and (2) similar to free jets, constant-velocity lines are approximately straight, emanating from the center of the jet orifice. Similar results have been found by other investigators.

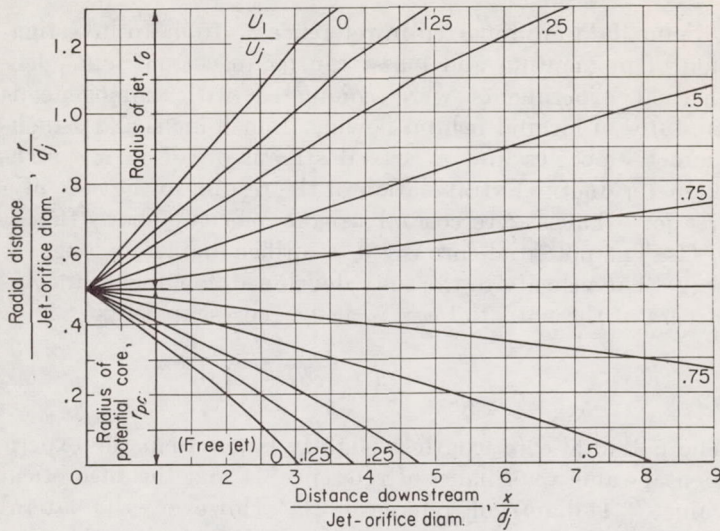


FIGURE 46.—Boundaries of jet and potential core in circular coaxial jets (ref. 31).

Normal jets: No theoretical data expressing the distribution of temperature or velocity in a fluid jet entering a fluid stream flowing normal to the jet were found. However, a theoretical analysis for the penetration of a cold jet into a hot fluid stream is presented in reference 32. Velocity and temperature distributions for free jets and a negligible pressure gradient at the mixing section were assumed. Results of the analysis indicated that penetration j of normal jets could be expressed as

$$j = F \left[\left(\frac{\text{Momentum of jet}}{\text{Momentum of fluid stream}} \right) \times \left(\frac{\text{Volume flow of fluid stream}}{\text{Total volume flow of fluid stream and jet}} \right)^2 \right] \quad (53)$$

For penetration of circular normal jets into fluid streams in rectangular ducts of width W_{dt} and depth b_{dt} , penetration at a distance x_j/b_{dt} from the orifice centerline is suggested as

$$\text{Relative penetration } \frac{j}{b_{dt}} = F \left[\frac{\frac{d_j U_j}{b_{dt} U_1} \sqrt{\frac{T_1}{T_j}}}{1 + \frac{\pi d_j^2 U_j}{4 b_{dt} W_{dt} U_1}} \right] \quad (54)$$

where

- d_j jet-orifice diameter
- T_1 temperature of fluid stream
- T_j temperature of jet fluid

Oblique jets: Jets entering a moving stream may enter at any angle from 0° to 180° . As such, the complex mixing problem does not lend itself to a ready solution. However, Ehrich (ref. 33) has analyzed the problem for oblique jets by means of a simplified two-dimensional potential-flow analysis. Essentially, Ehrich assumed that a jet entering a moving stream at an angle is separated from the main stream by a streamline and has a constant velocity. Thus, no discontinuities exist across the streamline. The jet wake downstream of the jet was assumed to be an area of dead fluid separated from the jet by a constant-pressure vortex sheet.

These assumptions oversimplify the problem of jet penetration into moving streams. However, the analysis does lead to a convenient method of calculating the relation between geometric and velocity parameters. In addition, qualitative agreement was obtained for the theoretical solution of flow from a two-dimensional orifice and experimental data for the approximately comparable case of a circular jet.

Multiple jets. Two expressions for the penetration of multiple jets into fluid streams are presented in reference 32. For the penetration of N jets entering a fluid stream at right angles through N circular orifices spaced laterally across a rectangular duct of width W_{dt} and depth b_{dt} , penetration at a distance x_j/b_{dt} from the orifice centerline is suggested as

$$\text{Relative penetration } \frac{j}{b_{dt}} = F \left[\frac{\frac{d_j U_j}{b_{dt} U_1} \sqrt{\frac{T_1}{T_j}}}{1 + N \frac{\pi d_j^2 U_j}{4 b_{dt} W_{dt} U_1}} \right] \quad (55)$$

No experimental data using this parameter were included in reference 32. For the penetration of N jets entering a fluid stream at right angles through N circular orifices equally spaced circumferentially around a duct of diameter d_{dt} , the expression suggested for a distance x_j/d_{dt} from the orifice centerline is

$$\text{Relative penetration } \frac{j}{d_{dt}} = F \left[\frac{\frac{d_j U_j}{d_{dt} U_1} \sqrt{\frac{T_1}{T_j}}}{1 + N \left(\frac{d_j}{d_{dt}} \right)^2 \frac{U_j}{U_1}} \right] \quad (56)$$

No experimental data using this parameter were included.

Experimental data.—Despite an abundance of theoretical analyses of jets issuing into gases at rest or in motion, many disagreements exist between theoretical and experimental results. Likewise, application of fundamental jet-penetration data to jet-engine combustors has given results in disagreement with theory. Disagreements may be attributed to various factors such as direction, size, shape, and orientation of the jets relative to the main fluid, and the presence of other jets resulting in possible jet interaction.

Free jets: Turbulent-flow velocity profiles: Much of the extant experimental data relative to gas jets concerns free jets mixing with air. In general, data are presented in terms of velocity distributions in both the potential core in axially symmetric jets and in the region of fully developed jet flow. Equations written to fit the experimental data for isothermal free jets mixing with air are presented in reference 34. Data are expressed in terms of momentum-flux velocity ratios, in which

$$\text{Momentum-flux velocity} = \sqrt{\frac{\rho U_x^2}{\bar{\rho}}} \quad (57)$$

where U_x is the instantaneous velocity in the jet in the x -direction at any radius r and longitudinal distance x , and ρ is the instantaneous density of the fluid. The value of ρU_x^2 is determined from impact tube measurements, and $\bar{\rho}$ is determined from static temperature and pressure. For incom-

pressible flow, the momentum-flux velocity is approximately $\sqrt{U_x^2}$. Momentum-flux velocity ratios of an isothermal free jet are presented in figure 47 for the potential core, a transition region at the end of the potential core, and the region of fully developed flow. Many of the data are presented, as in many references, in terms of a half-radius, that is, the jet radius at which the momentum-flux velocity equals half the momentum-flux velocity on the jet axis at the same longitudinal distance from the jet orifice. The data indicate that

(1) The potential core within which the flux velocity ratios are constant radially is approximately 3.5 jet-orifice diameters long.

(2) The radius of the potential core could be expressed as

$$\frac{r_{pc}}{d_j} = \frac{3.5 - \frac{x}{d_j}}{7.0} \quad (58)$$

where r_{pc} is the potential-core radius at any longitudinal distance x . Velocity ratios within the potential core (less than 3.5 diam downstream) closely approached a single generalized curve. Within the transition region, however, a different curve could be drawn from those for distances farther downstream. Radial flux velocity ratios, covering a range of jet velocities from 166 to 801 feet per second and distances from 10 to 30 jet diameters downstream of the jet orifice, were correlated by the following expression:

$$\sqrt{\frac{U_x^2}{U_{x,max}^2}} = e^{-\ln 2 (r/r_{1/2})^2} \quad (59)$$

Some data are reported in reference 35 from an investigation of momentum and mass transfer in coaxial jets. Isothermal experiments were conducted with homogeneous mixtures of air and helium flowing from $\frac{1}{4}$ -inch- and 1-inch-diameter nozzles into a coaxial stream of air in a 4-inch-diameter duct. Extrapolation of the results to the case of a free jet—that is, zero coaxial stream velocity—shows that

(1) The potential core is 4.0 jet-orifice diameters long.

(2) The velocity in the fully developed flow region (downstream of the potential core) can be represented by

$$\frac{U_x}{U_{x,max}} = \frac{1}{2} \left(1 + \cos \frac{\pi r}{2r_{1/2}} \right) \quad (60)$$

The potential-core length is slightly larger than the experimental value (3.5 diam) of reference 34 and the theoretical value (3.1 diam) of reference 31. However, the lateral velocity distribution agrees exactly with the theoretical distribution of Squire and Trouncer (eq. (52)) and fairly well with the experimental curve of reference 34 (eq. (59)), as shown in figure 47(c).

Axial velocity distribution within the fully developed flow region of the circular isothermal free jets of reference 34 could be closely approximated by

$$\frac{\sqrt{U_{x,max}^2}}{U_j} = \frac{1}{0.1508 \frac{x}{d_j}} \quad (61)$$

The curve of figure 48 and the experimental data agree closely with the previously discussed theoretical analysis of a symmetrical jet in which it was assumed, because of a

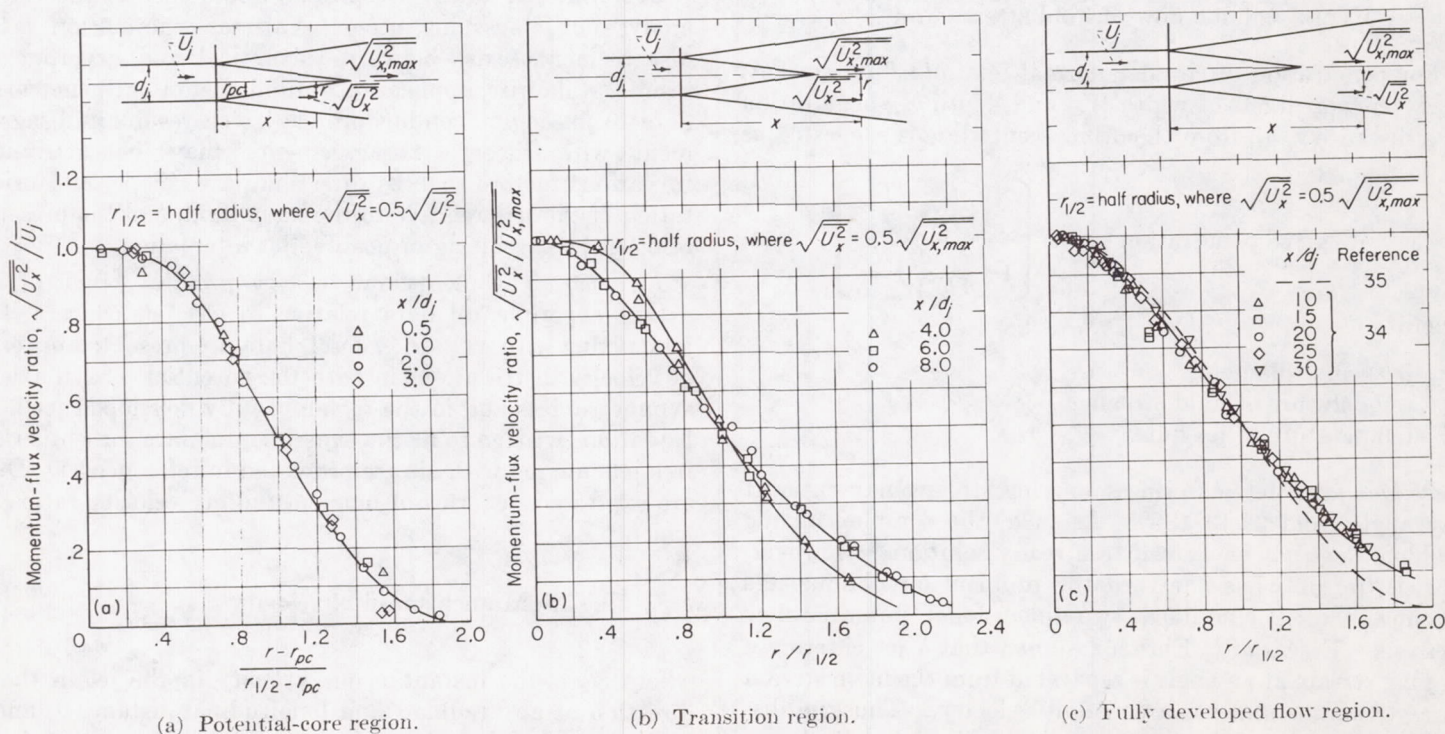


FIGURE 47.—Radial distribution of momentum-flux ratios in isothermal axisymmetric free jets of air. Long-throat, 0.9-inch-diameter nozzle; mean jet velocity, 390 feet per second (ref. 34).

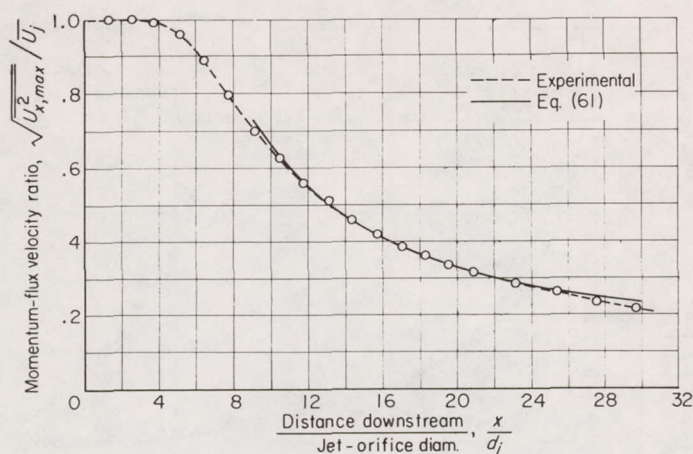


FIGURE 48.—Axial velocity distribution in axisymmetric isothermal free jet in air. Long-throat, 0.9-inch-diameter nozzle; mean jet velocity, 390 feet per second (ref. 34).

constancy of momentum at any jet section, that

$$U_{x,max} \propto \frac{1}{x} \quad (62)$$

This expression for axial velocity distribution agrees closely with an expression of Squire (ref. 36), who recommended use of the relation

$$\frac{U_{x,max}}{U_j} = \frac{6.5}{x/d_j} \quad (63)$$

Extrapolation of the data of reference 35 for coaxial jets to a free jet gives the axial velocity distribution as

$$\frac{U_{x,max}}{U_j} = \frac{4}{x/d_j} \quad (64)$$

The large discrepancy between equation (64) and equations (61) and (63) may be due in part to the experimental configuration of reference 35.

A large amount of data relative to axisymmetric free jets in air is summarized in reference 36. Half-velocity radii in the fully developed flow region of a free jet in air are presented in figure 49. Experimental data from references 34 and 37 and theoretical data from references 31 and 38 are also included. Reichardt (ref. 38) expressed the half-radius at any longitudinal position as

$$r_{1/2} = 0.0725 x \sqrt{\ln 4} \quad (65)$$

This expression and the experimental data of reference 34 agree closely with the data of figure 49, which indicate the lines of half-velocity radii to lie on a cone of half-angle of 5° , with the cone apex at the center of the jet orifice, for distances greater than 10 jet diameters from the orifice.

A small amount of data included in reference 36 for 0.1-velocity radii is also presented in figure 49. For the 0.1-velocity radii, straight lines emanate from the center of the jet orifice at an angle of 9.2° .

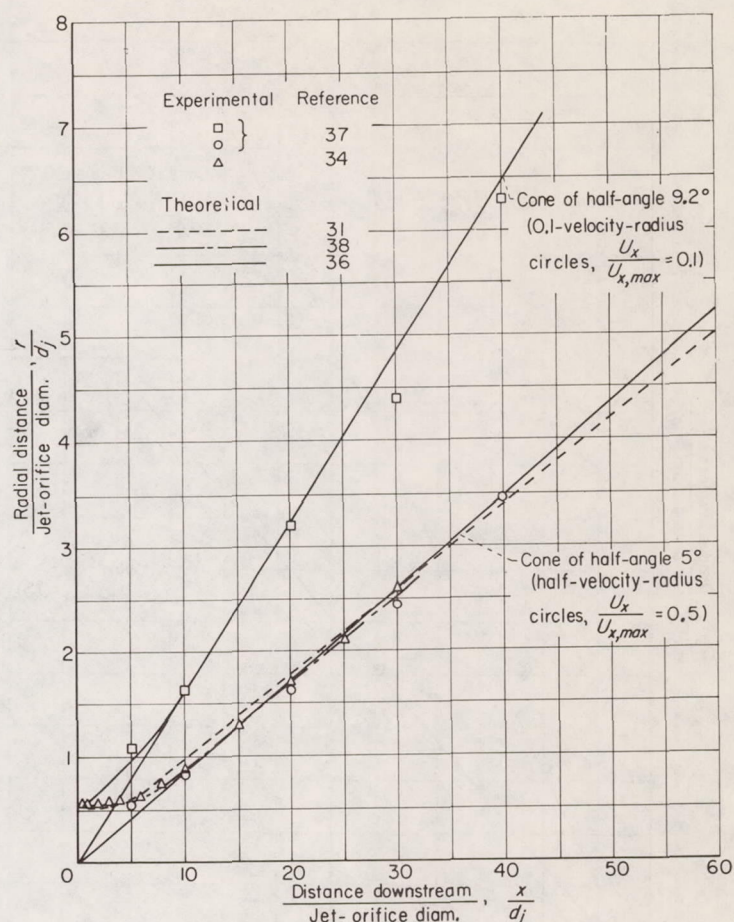


FIGURE 49.—Velocity distributions in axisymmetric free jets in air.

A small amount of experimental data pertaining to the velocity distribution in two-dimensional jets is available. For two-dimensional and axisymmetric free jets, theoretical analyses indicate that

- (1) For two-dimensional jets, $U_{x,max} \propto 1/x^{1/2}$
- (2) For axisymmetric jets, $U_{x,max} \propto 1/x$

Using these relations, Squire (ref. 36) infers that expressions applicable to axisymmetric jets may be applied to two-dimensional jets by replacing (x/d_j) with $(x/y)^{1/2}$ wherever (x/d_j) appears. Howarth (ref. 30) presents some experimental data from a previous investigator on the velocity profiles in a two-dimensional free jet and compares them with the theoretical distribution derived from the momentum-transfer and modified vorticity-transfer theories, both of which give the same theoretical velocity profile. Excellent agreement of experimental and theoretical data is indicated. The large amount of data on free jets includes many expressions for velocity distributions. For free jets (excluding the jets of ref. 35), recommended expressions for the radius of the potential core and lateral and axial velocity distributions are equations (58), (59), and (61), respectively. Half- and 0.1-velocity radii can be determined from figure 49.

Turbulent-flow temperature profiles: Experimental distributions of temperature in axisymmetric free jets are presented in figure 50. Results are expressed in terms of half-temperature- and 0.1-temperature-coefficient radii. In the

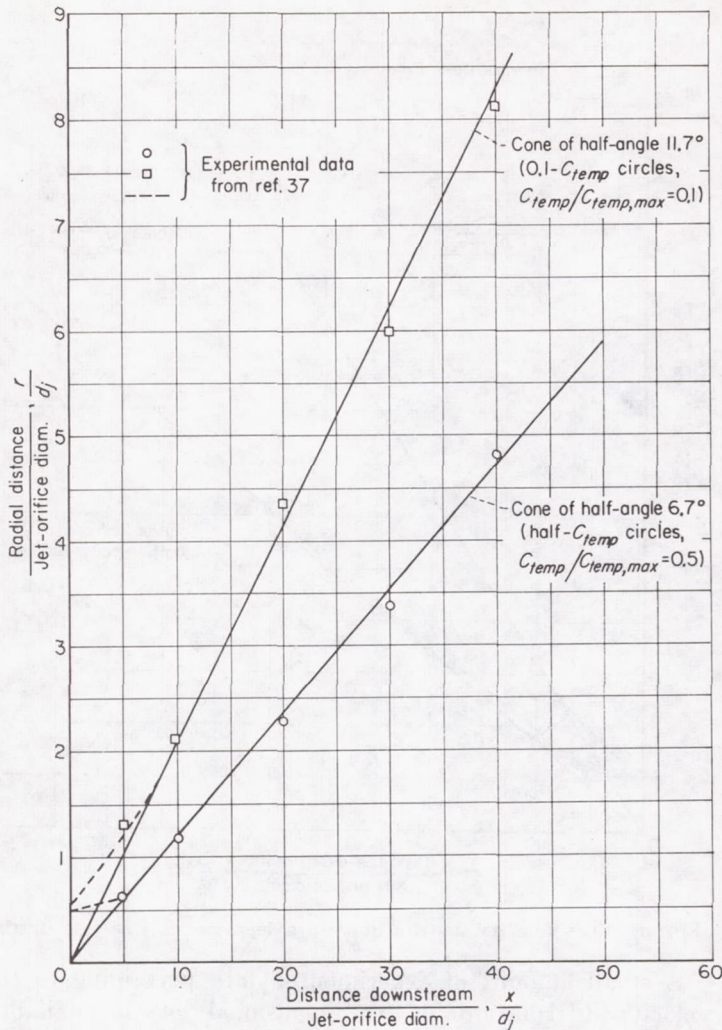


FIGURE 50.—Temperature distributions in axisymmetric free jets in air (ref. 36).

same manner as the velocity ratios, the temperature-coefficient ratios are defined as the ratio of the temperature coefficient C_{temp} at any point to the temperature coefficient $C_{temp,max}$ at a point on the axis in the same longitudinal plane. The temperature coefficient C_{temp} has been defined in the theoretical section considering temperature profiles in turbulent flow. For distances greater than 5 jet-orifice diameters downstream, straight lines of half-temperature-coefficient ratios lie on a cone of half-angle of 6.7° , with the apex of the cone at the center of the jet orifice. For 0.1-temperature-coefficient ratios, the distance downstream must be greater than 10 jet-orifice diameters, and the half-angle is 11.7° .

Longitudinal distribution of temperature in axisymmetric free jets is shown in figure 51. The temperature of the jet remains approximately constant for a distance of about 5 diameters, or the length of the potential core. For distances from 10 to 50 jet-orifice diameters from the orifice,

$$C_{temp,max} = \frac{4.8}{\frac{x}{d_j}} \quad (66)$$

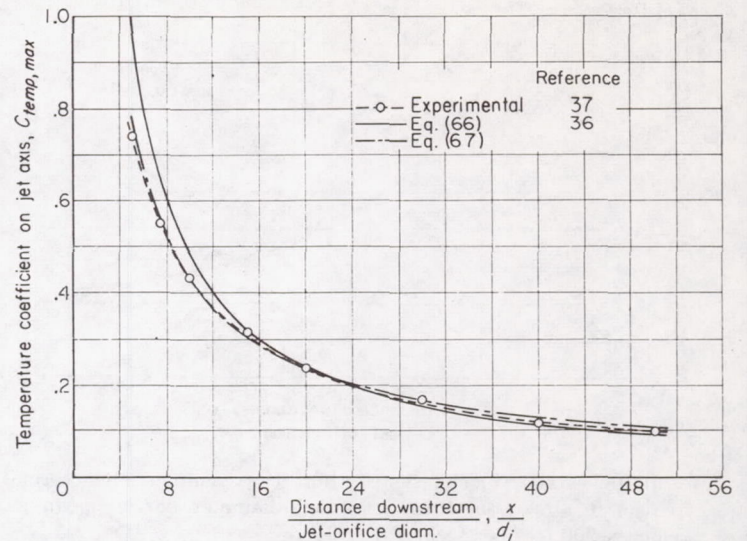


FIGURE 51.—Axial temperature distribution in axisymmetric free jets in air.

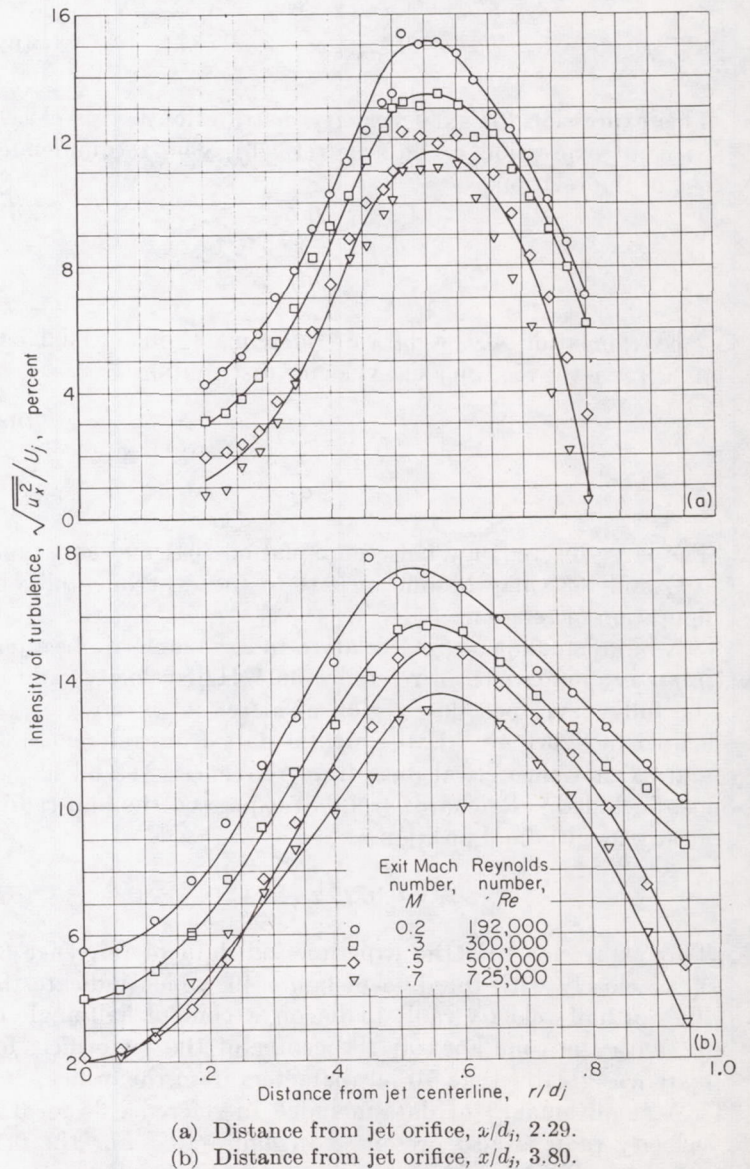


FIGURE 52.—Intensity of turbulence in percent of jet velocity at various exit Mach and Reynolds numbers (ref. 39).

This equation is recommended by Squire (ref. 36) as representative of the temperature distribution on the jet axis. A better expression for axial temperature distribution, for distances from 5 to 20 jet-orifice diameters from the orifice, is

$$C_{temp,max} = 3 \left(\frac{x}{d_j} \right)^{-0.845} \quad (67)$$

No experimental data showing the temperature distribution in two-dimensional free jets were found. However, Howarth (ref. 30) assumes that the agreement of experimental and theoretical temperature distributions in two-dimensional free jets is as good as with axisymmetric jets.

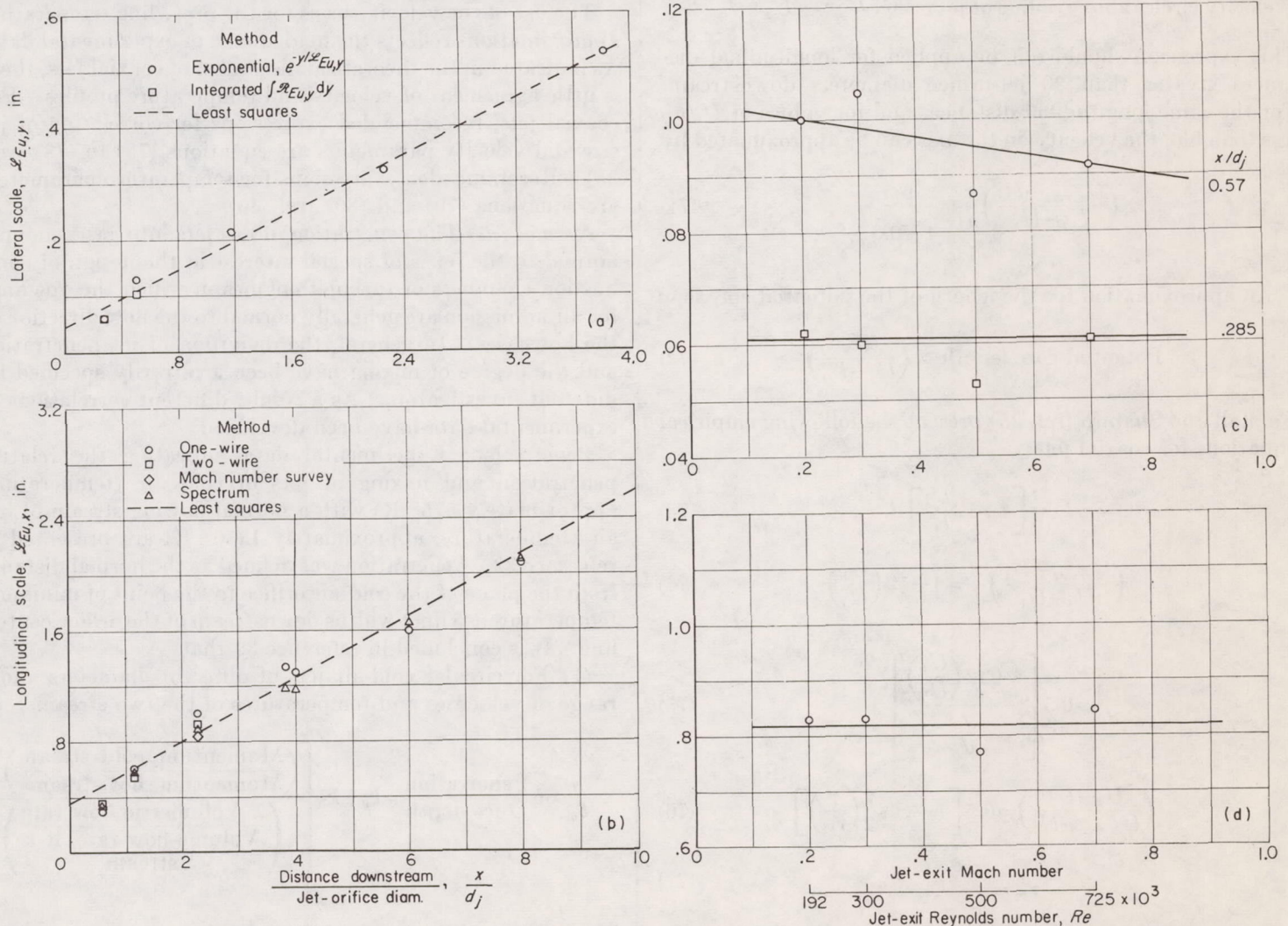
As will be indicated in the section **AERODYNAMIC MIXING**, the diffusions of mass and heat occur at approximately equal rates for the separate cases of mass and heat transfer. Thus, it has been concluded that the transport of heat and mass will result in similar mixing patterns.

Turbulence intensity and scale: Hot-wire-anemometer measurements of the intensity and scale of turbulence in free jets have been reported in various references. One of the most recent of these (ref. 39) describes tests conducted with

a 3.5-inch-diameter free air jet. The experiments included the effects of jet Mach number, which was varied from 0.2 to 0.7, and jet Reynolds number (based on jet radius), which was varied between 192×10^3 and 725×10^3 . The intensity of turbulence, which is expressed as the percentage ratio of the root-mean-square value of the fluctuating velocity component in the x -direction to the jet velocity, is shown in figure 52 as a function of the distance from the jet centerline and Mach and Reynolds numbers. The intensity of turbulence is a maximum at a distance of approximately 0.5 jet diameter from the jet centerline and decreases with increasing Mach and Reynolds numbers.

Lateral and longitudinal scales of turbulence are presented in figure 53. Both scales of turbulence vary proportionally with the distance from the jet orifice, and the lateral scale is much smaller than the longitudinal scale. As shown by the straight lines fitted to the experimental data by the method of least squares, the lateral scale of turbulence could be expressed by

$$\mathcal{L}_{Eu,y} = 0.036x + 0.043 \quad (68)$$



(a) Lateral scale.

(b) Longitudinal scale.

(c) Effect of jet-exit Mach and Reynolds numbers on lateral scale.

(d) Effect of jet-exit Mach and Reynolds numbers on longitudinal scale. Distance downstream, 2.2 jet-orifice diameters.

FIGURE 53.—Scale of turbulence in free air jet. Jet-orifice diameter, 3.5 inches; distance from jet-orifice centerline, 0.5 jet-orifice diameter; jet-exit Mach number, 0.3; jet-exit Reynolds number, 300,000 (ref. 39).

and the longitudinal scale of turbulence could be expressed by

$$\mathcal{L}_{Eu,x} = 0.064x + 0.35 \quad (69)$$

As shown in figure 53, the longitudinal and lateral scales of turbulence were nearly independent of Mach and/or Reynolds numbers. In addition, little variation of the lateral scale of turbulence was noted with distance from the jet centerline, while the longitudinal scale of turbulence was a maximum at a distance from the jet centerline of about 0.35 to 0.40 jet-orifice diameter.

Coaxial jets: Velocity measurements: In general, only a free jet spreads conically. Also, a boundary layer from the tube or nacelle containing the jet may have an important influence on the jet when the stream velocity is an appreciable fraction of the jet velocity. As a result, correlation of experimental data has led to general empirical rules concerning the characteristics of coaxial jets.

Squire (ref. 36) states that

$$\left(\text{Increase in radii of half-velocity or 0.1-velocity circles above radius of jet orifice} \right) \propto \left(\frac{U_j - U_1}{U_j} \right) \quad (70)$$

This expression should not be applied for longitudinal distances greater than 30 jet-orifice diameters downstream. For the same longitudinal distances and for values of U_1/U_j less than 0.6, the velocity on the axis can be approximated by

$$\left(\frac{U_{x,max} - U_1}{U_j - U_1} \right) \frac{x}{d_j} = \frac{6.5}{1 - 0.6 \frac{U_1}{U_j}} \quad (71)$$

An approximation for the length of the potential core is

$$\text{Potential-core length} \propto \left(\frac{U_j}{U_j - U_1} \right) \quad (72)$$

Forstall and Shapiro (ref. 35) present the following empirical equations for coaxial jets:

$$l_{pc} = \left[4 + 12 \frac{U_1}{U_j} \right] d_j \quad (73)$$

$$\left(\frac{U_{x,max} - U_1}{U_j - U_1} \right) \frac{x}{d_j} = 4 + 12 \left(\frac{U_1}{U_j} \right) \quad (74)$$

$$\frac{r_{1/2}}{d_j} = 0.5 \left[\frac{4 + 12 \left(\frac{U_1}{U_j} \right)}{\frac{x}{d_j}} \right]^{\frac{U_1 - U_i}{U_i}} \quad (75)$$

$$\left(\frac{U_x - U_1}{U_{x,max} - U_1} \right) = 0.5 \left[1 + \cos \frac{\pi}{2} \left(\frac{r}{r_{1/2}} \right) \right] \quad (76)$$

$$r_{1/2} \approx (x) \frac{U_i - U_1}{U_i} \quad (77)$$

$$r_o \approx (x) \frac{U_i - U_1}{U_i} \quad (78)$$

Discrepancies exist between these equations and the empirical correlations of reference 36. However, equation (76) approximates a similar theoretical equation of reference 31.

Temperature measurements: In general, temperature measurements in coaxial jets are less extensive than velocity measurements. However, Squire (ref. 36) suggests the following empirical relation based largely on the previous corresponding velocity relation:

$$\left(\text{Increase in radii of half-temperature- or 0.1-temperature-coefficient circles above radius of jet orifice} \right) \propto \left(\frac{U_j - U_1}{U_j} \right) \quad (79)$$

This approximation applies at longitudinal distances of less than 30 jet-orifice diameters from the jet orifice.

The temperature coefficient $C_{temp,max}$ at any point on the jet axis can be approximated by

$$\left(\frac{x}{d_j} \right) C_{temp,max} = \frac{4.8}{1 - 0.6 \frac{U_1}{U_j}} \quad (80)$$

The use of the velocity basis for the preceding temperature approximations reflects the inadequacy of experimental data. As indicated in the theoretical discussion of coaxial jets, there is little agreement of velocity and temperature profiles. For coaxial jets, recommended expressions for correlation of jet size and velocity parameters are equations (73) to (78) (ref. 35). Recommended expressions for temperature parameters are equations (79) and (80) (ref. 36).

Normal jets: The penetration of gas jets into gases moving normal to the jet is of special interest in the design of combustion chambers of turbojet engines in which the openings for air admission are generally normal to the flow direction of the hot gases. In general, the definition of jet penetration and the degree of mixing have been arbitrarily specified by different investigators. As a result, different correlations of experimental data have been developed.

Penetration: Experimental data indicating the relative penetration and mixing of jets of cold air (temperature, approximately 575° R) with a normal flowing stream of hot air (temperature, approximately 1350° R) are presented in reference 32. Penetration was defined as the normal distance from the plane of the cold-air orifice to the point of minimum temperature 1.5 duct widths downstream of the orifice centerline. It is concluded in reference 32 that

(1) For circular cold-air jets of different diameters and a range of velocities and temperatures of the two streams,

$$\frac{j}{b_{at}} \text{ or } \frac{\text{Penetration}}{\text{Duct depth}} = k_9 + k_{10} \left[\frac{\left(\frac{\text{Momentum, cold stream}}{\text{Momentum, hot stream}} \right)^{1/2}}{\left(\frac{\sum \text{Volumetric flow rate}}{\text{Volume-flow rate, h. t. stream}} \right)} \right] \quad (81)$$

This relation holds until the relative penetration becomes

approximately 0.6, at which time the edge of the cold-air jet approaches the opposite wall of the duct.

(2) For the same open area, circular and square holes give approximately the same penetration, while longitudinal and transverse rectangular holes give better and worse penetration, respectively (fig. 54).

(3) In general, mainstream turbulence reduces jet penetration. Data expressing the effect of turbulence on jet penetration are very meager in the literature. The qualitative results quoted herein may depend to some extent on how the mainstream turbulence is generated.

(4) Pressure losses are less for a given penetration by use of a small number of large holes than by use of a large number of small holes.

Results from a similar investigation in a 1½-inch-square duct in which hot-air jets (temperature, approximately 1040° R) entered normal flowing streams of cold air (temperature, approximately 600° R) through different shaped openings are presented in reference 40. Penetration was defined in the same manner as in reference 32, except that no limitations were imposed on the distance downstream of the orifice centerline. Relative penetration data were satisfactorily correlated in terms of either mass or momentum ratios of the hot stream to the cold stream. Relative penetration increased with increases in either mass or momentum ratios. The effect of hole shape on relative penetration was generalized by dividing the relative penetration of jets from equal-area holes of circular, square, and longitudinally rectangular shape (ref. 32) by the longitudinal length of the hole (fig. 54).

Penetration data for heated circular jets of air (temperature, approximately 860° R) entering normally a 2- by 20-inch duct filled with a stream of cold air (temperature, ambient) flowing at velocities of 260 or 360 feet per second are presented in reference 41. Penetration was defined as the distance to the point at which the temperature was 1° R greater than the free-stream total temperature. Data expressing the penetration were correlated by the expression

$$\left(\frac{j}{d_j}\right)^{1.65} = 2.91 \left(\frac{\rho_j U_j}{\rho_1 U_1}\right) \sqrt{\frac{x_j}{d_j}} \quad (82)$$

where U_j is the velocity of the jet at the vena contracta and ρ_j is the density of the jet fluid at the vena contracta. Penetration was unaffected by variations of Reynolds number from 0.6×10^5 to 5.0×10^5 , viscosity ratios of the two streams from 1.5 to 1.9, and ratios of duct width to jet diameter from 3.2 to 8.0.

A similar relation was found (ref. 42) for the penetration of liquid jets of water injected normally from small, simple, orifice-type nozzles into a high-velocity stream of air (velocity, approximately 700 ft/sec): Penetration, defined as the maximum penetration of liquid at any longitudinal position, was determined photographically. The data were correlated by the following empirical expression:

$$\left(\frac{j}{d_j}\right) = 0.450 \left(\frac{U_j}{U_1}\right)^{0.95} \left(\frac{\rho_j}{\rho_1}\right)^{0.74} \left(\frac{x_j}{d_j}\right)^{0.22} \quad (83)$$

Temperature distribution: No data indicative of the temperature profiles of a cold jet entering a normal moving

stream of hot gases were found. However, the entry of hot gases into a normal moving stream of cold air has been investigated (ref. 43). Temperatures of the hot gases ranged from 660° to 860° R; orifice diameters, from 0.250 to 0.625 inch; and free-stream velocities, from 160 to 390 feet per second. Orifice pressure ratios, which were much higher than would be encountered in turbojet combustors, ranged from 1.20 to 3.70. A method was presented for simple determination of the temperature profile downstream of the jet orifice. The procedure involves determination of the penetration of the jet at two positions and determination of the upper and lower slopes of the profile. The slopes of the profile are functions of several dimensionless exponential ratios in which the exponents are functions of the test equipment and conditions. The maximum temperature difference at any downstream position was found to be a function of the difference between jet and mainstream temperatures, and of the ratios of jet-orifice diameter to mainstream width and longitudinal distance downstream.

Figure 54 is recommended for determining the penetration of single cold-air jets entering a flowing stream of hot gases. This figure is more applicable to the design or analysis of turbojet combustors which have low orifice pressure ratios. For penetration of gas jets from orifices having high pressure ratios, equation (82) is recommended.

Oblique jets: Penetration: Data expressing the effect of fluid jets mixing with fluids flowing at angles other than 0° or 90° are meager. The investigators of reference 40 varied the entrance angle of hot circular jets to include angles of 22½°, 45°, 90°, and 135° with the direction of flow of the main stream. In general, maximum and minimum penetrations were obtained with jets at 90° and 22½° to the direction of flow of the main stream for all momentum ratios and distances downstream of the jet-orifice centerline. For angles of 135° or 45°, the better angle for penetration depended upon the position downstream and the momentum

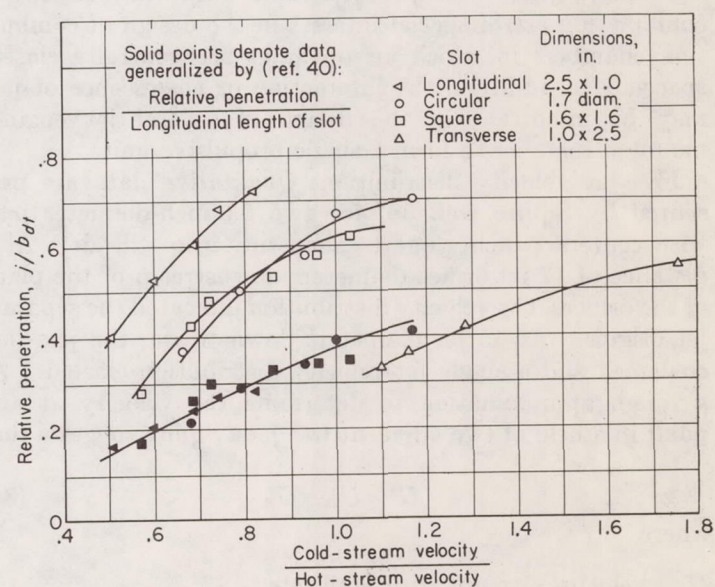


FIGURE 54.—Effect of opening shape on penetration of cold-air jets (temperature, 575° R) into normal hot airstream (temperature, 1350° R) (ref. 32). Hot stream velocity, approximately 280 feet per second.

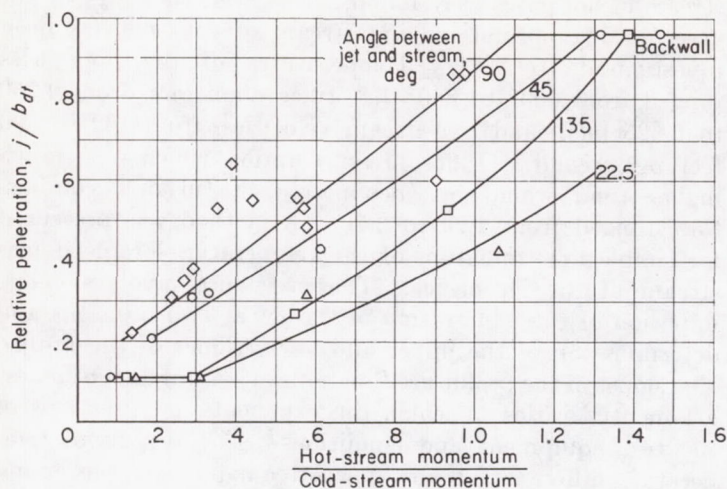


FIGURE 55.—Effect of angle between hot-air jets (temperature, 1040° R) and cold airstreams (temperature, 600° R) on penetration of 0.824-inch-diameter jets (ref. 40).

ratio of the two streams. Representative data are presented in figure 55 (ref. 40) in terms of relative penetration of the jets.

Temperature distribution: Data expressing the temperature distribution in oblique jets are meager. However, Squire (ref. 36) presents general data for the distribution of temperature in a hot jet entering a cold stream from a 1-inch-diameter circular orifice in the wall of a 3-inch-diameter body. The angle between streams was 15°. Representative data for this configuration are presented in figure 56. With increasing mainstream velocities, the spread of the jet is reduced and the centerline of the temperature profiles is bent downstream. In addition, at a stream-to-jet velocity ratio of approximately 0.4, the centerline of the jet becomes parallel to the mainstream flow at approximately 8 inches downstream of the center of the jet orifice.

Multiple jets: Multiple jets and their interaction or combination are of special interest in the design of combustion chambers in which air openings are generally closely spaced. In addition, the interaction or coalescence of jets may be important in the design of several jet engines mounted together to form a single propulsive unit.

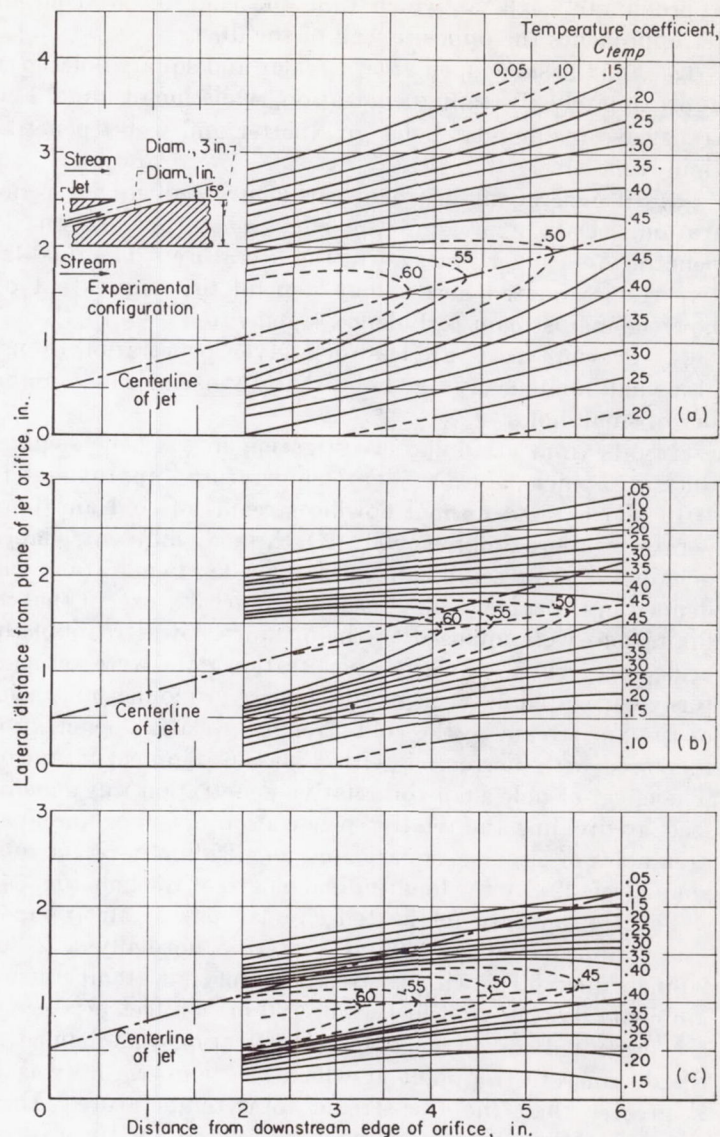
Free-jet velocity distribution: Qualitative data are presented by Squire (ref. 36) for two 0.6-inch-diameter jets, with centers 2 inches apart exhausting into still air. At a distance of 17 jet-orifice diameters downstream of the plane of the orifices, the velocity distribution indicated the separate jet origins. At 45 jet diameters downstream, the jets had coalesced and a single jet-velocity distribution existed. As a rough approximation to determine the velocity at any point in a field of two adjacent free jets, Squire suggests that

$$U^2 = U_D^2 + U_E^2 \quad (84)$$

where

U velocity at point with both jets
 U_D velocity at point in first jet
 U_E velocity at point in second jet

In addition, Squire states that a row of jets coalesces and behaves as a two-dimensional jet at sufficient distances from



(a) Stream velocity, 0.
 (b) Stream velocity, 120 feet per second.
 (c) Stream velocity, 240 feet per second.
 FIGURE 56.—Temperature distributions downstream of axisymmetric oblique jet. Jet velocity, 615 feet per second; jet temperature, 834° R (ref. 36).

the orifices. At distances greater than 10 times the distance between the centers of the individual orifices, the flow will approximate the flow for a two-dimensional jet of the same momentum per unit length.

Free-jet spreading and interaction: Baron and Alexander (ref. 44) determined the flow field in regions near a free jet of finite diameter by superposition of a number of solutions of the flow field for point sources. In reference 45 this method was also applied to regions well downstream of two parallel free jets. From the superposition of solutions,

$$\overline{\rho U^2} = \overline{\rho U_D^2} + \overline{\rho U_E^2} \quad (85)$$

where

$\overline{\rho U^2}$ momentum flux at point with both jets
 $\overline{\rho U_D^2}$ momentum flux at point in first jet
 $\overline{\rho U_E^2}$ momentum flux at point in second jet

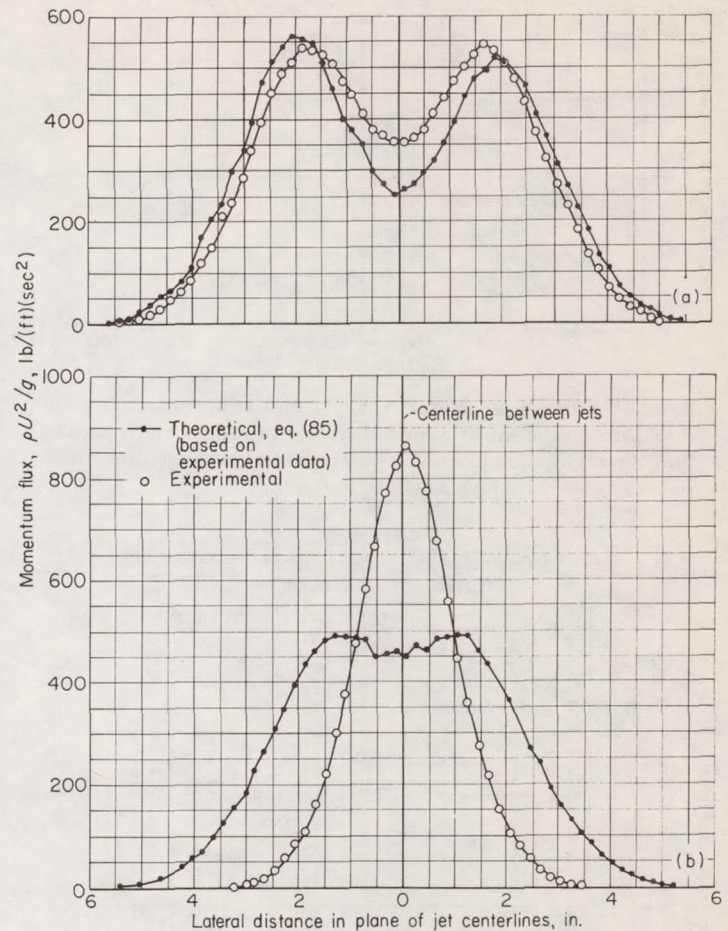
Equation (85) is very similar to the equation of Squire (eq. (84)). Figure 57(a) (ref. 46) gives a comparison of experimental data in the plane of the jet centerlines with values of ρU^2 predicted from equation (85). The general agreement is satisfactory. However, the comparisons for all the data indicate that the method of superposition tends to give values lower than the data in the region between the jets and values higher than the data in the outer regions (refs. 46 and 47). For parallel jets, the disagreement was not excessive.

For nonparallel or impinging jets, Baron and Bollinger (ref. 46) found the method of superposition to be unsatisfactory for determining the flow field. Figure 57(b) (ref. 46) illustrates the disagreement between predicted and experimental values for an included angle of 14° . The discrepancy between experimental and predicted values increased rapidly with increases in the included angle. Mutual entrainment and variation of static pressure in the region between the jets were suggested as probable causes for the large discrepancies between predicted and experimental values. Equation (85) should not be used when the angle between jet centerlines is greater than 14° .

Normal jets: Multiple gas jets entering normal flowing gas streams are discussed briefly in reference 32. No qualitative data are presented. However, included schlieren photographs indicate that two orifices in line in the flow direction give better penetration than orifices staggered in position. Reference 32 suggests that the mixing with circular openings in line is similar to that with longitudinal slots. For longitudinal slots, it is hypothesized that the wake of the upstream half of the jet allows the downstream half to penetrate farther into the hot stream than would be possible otherwise. It is also suggested that the optimum distance between jet centerlines should be approximately 2 jet-orifice diameters.

Orifice coefficients: Determination of mass flows through openings in combustion chambers requires a knowledge of the orifice pressure ratios and discharge coefficients. Much data are available pertaining to the discharge coefficients of orifices in a plane normal to a fluid flowing in a duct. However, in combustion chambers of ramjet or turbojet engines, the relative position of openings and the presence of flame and crossflow of gases generally limit the applicability of such data. As a result, various investigators have attempted to simulate the flow conditions in combustors for experimental determination of orifice coefficients.

Some of the parameters investigated in the experimental study of flow coefficients are orifice sizes, shapes, and pressure ratios, and velocities and Reynolds numbers of the gas streams. Callaghan and Bowden (ref. 48) determined the discharge coefficients of gas jets normal to airstreams as a function of orifice pressure ratios and jet Reynolds numbers for circular, square, and elliptical orifices. The effect of airstream velocity was also investigated. However, most of the data presented are for much higher orifice pressure ratios than would normally be encountered in jet-engine combustors. For orifices of the same area, elliptical orifices (with the major axis parallel to the direction of flow of the main stream) had higher discharge co-



(a) Two parallel jets. Distance between centerlines, 2.99 inches; jet velocities approximately the same.
(b) Two nonparallel intersecting jets. Included angle between jets, 14° ; distance between centerlines at plane of orifices, 2.99 inches; jet velocities approximately the same.

FIGURE 57.—Momentum flux distribution in two jets 23.6 inches downstream of jet orifices (ref. 46).

efficients, followed by square and circular orifices. The discharge coefficient increased with increases in major- to minor-axis ratios. These results agree in general with the results of reference 32, in which maximum penetration of jets from longitudinal slots was compared with that of circles and squares of the same area.

The experimental data of reference 48 were correlated in terms of jet Reynolds numbers and orifice pressure ratios. For jet Reynolds numbers from 0.3×10^5 to 3.6×10^5 and orifice pressure ratios from 1.15 to 2.09, the following correlations were obtained for jets emanating from sharp-edged orifices into still air:

Circular orifices:

$$\frac{C_h}{\Phi} = 0.948 + 4.83 (Re_j \times 10^{-4} + 53.8)^{-1} \quad (86)$$

$$\Phi = 0.151 \frac{P_{t,j}}{P_j} + 0.44$$

Square orifices:

$$\frac{C_h}{\Phi} = 0.916 + 7.50 (Re_j \times 10^{-4} + 74.0)^{-1} \quad (87)$$

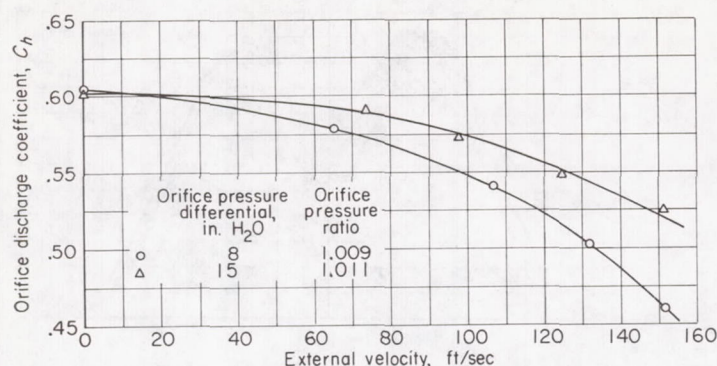


FIGURE 58.—Effect of external velocity and orifice pressure ratio on discharge coefficient of $\frac{3}{8}$ -inch-diameter orifice. Orifice parallel to flow direction; zero internal velocity; external static pressure, 44.2 pounds per square inch absolute (ref. 49).

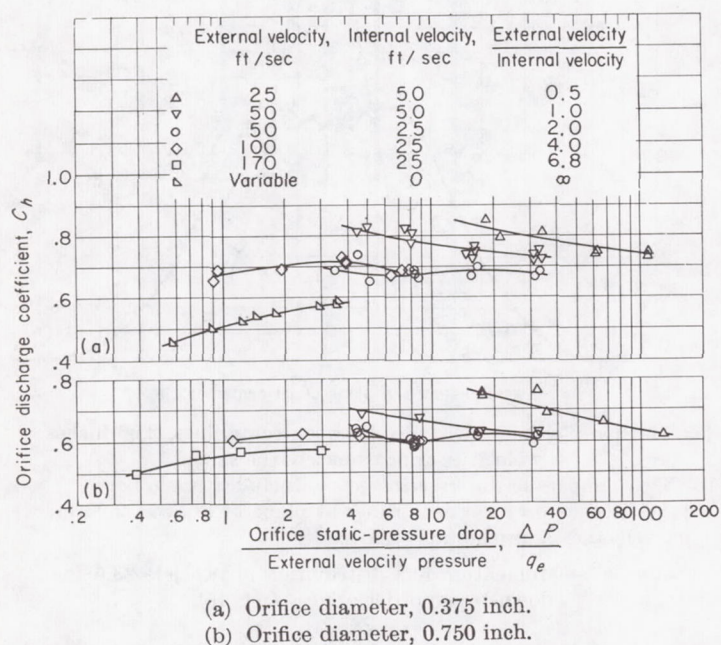


FIGURE 59.—Orifice discharge coefficients. Orifice parallel to flow direction; internal static pressure, 45 pounds per square inch absolute (ref. 49).

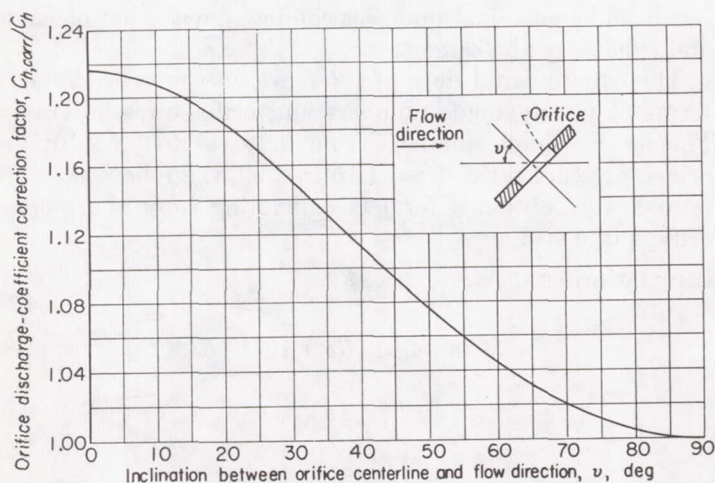


FIGURE 60.—Correction factor for orifices not parallel to flow direction (ref. 18).

$$\Phi = 0.150 \frac{P_{t,j}}{P_j} + 0.467$$

Elliptical orifices:

$$\frac{C_h}{\Phi} = 0.964 + 0.130 \left(\frac{Re_j \times 10^{-4}}{\varphi} + 0.63 \right)^{-1} \quad (88)$$

$$\Phi = 0.149 \frac{P_{t,j}}{P_j} + 0.469$$

$$\varphi = 5.97 \frac{P_{t,j}}{P_j} - 4.17$$

In addition, discharge coefficients for jets entering main streams having velocities as great as 380 feet per second can be calculated from the preceding formulas. However, the static pressure of the jet must be calculated from the static pressure of the main stream by use of the Bernoulli and continuity equations based on open area at the orifice, using the mainstream width minus the maximum width of the jet.

Some data indicating the effect of internal or external crossflow and orifice pressure ratios are available in reference 49. Representative data for zero internal flow and various external velocities with $\frac{3}{8}$ -inch-diameter orifices are presented in figure 58. For zero external crossflow, the orifice is similar to a normal ASME orifice in a straight pipe with a discharge coefficient of approximately 0.6. The discharge coefficient decreases with increasing external velocities and decreasing orifice pressure ratios. These trends agree qualitatively with the results of reference 48.

Much data within the range of orifice pressure ratios in the combustion chambers of jet engines are presented in reference 49. Representative discharge coefficients of two circular orifices are presented in figure 59 in terms of $\Delta P/q_e$ and various external-internal flow velocity ratios. In general, orifice discharge coefficients increased with decreases in external-internal flow velocity ratios and orifice diameters. The change in slope of the curves of figure 59 is hypothesized to be the result of opposite influences exerted by the internal and external lateral velocities. That is, an interaction that depends upon the velocity ratio occurs. For external-internal velocity ratios less than approximately 2, the internal velocity is more important, the external velocity being more important at velocity ratios greater than 2.

Reference 18 has stated that the effect of inclination of orifices to the direction of flow can be taken into account by multiplying the discharge coefficients read from figures 58 and 59 by a correction factor $C_{h,corr}/C_h$. This correction factor is plotted in figure 60 as a function of the angle of inclination between the orifice centerline and the direction of flow of the main stream. The orifice discharge coefficient increases with a decrease in the angle between the orifice centerline and the flow direction.

As a first approximation for use in combustion chambers of jet engines, 0.6 should be used for orifice discharge coefficients unless appreciable internal or external crossflow exists. In such cases, a discharge coefficient can be read from figure 58 or 59 and corrected for orifice inclination by the correction factor of figure 60.

AERODYNAMIC MIXING

The aerodynamic mixing of mass, heat, and momentum is of fundamental importance to many of the processes involved in converting the heat energy of fuel to an optimum distribution of momentum in the working fluid stream of jet engines. The processes involving aerodynamic mixing include fuel-air mixing, combustion, and jet mixing, all of which occur under turbulent-flow conditions. For this reason, the discussion of mixing emphasizes turbulent transport in high-velocity gas streams.

The mixing of quantities such as mass, heat, and momentum in turbulent gas streams is accomplished by the gross transport of large groups of gas molecules by means of the turbulent fluid motion, with local mixing proceeding by means of molecular motion. The turbulent and molecular mixing of heat and mass follows the same general laws, from which differential equations may be formed for use in the solution of problems in the diffusion of mass and heat in turbulent streams. Solution of the differential equations of diffusion is complicated by the dependence of the molecular diffusion coefficients on temperature and pressure, and the dependence of the turbulent diffusion coefficients on time. For applications where the molecular diffusion coefficient is constant or negligible compared with the turbulent diffusion coefficient, a generalized form of the differential equation of diffusion may be used to obtain exact or graphical solutions for a wide variety of transport problems encountered in jet-engine combustor design. The following sections include a general discussion of the theory of turbulent diffusion, a discussion of the solution of the differential equations of diffusion, a tabulation of solutions of transport problems for a wide variety of boundary conditions, a discussion of the effect of periodic flow fluctuations on transport, and applications of turbulent diffusion theory to problems in fuel-air mixing. For the most part, the discussion and solutions pertain to the time-mean concentration of mass or heat at fixed points in fluid streams.

DIFFUSION

Fundamental equations.—*Empirical laws of heat, mass, and momentum transfer:* The differential equations describing the transfer of heat, mass, and momentum arise from a set of similar empirical laws, each of which states that the flux of a quantity being transferred through a unit area is equal to the concentration gradient of the diffusing quantity multiplied by a coefficient. As shown in reference 35, these laws may be tabulated for comparison between the molecular and turbulent cases as follows:

Empirical law	Diffusion of	Laminar flow (molecular)	Turbulent flow
Fick-----	Mass-----	$\frac{w}{A} = D_M \frac{\partial \mathcal{C}}{\partial X}$	$\frac{w}{A} = D_{T,M} \frac{\partial \mathcal{C}}{\partial X}$
Biot-Fourier-	Heat-----	$\frac{Q}{\rho c_p A} = \frac{\kappa}{\rho c_p} \frac{\partial T}{\partial X}$	$\frac{Q}{\rho c_p A} = D_{T,H} \frac{\partial T}{\partial X}$
	Momentum-	$\frac{\tau g}{\rho} = \frac{\mu}{\rho} \frac{\partial U}{\partial X}$	$\frac{\tau g}{\rho} = D_{T,mom} \frac{\partial U}{\partial X}$

These empirical laws may be correlated by the Prandtl and Schmidt numbers for both laminar and turbulent flow:

Number	Laminar	Turbulent
Prandtl-----	$Pr = \left(\frac{\mu}{\rho}\right) / \frac{\kappa}{\rho c_p}$	$Pr_T = \frac{D_{T,mom}}{D_{T,H}}$
Schmidt-----	$Sc = \left(\frac{\mu}{\rho}\right) / (D_M)$	$Sc_T = \frac{D_{T,mom}}{D_{T,M}}$

Experimental data on the diffusion of mass, heat, and momentum are summarized in reference 35 as follows:

Fluid flowing	Diffusing material	Laminar flow		Turbulent flow	
		Pr	Sc	Pr_T	Sc_T
Air-----	Warm air-----	0.74	-----	0.76	-----
Air-----	Helium-----	-----	0.34	-----	0.70
Water-----	Salt water-----	-----	785	-----	.64

From the preceding experimental results, it may be concluded that the turbulent diffusions of heat and mass occur at equal rates, since the turbulent Prandtl and Schmidt numbers are essentially equal for the separate cases of mass and heat transfer. The latter conclusion is in agreement with the statistical theory of turbulent diffusion, which is discussed in the following paragraphs. A necessary prerequisite to the use of the empirically determined turbulent diffusion coefficients is that the turbulent-flow fields to be correlated must have proportional turbulence levels and similar turbulent velocity autocorrelation coefficients. A further limitation to the use of the dimensionless Prandtl and Schmidt numbers arises from the assumption of a constant coefficient of diffusion, which in subsequent sections is shown to be a function of time.

Differential equations of diffusion: The differential equations of diffusion may be derived from the empirical Fick and Biot-Fourier laws by equating the amount of the diffusing quantity entering an infinitesimal volume to the time rate of change of the total amount of the diffusing quantity in that infinitesimal volume (refs. 50 and 51, p. 7). For the combined turbulent and molecular diffusion of mass without local sources or sinks, the differential equation becomes

$$\frac{\partial \mathcal{C}}{\partial t} = \frac{\partial}{\partial X_i} \left[(D_{T,M,i} + D_{M,i}) \frac{\partial \mathcal{C}}{\partial X_i} \right] \quad (i=1,2,3) \quad (89)$$

where the X_i are rectangular coordinates. If the turbulent field is homogeneous and isotropic, equation (89) may be simplified to

$$\frac{\partial \mathcal{C}}{\partial t} = (D_{T,M} + D_M) \frac{\partial^2 \mathcal{C}}{\partial X_i^2} \quad (i=1,2,3) \quad (90)$$

The differential equation for the combined turbulent and molecular transport of heat without local sources or sinks is

$$\rho c_p \frac{\partial T}{\partial t} = \frac{\partial}{\partial X_i} \left[(\rho c_p D_{T,H,i} + \kappa_i) \frac{\partial T}{\partial X_i} \right] \quad (i=1,2,3) \quad (91)$$

A transformation of the independent variable T (temperature) similar to that presented in reference 52 may be employed:

$$h = \int_{T_{ref}}^T \rho c_p dT \quad (92)$$

With the use of this transformation, equation (91) may be written as

$$\frac{\partial h}{\partial t} = \frac{\partial}{\partial X_i} \left[\left(D_{T,H,i} + \frac{\kappa_i}{\rho c_p} \right) \frac{\partial h}{\partial X_i} \right] \quad (i=1,2,3) \quad (93)$$

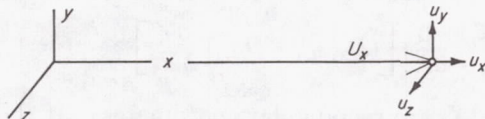
If the turbulent field is homogeneous and isotropic, and if the molecular diffusivity $\kappa_i/\rho c_p$ is small, or nearly constant, and equal in all directions, equation (93) may be simplified to

$$\frac{\partial h}{\partial t} = \left(D_{T,H} + \frac{\kappa}{\rho c_p} \right) \frac{\partial^2 h}{\partial X_i^2} \quad (i=1,2,3) \quad (94)$$

Exact solutions of the preceding differential equations can be made for a variety of transport problems only if the functional forms of the diffusion coefficients are known. The effect of temperature and pressure on the molecular transport coefficients D_M and $\kappa/\rho c_p$ for most gaseous systems can be found in the literature. The turbulent diffusion coefficients $D_{T,M}$ and $D_{T,H}$ can be determined experimentally or may be predicted theoretically from knowledge of two fundamental parameters of the turbulent field. The relation between the turbulent diffusion coefficient and the parameters of the turbulent field is found in the Taylor theory of diffusion by continuous movements, which is summarized in the following section.

Homogeneous, isotropic, turbulent fields.—*Diffusion by continuous movements:* The theory of diffusion by continuous movements, first presented in reference 53, is generally considered to give a fundamental description of the mechanism of turbulent diffusion. The theory provides a coefficient of turbulent diffusion that may be used directly in equations (89), (90), (93), and (94). As shown in subsequent paragraphs, this diffusion coefficient is a function of two parameters that characterize all turbulent fields.

The first of the two turbulence parameters is called the intensity $\sqrt{u_z^2}$, $\sqrt{u_y^2}$, or $\sqrt{u^2}$, which defines the magnitude of the turbulent velocities in the three Cartesian coordinate directions:



Sketch (e)

where U_x is the mean stream velocity, and the time-averages $\overline{u_x}$, $\overline{u_y}$, and $\overline{u_z}$ are all zero. The second turbulence parameter used in the Taylor theory is the Lagrangian double velocity correlation coefficient \mathcal{R}_{La} (sometimes called the autocorrelation coefficient), which describes the degree of cor-

relation between the turbulent velocities of a particular fluid particle at time zero and at time t :

$$\mathcal{R}_{La,x} = \frac{\overline{u_{x,0} u_{x,t}}}{\sqrt{\overline{u_{x,0}^2}} \sqrt{\overline{u_{x,t}^2}}} \quad \mathcal{R}_{La,y} = \frac{\overline{u_{y,0} u_{y,t}}}{\sqrt{\overline{u_{y,0}^2}} \sqrt{\overline{u_{y,t}^2}}} \quad \mathcal{R}_{La,z} = \frac{\overline{u_{z,0} u_{z,t}}}{\sqrt{\overline{u_{z,0}^2}} \sqrt{\overline{u_{z,t}^2}}}$$

where the \mathcal{R}_{La} are functions of the time interval t , and the double bar over the product of instantaneous velocities denotes an average of a large number of particle motions.

When the turbulent field is homogeneous ($\sqrt{\overline{u_{x,0}^2}} = \sqrt{\overline{u_{x,t}^2}}$, etc.), the Lagrangian correlation coefficients may be written as

$$\mathcal{R}_{La,x} = \frac{\overline{u_{x,0} u_{x,t}}}{\overline{u_x^2}} \quad \mathcal{R}_{La,y} = \frac{\overline{u_{y,0} u_{y,t}}}{\overline{u_y^2}} \quad \mathcal{R}_{La,z} = \frac{\overline{u_{z,0} u_{z,t}}}{\overline{u_z^2}}$$

From the definition of the correlation coefficient $\mathcal{R}_{La,y}$, an integral equation may be written:

$$\overline{u_{y,0} \int_0^t u_{y,t} dt} = \overline{u_y^2} \int_0^t \mathcal{R}_{La,y} dt \quad (95)$$

Since the mean displacement \overline{Y} of a large number of fluid particles is given by

$$\overline{Y} = \int_0^t \overline{u_y} dt$$

and since

$$\overline{Y u_{y,0}} = \overline{Y} \frac{d\overline{Y}}{dt} = \frac{1}{2} \frac{d\overline{Y^2}}{dt}$$

equation (95) may be written as

$$\frac{1}{2} \frac{d\overline{Y^2}}{dt} = \overline{u_y^2} \int_0^t \mathcal{R}_{La,y} dt \quad (96)$$

As shown in references 54 and 55, the quantity $\frac{1}{2} \frac{d\overline{Y^2}}{dt}$ corresponds directly to the turbulent diffusion coefficient D_T , so that

$$D_{T,x} = \overline{u_x^2} \int_0^t \mathcal{R}_{La,x} dt \quad (97)$$

$$D_{T,y} = \overline{u_y^2} \int_0^t \mathcal{R}_{La,y} dt \quad (98)$$

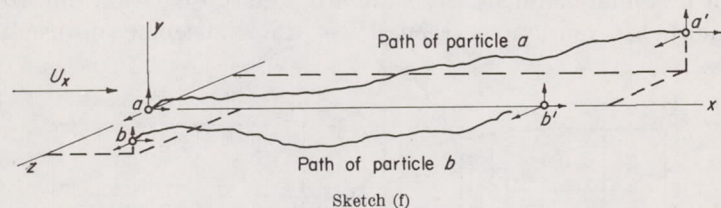
$$D_{T,z} = \overline{u_z^2} \int_0^t \mathcal{R}_{La,z} dt \quad (99)$$

The turbulent diffusion coefficients derived in the previous equations make no distinction between the transport of heat and mass, and are therefore considered to be applicable to both equations (90) and (94). It is of particular significance to note that the Taylor theory assumes a homogeneous turbulent field where the values of the various intensities and correlation coefficients do not change with position in the field. If the field is also isotropic, then $D_{T,x}$, $D_{T,y}$, and $D_{T,z}$ should be identical.

Correlation coefficient: Direct measurement of the Lagrangian correlation coefficient R_{La} does not appear to be feasible by conventional anemometry techniques, since by definition the motion of a particular particle must be observed over a finite length of time. An Eulerian double velocity correlation coefficient R_{Eu} has been defined by Taylor in reference 56 and generalized by von Kármán and Howarth in reference 57. The Eulerian correlation coefficient R_{Eu} describes the degree of correlation between fluid-particle turbulent velocities at two different points in the field at the same instant. For a homogeneous turbulent field, the Eulerian correlation coefficients of interest in the present discussion are those relating the turbulent velocity components at the point $(0,0,0)$ and $(x,0,0)$, $(0,y,0)$ or $(0,0,z)$:

$$R_{Eu,x} = \frac{\overline{u_{x,0}u_x}}{\overline{u_x^2}} \quad R_{Eu,y} = \frac{\overline{u_{y,0}u_y}}{\overline{u_y^2}} \quad R_{Eu,z} = \frac{\overline{u_{z,0}u_z}}{\overline{u_z^2}}$$

If the turbulent field is also isotropic, then $R_{Eu,x}$, $R_{Eu,y}$, and $R_{Eu,z}$ are all identical. The correlation coefficient R_{Eu} can be measured directly by conventional anemometry techniques (refs. 58 and 59), but to date no theoretical relation has been found between the Lagrangian and Eulerian correlation coefficients. The distinction between the two correlation coefficients is illustrated in the following diagram of particle position and turbulent velocity components:



It is evident from this diagram that measurement of velocity components at the points $(0,0,0)$ and $(x,0,0)$ cannot result in the true Lagrangian correlation R_{La} of either particle a or b.

A turbulent diffusion experiment reported in reference 60 indicates that the Eulerian scale of turbulence L_{Eu} may be roughly equal to the Lagrangian scale of turbulence L_{La} for turbulence Reynolds numbers $(\sqrt{\overline{u_x^2}} L_{Eu})/\nu > 100$, where the Eulerian and Lagrangian scales are defined by

$$\begin{aligned} L_{Eu,x} &= \int_0^\infty R_{Eu,x} dx \\ L_{Eu,y} &= \int_0^\infty R_{Eu,y} dy \\ L_{Eu,z} &= \int_0^\infty R_{Eu,z} dz \\ L_{La,x} &= \sqrt{\overline{u_x^2}} \int_0^\infty R_{La,x} dt \\ L_{La,y} &= \sqrt{\overline{u_y^2}} \int_0^\infty R_{La,y} dt \\ L_{La,z} &= \sqrt{\overline{u_z^2}} \int_0^\infty R_{La,z} dt \end{aligned}$$

In a recent experiment (ref. 61), a direct comparison was made between the Lagrangian and Eulerian correlation coefficients. The Lagrangian correlation coefficient was deduced from helium mixing data downstream of a point source, and the Eulerian correlation coefficient was measured directly by anemometry. The Lagrangian and Eulerian correlation coefficients were found to have the same shape when related by the expression

$$R_{Eu}(y) \text{ compared with } R_{La} \frac{y}{\mathcal{B}\sqrt{\overline{u_y^2}}} \quad (100)$$

The factor \mathcal{B} was constant for any particular stream condition and varied from 0.56 to 0.72 over a range of stream velocities.

Dryden (ref. 62) notes that measured correlation coefficients commonly follow the exponential form and suggests that the Lagrangian correlation coefficient might have the form

$$R_{La,y} = e^{-t/t_{La}} \quad (101)$$

where t_{La} is a characteristic time related to the Lagrangian scale by definition:

$$t_{La} = \frac{L_{La,y}}{\sqrt{\overline{u_y^2}}}$$

The exponential form of the Lagrangian correlation coefficient, which was found in a diffusion experiment reported in reference 63, is used for illustration herein. An exponential correlation coefficient is shown in figure 61 for typical ramjet-combustor approach-stream conditions of 300-feet-per-second mean stream velocity, 15-feet-per-second turbulence intensity, and 0.15-foot Lagrangian scale.

In practice, the Lagrangian microscale of turbulence λ_{La} may have an appreciable effect on the form of the correlation coefficient (ref. 60). The microscale is defined by the relation

$$R_{La} = 1 - \frac{t^2}{\lambda_{La}^2} \quad (t \ll \lambda_{La}, t) \quad (102)$$

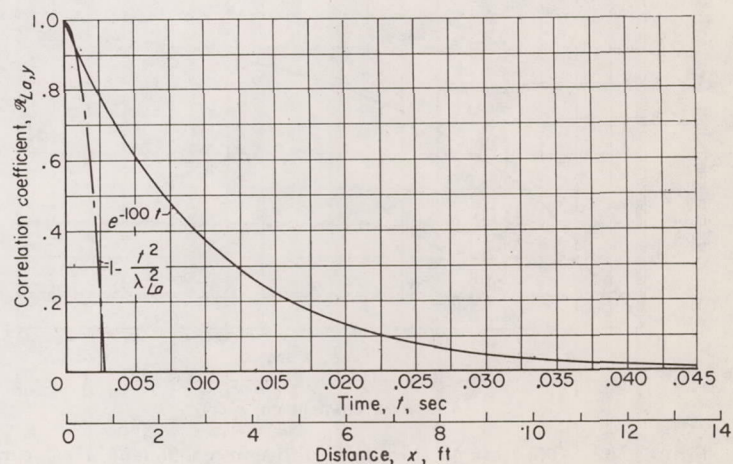


FIGURE 61.—Correlation coefficient $R_{La,y}$ of form $R_{La,y} = e^{-t/t_{La}}$. Mean stream velocity, 300 feet per second; turbulence intensity, 15 feet per second; turbulence scale, 0.15 foot; turbulence microscale, 0.0416 foot.

and its effect on the correlation coefficient is shown in figure 61 for a microscale value of 0.0416 foot.

The turbulent diffusion coefficient $D_{T,y}$, which results from the correlation coefficient $\mathcal{R}_{La,y}$ shown in figure 61, is plotted in figure 62 as a function of time t and of the distance downstream x through the transformation $x = U_x t$. In order to illustrate the effect of turbulence scale on the turbulent diffusion coefficient, curves are also shown in figure 62 for a range of scale values, all other parameters remaining the same. The curves show two characteristics of the turbulent diffusion coefficient:

(1) For small times ($t \ll t_{La}$), or short distances ($x \ll U_x t_{La}$), the eddy diffusion coefficient follows the form

$$D_{T,y} = \bar{u}_y^2 t$$

(2) For large times ($t \gg t_{La}$), or large distances ($x \gg U_x t_{La}$), the eddy diffusion coefficient follows the form

$$D_{T,y} = \sqrt{\bar{u}_y^2} \mathcal{L}_{La,y}$$

It is of particular significance to note that the turbulent diffusion coefficient is not constant, as assumed in empirical treatments of diffusion, but is in reality a function of time, which may have a very large variation in the range of interest of processes such as fuel-air mixing.

Turbulence spectrum: Taylor has shown (ref. 64) that the Eulerian correlation coefficient \mathcal{R}_{Eu} is related to the one-dimensional turbulence energy spectrum by the Fourier transform integral

$$\mathcal{R}_{Eu} = \int_0^\infty F(f_T) \cos \frac{2\pi f_T x}{U_x} df_T \quad (103)$$

where the spectrum density function $F(f_T)$ represents the fraction of the total kinetic energy which lies between the frequencies f_T and $f_T + df_T$, so that

$$\int_0^\infty \bar{u}_x^2(f_T) F(f_T) df_T = \bar{u}_x^2 \quad (104)$$

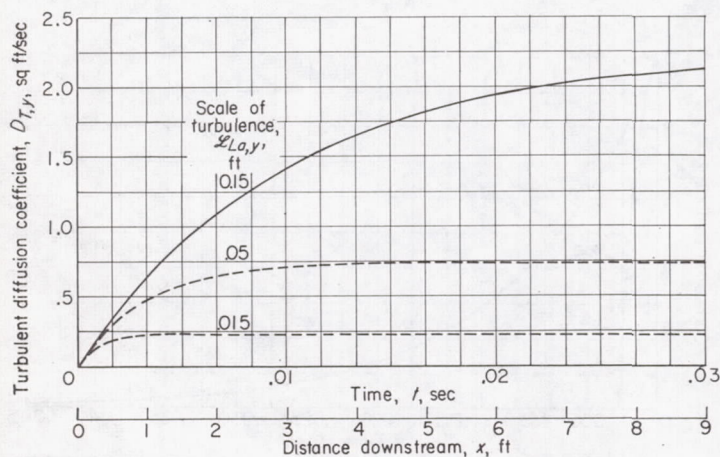


FIGURE 62.—Theoretical turbulent diffusion coefficient $D_{T,y}$ corresponding to Lagrangian correlation coefficient $\mathcal{L}_{La,y} = e^{-t/t_{La}}$. Mean stream velocity, 300 feet per second; turbulence intensity, 15 feet per second.

The spectrum density function $F_y(f_T)$ shown in figure 63 corresponds to an Eulerian correlation coefficient of the exponential form

$$\mathcal{R}_{Eu,y} = e^{-\frac{y}{\mathcal{L}_{Eu,y}}} \quad (105)$$

This short discussion of the relation between the correlation coefficient and the spectrum density function is presented to serve as a possible insight into the nature of the Lagrangian correlation coefficient in cases where flow fluctuations are present in addition to those due to turbulence proper. The effect of abnormal spectra on turbulent diffusion is discussed in a succeeding section.

Comparison of turbulent and molecular diffusion: An excellent measure of diffusion is given by the quantity ω , which is equivalent to the square of the standard deviation used in the theory of statistics. The standard square deviation ω due to turbulence is related to the turbulent diffusion coefficient by the expression

$$\omega_T = \frac{\bar{Y}_T^2}{2} = \int_0^t D_{T,y} dt \quad (106)$$

In a similar manner, the standard square deviation due to molecular motion is related to the molecular diffusion

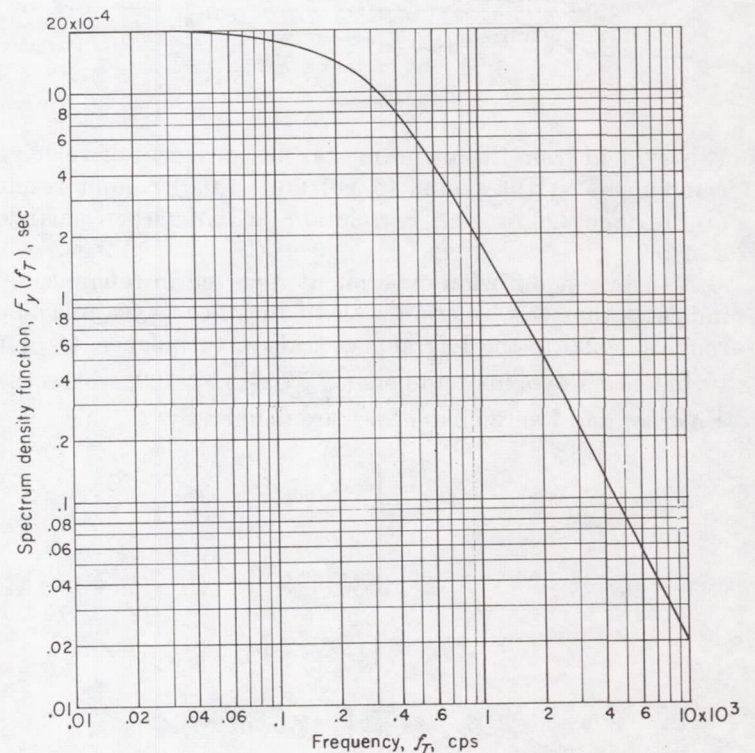


FIGURE 63.—One-dimensional spectrum of turbulence when $\mathcal{R}_{Eu,y} = e^{-y/\mathcal{L}_{Eu,y}}$. Mean stream velocity, 300 feet per second; Eulerian scale $\mathcal{L}_{Eu,y}$, 0.15 foot; negligible microscale.

coefficient by (ref. 54)

$$\omega_{mol} = \frac{\overline{Y_{mol}^2}}{2} = \int_0^t D_M dt \quad (107)$$

Methods for the determination of the total standard square deviation ω , where

$$\omega = \omega_T + \omega_{mol}$$

are discussed in a subsequent section on the standard square deviation. At present, it will suffice to note that the greater the value of the parameter ω , the greater will be the degree of mixing. Comparison of the turbulent and molecular standard square deviations must be based on the form of the correlation coefficient, since the turbulent diffusion coefficient depends directly on the correlation coefficient as shown by equations (97) to (99). For purposes of comparison, a correlation coefficient of the form given by equation (101) is assumed, and the turbulent and molecular mean square deviations are plotted in figure 64 as functions of time for various values of the parameters $D_M/\mathcal{L}_{La,y}^2$ and $\sqrt{u_y^2}/\mathcal{L}_{La,y}$.

On the basis of the preceding discussion, a comparison can be made for a model of practical interest: the diffusion of isooctane in a turbulent airstream. For this comparison, the molecular diffusion coefficient is maximized by assuming a low static pressure of 0.25 atmosphere and a high static temperature of 1100° R. At these conditions, the molecular diffusion coefficient D_M has a value of 0.000774 square foot per second. The turbulent standard square deviation ω_T for a mean stream velocity U_x of 300 feet per second, a turbulence intensity $\sqrt{u_y^2}$ of 15 feet per second, and a Lagrangian scale of 0.15 foot, was calculated from equation (106) using the turbulent diffusion coefficient shown in figure 62. The turbulent and molecular standard square deviations are shown in figure 65 as functions of time. While the molecular standard square deviation is negligible in this diffusion model over the range of interest, this may not always be the case. For example, the times and distances over which diffusion occurs in flame fronts are so small that the molecular diffusion coefficient might become significant.

Generalized form of differential equations of diffusion: Solutions of the differential equation of diffusion with constant coefficients are treated for a wide variety of boundary conditions in references 51 and 65. Equations (90) and (94) for the combined turbulent and molecular diffusion of mass and heat, respectively, have coefficients that are functions of the independent variable t , but may be transformed to equations with constant coefficients through the relations

$$\omega_M = \int_0^t (D_{T,M} + D_M) dt \quad (108)$$

$$\omega_H = \int_0^t \left(D_{T,H} + \frac{\kappa}{\rho c_p} \right) dt \quad (109)$$

Methods for the determination of the standard square

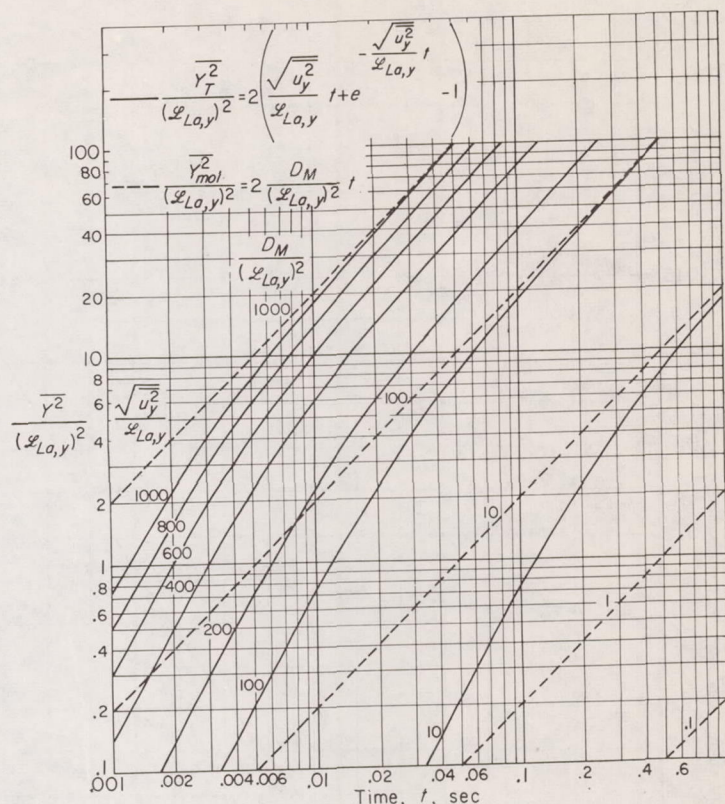


FIGURE 64.—Comparison of turbulent and molecular standard square

deviations, based on $\mathcal{R}_{La,y} = e^{-\frac{\sqrt{u_y^2}}{\mathcal{L}_{La,y}} t}$.

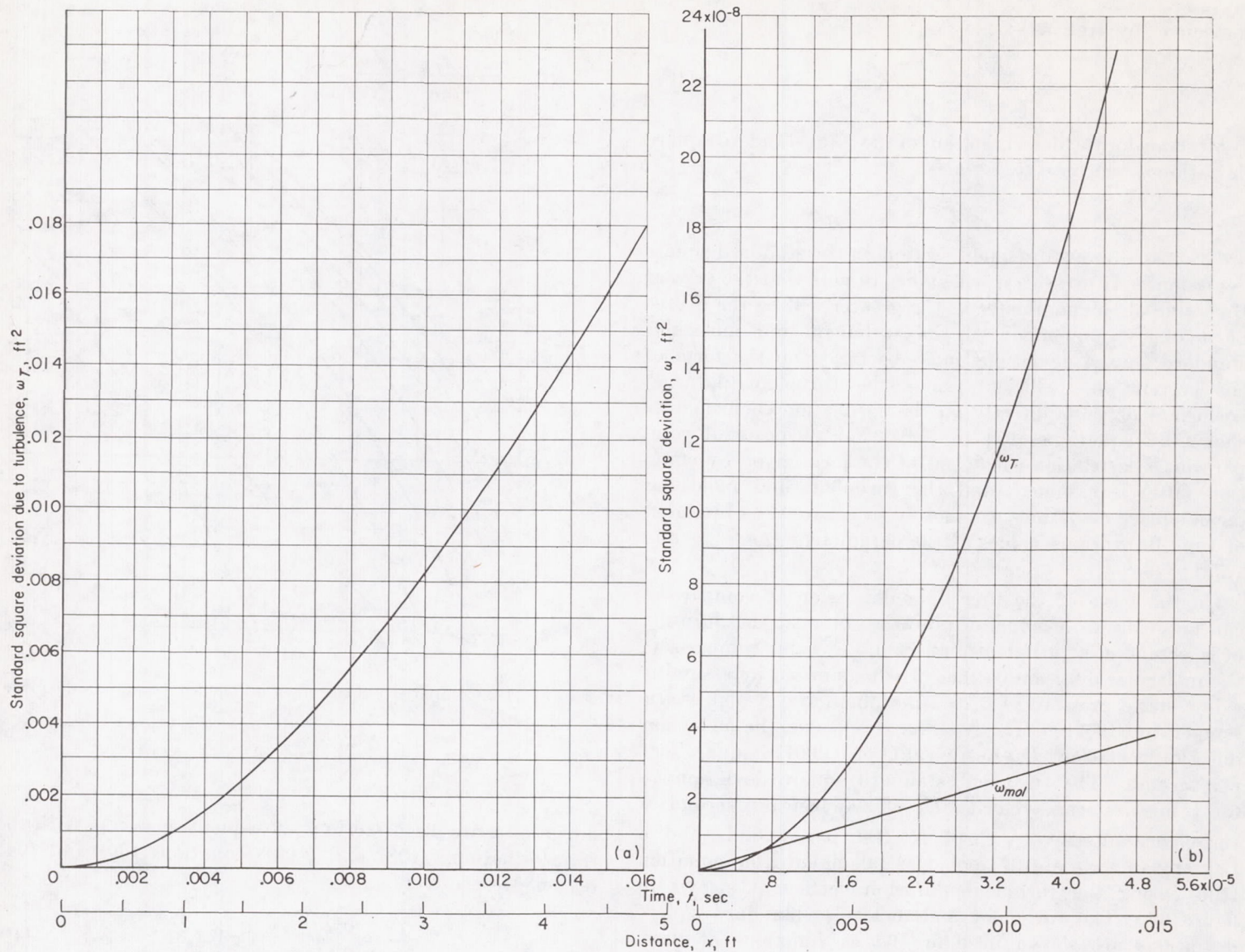
deviation ω are discussed in a subsequent section. With the transformations (108) and (109), equations (90) and (94) become, respectively,

$$\frac{\partial \mathcal{C}}{\partial \omega_M} = \frac{\partial^2 \mathcal{C}}{\partial X_i^2} \quad (i=1, 2, 3) \quad (110)$$

$$\frac{\partial h}{\partial \omega_H} = \frac{\partial^2 h}{\partial X_i^2} \quad (i=1, 2, 3) \quad (111)$$

which are amenable to the same solutions as the differential equations of diffusion with constant coefficients.

Several methods have been evolved for the solution of the differential equations of diffusion for the various boundary conditions corresponding to the type of diffusion source. The method to be followed herein is that which utilizes the instantaneous point source in derivations for all source configurations. In addition to its value in the more complex derivations, the point-source model adequately describes some diffusion systems of practical interest and is therefore treated in more detail than the complex models. Since equations (110) and (111) are identical except for the symbols defining the dependent variables, their solutions are also identical. Hereinafter, the equation for the diffusion of mass will be used, with the understanding that its solutions and those for the diffusion of heat are identical in form.



(a) Standard square deviation over a range of interest in jet-engine applications.

(b) Comparison of turbulent and molecular standard square deviations.

FIGURE 65.—Standard square deviation based on turbulent diffusion coefficient shown in figure 62 for Lagrangian scale of turbulence of 0.15 foot.

Point source: The solution for a point source of diffusion is given in reference 65 (p. 338):

$$\mathcal{C} = \frac{K_{ps}}{(4\pi\omega)^{3/2}} e^{-\frac{[(x-U_zt)^2 + r^2]}{4\omega}} \quad (112)$$

where

- \mathcal{C} concentration of diffusing quantity at point (x,r) and time t , lb/cu ft
- K_{ps} strength of point source, lb
- ω standard square deviation of fluid particles, sq ft
- x distance downstream from point source, ft
- r radial distance from streamline passing through point source, ft

The value ω is a function of time, as illustrated in figure 65(a), and may be determined from equation (108) or by methods discussed in the next section.

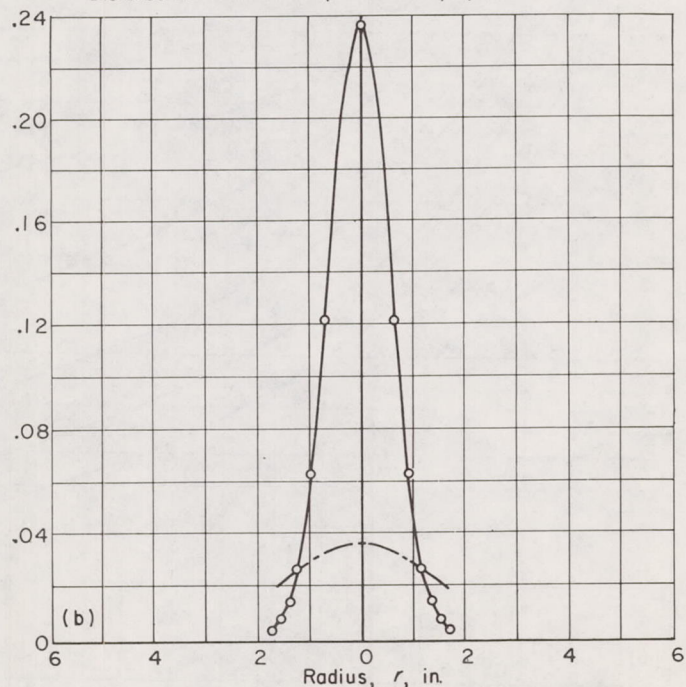
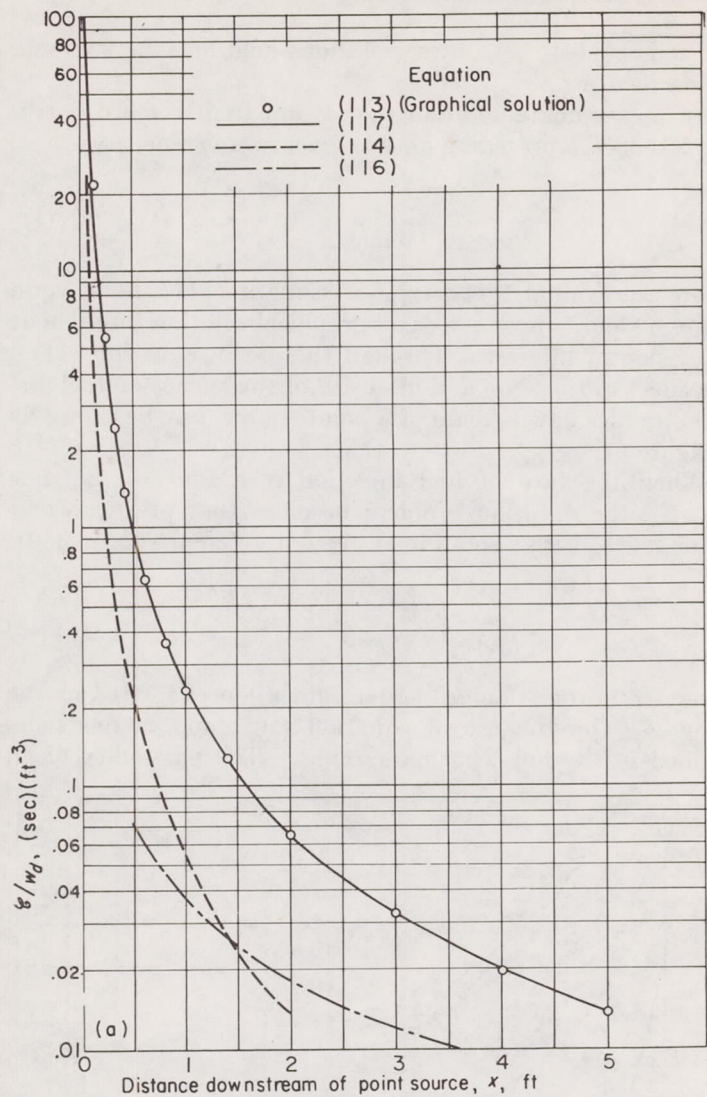
As shown in reference 55, the instantaneous point-source solution may be used to solve for the case of a continuous point source. The concentration \mathcal{C} at a point (x,r) is obtained by a summation of contributions to that point

by instantaneous point sources located at the points $((x-U_zt), 0, 0)$:

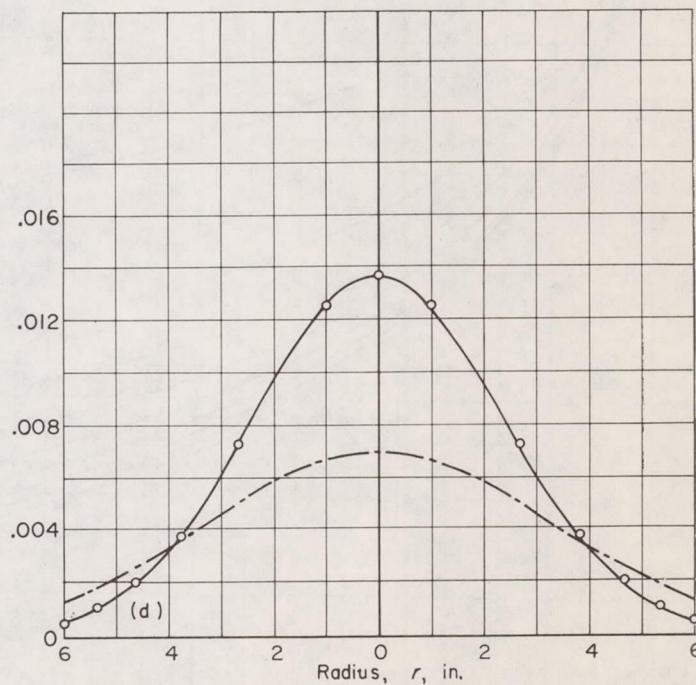
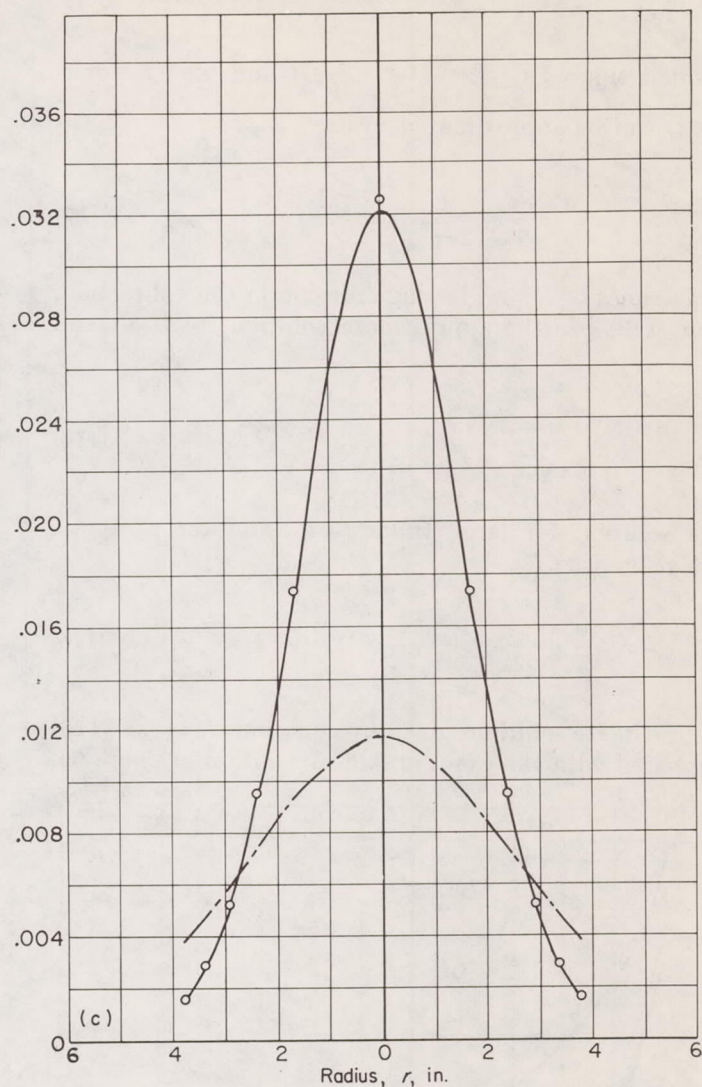
$$\mathcal{C} = \frac{w_d}{(4\pi)^{3/2}} \int_0^\infty \frac{1}{\omega^{3/2}} e^{-\frac{(x-U_zt)^2 + r^2}{4\omega}} dt \quad (113)$$

where w_d is the weight-flow rate (lb/sec) of material issuing from the point source. With the exception of the limiting cases of very small and very large distances from the point source, the functional form of ω does not permit direct integration of equation (113). To permit comparison with several approximate forms to be discussed, equation (113) was solved graphically and is plotted in figure 66 for the following conditions:

Fluid	-----	Air
Mean velocity, U_z , ft/sec	-----	300
Static pressure, atm	-----	0.25
Static temperature, °R	-----	1100
Turbulent intensity, $\sqrt{u_z^2} = \sqrt{u_r^2} = \sqrt{u_\theta^2}$, ft/sec	-----	15
Turbulence scale, $L_{La,x} = L_{La,y} = L_{La,z}$, ft	-----	0.15
Correlation coefficient, $R_{La,x} = R_{La,y} = R_{La,z}$	-----	$e^{-t/t_{La}}$
Fuel	-----	Isooctane
Molecular diffusion coefficient, sq ft/sec	-----	0.000774



(a) Mean concentrations along x -axis.
 (b) Radial concentration profile at $x=1$ foot.



(c) Radial concentration profile at $x=3$ feet.
 (d) Radial concentration profile at $x=5$ feet.

FIGURE 66.—Comparison of solutions for point source of diffusion. Mean stream velocity, 300 feet per second; turbulence intensity, 15 feet per second; turbulence scale, 0.15 foot; correlation coefficient, $e^{-t/lLa}$; stream static pressure, 0.25 atmosphere; stream temperature, 1100° R; isooctane vapor diffusing through air.

For small times $t \ll t_{La}$, $\frac{\sqrt{u_y^2}}{U_x} \ll \frac{x}{\sqrt{x^2 + r^2}}$, and $x \gg y, z$, equation (113) can be approximated by (ref. 55)

$$\frac{\mathcal{C}}{w_d} = \frac{U_x}{2\pi u_y^2 x^2} e^{-\frac{U_x^2 r^2}{2u_y^2 x^2}} \quad (114)$$

For large times $t \gg t_{La}$, neglecting diffusion in the x -direction, equation (113) has the approximate solution (refs. 55 and 66):

$$\frac{\mathcal{C}}{w_d} = \frac{1}{4\pi \sqrt{u_y^2} L_{La,y} (x^2 + r^2)^{1/2}} e^{\frac{U_x [x - (x^2 + r^2)^{1/2}]}{2\sqrt{u_y^2} L_{La,y}}} \quad (115)$$

Another solution for large times $t \gg t_{La}$ and for $x > y, z$ is given in reference 67:

$$\frac{\mathcal{C}}{w_d} = \frac{1}{4\pi \sqrt{u_y^2} L_{La,y} x} e^{-\frac{U_x r^2}{4\sqrt{u_y^2} L_{La,y} x}} \quad (116)$$

The approximate solutions given by equations (114) to (116) are compared with the exact graphical solution in figure 66,

and it is evident that these solutions hold only for extreme values of x or t .

An approximate solution that is apparently more nearly exact than the preceding ones is given in reference 68:

$$\frac{\mathcal{C}}{w_d} = \frac{1}{4\pi U_x \omega} e^{-\frac{r^2}{4\omega}} \quad (117)$$

where ω is evaluated at $t = x/U_x$. Equation (117) is shown in figure 66 and follows the exact graphical solution throughout the range of interest. Through the use of equation (117), the effect of the scale and intensity of turbulence on fuel-air-ratio profiles downstream of a point source may be shown as in figure 67.

When the rate of fuel injection is a function of time $w'_{d,f}(t')$, the diffusion problem becomes that of a transient point source with a solution as given in reference 65 (p. 339):

$$\mathcal{C} = \frac{1}{(4\pi)^{3/2}} \int_0^t \frac{w'_{d,f}}{(\omega')^{3/2}} e^{-\frac{[(x-U_x t')^2 + r^2]}{4\omega'}} dt' \quad (118)$$

where ω' is the standard square deviation evaluated at the time $t-t'$ by the use of equation (108) and methods described in the following paragraphs. The possibility of an

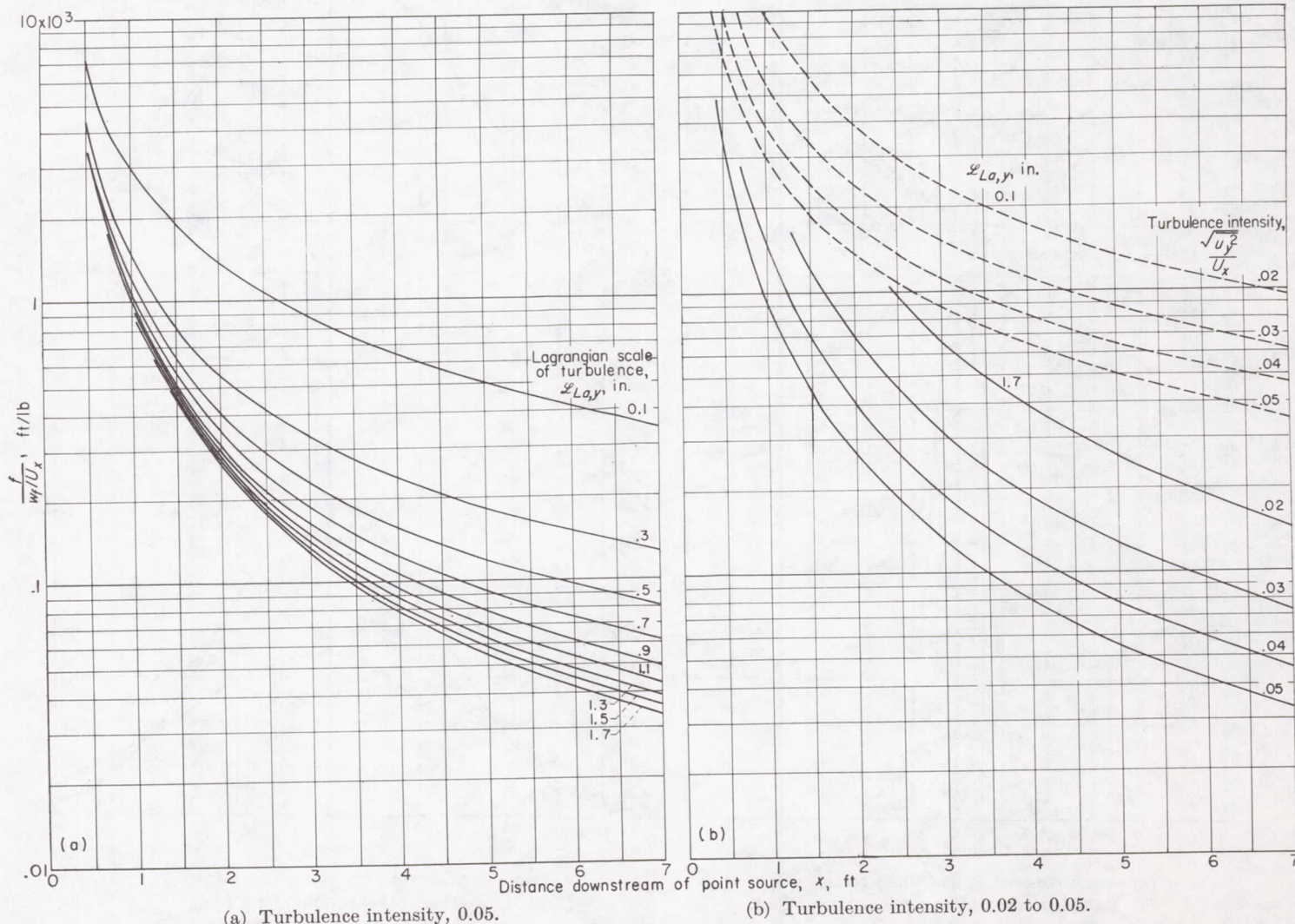


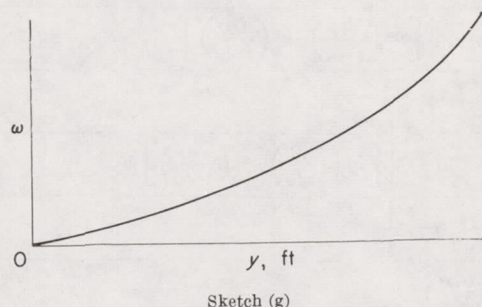
FIGURE 67.—Effect of scale of turbulence on axial fuel-air-ratio profile downstream of continuous point source of diffusion. Profiles based on equation (117); air density, 0.0764 pound per cubic foot.

analytic solution to equation (118) depends upon the functional form of $w'_{d,r}$, even when diffusion in the x -direction is neglected, with the integration performed over x . In cases where analytic solutions are impossible, recourse must be made to graphical integration or to differential analyzers (analog computers) such as described in reference 69.

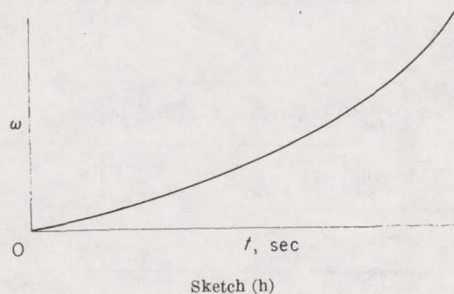
Standard square deviation: As discussed in a preceding section on the correlation coefficient, the Lagrangian parameters of turbulence cannot be measured by existing anemometry techniques; and, further, a theoretical relation between the Lagrangian and Eulerian parameters has not yet been found. This state of the science does not allow direct mathematical or graphical determination of the standard square deviation ω through equations (97), (98), (99), (108), and (109). Two alternatives are possible, the first of which is based on the results of reference 61. If the Eulerian correlation coefficient \mathcal{R}_{Eu} is known for the fluid stream in question, then the standard square deviation ω may be calculated from the equation

$$\omega = \int_0^y \int_0^y \mathcal{R}_{Eu} dy dy \quad (119)$$

so that a graph of ω is



Anemometry techniques for quick and simple measurement of $\mathcal{R}_{Eu}(y)$ are discussed in detail in reference 61. To obtain a graph of ω against t , the abscissa values are divided by $\mathcal{B}\sqrt{u_y^2}$, where \mathcal{B} was found to be 0.6 in reference 61:



When a functional relation between ω and t is obtained, the mixing problem may be solved analytically or graphically.

The second alternative involves the indirect measurement of the standard square deviation ω in the field of turbulence by utilizing known solutions for continuous point or line sources. This method has essentially been employed in references 60, 61, and 63, and is described briefly herein for a continuous point source of diffusion. Inspection of equation (117) reveals that, if the concentration \mathcal{C} of a gas were known at a number of points (x,r) downstream

of a point source emitting the gas at a continuous known rate w_f into a turbulent stream flowing at a known velocity U_x , the standard square deviation ω could be determined as a function of $t=x/U_x$. The instrumentation and equipment for such measurements would consist of a gas supply and tube injector, sampling probe(s), and a gas-concentration sensing instrument. The standard square deviation ω determined from such measurements could then be used in any equation shown in table III for the solution of diffusion problems having more complex source configurations, boundary conditions, or both. Of the two alternatives, this method seems to offer the best promise for accurate results but is far more cumbersome than the method described in the preceding paragraph.

Line, plane, surface, and volume sources: As mentioned previously, the instantaneous point-source solution may be used in the solution of all diffusion source configurations. The concentration \mathcal{C} at a point (x,r) is found by summing the contributions to that point from the infinite number of point sources which form the particular source configuration under study. Derivations of solutions for the various source configurations are not given herein, but a summary of equations is given in table III. Detailed derivations of these equations can be found in the references listed in the table. Many of the equations in table III do not have analytic solutions; hence, resort must be made to simplifying assumptions, graphical solution, or analog computers before direct solutions can be obtained.

Nonisotropic turbulent-flow fields.—The preceding discussion on the theory of turbulent diffusion and solution of the differential diffusion equations has assumed that the turbulent field is homogeneous and isotropic, which may reduce the applicability of the results in most jet-engine flow fields. Several methods for treating fields other than isotropic or homogeneous have been found and are discussed in following paragraphs.

Homogeneous fields: Frenkiel has suggested (ref. 55) solutions to diffusion problems where the turbulent diffusion coefficients are linearly related by

$$D_{T,x} = k_y^2 D_{T,y} = k_z^2 D_{T,z}$$

where k_y and k_z are constants of proportionality. If the molecular diffusion coefficient is negligible, equation (89) may be written

$$\frac{1}{D_{T,x}} \frac{\partial \mathcal{C}}{\partial t} = \frac{\partial^2 \mathcal{C}}{\partial x^2} + \frac{1}{k_y^2} \frac{\partial^2 \mathcal{C}}{\partial y^2} + \frac{1}{k_z^2} \frac{\partial^2 \mathcal{C}}{\partial z^2} \quad (120)$$

which may be transformed by the relation

$$\omega_x = \int_0^t D_{T,x} dt$$

into a generalized form

$$\frac{\partial \mathcal{C}}{\partial \omega_x} = \frac{\partial^2 \mathcal{C}}{\partial x^2} + \frac{\partial^2 \mathcal{C}}{\partial (k_y y)^2} + \frac{\partial^2 \mathcal{C}}{\partial (k_z z)^2} \quad (121)$$

The solution to equation (121) for an instantaneous point source of diffusion is

$$\mathcal{C} = \frac{w_d k_y k_z}{(4\pi \omega_x)^{3/2}} e^{-\frac{[(x-U_x t)^2 + k_y^2 y^2 + k_z^2 z^2]}{4\omega_x}} \quad (122)$$

TABLE III.—EQUATIONS FOR CONCENTRATION OF HEAT OR MASS DOWNSTREAM OF VARIOUS SOURCES^a

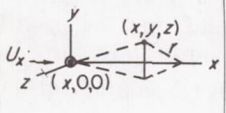
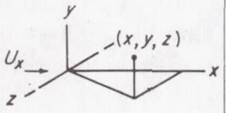
Source configuration	Type solution	Reference	Conditions	Range	Concentration equation, $\mathcal{C} =$
 <p>Point</p>	(b,c)	65 (p. 338)	-----	All t	$\frac{K_{ps}}{(4\pi\omega)^{3/2}} \exp\left\{-\frac{1}{4\omega}[(x-U_x t)^2 + r^2]\right\}$ (112)
	(c,d)	55	-----	All t	$\frac{w_d}{(4\pi)^{3/2}} \int_0^\infty \omega^{-3/2} \exp\left\{-\frac{1}{4\omega}[(x-U_x t)^2 + r^2]\right\} d\omega$ (113)
				$t \ll t_{La}$	$\frac{w_d \exp\left(-\frac{U_x^2 t^2}{2u_y^2}\right)}{(2\pi)^{3/2} \sqrt{u_y^2(x^2+r^2)}} \left\{1 + \frac{\pi}{2} \exp\left[\frac{x^2 U_x^2}{2u_y^2(x^2+r^2)}\right] \operatorname{erfc}\left[\frac{x U_x}{\sqrt{2} \sqrt{u_y^2(x^2+r^2)}}\right]\right\}$ (152)
	(d,e)	55	$\frac{\sqrt{u_y^2}}{U_x} \ll \frac{x}{\sqrt{x^2+r^2}}$ $0 < x > y, z$	$t \ll t_{La}$	$\frac{w_d U_x}{2\pi u_y^2 x^2} \exp\left(-\frac{U_x^2 r^2}{2u_y^2 x^2}\right)$ (114)
		51, 66	$\frac{\partial \mathcal{C}}{\partial x} \neq 0$	$t \gg t_{La}$	$\frac{w_d}{4\pi \sqrt{u_y^2} \mathcal{L}_{La,y}(x^2+r^2)^{1/2}} \exp\left\{\frac{U_x[x-(x^2+r^2)^{1/2}]}{2 \sqrt{u_y^2} \mathcal{L}_{La,y}}\right\}$ (115)
		67	$\frac{\partial \mathcal{C}}{\partial x} \neq 0, x > y, z$	$t \gg t_{La}$	$\frac{w_d}{4\pi \sqrt{u_y^2} \mathcal{L}_{La,y} x} \exp\left(-\frac{U_x r^2}{4 \sqrt{u_y^2} \mathcal{L}_{La,y} x}\right)$ (116)
		68	$\frac{\partial \mathcal{C}}{\partial x} = 0$	All t	$\frac{w_d}{4\pi U_x \omega} \exp\left(-\frac{r^2}{4\omega}\right)$ (117)
	(c,f)	65 (p. 339)	-----	All t	$\frac{1}{(4\pi)^{3/2}} \int_0^t \frac{w_d'}{(\omega')^{3/2}} \exp\left\{-\frac{1}{4\omega'}[(x-U_x t')^2 + r^2]\right\} dt'$ (118)
 <p>Line</p>	(b,c)	-----	Line source lying between $z=j, z=-j$ K_{ps} variable	All t	$\frac{1}{(4\pi)^{3/2}} \int_{-j}^j \frac{K_{ps}(z')}{\omega^{3/2}} \exp\left\{-\frac{1}{4\omega}[(x-U_x t)^2 + y^2 + (z-z')^2]\right\} dz'$ (153)
			Line source lying between $z=j, z=-j$	All t	$\frac{K_{ps}}{8\pi\omega} \exp\left\{-\frac{1}{4\omega}[(x-U_x t)^2 + y^2]\right\} \left[\operatorname{erf}\left(\frac{z+j}{2\sqrt{\omega}}\right) - \operatorname{erf}\left(\frac{z-j}{2\sqrt{\omega}}\right)\right]$ (154)
			Infinite length or bounded	All t	$\frac{K_{ps}}{4\pi\omega} \exp\left\{-\frac{1}{4\omega}[(x-U_x t)^2 + y^2]\right\}$ (155)
	(c,d)	-----	Line source lying between $z=j, z=-j$	All t	$\frac{w_d}{8\pi} \int_0^\infty \frac{1}{\omega} \exp\left\{-\frac{1}{4\omega}[(x-U_x t)^2 + y^2]\right\} \left[\operatorname{erf}\left(\frac{z+j}{2\sqrt{\omega}}\right) - \operatorname{erf}\left(\frac{z-j}{2\sqrt{\omega}}\right)\right] d\omega$ (156)
			Infinite length or bounded	All t	$\frac{w_d}{4\pi} \int_0^\infty \frac{1}{\omega} \exp\left\{-\frac{1}{4\omega}[(x-U_x t)^2 + y^2]\right\} d\omega$ (157)
	(d,e)	55	$\frac{y}{x} \frac{\sqrt{u_y^2}}{U_x} \ll 1$	$t \ll t_{La}$	$\frac{w_d}{\sqrt{2\pi} U_x \mathcal{L}_{La,x}} \exp\left(-\frac{U_x y^2}{2u_y^2 x^2}\right)$ (158)
			-----	$t \gg t_{La}$	$\frac{w_d}{2\pi U_x \mathcal{L}_{La}^2} \exp\left(-\frac{U_x x}{2 \sqrt{u_y^2} \mathcal{L}_{La}}\right) J_2\left(\frac{U_x \sqrt{x^2+y^2}}{2 \sqrt{u_y^2} \mathcal{L}_{La}}\right)$ (159)
			$\frac{y}{x} \ll 1$	$t \gg t_{La}$	$\frac{w_d (\sqrt{u_y^2})^{1/2}}{2 \sqrt{\pi} (U_x \mathcal{L}_{La})^{3/2} x^{1/2}} \exp\left(-\frac{U_x y^2}{4u_y^2 \mathcal{L}_{La} x}\right)$ (160)
			$\frac{y}{x} \frac{\sqrt{u_y^2}}{U_x} \ll 1$	All t	$\frac{w_d \sqrt{u_y^2}}{\sqrt{4\pi\omega} U_x \mathcal{L}_{La}} \exp\left(-\frac{y^2}{4\omega}\right)$ (161)
	(c,f)	-----	Line source lying between $z=j, z=-j$	All t	$\frac{1}{(4\pi)^{3/2}} \int_0^t \left(\int_{-j}^j \frac{w_d'(z',t')}{(\omega')^{3/2}} \exp\left\{-\frac{1}{4\omega'}[(x-U_x t')^2 + y^2 + (z-z')^2]\right\} dz'\right) dt'$ (162)
					$\frac{1}{8\pi} \int_0^t \frac{w_d'}{\omega'} \exp\left\{-\frac{1}{4\omega'}[(x-U_x t')^2 + y^2]\right\} \left[\operatorname{erf}\left(\frac{z+j}{2\sqrt{\omega'}}\right) - \operatorname{erf}\left(\frac{z-j}{2\sqrt{\omega'}}\right)\right] dt'$ (163)
			Infinite length or bounded	All t	$\frac{1}{4\pi} \int_0^t \frac{w_d'}{\omega'} \exp\left\{-\frac{1}{4\omega'}[(x-U_x t')^2 + y^2]\right\} dt'$ (164)
	(b,c)	51	Ring source of radius r_{rs}	All t	$\frac{K_{ps} r_{rs}}{4 \sqrt{\pi\omega^{3/2}}} \exp\left\{-\frac{1}{4\omega}[(x-U_x t)^2 + r^2 + r_{rs}^2]\right\} J_1\left(\frac{r_{rs} r}{2\omega}\right)$ (165)
	(d,e)	-----	Ring source of radius r_{rs}	All t	$\frac{w_d r_{rs}}{4 \sqrt{\pi}} \int_0^\infty \frac{1}{\omega^{3/2}} \exp\left\{-\frac{1}{4\omega}[(x-U_x t)^2 + r^2 + r_{rs}^2]\right\} J_1\left(\frac{r_{rs} r}{2\omega}\right) d\omega$ (166)
	(c,f)	-----	Ring source of radius r_{rs}	All t	$\frac{r_{rs}}{4 \sqrt{\pi}} \int_0^t \frac{w_d'}{(\omega')^{3/2}} \exp\left\{-\frac{1}{4\omega'}[(x-U_x t')^2 + r^2 + r_{rs}^2]\right\} J_1\left(\frac{r_{rs} r}{2\omega'}\right) dt'$ (167)
	(d,e)	73	Ring source of radius r_{rs} ; $\partial \mathcal{C} / \partial x = 0$	All t	$\frac{w_d}{4\pi U_x \omega} \exp\left[-\frac{1}{4\omega}(r_{rs}^2 + r^2)\right] J_1\left(\frac{r_{rs} r}{2\omega}\right)$ (168)

TABLE III.—EQUATIONS FOR CONCENTRATION OF HEAT OR MASS DOWNSTREAM OF VARIOUS SOURCES ^a—Concluded

Source configuration	Type solution	Reference	Conditions	Range	Concentration equation, $\mathcal{C} =$
Plane	(b,e)	-----	Plane lying between $y' = \pm a, z' = \pm b$	All t	$\frac{K_{ps}}{4\sqrt{4\pi\omega}} \exp\left[-\frac{(x-U_zt)^2}{4\omega}\right] \left[\operatorname{erf}\left(\frac{y+a}{2\sqrt{\omega}}\right) - \operatorname{erf}\left(\frac{y-a}{2\sqrt{\omega}}\right) \right] \left[\operatorname{erf}\left(\frac{z+b}{2\sqrt{\omega}}\right) - \operatorname{erf}\left(\frac{z-b}{2\sqrt{\omega}}\right) \right]$ (169)
			Infinite plane; $(y+a), (z+b) \gg \sqrt{4\omega}$	All t	$\frac{K_{ps}}{\sqrt{4\pi\omega}} \exp\left[-\frac{(x-U_zt)^2}{4\omega}\right]$ (170)
	(e,d)	-----	Infinite plane	All t	$\frac{w_d}{\sqrt{4\omega}} \int_0^\infty \frac{1}{\omega^{1/2}} \exp\left[-\frac{(x-U_zt')^2}{4\omega}\right] dt'$ (171)
	(e,f)	-----	Infinite plane	All t	$\frac{1}{\sqrt{4\omega}} \int_0^t \frac{w_d'}{(\omega')^{1/2}} \exp\left[-\frac{(x-U_zt')^2}{4\omega}\right] dt'$ (172)
	(b,e)	-----	Disk source of radius r_{ds}	All t	$\frac{K_{ps}}{4\sqrt{\pi\omega}} \exp\left\{-\frac{1}{4\omega}[(x-U_zt)^2+r^2]\right\} \left[\int_0^{r_{ds}^2/4\omega} e^{-\alpha} J_1\left(r\sqrt{\frac{\alpha}{\omega}}\right) d\alpha \right]$ (173)
	(e,d)	-----	Disk source of radius r_{ds}	All t	$\frac{w_d}{4\pi^{1/2}} \int_0^\infty \frac{1}{\omega^{1/2}} \exp\left\{-\frac{1}{4\omega}[(x-U_zt')^2+r^2]\right\} \left[\int_0^{r_{ds}^2/4\omega} e^{-\alpha} J_1\left(r\sqrt{\frac{\alpha}{\omega}}\right) d\alpha \right] dt$ (174)
	(e,f)	-----	Disk source of radius r_{ds}	All t	$\frac{1}{4\pi^{1/2}} \int_0^t \frac{w_d'}{(\omega')^{1/2}} \exp\left\{-\frac{1}{4\omega}[(x-U_zt')^2+r^2]\right\} \left[\int_0^{r_{ds}^2/4\omega'} e^{-\alpha} J_1\left(r\sqrt{\frac{\alpha}{\omega}}\right) d\alpha \right] dt'$ (175)
	(d,e)	73	Disk source of radius r_{ds} ; $\partial\mathcal{C}/\partial x=0$	All t	$\frac{w_d}{2\pi U_z r_{ds}^2 \omega} \exp\left(-\frac{r^2}{4\omega}\right) \int_0^{r_{ds}} r' \exp\left(-\frac{r'^2}{4\omega}\right) J_1\left(\frac{r r'}{2\omega}\right) dr'$ (176)
Surface	(b,e)	-----	Cylindrical surface of radius r_{cs} between $x=a, x=-a$	All t	$\frac{K_{ps} r_{cs}}{4\omega} \exp\left(-\frac{r^2+r_{cs}^2}{4\omega}\right) J_1\left(\frac{r r_{cs}}{2\omega}\right) \left\{ \operatorname{erf}\left[\frac{(x-U_zt)+a}{\sqrt{4\omega}}\right] - \operatorname{erf}\left[\frac{(x-U_zt)-a}{\sqrt{4\omega}}\right] \right\}$ (177)
			Cylindrical surface of radius r_{cs} with infinite length	All t	$\frac{w_d r_{cs}}{2\omega} \exp\left(-\frac{r^2+r_{cs}^2}{4\omega}\right) J_1\left(\frac{r r_{cs}}{2\omega}\right)$ (178)
	(e,d)	-----	Cylindrical surface of radius r_{cs} with infinite length	All t	$\frac{w_d r_{cs}}{2} \int_0^\infty \frac{1}{\omega} \exp\left(-\frac{r^2+r_{cs}^2}{4\omega}\right) J_1\left(\frac{r r_{cs}}{2\omega}\right)$ (179)
	(e,f)	-----	Cylindrical surface of radius r_{cs} with infinite length	All t	$\frac{r_{cs}}{2} \int_0^t \frac{w_d'}{\omega'} \exp\left(-\frac{r^2+r_{cs}^2}{4\omega'}\right) J_1\left(\frac{r r_{cs}}{2\omega'}\right) dt'$ (180)
	(b,e)	-----	Spherical surface of radius r_{ss}	All t	$\frac{K_{ps} r_{ss}}{\sigma(4\pi\omega)^{1/2}} \left\{ \exp\left[-\frac{(\sigma-r_{ss})^2}{4\omega}\right] - \exp\left[-\frac{(\sigma+r_{ss})^2}{4\omega}\right] \right\}$ (181)
	(e,d)	-----	Spherical surface of radius r_{ss}	All t	$\frac{w_d r_{ss}}{(4\pi)^{1/2}} \int_0^\infty \frac{1}{\sigma\omega^{1/2}} \left\{ \exp\left[-\frac{(\sigma-r_{ss})^2}{4\omega}\right] - \exp\left[-\frac{(\sigma+r_{ss})^2}{4\omega}\right] \right\} d\sigma$ (182)
	(e,f)	-----	Spherical surface of radius r_{ss}	All t	$\frac{r_{ss}}{(4\pi)^{1/2}} \int_0^\infty \frac{w_d'}{\sigma'(\omega')^{1/2}} \left\{ \exp\left[-\frac{(\sigma'-r_{ss})^2}{4\omega'}\right] - \exp\left[-\frac{(\sigma'+r_{ss})^2}{4\omega'}\right] \right\} d\sigma'$ (183)
	(b,e)	65 (p. 338)	K_{ps} variable over volume	All t	$\frac{1}{(4\pi\omega)^{3/2}} \iiint_{V'} K_{ps} \exp\left\{-\frac{1}{4\omega}[(x-x')^2+(y-y')^2+(z-z')^2]\right\} dV'$ (184)
Volume	(e,d)	-----	w_d' variable over volume	All t	$\frac{1}{(4\pi)^{3/2}} \int_0^\infty \frac{1}{\omega^{3/2}} \left(\iiint_{V'} w_d' \exp\left\{-\frac{1}{4\omega}[(x-x')^2+(y-y')^2+(z-z')^2]\right\} dV' \right) dt$ (185)

^a Symbols are explained as follows:

$$\operatorname{erf}(a) = \frac{2}{\sqrt{\pi}} \int_0^a e^{-\alpha^2} d\alpha$$

$$\operatorname{erfc}(a) = 1 - \operatorname{erf}(a)$$

$J_2(a)$ = modified Bessel function, second kind, zero order

$J_1(a)$ = modified Bessel function, first kind, zero order

$$r^2 = y^2 + z^2, \sigma^2 = (x - U_z t)^2 + y^2 + z^2$$

K_{ps} , w_d , and w_d' are independent of x , y , and z except where noted.

^b Instantaneous.

^c Exact.

^d Continuous.

^e Approximate.

^f Transient.

Solutions for other source configurations may be obtained by the summation method described in the preceding sections.

Nonhomogeneous fields: Diffusion processes may occur in portions of the jet-engine stream having appreciable turbulence intensity and velocity gradients, so that the turbulent diffusion coefficient may be a function of both time and space (assuming negligible molecular diffusion):

$$D_{T,x} = \mathcal{F}_x(t) F_x(x)$$

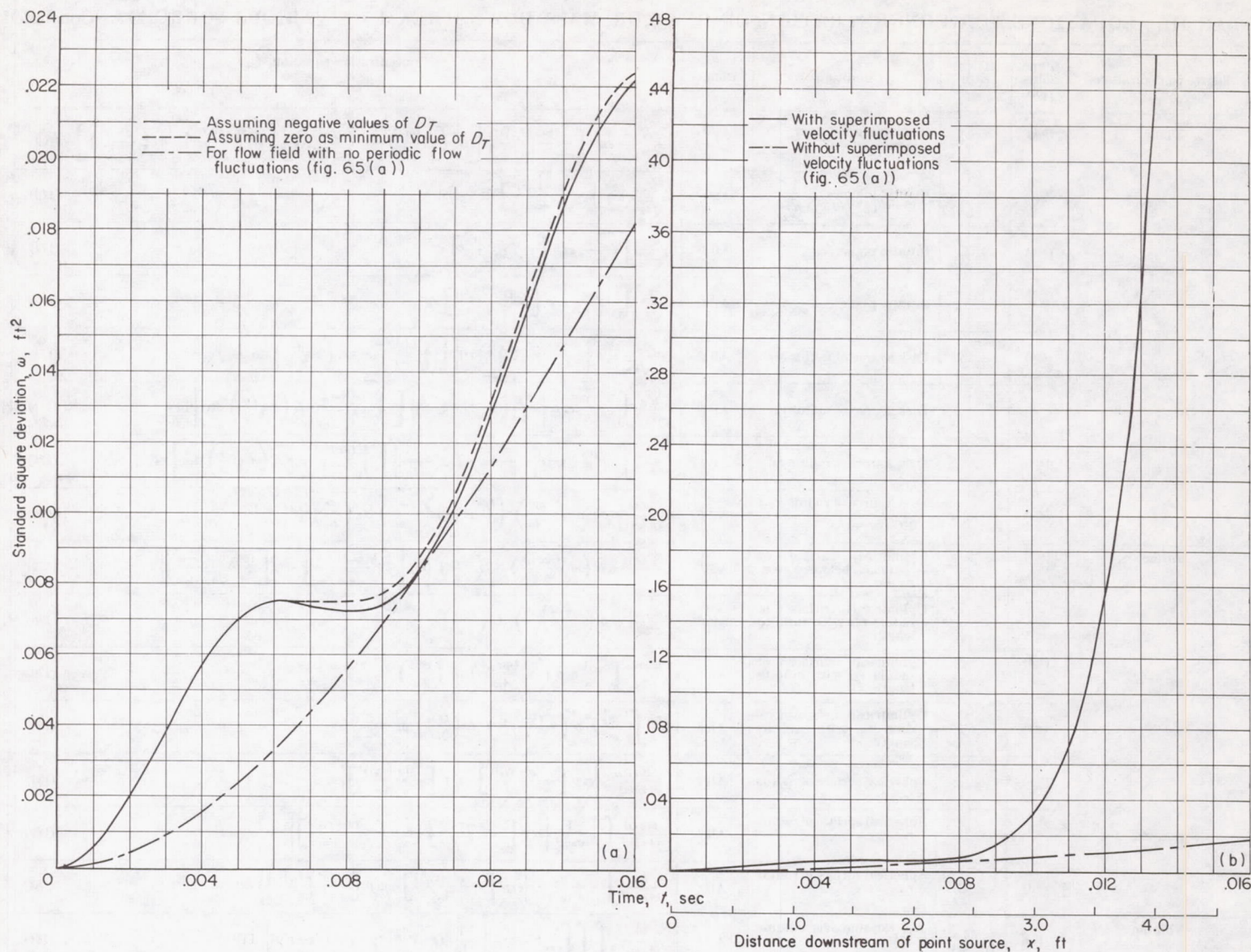
$$D_{T,y} = \mathcal{F}_y(t) F_y(y)$$

$$D_{T,z} = \mathcal{F}_z(t) F_z(z)$$

In this case, the differential equation of diffusion becomes

$$\frac{\partial \mathcal{C}}{\partial t} = \mathcal{F}_x(t) \frac{\partial}{\partial x} \left[F_x(x) \frac{\partial \mathcal{C}}{\partial x} \right] + \mathcal{F}_y(t) \frac{\partial}{\partial y} \left[F_y(y) \frac{\partial \mathcal{C}}{\partial y} \right] + \mathcal{F}_z(t) \frac{\partial}{\partial z} \left[F_z(z) \frac{\partial \mathcal{C}}{\partial z} \right] \quad (123)$$

Successful solution of equation (123) depends on the complexity of the space-time equations for the diffusion coefficients $D_{T,x}$, $D_{T,y}$, and $D_{T,z}$.



(a) Superimposed discrete velocity fluctuation.

(b) Superimposed velocity fluctuations over finite band width.

FIGURE 68.—Standard square deviation for turbulent-flow field with superimposed velocity fluctuations.

Turbulent-flow fields containing periodic flow fluctuations.—As mentioned in preceding sections of this chapter, flow fields encountered in jet engines may be substantially different from those found in fully developed turbulent flow in pipes or in turbulent flow behind grids. Since theoretical and experimental work in turbulent diffusion has mainly been confined to turbulent pipe flow or to flow fields behind grids, it is of interest to consider the effect of abnormal flow fields on diffusion.

Measurements of axial and lateral kinetic-energy spectra (ref. 70, fig. 14) and of sound spectra (ref. 70 and discussion in ch. VIII) indicate that flow fluctuations may be present in the form of discrete periodicities or in finite frequency bands. The spectrum density function for such turbulent fields may be written as

$$F(f_T) = \frac{\overline{u_y^2}}{\overline{u_{y,t}^2}} F(f_T) + \frac{\overline{u_{y,per}^2}}{\overline{u_{y,t}^2}} \delta(f_T - f_{per}) + \frac{\overline{u_{y,w}^2}}{\overline{u_{y,t}^2}} F(f_{per}) \quad (124)$$

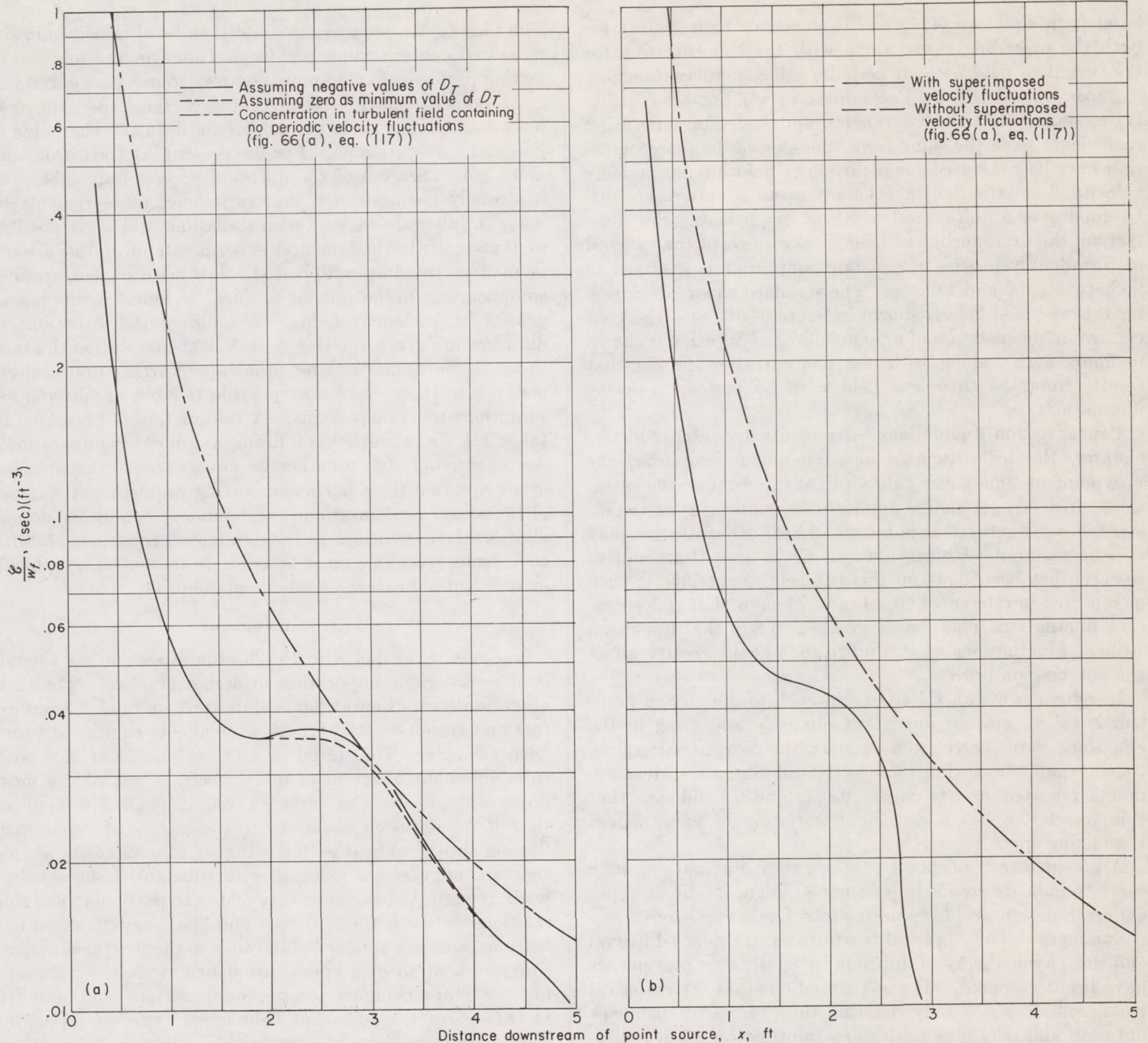
where $\overline{u_{y,per}^2}$ is the mean square of periodic velocity fluctuations; $\overline{u_{y,w}^2}$ is the mean square of periodic velocity fluctuations

having finite band width; and $\overline{u_{y,t}^2}$ is the total mean square of all velocity fluctuations, equal to

$$\overline{u_{y,t}^2} = \overline{u_y^2} + \overline{u_{y,per}^2} + \overline{u_{y,w}^2} \quad (125)$$

If the energy spectrum of a flow field is known and can be represented by an equation such as equation (124), the Eulerian correlation coefficient can be calculated from equation (103). Although a direct theoretical relation has not been determined between the Eulerian correlation coefficient \mathcal{R}_{Eu} and the Lagrangian correlation coefficient \mathcal{R}_{La} , it will be assumed herein that they are of the same form, so that the coefficient \mathcal{R}_{La} can be estimated for turbulent fields having abnormal spectra.

Superimposed discrete periodicities: To illustrate the possible effect of a discrete periodic velocity fluctuation at a particular frequency on turbulent diffusion, the flow field used for figure 66 is assumed to have an additional discrete velocity-fluctuation contribution at 100 cycles per second with a magnitude of 30 feet per second. The spectrum density function for this field is



(a) Superimposed discrete periodic velocity fluctuation.

(b) Superimposed velocity fluctuations over finite band width.

FIGURE 69.—Concentration downstream of point source of diffusion in turbulent-flow field with superimposed velocity fluctuations.

$$F_v(f_T) = \frac{4 \frac{L_{Eu,v}}{U_x} \frac{\overline{u_y^2}}{U_x^2} + \frac{\overline{u_{y,per}^2}}{U_x^2} \delta(f_T - 100)}{1 + \left(\frac{2\pi L_{Eu,v}}{U_x} \right)^2 f_T^2 \frac{\overline{u_y^2}}{U_x^2} + \frac{\overline{u_{y,per}^2}}{U_x^2}} \quad (126)$$

so that the Eulerian correlation coefficient becomes

$$R_{Eu,v} = \frac{\overline{u_y^2}}{U_x^2} e^{-\frac{x}{L_{Eu,v}}} + \frac{\overline{u_{y,per}^2}}{U_x^2} \cos \frac{2\pi f_T x}{U_x} \quad (127)$$

It will be assumed that the Lagrangian correlation coefficient has the same form as the Eulerian correlation coefficient:

$$R_{La,v} = \frac{\overline{u_y^2}}{U_x^2} e^{-t/L_{La}} + \frac{\overline{u_{y,per}^2}}{U_x^2} \cos 2\pi f_T t \quad (128)$$

from which the standard square deviation ω may be obtained:

$$\omega = 2.24 t + 0.0225 (e^{-100t} - 1) + 0.00057 (1 - \cos 200\pi t) \quad (129)$$

The standard square deviation as given by equation (129) is shown in figure 68(a) for two cases:

- (1) Assuming that the turbulent diffusion coefficient may have negative values
- (2) Assuming that the turbulent diffusion coefficient cannot have negative values and that, where the theoretical relations have negative values, the turbulent diffusion coefficient is zero

The standard square deviation shown in figure 65(a) is shown again in figure 68(a) for comparison. The concentration downstream of a point source of diffusion in the turbulent field containing the discrete velocity fluctuation was calcu-

lated from equation (117) and is shown in figure 69(a) for both the preceding cases, along with the concentration for the turbulent field without periodic velocity fluctuations.

Superimposed velocity fluctuations with finite band width: By assuming that the Lagrangian and Eulerian correlation coefficients have the same form, the standard square deviation may be evaluated for a turbulent field having periodic velocity fluctuations of a constant mean square value distributed over a finite band width of frequencies. For illustration, the same turbulent field is taken, except that a band of turbulent velocities of constant amplitude is assumed to lie between 100 and 130 cps. The standard square deviation for this assumed field is shown in figure 68(b), and the concentration downstream of a point source of diffusion is shown in figure 69(b), along with the concentration profile that results from the turbulent field with no periodic velocity fluctuations.

Concentration fluctuations.—As mentioned earlier in this chapter, the text discusses aerodynamic mixing from the viewpoint of time-mean values of heat and mass concentration. In many jet-engine applications, knowledge of the instantaneous fluctuations of mass and heat concentration may also be required. Unfortunately, only a limited amount of research has been done on this subject. Experiments such as reported in references 60, 71, and 72 show that concentration fluctuations may be as great as 0.8 of the time-mean value. Fluctuations of this magnitude could greatly affect the combustion process.

In reference 60, an Eulerian approach to the mixing problem is taken, and an important quantity appearing in the equations is the correlation between the concentration fluctuations and the turbulent velocity fluctuations. Measurements reported in references 60, 71, and 72 indicate that this correlation has a consistent variation in value across the mixing space.

Although the concept of concentration fluctuations may serve to indicate trends in jet-engine design, its direct application to design problems must await further research.

Summary.—The empirical treatment of turbulent diffusion and the Taylor theory of diffusion by continuous movements have been compared. It was pointed out that the empirical treatment does not fully describe the process of turbulent diffusion and may give misleading information when fundamental data are applied to full-scale engine design. The Taylor theory of diffusion requires quantitative knowledge of the Lagrangian parameters of the turbulent field under consideration before solution of particular mixing problems can be made. Since only the Eulerian parameters of the turbulent field can be measured by conventional anemometry techniques, two alternatives are suggested to obtain the Lagrangian parameters. The first alternative is to convert the Eulerian correlation coefficient to the Lagrangian correlation coefficient by means of an empirical method described in the section on standard square deviation. This requires either experimental measurement of the Eulerian coefficient by anemometry, or estimation from previous experience. The second alternative would employ a simple point or line source of diffusion of mass or heat, respectively, installed in the flow region of interest, and concentration-sensing instrumentation at points downstream of the diffusion source.

The Lagrangian parameters could then be obtained from the measured concentration profiles and used in the solution of mixing problems having more complex source configurations.

As pointed out in the preceding sections, periodic flow disturbances may seriously affect the diffusive character of jet-engine flow streams. For the present, at least, this may make generalization of the diffusion process impossible. It is strongly recommended that turbulence measurements be made in full-scale-engine test installations whenever possible so that realistic fundamental experiments on diffusion may be made. In addition to periodic flow disturbances, another complication of the mixing problem is found in nonhomogeneity of turbulent fields. The differential equations of diffusion are given for this case, but their solution depends upon the particular mixing problem. Further practical experience in these cases may provide reliable simplifying assumptions to the equations. A compilation is presented in table III for a variety of diffusion source configurations. Accompanying each equation are notes to assist the choosing of an equation for a particular mixing problem. A number of the source configurations and boundary conditions do not allow analytic solutions to the differential equations of diffusion; hence, recourse must be made to numerical, graphical, or differential-analyzer methods of solution.

FUEL-AIR MIXING

The mixing of fuel with the flowing stream in jet engines is of considerable importance in design practice. The fuel-air-ratio distribution at flame stabilizers in ramjet combustors and turbojet afterburners often affects engine performance strongly. The initial mixing of fuel and air, with subsequent introduction of dilution air, is one of the most important processes in turbojet combustors. The application of the diffusion equations to the mixing of vapor with flowing air and of heat with flowing air to some of the simple source configurations has met with substantial success, but much remains to be done in this field. In particular, suitable relations between the Eulerian and the Lagrangian turbulence parameters are needed in order to predict the standard square deviation of a given turbulent-flow field. Solutions for the more complex source configurations and detailed knowledge of the turbulent field in all types of jet-engine combustors would be of considerable utility to both design practice and research. The following sections discuss the current status of practical application of theory to fuel-air mixing and present suggested extensions to existing information on the fuel-air mixing of evaporating sprays in high-velocity airstreams.

Experiments on diffusion from simple point and line sources.—The turbulent diffusion of hydrogen and carbon dioxide from a point source in a flowing airstream conforms to equations (115) or (116), as reported in reference 68. As predicted by the Taylor theory of diffusion by continuous movements, the turbulent diffusion coefficient was found (1) to approach an asymptotic value with increase in distance downstream, (2) to be approximately directly proportional to the mean-stream velocity U_x (and hence $\sqrt{u_y^2}$, since $\sqrt{u_y^2}/U_x$ is substantially constant in fully developed pipe flow), and (3) to be proportional to duct size (and hence

$\mathcal{L}_{La,y}$, since $\mathcal{L}_{La,y}$ is proportional to pipe diameter in fully developed pipe flow). A similar experiment, reported in reference 63, shows that the diffusion of salt water from a point source in a turbulent water stream follows equation (117), and that the Lagrangian correlation coefficient follows the form given by equation (101).

The diffusion of naphtha injected at low velocity from a small tube into a high-velocity gas stream was found in reference 73 to follow equation (116) when an empirically determined turbulent diffusion coefficient was used. The turbulent diffusion coefficient was independent of stream static pressure (over a range of 4 to 55 lb/sq in. abs) as predicted by the theory of diffusion by continuous movements.

The diffusion of heat from a line source is reported in reference 74 to follow equation (161) (table III), where

$$\omega = \frac{1}{2} \overline{u_x^2} t^2 + \frac{\kappa}{\rho c_p} t \quad (130)$$

which is in agreement with the theoretical standard square deviation for $t \ll t_{La}$, as discussed previously.

The diffusion of heat from a line source in a turbulent stream has also been investigated (ref. 60) through a range of time such that the Lagrangian correlation coefficient could be evaluated. The mean temperatures in the heat wake behind the line source were found to follow a simple form of equation (161) (table III):

$$\frac{\Delta T}{(\Delta T)_0} = e^{-\frac{y^2}{4\omega}} \quad (131)$$

where the mean square deviation ω was a function of time and asymptotically approached a constant value.

Fuel droplet trajectories and impingement.—Aerodynamic mixing includes not only diffusion mixing of unlike gases but also the contact of liquid-fuel droplets with a gaseous medium into which the fuel may vaporize. In a turbojet combustor, liquid fuel generally is introduced in the form of a hollow-cone spray composed of fuel droplets that vary widely in size. The fuel is rapidly disintegrated by recirculatory currents induced in the primary combustion zone. In ramjet combustors, however, liquid fuel may be in the form of a fine spray introduced longitudinally into a high-velocity airstream. Much of the spray may be deposited on the flameholders, the amount depending on the fineness of the spray and the gas-stream velocity. Reference 75 suggests that the stability of flames behind a flameholder depends, among other things, upon the liquid fuel that collects upon the bluff object. A possible explanation of the entry of the collected fuel into the recirculatory zone downstream of the flameholder is the rearward flow of the liquid fuel to a downstream point on the flameholder, at which point the fuel is either sheared from the rod surface by the high-velocity airstream or is partially vaporized by heat conducted from the flameholder. Under either condition, much of the fuel is swept into the recirculatory zone. With such a combustion system, the rate at which fuel collects upon the bluff object, or the manner in which it is carried past (fuel droplet trajectories) can be important in stable and efficient combustion.

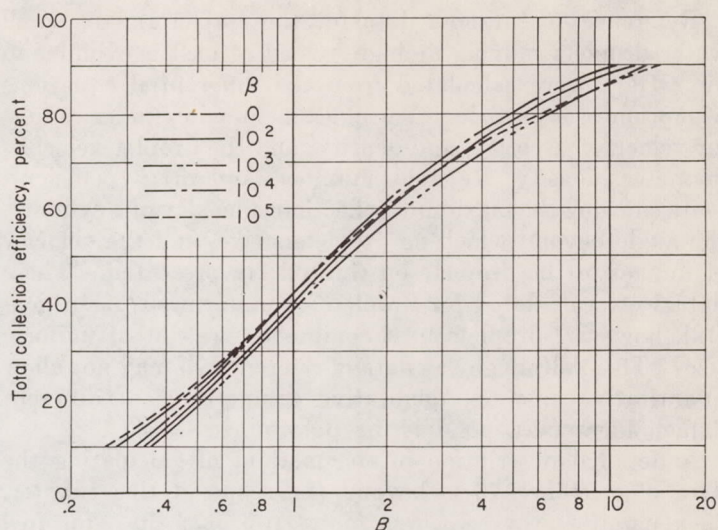


FIGURE 70.—Total liquid droplet collection efficiency of cylindrical rod in moving airstream (ref. 78).

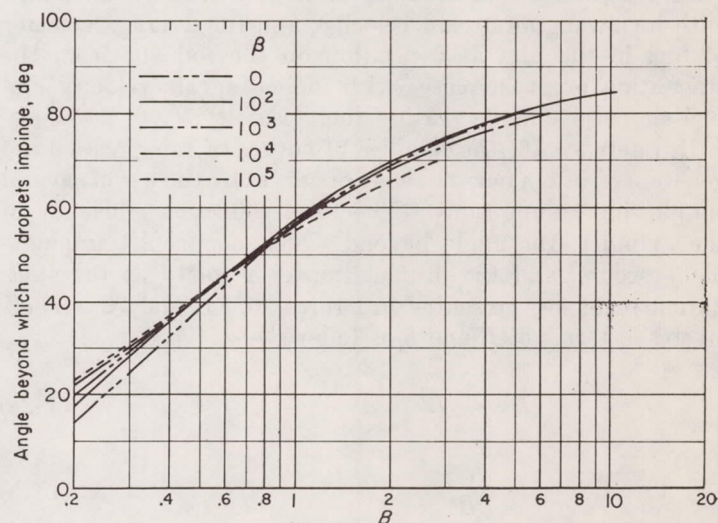


FIGURE 71.—Angle beyond which no liquid droplets impinge on cylindrical rod in moving airstream (ref. 78).

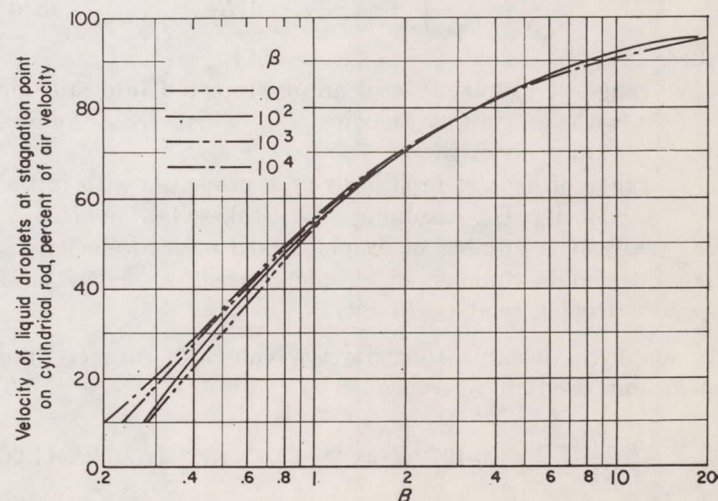


FIGURE 72.—Impact velocity of liquid droplets at stagnation point on cylindrical rod in moving airstream (ref. 78).

Reference 76 presents data for the trajectories of small water droplets moving at high velocities past a cylinder in air. Data were calculated from the differential equations of motion of a particle. Variables included cylinder radius, air velocity, viscosity, and density, and the droplet velocity, diameter, density, Reynolds number, and drag coefficient. Data showing the maximum collection efficiency of a cylinder, the angle beyond which no droplets strike, and the velocity of impact of the droplets on the rod are presented. These data were calculated for droplets of uniform size. In general, however, droplets in a combustor are not of uniform size. Thus, although the data of reference 76 may not allow quantitative answers, qualitative comparisons of different flameholders may possibly be determined.

A detailed description of the method of calculating the data of reference 76 is beyond the scope of this chapter. In general, however, it was found (ref. 77) that, for fuel collected on a cylindrical rod, the thickness of the fuel film decreases with decreasing fuel-air ratios and decreasing fuel viscosity, the point of maximum film thickness moves rearward and the film shape undergoes a marked change with increasing airstream velocity, and the average velocity of fuel in the film at a position on the rod 90° from the stagnation point increases with increasing air velocity and fuel-air ratio and decreasing fuel viscosity.

In reference 78, the families of curves of reference 76 are generalized into a narrow range of curves by the use of several simplifying assumptions. The total collection efficiency of the cylinder, the angle beyond which no droplet impingement occurs, and the droplet impact velocity at the stagnation point are presented in figures 70, 71, and 72, respectively, in terms of B and β as follows:

$$B = \frac{\Lambda}{\Lambda_s} B' \quad (132a)$$

$$\beta = \frac{Re_a^2}{B'} \quad (132b)$$

$$B' = \frac{4r_{dr}^2 U_a \rho_a}{9d_{cy} \mu_a} \quad (132c)$$

$$\frac{\Lambda}{\Lambda_s} = \frac{1}{Re_a} \int_0^{Re_a} \frac{24}{C_{D,dr} Re_{dr}} d(Re_{dr}) \quad (132d)$$

where

Λ range of droplet in still air if projected into still air with an initial velocity U_a , when $C_{D,dr}$ follows values given in ref. 76

Λ_s range of droplet in still air as a projectile with initial velocity U_a , assuming that Stokes' law holds

Re_a Reynolds number of droplet based on air velocity U_a

Re_{dr} Reynolds number of droplet based on velocity of droplet relative to air, $|U_{dr} - U_a|$

An empirical formula that fits the values of droplet drag coefficient used in reference 76 is

$$\frac{C_{D,dr} Re_{dr}}{24} = 1 + 0.197 (Re_{dr})^{0.63} + (2.6 \times 10^{-4}) (Re_{dr})^{1.38} \quad (133)$$

These data, like the data of reference 76, can be used best for qualitative comparisons of different flameholders.

Turbulent spreading of evaporating liquid-fuel droplets from fuel injectors.—Information pertaining to the liquid-fuel distribution in fuel sprays in high-velocity airstreams is limited mainly to simple-orifice contrastream injectors. Reference 42 relates the boundary geometry of liquid sprays from single-orifice injectors to spray variables such as injection angle, injection pressure, liquid density, and jet velocity; to injector variables such as strut shape and orifice diameter; and to airstream variables such as stream velocity and density. Liquid concentration profiles resulting from oblique injectors and from complex fuel injectors have not been reported.

The initial spreading of the fuel spray is due to the radial momentum imparted to the fuel droplets by the injector and depends on the variables discussed in chapter I. Further spreading takes place by virtue of the mixing action of the turbulent field and follows the same general laws as the diffusion of vapor or gas when initial spreading has been accounted for by assigning an appropriate source configuration. Diesel oil concentration profiles downstream of a simple-orifice contrastream fuel injector and of a hollow-cone spray nozzle are reported in reference 73. For a low liquid jet velocity, the concentration profiles follow the equation

$$f_l = \frac{w_f U_x}{4\pi G_a D_{Tx}} e^{-\frac{U_x r^2}{4D_{Tx}}} \quad (134)$$

(where f_l is liquid fuel-air ratio), which is identical to equation (116) (table III) if $D_T = \sqrt{u_y^2} \mathcal{L}_{La,y}$ as assumed in the reference. For a higher liquid jet velocity with the simple-orifice contrastream injector, the data of reference 73 fit the diffusion equation for a disk source:

$$f_l = \frac{w_f}{G_a r_{ds}^2} \psi \quad (135)$$

where f_l is total fuel-air ratio, and

$$\psi = \frac{U_x}{2\pi D_{Tx}} e^{-\frac{U_x r^2}{4D_{Tx}}} \int_0^{r_{ds}} r' e^{-\frac{U_x r'^2}{4D_{Tx}}} J_1 \left(\frac{U_x r' r}{2D_{Tx}} \right) dr'$$

so that equation (135) is identical to equation (176) (table III) if $\omega = D_T \frac{x}{U_x}$. The function ψ is plotted in reference 73 for a range of values of r/r_{ds} and $U_x r_{ds}^2 / 2D_{Tx}$, where the disk-source radius r_{ds} follows the empirical relation

$$\frac{r_{ds}}{r} = 11.2 \left(\frac{\rho_a U_x^2}{\rho_f U_{x,f}^2} \right)^{-1/4} \quad (136)$$

Concentration profiles downstream of the hollow-cone spray nozzle also followed equation (135) when an appropriate disk radius was used. It was found that the empirically determined diffusion coefficient for liquid-fuel droplets was identical for the three fuel-injection systems when airstream conditions were held constant.

The experimental work discussed in the preceding paragraph suggests that liquid-fuel spreading proceeded at a rate independent of fuel droplet size, since the concentration profiles conform to equations derived for continuous mediums. A detailed photographic study of isooctane fuel sprays

reported in reference 79 shows that the acceleration of evaporating fuel droplets to stream velocity was independent of drop size for the stream conditions investigated. Analysis of the data reported in reference 79 shows that, for the spray system studied, the droplet velocity conformed to the equation

$$U_{dr} = U_x(1 - e^{-337t}) \quad (137)$$

The time required for a fuel droplet to reach any station x downstream of the fuel injector was

$$x = U_x \left[t - \frac{1}{337} (1 - e^{-337t}) \right] \quad (138)$$

Two such distance-time curves based on the data from reference 79 are shown in figure 73, along with the linear time-distance curves $x = U_x t$ corresponding to the two stream velocities investigated in the reference.

The significance of equation (138) is shown by further analysis of liquid-fuel concentration profiles measured in the same fuel-injection system as the data of reference 79. These liquid-fuel concentration data (unpublished) were obtained during the fuel-spreading program reported in reference 80. The liquid-fuel concentration profiles follow a form based on equation (117) (table III):

$$f_i = \frac{w_f(1 - \epsilon_v)}{4\pi\rho_a U_x \omega_{lf}} e^{-\frac{r^2}{4\omega_{lf}}} \quad (139)$$

Values of ω_{lf} were determined from the liquid-fuel profiles at three different stations downstream of the fuel injector for the same stream conditions used in reference 79. Through the use of figure 73, the liquid-fuel standard square deviation can be plotted as a function of time, as shown in figure 74(a). As seen from the figure, the diffusion coefficient $D_{T,lf}$ for the liquid-fuel droplets is independent of both time and stream velocity over the range investigated. The experimental data of reference 73 include values of the diesel oil

droplet diffusion coefficient $D_{T,lf}$ at a fixed station downstream of the point-source injector for a range of stream velocities from 200 to 460 feet per second. The droplet diffusion coefficient $D_{T,lf}$ was found to be constant over this velocity range, which corroborates the data of figure 74(a). At the present time, no straightforward analysis is available that explains the independence of the liquid-fuel droplet diffusion coefficient from stream velocity.

A summary of unpublished data obtained in conjunction with the research reported in reference 80 is shown in figure 74(b), where the isooctane liquid-fuel droplet standard square deviation is plotted as a function of time. The time t was found from equation (138) for each data point, with the assumption that the liquid droplet acceleration was independent of stream pressure and temperature. The data scatter indicates that either the liquid droplet diffusion coefficient $D_{T,lf}$ or the liquid droplet axial acceleration, or both, may have a relation to stream temperature and pressure. Further experimental data on the acceleration of evaporating fuel droplets over a range of stream pressures and temperatures would be of great utility in evaluating the numerical constant in equations such as (137) and (138).

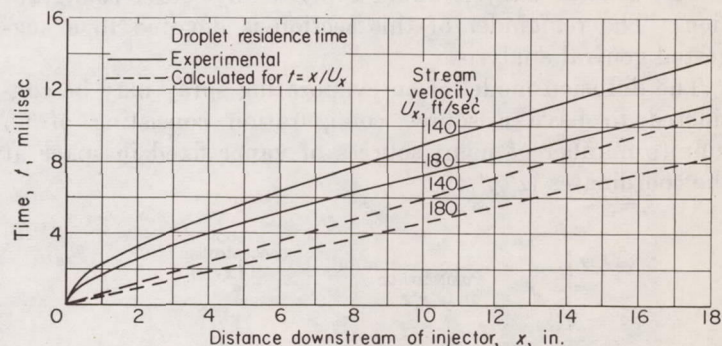


FIGURE 73.—Fuel droplet residence time in simple-orifice, contra-stream, isooctane evaporating spray (ref. 79).

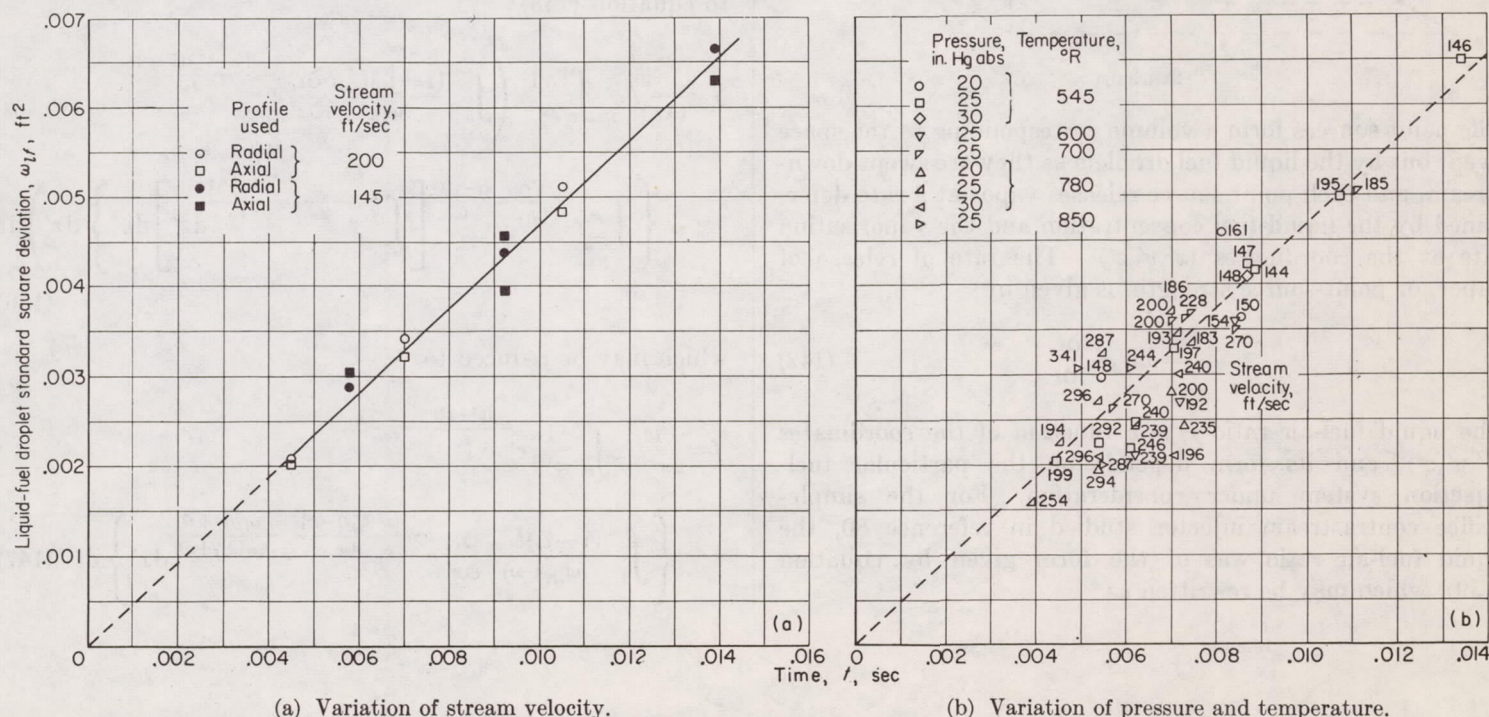


FIGURE 74.—Isooctane liquid-fuel droplet standard square deviation downstream of simulated point source.

Combined spreading of liquid and vapor fuel in high-velocity airstreams.—The spreading of evaporating liquid-fuel sprays is treated in reference 80, where isooctane was injected from a simple-orifice contrastream injector into a high-velocity airstream. The stream pressure and temperatures were varied over wide ranges, and vaporization rates (ch. I) and total fuel-spreading parameters were evaluated from the total fuel-concentration profiles, which followed the form

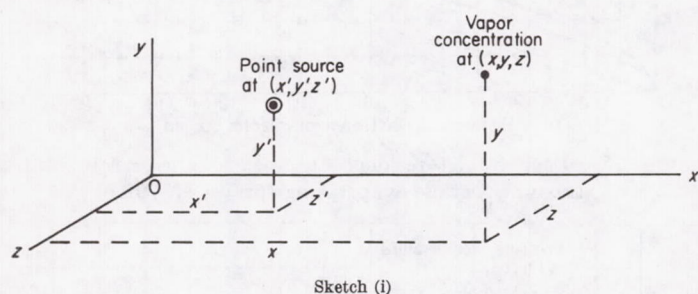
$$f_i = \frac{f_{ov} r_{ds}^2}{S} e^{-\frac{r^2}{S}} \quad (140)$$

Equation (140) is identical to equation (117) (table III) if $S=4\omega$. The total fuel-spreading parameter S was found to follow the correlation

$$S = 0.0598 \left(\frac{T}{1000} \right)^{0.67} P_f^{0.49} a^{0.79} \left(\frac{U_x}{100} \right)^{-0.85} P_a^{-0.57} x^{0.76} + 0.0042 \quad (141)$$

While the correlations presented in reference 80 hold for fuel injectors and airstream conditions used in the investigation, a more general analysis would apply to any source configuration. The remainder of this section is devoted to a suggested general analysis.

The diffusion model of an evaporating spray may be considered to have a source configuration consisting of an infinite number of point sources of vapor fixed in space at the coordinates (x', y', z') :



The point sources form a volume corresponding to the space swept out by the liquid fuel droplets as they are swept downstream, and each point source releases vapor at a rate determined by the liquid-fuel concentration and the vaporization rate at the coordinates (x', y', z') . The rate of release of vapor, or point-source strength, is given by

$$w_{a,f} = \rho_a U_x f_i \frac{\partial \iota_v}{\partial t} \quad (142)$$

The liquid fuel-air ratio f_i is a function of the coordinates (x', y', z') , and its form depends on the particular fuel-injection system under consideration. For the simple-orifice contrastream injector studied in reference 80, the liquid fuel-air ratio was of the form given by equation (139), which may be rewritten as

$$f_i = \frac{w_{a,f}(1-\iota_v)}{4\pi\rho_a U_x \omega_{lf}} e^{-\frac{(x'^2+y'^2)}{4\omega_{lf}}} \quad (143)$$

The vaporization rate $\partial \iota_v / \partial t$ appearing in equation (142) is discussed in chapter I. If the drop-size distribution is constant across a particular station, as was the case for the fuel sprays investigated in references 79 and 80 (and apparently in ref. 73), the vaporization rate $\partial \iota_v / \partial t$ is a function only of the distance x' . The functional relation between $\partial \iota_v / \partial t$ may be found by the equation

$$\frac{\partial \iota_v}{\partial t} = \frac{\partial \iota_v}{\partial x'} \frac{\partial x'}{\partial t} = U_{dr} \frac{\partial \iota_v}{\partial x'} \quad (144)$$

where the droplet velocity U_{dr} may be obtained from data such as those of reference 79 (shown in eq. (137)) and the axial gradient of the evaporated fraction $\partial \iota_v / \partial x'$ from data such as those of reference 80. The fraction of the total fuel evaporated at any particular station can be obtained as a function of the distance x' from data such as those of reference 80, as discussed in chapter I.

The vapor concentration at a point (x, y, z) (see sketch (i)) is given by equation (185) (table III), which may be written in terms of vapor fuel-air ratio as follows:

$$f = \frac{1}{(4\pi)^{3/2} \rho_a} \int_0^\infty \frac{1}{\omega^{3/2}} \left(\int_0^\infty e^{-\frac{[(x-U_x t)-x']^2}{4\omega}} \left\{ \int_{-\infty}^\infty e^{-\frac{(y-y')^2}{4\omega}} \left[\int_{-\infty}^\infty w_{a,f} e^{-\frac{(z-z')^2}{4\omega}} dz' \right] dy' \right\} dx' \right) dt \quad (145)$$

For the fuel-injection system described in reference 80, the relations given by equations (142) to (144) may be applied to equation (145):

$$f = \frac{w_f}{(4\pi)^{5/2} \rho_a} \int_0^\infty \frac{1}{\omega^{3/2}} \left(\int_0^\infty \frac{(1-\iota_v) U_{dr}}{\omega_{lf}} \frac{\partial \iota_v}{\partial x'} e^{-\frac{[(x-U_x t)-x']^2}{4\omega}} \left\{ \int_{-\infty}^\infty e^{-\frac{y'^2}{4\omega_{lf}}} e^{-\frac{(y-y')^2}{4\omega}} \left[\int_{-\infty}^\infty e^{-\frac{z'^2}{4\omega_{lf}}} e^{-\frac{(z-z')^2}{4\omega}} dz' \right] dy' \right\} dx' \right) dt \quad (146)$$

which may be reduced to

$$f = \frac{w_f}{2\pi^{3/2} \rho_a} \int_0^\infty \frac{1}{\omega^{3/2}} e^{-\frac{(y^2+z^2)}{4\omega}} \left\{ \int_0^\infty \frac{(1-\iota_v) U_{dr}}{(\omega_{lf} + \omega)} \frac{\partial \iota_v}{\partial x'} e^{-\frac{[(x-U_x t)-x']^2}{4\omega}} e^{-\frac{\omega_{lf}(y^2+z^2)}{\omega(\omega_{lf} + \omega)}} dx' \right\} dt \quad (147)$$

While ϵ , and ω , are known functions of x' , the integration over x' must be carried out for a number of values of t for each particular point (x, y, z) , so that the graphical solution of equation (147) would be tedious, even with the aid of a differential analyzer.

Effect of solid boundaries and flow-area changes on fuel spreading.—The effect of duct walls or other solid boundaries on both liquid-fuel droplet and fuel vapor concentrations is discussed in reference 73. The effect of walls on the liquid-fuel concentration is indeterminate, since the liquid may either adhere to the wall or reatomize back into the stream (ref. 73). For the vapor case, an exact solution has been obtained (ref. 73) for the vapor-fuel concentration profiles downstream of a point source located on the centerline of a circular duct. A graphical method for wall correction is proposed in the same reference, which compares well with both experimental data and the exact theoretical solution. The method essentially assumes that vapor is reflected from the walls and is directly additive to the theoretical concentration profile for an infinite duct. An empirical method for graphically determining fuel concentration profiles in ducts of changing area is discussed in reference 73.

Assumptions and procedure necessary for application to jet-engine design.—The information contained in the preceding portions of this chapter on aerodynamic mixing may be used to solve practical problems in jet-engine design. A typical problem is the positioning and spacing of fuel injectors in combustors. By following the procedure listed below, a direct solution to this problem may be obtained:

- (1) Determine the physical properties of the flow field:
 - (a) The radial velocity profile must be fairly flat.
 - (b) Reasonable variations in the axial velocity profile are permissible if the mixing process is considered on a time scale only.
 - (c) The turbulence must be fairly homogeneous throughout the mixing region. (Struts, fuel injectors, etc., may introduce considerable vortex streets.)
- (2) Determine the appropriate configuration of the mixing source. (See ref. 73 for some information on spray nozzles.)
- (3) Determine the functional relation between the standard square deviation and time, by one of the following methods:
 - (a) The experimental diffusion method described in the summary of the **Diffusion** section
 - (b) By hot-wire-anemometer measurements and the empirical relations in reference 61
 - (c) From estimation based on experience with similar flow fields
- (4) Solve for the fuel-air ratio (fuel concentration) at points of interest:

- (a) Use appropriate equation from table III.
- (b) Use summation principle for multiple source configurations.
- (c) Use instantaneous point-source solution (eq. (112)) and sum by integration for solution to configurations not listed in table III. (See eqs. (142) to (147) for an example.)

Summary.—Experiments on the diffusion of vapor and of heat from simple point and line sources substantiate many points in the Taylor theory of diffusion and in the analytical solutions of the differential equations of diffusion for such source configurations. The mean square deviation ω is a function of time asymptotically approaching a constant value and is independent of local static pressure.

In addition to the spreading of liquid-fuel droplets due to initial momentum imparted by the injection and atomization processes, liquid-fuel sprays mix further with the airstream because of turbulence present in the stream. Little work has been done on this subject to date, and available information seems to indicate that the turbulent mixing of fuel droplets follows the same general laws as those for vapor if special consideration is given to the aerodynamics of the droplet. Data taken over a limited range of stream and vaporization rate conditions seem to indicate that the turbulent diffusion coefficient for liquid-fuel droplets is constant, but no general laws have been substantiated by experiment. A suggested model for the combined spreading of liquid and vapor fuel is presented, and the mathematical analysis is carried to an integral form not subject to analytic solution in its present form.

JET MIXING

Mixing of gases having different temperatures or different components may occur in laminar flow or in flow having a turbulence that is either microscopic or macroscopic in character. In laminar flow, mixing is usually slow and depends upon molecular diffusion. In turbulent flow, mixing depends upon eddy diffusion, whereby eddies in one stream diffuse into the other streams, with a resulting increase in the mixing rate. Microscopic turbulence arises from flow in a smooth pipe at Reynolds numbers greater than the critical value, while macroscopic turbulence results from obstruction or path changes in the mixing chamber. Mixing in turbulent flow, especially macroscopic mixing, is probably of greater importance in combustor design than any of the other forms of mixing. In general, mixing of gases can be achieved by two major methods:

- (1) Subdivision of streams
- (2) Creation of turbulence

Mixing of gas streams by stream subdivision is discussed by Minchin in reference 81. For two parallel streams of gases having equal velocities but different temperatures, the

lateral temperature gradient due to microscopic mixing alone could be approximated by

$$\text{Temperature gradient} \approx 500(x)^{-0.61} \quad (148)$$

where x equals the distance from the junction of the two streams, and the temperature gradient, expressed in percentage of the maximum temperature difference per inch, is measured over a distance of $0.04 x$. These results were found to be independent of the absolute velocities of the gas stream, as long as the velocities were equal and the Reynolds numbers were above the critical value. For mixing between parallel streams varying both in temperature and velocity, little change was discerned in the mixing near the mixing origin. However, the effect of the different velocity became marked at distances farther downstream. It was immaterial which of the different temperature streams was the faster.

Variation of the angle of mixing between jets influences mixing. However, as shown in the following table, the effect of the angle is negligible for included angles of less than 45° :

Total angle between jets, deg	Temperature gradients, percent/in.			
	Distance downstream from junction, in.			
	2.5	5.5	8.5	11.5
0		157	114	95
10	309	160	114	92.5
20	279	159	141	102.0
30	254	163	122	100.5
45	205	131	95.5	60.0
60	197	101	72	41.0
75	172	67	37	18.0
90	164	54	31.7	11.7

In general, mixing due to microscopic turbulence between parallel streams of gases is quite slow. Mixing can be accelerated either by creation of macroscopic turbulence in the entering streams (e. g., by use of sharp S-bends before junction of the stream) or by use of a turbulence-producing device at the stream junctions. With the latter method, turbulence-producing devices introduced at the interface between streams to cause interlacing of the streams produced best results. Such devices are similar to the flameholders used in some ramjet engines.

A possible method of mixing discussed in reference 81 is the use of a cylindrical obstacle at the interface between two parallel gas streams. This mixing roll creates a vortex trail composed alternately of gases from the two different streams and provides gaps for penetration of gases from the opposite stream. Some data are reported in which the diameter of a cylinder between two parallel streams of gases at different temperatures was varied. Increasing mixing was obtained with diameter increases from $\frac{1}{4}$ to $\frac{3}{4}$ inch. However, the increased mixing was obtained at the expense of an increased pressure loss. Cylinders larger than $\frac{3}{4}$ inch in diameter effected no improvements in mixing.

The absolute velocity of the two streams with the mixing roll affects the degree of mixing in that similar temperature distributions require the same time interval for mixing. Differences in velocities of the two parallel streams hindered formation of the vortex trail and reduced the degree of mixing, although little effect was noted at velocity ratios greater than 2. As with mixing with parallel streams alone, it is immaterial which stream is the faster.

Some data have been recorded in which macroscopic turbulence was created in each of the individual gas streams before mixing. Data in which $\frac{1}{2}$ -inch-diameter cylinders or sharp S-bends were installed upstream of the junction of parallel gas streams indicate that large-scale upstream macro-turbulence reduces the mixing when the mixing-roll method is employed. However, in plain mixing between parallel gas streams, mixing was improved by the introduction of upstream turbulence-producing obstructions. Mixing between two concentric gas streams differing in temperature is similar to the mixing of two parallel gas streams. However, the mixing-roll method seems to be more effective with concentric gas streams than with parallel streams.

Pressure losses due to mixing of gas streams in the following three configurations are discussed in reference 82 (complete mixing of the two streams after their junction is assumed):

(1) For normal gas streams, expressions similar to those defining pressure losses due to heat addition can be utilized if the total-temperature ratio $T_{t,4}/T_{t,3}$ in equation (23) and figure 39 is replaced by

$$\frac{T_{t,4}}{T_{t,3}} = \frac{R_3 \gamma_3 (\gamma_4 - 1)}{R_4 \gamma_4 (\gamma_3 - 1)} \left(1 + \frac{w_{3b}}{w_3} \right) \left[1 + \frac{w_{3b} R_{3b} \gamma_{3b} T_{t,3b} (\gamma_3 - 1)}{w_3 R_3 \gamma_3 T_{t,3} (\gamma_{3b} - 1)} \right] \quad (149a)$$

where w_3 and w_{3b} are defined in table IV. For rapid approximation, the difference in the R 's and γ 's may be neglected, and equation (149a) reduces to

$$\frac{T_{t,4}}{T_{t,3}} = \left(1 + \frac{w_{3b}}{w_3} \right) \left(1 + \frac{w_{3b} T_{t,3b}}{w_3 T_{t,3}} \right) \quad (149b)$$

By use of this new value of over-all total-temperature ratio, the exit Mach number M_4 can be determined and the total-pressure losses due to complete mixing of two perpendicular gas streams can be found from either equation (22) or figure 39.

(2) The mixing of oblique gas streams is somewhat more complicated than the mixing of perpendicular gas streams. Additional parameters derived in reference 82 include

$$B^* = \left(1 + \frac{w_{3b} U_{3b}}{w_3 U_3} \cos \alpha \right) \quad (150a)$$

$$\begin{aligned} C^* &= \left(1 + \frac{w_{3b}}{w_3} \right) \sqrt{\frac{T_{t,4}}{T_{t,3}}} \\ &= \sqrt{\left(1 + \frac{w_{3b}}{w_3} \right) \left(\frac{R_3 \gamma_3}{R_4 \gamma_4} \right) \left(\frac{\gamma_4 - 1}{\gamma_3 - 1} \right) \left[1 + \frac{(w_{3b} R_{3b} \gamma_{3b} T_{t,3b} (\gamma_3 - 1))}{(w_3 R_3 \gamma_3 T_{t,3} (\gamma_{3b} - 1))} \right]} \end{aligned} \quad (150b)$$

where α is the included angle between the gas streams. As

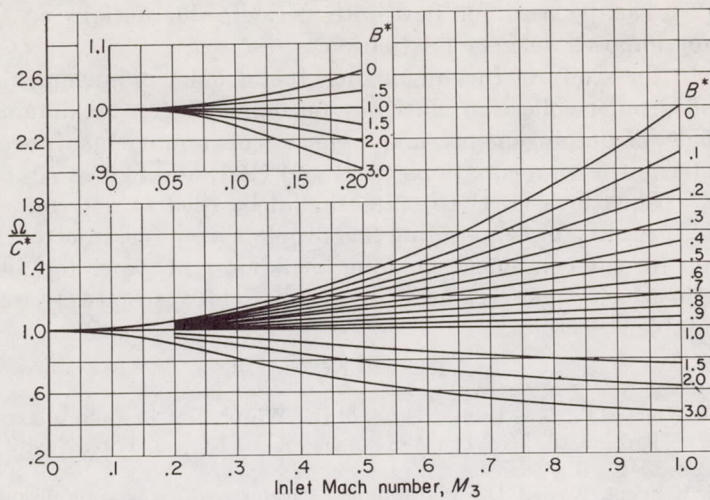


FIGURE 75.—Values of parameter Ω for determination of mixing pressure losses of oblique and parallel gas streams (ref. 82).

before, the differences in R 's and γ 's may be neglected for rapid approximations, and equation (150b) reduces to

$$C^* = \sqrt{\left(1 + \frac{w_{3b}}{w_3}\right) \left(1 + \frac{w_{3b} T_{t,3b}}{w_3 T_{t,3}}\right)} \quad (150c)$$

A new parameter Ω , which is defined as

$$\frac{\Omega}{C^*} = \frac{1 + \gamma_3 M_3^2}{1 + B^* \gamma_3 M_3^2} \quad (150d)$$

is used in determining the exit Mach number. Values of Ω/C^* for various inlet Mach numbers and values of B^* , and γ_3 of 1.4 are presented in figure 75. The value of exit Mach

number M_4 can be found by substituting Ω^2 for $T_{t,4}/T_{t,3}$ in figure 39 or equation (23). Total-pressure losses due to mixing of the two oblique streams can then be found from

$$\left(\frac{\Delta P_t}{P_{t,3}}\right)_{ob} = 1 - \left(\frac{1 + \gamma_3 B^* M_3^2}{1 + \gamma_4 M_4^2}\right) \frac{\left(1 + \frac{\gamma_4 - 1}{2} M_4^2\right)^{\frac{\gamma_4}{\gamma_4 - 1}}}{\left(1 + \frac{\gamma_3 - 1}{2} M_3^2\right)^{\frac{\gamma_3}{\gamma_3 - 1}}} \quad (150e)$$

(3) Mixing in parallel gas streams is treated in reference 82 in much the same manner as oblique streams, except that a term which includes the area ratio is added. For mixing of parallel gas streams, as shown in table IV, the parameters B^* and C^* are defined as

$$B^* = \mathcal{A} \left(1 + \frac{w_{3b} U_{3b}}{w_3 U_3}\right) \quad (151a)$$

$$C^* = \mathcal{A} \left(1 + \frac{w_{3b}}{w_3}\right) \sqrt{\frac{T_{t,4}}{T_{t,3}}} \\ = \mathcal{A} \sqrt{\left(1 + \frac{w_{3b}}{w_3}\right) \left(\frac{R_3 \gamma_3}{R_4 \gamma_4}\right) \left(\frac{\gamma_4 - 1}{\gamma_3 - 1}\right) \left[1 + \frac{(w_{3b} R_{3b} \gamma_{3b} T_{t,3b})(\gamma_3 - 1)}{(w_3 R_3 \gamma_3 T_{t,3})(\gamma_3 - 1)}\right]} \quad (151b)$$

where \mathcal{A} is the ratio of jet flow area A_3 to mixed-jet flow area A_4 . For constant R and γ , equation (151b) reduces to

$$C^* = \mathcal{A} \sqrt{\left(1 + \frac{w_{3b}}{w_3}\right) \left(1 + \frac{w_{3b} T_{t,3b}}{w_3 T_{t,3}}\right)} \quad (151c)$$

The parameter Ω , which can be determined either from equation (150d) or from figure 75, applies to parallel-jet mixing as well as to the mixing of oblique jets. However, the appropriate values of B^* and C^* from equations (151a, b, or

TABLE IV.—ARRANGEMENTS FOR MIXING OF GAS STREAMS (Ref. 82)

Gas stream	Arrangement	B^*	C^* (for constant R and γ)	$\frac{\Omega}{C^*}$
Normal		1	$\sqrt{\left(1 + \frac{w_{3b}}{w_3}\right) \left(1 + \frac{w_{3b} T_{t,3b}}{w_3 T_{t,3}}\right)}$	1
Oblique		$\left(1 + \frac{w_{3b} U_{3b}}{w_3 U_3} \cos \alpha\right)$	$\sqrt{\left(1 + \frac{w_{3b}}{w_3}\right) \left(1 + \frac{w_{3b} T_{t,3b}}{w_3 T_{t,3}}\right)}$	From fig. 75 or eq. (150d)
Parallel		$\mathcal{A} \left(1 + \frac{w_{3b} U_{3b}}{w_3 U_3}\right)$	$\mathcal{A} \sqrt{\left(1 + \frac{w_{3b}}{w_3}\right) \left(1 + \frac{w_{3b} T_{t,3b}}{w_3 T_{t,3}}\right)}$	From fig. 75 or eq. (150d)

c) must be used. As with the mixing of oblique gas streams, the exit Mach number can be found by substituting Ω^2 for $T_{t,4}/T_{t,3}$ in figure 39 or equation (23). The pressure drop due to mixing of two parallel gas streams can then be found from equation (150e), which also applies to normal gas streams.

DESIGN SUMMARY

The object of this chapter has been to present aerodynamic relations applicable to the design of the combustion chambers of jet engines. The designers of combustion chambers are generally interested in the combustor approach-stream parameters, combustor pressure losses, jet penetration and mixing, orifice coefficients, turbulence levels, and fuel injection and spreading.

For the designer of combustion chambers of turbojet or ramjet engines, equations (1) to (14) and figures 31 to 33 are suitable for determining approach-stream parameters of pressure, temperature, and velocity. Equation (15) and figure 34 may be used to estimate the effect of combustor pressure losses on over-all cycle performance. In accounting for the effect on combustor pressure losses of abrupt changes in cross-sectional flow area, bluff bodies or flameholders, friction forces, and momentum changes imparted to the gases, equations (16) to (34) and figures 35 to 41 can be used. Pressure losses due to jet mixing can be estimated from equations (149) to (151) and figure 75. Equation (35) can be used to correlate combustor pressure losses.

Many applications in combustion chambers require a knowledge of jet mixing parameters. Theoretical velocity profiles in free jets are best expressed by equations (41) and (43) and figure 43. Theoretical free-jet temperature profiles are best expressed by equation (49) and figure 44. For coaxial jets, theoretical parameters can be obtained from figures 45 and 46. Equations (53) to (56) theoretically relate the penetration of air jets to duct dimensions and jet and stream parameters.

Recommended experimental data on velocity profiles in free jets are contained in equations (58) to (61) and figures 47 to 49. Experimental temperature profiles in free jets can be determined from equation (67) and figures 50 and 51. Turbulence intensities in free jets can be determined from figure 52, and the scale of turbulence in jets can be found from equations (68) and (69) or figure 53. If the jets are coaxial, equations (73) to (78) are recommended for experimental correlation of jet size and velocity parameters. Experimental data on jet penetration and temperature distributions are contained in figures 54 to 56. To account for jet interaction, equations (84) and (85) and figure 57 are suitable. Orifice coefficients, required to calculate the flow through combustion-chamber openings, can be determined from figures 58 to 60.

For theoretical background in the study of diffusion in the combustor, equations (89) to (111) may be used. Useful expressions for instantaneous and continuous point sources of diffusion are equations (112) to (118). In addition, table III contains a large number of equations giving the concentration at a point for many conditions with point, line, plane, surface, and volume sources. For nonisotropic fields, equations (120) to (123) are available. Equations (124) to

(129) can be used for flow with periodic fluctuations or a superimposed velocity fluctuation.

In the study of fuel-air mixing, fuel droplet impingement and droplet collection efficiency on flameholders, maximum angle of impingement, and velocity of impingement are determined from equations (132) and (133) and figures 70 to 72. Equations (134) to (139) should be used to determine the spreading of evaporating fuel droplets from fuel injectors. And for the combined spreading of liquid and vapor fuel in high-velocity gas streams, equations (140) to (147) are suitable.

REFERENCES

1. Whittle, F.: The Early History of the Whittle Jet-Propulsion Gas Turbine, pt. II. The Aeroplane, vol. LXIX, no. 1797, Nov. 2, 1945, pp. 503-507.
2. Sanders, Newell D.: Performance Parameters for Jet-Propulsion Engines. NACA TN 1106, 1946.
3. Wallner, Lewis E., and Fleming, William A.: Reynolds Number Effect on Axial-Flow Compressor Performance. NACA RM E9G11, 1949.
4. Fleming, William A.: Turbojet Performance Characteristics and Research Techniques. Lecture 3, Gas Turbine and Free Piston Engine Lectures, Frank L. Schwartz, ed., Dept. Mech. and Ind. Eng., Univ. of Mich., June 13-17, 1955.
5. Lloyd, Peter: Combustion in the Gas Turbine—A Survey of War-Time Research and Development. R. & M. No. 2579, British ARC., May 1946.
6. Lovesey, A. C.: Modern Methods of Testing Aero-Engines and Power Plants. Jour. Roy. Aero. Soc., vol. 54, no. 474, June 1950, pp. 327-358.
7. DeZubay, E. A.: Combustion Processes and Their Application in Gas Turbines. Gas Turbine Lectures, Dept. Mech. and Ind. Eng., Univ. Mich., June 29-July 9, 1953, pp. 510-558.
8. Yellott, J. I., and Lype, E. F.: Some Effects of Pressure Loss on the Open-Cycle Gas-Turbine Power Plant. Trans. ASME, vol. 69, no. 8, Nov. 1947, pp. 903-911.
9. Schutt, H. C.: Losses of Pressure Head Due to Sudden Enlargement of a Flow Cross-Section. Trans. ASME (Hydraulics), vol. 51, no. 15, May-Aug. 1929, pp. 83-87.
10. Committee A-9, Aircraft Air Conditioning Equipment: Airplane Heating and Ventilating Equipment—Engineering Data—Fluid Dynamics. Aero. Info. Rep. No. 23, SAE, 1951, pp. 5-8.
11. Patterson, G. N.: Modern Diffuser Design. The Efficient Transformation of Kinetic Energy to Pressure. Aircraft Eng., vol. X, no. 115, Sept. 1938, pp. 267-273.
12. Sanger, E., and Bredt, I.: A Ram-Jet Engine for Fighters. NACA TM 1106, 1947.
13. Valentine, E. Floyd, and Carroll, Raymond B.: Effects of Several Arrangements of Rectangular Vortex Generators on the Static-Pressure Rise Through a Short 2:1 Diffuser. NACA RM L50L04, 1951.
14. Reid, Elliott G.: Performance Characteristics of Plane-Wall Two-Dimensional Diffusers. NACA TN 2888, 1953.
15. Perry, John H., ed.: Chemical Engineers' Handbook. Third ed., McGraw-Hill Book Co., Inc., 1950, pp. 387-388.
16. Friedman, J., Bennet, W. J., and Zwick, E. B.: The Engineering Application of Combustion Research to Ramjet Engines. Fourth Symposium (International) on Combustion, The Williams & Wilkins Co., 1953, pp. 756-764.
17. McAdams, W. H.: Heat Transmission. Second ed., McGraw-Hill Book Co., Inc., 1942, p. 119.
18. Knight, H. A., and Walker, R. B.: The Component Pressure Losses in Combustion Chambers. Rep. No. R.143, British N.G.T.E., Nov. 1953.
19. Shapiro, Ascher H., and Hawthorne, W. R.: The Mechanics and Thermodynamics of Steady One-Dimensional Gas Flow. Jour. Appl. Mech., vol. 14, no. 4, Dec. 1947, pp. A317-A336.

20. Younger, George G., Gabriel, David S., and Mickelsen, William R.: Experimental Study of Isothermal Wake-Flow Characteristics of Various Flame-Holder Shapes. NACA RM E51K07, 1952.
21. Goldstein, Sydney, ed.: Modern Developments in Fluid Dynamics. Vols. I and II. The Clarendon Press (Oxford), 1938.
22. Williams, G. C., Hottel, H. C., and Scurlock, A. C.: Flame Stabilization and Propagation in High Velocity Gas Streams. Third Symposium on Combustion and Flame and Explosion Phenomena, The Williams & Wilkins Co. (Baltimore), 1949, pp. 21-40.
23. Prandtl, L., and Tietjens, O. G.: Applied Hydro- and Aeromechanics. McGraw-Hill Book Co., Inc., 1934, pp. 130-136.
24. Pinkel, I. Irving, and Shames, Harold: Analysis of Jet-Propulsion-Engine Combustion-Chamber Pressure Losses. NACA Rep. 880, 1947. (Supersedes NACA TN 1180.)
25. Lubbock, I.: Combustion Problems of the Gas Turbine. Aircraft Eng., vol. XXIII, no. 269, July 1951, pp. 196-202; 213.
26. Childs, J. Howard, McCafferty, Richard J., and Surine, Oakley W.: Effect of Combustor-Inlet Conditions on Performance of an Annular Turbojet Combustor. NACA Rep. 881, 1947. (Supersedes NACA TN 1357.)
27. Tollmien, Walter: Calculation of Turbulent Expansion Processes. NACA TM 1085, 1945.
28. Taylor, G. I.: The Transport of Vorticity and Heat Through Fluids in Turbulent Motion. Proc. Roy. Soc. (London), ser. A, vol. 135, no. A828, Apr. 1, 1932, pp. 685-702.
29. Abramovich, G. N.: The Theory of a Free Jet of a Compressible Gas. NACA TM 1058, 1944.
30. Howarth, L.: Concerning the Velocity and Temperature Distributions in Plane and Axially Symmetric Jets. Proc. Cambridge Phil. Soc., vol. 34, 1938, pp. 185-203.
31. Squire, H. B., and Trouncer, J.: Round Jets in a General Stream. R. & M. No. 1974, British A.R.C., 1944.
32. Hawthorne, W. R., Rogers, G. F. C., and Zaczek, B. Y.: Mixing of Gas Streams—The Penetration of a Jet of Cold Air into a Hot Stream. Tech. Note No. Eng. 271, British R.A.E., Mar. 1944.
33. Ehrich, Fredric F.: Penetration and Deflection of Jets Oblique to a General Stream. Jour. Aero. Sci., vol. 20, no. 2, Feb. 1953, pp. 99-104.
34. Taylor, J. F., Grimmer, H. L., and Comings, E. W.: Isothermal Free Jets of Air Mixing with Air. Chem. Eng. Prog., vol. 47, no. 4, Apr. 1951, pp. 175-180.
35. Forstall, Walton, Jr., and Shapiro, Ascher H.: Momentum and Mass Transfer in Coaxial Gas Jets. Meteor. Rep. No. 39, Dept. Mech. Eng., M. I. T., July 1949. (Bur. Ord. Contract NOrd 9661.)
36. Squire, H. B.: Jet Flow and Its Effects on Aircraft. Aircraft Eng., vol. XXII, no. 253, Mar. 1950, pp. 62-67.
37. Corrsin, Stanley: Investigation of Flow in an Axially Symmetrical Heated Jet of Air. NACA WR-94, 1943. (Supersedes NACA ACR 3L23.)
38. Reichardt, H.: On a New Theory of Free Turbulence. R.T.P. Trans. No. 1686, British M.A.P. (See also Z.a.M.M., Bd. 21, Heft 5, Oct. 1941, pp. 257-264.)
39. Laurence, James C.: Intensity, Scale, and Spectra of Turbulence in Mixing Region of Free Subsonic Jet. NACA Rep. 1292, 1956. (Supersedes NACA TN's 3561 and 3576.)
40. Pfeiffer, Arthur, Murati, George T., and Engel, Arthur B.: Mixing of Gas Streams. M. S. Thesis, M. I. T., 1945.
41. Callaghan, Edmund E., and Ruggeri, Robert S.: Investigation of the Penetration of an Air Jet Directed Perpendicularly to an Air Stream. NACA TN 1615, 1948.
42. Chelko, Louis J.: Penetration of Liquid Jets into a High-Velocity Air Stream. NACA RM E50F21, 1950.
43. Callaghan, Edmund E., and Ruggeri, Robert S.: A General Correlation of Temperature Profiles Downstream of a Heated-Air Jet Directed Perpendicularly to an Air Stream. NACA TN 2466, 1951.
44. Baron, Thomas, and Alexander, L. G.: Momentum, Mass, and Heat Transfer in Free Jets. Chem. Eng. Prog., vol. 47, no. 4, Apr. 1951, pp. 181-185.
45. Alexander, Lloyd G., Baron, Thomas, and Comings, Edward W.: Transport of Momentum, Mass, and Heat in Turbulent Jets. Bull. Ser. No. 413, Univ. of Ill., 1953.
46. Baron, T., and Bollinger, E. H.: Mixing of High-Velocity Air Jets. Tech. Rep. No. CML-3, Eng. Exp. Station, Univ. of Ill., Mar. 1, 1952. (Contract DA-18-064-CML-445, Army Chem. Corps, Army Dept.)
47. Grimmer, Howard L.: Entrainment in Air Jets. Ph.D. Thesis, Univ. of Ill., 1950.
48. Callaghan, Edmund E., and Bowden, Dean T.: Investigation of Flow Coefficient of Circular, Square, and Elliptical Orifices at High Pressure Ratios. NACA TN 1947, 1949.
49. Seglem, Clifford E.: The Discharge Coefficient of a Combustor Air Inlet Hole. M. S. Thesis, Univ. of Pittsburgh, 1952.
50. Churchill, Ruel V.: Fourier Series and Boundary Value Problems. McGraw-Hill Book Co., Inc., 1941.
51. Carslaw, H. S., and Jaeger, J. C.: Conduction of Heat in Solids. Univ. Press (Oxford), 1947.
52. Van Dusen, M. S.: Note on the Theory of Heat Conduction. Bur. Standards Jour. Res., RP 178, vol. 4, no. 6, June 1930, pp. 753-756.
53. Taylor, G. I.: Diffusion by Continuous Movements. Proc. London Math. Soc., vol. 20, 1922, pp. 196-212.
54. Glasstone, Samuel: Text-Book of Physical Chemistry. Second ed., D. Van Nostrand Co., Inc., 1946.
55. Frenkiel, F. N.: Turbulent Diffusion: Mean Concentration Distribution in a Flow Field of Homogeneous Turbulence. Vol. III of Advances in Appl. Mech., Richard von Mises and Theodore von Kármán, eds., Academic Press, Inc., 1953, pp. 61-107.
56. Taylor, G. I.: The Statistical Theory of Turbulence, pt. II. Proc. Roy. Soc. (London), ser. A, vol. 151, no. 833, 1935, pp. 444-454.
57. von Kármán, Theodore, and Howarth, Leslie: On the Statistical Theory of Isotropic Turbulence. Proc. Roy. Soc. (London), ser. A, vol. 164, Jan. 21, 1938, pp. 192-215.
58. Laurence, James C., and Landes, L. Gene: Auxiliary Equipment and Techniques for Adapting the Constant-Temperature Hot-Wire Anemometer to Specific Problems in Air-Flow Measurements. NACA TN 2843, 1952.
59. Kovátszay, Leslie S. G.: Development of Turbulence-Measuring Equipment. NACA Rep. 1209, 1954. (Supersedes NACA TN 2839.)
60. Uberoi, Mahinder S., and Corrsin, Stanley: Diffusion of Heat from a Line Source in Isotropic Turbulence. NACA Rep. 1142, 1953. (Supersedes NACA TN 2710.)
61. Mickelsen, William R.: An Experimental Comparison of the Lagrangian and Eulerian Correlation Coefficients in Homogeneous Isotropic Turbulence. NACA TN 3570, 1955.
62. Dryden, Hugh L.: A Review of the Statistical Theory of Turbulence. Quart. Appl. Math., vol. 1, no. 1, Apr. 1943, pp. 7-42.
63. Kalinske, A. A., and Pien, C. C.: Eddy Diffusion. Ind. and Eng. Chem., vol. 36, no. 3, Mar. 7, 1944, pp. 220-222.
64. Taylor, G. I.: The Spectrum of Turbulence. Proc. Roy. Soc. (London), ser. A, vol. 164, Feb. 18, 1938, pp. 476-490.
65. Jakob, Max: Heat Transfer. Vol. 1. John Wiley & Sons, Inc., 1949.
66. Wilson, H. A.: Convection of Heat. Proc. Cambridge Phil. Soc., vol. 12, Apr. 1904, pp. 406-423.
67. Roberts, D. F. T.: The Theoretical Scattering of Smoke in a Turbulent Atmosphere. Proc. Roy. Soc. (London), ser. A, vol. 104, 1923, pp. 640-654.
68. Towle, W. L., and Sherwood, T. K.: Eddy Diffusion—Mass Transfer in the Central Portion of a Turbulent Air Stream. Ind. and Eng. Chem., vol. 31, no. 4, Apr. 1939, pp. 457-462.
69. Bush, V., and Caldwell, S. H.: A New Type of Differential Analyzer. Jour. Franklin Inst., vol. 240, no. 4, Oct. 1945, pp. 325-326.
70. Mickelsen, William R., and Laurence, James C.: Measurement and Analysis of Turbulent Flow Containing Periodic Flow Fluctuations. NACA RM E53F19, 1953.

71. Corrsin, Stanley, and Uberoi, Mahinder S.: Further Experiments on the Flow and Heat Transfer in a Heated Turbulent Air Jet. NACA Rep. 998, 1950. (Supersedes NACA TN 1865.)
72. Townsend, A. A.: The Diffusion Behind a Line Source in Homogeneous Turbulence. Proc. Roy. Soc. (London), ser. A, vol. 224, no. 1159, July 22, 1954, pp. 487-512.
73. Longwell, John P., and Weiss, Malcolm A.: Mixing and Distribution of Liquids in High-Velocity Air Streams. Ind. and Eng. Chem., vol. 45, no. 3, Mar. 1953, pp. 667-677.
74. Schubauer, G. B.: A Turbulence Indicator Utilizing the Diffusion of Heat. NACA Rep. 524, 1935.
75. Scurlock, A. C.: Flame Stabilization and Propagation in High-Velocity Gas Streams. Meteor Rep. No. 19, Fuels Res. Lab., M.I.T., May 1948. (Contract NOrd 9661.)
76. Langmuir, Irving, and Blodgett, Katherine B.: A Mathematical Investigation of Water Droplet Trajectories. Tech. Rep. No. 5418, Air Materiel Command, AAF, Feb. 19, 1946. (Contract No. W-33-038-ac-9151 with General Electric Co.)
77. Scull, Wilfred E.: Measurements of Liquid Fuel Films on a Rod Flame-Holder. Rep. of Exp. Res. Problem in Chem. Eng., M.I.T., Jan. 19, 1951.
78. Sherman, P., Klein, J. S., and Tribus, M.: Determination of Drop Trajectories by Means of an Extension of Stokes' Law. Eng. Res. Inst., Univ. Michigan, Apr. 1952. (Air Res. and Dev. Command, USAF, Contract AF 18(600)-51, Proj. M992-D.)
79. Ingebo, Robert D.: Vaporization Rates and Drag Coefficients for Isooctane Sprays in Turbulent Air Streams. NACA TN 3265, 1954.
80. Bahr, Donald W.: Evaporation and Spreading of Isooctane Sprays in High-Velocity Air Streams. NACA RM E53I14, 1953.
81. Minchin, L. T.: The Mixing of Gas Streams. Rep. No. E.3965, British RAE., Jan. 1943.
82. Hawthorne, W. R., and Cohen, H.: Pressure Losses and Velocity Changes Due to Heat Release and Mixing in Frictionless, Compressible Flow. Rep. No. E.3997, British RAE., Jan. 1944.

CHAPTER III

IGNITION AND FLAMMABILITY OF HYDROCARBON FUELS

By FRANK E. BELLES and CLYDE C. SWETT

INTRODUCTION

Many physical and chemical influences set limits on ignition or flame propagation in fuel-air mixtures. The importance of these limits in high-speed combustors is evident; they may give rise to conditions in which the mixture cannot be ignited or, if ignited, is incapable of sustained burning. This chapter discusses the experimental observations of flame quenching and of the limits of flammability, flame propagation, and ignition and draws from them some insight into the basic mechanisms that set the limits. Although most of the results in the literature have been obtained for homogeneous mixtures and for single fuels rather than multicomponent fuels such as those used in practical engines, there are many applications of both the data and the ideas to the operating problems of high-speed combustors.

A flammable mixture is defined as one capable of propagating flame indefinitely away from, and in the absence of, a source of ignition. That is, an ignition source such as an electric spark must be provided initially, but a flammable mixture will continue to propagate the flame even after the spark has been turned off, while a nonflammable one will not. In the nonflammable case, emission of light or some other evidence of chemical reaction may be observed, but this persists only while the ignition source is in operation.

A flammable mixture of fuel and air may be progressively diluted with either constituent until eventually a mixture results that is nonflammable. The limit of flammability is the borderline composition that separates mixtures capable of propagating a flame from those that are not. If the diluting agent is air, the limit mixture contains too little fuel to be capable of sustained flame propagation; and the borderline concentration is termed the lean or lower flammability limit. Conversely, if the diluting agent is fuel, the rich or upper flammability limit is reached. The flammability limits at a particular temperature and pressure obtained in this manner are often called the concentration limits. They may be made independent of any apparatus effects; therefore, these limits are physicochemical constants for each fuel. Mixtures of fuel concentrations between the lean and rich limits are said to lie within the flammable range.

It is sometimes observed that a flame in a mixture well within the flammable range will be extinguished if it is forced to propagate through a constriction. The walls are evidently able to exert some repressive influence on the flame. The effect is observable in Bunsen burners when the flow of mixture is suddenly stopped. If the burner tube is

sufficiently wide, the flame will flash back and propagate into the stationary mixture; whereas, with a smaller tube, it will be extinguished at the port. This effect of the walls on flame propagation is termed quenching. It is possible to determine a minimum diameter or a minimum rectangular opening through which a flame will travel, and such a dimension is a quenching distance.

Although the walls are able to set limits of flame propagation, these limits are not flammability limits in the true sense, since they are not physicochemical constants of the fuel. Rather, the limits are conditioned by the presence of walls.

SYMBOLS

The following symbols are used in this chapter:

\mathcal{A}	Avogadro number
B	geometrical factor
\mathcal{B}	dimensionless factor, value of which depends only on geometry of quenching surface
b	constant
C	constant
c	capacitance of condenser
c_p	specific heat at constant pressure
D	diffusion coefficient at 77° F and 1 atm
d	diameter
d_q	quenching distance
d_{slit}	critical slit opening
d_{tube}	critical tube diameter
E_{act}	apparent energy of activation
E_c	energy from capacitance
E_{ig}	total ignition energy
E_L	energy from inductance
E_{ls}	energy in line source
F	constant relating total number of reaction events that occur during passage of a flame to number that must occur in reaction zone for the flame to propagate
$\mathcal{F}\sqrt{u^2}$	function of intensity of turbulence, ft/sec
G	constant
i	current, amp
K	constant
\mathcal{K}	constant
k_{av}	average rate constant for reaction of active particles with fuel molecules
L	inductance
N_f	number of fuel molecules per unit volume
p	pressure
R	universal gas constant

r	radius
s	electrode spacing
T	temperature
T_F	equilibrium adiabatic flame temperature
T_o	initial mixture temperature
t_{ig}	ignition lag
t_s	spark duration
U_F	burning velocity
U_g	gas velocity
v	voltage
X_f	mole fraction of fuel
ϵ_{mol}	fraction of molecules present in gas phase that must react for flame to continue to propagate
κ	thermal conductivity
ω	reaction rate
Subscripts:	
a	air
dr	droplet
min	minimum
r	rod
re	in reaction zone
S	sphere

FLAME QUENCHING

Before discussing flammability and ignition, it is desirable to consider flame quenching. This phenomenon affects the process of flame propagation, with which flammability is concerned, and also that of ignition. The effects of quenching must either be accounted for or eliminated in the measurement of limits of flammability and of ignition energies, if meaningful interpretations of the data are to be made. In older literature, the importance of flame quenching was not understood, with the result that many misleading conclusions were reached.

As stated in the **INTRODUCTION**, quenching may be observed when a Bunsen flame is allowed to flash back into the burner tube. This fact serves as the basis for a standard means of measuring quenching distance. A flame is established on the burner port, and the mixture flow is then suddenly stopped. If the flame flashes back and propagates down the burner tube, a smaller one is substituted until the tube will just permit the flame to propagate. The diameter of the tube is thus the quenching distance for the given fuel-oxidant mixture under the specified conditions of temperature and pressure. In practice, a rectangular burner with a continuously variable width is often used, to avoid the frequent changes of tubes and to improve the precision of the measurements. An alternative procedure is to employ a fixed burner opening and to change one of the conditions, such as pressure or mixture composition, until the condition corresponding to the specified quenching distance is determined.

Quenching distances may be measured by entirely different means from the ones just described. This is possible because of the existence of quenching effects in measurements of flammability and spark-ignition energies of fuel-oxidant mixtures. Before these aspects are discussed, however,

some of the data on the effects of variables on straightforward quenching-distance measurements will be presented.

EFFECTS OF VARIABLES ON FLAME QUENCHING

All the experiments described in this section were conducted with homogeneous mixtures of gaseous or vapor fuel and air or some other oxidant. In addition, all the quenching distances were measured by means of the flashback of burner flames into quiescent mixtures.

Geometry of quenching surface.—Reference 1 reports quenching distances measured by establishing a flame on a burner and then suddenly stopping the mixture flow. The flame either flashed back through the burner or was quenched at the port, depending upon the size of the burner. Various cylindrical and rectangular tubes were used, and the fuels were methane and propane in air at room temperature and atmospheric pressure.

The critical tube diameters and critical slit openings for flame propagation—that is, the quenching distances—were not the same. The critical diameters were larger than the critical slit openings. A geometrical factor B may be defined as

$$B = \frac{d_{tube}}{d_{slit}} \quad (1)$$

The data of reference 1 show that, for lean to stoichiometric mixtures, the average value of B is 1.25 for methane-air mixtures and 1.45 for propane-air mixtures. Reference 2 extended the study of geometry effects to include annuli and rectangular slots of various length-to-width ratios. It was found that a very small centerbody has a large quenching action in the annular case.

Hydrocarbon type.—Friedman and Johnston have measured the quenching distances of mixtures of propane, benzene, *n*-heptane, and isooctane in air by determining the smallest opening of a rectangular burner that will permit a flame to flash back when the mixture flow is stopped (ref. 3). The data are presented in figure 76, where quenching distance is plotted against percent stoichiometric fuel-air ratio. The experiments were carried out at 1-atmosphere pressure and 212° F ambient temperature.

Figure 76 shows that mixtures slightly richer than stoichiometric are able to propagate flame through the narrowest channels. For lean and stoichiometric mixtures, the quenching distances decrease in the following order: isooctane > *n*-heptane > propane > benzene. Reference 3 notes that this order is the same as the order of increasing burning velocities for the four compounds. In the case of rich mixtures, there are changes in the order of quenching distances, and it is not certain that there is any simple relation with burning velocity. Although in all cases the quenching distances are small under the conditions of the experiment, there are considerable percentage differences from fuel to fuel. For example, the quenching distance of a stoichiometric mixture of benzene in air at 1 atmosphere and 212° F is about 80 percent of that of a stoichiometric isooctane-air mixture.

Inert diluents.—For his work on the effects of inert gases on quenching, Friedman (ref. 4) used hydrogen as the fuel

and conducted the experiments at ambient pressure and temperature. The inert gases used were helium, argon, nitrogen, and carbon dioxide. Mixtures of hydrogen, oxygen, and inert gas were prepared with a quantity of inert gas such that the calculated flame temperature of the stoichiometric mixture was 4244° F in all four cases. Some of the data of reference 4 are shown in figure 77. The figure shows that, for a given mixture, the quenching distance decreases with the inert diluent used in the order helium > argon > nitrogen > carbon dioxide; that is, the quenching effect of the walls on the flame is greater if the diluent is helium than if it is carbon dioxide.

Analogous results for hydrocarbon fuels were found in reference 5 for methane and in reference 6 for propane. Replacement of helium by argon in the "air" does not change the equilibrium flame temperature or composition, but the quenching distance is nevertheless strongly affected. In all cases, the quenching distance is decreased when the inert diluent decreases the coefficients of transport of heat and mass. In other words, the flame is in effect more insulated from the walls by argon than by helium.

The results for hydrogen in reference 4 were interpreted on the basis of a thermal model of quenching, in which heat

is conducted away from the flame by the walls. This analysis indicated that the quenching should be proportional to the factor

$$\frac{\kappa}{U_p c_p} \quad (2)$$

where c_p is the heat capacity per unit volume of unburned gas. This parameter correlated the quenching-distance data for various inert diluents in a satisfactory manner. However, it is emphasized (ref. 4) that no conclusion could be drawn as to the true mechanism of quenching and that diffusion of active particles to the walls might be important.

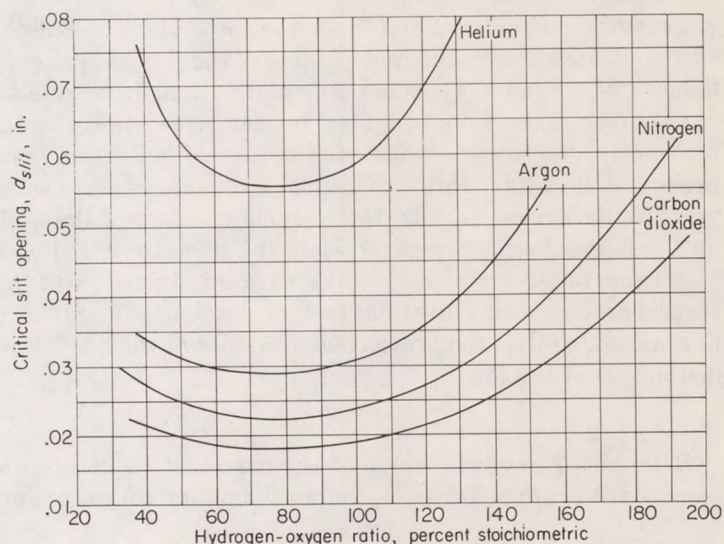


FIGURE 77.—Effects of various inert gases on quenching distance (ref. 4).

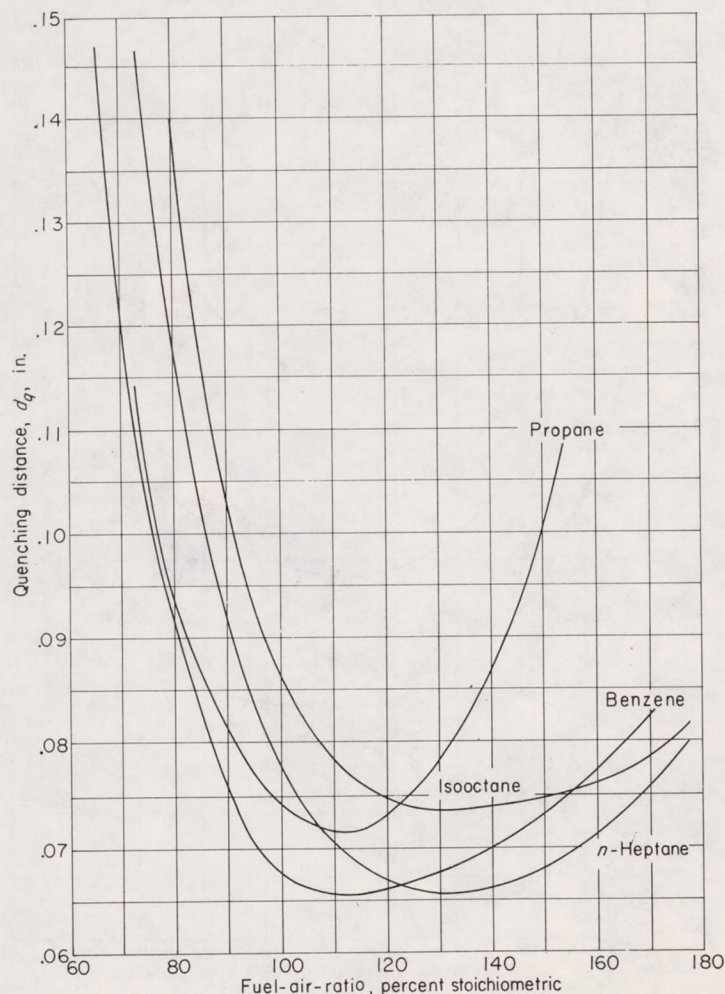


FIGURE 76.—Variation of quenching distance with hydrocarbon type. Pressure, atmospheric; temperature, 212° F (by permission from ref. 3).

A more complete theoretical discussion is given in reference 6. The theory, which will be described in more detail later, avoids empirical terms such as the burning velocity that appears in equation (2). It was hoped that a decision could be reached as to the importance of loss of heat as opposed to loss of active particles at the walls. The following table compares the observed ratios of quenching distances at atmospheric pressure for propane-oxygen-argon and propane-oxygen-helium with ratios predicted by a "diffusional" and by a "thermal" theory:

Stoichiometric fuel-oxidant ratio, percent	$\frac{d_{slit}(\text{argon})}{d_{slit}(\text{helium})}$		
	Observed	Predicted (thermal)	Predicted (diffusional)
73.8	0.35	0.47	0.67
100	.41	.48	.68
149	.44	.50	.72

The observed ratios are in better agreement with the thermal than with the diffusional values. Reference 6 points out, however, that conclusive proof is still lacking, because the theories are actually quite approximate.

Temperature.—Friedman and Johnston (ref. 7) have studied the effects of temperature on quenching distance. Increased temperature decreases the quenching distance; that is, the flame is able to pass through smaller openings. The results shown in figure 78(a) for propane-air mixtures at about 1-atmosphere pressure are consistent with the general observation that chemical reactions are promoted by increase in temperature. The magnitude of the temperature effect varies with mixture composition. For rich and stoichiometric propane-air mixtures, quenching distance is approximately proportional to the -0.5 power of the absolute temperature; while for lean mixtures the exponent increases.

Pressure.—Friedman and Johnston have also studied the effects of pressure on the quenching distances of propane-air flames (ref. 7) and of benzene-, *n*-heptane-, and isooctane-air flames (ref. 3). A rectangular burner was employed, as previously described. Some of the data of reference 7 are presented in figure 78(b). Quenching distance increases as pressure decreases; that is, the quenching effect of the walls on the flames becomes greater when the pressure is reduced.

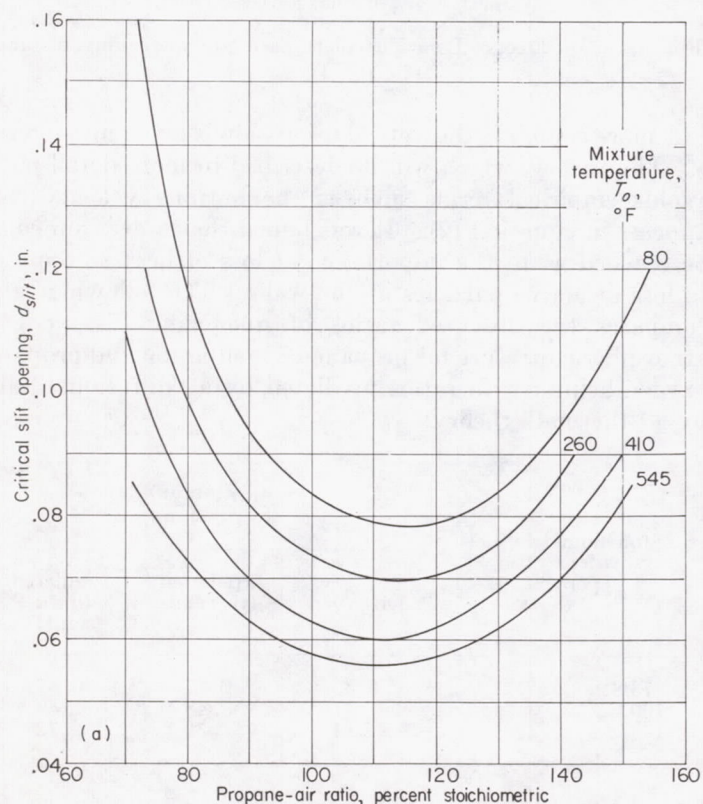
A logarithmic cross plot of the data of figure 78(b) for several propane concentrations is shown in figure 79. Straight lines result, so that the pressure-dependence of the quenching distance is of the form

$$d_{slit} \propto p^{-b} \quad (3)$$

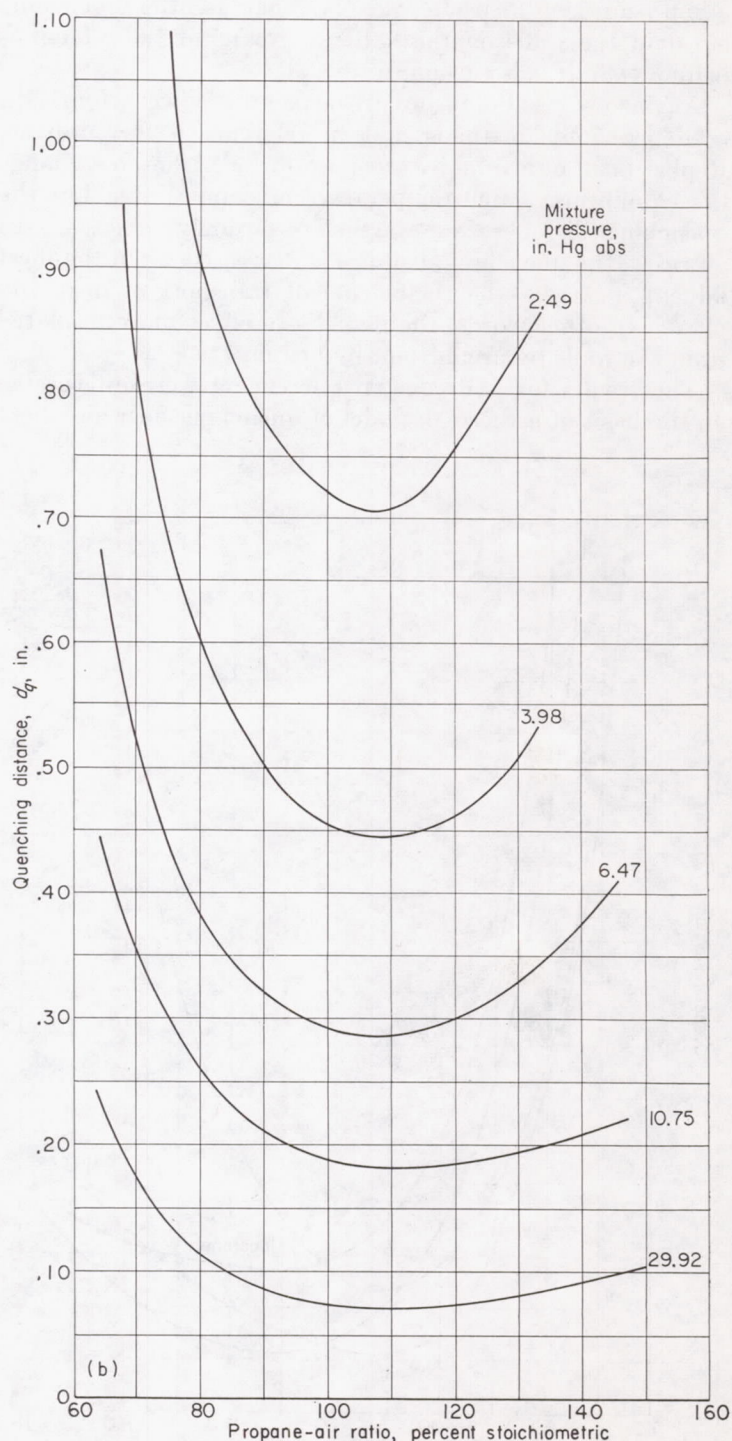
Reference 7 gave the value of the exponent b for the propane concentration corresponding to the minimum quenching

distance as 0.91. Reference 3 subsequently showed that the pressure-dependence of the minimum quenching distances of benzene-, *n*-heptane-, and isooctane-air flames is almost identical to that of propane-air flames. Therefore, it appears that, as a rough approximation for hydrocarbons burning in air,

$$d_{slit, min} \propto \frac{1}{p} \quad (4)$$



(a) Effect of temperature. Pressure, 29.02 inches of mercury absolute.



(b) Effect of pressure. Ambient temperature, about 75° F.

FIGURE 78.—Effect of temperature and pressure on quenching distance of propane-air flames (by permission from ref. 7).

In the case of propane-air mixtures, however, the value of the exponent of the pressure is slightly dependent on the propane concentration and increases from lean to rich mixtures. The effect was noted in reference 8, using the data of reference 7, and also in reference 9. The following table shows the variation of the pressure-dependence of quenching distance of propane-air flames with fuel concentration:

Stoichiometric fuel-air ratio, percent	Negative exponent of pressure, b	Reference
74-----	0.83	^a 8
74-----	.85	9
86-----	.84	9
87-----	.85	^a 8
100-----	.88	^a 8
100-----	.89	9
110-----	.91	7
124-----	.95	9
149-----	.98	9

^a Using data of ref. 7.

The variations in b shown by this table do not appear very large, but, as can be seen in figure 79, they are quite apparent in a logarithmic plot of quenching distance against pressure.

Oxygen concentration.—Reference 9 describes the effects of pressure on the quenching distances of flames in various propane-oxygen-nitrogen systems. The measurements were made with a variable-width rectangular burner over a pressure range from 2.99 to 29.92 inches of mercury absolute. Five oxidant atmospheres were used, containing 17, 21, 30, 50, and 70 percent oxygen by volume. The effects of pressure on the quenching distances of flames in any given oxidant were very similar to those described in the preceding section.

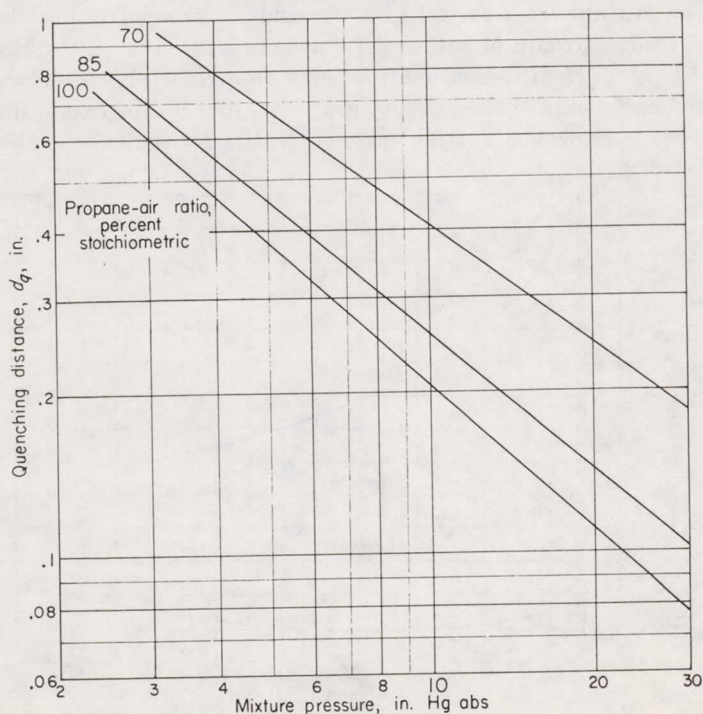


FIGURE 79.—Pressure-dependence of quenching distance of propane-air flames (ref. 7).

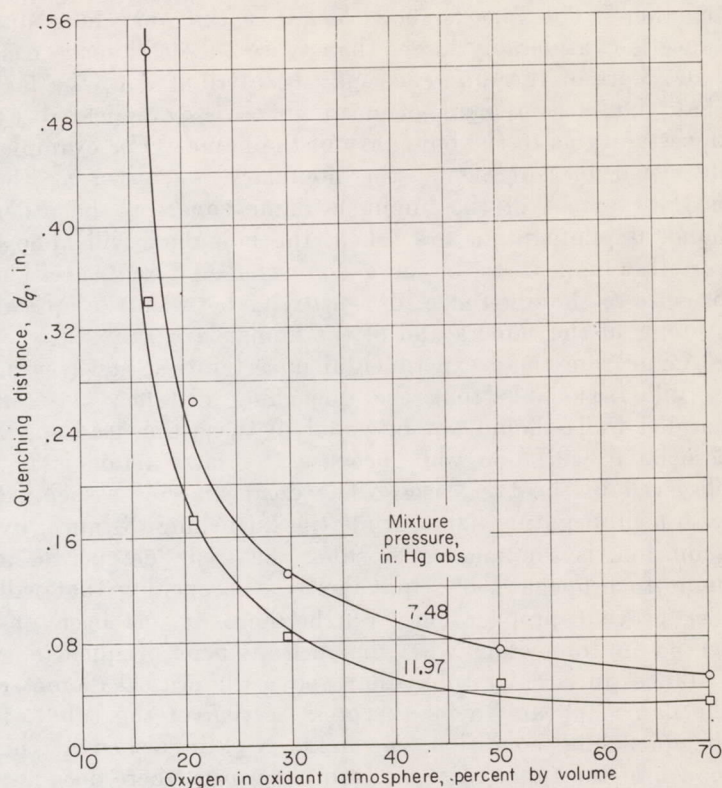


FIGURE 80.—Effect of oxygen concentration in oxidant on quenching distances of stoichiometric propane-oxygen-nitrogen mixtures (ref. 9).

At any given pressure and percent stoichiometric propane, the quenching distance decreased as the oxygen concentration of the oxidant increased. The effects are shown graphically in figure 80, where data for stoichiometric mixtures and two pressures are presented. The decrease in quenching distance with increase in the amount of oxygen in the oxidant atmosphere is very rapid up to about 25 percent oxygen (air=21 percent) and then becomes more gradual.

DEAD SPACE

When a flame is adjacent to a surface, the luminous zone does not extend completely to the surface. There is a region, the width of which depends on the experimental conditions, where the reactions appear to be quenched by the wall. The distance from the end of the luminous zone to the wall is called dead space. The dead space may easily be observed, for example, by sighting across the top of a Bunsen burner; the base of the flame cone is situated a small distance above the burner port. Thus, it is evident that the wall quenches the flame reactions in the gas adjacent to it. It is therefore logical to consider dead space in connection with a discussion of quenching distance.

It might at first appear that, if the dead space associated with a flame propagating through a rectangular duct were measured, the dead space should be equal to half the quenching distance under the same conditions. This interpretation is based on the idea that the quenching distance corresponds to a situation in which the flame has zero width because of the merging of the dead spaces associated with two walls when the walls are brought sufficiently close

together. The fact is, however, that the quenching distance is considerably larger than twice the dead space (ref. 10). Part of the difference may be attributed to the fact that the measurement of dead space is complicated by uncertainty as to the boundary of the flame. For example, in visual measurements, the boundary is chosen as the farthest extent of the luminous flame zone; on the other hand, if photographs are taken, the boundary will almost certainly appear to be in a somewhat different position because of the differences in sensitivity between the optical systems of the camera and of the human eye.

Aside from these experimental uncertainties, however, it is still reasonable that the quenching distance between parallel walls should not be equal to twice the dead space associated with one wall, because the same flame is not observed in the two cases. The dead space is associated with a propagating flame, while the quenching distance, by definition, is the smallest opening that will just permit a flame to propagate, or, equivalently, the opening that will just prevent propagation. Furthermore, it has been observed in connection with the measurement of quenching distances in circular tubes that above the critical diameter the flame appears to fill the cross section of the tube; at the quenching condition, the flame is extinguished at the mouth of the tube (ref. 8). In other words, there does not appear to be any marked diminution in the size of the flame as the quenching condition is approached.

Thus, the dead space is a characteristic distance associated with a flame; it arises through the quenching action of the walls, but it is not equivalent to the quenching distance.

There have not been many experimental studies of dead space. Reference 10 summarizes the work. Qualitatively, dead space varies with fuel concentration and with pressure in much the same way as does quenching distance. For example, the minimum dead space occurs in butane-air mixtures that are slightly richer than stoichiometric and increases as the pressure is decreased (ref. 10).

HOMOGENEOUS QUENCHING

The discussion of quenching has heretofore been concerned with the effects of walls on the flame. The effects must occur because the walls absorb heat or free-radical chain carriers of the flame reactions, one or both of which must be transferred ahead of the flame to the unburned gas in sufficient quantity if the flame is to continue propagating (see ch. IV). These considerations suggest the possibility that a flame might be quenched by the combustible gas itself. Such homogeneous quenching might occur, for example, with a flame propagating in a turbulent mixture. If the turbulent intensity were sufficiently high, the dilution of the flame zone with cold unburned gas might overwhelm the transfer of heat and chain carriers from the burning zone to the surrounding fresh gas, and the flame would then be extinguished.

The situation described has received only limited experimental attention. In one article concerning this phenomenon (ref. 11), the spread of flame from a nucleus in a flowing turbulent stream through a tube was studied. The turbulence was pipe turbulence, and the mixture of propane and

air was periodically ignited by a spark across the full width of flow. Inasmuch as there was no flameholder, the flame traveled downstream with the flow and was observed stroboscopically. At the limits of flame propagation, the mixture was ignited at the spark, but the flame nucleus decreased in size and was finally extinguished as it traversed the test section. The range of propane concentrations over which propagating flames were obtained was determined for flow velocities up to 250 feet per second. Typical curves, obtained at a static pressure of 30.7 inches of mercury absolute, are shown in figure 81, where the concentration range of propagation is seen to narrow with increasing flow velocity. The lean limit of flame propagation changes less rapidly than the rich limit when the data are plotted in terms of percent stoichiometric, and the two limits tend to converge on the stoichiometric propane concentration. A Reynolds number of 2000 in these tests corresponded to a flow velocity of about 12 feet per second; therefore, the data apply to the turbulent regime. In one series of experiments, a screen was inserted upstream of the spark; this reduced the turbulent scale but had no appreciable effect on the range of mixtures capable of propagating flame at a given velocity. Reference 11 offers no conclusive explanation of the behavior of the lean-limit curve at flow velocities less than 50 feet per second.

Inasmuch as the turbulence intensity increases with increasing flow velocity, the experiments indicate that the idea of homogeneous quenching by dilution with a combustible mixture may have some physical reality. Reference 11 suggests this mechanism to explain curves similar to those of figure 81.

Gas-phase quenching is also reported in references 12 and 13. Small flame kernels were photographed as they expanded from spark electrodes in a free turbulent jet. The turbulence was induced by grids. Nonisotropic fields just downstream of sufficiently large grids increased the rate of kernel growth; the flow property thought responsible was the magnitude of the velocity gradients met by the expanding flame. However, further increase in the gradients quenched

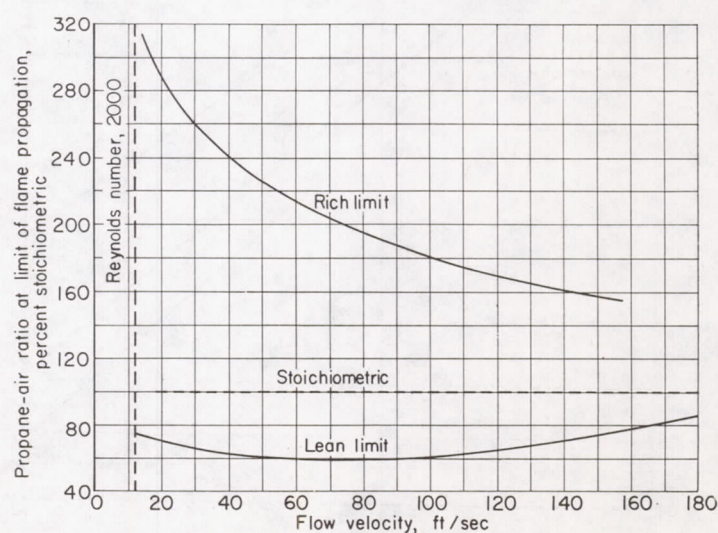


FIGURE 81.—Effect of flow velocity on limits of flame propagation in propane-air mixtures. Static pressure, 30.7 inches of mercury absolute (ref. 11).

the flame, indicating an optimum gradient for flame spreading.

INTERPRETATIONS OF WALL QUENCHING

In order to interpret the observed ability of walls to quench flames in terms of fundamental processes, it is necessary first to decide upon the mechanism by which a flame is presumed to propagate, and then to examine the influence of the presence of walls upon this mechanism. Inasmuch as a flame is a zone of intense chemical reaction accompanied by the evolution of heat and the formation of new products from the reacting fuel and air, there exist steep gradients of temperature and concentration from the flame to the unburned gas.

It is possible to set up differential equations that govern the flow of heat and of various molecular species that must occur as a result of these gradients. In order to use the equations and to obtain solutions by ordinary means, however, it is necessary to make certain assumptions. This matter is discussed in chapter IV. At this point, it may suffice to say that, although both heat and matter must flow from the flame because of the gradients that exist, and although the transfer of both heat and matter are probably essential features of the basic mechanism of flame propagation, in the past one or the other of these two types of transfer has been chosen as most important. In other words, in order to make the basic differential equations amenable to solution in closed form, it has sometimes been assumed that the transfer of heat from the flame to the unburned gas is the most important process in flame propagation and that the diffusion of matter is much less important. In other cases, the opposite point of view has been adopted. In either case, the assumption made can be justified in various ways.

As a result of the considerations discussed, two schools of thought have arisen concerning the most important mechanism responsible for flame propagation. One emphasizes the importance of heat conduction from the hot to the cold gas, since it is known that chemical reactions can be started and accelerated by an increase in temperature. The

other stresses the importance of the diffusion of certain active particles (free radicals and atoms) known to be produced in flames; because of their highly reactive and energetic nature, these active particles are supposed to be able to initiate chemical reactions in the cold gas. Actually, as stated previously, both features may be important.

Thus, interpretations of the quenching effect start with the assumption of one of these two processes as the more important one and then identify the walls as a sink for either heat or active particles. On the basis of these models, the flame is quenched if the walls abstract more than some critical amount of heat or active particles. The resulting interpretations may be described as either thermal or diffusional interpretations.

Actually, the distinction is not always as clear as might be inferred. For example, references 4 and 14 present interpretations of quenching distance that are based on heat transfer to the cold walls; but in both cases the equations involve the experimental burning velocity of the mixture (see ch. IV). Consequently, there is the possibility that, if the burning velocity depends upon diffusion of active particles, these quenching theories are not uniquely thermal.

The theory developed in reference 4 was used, as described, to correlate data on the effects of various inert diluents on the quenching distances of hydrogen-oxygen-diluent mixtures. The correlating parameter (eq. (2)) was quite successful; it has not been applied to other types of quenching data.

The theory of reference 14 is based on the combustion-wave theory of Lewis and von Elbe (ref. 5) and has been applied to quenching distances of methane-oxygen-nitrogen mixtures at atmospheric pressure. With the use of an experimental burning velocity, it is possible to solve the equations to obtain an estimate of the absolute value of the quenching distance of a mixture. In reference 14, these calculations are made and the results compared with experimental values. Quenching by tubes and by rectangular burners was considered. Some of the results are reproduced in the following table:

Mixture, percent by volume										
Methane.....	10	15	25	40	50	52.5	10.0	16.3	21.5	26.4
Oxygen.....	90	85	75	60	50	47.5	18.8	29.3	39.8	49.1
Nitrogen.....	0	0	0	0	0	0	71.2	54.4	39.7 [sic]	24.5
Quenching distance, d_q , in.										
Critical slit openings, d_{slit}										
Experimental.....	0.086	0.046	0.028	0.043	0.15	0.22	0.28	0.079	0.053	0.045
Calculated.....	.086	.039	.019	.033	.09	.14	.17	.056	.038	.039
Percent deviation.....	0	-15	-32	-23	-40	-36	-39	-29	-28	-13
Critical diameters, d_{tube}										
Experimental.....	0.118	0.068	0.048	0.069	0.215	0.325	0.335	0.142	0.092	0.070
Calculated.....	.190	.094	.039	.065	.190	.340	.354	.117	.075	.061
Percent deviation.....	61	38	-19	-6	-12	5	6	-18	-18	-13
$B = \frac{d_{tube}}{d_{slit}}$										
Experimental.....	1.37	1.48	1.71	1.60	1.43	1.48	1.20	1.80	1.74	1.56
Calculated.....	2.21	2.41	2.05	1.97	2.11	2.43	2.08	2.09	1.97	1.56

These data show that the theory of reference 14 is capable of predicting reasonably well the observed values of d_{tube} , d_{slit} , and B .

In contrast to the two thermal treatments of quenching described, reference 8 presents a diffusional interpretation based on the destruction of active particles at the wall. It was assumed that the diffusion of active particles ahead of the flame, where they react with fuel molecules, is responsible for flame propagation, and that, when the flame is near a wall, a certain proportion of the active particles is lost by collision with the surface. On this basis, it was possible to set up a balance between the number of collisions of active particles and fuel molecules required to propagate the flame and the number of active particles lost by diffusion to the wall. The important active particles were assumed to be the light, rapidly diffusing species H, O, and OH. The quenching distances for lean to stoichiometric mixtures could be calculated from the resulting equations with surprisingly good accuracy. Separate equations were developed for two cases:

(1) The critical diameter for flame propagation in a cylindrical tube:

$$d_{tube} = \left[\frac{32T_p^2}{(298)^2 N_f} \left(\frac{\epsilon_{mol}}{k_{av}} \right) \left(\frac{1}{\frac{p_H}{D_H} + \frac{p_O}{D_O} + \frac{p_{OH}}{D_{OH}}} \right) \right]^{1/2} \quad (5)$$

where d_{tube} is the critical tube diameter for propagation in a given fuel-air mixture at a particular pressure; and p_H , p_O , and p_{OH} are the equilibrium partial pressures of H, O, and OH in flame.

(2) The minimum width of the opening for propagation through a rectangular slit:

$$d_{slit} = \left[\frac{12T_p^2}{(298)^2 N_f} \left(\frac{\epsilon_{mol}}{k_{av}} \right) \left(\frac{1}{\frac{p_H}{D_H} + \frac{p_O}{D_O} + \frac{p_{OH}}{D_{OH}}} \right) \right]^{1/2} \quad (6)$$

Equations (5) and (6) were used to make absolute calculations of quenching distances for propane-air mixtures over a range of concentrations from lean to stoichiometric and pressures less than 1 atmosphere, and for stoichiometric ethene-air and isooctane-air mixtures in a similar pressure range (ref. 8). All quantities in the equations were calculated or estimated, except the constants ϵ_{mol} and k_{av} . It was found that ϵ_{mol} could be approximated by the lean concentration limit of flammability measured at atmospheric pressure, and that a suitable value of k_{av} could be derived from burning-velocity data. These constants have specific values for a given fuel and oxidant; therefore, a separate experimental value for the calculation of quenching distance at each condition is not required. It will be recalled that the theory of reference 14 requires a value of the burning velocity for each condition at which an absolute calculation of quenching distance is made. The agreement between observed and calculated quenching distances shown in reference 8 was quite striking, with an average difference of ± 3 percent. The agreement was probably in some degree fortuitous, depending in part on the choice of the diffusion coefficients and the choice of the temperature-dependence of the diffusion coefficients.

However, equations (5) and (6) may be used to correlate quenching-distance data if the ratio ϵ_{mol}/k_{av} is left as an

undetermined constant. This was done in reference 8, and also in reference 9, where the effects of pressure, propane concentration, and oxygen concentration in the oxidant were correlated. Reference 9 found that the choice of diffusion coefficients and temperature-dependence did not affect the result. Reference 15, however, analyzed all the available types of propane quenching data, including those that show the effects of initial temperature (ref. 7), and concluded that there is a slight influence of the choice of diffusion coefficients and their temperature-dependence. Reference 15 also presented quenching equations for the cases in which there is chain breaking and branching in the gas phase and in which there is not total destruction of active particles at the walls; evidence was shown that these factors need not be considered in correlating propane quenching data.

As a straightforward result of the boundary conditions, the diffusional treatment predicts the following value for the geometrical factor B :

$$B = \frac{d_{tube}}{d_{slit}} = \left(\frac{32}{12} \right)^{1/2} = 1.64 \quad (7)$$

This result is in agreement with experiment. Reference 2 extends the ideas and shows how to calculate the geometrical factors for annuli, equilateral triangles, ellipses, and rectangular slots of various length-to-width ratios. Quenching data obtained for some of the geometries correspond very well to predicted behavior. One striking result of both theory and experiment is that a very small annular center-body may have a severe quenching effect.

Using the diffusional treatment of reference 8 as a basis, reference 16 presents a thermal equation for quenching distance. The equation was derived by changing the first assumption of reference 8—namely, that in order for a flame to propagate the number of reaction events per unit volume that occur in the gas ahead of the flame must be above some minimum value. The authors of reference 16 assumed instead that the necessary number of reaction events is a constant fraction F of the total number of events per unit volume that normally occur during passage of a flame. The following equation was obtained:

$$d_q^2 = \frac{F \mathcal{A} B \kappa_{re} X_f}{c_{p, re} \omega} \quad (8)$$

where \mathcal{B} is a dimensionless factor, the value of which depends only on the geometry of the quenching surface and is the same as for the diffusional treatment, and $c_{p, re}$ is the heat capacity of the mixture in the reaction zone. The important feature of equation (8) is that the form of the reaction-rate term ω need not be specified. Two specific forms of rate-controlling reactions were tested in reference 16: (1) reaction between active particles and fuel molecules, and (2) reaction between oxygen molecules and fuel molecules.

Now, the diffusional equations of reference 8 do not correlate quenching data for mixtures much richer than stoichiometric. But the thermal equation (8), with assumption (2) as to the rate-controlling reaction, does correlate both lean and rich data. From this standpoint, equation (8) is very useful, and is an improvement on the equations of reference

8. However, in the work on effects of diluents (ref. 6), the best agreement between observed and predicted ratios of quenching distances was obtained with the thermal equation plus the assumption that the reaction of active particles and fuel is rate-controlling.

Thus, no completely satisfactory single treatment of quenching distance has yet been advanced. References 8 and 16 provide useful equations, and the conditions for which they apply have been described. However, all the analyses of flame quenching have not answered the important basic question: Does hydrocarbon flame propagation depend mainly on mass or heat transfer? In view of the partial success of both ideas, it is probably true that both mechanisms are important.

QUENCHING IN FLAMMABILITY AND SPARK-IGNITION MEASUREMENTS

It was stated at the beginning of the discussion of quenching that measurements of flammability and spark-ignition energy may be affected by quenching. Therefore, it is sometimes possible to determine quenching distances from such measurements. The way these effects appear will now be shown briefly.

Flammability measurements.—The concentration limits of flammability are, if measured properly, true physico-chemical constants for each fuel. Limits of this type are discussed in the next main section. Determination of these limits has generally been limited to work at atmospheric

pressure. However, some work has been done at lower pressures. Most of the observations at reduced pressures indicate that the lean and rich limits of homogeneous mixtures progressively converge and finally meet at some pressure below which no flame will propagate. Most of the older literature on low-pressure limits should be regarded critically. In most cases, insufficient cognizance was taken of the effects of the size of the test vessel and the need for a powerful ignition source. Thus, many of the limits recorded are actually ignition limits for the particular source used, or are the result of quenching by the walls. For example, it was believed that mixtures of ordinary hydrocarbon fuels in air could not sustain flame propagation below a pressure of about 1.2 inches mercury; it is now known that this minimum pressure is actually set by quenching due to the walls of the usual 2-inch-diameter tubes used in the experiments. The minimum pressure is lowered if larger tubes are used. Another difficulty in measuring limits at pressures other than atmospheric is the need to maintain the pressure constant during the propagation of the flame.

Recent work has avoided these difficulties and has clarified the meaning of the limits at reduced pressures (ref. 8). Care was taken to eliminate any effects of the ignition source, and the flame tubes were connected to a large plenum so that the flames propagated at essentially constant pressure. The limits were measured for homogeneous fuel-air mixtures in flame tubes of several diameters. Typical results for propane-air are shown in figure 82 (from ref. 8). The lean-limit concentration is lower for the larger tubes, as is the minimum pressure for flame propagation. The rich limit, although not shown in figure 82, also increases with increasing tube diameter. Therefore, the flammable range at a given pressure is wider for the larger tubes.

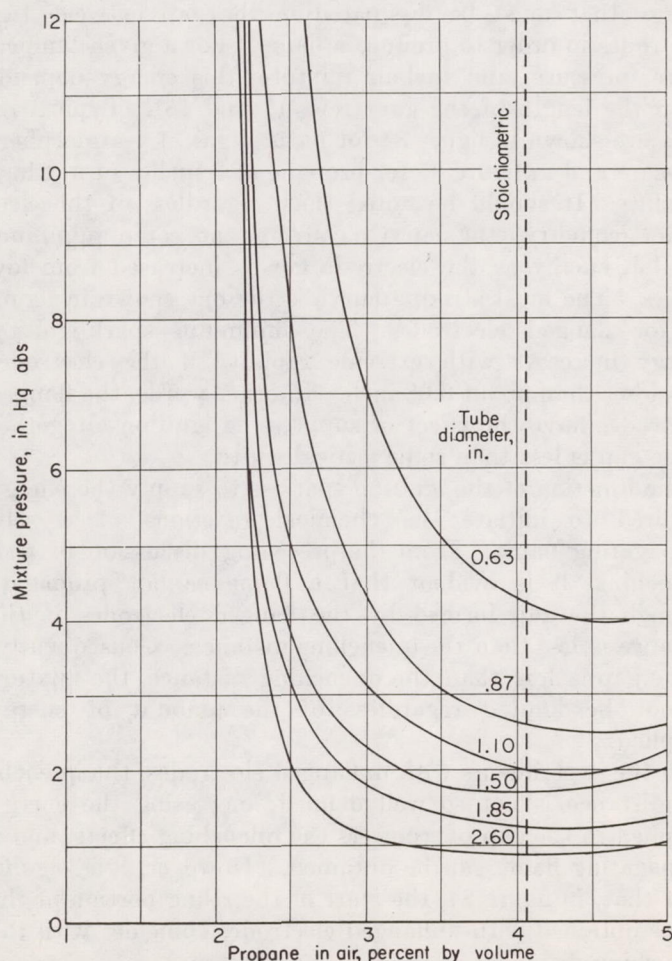


FIGURE 82.—Effect of tube diameter on low-pressure limits of flame propagation (ref. 8).

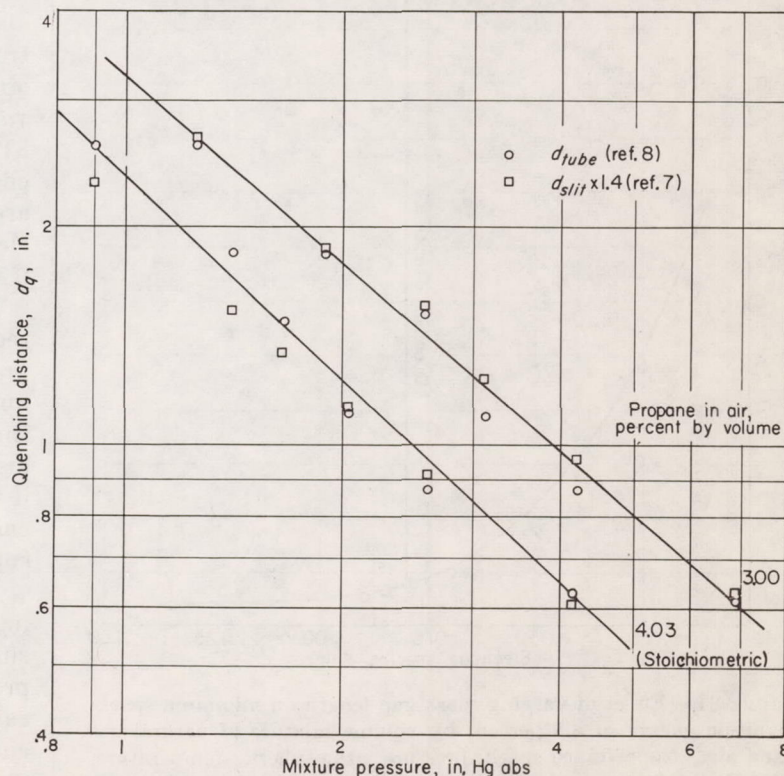


FIGURE 83.—Relation of quenching distance and low-pressure limits of flame propagation.

Since the diameter of the flame tube affects the results, it is evident that these limits are not true flammability limits; that is, they are not physico-chemical constants of the fuel. They are better termed limits of flame propagation at reduced pressures. The behavior of the data suggests that the limits are set by quenching action of the tube walls; and, in order to test this idea, logarithmic cross plots of the data of figure 82 were made at constant propane concentrations on the lean side of stoichiometric (fig. 83).

Friedman and Johnston (ref. 7) measured quenching distances for propane-air flames in terms of the critical width of a rectangular slit that would allow flashback of a Bunsen flame when the mixture flow was reduced. Some of their data are also shown in figure 83; the critical slit widths are multiplied by an empirical factor of 1.4 to account for the geometrical differences between the experiments. Figure 83 shows that the two types of data nearly coincide. Therefore, it is concluded that the measured pressure limit of flame propagation of a given mixture in a tube of a particular size is actually a measurement of the critical diameter, or quenching distance, for flame propagation in the mixture at the pressure of the limit (ref. 8).

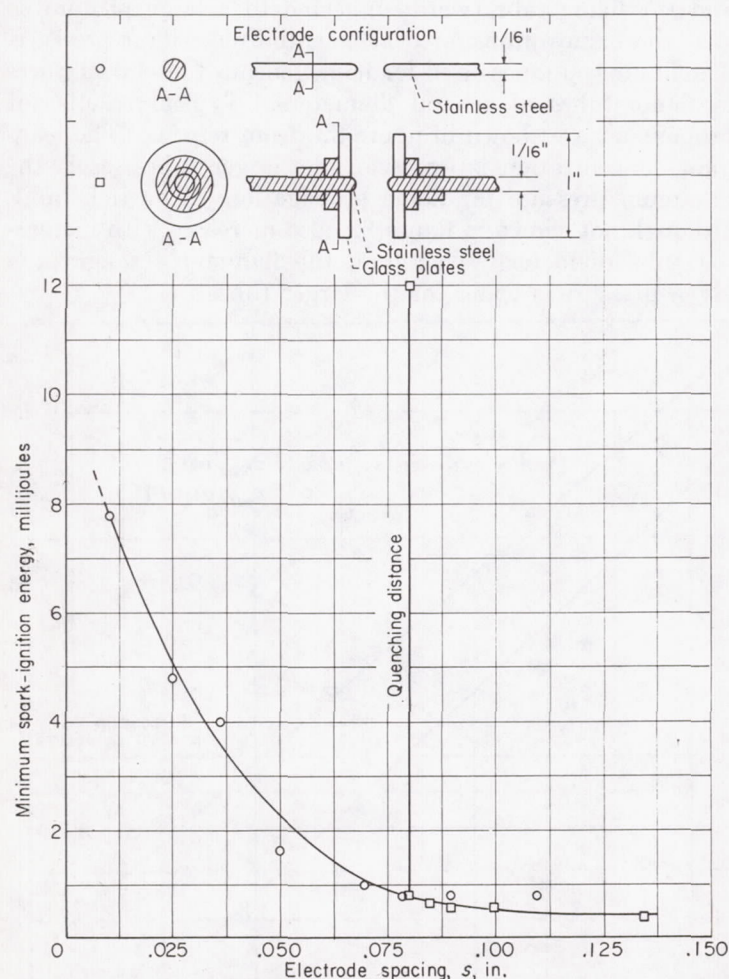


FIGURE 84.—Effect of varying spark-gap length on minimum spark-ignition energy of 8.5 percent by volume mixture of natural gas and air. Capacitance spark; pressure, atmospheric; temperature, 77° F (ref. 17).

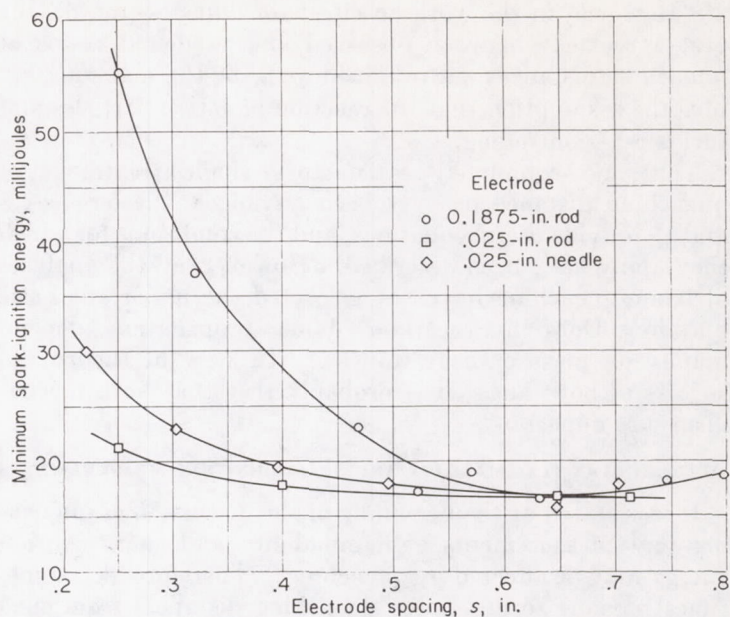


FIGURE 85.—Effect of electrode configuration and electrode spacing on minimum spark-ignition energy of flowing 5.2 percent by volume mixture of propane in air. Long-duration (600 microsec) capacitance spark; pressure, 3 inches of mercury absolute; temperature, 80° F (ref. 18).

Spark-ignition-energy measurements.—Spark-ignition energy is measured by determining the minimum amount of energy that must be dissipated in the gap between two electrodes in order to produce a flame. For a given temperature, pressure, and fuel-air mixture, this energy depends upon the length of the gap (refs. 17 and 18). Typical results are shown in figure 84 for natural gas at 1-atmosphere pressure and in figure 85 for propane at 3 inches of mercury absolute. It should be noted that, regardless of the electrode geometry, the curves converge at some minimum ignition energy as the electrode gap is increased from low values. The most striking curve is the one shown in figure 84 for flanged electrodes. The minimum spark-ignition energy increases with extreme rapidity if the electrodes are closer than about 0.08 inch. In other words, the flanged electrodes have the effect of suppressing ignition altogether if the gap is less than some critical width.

The function of the ignition spark is to supply the energy required to initiate the chemical reactions of a self-propagating flame. From the preceding discussion of wall quenching, it is evident that a flame cannot propagate through the gap formed by the flanged electrodes if the distance is less than the quenching distance. Consequently, if the gap is less than the quenching distance, the mixture cannot be ignited regardless of the amount of energy supplied.

In the experiments with unflanged electrodes, the quenching distance is not so well defined; increasing the energy supplied to the gap overpowers the quenching effects, and a propagating flame can be obtained. However, it is significant that, in figure 84, the start of the rising portion of the curve obtained with unflanged electrodes coincides with the quenching distance.

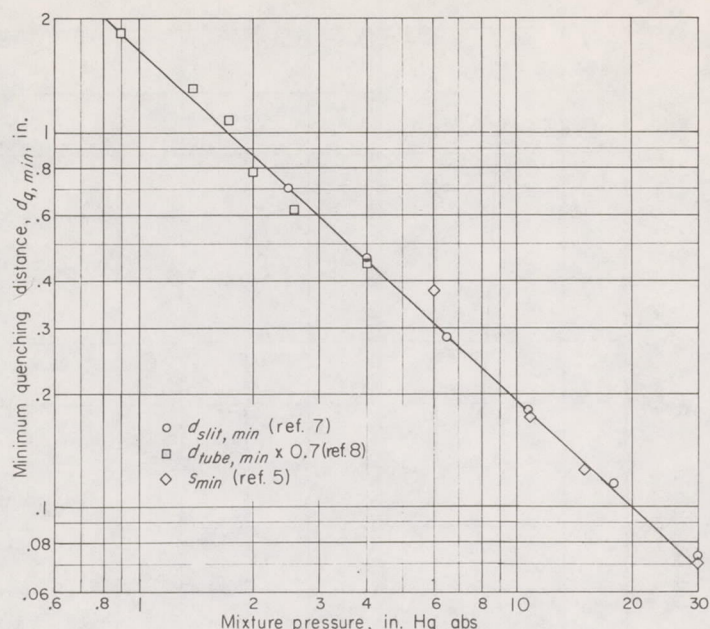


FIGURE 86.—Minimum quenching distance at various pressures. Propane in air, approximately 110-percent stoichiometric (ref. 8).

Finally, the quenching distance obtained from spark-ignition experiments is the same or very nearly the same as that obtained by the usual means, that is, by determining the critical slit opening for flashback of a Bunsen flame. It is also the same as the critical diameter obtained from low-pressure limits of flame propagation, as described in the preceding section, multiplied by a constant to account for the geometrical differences in quenching effect by cylindrical

and plane-parallel surfaces. Data of all three types are plotted in figure 86, and the points conform very well to a single line (ref. 8).

Thus, the same quenching effects that have been studied by means of flashback also extend to measurements of flammability at reduced pressures and to measurements of spark-ignition energy. Wall quenching is therefore an important phenomenon at all stages of the combustion process and must be considered if unambiguous interpretations of combustion data are to be made.

FLAMMABILITY LIMITS

EFFECTS OF VARIABLES ON FLAMMABILITY LIMITS AT ATMOSPHERIC PRESSURE

In the measurement of lean and rich concentration limits of flammability it is necessary to eliminate all external effects, so that the limit is a property only of the fuel at a given temperature and pressure. Coward and Jones (ref. 19) have critically reviewed the literature on flammability limits and have recommended the experimental procedure that will lead to the determination of true limits.

As previously stated in the definition of flammable mixtures, the ignition source must not affect the results. If a weak source is used, some mixtures may not inflame, especially if they are near the limit concentration, while a stronger source would succeed in igniting them. The limits determined with the weak igniter would consequently not be limits of flammability, but merely limits of ignitibility for the particular source used. Thus, it is essential to use a strong source, such as a spark several millimeters long or a small naked flame.

In order to minimize quenching action by the walls, the

TABLE V.—FLAMMABILITY LIMITS IN AIR AT ATMOSPHERIC PRESSURE AND ROOM TEMPERATURE (Ref. 19)

Fuel	Lean limit		Rich limit	
	Volume percent	Fuel-air ratio, percent stoichiometric	Volume percent	Fuel-air ratio, percent stoichiometric
<i>n</i> -Paraffins				
Methane.....	5.3	53.5	14	156
Propane.....	2.2	53.8	9.5	251
Butane.....	1.9	60.1	8.5	288
Pentane.....	1.5	58.2	7.8	323
Hexane.....	1.2	55.2	7.5	368
Heptane.....	1.2	63.9	6.7	378
Octane.....	1.0	60.3	-----	-----
Isoparaffins				
2,2-Dimethylpropane.....	1.4	54.2	7.5	201
2-Methylpentane.....	1.2	55.2	7.0	342
2,2,4-Trimethylpentane.....	1.1	66.3	-----	-----
2,2,3,3-Tetramethylpentane.....	.8	53.9	4.9	345
Olefins				
Ethene.....	3.1	45.8	32	676
Propene.....	2.4	52.8	10.3	247
1-Butene.....	1.6	46.8	9.3	294
Aromatics				
Benzene.....	1.4	50.9	7.1	275
Toluene.....	1.4	61.1	-----	-----
Ethylbenzene.....	1.0	50.7	-----	-----

vessel in which the flame is observed should be at least 2 inches in diameter for observations at atmospheric pressure. It should also be long enough (4 ft) to allow the observer to judge whether the mixture is truly capable of propagating a flame indefinitely away from the ignition source. A glass tube of these dimensions is a suitable vessel. The ignition end of the tube should be open during the test to avoid a change in pressure.

Finally, it is important to specify the direction of flame propagation. Since it may be stated as a rough approximation that a flame cannot propagate downward in a mixture if the convection current it produces is faster than the speed of the flame, the limits for upward propagation are usually slightly wider than for downward or horizontal propagation. The experimental results discussed are limited to those obtained with upward propagation and subject to the precautions described, unless otherwise noted. In addition, only concentration limits of flammability at atmospheric pressure are discussed; the effects of pressure are considered in a subsequent section.

Hydrocarbon type.—The flammability limits of various hydrocarbon types in air at atmospheric pressure and room temperature are listed in table V (ref. 19). For the comparison shown in this table, the limits are expressed in terms of the percent of stoichiometric fuel-air ratio (by weight).

Although the results of table V indicate no striking effects of hydrocarbon type (above propane and propene) on the lean flammability limits, considerable variation among the rich limits is apparent. Among the saturated compounds (normal and isoparaffins), the rich limit tends to increase with molecular weight. Since the lean limits are about the same for all the fuels, the range of flammability increases with molecular weight. Ranges of flammability calculated from the data of table V are plotted to show this increase graphically in figure 87. A more complete set of data (ref. 20) indicates that the flammable range for normal paraffins passes through a maximum at *n*-heptane and decreases to *n*-decane. However, these data (ref. 20) are less accurate than those of table V because the work was done at reduced pressures, and extrapolations must be made to estimate the limits at 1-atmosphere pressure. In spite of these extrapolations, it is believed that the proper trends are indicated.

The branched-chain hydrocarbons (isoparaffins) have somewhat smaller flammable ranges than the corresponding straight-chain fuels (fig. 87).

Among the three monoolefins listed in table V, ethene stands out because of its extremely wide range of flammability (45.8 to 676 percent stoichiometric). The results for propene and 1-butene are similar to those for the corresponding saturated compounds. Figure 87 emphasizes the anomalous nature of ethene. An extension of the curve for olefins, by means of the data of reference 20, would show that the flammable range increases rapidly from propene to 1-hexene, and then levels off through 1-decene.

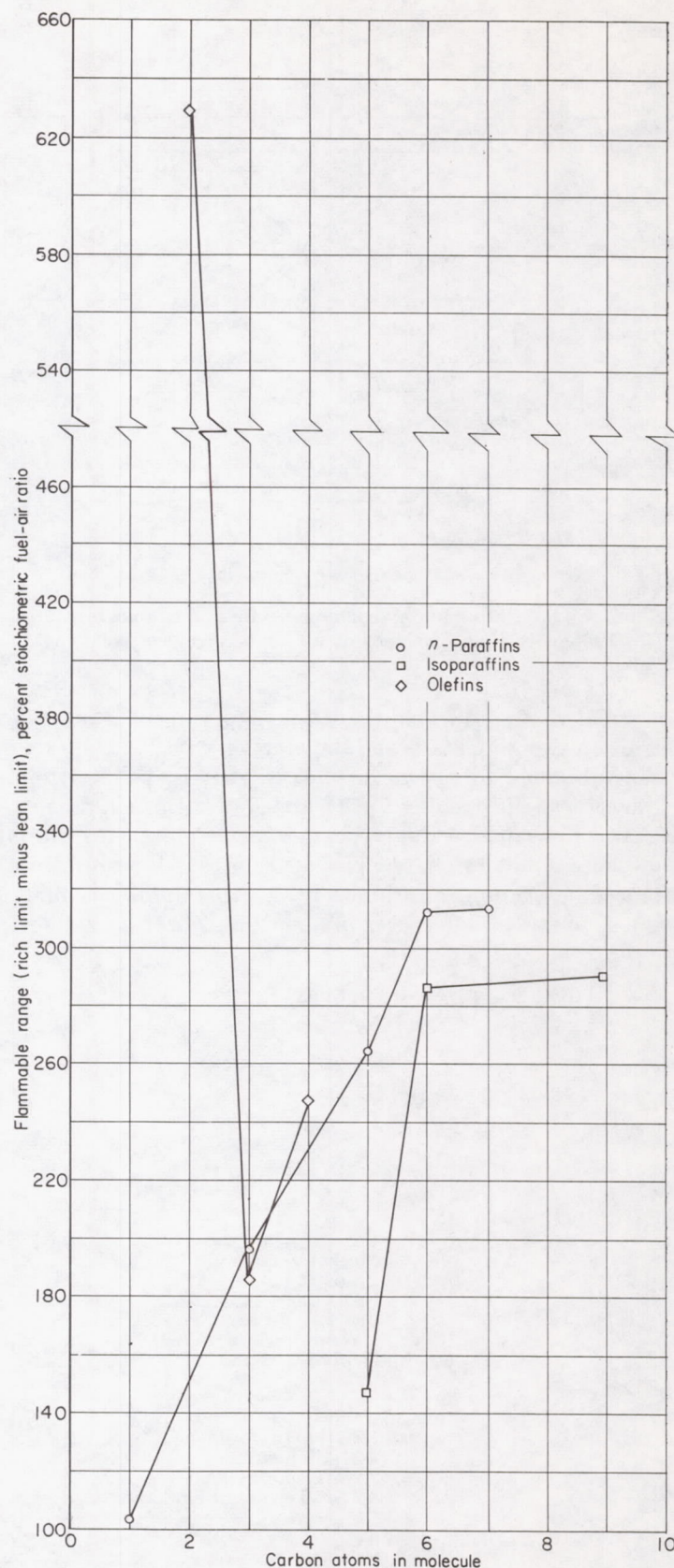


FIGURE 87.—Effect of hydrocarbon type on flammable range of pure fuels (ref. 19).

TABLE VI.—TYPICAL DISTILLATION DATA FOR AIRCRAFT FUELS (Ref. 21)

ASTM distillation D86-52, percent evaporated	Temperature, °F			
	AN-F-48, 100/130	MIL-F- 5616, JP-1	MIL-F-5624A	
			JP-3	JP-4
Initial point-----	105	338	113	148
10-----	144	362	169	218
20-----	162	366	198	255
30-----	178	369	218	288
40-----	191	373	236	319
50-----	202	377	254	349
60-----	210	381	270	378
70-----	219	387	293	409
80-----	225	393	324	441
90-----	236	404	388	475
End point-----	299	424	473	561

The data for aromatic compounds are incomplete. The flammable range for benzene is smaller than that for a six-carbon-atom branched-chain fuel.

The flammability limits for cycloparaffins are not included in table V, but reference 19 shows them to be very similar to the limits of normal paraffins with the same number of carbon atoms.

Petroleum fuels.—The discussion thus far has been concerned with the flammability limits of pure hydrocarbons. On the other hand, practical aircraft fuels are complex mixtures of many hydrocarbons, each with its own effect on the limits of the mixed fuel. The limits of such fuels, however, may be measured in the manner previously described, if the apparatus is maintained at a temperature high enough to keep all constituents in the vapor phase.

Inspection of the data in table VI (ref. 21) shows that, in order to obtain a consistent set of flammability limits for the four fuels, the limits of all would have to be determined at a rather high temperature. Perhaps the closest approach to the required conditions is found in experiments reported in reference 22. The limits determined at 300° F and atmospheric pressure for three fuels are listed in table VII. The data of reference 22 were reported only in terms of fuel-air ratios; in order to express the limits in volume-percent fuel vapor in air, it was necessary to estimate some average molecular weight for each fuel. This was done by

TABLE VII.—FLAMMABILITY LIMITS OF AIRCRAFT FUELS AT 300° F

Fuel	Flammability limits			
	Fuel-air ratio ^a		Volume percent ^b	
	Lean	Rich	Lean	Rich
100/130 gasoline-----	0. 041	0. 27	1. 17	7. 27
JP-1-----	. 037	. 31	. 71	5. 65
JP-3-----	. 037	. 30	. 93	7. 08

^a Ref. 22. ^b Estimated.

the methods described in reference 20, with the following results: average molecular weight of 100/130 grade gasoline, 100; JP-1, 150; JP-3, 114. Assuming that the fuels are mainly composed of paraffin hydrocarbons, these molecular weights correspond approximately to heptane, decane, and octane, respectively. The limits for these compounds (table V) compare fairly well with the limits in table VII, considering the approximations and the differences in temperature involved. It seems definite, from these and other data, that the flammable range of aircraft fuels completely vaporized and mixed with air is about 1 to 7 percent by volume.

If multicomponent liquid fuels are not completely vaporized, quite different results may be obtained. Thus, if the tests are carried out at low temperatures and only part of the liquid sample is vaporized, the vapors will be composed mainly of the lower-boiling constituents. Mixtures of these vapors with air may be prepared and the limits determined in the manner previously described. Both lean and rich limits should lie at higher concentrations (volume percent) than if the entire sample were vaporized, because the limits of the lighter hydrocarbons behave in this manner (table V). This expectation is verified by experiment; the lower the temperature (and, hence, the smaller the fraction of liquid fuel that serves as the source of vapor for making fuel-air mixtures), the higher the concentrations of the limits (ref. 22).

It is evident that the history of an aircraft fuel has an effect on its limits of flammability. For example, a fuel containing quantities of volatile hydrocarbons may be stored under conditions that permit their gradual escape, and the limits will be more and more controlled by the heavier compounds. Consequently, it is difficult to predict the flammability of a given sample, and even more difficult to obtain reproducible results if the supply of fuel vapor is obtained from, for example, the first 10 percent of the liquid to evaporate.

The preceding discussion refers to unsaturated vapor-air mixtures. If a liquid fuel and its vapors are allowed to come to equilibrium in a volume of air, so that the air is saturated at the given temperature, the temperature itself sets the lean

and rich limits. For example, grade 100/130 gasoline and JP-3 jet fuel have such high equilibrium vapor pressures at a temperature of about 78° F that saturated vapor-air mixtures are beyond the rich limit and are therefore non-flammable. As the temperature is lowered, however, a point will be reached on the vapor-pressure curve of the fuel that corresponds to the concentration of fuel in air at the rich limit. With still further reduction in temperature, the saturated mixtures will be flammable until a temperature is reached that corresponds to the vapor concentration for the lean limit. The two temperatures are referred to as the rich and lean temperature limits of flammability (at a given pressure). The range of temperatures corresponding to flammable saturated mixtures is lower for volatile fuels, such as 100/130 gasoline or JP-3, than for the less volatile JP-1 or JP-4. The temperature limits are discussed in reference 21.

It is not clear whether the temperature limits of flammability of saturated mixtures have any application to flowing mixtures of fuel droplets in air. It is perhaps conceivable that a spray of fuel droplets might come to equilibrium in the moving airstream if the turbulence level were sufficiently high to effect very rapid heat transfer and mixing of the vapor and air. Even if equilibrium were attained, however, the situation would be complicated by the effects of fuel droplets on the flammability of the vapor fuel-air and fuel-droplet mixture, as well as by the effects of velocity and turbulence.

Mists and sprays.—Relatively little work has been done on the flammability of vapor fuel-air and liquid fuel mixtures. There are obvious difficulties in measuring flammability limits in quiescent mixtures because of the need to prepare reasonably stable mists, in which the droplets will not settle out before the ability to sustain flame propagation can be tested. In addition, it is necessary to characterize the average droplet size, or else prepare mists of uniform droplets.

The observations of reference 23 show that there should be some mists with limits about the same as for vaporized fuels. In that investigation, kerosene droplets were fed into the approach streams of premixed Bunsen flames. If the droplets were small enough (9 to 30 microns in a butane-air mixture), they were completely vaporized and disappeared before reaching the inner cone. Larger droplets (of the order of 80 microns) completed evaporation definitely above the inner cone. Reference 23 also noted that, when the drops were carried by a fast-burning acetylene-air mixture, conditions were less favorable for vaporization, presumably because of the higher gas velocity and narrower preheat zone of the acetylene flame. Thus, a flame burning slowly enough, through a mist of small enough droplets, may actually be equivalent to a flame in a homogeneous vapor-air mixture.

This expectation of similar limits for the right kind of mist is borne out, for example, by reference 22 (p. 40). JP-1 vapor-air mixtures were chilled to condense some of the fuel. The average droplet size, measured immediately after formation, was 10 microns at 32° F. Under these conditions, the flammability limits were at fuel-air ratios of 0.043 (lean limit) and 0.23 (rich limit). Considering the difference in temperature, the limits of JP-1 mists are similar to the limits of JP-1 vapor-air mixtures at 300° F given in table VII (fuel-air

ratios, 0.037 and 0.31). More specifically, an estimate of the effect of the 268° F temperature difference on the limits, based on the temperature effects on limits of homogeneous mixtures (to be discussed in a subsequent section), shows that the lean limit of the mist corresponds very closely to that of the vapor. The rich limit of the mist, however, is at a lower concentration than would be estimated from the data on homogeneous mixtures.

The results of similar experiments (ref. 24) are presented in table VIII. While drop sizes were not measured, they must have been small to permit the formation of stable mists. Lean limits are again in the region anticipated for hydrocarbon vapors, and rich limits are at somewhat lower fuel-air ratios than are usually observed for heavy hydrocarbon vapors. This behavior of the rich limits is perhaps not too surprising, since the rich limit is more susceptible to slight effects, such as direction of flame propagation (e. g., for hexane with upward propagation, the rich limit is 0.242; with downward propagation, the limit is 0.112 (ref. 19)). Reference 24 also reports that the percentages of nitrogen or carbon dioxide that must be added to air to render mists of cutting oil number 3 nonflammable are: nitrogen, 30 percent; carbon dioxide, 22 percent. These values are somewhat smaller than the equivalent figures for hydrocarbon vapors (for *n*-heptane, the amounts required are: nitrogen, 42 percent; carbon dioxide, 29 percent) and suggest that the combustion of mists is more easily suppressed.

TABLE VIII.—LIMITS OF FLAMMABILITY OF OIL MISTS
(Ref. 24)

[Tube diam., 1½ in.]

Fuel	Fuel-air ratio	
	Lean limit	Rich limit
Cutting oil no. 1.....	0. 033	0. 118
Cutting oil no. 2.....	. 043	. 134
Cutting oil no. 2, distilled once.....	. 043	. 214
Cutting oil no. 3.....	. 038	-----
Sperm quenching oil.....	. 035	159
Diesel oil.....	. 038	-----

On the other hand, the spray flammability test of reference 25 does not indicate this difference. In this test, fuel was introduced as a spray into a cylinder 2½ inches in diameter and 15 inches long, through which an oxygen-nitrogen mixture was flowing. The spray flammability limit was defined by the minimum volume percent of oxygen for which ignition took place. In table IX, spray flammability limits for a number of hydrocarbons are listed, and minimum oxygen concentrations for combustion of hydrocarbon vapors are also included for purposes of comparison. While the empirical nature of the spray flammability test is stressed, it is of interest to note that these limits correspond closely to the values for hydrocarbon vapors. It is impossible to say whether the higher limits for lubricating oils were real or whether they were due to a failure of the spray to deliver sufficient fuel to the ignition region of the apparatus when more viscous oils were tested.

Recent work has extended and refined the study of mist flammability. In reference 26, uniform mists were prepared

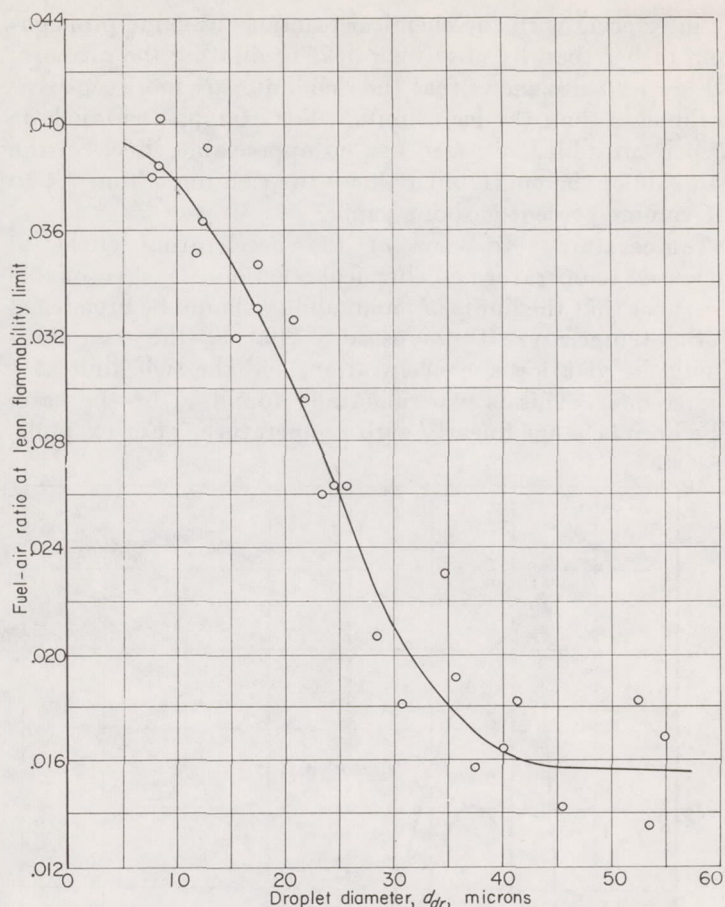


FIGURE 88.—Effect of droplet diameter on lean flammability limits of uniform tetralin mists (ref. 26).

by condensing fuel vapor on nuclei supplied by vaporizing sodium chloride with a heating coil. Various uniform drop sizes could be produced. Using tetralin as the fuel, nearly monodisperse mists were produced in the size range 7 to 55 microns. The mixtures had to be kept moving, but the maximum speed was only about 3 centimeters per second in the flammability-limit tube. The droplets did not aggregate appreciably during flow through the tube. The mists flowed downward and were ignited at the bottom, so that flame propagation was upward.

Reference 26 showed that there is a complete change in the nature of the flame between 7 and 55 microns. Figure 88 is

a plot of the lean limits of tetralin mists as a function of droplet diameter. The limit for small droplets is at a fuel-air ratio of 0.039, about the value expected for vapor-air mixtures. As the drops become larger, the lean limit decreases. Over this range of sizes, there is at the same time a continuous change in flame nature; for the small drops the flame has every appearance of a gaseous lean-limit flame, but as the drops become larger the flame is more and more composed of discrete centers of burning around individual drops.

Reference 26 reports a few experiments with downward propagation. Limits for this case could be measured accurately only for the smallest drops. For 9-micron drops, the upward limit was at a fuel-air ratio of 0.039, and the downward limit at 0.044. This is the same order of difference as observed for gaseous lean limits.

Reference 26 also showed the effects of added nitrogen on the lean limits for drops of 10, 19, and 45 microns diameter. The results are shown in figure 89. There is a gradual increase in lean limit up to the limiting nitrogen concentration, followed by an abrupt rise. Note that more nitrogen is required to prevent flame propagation through mists of larger drops. This indicates that the nitrogen extinction limit depends on the value of the lean limit in air. It is interesting to note that the oxygen concentration at the limit, for the small drops already shown to burn like a gaseous mixture, is close to 12 percent, just as in other gaseous hydrocarbon flames (table IX).

In summary, from the information available, it seems clear that flames can propagate in mixtures of vapor fuel-air and liquid fuel at over-all fuel-air ratios similar to those found for the limits of homogeneous vapor-air mixtures.

The observations that are sometimes made of burning at extremely lean or rich over-all fuel-air ratios may be a result of the existence of regions in which the mixture is actually within the flammable range; these regions may serve as sources of piloting combustion.

Diluents.—As increasing amounts of an incombustible gas or vapor are added to the atmosphere, the flammability limits of a gaseous fuel in the atmosphere approach one another, and finally meet. Inert diluents, such as carbon dioxide, nitrogen, or argon, merely replace part of the oxygen in the mixture; but they do not all have the same extingutive power. The order of efficacy is the same as that of the heat capacities

TABLE IX.—SPRAY FLAMMABILITY LIMITS COMPARED WITH MINIMUM OXYGEN CONCENTRATIONS FOR COMBUSTION OF HYDROCARBON VAPORS IN OXYGEN-NITROGEN MIXTURES

Fuel (liquid)	Spray flammability limit, ^a % O ₂ in O ₂ -N ₂	Fuel (vapor)	Min. O ₂ concentration for fuel-vapor combustion, ^b % O ₂ in O ₂ -N ₂
Benzene.....	12	Benzene.....	11. 2
n-Hexadecane.....	12	Methane.....	12. 1
Cumene.....	12	Propane.....	11. 4
Aviation hydraulic fluid AN-VV-O-366B.....	12	Pentane.....	12. 1
Naval lubricating oil N. S. 2135.....	34	Hexane.....	11. 9

^a Ref. 25.

^b Ref. 19.

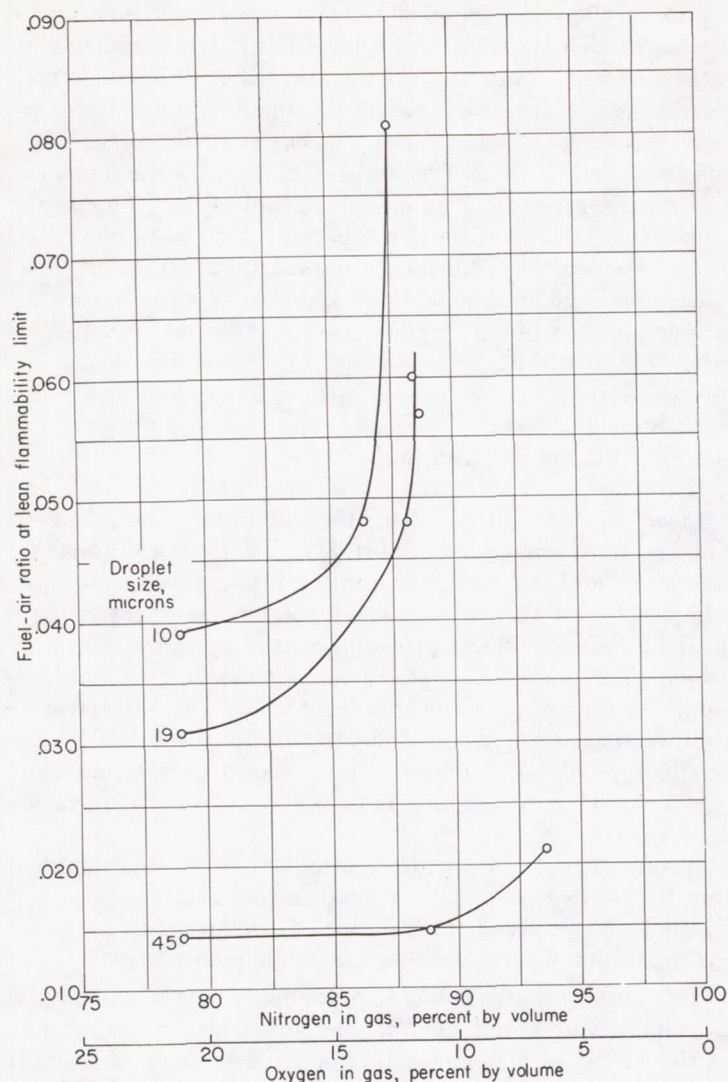


FIGURE 89.—Effect of nitrogen dilution on lean flammability limits of tetralin mists (ref. 26).

of these three gases: carbon dioxide $>$ nitrogen $>$ argon. For example, the minimum percentage of oxygen that will permit flame propagation in mixtures of methane, air, and carbon dioxide is 14.6 percent by volume; if nitrogen is the diluent, more is required to reduce the oxygen to 12.1 percent; and, in the case of argon, still more is needed to reduce the oxygen to 9.8 percent (ref. 19, p. 49).

Other types of diluent are far more effective than the inert gases. Certain halogen-containing organic compounds, in particular, have very powerful effects. Figure 90 is a plot of the lean and rich limits of flammability of gasoline in atmospheres of air plus several diluents. The compositions given are volume percentages of the total mixture. Methyl bromide and chlorobromomethane (ref. 27) are much more effective extinguishants than nitrogen, exhaust gas, or carbon dioxide (ref. 5, p. 764); that is, smaller concentrations are required to prevent flame propagation in any mixture of gasoline vapor and air. References 28 and 29 contain thorough discussions of this subject.

Since the halogenated compounds are in an entirely different class of efficacy from the other three gases shown in figure 90, it is believed that they exert their extinctive action

by interfering with the chemical reactions of flame propagation, rather than by absorbing heat or diluting the mixture.

Figure 90 also shows that the rich limits are more sensitive to diluents than the lean limits. For example, as much as 15 percent added nitrogen has no appreciable effect on the lean side of the curve but reduces the rich limit from 7.4 to 5.4 volume-percent gasoline vapor.

Temperature.—In view of the accelerating effect of increased temperature on chemical reactions, it is reasonable to expect that the limits of flammability should be broadened if the temperature is increased. That is, the lean limit should lie at a lower concentration, and the rich limit at a higher one. This is experimentally found to be the case. The limits change linearly with temperature. For example,

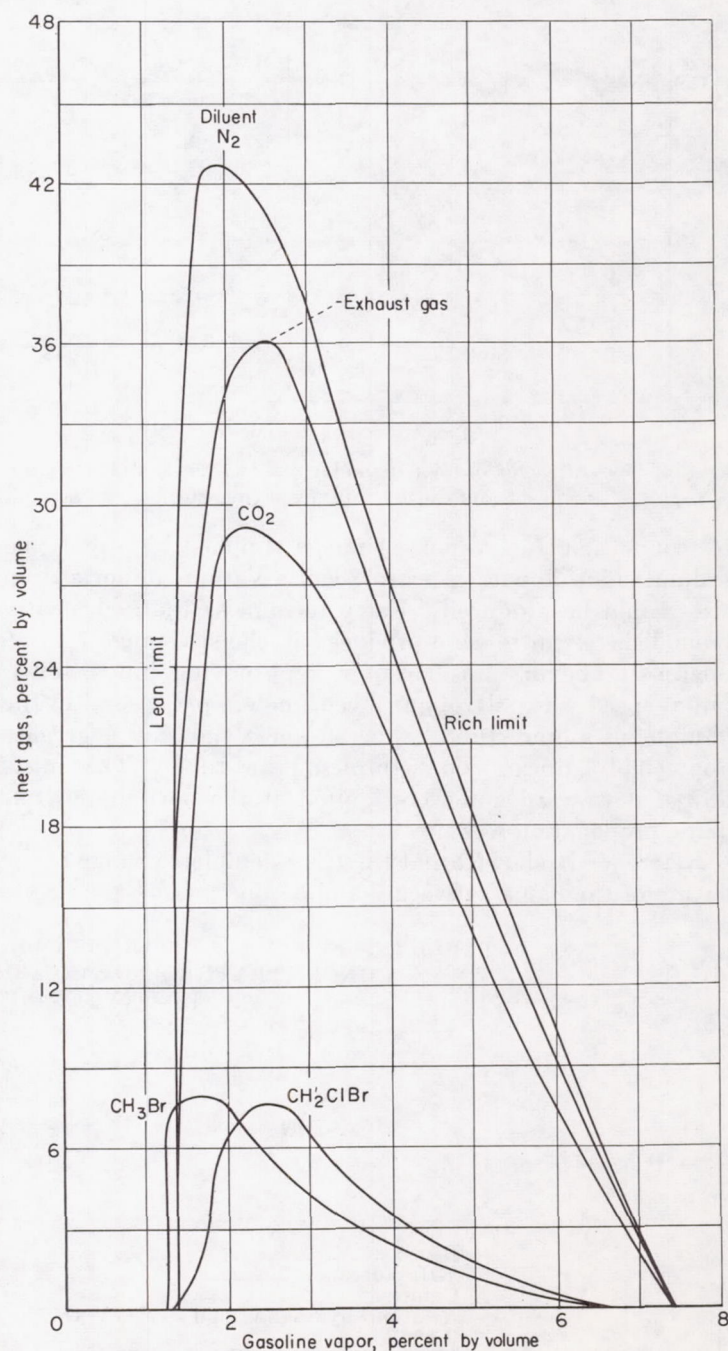


FIGURE 90.—Effect of diluents on flammability limits of gasoline (refs. 5 and 27).

the lean limit of *n*-pentane decreased from 1.53 volume percent at room temperature to 1.22 percent at 570° F, so that the lean limit decreased at a rate of about 6.1×10^{-4} volume percent per °F. The rich limit increased at a higher rate, approximately 17×10^{-4} volume percent per °F (ref. 19, p. 63). These data were obtained with downward flame propagation, but upward propagation leads to analogous results (ref. 20). The figures quoted for *n*-pentane appear to be characteristic of other hydrocarbon fuels. Thus, increases in the temperature of homogeneous hydrocarbon-air mixtures produce widened limits of flammability; however, the effects are relatively small.

Velocity and turbulence.—Most of the flammability-limit studies discussed previously have been concerned with quiescent, homogeneous mixtures. Information on the flammability limits of flowing streams of mixture is of considerable practical interest, but very few such observations have been made. It is known that mixtures may be circulated slowly through a flame tube by means of a fan in an external bypass without any effect on the limits (ref. 30). This observation cannot be considered to apply to the fast streams in high-speed combustors.

A flame burning in a laminar stream cannot propagate upstream against normal components of the flow velocity greater than the laminar burning velocity; in this sense, such a stream might be nonflammable. If the stream is turbulent, the over-all burning rate is increased, as described in chapter IV, and the flame may be able to propagate. Therefore, it appears that the effects of velocity in laminar streams are of little practical value. The effects of turbulence and of velocity in turbulent streams are the important ones, because the flow in practical combustors is invariably turbulent and has a mean velocity greater than the laminar burning velocity.

Only a few experiments have been made to elucidate the effects of turbulence on the limits. The lean limits of methane and ethane are somewhat extended by a suitable amount of turbulence produced by a fan or by stream velocity; that is, flames will propagate in turbulent mixtures that are too lean to sustain propagation in the quiescent condition (ref. 19). However, the turbulence was not characterized; and, in the case of the mixtures stirred by a fan, it is possible that true turbulence—that is, completely random disturbances—may not have existed. An opposite effect was found for propane-air mixtures in a different experiment. In this experiment, an axial rotor as long as the flame tube was rotated at various speeds. Above 850 rpm, the lean limit was markedly narrowed (ref. 31); no attempt was made to characterize the turbulence.

A more meaningful experiment is the one described in reference 11 and discussed previously in connection with homogeneous quenching. In that case, the range of fuel concentrations capable of propagating a flame was narrowed by an increase in flow velocity. At flow velocities between 12 and 50 feet per second, however, the lean limit was extended. In the experiment of reference 11, the flow disturbances were due to pipe turbulence; it is believed that the fluctuations were more likely to be random and thus constitute true turbulence than in experiments employing fans or rotors.

Reference 11 suggests that the narrowing of the limits with

increase in velocity may be due to the fact that turbulent intensity also increases, so that the flame zone is more diluted with cold unburned mixture. However, a different interpretation is also possible. Karlovitz has observed the stability of turbulent burner flames stabilized on the burner port by a small annular pilot flame (ref. 32). At sufficiently high flow velocities, broken-off flames were obtained such that a flame burning in one part of the combustible mixture would not propagate through the mixture. The situation is roughly similar to the experiment of reference 11. The explanation given in reference 32 is that flame propagation is arrested by the high velocity gradients across the flame front.

It is not yet possible to draw definite conclusions about the effects of velocity and turbulence on the flammability limits. Various observers have reported contradictory results; it may be that a suitable type of turbulence broadens the limits up to a certain level of turbulent intensities and narrows the limits at higher intensities. In view of the work of reference 11, it is tentatively suggested that, in high-speed combustors employing homogeneous fuel-air mixtures, the flammable range of homogeneous mixtures is reduced by increase in velocity and turbulence. It would, however, be unsafe to apply this idea to heterogeneous mixtures.

EFFECTS OF VARIABLES ON FLAMMABILITY LIMITS AT NONATMOSPHERIC PRESSURES

All the flammability limits discussed thus far have been at atmospheric pressure. Less work has been carried out at pressures above and below 1 atmosphere. The behavior of the limits at elevated pressures is somewhat surprising and has not been completely explained. For the simple hydrocarbons, ethane, propane, butane, and pentane, it appears that the rich limits extend linearly with increasing pressure at a rate of about 0.13 volume percent per atmosphere increased pressure above atmospheric. The lean limits, on the other hand, are at first extended slightly, but between 1.3 and 2.5 atmospheres they pass through a minimum concentration and are thereafter narrowed as pressure is increased to 6 atmospheres (ref. 19, p. 56).

For flammability limits at reduced pressures, most of the older work indicated that the rich and lean limits converge as the pressure is reduced until a pressure is reached below which no flame can propagate (ref. 19, p. 3). However, as pointed out in the discussion of quenching, it has been found that this behavior is due to wall quenching by the tube in which the experiments are conducted (ref. 8). The limits are actually as wide at low pressure as at 1 atmosphere, provided the tube is sufficiently wide, and provided an ignition source can be found that will ignite the mixtures. For example, recent work (ref. 33, p. 5), in which a 4-inch tube was used, has shown this to be true for gasoline vapor-air mixtures down to pressures less than 1 inch of mercury. Consequently, the limits obtained at reduced pressures are not generally true limits of flammability, since they are influenced by the tube diameter and are therefore not physicochemical constants of a given fuel. These low-pressure limits might better be termed limits of flame propagation, and should be accompanied by a specification of the tube diameter.

Hydrocarbon type.—Investigations have been conducted at the NACA Lewis laboratory to measure the low-pressure limits of flame propagation of a large number of fuels. The experiments were carried out in a flame tube 2 inches in diameter with a hot wire as the igniter. The apparatus was not provided with a plenum, so the flames did not propagate at constant pressure; however, all the limits were determined in the same manner, and the data are consistent. The results are presented in references 20 and 34.

Both the lean and rich limits are virtually unaffected by decrease in pressure from 1 atmosphere to about 10 inches of mercury. This result is in agreement with the data of figure 82. Furthermore, the relative order of concentrations of the limits for the various fuels is the same as at atmospheric pressure. Therefore, table V, which gives the limits at 1 atmosphere for several pure compounds, also qualitatively describes the results at pressures down to 10 inches of mercury. Further decrease in pressure introduces the quenching effect of the walls and causes both lean and rich limits to converge quite rapidly. The limits finally meet at a minimum pressure below which flame cannot propagate in homogeneous mixtures in a 2-inch tube. This minimum was about 1.3 inches of mercury for most of the fuels investigated.

The relative order of the rich limits for a series of fuels was not the same at pressures below 6.5 inches of mercury as above that pressure. This change occurred through a peculiar behavior of the limit curves. Several typical examples for normal paraffins in air are shown in figure 91. The rich side of the curve contains an additional lobe; this type of pressure-limit curve was found for all hydrocarbon fuels except methane (refs. 20 and 34). It has been suggested that the lean lobe corresponds to the limits of propagation of normal flames, while the rich lobe is due to "cool flames" which are capable of propagating in rich hydrocarbon-air mixtures by means of a different mechanism (ref. 34).

Petroleum fuels.—Reference 22 reports the effect of reduced pressure on the limits of flame propagation of several petroleum fuels. The data were obtained in a closed 2-inch-diameter tube, in an apparatus similar to the one described in reference 34. However, in the tests of reference 22, a spark-ignition source was used in place of a hot wire. Reference 34 states that doubt exists as to the possibility of initiating cool flames with a spark source; the data of reference 22 support this idea, for the curves do not show cool-flame lobes such as those in figure 91. Curves are presented in figures 92(a) and (b) for 100/130 grade aviation gasoline and for JP-3 fuel. The data were obtained at 77° to 81° F with fuel-air mixtures prepared only from the first 20 percent of vapor that distilled from the multicomponent petroleum fuels. Therefore, the percentages of heavy vapors in the mixtures were small. It should also be noted that the previous history of the fuels must have had an effect on the results, as discussed previously in connection with the limits of flammability of petroleum fuels at atmospheric pressure. In view of the uncertain average molecular weight of the combustible vapors, the data in figure 92 are plotted in terms of volume percent of combustible in air.

The facts that a closed flame tube was used in these experiments and that the type of spark-ignition source

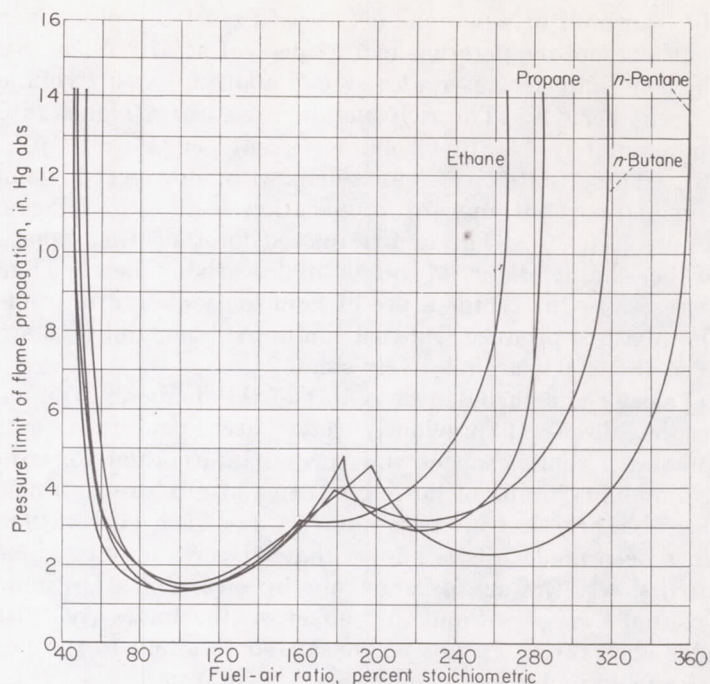


FIGURE 91.—Low-pressure limits of flame propagation of normal paraffins in air in 2-inch tube (by permission from ref. 34).

affected the results indicate that the data of figure 92 are of value mainly for comparative purposes. It is believed that they are not true flammability-limit data. However, it is interesting to note that flame propagation may occur at pressures less than 1 inch of mercury, and that the roughly vertical portions of the curves lie at fuel concentrations similar to the true flammability limits at 1 atmosphere of pure normal-paraffin fuels in the butane-heptane range.

SIGNIFICANCE OF FLAMMABILITY LIMITS

Limits of flame propagation.—The significance of the observations discussed in the foregoing sections must necessarily be considered in terms of the experimental conditions. The true limits of flammability, which are physicochemical constants of the fuel at a given temperature and pressure, are not affected by the size and shape of the vessel or by the igniter. As has been pointed out, measurement of these true flammability limits has been confined mainly to atmospheric pressure, because at lower pressures the quenching influence of the walls occurs. The limits at lower pressures are therefore properly termed limits of flame propagation and may be related to quenching distances. That is, limits of flame propagation at low pressures occur in mixtures that are actually flammable, and in sufficiently large vessels it appears that flame may propagate in these mixtures down to very low pressures.

In addition, it is not yet certain that true limits of flammability may be measured in any but homogeneous mixtures of fuel vapor and air because of the difficulty of defining precisely the physical state of heterogeneous mixtures of liquid and vapor fuel with air.

The limits of flame propagation at reduced pressure have already been discussed, and the relation to quenching has been described. The true limits of flammability, determined for homogeneous mixtures at atmospheric pressure, remain to be considered.

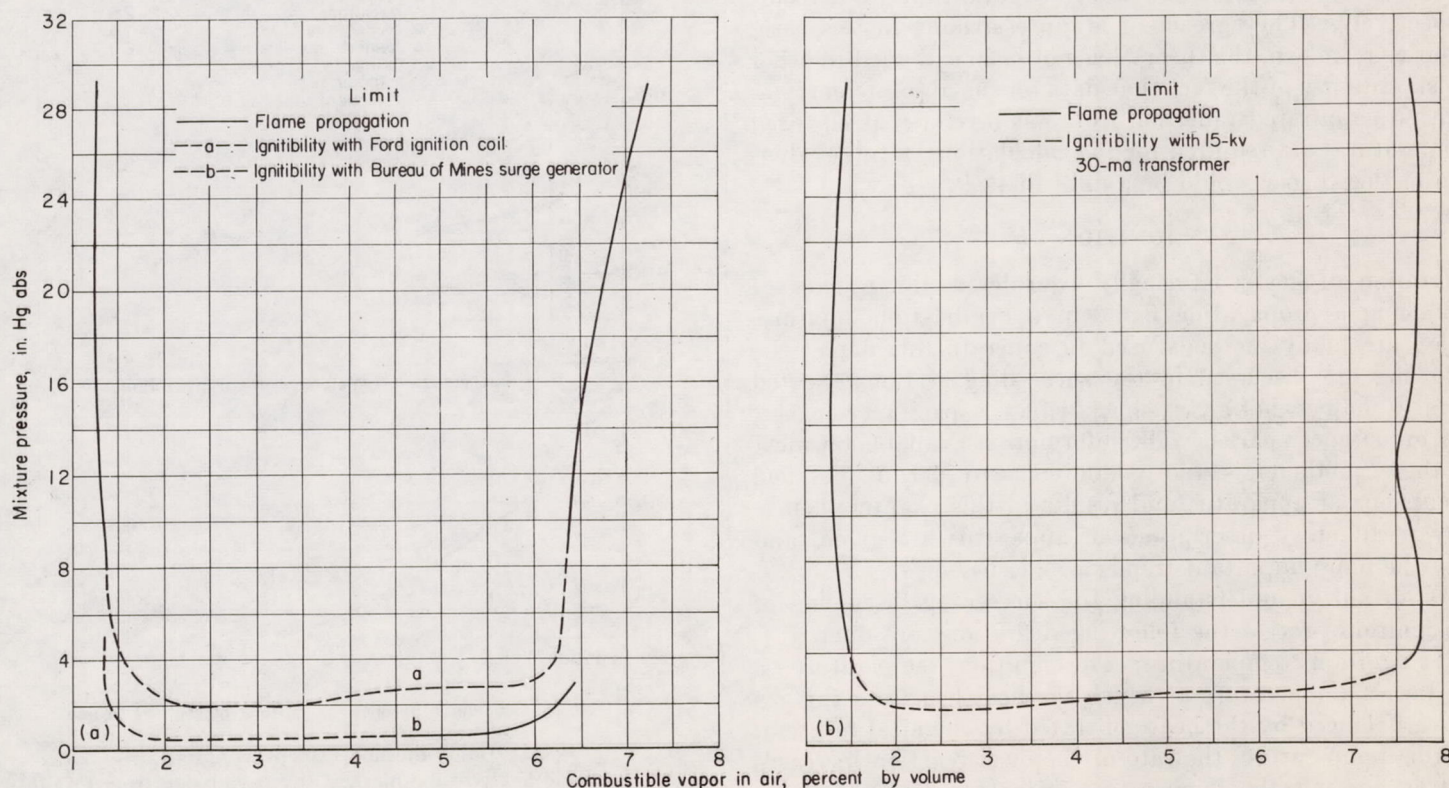
True flammability limits.—If a flame is to propagate through a mixture, it is evident that each layer of fresh gas just ahead of the flame must be ignited so that the flame overtakes it just as the chemical reactions of combustion reach the state characteristic of the flame. It is therefore reasonable that the true limits of flammability should occur at fuel concentrations such that just sufficient energy is transmitted from the flame to the gas ahead to allow this continuous ignition to take place. Dilution of the limit mixture by fuel at the rich limit, or air at the lean limit, would upset the balance, and flame would propagate only if aided by some external energy supply such as the ignition source.

It was pointed out previously that diffusion of active particles and conduction of heat from the flame zone to the cold gas are probably both important in the process of flame propagation. It is not yet established which of these two mechanisms will be more successful in explaining the observed combustion phenomena. Regardless of the mechanism of energy transfer, however, it is logical to expect that the limit concentration should be related to the amount of chemical enthalpy (heat of combustion) available in the mixture for transfer to the unburned gas. This expectation is experimentally verified, at least for the lean flammability limits of hydrocarbon fuels. On the average, lean-limit mixtures of most hydrocarbons have a combustion heat release of 10.4 kilocalories per mole of fuel-air mixture (ref. 20). Also, Egerton and Powling (ref. 35) have shown a very striking correlation between the heat of combustion of the fuel and the reciprocal of the lean-limit concentration (ref. 5, p. 334). Similar correlations between the heat of combustion and the rich flammability limits have not been

so successful. However, it has been found that the calorific values of rich-limit mixtures are approximately the same for several hydrocarbon fuels (ref. 19, p. 12). The same general ideas of flammability limits may therefore apply to both rich and lean limits.

The foregoing discussion implies that there may be a characteristic temperature associated with the limit flames of each fuel. It will be recalled that increased initial mixture temperature widens the limits, so that the heat of combustion per mole of mixture is decreased. If there is a characteristic limit flame temperature, the decrease in heat of combustion should be just balanced by the gain in heat content due to the higher initial temperature. This is found to be approximately true for several hydrocarbons and may explain the linear dependence of limits of flammability on initial mixture temperature that is usually observed (ref. 19, p. 12).

The general ideas of flammability limits discussed have not as yet been implemented with a useful theory. The theoretical approach of Lewis and von Elbe (ref. 5, p. 369) has not led to a means of calculating the limits from basic physical and chemical properties of fuel-air mixtures. The ideas expressed in reference 36 have been somewhat more successful. This work points out, both on the basis of the thermal theory of flame propagation of Zeldovich and from experimental evidence, that the burning velocity does not fall to zero in a limit mixture. Consequently, there must be some factor than prevents the propagation of slower flames in mixtures more dilute than the limit mixtures. It was suggested that this factor is the loss of heat due to radiation. The radiation in question is chiefly infrared. On the basis of necessarily crude calculations, which were not described in detail in the reference, it was estimated that radiation



(a) Aviation gasoline, grade 100/130. Temperature, $78^{\circ} \pm 1^{\circ}$ F. (b) Aviation jet fuel, grade JP-3. Temperature, $79^{\circ} \pm 2^{\circ}$ F.
FIGURE 92.—Limits of flame propagation of petroleum fuels at reduced pressures in closed 2-inch-diameter tube (ref. 22).

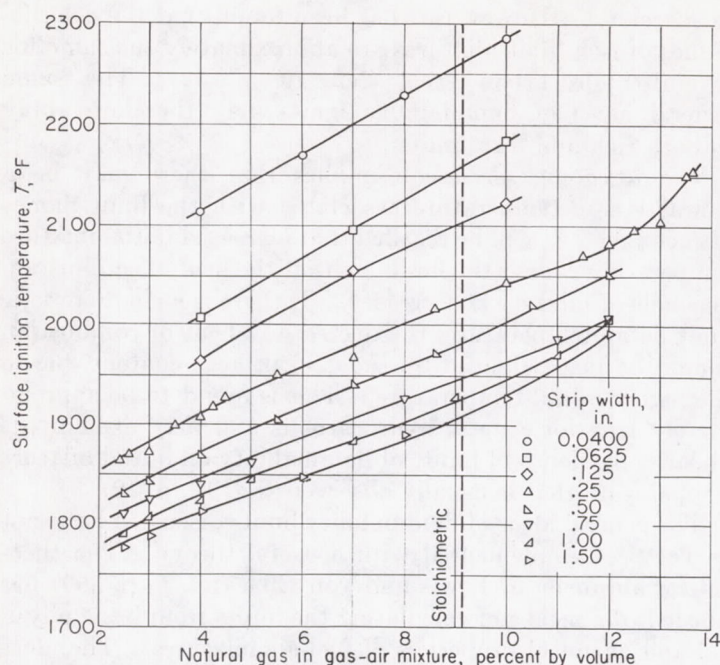


FIGURE 93.—Effect of mixture composition on surface ignition temperature of various quiescent mixtures of natural gas and air. Ignition by electrically heated $\frac{1}{2}$ -inch-long nickel strips cut from sheet of No. 18 B&S gage commercial nickel (ref. 43).

makes it impossible for a flame to propagate in carbon monoxide mixtures at a velocity less than 0.065 foot per second. The lean limit of carbon monoxide in air was calculated to be between 10 and 13.5 percent carbon monoxide by volume, and the rich limit between 81 and 87.5 percent. These figures may be compared with those of reference 19, which gives the limits as 12.5 and 74 percent, respectively. The agreement is quite striking in this case; so far as is known, the theory has not been extended to other fuels. In view of the fact that data on the absolute energies emitted as infrared radiation from gas mixtures at elevated temperatures are required for the calculations, a full evaluation of this theory would be a difficult task.

IGNITION

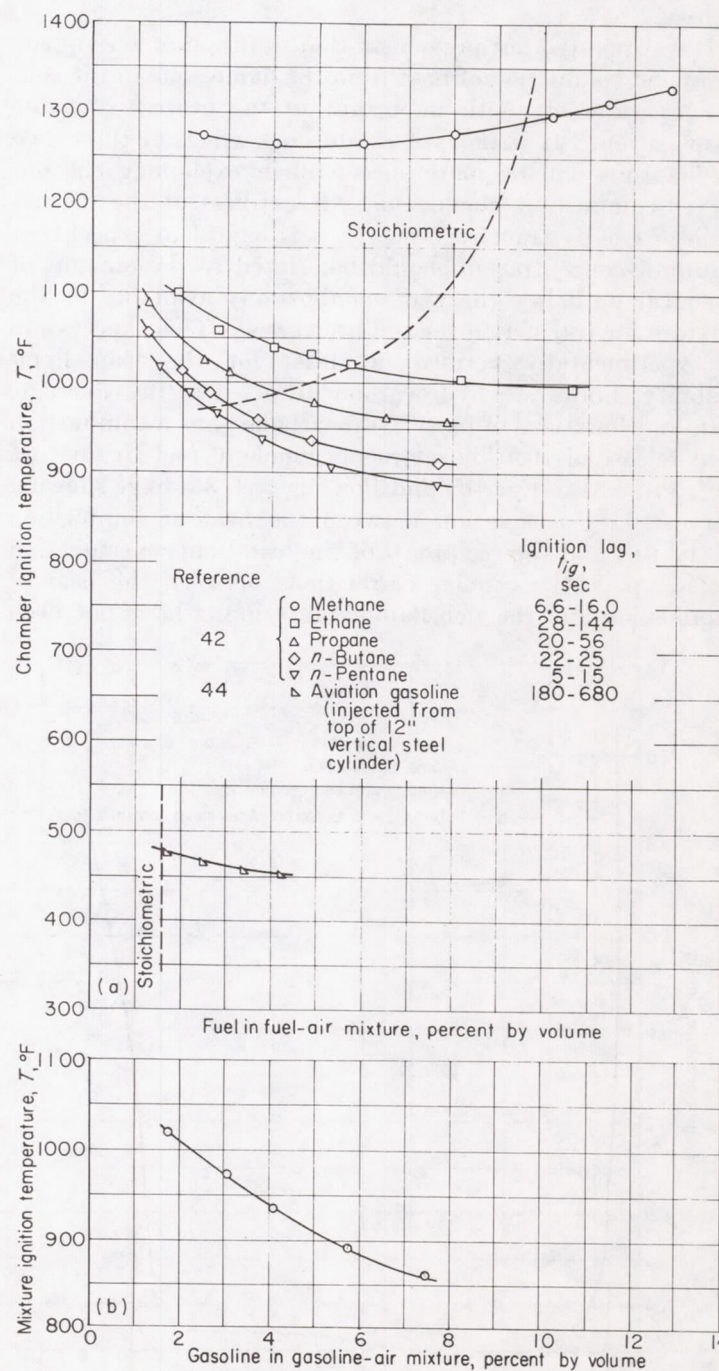
Ignition of gases is usually considered the process of producing a propagating flame in a combustible mixture. There are many methods used to generate this flame; the following are discussed in the succeeding sections: heated surfaces, flames, hot gases, shock waves, capacitance sparks, and inductance sparks. The information available on most of these methods is too voluminous to permit detailed discussions of apparatus and results in this chapter; hence, only perfunctory descriptions of apparatus are given, and only the more important trends are discussed.

As an aid in understanding the succeeding discussion of the ignition process the following definitions are offered:

(1) Ignition temperature: The ignition temperature is the lowest temperature at which the heat lost from the gas is overbalanced by the heat generated by chemical reaction. At this temperature, the rate of chemical reaction increases and as a result the temperature is increased to the flame temperature. However, when it is desired to determine

ignition temperatures, it becomes necessary to employ various types of apparatus which in themselves do not give the true temperature of the gas but rather a temperature of part of the apparatus. Hence, temperatures reported hereinafter for various ignition methods are equipment temperatures.

(2) Ignition limits: Ignition limits of a mixture are those proportions of fuel in air or oxygen that are just capable of permitting flame in a portion of the mixture for a specific ignition method. Because ignition is considered as the process of initiating a propagating flame, ignition is limited by the limits of flammability previously discussed.



(a) Bomb method (except as noted).
(b) Dynamic heated-tube method (by permission from ref. 45).
FIGURE 94.—Effect of mixture composition on ignition temperatures of different fuels.

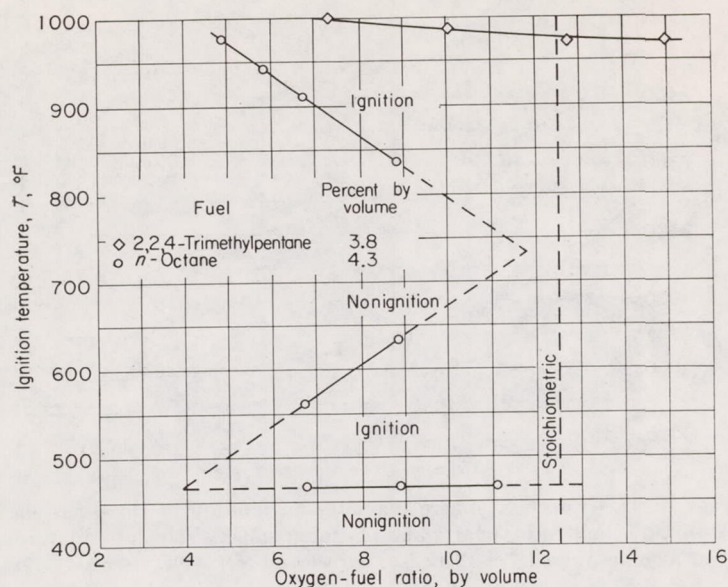


FIGURE 95.—Ignition characteristics of *n*-octane and 2,2,4-trimethylpentane in mixtures of fuel, oxygen, and nitrogen. Ignition by dynamic heated-tube method; supporting atmosphere flow, 230 cc per minute at atmospheric pressure and temperature (by permission from ref. 45).

(3) Ignition lag: Ignition lag is the time between the introduction of the mixture to the ignition source and the first indication of ignition.

IGNITION BY HEATED SURFACES

The most important methods used to obtain basic data on surface ignition temperatures of fuels are: (1) crucible methods, static and dynamic; (2) heated surfaces of various geometries; (3) adiabatic compression method, and (4) bomb method.

The crucible methods have been most widely used to obtain ignition temperatures of liquid fuels. In this method, a drop of fuel is dropped through an opening into a heated container filled with either quiescent or flowing air or oxygen (depending upon whether static or dynamic tests are to be made). The crucible temperature and ignition lag are determined at the instant the drop bursts into flame. The disadvantages are that the mixture composition is not obtained and that the heat of vaporization must be supplied by the crucible. The ignition temperature is the surface temperature of the crucible. This method has been derived from the methods described in references 37 and 38 and yields ignition temperatures that are among the lowest found in the literature. The crucible method has been critically evaluated and refined by Setchkin (ref. 39).

The dynamic heated-tube method (ref. 40) utilizes concentric quartz or Pyrex tubes in which the flammable vapor and supporting atmosphere are flowing and are separately heated. The flammable vapor is metered into the large tube containing the supporting atmosphere by means of a small orifice in the end of the small tube. The measured ignition temperature is the mixture temperature at which flame appears after a measured time lag. The mixture composition is controllable in this method.

The adiabatic-compression method was originally developed by Tizard and Pye (ref. 41) to eliminate the effects of

the surface on ignition temperature. The apparatus was constructed with a piston that moved forward very rapidly to compress a volume of fuel-air mixture in a cylinder; the piston was locked at the end of the stroke. Reasonable calculations showed that the time required for any appreciable heat loss from the gas to the cylinder walls was much greater than the observed ignition lags. The ignition lags depend upon the temperature reached in the compression process; the temperature is calculated from the compression ratio as determined from a pressure record.

The original intention of Tizard and Pye, that the ignition temperatures obtained by the adiabatic-compression method should be those for homogeneous gas-phase ignition, does not appear to have been fulfilled. The experiments of reference 41 showed that, although the ignition lags were only of the order of 10^{-3} second up to a few tenths of a second, significant heat transfer to the cylinder walls occurred. Lewis and von Elbe, in a discussion of the adiabatic-compression method, point out that all experimenters have found it necessary to condition the walls of the reaction chamber in order to obtain consistent results (ref. 5, p. 162). This fact plainly indicates a wall effect on the ignition temperatures. Furthermore, strong evidence for a wall effect has been obtained in photographs taken through the end of the compression chamber fitted with a window; the pictures show that luminous spots appear first at the surface of the cylinder and grow inward (ref. 5, p. 163). Thus, ignition definitely does not occur uniformly throughout the compressed mixture. For these reasons, it appears that the adiabatic-compression method, like the other methods under discussion, gives some sort of apparatus temperature rather than an absolute ignition temperature.

The bomb method (ref. 42) utilizes an evacuated chamber heated to a known temperature. The flammable mixture is introduced into the chamber and time lag is measured. The chamber has possible catalytic effects, and errors may result because the mixture must be heated before ignition can occur.

Data from all these methods cannot be compared because of the difference in experimental apparatus and technique. However, data from one source can be used to show the trends of different variables.

Mixture composition.—The effect of mixture composition on the surface ignition temperature of electrically heated nickel strips (ref. 43) is shown in figure 93. The approximately linear relations show that the ignition temperature increases as the percentage of fuel in the fuel-air mixture increases and as the strip width decreases. This trend of increasing temperature with increasing proportions of fuel does not hold for all fuels. Figure 94 shows that, for some hydrocarbons of the paraffin series, the temperature decreases with increasing fuel proportions (refs. 42 and 44), although it might be expected that the curves will eventually turn back up at richer mixtures. Gasoline shows a trend similar to the paraffin hydrocarbons (fig. 94).

A fuel may exhibit two ignition temperatures at certain oxygen-fuel ratios (ref. 45). For example, figure 95 shows the ignition temperatures for *n*-octane and 2,2,4-trimethylpentane as a function of oxygen-fuel ratio. For 2,2,4-tri-

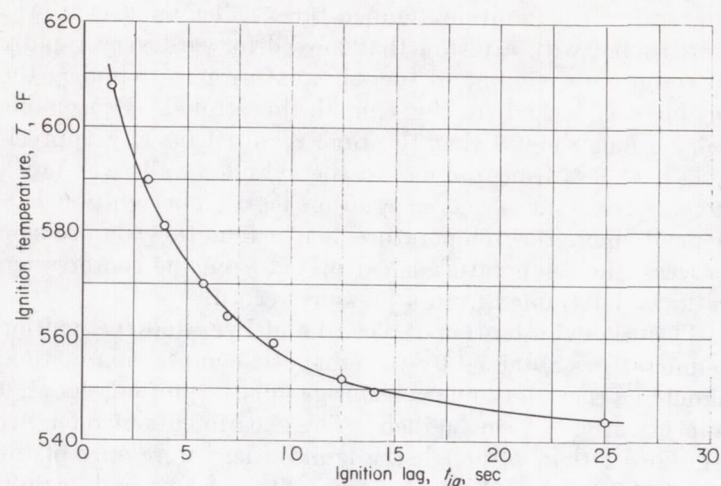


FIGURE 96.—Variation of ignition temperature of gasoline in oxygen with varying ignition lags as determined by dynamic-drop method in platinum crucible (ref. 48).

methylpentane, the temperature gradually decreases with increasing oxygen-fuel ratio. However, with the *n*-octane fuel and, for example, an oxygen-fuel ratio of 8, an ignition region is found between 465° and 605° F, a nonignition region between 605° and 865° F, and another ignition region above 865° F. Hence, there are two types of ignition: (1) a low-temperature ignition that is substantially constant regardless of fuel concentration, and (2) a high-temperature ignition that is affected by fuel concentration. The readily ignited hydrocarbons, such as cetane, heptane, decane, and decahydronaphthalene, exhibit zones of nonignition above the minimum ignition temperature (ref. 46). Reference 47 shows that mixtures of air and straight-chain paraffins containing three or more carbon atoms exhibit zones of nonignition. Oxidation-resistant hydrocarbons such as ben-

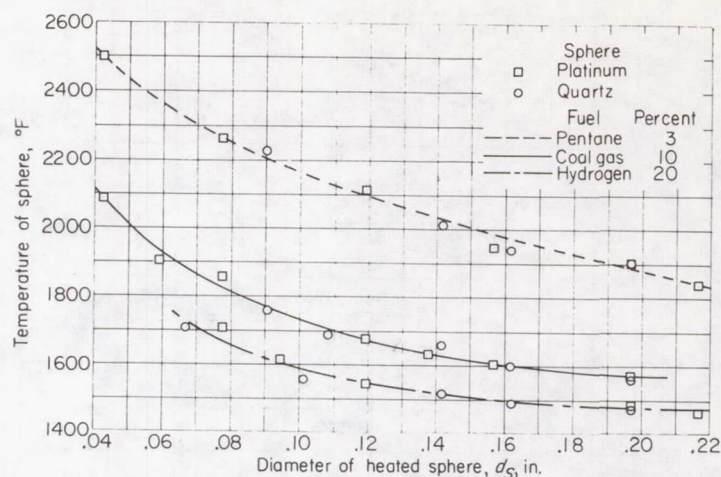
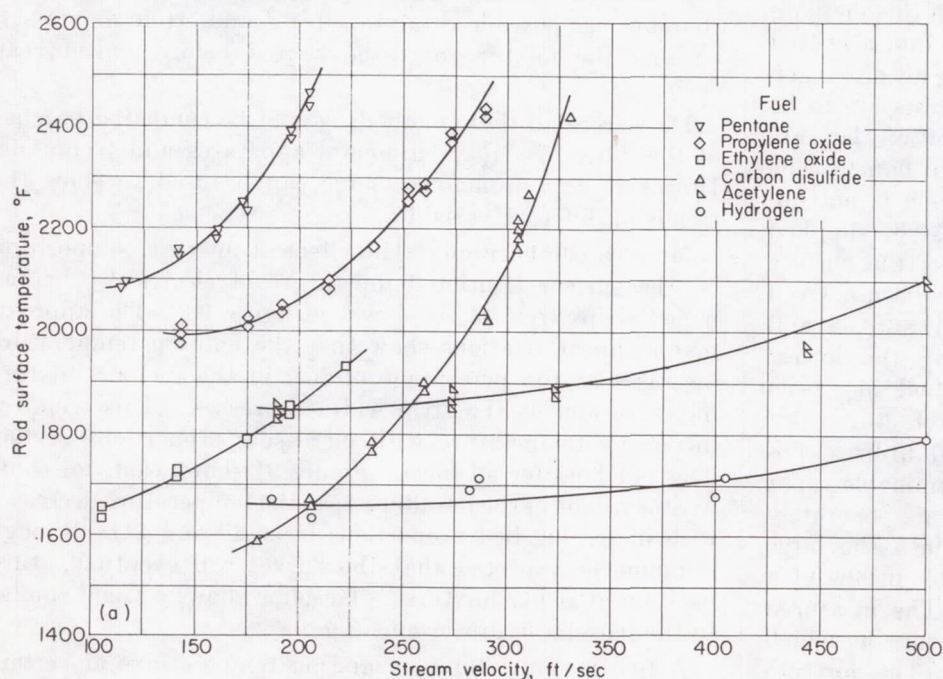


FIGURE 97.—Effect of sphere diameter on ignition of three gas-air mixtures ignited by quartz and platinum spheres shot into mixture at average velocity of 13.12 feet per second (ref. 49).

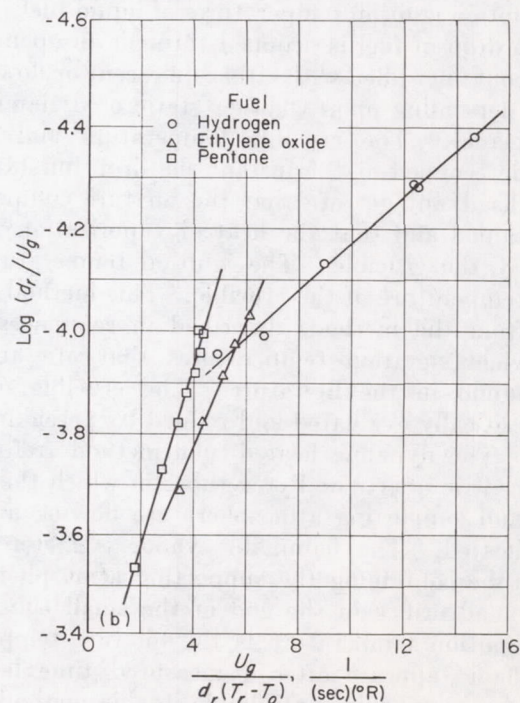
zene, toluene, and 2,2,4-trimethylpentane exhibit no zones of nonignition. The phenomena of zones of nonignition may be due to chain-making and -breaking mechanisms.

Ignition lag.—The ignition temperature of a flammable depends upon the time interval between the introduction of the flammable to the ignition source and the actual appearance of flames. Figure 96 shows the effect of this lag on the ignition temperature of a gasoline-oxygen mixture (ref. 48). The temperature decreases almost hyperbolically with increasing ignition lag. The minimum ignition temperature is reached when the temperature no longer decreases with increasing lag. This same trend is observed with other fuels and other types of ignition source (except sparks).

The importance of ignition lag in ignition by heated surfaces is indicated in figure 96. The times shown are unreasonably long compared with the residence time of a fuel



(a) Experimental data.



(b) Data correlation.

FIGURE 98.—Variation of ignition temperature of various fuels in air with gas-stream velocity. Ignition by $\frac{1}{4}$ -inch heated rods; stoichiometric mixtures; pressure, atmospheric; temperature, 155° F (ref. 50).

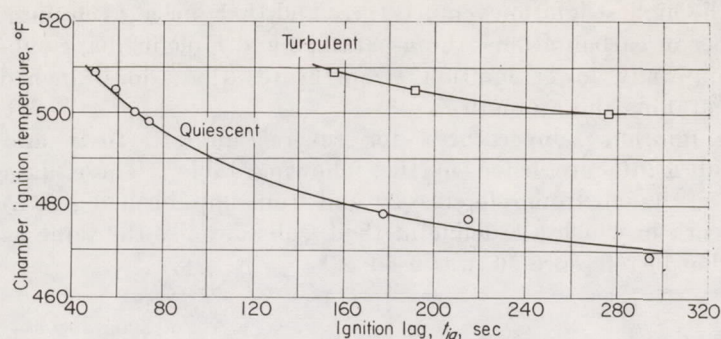


FIGURE 99.—Influence of mild turbulence on minimum ignition temperature of liquid aviation gasoline injected into 12-inch-diameter 12-inch vertical steel cylinder (ref. 44).

in a combustion chamber. Therefore, for such applications, the surface temperature must be markedly increased or else some means provided to prolong contact between fuel and surface.

Heated spheres and rods.—Heated spheres shot into the combustible have also been used as ignition sources, with the results shown in figure 97. Ignition temperature decreased as the diameter of the sphere increased because of the greater surface area. In this study (ref. 49), the criterion for setting up a theory was that the rate of heat generated by reaction should be greater than that lost by conduction. It is shown that, for a specific sphere velocity,

$$\frac{T_s - T_o}{r_s} = K e^{-E_{act}/RT_s} \quad (9)$$

where T_s is the heated-sphere temperature and E_{act} is the apparent energy of activation.

Because of the ignition criterion that considered heat losses by conduction only, the equation does not contain any factor relating to the duration of contact of the fuel with the ignition source.

Heated rods have been used as ignition sources for high-velocity gas streams (ref. 50), as shown in figure 98(a). High mixture velocities correspond to short ignition lags; thus, the ignition temperature of a flammable mixture increases with increasing velocity of the mixture. These data have been correlated (fig. 98(b)) in accordance with the following equation:

$$\frac{d_r}{U_g} e^{-\frac{E_{act}}{R T_g}} \left[\frac{C_g}{d_r(T_r - T_o)} \right] = K \quad (10)$$

where U_g is the velocity past the heated rod.

Turbulence.—Data on the effect of turbulence on ignition are not extensive, and the little information that is available does not include quantitative measurements of turbulence. Reference 43 shows that mild turbulence decreases the ignition temperature. However, an opposite trend is reported in reference 44, where the ignition temperature was increased approximately 30° F by stirring the mixture (fig. 99).

Surface condition and composition.—The condition of the heated surface may affect ignition in that the scale or ash forms an insulating coating which requires the whole material to be heated to a much higher temperature for ignition than

would otherwise be necessary. A gas film (e. g., adsorbed water or carbon dioxide vapor) may act in the same manner.

The composition of the ignition surface affects the ignition temperature (refs. 43 and 51) of flammable mixtures. The effects of various surfaces are shown in figure 100. Differences shown for the various surfaces are probably due to thermal conductivity, catalytic activity, or oxidation properties. Except for molybdenum and platinum, the surface temperature increases with the amount of fuel in the mixture. Molybdenum oxidizes rapidly at these ignition temperatures, which probably explains the trend opposite to other metals. Platinum is catalytically active, and the results may be explained on that basis. With platinum, a reaction of fuel and oxygen takes place with liberation of heat at the surface. This heat affects the temperature gradient in such a manner that less heat will flow from the heated surface, thereby inhibiting ignition. The rate of the catalytic reaction attains a maximum at stoichiometric mixture composition, causing the heat flow from the surface to be minimum. Therefore, to compensate for the smaller heat flow, it is necessary to raise the surface temperature in order to obtain ignition, as shown by the peak in figure 100.

This effect of type of surface upon the ignition temperature depends upon the particular method of ignition used. For example, reference 52 shows that, in the dynamic-bomb method of ignition, changing the metal surfaces has substantially no effect on the ignition temperature. Glass surfaces, however, ignite flammables at lower temperatures (ref. 53).

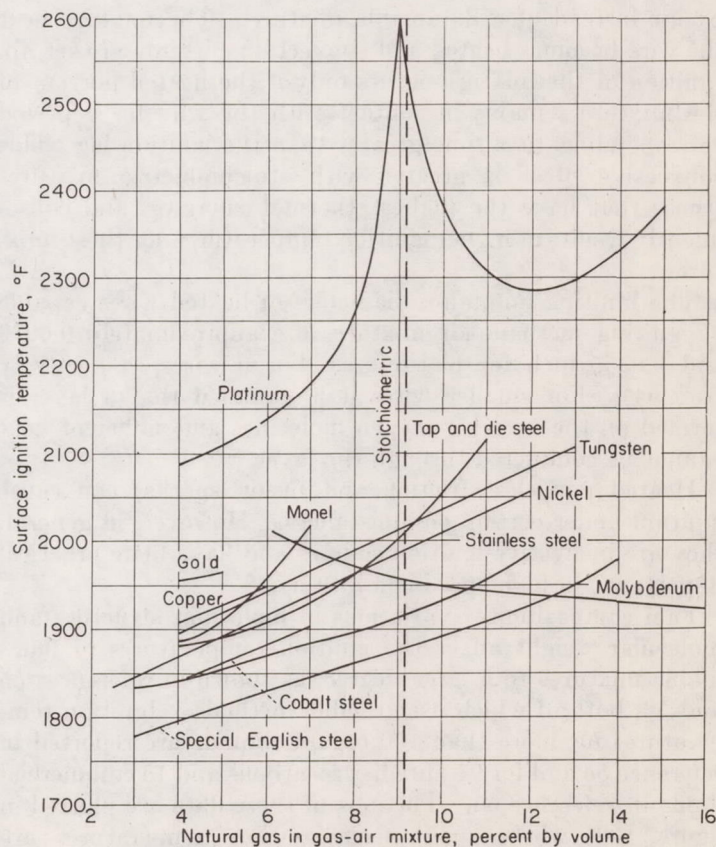


FIGURE 100.—Effect of fuel composition on surface ignition temperature. Ignition of natural gas by electrically heated $4.25 \times 0.50 \times 0.04$ -inch metal strips (ref. 43).

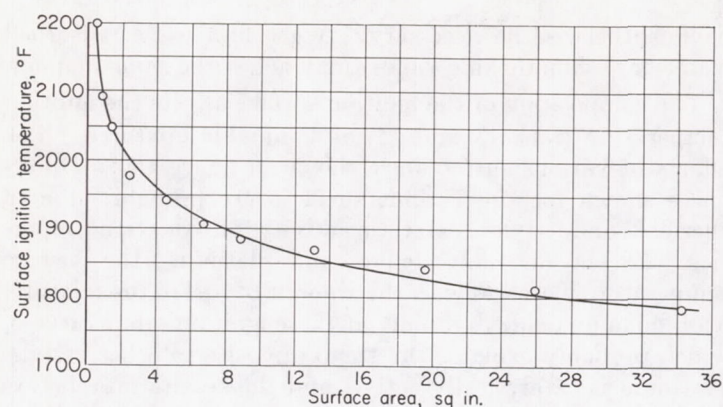


FIGURE 101.—Effect of surface area on surface ignition temperature of quiescent mixture of 7 percent natural gas and air. Ignition by electrically heated surface (ref. 44).

Surface area.—The effect of increasing the surface area of a heated plate (ref. 44) is shown in figure 101, in which an increase in area lowers the ignition temperature. Increasing the area from which heat may be transferred increases the amount of heat output and correspondingly lowers the ignition temperature. The curve appears to approach a minimum temperature below which it is impossible to obtain ignition regardless of area.

Small wires can cause ignition when heated electrically to incandescence. In the case of platinum, difficulties are caused, however, by combustion without flame that takes place on the surface of the wires. This combustion causes the wire to have a temperature higher than when surrounded by air instead of a flammable mixture. The mixture near the wire becomes heated and convection currents are set up. Ignition of the mixture occurs only if the heated portion of the mixture remains in contact with the wire for a period corresponding to a time greater than the ignition lag. This convective effect is greater with stoichiometric mixtures (those that have the highest thermal energies) and consequently results in higher ignition temperatures at these mixtures.

The limiting minimum diameters of heated wires capable of igniting methane-air mixtures are approximately 0.0079 and 0.0355 inch for platinum and iron wires, respectively (ref. 54). For smaller wires it is assumed that a layer is formed on the wire by oxygen molecules and sufficient heat cannot be conducted through the layer.

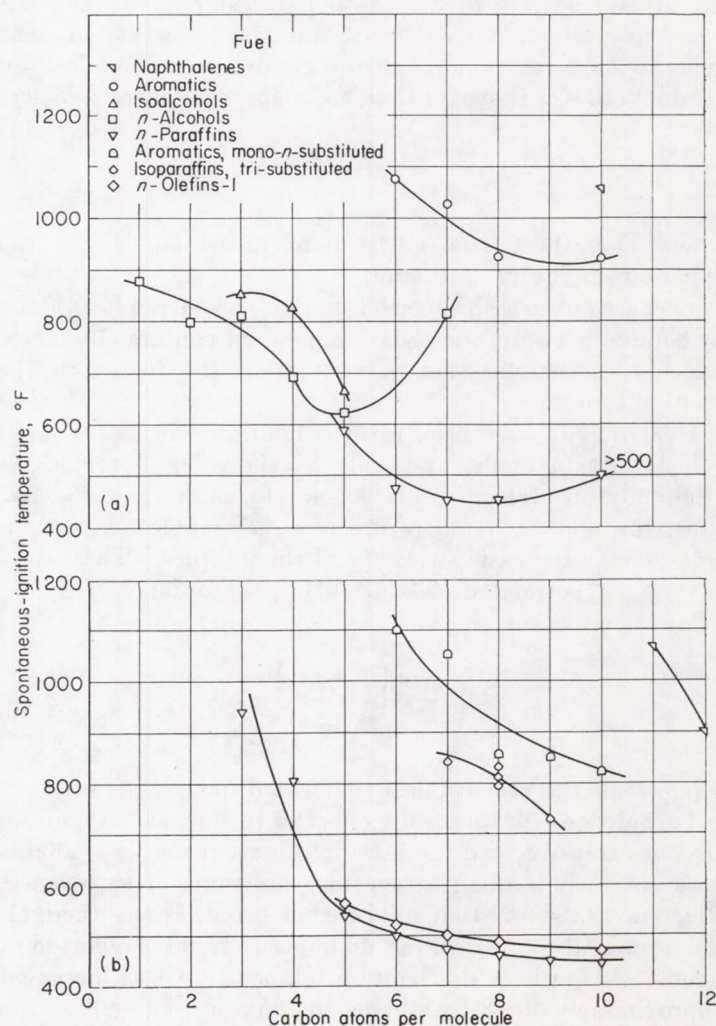
Heated particles (friction and fusion sparks) can cause ignition under certain circumstances. However, in general, they are ineffective ignition sources and have little practical importance in high-speed combustors.

Fuel composition.—Variations in molecular structure and molecular weight affect the ignition temperatures of flammable mixtures to a large degree, as shown in references 55 and 56, both of which use crucible methods. Ignition temperatures for more than 100 organic liquids are reported in reference 55 and for 94 pure hydrocarbons and 15 commercial fluids in reference 56. Portions of these data are plotted in figure 102, where spontaneous-ignition temperatures are shown as functions of the number of carbon atoms per molecule for several types of compound. These figures show that the compounds with the lowest molecular weight have

the highest ignition temperatures and that, for a given number of carbon atoms, the *n*-paraffins and *n*-olefins have substantially lower ignition temperatures than do branched paraffins and aromatics.

Ignition temperatures for several aircraft fuels and lubricants are listed in the following table. These data were taken from reference 56 and from unpublished NACA work in which a crucible method, substantially the same as that of reference 56, was used:

Fuel or lubricant	Spontaneous-ignition temperature, °F
100/130 Grade aviation gasoline.....	844
Low-volatility aviation gasoline.....	900
Unleaded 62-octane motor gasoline.....	568
Kerosene.....	480
Grade JP-3 jet fuel	
Sample A.....	484
Sample B.....	502
Grade JP-4 jet fuel.....	484
Grade JP-5 jet fuel	
Sample A.....	473
Sample B.....	477
SAE No. 10 lube oil.....	720
SAE No. 60 lube oil.....	770



(a) By permission from reference 55.

(b) Reference 56.

FIGURE 102.—Effect of number of carbon atoms per molecule on spontaneous-ignition temperatures of various liquid fuels.

The ignition temperatures for the jet fuels are among the lowest found for hydrocarbons.

There is no exact relation between octane number and ignition temperature, but references 51 and 57 indicate that ignition temperatures of unleaded fuels generally increase with increasing octane number. Data from references 46, 53, and 58 show that the effect of decreasing fuel quality or cetane number is to increase the ignition temperature (fig. 103). Addition of tetraethyl lead also increases the ignition temperature (ref. 46).

Pressure.—The effect of pressure on the ignition temperature of methane-air mixtures as determined by a dynamic heated-tube method is shown in figure 104(a) (ref. 40), and its effect on the bomb-ignition temperature for four liquid hydrocarbons is shown in figure 104(b) (ref. 59). Ignition temperatures decreased continually with increasing pressure over the pressure range investigated, which was to 30 atmospheres in reference 59. The effects of increasing pressure on crucible-method ignition temperatures are shown in the following table for JP-4 and JP-5 fuels (unpublished NACA data):

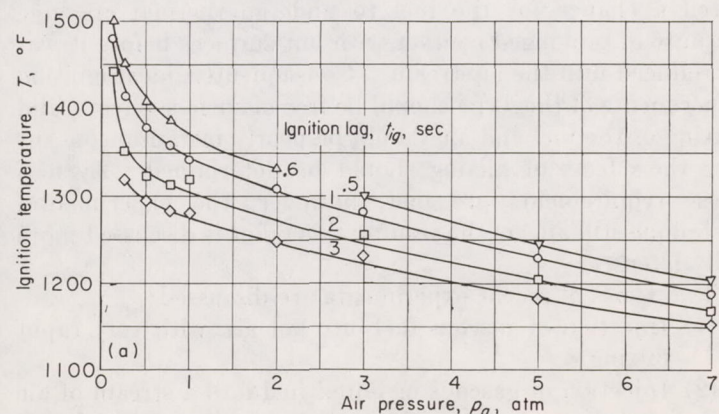
Pressure, atm	Ignition temperature, °F	
	JP-4	JP-5
1-----	484	477
5-----	376	415
9-----	378	408

A considerable decrease in ignition temperature is seen when pressure is increased from 1 to 5 atmospheres. Further increases to 9 atmospheres had little effect.

Diluents.—The effect of adding diluents to flammable mixtures is to increase the ignition temperatures, because the amount of oxygen is correspondingly reduced (ref. 45). However, in the low-temperature type of ignition previously described, the effect of diluents is negligible, the ignition temperature remaining substantially constant.

IGNITION BY FLAMES

The energy required to initiate the chemical reactions characteristic of a propagating flame may be supplied to a



(a) Ignition of methane in air using dynamic heated-tube method (ref. 40).

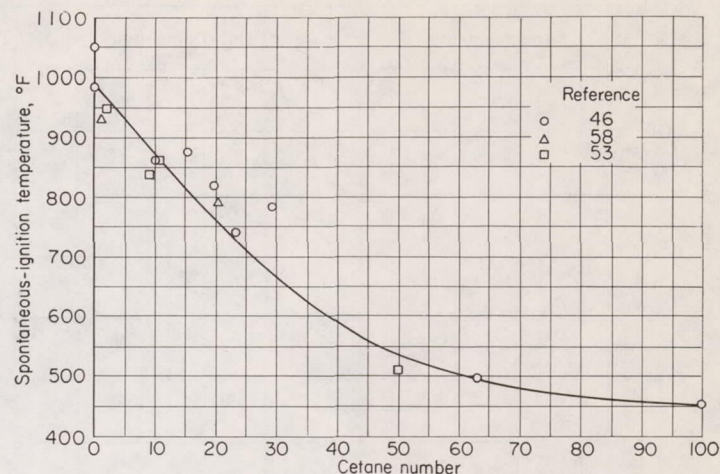
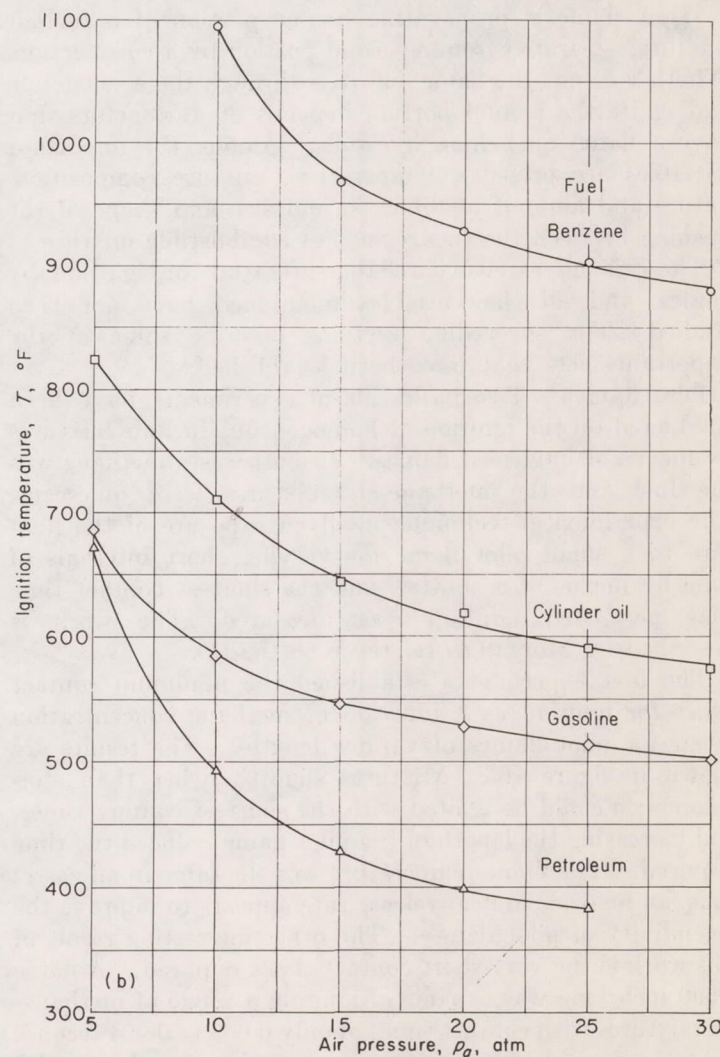


FIGURE 103.—Effect of cetane number on spontaneous-ignition temperature of various fuels in air. (Cetane numbers are converted ASTM-CFR octane numbers.)

fuel-air mixture by means of flames. Two separate situations may be considered:

(1) A pilot flame is immersed in the fuel-air mixture. Whether or not the mixture will be ignited depends upon



(b) Bomb ignition with fuel sprayed in (ref. 59).

FIGURE 104.—Effect of air pressure on ignition temperature.

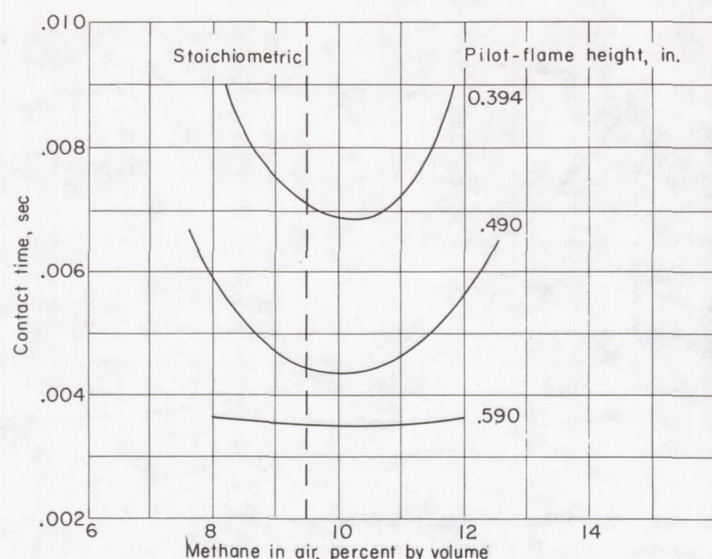


FIGURE 105.—Effects of pilot-flame contact time and size on ignition (ref. 60, p. 45).

mixture composition, duration of contact between flame and mixture, size and temperature of the flame, pressure, turbulence level, and the nature and amount of diluents.

(2) A flame is propagating in one portion of a fuel-air mixture, separated from a second portion by a constriction. Whether or not the flame will pass through the constriction and ignite the second portion depends on the factors that govern flame quenching by walls. Among the important variables are pressure, temperature, mixture composition, nature and amount of diluents, and size and shape of the opening between the two regions of combustible mixture.

There is no extensive reliable literature on ignition by flames, and all the variables mentioned have not been studied. The succeeding sections describe some of the important facts that have been established.

Pilot flames.—Two basic sets of experiments have been conducted on the ignition of homogeneous fuel-air mixtures by means of immersed flames. In both cases methane was the fuel and the methane-air mixtures were quiescent. The experimental technique involved exposure of the mixture to a small pilot flame for varying short intervals of time by means of a shutter, and the shortest contact time that permitted ignition was measured. The work is described by Morgan in reference 60 (p. 44).

The first experiments established the minimum contact times for ignition as a function of methane concentration in air for pilot flames of various lengths. The results are shown in figure 105. Mixtures slightly richer than stoichiometric could be ignited with the shortest contact times, and increasing the length of the pilot flame reduced the time required. The flame temperature was the same in all cases; thus, an increase in heat-release rate appears to improve the incendiarity of pilot flames. The other interesting result of this work is the very short contact times required. A flame 0.590 inch long was capable of igniting a range of methane-air mixtures with contact times of only 0.003 to 0.004 second.

In the second series of experiments, the size of the pilot flame was kept constant, but the temperature was varied

by adjustment of the mixture. In this way, it was found that the minimum contact time for ignition of methane-air mixtures by a pilot flame burning at 3215° F was only about one-sixth the time required with a flame at 2770° F.

These two series of tests therefore establish the importance of both pilot heat and pilot-flame temperature in the ignition of quiescent mixtures.

Propagating flames through constrictions.—It is apparent from a previous discussion of flame quenching by walls that, if the quenching distance is known, the possibility that a flame propagating in one portion of a mixture will pass through a constriction and ignite a second portion can be determined. All evidence indicates that, if the flame succeeds in passing through the constriction, ignition of the second portion is automatically ensured. It is therefore appropriate to consider the factors that affect quenching distance in connection with this type of flame ignition (see **FLAME QUENCHING**).

IGNITION BY HOT GASES

Ignition by hot gases generally applies to the case in which fuel is injected into hot air. The mixing process is an essential part of the sequence of events leading to ignition. In addition, the chemical nature and physical state of the fuel, and the temperature, pressure, and composition of the hot gas will influence ignition.

Some of the factors governing ignition of fuels injected into hot airstreams are discussed in this section. The criterion for ignition is the appearance of flame. Oxidation is accelerated by increased temperature; therefore, the time lag, or ignition lag, from the instant of fuel injection until the flame appears is a function of the air temperature. In addition, some of the experiments show that the relative amounts of fuel and air affect the temperature required for ignition after a given ignition lag. It is therefore evident that quoting an ignition temperature for a fuel is meaningless unless the fuel-air ratio and the time lag before ignition are also specified.

One of the major difficulties in the measurement of such ignition temperatures is that a mixing process is superimposed on the results. In the older work the fuel concentration varied from point to point in the apparatus, and no attempt was made to determine the concentration at the point where flame first appeared. In addition, there was often a chance for the fuel to undergo thermal cracking because of prolonged contact with hot surfaces before it was introduced into the airstream. Consequently, ideal ignition experiments of this type should be free of surface effects, and mixing of the fuel and air should be nearly instantaneous, or else the effects of mixing should be determined. Even if these requirements are met, however, the experimental technique still affects the results; this point is discussed more fully later.

Two types of recent experiments are discussed:

- (1) Injection of gaseous fuel into hot air, with very rapid mixing
- (2) Injection of gaseous or liquid fuel into a stream of air plus hot products of combustion from a "slave" burner, with no special attempt to secure rapid mixing.

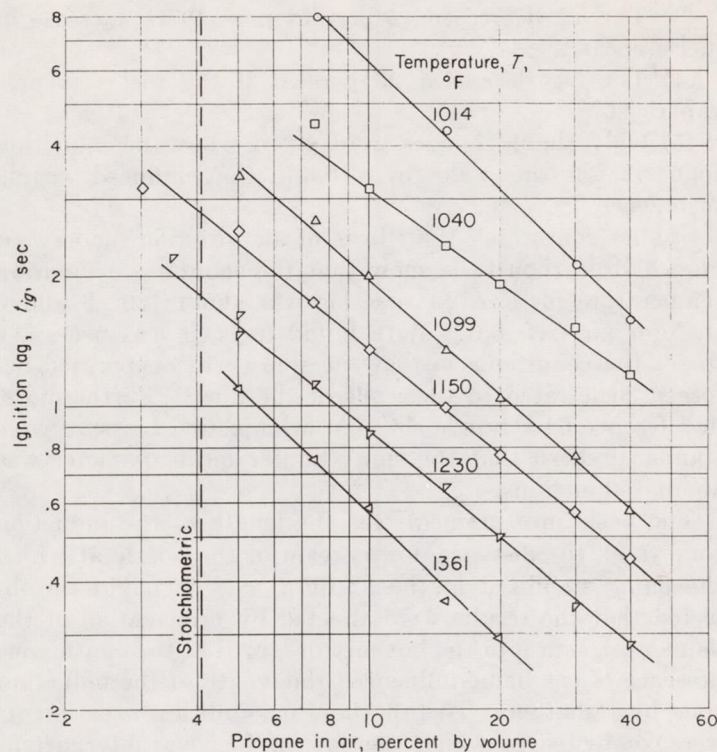


FIGURE 106.—Effect of propane concentration and temperature on ignition lags of propane-air mixtures in 1-inch tubes. Flow rate approximately that for minimum ignition lag (ref. 61).

Heated air.—A spontaneous-ignition apparatus that overcomes some of the experimental objections to the measurement of ignition temperatures was designed and used to study the ignition of propane by hot air (ref. 61). The propane and the air were very rapidly mixed in a specially designed chamber; the mixing time with the low flow rates used was 6×10^{-3} second or less. Consequently, it is believed that no significant thermal cracking of the fuel occurred before it was mixed with the air. The mixture was allowed to flow upward in a glass flame tube, and the ignition lag was measured by means of a photocell that responded to light from the flame, or by a pressure pickup that recorded a pulse when ignition occurred. By means of several electric heating elements, conditions were controlled so that the mixture, mixing chamber, and flame tube were all the same temperature. The flame tubes were 36 inches long and 1 or 2 inches in diameter.

The results did not depend appreciably on the flame-tube diameter (ref. 61). There was, however, an effect of flow rate. Curves of ignition lag against flow rate, at constant temperature and propane concentration, showed minimums for ignition lag. The flow rate corresponding to the minimum lag shifted to higher values for richer mixtures.

Nevertheless, the data of reference 61 definitely show that ignition lag decreases as propane concentration increases. Typical data are shown in figure 106 in the form of a logarithmic plot. The ignition lags vary from 0.3 to 8 seconds over a range of propane concentrations of 3 to 40 percent by volume and a range of temperature from 1014° to 1361° F. The straight lines of figure 106 show that the dependence of

ignition lag on propane concentration may be expressed by the following equation:

$$\frac{1}{t_{ig}} = G [C_3H_8]^b \quad (11)$$

where $[C_3H_8]$ is propane concentration. The value of the exponent b may be determined from the slopes of the lines of figure 106. These slopes have an average value of -0.93 , so that the exponent b in equation (11) may be approximated by unity.

Reference 61 also describes experiments in which the oxygen concentration was varied independently of the propane concentration. In this way, it was found that there is a slight dependence of ignition lag on oxygen concentration. The following equation expresses the combined effects of propane and oxygen concentrations on the ignition lags at a given temperature:

$$\frac{1}{t_{ig}} = G [C_3H_8] [O_2]^{1/4} \quad (12)$$

Reference 61 showed that the temperature-dependence of ignition lag is not of the simple Arrhenius type; the data indicate that the activation energy is not constant over the range of temperatures studied. However, the ignition-lag data could be reasonably well expressed (within 30 percent) by the following equation, which accounts for all the variables studied:

$$t_{ig} [C_3H_8] [O_2]^{1/4} = 0.030 + 5.4 \times 10^{-9} e^{26100/T} \quad (13)$$

where $[C_3H_8]$ and $[O_2]$ are the concentrations in mole fractions, and T is in °R.

The preceding experiment is subject to apparatus variables that appear to be inevitable, even though some of the objections to the measurement of spontaneous-ignition temperatures have been removed. If the essential processes are assumed to take place in the gas phase, ignition cannot occur until the rate of heat release from the preignition reactions (or perhaps the rate of production of certain active particles) overcomes the rate of loss to the walls of the test section and to the air or inert gas that precedes the fuel-air mixture through it. Such a transfer must occur even though the walls are maintained at the same temperature as the entering stream of mixture, for the oxidation reactions release heat even before ignition takes place, so that the temperature of the stream rises as it progresses through the flame tube. Consequently, gradients in temperature and in concentration will exist between the center of the tube and the walls, and the diameter of the test section should have some effect on the results. The material of the walls might also be of some importance. In addition, the flow rate should affect the ignition lags at a given spontaneous-ignition temperature, since it influences the heat transfer to the walls. Similar considerations apply if processes at the wall are assumed to be controlling. There is also the possibility that both gas-phase and surface reactions are important, perhaps in different ranges of concentration and temperature.

Reference 61 shows that some of the results can be qualitatively explained both in terms of gas-phase reactions, using a reaction mechanism based on low-temperature oxidation studies, and in terms of a postulated surface reaction between adsorbed oxygen and propane. In the latter case, it would be expected that the ignition lags should depend upon the diameter of the flame tube; however, as has been pointed out, there was little difference between the ignition lags measured in 1- and 2-inch tubes. Reference 61 suggests that the explanation may lie in the fact that, whereas the smaller tube with its larger surface-volume ratio gives greater concentrations of reactants per unit volume of gas, the smaller tube also provides a larger relative area for loss of heat or destruction of active particles.

Concerning the other variables, the data of reference 61 show that ignition lag depends upon flow rate. Additional work, reported in reference 62, describes the effects of pressure, nature of walls, and nature of inert gas. Decrease in pressure caused an increase in ignition lag; at 1 atmosphere and 1125° F, tubes of Vycor, stainless steel, and Vycor coated with potassium chloride all gave identical ignition lags; and substitution of helium for nitrogen in the air increased lags about 10 percent, while substitution of argon caused no change.

Vitiated air.—Mullins (ref. 63) has provided some data on short ignition lags obtained under rather specialized conditions. The objective was to simulate the situation in current types of turbojet combustors. In this case no flameholders are provided in the combustors, and the fuel must be ignited by spraying it into a primary zone of air plus hot products of combustion introduced by recirculation from the flame zone. In the apparatus described in reference 63, the air was heated by addition of the hot exhaust from a "slave" combustion chamber situated upstream of the test section. The fuel was injected through a nozzle (both vapor and liquid fuels were studied). The ignition lag was determined from the known flow rate and a measurement of the distance from the nozzle to the point at which the spontaneously ignited flame stabilized in a gradually tapering diffuser downstream of the injection nozzle.

Such an experiment must be subject to the effects of evaporation, mixing, drop size, drop-size distribution, and turbulence. In addition, the air supply is vitiated by the added combustion products, so that the oxygen concentration varies below 21 percent as a function of the temperature required in the airstream. Mullins has attempted to account for many of these effects in reference 64, which describes the results of studies on the ignition lags of kerosene-air mixtures. Several physical variables were examined, with the following results:

(1) Fuel-air ratio and velocity had negligible effects on ignition lag.

(2) At a given air temperature, the lag increased about 1 percent per 3-micron increase in spray Sauter mean diameter.

(3) The lag decreased 15 percent per 140° F increase in fuel preheat.

(4) The lag decreased 25 percent if the fuel was pre-vaporized.

(5) Only slight changes were noted when the induction zone was in the wake of a baffle that induced coarse turbulence.

Studies concerning the effects of air vitiation made with pure hydrocarbon fuels show that the spontaneous-ignition temperature for a given time lag was about 120° F above that for air (ref. 65). With liquid fuels, it was necessary to set the conditions so that the spray was evaporated before it penetrated to the walls of the duct. Furthermore, in reference 64 a nozzle size and an injection pressure were standardized so that the spray Sauter mean diameter was about 100 microns.

The basic measurement was the length of the induction zone (i. e., the distance downstream of the nozzle at which the flame stabilized in the 3° diffuser). It might be objected that the results were affected by propagation of the flame upstream into the hot mixture, or that the continuous presence of the flame influenced the length of the induction zone by radiation. To test these possibilities, experiments were conducted in which the flow of fuel was intermittent (ref. 64). The flashes from ignited mixture appeared 1 to 3 inches downstream of the corresponding continuous-flame-front position. This result seems to indicate that the continuous presence of the flame did have some effect, but it was pointed out that intermittent operation may not have allowed time for the nozzle to develop its normal spray. Therefore, the difference between continuous and intermittent ignition lags may have been due to a difference in spray characteristics. In any event, the discrepancies were small in absolute magnitude, although percentagewise they were as high as 15 percent.

Although subject to the preceding experimental variables, Mullins' work provides the only measurements of the very short ignition lags of interest in present turbojet combustors. The measurements covered the range of 0.5 to 30 milliseconds ignition lag. Typical data for kerosene, taken from reference 64, are shown in figure 107. The effects of pressure were also studied, and figure 107 includes lines for pressures from 9.88 to 29.92 inches of mercury. At a given temperature, the ignition lag for kerosene under the particular set of spray and stream conditions was proportional to the reciprocal of the pressure. Different pressure dependences were found for other fuels. Figure 107 also includes a line for a gaseous hydrocarbon fuel, "calor gas," composed of C₄ hydrocarbons (ref. 65).

From the experimental data, activation energies were calculated and corrected for the effect of air vitiation, so that the results corresponded to pure air. The activation energy for ignition of kerosene was calculated to be 45.5 kilocalories per mole; for "calor gas," 52 kilocalories per mole.

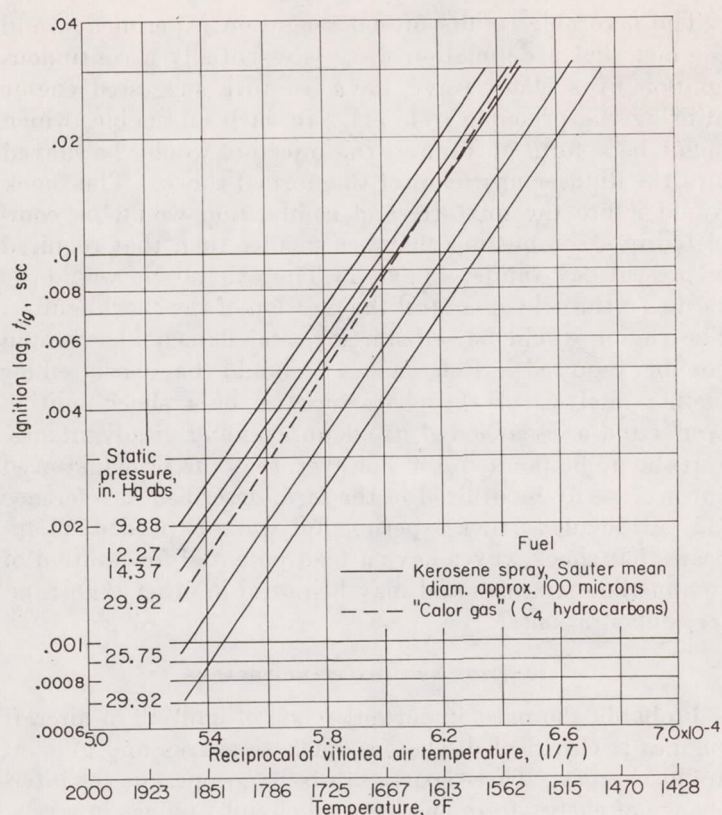


FIGURE 107.—Ignition lags on injection of fuel into hot vitiated airstream (refs. 64 and 65).

There are several striking differences among the experiments discussed:

(1) Reference 61 found that the ignition-lag data for propane did not follow an Arrhenius-type plot; hence, a constant activation energy was not obtained. However, the empirical equation (12) used to express the data includes an exponential term $e^{26100/T}$. This temperature-dependence is much less than found in references 64 and 65; the analogous exponential terms, with activation energies of 45.5 and 52 kilocalories per mole, would be $e^{41200/T}$ or $e^{47200/T}$. Although different fuels are involved, other experience indicates that the temperature coefficients for propane and "calor gas," in particular, should agree more closely.

(2) Reference 64 reports no effect of fuel concentration on ignition lag, whereas reference 61 found that the lag at a given temperature was proportional to the inverse of the propane concentration.

(3) The data of reference 61 indicate a low order of dependence of ignition lag on oxygen concentration, while reference 66 reports that the lag varied inversely as the square of the oxygen concentration.

It is impossible at present to ascertain the reasons for these discrepancies, because the experiments are so different and the effects of variables are incompletely understood. The need for caution in the interpretation of spontaneous-

ignition measurements is emphasized. In the present stage of knowledge, the safest procedure for practical application of the data to high-speed combustors is to choose an experiment that most nearly matches the actual conditions. For example, the work of Mullins provides measurements suitable for such application to present types of turbojet combustors. More basic experiments, such as those of references 61 and 62, will eventually lead to a better understanding of ignition by hot gases.

IGNITION BY SHOCK WAVES

The possibility of ignition of fuel-air mixtures by shock waves may readily be seen by a brief examination of the properties of the waves. It is not within the scope of this discussion to present the details of the formation and propagation of shocks; many excellent works may be consulted on these subjects (e. g., ref. 5, p. 590).

A shock wave travels through a gas at a velocity greater than the local sound velocity. As the gas flows through the wave, it undergoes abrupt increases in pressure and temperature. The temperature is considerably greater than that obtained by adiabatic compression, in which case the assumption is that the piston moves so slowly that equilibrium always exists. This condition is met in practical cases as long as the piston velocity is small compared with the average molecular velocity. In the case of a shock wave, the wave itself is the piston head, and, as already stated, its velocity is high. Consequently, the compression is accompanied by the degradation of kinetic energy into random molecular motion, that is, thermal energy.

An idea of the properties of shock waves may be obtained from the following table (ref. 5, p. 594). The quantities in the table were calculated from the appropriate hydrodynamic equations for shock waves in air at an initial temperature of 32° F:

Ratio of pressure behind shock wave to initial pressure	Shock-wave velocity, ft/sec	Temperature behind shock, °F	Temperature resulting from adiabatic compression to same pressure ratio, °F
2-----	1,483	145	135
5-----	2,290	408	307
10-----	3,209	810	468
50-----	7,050	3,610	970
100-----	9,910	6,490	1250
1000-----	30,200	33,900	2620
2000-----	42,300	51,700	3270

The extremely high temperatures produced in the shock are sufficient to indicate the potential of shock waves as ignition sources, particularly when the temperatures in the table are compared with the spontaneous-ignition temperatures that have been quoted previously. In addition, the shock contains free atoms and radicals that can promote rapid chemical reaction; shocks are often observed to be luminous, even in inert gases.

Thus far, only shock waves in noncombustible gases have been considered. If the gas is a combustible mixture, a mathematical analysis of the hydrodynamic processes that occur when a wave of chemical reaction sweeps through the mixture shows that two different types of process satisfy the conservation laws. In one case, the pressure and density behind the wave are both lower than those ahead of the wave; this is called a deflagration, and constitutes the usual flame with which this chapter is concerned. In the other case, pressure and density increase behind the wave; this is a detonation. (For a complete discussion, see ref. 67.)

Ordinary flames propagating in tubes are often observed to accelerate and transform to detonation waves if the tube is long enough and the mixture is within the concentration limits of detonability. The processes involved are not yet completely understood. It may be sufficient to state that the detonation wave is a shock wave that continuously ignites the mixture into which it propagates and is sustained at a velocity very much greater than the normal burning velocity by the energy released in combustion.

Thus, the possibility of ignition by shock waves is established by the very existence of the phenomenon of detonation. In the situation just described, however, flame is present initially. Recent studies show that ignition by shock waves can be accomplished without the presence of a preliminary, slowly propagating flame. In general, the technique has been to employ a shock tube, in which an inert gas at high pressure is separated by a diaphragm from a combustible mixture. When the diaphragm ruptures, a shock wave with a strength dependent on the bursting pressure and the properties of the inert gas travels into the combustible mixture. The properties of this incident shock may be calculated from shock-tube theory, and the shock of minimum strength required to ignite the mixture can be determined. The technique has been used by Shepherd (ref. 68) with methane-oxygen, methane-air, and ethene-oxygen mixtures, and by Fay (ref. 69) with hydrogen-oxygen mixtures. In general, ignition resulted in a detonation if the mixtures were within the concentration range of detonability, as might be expected. However, the incident shock did not by any means need to be as strong as the detonation that resulted from it. For example, reference 68 showed that methane-oxygen mixtures could be ignited by shocks in which the calculated temperature was 410° to 482° F; the calculated temperature in reference 69 for a $2\text{H}_2\text{-O}_2$ mixture was 266° to 680° F. Ranges of temperature are given because the results depended somewhat upon the experimental arrangement, and the technique has not yet been sufficiently refined to eliminate all extraneous effects. Nevertheless, the indicated ignition temperatures are in a strikingly lower range than those determined by methods previously discussed, especially when the very short lags associated with shock-wave ignition are considered. More recent work suggests that the low shock-ignition temperatures are illusory, and are due to various effects in the region of the bursting diaphragm and in regions where the tube walls are not flat (ref. 70). When care was taken to eliminate these effects, the temperatures required for shock ignition were as high as or higher than those required for other forms of ignition.

The favorable results of shock-ignition experiments, and the fact that a detonation wave is essentially a continuous ignition by a shock wave, have led to a suggested engine utilizing the principle (ref. 71). In such an engine, which might be a form of ramjet, the injectors would be moved into the diffuser upstream of the normal shock. The shock would ignite the mixture, and combustion would be completed in a combustion chamber smaller than that required in present-day ramjet engines. The exit nozzle would be used as a throttle to control the position of the shock igniter. The engine would be self-starting, and flameholders would not be required. Reference 71 should be consulted for further analysis of the characteristics of a shock-ignition ramjet and a discussion of its advantages and disadvantages.

It should be pointed out, however, that the principal need not necessarily be utilized in the form described in reference 71. Although further experimental work is needed, it appears that shock waves have a high potential for ignition of combustible mixtures and may be useful in other than ramjet configurations.

IGNITION BY CAPACITANCE SPARKS

Probably the most important mode of ignition in aircraft engines is electrical discharges, such as sparks and glow or arc discharges. These sparks or discharges permit the interchange of energy from an electrical circuit to a gas in a relatively efficient manner and in a minute volume compared with heated surfaces, flames, or hot gases. Complete control can be exercised over the amount of energy and the duration of the discharge. Although spark ignition has been the subject of many investigations and has found wide use in practical applications, there is still much to be learned about the mechanism whereby stored energy is converted to flame. The most complete summary available on spark ignition is that of reference 72.

Three types of discharges have been used to obtain ignition: capacitance sparks, inductance sparks, and capacitance sparks of long duration. The rate at which energy is released is different for these sparks and accounts for the difference in igniting ability. Capacitance sparks are produced by the discharge of charged condensers into a gas. The duration of such a discharge may be extremely short (<0.01 microsec) for low energies and can be as high as 100 microseconds for larger energies (>1 j) because of inherent properties of the circuitry. The appearance of the spark is bright, and the spectrum of the spark corresponds to that of the gas in which the spark occurs. The current is high because of the low impedance of the spark gap. Inductance sparks are obtained from transformers, ignition coils, and magnetos, or when an inductive circuit is interrupted by opening contacts. Because inductance sparks usually are generated by high-impedance sources, the current is low; hence, the sparks have a weak appearance. The duration is long and the spectrum corresponds to the vapor of the metal electrodes. Capacitance sparks of long duration are produced when resistance is added to a capacitance discharge ignition system, the duration being controlled by the relative values of resistance and capacitance. When resistance is added, the characteristics of the discharge (i. e., current, duration, and appearance) become very similar to those of

an inductance spark. Because of losses in the resistance, such sparks are only useful for fundamental research. The energy at the gap must be measured by oscillographic or calorimetric methods.

The energy in a capacitance spark as obtained from the discharge of a capacitance is calculated by the following equation:

$$E_c = \frac{1}{2} c (v_2^2 - v_1^2) \quad (14)$$

where

E_c energy obtained from capacitance, joules

c capacitance of condenser, farads

v_2 voltage on condenser just before spark occurs, volts

v_1 voltage remaining on condenser at instant spark ceases, volts

This equation gives the energy released from the condenser, which may be higher than that actually dissipated in the spark gap because of losses in the circuit unless extreme care is taken to minimize the losses. Usually v_1 is small compared with v_2 , and hence may be neglected. However, in systems using large capacitors and relatively low voltage, v_1 can be important.

In the succeeding discussion of the effects of variables on ignition by capacitance sparks, the following definitions will aid in consideration of the results:

(1) Minimum spark-ignition energy: The minimum spark-

ignition energy of a flammable mixture is the total energy dissipated in the weakest spark that will just cause ignition.

(2) Quenching distance: The quenching distance is the electrode spacing marking the farthest penetration of the flame-quenching effect of the solid material. At this spacing, the ignition energy is a minimum; below this spacing, the energy increases.

(3) Electrostatic sparks: Electrostatic sparks are those sparks generated by friction, impact, pressure, cleavage, induction, successive contact and separation of unlike surfaces, and transference of fluids. They are the same as capacitance sparks, the only difference being in the manner in which the energy is generated. Data for electrostatic ignition energies would be the same as those determined for capacitance-spark ignition energies.

(4) Breakdown voltage of spark gap: The breakdown voltage of a spark gap is the lowest voltage that may be applied to a spark gap and yet cause a spark to be formed. This voltage should be distinguished from the spark discharge voltage, which is the voltage appearing across the spark gap during the life of the spark or discharge.

(5) Spark discharge: A spark occurs upon the electrical breakdown of a gap. It marks a transition from a non-self-sustaining discharge (sometimes called dark discharge) to one of several types of self-sustaining discharge and usually takes place with explosive suddenness. The most

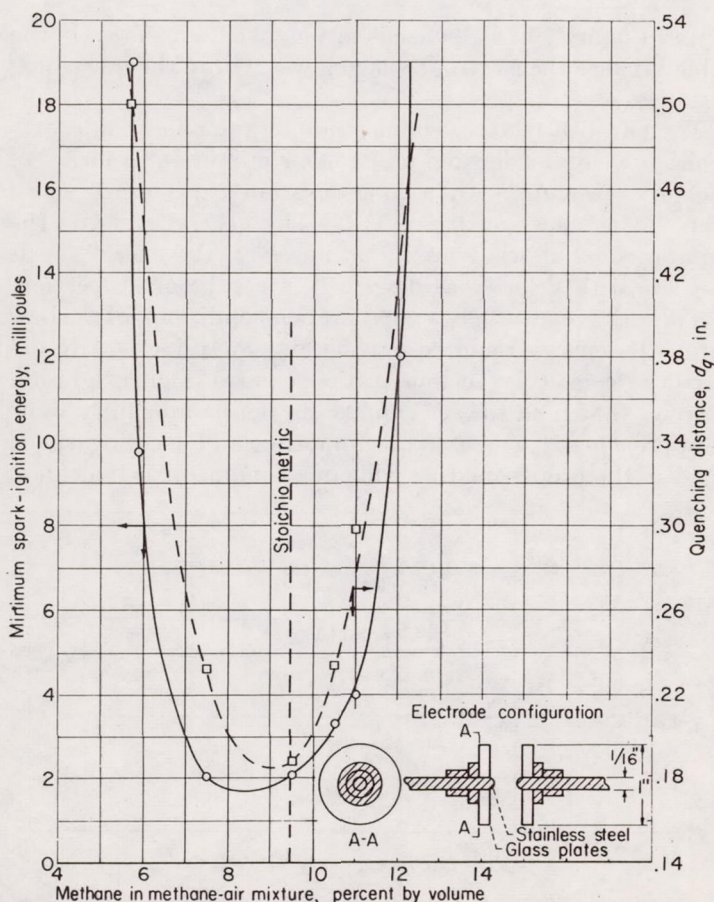


FIGURE 108.—Effect of mixture composition on minimum spark-ignition energy and quenching distance of methane-air mixtures. Capacitance spark; pressure, 9.98 inches of mercury absolute; temperature, 77° F (ref. 17).

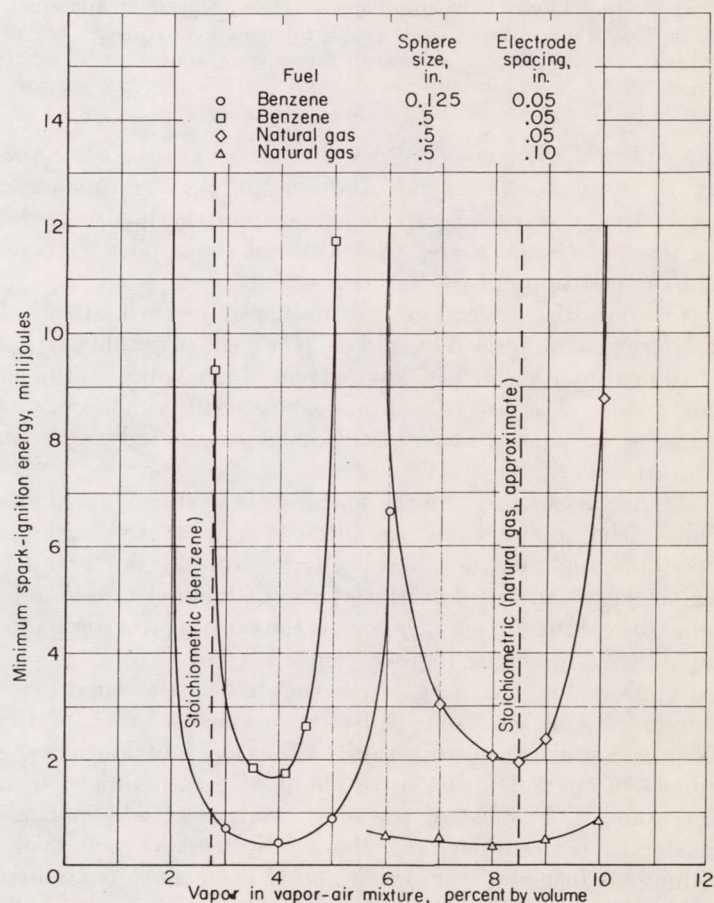


FIGURE 109.—Effect of mixture composition on minimum spark-ignition energy of mixtures of benzene and air or natural gas and air. Capacitance spark; pressure, atmospheric; room temperature; electrode spacing not maintained at quenching distance; electrodes, stainless-steel spheres (ref. 73).

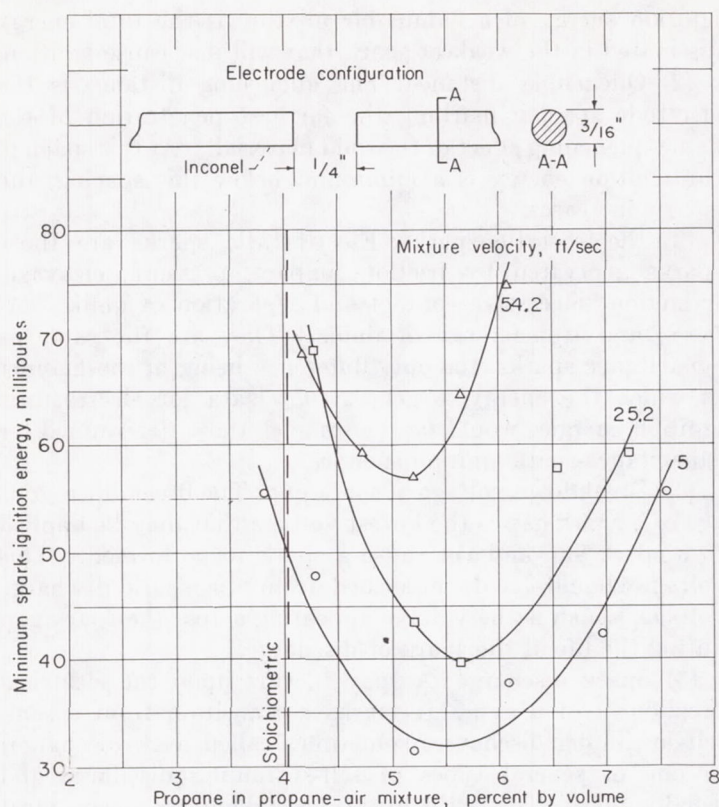


FIGURE 110.—Effect of mixture composition and velocity on minimum spark-ignition energy of flowing propane-air mixtures. Long-duration (600 to 900 microsec) capacitance spark; pressure, 3 inches of mercury absolute; temperature, 80° F; electrode spacing, 0.25 inch (within quenching distance) (ref. 75).

important of the self-sustaining discharges are the glow and arc discharges. The type of discharge that results upon spark breakdown of a gap depends upon the gas pressure, the gap length and shape, the nature of the applied voltage, and the constants of the external circuit.

(6) Glow discharge: The glow discharge is a self-sustained discharge characterized by a glow over a considerable portion of the cathode electrode, low current, high voltage drop in the region close to the cathode electrode, small current densities at the cathode electrode, and generally a weak appearance.

(7) Arc discharge: The arc discharge is a self-sustained discharge characterized by an intense spot at the cathode electrode, high current, low voltage drop at the cathode region, large current densities at the cathode electrode, and generally strong appearance. It is the only type of discharge capable of supporting high currents.

In discussing the parameters that affect the energy required for ignition using capacitance sparks, much of the older data is disregarded, because it does not contribute to the subject of spark ignition in the light of present knowledge. For example, in most of the older work electrode spacings shorter than the quenching distance were used, and many deductions using such information are erroneous, as pointed out in reference 5. Therefore, such information is used only where necessary to show a trend, and it is indicated that such data were obtained within the quenching distance. The important test conditions are generally included in the figure legends.

Mixture composition.—The effect of mixture composition on minimum ignition energy of quiescent mixtures (refs. 17 and 73) is shown in figures 108 and 109 for three electrode configurations, various spacings, three fuels, and two pressures. The curves show that well-defined upper and lower ignition limits exist and that a minimum value of energy is required at a fuel composition of the order of stoichiometric. For most fuels, the minimum falls on the rich side of stoichiometric. For example, the following table (obtained from ref. 74) shows the minimum points of the curves for a number of different hydrocarbon fuels ignited at atmospheric pressure with the same electrodes used to obtain the data in figure 108:

Flammable	Fuel in fuel-air mixture, percent by volume	Percent fuel in fuel-air mixture Percent fuel in stoichiometric fuel-air mixture	Least energy, millijoule
Methane----	8.45	0.88	0.28
Ethane----	6.61	1.17	.25
Propane----	5.07	1.26	.26
<i>n</i> -Butane----	4.53	1.47	.26
<i>n</i> -Hexane----	3.64	1.71	.24
<i>n</i> -Heptane----	3.36	1.82	.25
Cyclopropane----	6.34	1.45	.18
Cyclohexane----	3.94	1.75	.24
Benzene----	4.67	1.75	.21
Diethyl ether----	5.30	1.57	.19

Data in figure 109 for benzene are higher than shown in the table because the electrode spacing was within the quenching distance.

The effect of mixture composition on the minimum spark-ignition energy of flowing propane-air mixture at 3 inches of mercury absolute with a long-duration capacitance spark (ref. 75) is shown in figure 110. The general trend is the same as for quiescent mixtures; however, the energy levels increase with velocity as described in a subsequent section.

The data show that, under proper conditions of fuel-air ratio, the energy required can be extremely low. Any departure from this fuel-air ratio requires higher ignition energies that tend toward infinity as the flammability limit is approached. The extreme importance of locating spark plugs in the proper mixture zone in a combustor is indicated.

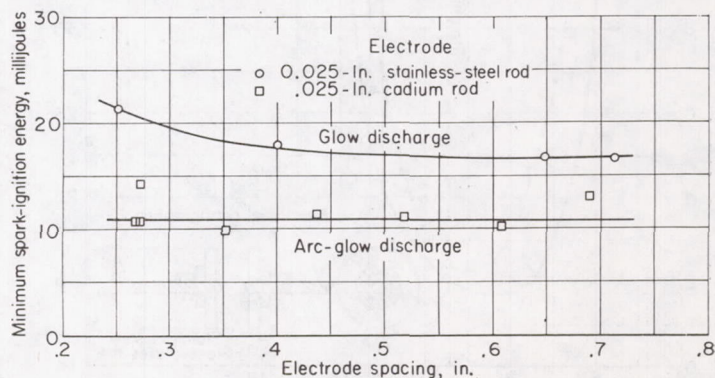


FIGURE 111.—Effect of electrode material and electrode spacing on minimum spark-ignition energy of flowing 5.2 percent by volume mixture of propane in air. Long-duration (600 microsec) capacitance spark; pressure, 3 inches of mercury absolute; temperature, 80° F (ref. 18).

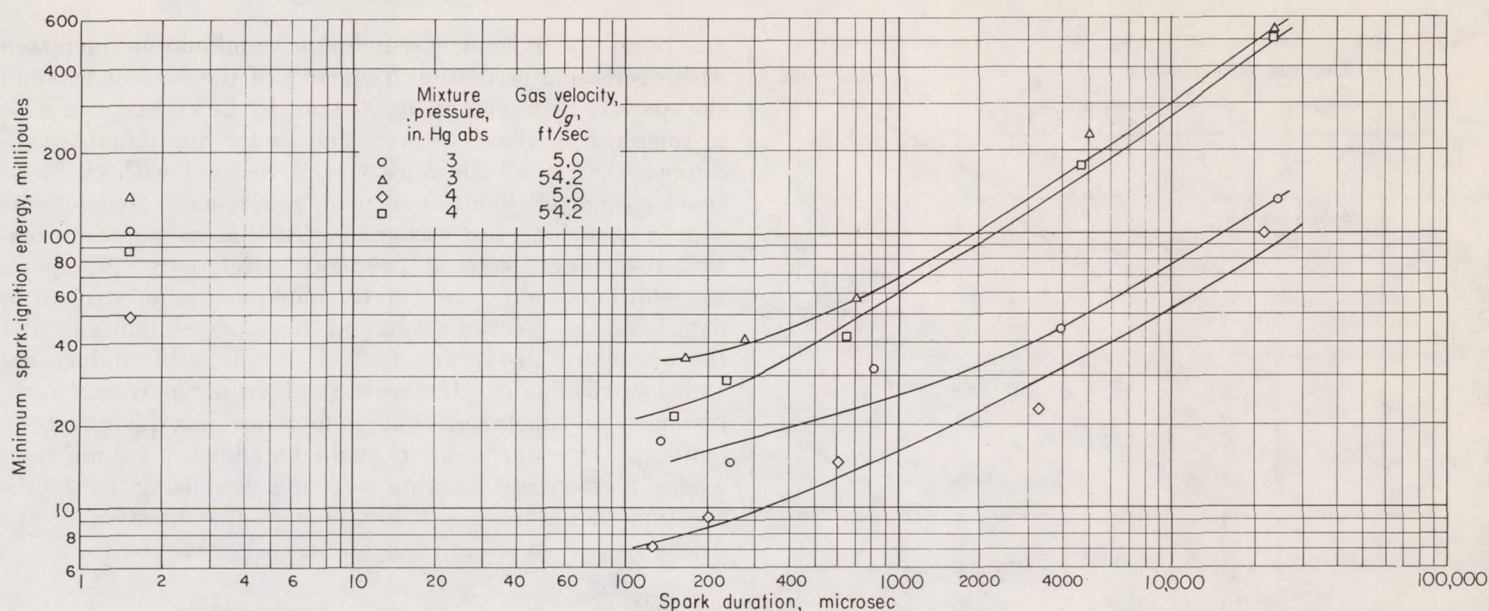


FIGURE 112.—Effect of spark duration on minimum spark-ignition energy of flowing 5.2 percent by volume mixture of propane in air. Long-duration capacitance spark; temperature, 80° F; electrode spacing, 0.25 inch (within quenching distance) (ref. 75).

Fuel type.—The type of fuel has a definite influence on the minimum ignition energy, as shown in the appendix. Reference 76 presents analyses of a number of fuels with respect to molecular weight and arrangement of compounds with the following conclusions:

(1) Hydrocarbon ignition energies decrease in the order: alkanes > alkenes > alkynes.

(2) An increase in chain length or chain branching increases ignition energy.

(3) Conjugation generally lowers the ignition energy.

(4) For long chains, the effect of structural variation is small, but for short chains, the effects are much larger.

(5) Negative substituent groups result in increasing ignition energy in the order: mercaptan < alcohol < chloride < amine. The effects of chlorine and amine groups are particularly large.

(6) Primary amines increase ignition energy more than secondary or tertiary amines.

(7) Ethers and thioethers increase ignition energy.

(8) The peroxide group lowers the ignition energy greatly.

(9) Esters and ketones increase ignition energy greatly, but aldehydes raise ignition energy only slightly.

(10) Ignition energies for compounds containing three-membered rings are very low, particularly when oxygen is in the ring.

(11) Saturated compounds containing six-membered rings have relatively high ignition energies, but those of five-membered rings are about average.

(12) Ignition energies for aromatics are similar to those for linear hydrocarbons containing the same number of carbon atoms.

Basic studies of ignition of fuel mists or sprays in air, a very important aspect of fuel type, have not appeared in the literature because of problems associated with wetting of electrodes, energy absorbed by heat of vaporization, measurement of drop size, partial vaporization of droplets, and volatility of fuel. These variables may affect the energy to such an extent that theories and empirical correla-

tions formulated for gaseous fuel mixtures may not be applicable to liquid fuels.

Electrode spacing.—The effect of electrode spacing for various electrode configurations on the minimum spark-ignition energy (refs. 17 and 18) is shown in figures 84 and 85. With the unflanged electrodes and irrespective of pressure, as the spacing is increased from low values, the energy required decreases. At atmospheric pressure, the energy remains constant with further increase in spacing. Eventually, the energy will rise again at much larger spacings. This constant energy portion is not observed at low pressure. With flanged electrodes, a spacing can be found below which ignition cannot be obtained regardless of the energy supplied. This spacing defines the quenching distance that has been previously described.

The quenching distance also varies with composition, as shown in figure 108. The shape of the curve roughly parallels that of the energy curve. The data show that, to obtain easiest ignition, electrode spacing must be changed as the fuel-air ratio is changed.

Electrode type.—Varying the electrode material has no significant effect on the ignition energy of a flammable mixture with capacitance sparks of short duration. Ignition of gaseous mixtures by sparks from platinum, nickel, zinc, aluminum, lead, brass, and steel electrodes was unaffected by electrode material (refs. 60 and 77). However, reference 18 shows that, with long-duration capacitance sparks, there may be an indirect effect of electrode material. This reference indicates that ignition energies can be different for the different materials, depending upon the type of discharge produced. Figure 111 shows that stainless-steel electrodes, which produced a glow discharge, had ignition energies 50 percent higher than cadmium electrodes, which produced a discharge starting as an arc discharge and changing to a glow discharge. If the type of discharge was a glow discharge, varying the electrode material had a negligible effect.

The effect of electrode configuration is also shown in figure 85. It may be concluded that the effect of electrode size is negligible at the quenching distance (0.56 in. at this condi-

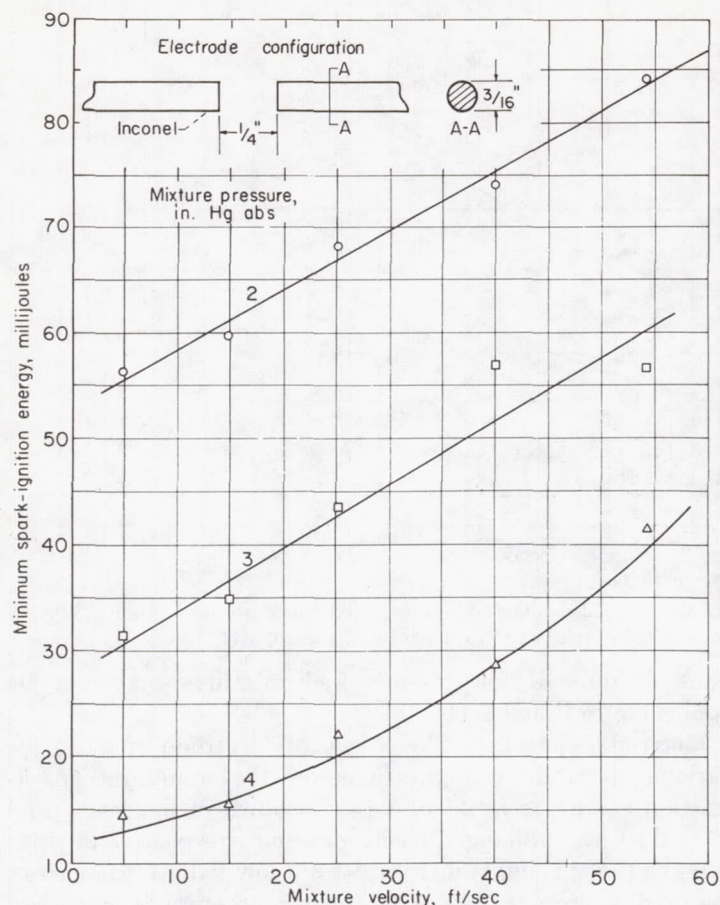


FIGURE 113.—Effect of mixture velocity and pressure on minimum spark-ignition energy of flowing 5.2 percent by volume mixture of propane in air. Long-duration (600 microsec) capacitance spark; temperature, 80° F; electrode spacing 0.25 inch (within quenching distance) (ref. 75).

tion). At spacings less than the quenching distance, the larger electrodes require more energy than the smaller electrodes because of the increased area for quenching to take place.

Condenser voltage.—The effect of condenser voltage on the ignition energy of a flammable mixture is negligible. That is, the ignition energy required is unaffected by increasing the condenser voltage as long as the capacitance is reduced to maintain the same stored energy. Reference 78 reports that the voltage could be varied from 1.6 to 5.8 kilovolts without changing the ignition energy required.

Spark duration.—The effect of increasing the spark duration in the range of 125 to 25,000 microseconds (ref. 75) is to increase the energy required approximately as a power function of the spark duration (fig. 112). This increase is due to distribution of the energy over a larger volume. However, at extremely short spark durations (2 microsec), the energy is considerably higher than that of the majority of the longer-duration sparks. Reference 18 suggests that the increased energy is due to the energy distribution along the spark length.

Oscillation frequency.—Some references (e. g., ref. 79) state that electrical processes are more important in the spark-ignition process than any thermal processes. The research used as a basis for this viewpoint is that described in reference 80, in which the igniting power of a spark

generated by a condenser-inductor combination increased with decreasing oscillation frequency of the current wave of the spark. However, as pointed out by Lewis and von Elbe in reference 5, the tests were run under questionable conditions; that is, all the work was carried out with electrode spacings shorter than the quenching distance. Hence, some sort of quenching test was conducted that gave no information regarding electrical processes. Reference 78 reports the addition of inductance to the apparatus in an attempt to determine the effect of oscillation frequency on ignition. At the quenching distance, no effect of reasonable inductance addition was found. Hence, in the light of the recent work, it must be concluded that inductance has no effect on ignition. One qualification might be added: In some cases where high-energy ignition systems are being used, the addition of inductance might change the duration of the discharge and so affect the ignition energy required.

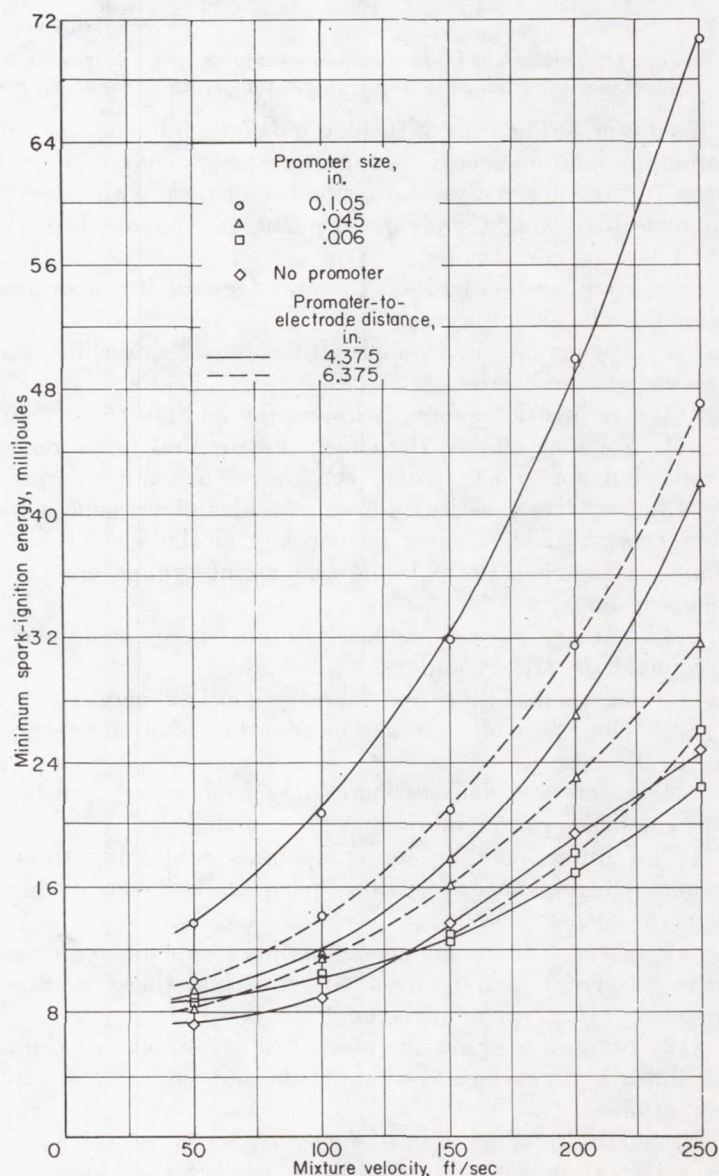


FIGURE 114.—Effect of mixture velocity, promotor size, and distance from promotor to spark electrodes on minimum spark-ignition energy of 5.2 percent by volume mixture of propane in air. Long-duration (approx. 500 microsec) capacitance spark; pressure, 5 inches of mercury absolute; temperature, 80° F; electrode spacing, 0.37 inch (quenching distance) (ref. 82).

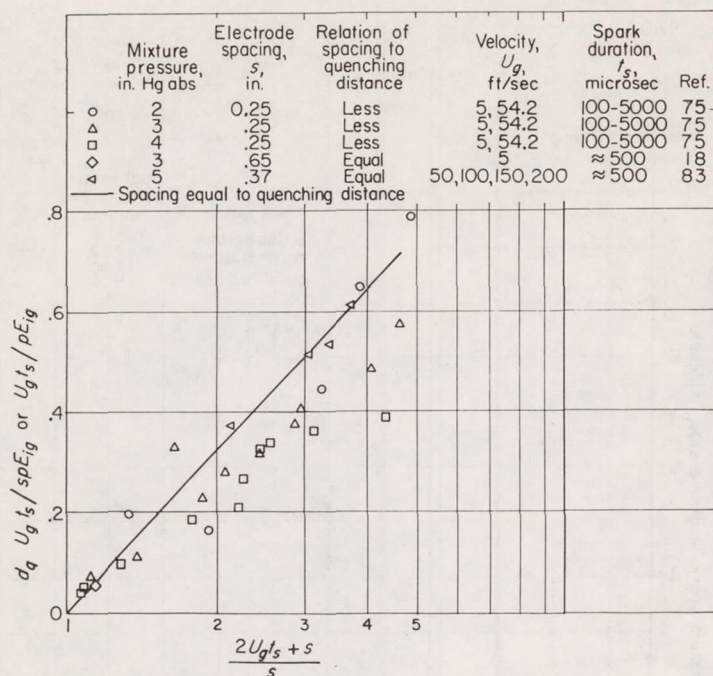


FIGURE 115.—Correlation of non-turbulent-flow ignition-energy data. Fuel, propane; fuel-air ratio, 0.0835.

Sparkling rate.—The effect of sparking rate is described briefly in reference 81, in which an induction coil was used to produce sparks. However, the sparks produced were a series of capacitance sparks from a characteristic capacitance in the circuit. The first spark caused ignition if ignition occurred at all. The passage of two to ten additional sparks had no effect. This was believed to be because of somewhat lower voltage (and energy) in sparks following the first. These tests were conducted with spacing within the quenching distance and are therefore open to question. It is conceivable that, if the sparking rate is sufficiently high and sparks following the first could be generated in the heated zone left by the first spark, some effect could be observed.

Mixture velocity.—Increasing the velocity of flow of a combustible past the electrodes increases the energy required for ignition (ref. 75), as shown in figure 113. Over the range of velocities indicated (5 to 54 ft/sec), the energy increases approximately linearly with velocity. At higher velocities (ref. 82), the energy increases much more rapidly (fig. 114). The velocity causes the spark to be blown downstream, thereby lengthening the spark path and causing the energy to be distributed over a much larger volume. Such distribution depends on the gas velocity and spark duration. A theory is proposed in reference 83 to correlate the parameters of density, velocity, spark duration, electrode spacing, fuel constants, and energy. This theory is based on the idea that the total energy E_{ig} of the spark may not be the important factor in ignition of flowing gases with long-duration sparks. The spark is considered to move downstream at stream velocity U_g in the form of a square-cornered U. The legs of the U will be continuously lengthening, but the length s (corresponding to electrode spacing) will remain constant. It is considered that this length s is a line source of ignition moving at mean stream velocity and is the important part of the spark. The energy in this line source E_{ls} is calculated by making certain assumptions as

to the manner in which and the rate at which the energy goes into the spark. The energy is calculated as follows:

$$E_{ls} = \frac{s E_{ig}}{2 U_g t_s} \log \frac{2 U_g t_s + s}{s} \quad (15)$$

where

E_{ls} energy in line source, joules

s electrode spacing, ft

E_{ig} total ignition energy, joules

U_g gas velocity, ft/sec

t_s spark duration, sec

The energy E_{ls} heats a cylindrical volume of the combustible of length s and radius r . The radius is found by assuming the requirement of ignition is that r must be of such size that the rate of heat generated in the volume must be equal to the rate of heat lost by conduction. An equation relating the rate of heat generated and rate of heat lost determines the critical size of r . Once r is determined, the amount of heat required to heat the volume of radius r and length s to flame temperature can be calculated. This heat should be equal to the heat E_{ls} from the spark, resulting in

$$\frac{d_q U_g t_s}{p s E_{ig}} \propto \log \frac{2 U_g t_s + s}{s} \quad (16)$$

for electrode spacings equal to or less than quenching distance d_q ; or

$$\frac{U_g t_s}{p E_{ig}} \propto \log \frac{2 U_g t_s + s}{s} \quad (17)$$

for electrode spacing greater than d_q . A plot of equations (16) and (17) is shown in figure 115 for data obtained from references 75 and 83. Hence, from this analysis it may be concluded that only a portion of the spark length is important in ignition of flowing gases by long-duration sparks. Energy in the remainder of the spark is dissipated without any help to the ignition process.

Turbulence.—If a turbulence promoter such as a wire screen is placed upstream of the electrodes in a flowing combustible gas (ref. 82), the energy required increases with the

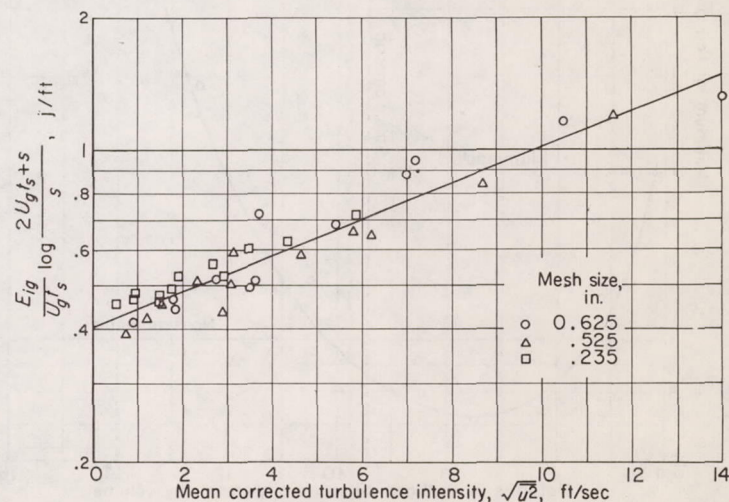


FIGURE 116.—Correlation of ignition energy with velocity, spark duration, electrode spacing, and intensity of turbulence. Pressure, 5.0 inches of mercury absolute; velocity, 50 to 200 feet per second; propane-air ratio, 0.0835 by weight; spark duration, approximately 500 microseconds; electrode spacing, 0.37 inch (ref. 82).

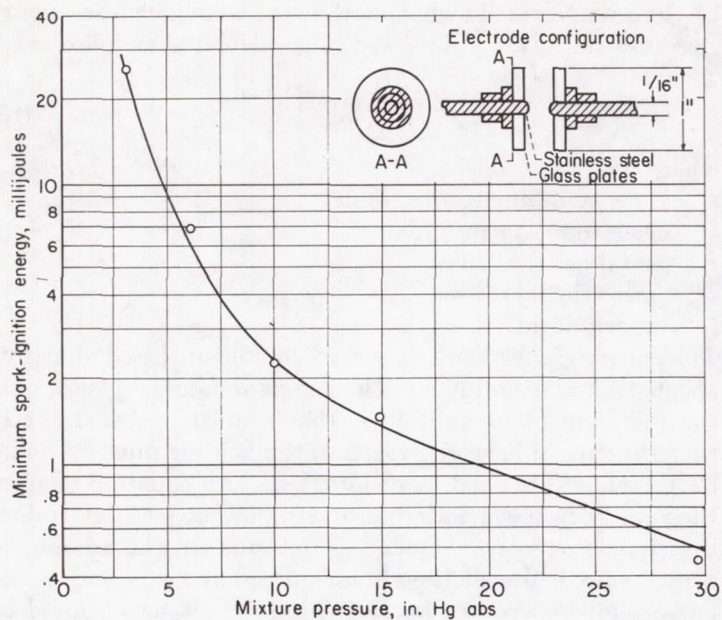


FIGURE 117.—Effect of varying pressure of 8.5 to 9.5 percent by volume mixture of methane and air on minimum spark-ignition energy. Capacitance spark; temperature, 77° F (ref. 78).

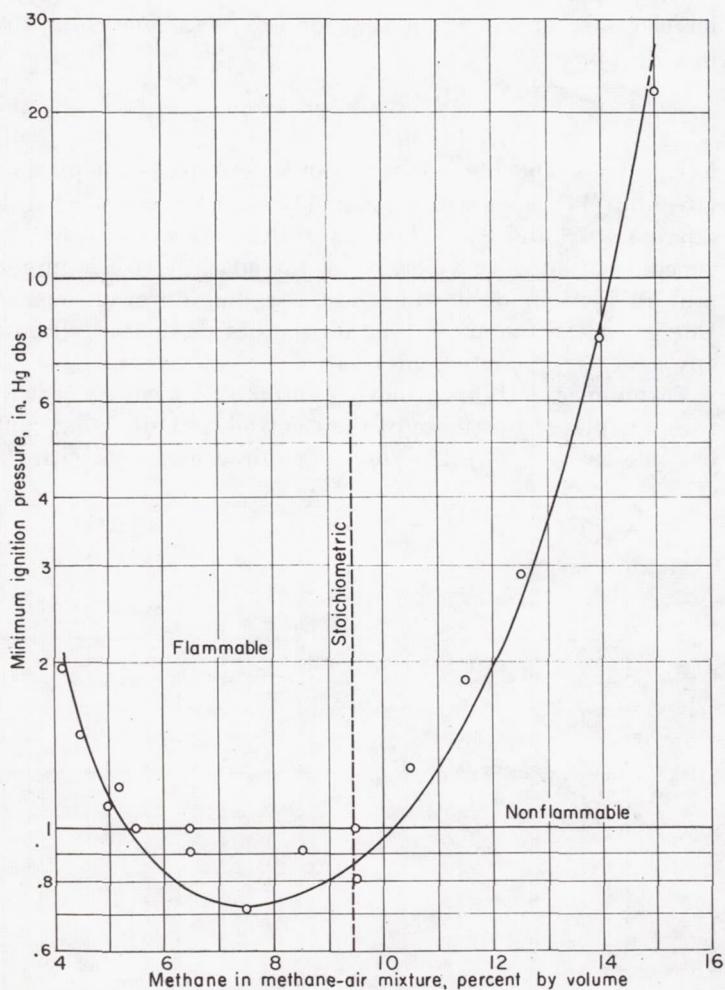


FIGURE 119.—Effect of mixture composition on minimum ignition pressure of methane-air mixtures. Capacitance spark; temperature, 78° to 87° F; spark-plug electrodes; electrode spacing, 0.11 inch (within quenching distance); ignition energy, 8640 millijoules (ref. 84).

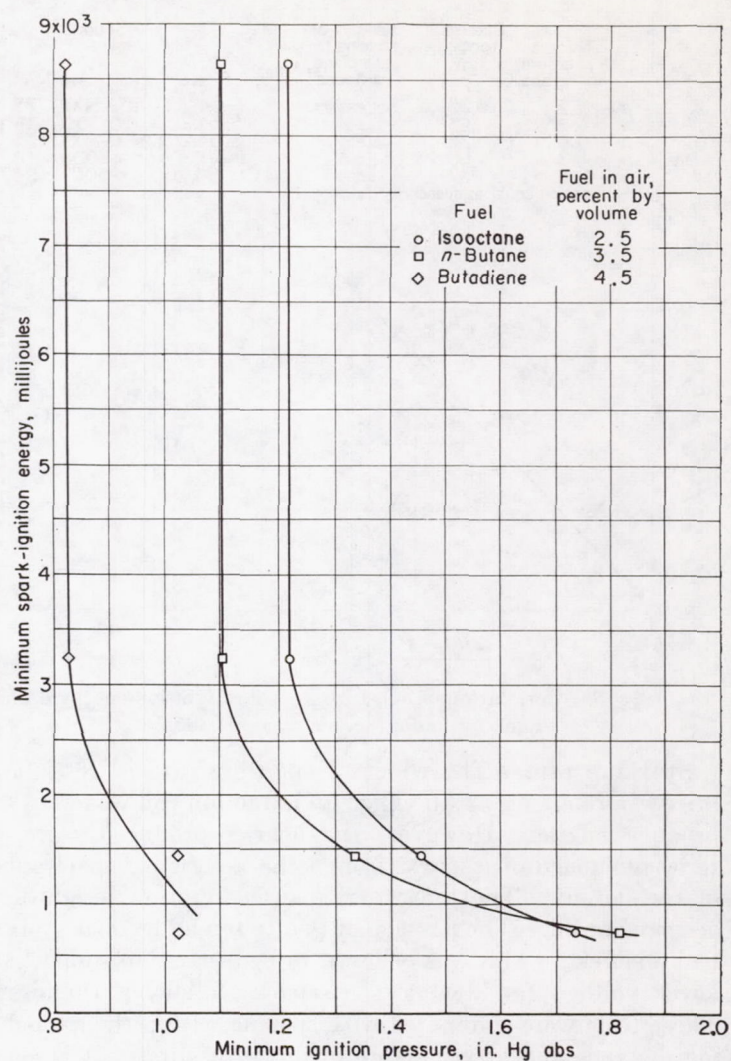


FIGURE 118.—Effect of mixture pressure on minimum spark-ignition energy of one electrode configuration. Capacitance spark; electrode spacing, 0.11 inch (within quenching distance); spark voltage, 600 volts; mixtures slightly richer than stoichiometric (ref. 84).

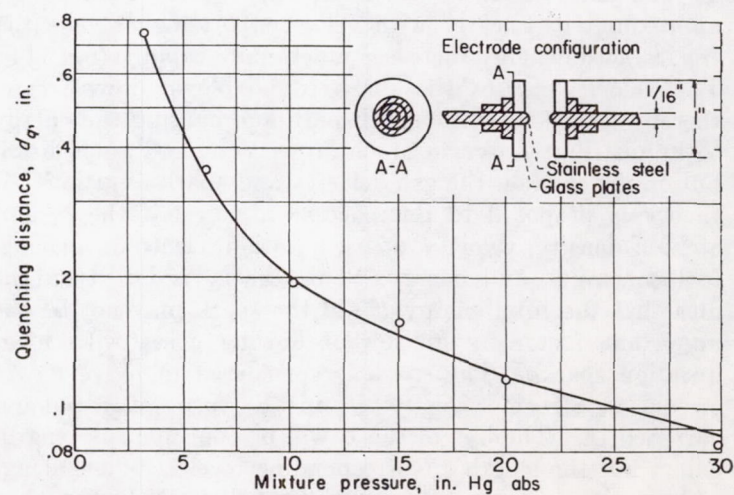


FIGURE 120.—Effect of mixture pressure of 8.5 to 9.5 percent by volume mixture of methane and air on quenching distance of one electrode configuration. Capacitance spark; temperature, 77° F (by permission from ref. 78).

wire size of the turbulence promoter and with decreasing distance from turbulence promoter to electrodes (fig. 114). The energy increases with those factors that increase the intensity of turbulence. The idea of a line source of ignition has been applied to turbulent ignition data similar to those shown in figure 115 (ref. 83). All the concepts considered in the previous section were used except that the rate of heat loss was assumed to depend upon the intensity of turbulence. This analysis showed that, at constant pressure,

$$\frac{E_{ig}}{U_{gs} t_s} \log \frac{2U_{gs} t_s + s}{s} \propto \mathcal{F} \sqrt{u^2} \quad (18)$$

A plot of this relation is shown in figure 116. Hence, the energy in the line source of ignition depends directly on the intensity of turbulence. The effect of scale of turbulence is negligible at this condition.

Pressure.—Pressure has a pronounced effect on the ignition of a flammable mixture (ref. 78), as shown in figure 117, in which the minimum ignition energy increases with decreasing pressure. For most fuels, the energy varies inversely as the b^{th} power of pressure, where b is approximately 2. If the pressure is reduced sufficiently, a pressure will be reached (minimum ignition pressure) below which ignition is limited by some factors of the apparatus such as electrode spacing, size of ignition chamber, or available energy. Whether there is an ultimate limiting pressure has not been determined. Therefore, all the following data are apparatus-limited.

Figure 118 shows the energy increasing as the pressure decreases toward the minimum ignition pressure in tests (ref. 84) with constant electrode spacing. This curve is a combination of two separate effects, pressure and quenching. That is, as the pressure is reduced, the electrode spacing is effectively moved farther within the quenching distance, since the quenching distance increases with decreasing pressure. Different fuels exhibit different minimum pressures, as shown in figure 118 and the following table (ref. 84):

Fuel	Minimum ignition pressure, ^a in. Hg abs
Hydrogen.....	0.45
Methane.....	.75
1,3-Butadiene.....	.83
2-Butene.....	1.14
n-Butane and isobutane.....	1.14
Benzene.....	1.10
2,4-Dimethyl-1,3-pentadiene.....	1.30
n-Nonane.....	1.30

^a Obtained with capacitance spark; temperature, 75° to 85° F; electrode spacing, 0.110 in. (less than quenching distance); energy, 8.64 j.

Lower pressures than these could have been obtained if the tests had been conducted in apparatus of sufficiently large size so that quenching could not occur. The importance of apparatus size has been emphasized in the quenching discussions.

Pressure limits for some of the petroleum fuels in air at room temperature have been determined as follows:

Fuel	Minimum ignition pressure, ^a in. Hg abs	Reference
100/130 Grade aviation gasoline.....	0.63	22
115/145 Grade aviation gasoline.....	1.50	22
Grade JP-3 jet fuel.....	1.50	22
Grade JP-4 jet fuel.....	.51	85

^a Obtained with capacitance spark; temperature, 78° F; electrode spacing, 1.0 in.

Minimum ignition pressures are also a function of the mixture composition (ref. 84), as shown in figure 119. The lowest pressure occurs at about 7.5 percent mixture ratio and on the lean side of stoichiometric for methane. Hydrogen also has the minimum on the lean side (ref. 84). For heavier hydrocarbons, such as propane and *n*-butane, the lowest pressure occurs on the rich side of stoichiometric. This phenomenon may be due to relative differences in diffusivities of air and the fuels. Air has a diffusivity less than hydrogen and methane and greater than propane and *n*-butane.

In determining the effect of pressure on ignition energy, consideration must be given to the choice of electrode spacing to be used, since the quenching distance is also a function of the pressure (ref. 76). This is demonstrated in figure 120, which shows that the quenching distance increases with decreasing pressure. A complete relation between electrode spacing, pressure, and minimum ignition energy is shown in figure 121.

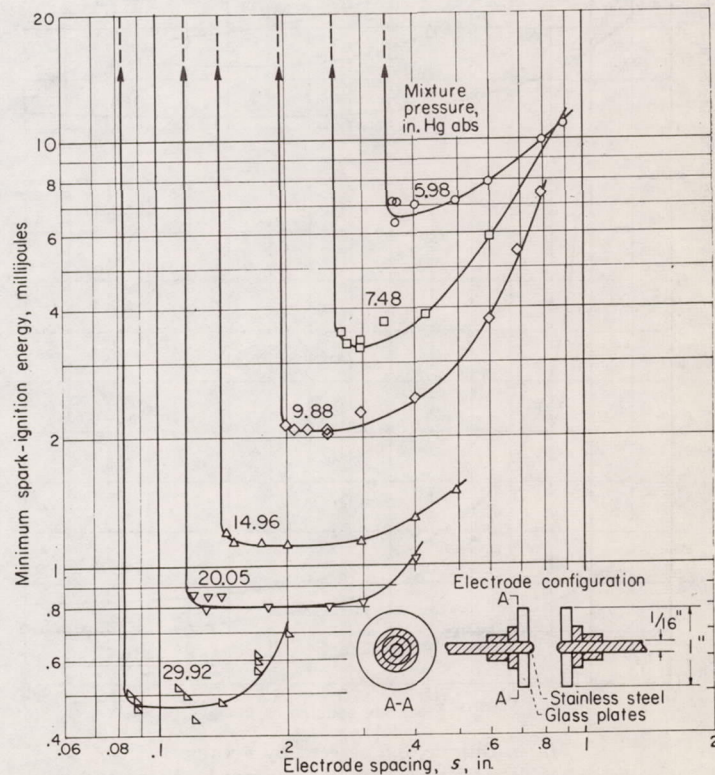
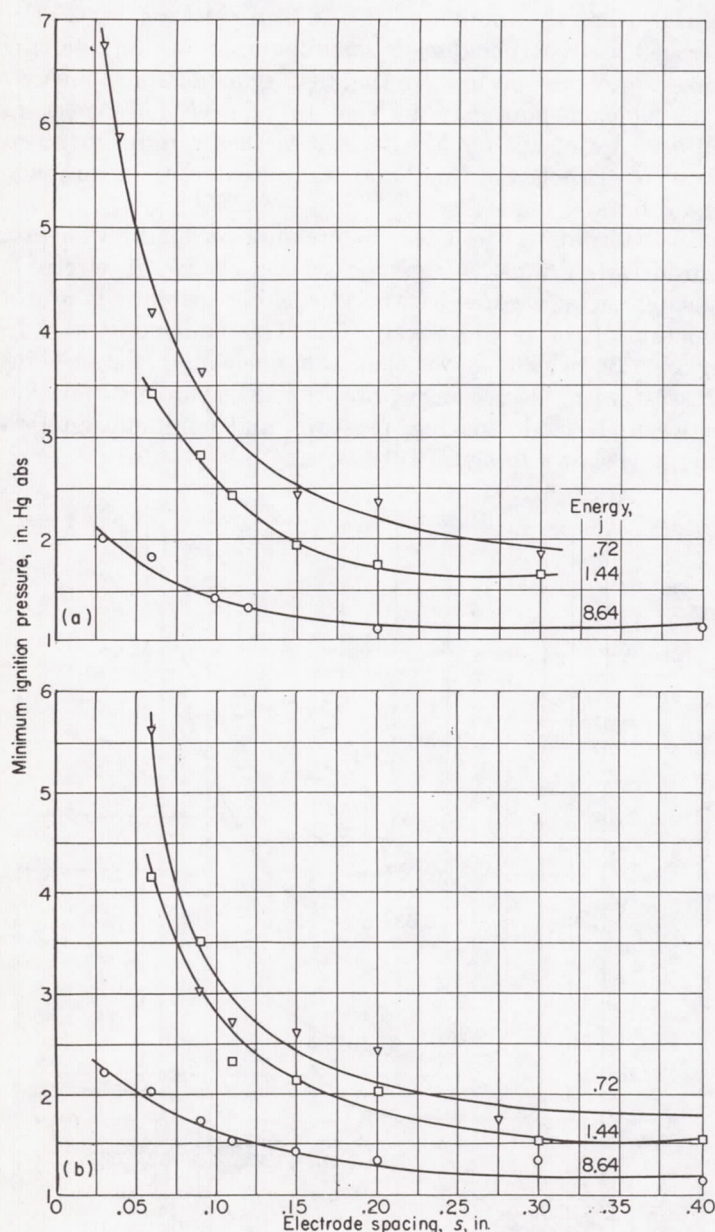


FIGURE 121.—Effect of electrode spacing and pressure on minimum spark-ignition energy of 9.5 percent by volume methane in air. Capacitance spark; temperature, 77° F (by permission from ref. 78).

The fact that the electrode spacing for minimum ignition energy increases with decreasing pressure may be explained by assuming that a certain spark-ignition energy can initially ignite a certain mass of flammable mixture. If the pressure is decreased, the mass occupies a larger volume, and hence the electrode spacing must be increased so that the spark will be of sufficient size to ignite the larger volume.

In the determination of minimum ignition pressures, capacitance sparks of high energy have been used to overcome the quenching effect of the electrodes (ref. 84). Figure 122 shows the effect of electrode spacing and energy on minimum ignition pressure for *n*-butane and 2,2,4-trimethylpentane. The data show that the higher the energy, the less the effect of spacing on pressure. The energy of 8.64



(a) *n*-Butane, 3.5 percent by volume.

(b) 2,2,4-Trimethylpentane, 2.5 percent by volume.

FIGURE 122.—Effect of electrode spacing on minimum ignition pressure. Capacitance spark; temperature, 70° to 75° F; sparkplug electrodes (ref. 84).

joules that is used with a spacing of 0.110 inch ignites at pressures close to the minimum of the curves; and, consequently, not much is gained by the wider spacing, although the optimum spacing would be greater than 1 inch.

Temperature.—The effect of increasing the temperature is to lower the minimum ignition energy, as shown in the following table taken from reference 86:

Fuel	Temperature, °F	Ignition energy, ^a millijoules
Carbon disulfide.....	77	0.76
	212	.5
<i>n</i> -Heptane.....	77	14.5
	212	6.7
	340	3.2
Isooctane.....	77	27.0
	212	11.0
	340	4.8
<i>n</i> -Pentane.....	-22	45.0
	-4	14.5
	77	7.8
	212	4.2
	340	2.3
	347	2.5
Propane.....	-40	11.7
	-22	9.7
	-4	8.4
	77	5.5
	135	4.2
	180	3.6
	212	3.5
	399	1.4
Propene oxide.....	77	2.4
	212	1.5
	360	.9

^a Determined with capacitance spark, atmospheric pressure, and flanged electrodes.

From these data, a correlation was obtained relating energy and initial temperature of the mixture. This relation was of the form

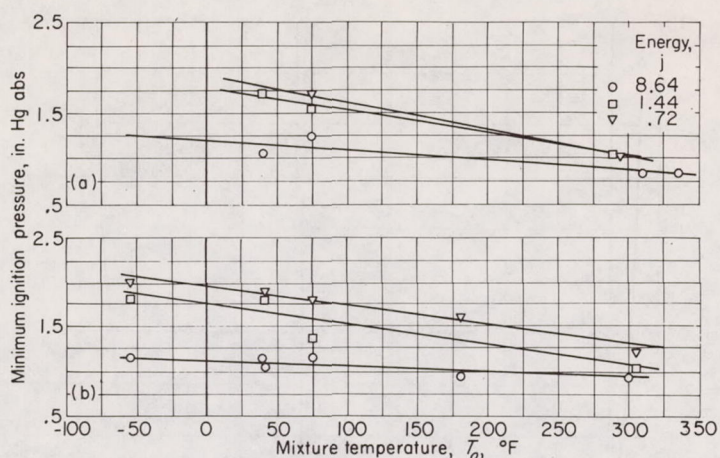
$$E_{ig} = C e^{\mathcal{K} T_o} \quad (19)$$

where C and \mathcal{K} are constants that are different for the various compounds.

The same trend of lower ignition energies with increased temperatures is shown in reference 87 for a flowing propane-air mixture and long-duration capacitance discharge. The correlation of this data was based on theoretical considerations which resulted in the relation

$$\ln \frac{E_{ig}}{\kappa C_p \left(1962 + \frac{1}{2} T_o\right) \left(1962 - \frac{1}{2} T_o\right)^2} \propto \frac{1}{1962 + \frac{1}{2} T_o} \quad (20)$$

The minimum ignition pressure is not affected greatly by changing the temperature from -50° to 300° F (ref. 84). Figure 123 shows a slight linear decrease in pressure with an increase in temperature in this range. This decrease is in the proper direction to be the result of decreased quenching caused by increased temperature, as discussed previously.



(a) 2,2,4-Trimethylpentane in air, 2.5 percent by volume.
(b) *n*-Butane in air, 3.5 percent by volume.

FIGURE 123.—Effect of mixture temperature on minimum spark-ignition pressure of mixtures of 2,2,4-trimethylpentane or *n*-butane in air. Capacitance spark; sparkplug electrodes; electrode spacing, 0.11 inch (within quenching distance) (ref. 84).

Diluents.—The addition of a diluent to a combustible gas has a marked effect on the minimum ignition energy (ref. 78). It should be expected that the minimum ignition energy depends upon the absorptive and conductive qualities of any additive that might be present in the fuel, as well as upon the fuel itself. This is shown to be true in figure 124(a). If the nitrogen in a methane-air mixture is replaced with helium, the energy increases; if replaced by argon, the energy decreases. With the exception of the methane-oxygen-argon mixtures, the minimum ignition energies increase with increasing diffusivity of the mixture according to reference 88. The quenching-distance curves (fig. 124(b)) are similar to the energy curves.

The effects of diluents on minimum ignition pressure of mixtures of *n*-butane and oxygen with argon, nitrogen, carbon dioxide, and helium (ref. 84) are shown in figure 125. In all cases, mixtures containing argon are the most easily ignited; mixtures containing carbon dioxide are the least easily ignited. Humidity, which might be considered as a diluent, would replace some of the oxygen and would thus cause higher ignition energies. This effect has not been determined experimentally. The effect, if any, is probably small and can be neglected in most cases.

IGNITION BY INDUCTANCE SPARKS

The difference between inductance sparks and capacitance sparks has been explained previously. The energy stored in an inductance is

$$E_L = \frac{1}{2} Li^2 \quad (21)$$

where

E_L energy, joules

L inductance, henry

i current in circuit at instant of sparking, amp

Mixture composition, pressure, and temperature.—The effect of mixture composition, pressure, and temperature on minimum ignition energy with inductance sparks is similar to that obtained with capacitance sparks. However, with

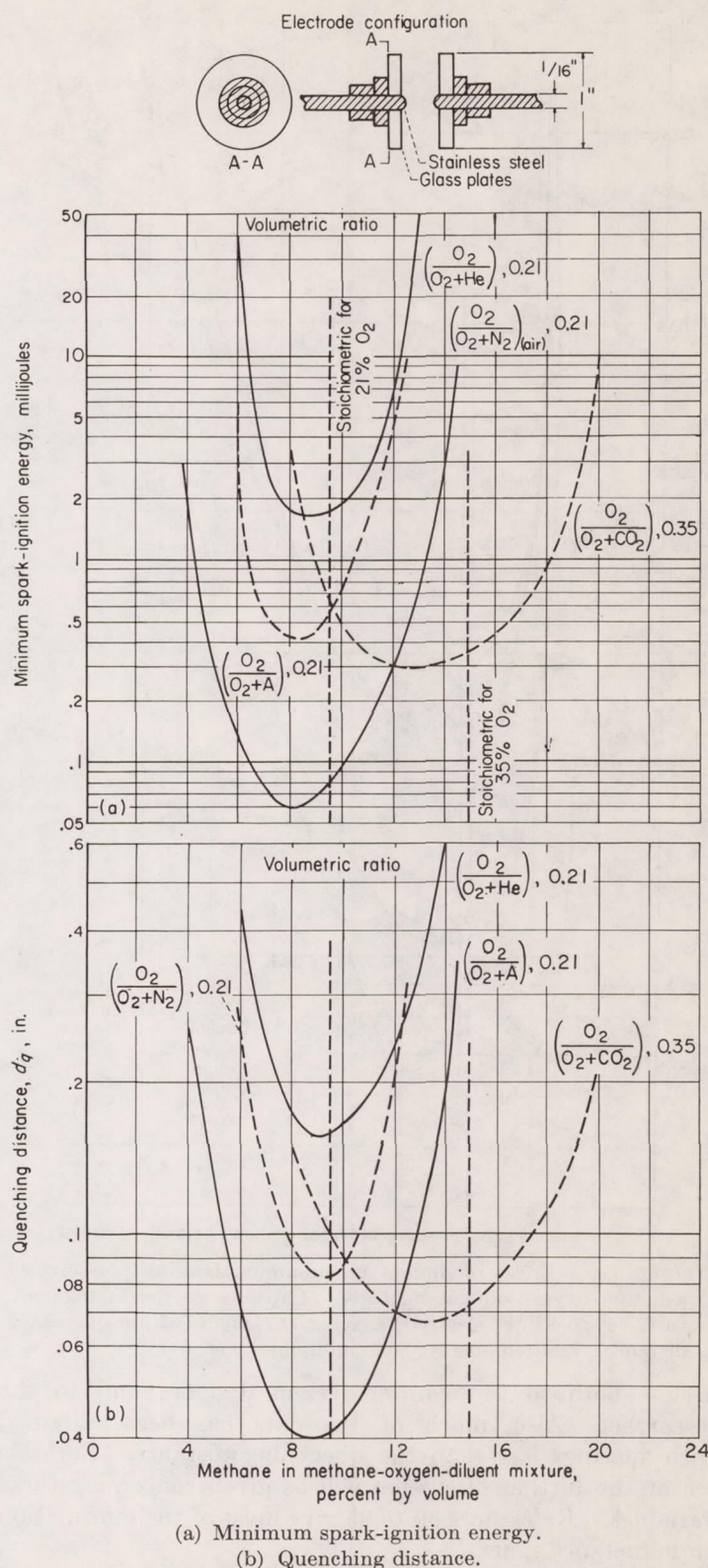


FIGURE 124.—Effect of diluents on minimum spark-ignition energy and quenching distance of methane-oxygen-diluent mixtures. Capacitance spark; pressure, atmospheric; temperature, 77° F (by permission from ref. 78).

inductance sparks, much of the data have been obtained using the current in the primary of a transformer as an indication of the energy in the spark gap. Since this method does not give actual energies, the data are practically

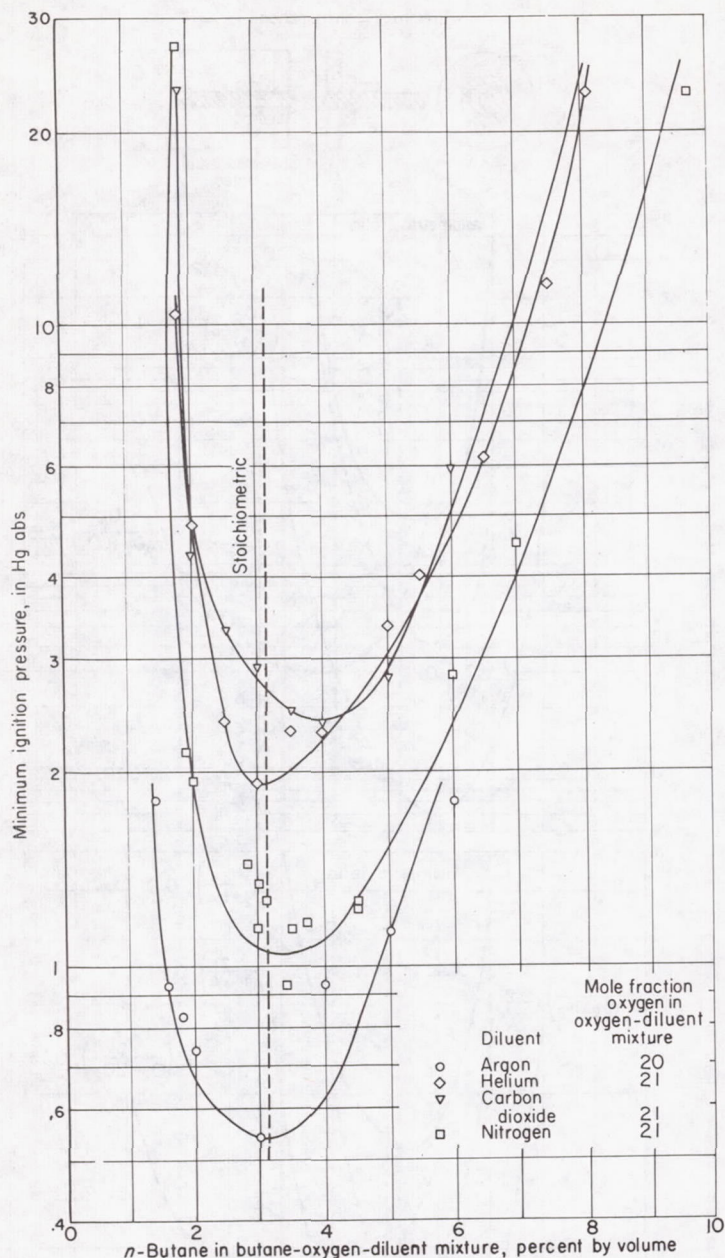


FIGURE 125.—Effect of diluent on minimum ignition pressures of *n*-butane-oxygen-diluent mixtures. Capacitance spark; temperature, 74° to 82° F; electrode spacing, 0.11 inch (within quenching distance); ignition energy, 8640 millijoules (ref. 84).

useless both to the ignition-system designer and to the researcher. Also, much of the data has been obtained with spacings less than the quenching distance. For this reason, no further discussion will be given concerning these variables. References 89 to 95 give most of the information on inductance sparks.

Electrode spacing.—As shown in figure 126, the curve of minimum electrode spacing against composition is very similar to those obtained with the capacitance spark (fig. 124(b)). The quenching distances with inductance sparks appear to be slightly lower than those obtained with capacitance sparks.

Electrode material.—The available data on inductance sparks indicate that, unlike capacitance sparks, ignition energies of flammables are affected by changes in electrode materials. Electrodes of platinum, nickel, copper, alumi-

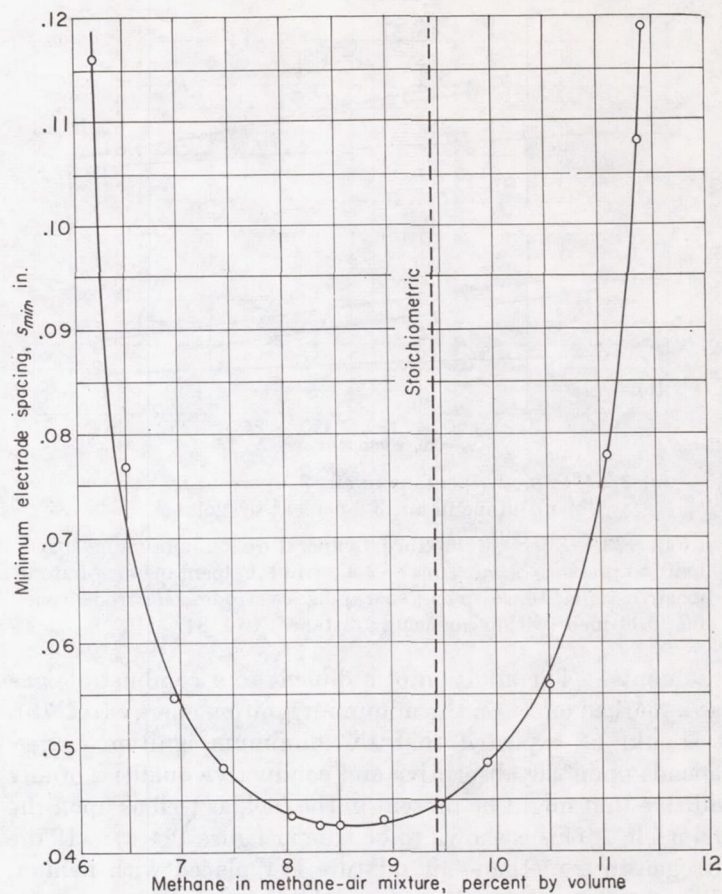


FIGURE 126.—Effect of mixture composition on minimum electrode spacing in ignition of methane-air mixture. Inductance spark; atmospheric pressure and temperature; electrode configuration, 0.394-inch-diameter platinum disk and sharply pointed platinum cone; primary-circuit current, 1.0 ampere (ref. 90).

num, and iron have been used to ignite ethane-air and carbon monoxide-air mixtures (ref. 91). Decreasing the density of the electrode material generally decreased the amount of energy required to ignite the flammable mixture. No separation of the types of discharge (i. e., arc or glow) was made; therefore, no comparison can be made with the results obtained with the long-duration capacitance sparks.

Circuit inductance and voltage.—The energy stored in an inductance is determined by a simple relation with inductance and current; however, two factors that can be present may cause errors in calculations. These factors are the type of inductance used and the circuit voltage. Sometimes, in order to obtain large energies, it is necessary to use inductances with metal cores, in which case some energy losses occur in the core material, as can be concluded from the following table (ref. 92) (14 layers of inductance-core winding in each case):

Core of coil	Circuit inductance, <i>L</i> , henry	Circuit current, <i>i</i> , amp	Ignition energies,* millijoules
Air.....	0.01	0.35	0.6
Straight iron bar.....	.07	.15	.8
Rectangular iron frame.....	.56	.09	2.3

* Ignition of coal gas and air at atmospheric pressure and temperature.

Hence, the effect of type of inductance (if losses are present) is higher readings than are actually present in the spark.

When sparks are generated by opening contacts through which current is flowing, a sufficiently high circuit voltage causes current to flow across the gap for a short time after the stored energy is dissipated. The amount of extraneous energy caused by this aftercurrent increases with the circuit voltage. Therefore, since the actual ignition energy in the spark gap is the sum of the stored energy plus the extraneous energy, any ignition-energy values based on calculated stored energy will be too low. This effect is shown in the following table from reference 93:

Circuit inductance, <i>L</i> , henry	Circuit potential, volts	Circuit current, <i>i</i> , amp	Spark- ignition energy, ^a millijoules
0.0214-----	4 220	0.77 .35	6.35 1.30
0.012-----	4 220	1.025 .4	6.30 .96

^a Ignition of 8.5 percent by volume mixture of methane in air at atmospheric pressure and temperature.

Current type.—Whether the current is alternating or direct appears to have no effect on ignition with inductance sparks (ref. 94).

SIGNIFICANCE OF BASIC QUENCHING, FLAMMABILITY, AND IGNITION DATA IN RELATION TO AIRCRAFT PROPULSION PROBLEMS

The data presented show the environmental conditions under which ignition and flame propagation in hydrocarbon-air mixtures may be obtained. With a fuel-air mixture contained in an apparatus large enough to preclude quenching, there are practically no limits to the conditions under which ignition and flame propagation may be obtained except the concentration limits of flammability. Hence, if proper mixtures can be produced in an aircraft combustor, there should be no basic limitation insofar as ignition and flammability are concerned in the over-all aircraft propulsion problem. However, practical limitations arise at present because of the finite size of combustors, the presence of turbulent flow, and the limited energy available from ignition sources. There are some areas in which more work is needed. The quenching, flammability, and ignition of fuel sprays and mists have not yet been studied sufficiently. The effects of velocity and turbulence on flammability are still somewhat in doubt.

As yet, there is no unified theory that is able to predict quantitatively the limits imposed on combustion by quenching, flammability, and ignition from a knowledge of the basic physical and chemical properties of a combustible mixture. However, some qualitative ideas can be presented on the basis of present knowledge. The ideas are discussed under the three main types of work described in this chapter. Correlations of fundamental combustion properties and combustor performance, which at present must largely take the place of a general quantitative theory, are given in subsequent chapters.

QUENCHING

The quenching effect of walls is always present when a flame is enclosed by a duct. If flame propagation is to occur, the dimensions of the volume to be burned must be larger than the quenching distance at the lowest pressure and most unfavorable fuel-air ratio encountered. Even if the flame is stabilized and is in no danger of being quenched by the walls, the dead space still exists and may be appreciable under some conditions. Thus, it should be noted that the full cross section of the chamber is not available for heat release.

In some current tubular-combustor turbojet engines, only two of the chambers are fitted with spark plugs. The remaining chambers must be ignited by the spread of flame through cross-fire tubes. Altitude starting performance should therefore be adversely affected by quenching of the igniting flame if the cross-fire tubes are too narrow.

Recent work indicates that homogeneous gas-phase quenching may also occur because of turbulent motion. Thus, it is possible that measures taken to increase turbulence and thereby improve mixing or extend the residence time of the fuel in the combustor may actually result in no change or even a decrease in combustor performance.

FLAMMABILITY

A self-sustained flame cannot exist in a mixture unless the fuel concentration is within the flammable range under the given conditions. Consequently, excessive dilution of the burning zone with either fuel or air must be avoided. It should again be pointed out, however, that flames sustained by a continuous ignition source such as a pilot may sometimes exist at over-all fuel-air ratios outside the range of flammability.

The effects of diluents must also be considered. For example, if it is required to burn fuel in an atmosphere containing exhaust products, substitution of carbon dioxide and water vapor for some of the oxygen originally present will narrow the flammable range. If the exhaust products are hot, the increased temperature may tend to compensate for this narrowing. Such questions might arise, for example, if a pilot flame is required to burn in the presence of recirculation from the main combustion zone of the combustor, or in the case of an afterburner.

IGNITION

Ignition in the high-speed combustor can be accomplished by any of the methods discussed; however, practical considerations may make some of them infeasible. For example, ignition by electrically heated surfaces is very inefficient compared with ignition by electrical discharges. Not only must the mass of the heated surface be raised to the required temperature, but also a larger volume of gas must be heated because of the longer times required to attain ignition.

Flames or hot gases can be effective ignition sources, but there must be available an additional ignition source to produce the flame or hot gas in the first place. In aircraft at adverse starting conditions, it may be just as difficult to ignite the pilot as it would be to ignite the main combustible. Ignition by electrical discharge, therefore, appears to be the most feasible method.

The ideal environmental conditions for ignition by electrical discharges are as follows:

- (1) High pressure
- (2) High temperature
- (3) Low gas velocity and turbulence
- (4) Location of spark in zone of best mixture composition
- (5) Gaseous fuel-air mixture
- (6) Electrode spacing maintained at quenching distance
- (7) Optimum spark duration

Obviously, it would be impossible to satisfy all these requirements in an actual combustor, but any attempt to satisfy as many as possible would result in lower ignition energies and lower-weight ignition systems.

Whether capacitance or inductance sparks are the better for ignition is a point for consideration. The data presented herein show that capacitance sparks can be varied readily over a tremendous energy range, whereas inductance sparks may possibly be limited to those applications where low energy is required. On the other hand, if the data on the effect of spark duration using long-duration sparks are used as an indication of what might happen with inductance sparks, there may be some instances where inductance sparks are superior to capacitance sparks. It appears, then, that a choice between the two systems depends upon the actual energy required. Design and operation of the ignition systems producing these two types of sparks might be the important factor in selecting the type of spark to be used.

The fact that there is a minimum contact time, or ignition lag, for ignition by heated surfaces, hot gases, or pilot flames, introduces the possibility of an effect of such ignition sources on the combustion efficiency of combustors that utilize them. If the flow rate in a given burner is fixed, 100-percent combustion efficiency can be obtained only if there is sufficient residence time for the mixture to be ignited and for the flame to consume the mixture as rapidly as it flows into the chamber. The consumption time depends upon the burning velocity under the given conditions. Therefore, if the required time for contact with the ignition source is excessively long, insufficient time for burning may remain before the mixture leaves the burner; that is, only part of the fuel may be consumed, and the combustion efficiency may fall below 100 percent.

REFERENCES

1. Harris, Margaret E., Grumer, Joseph, von Elbe, Guenther, and Lewis, Bernard: Burning Velocities, Quenching, and Stability Data on Non-turbulent Flames of Methane and Propane with Oxygen and Nitrogen. Third Symposium on Combustion and Flame and Explosion Phenomena, The Williams & Wilkins Co. (Baltimore), 1949, pp. 80-89.
2. Berlad, A. L., and Potter, A. E., Jr.: Effect of Channel Geometry on the Quenching of Laminar Flames. NACA RM E54CO5, 1954.
3. Friedman, Raymond, and Johnston, W. C.: Pressure Dependence of Quenching Distance of Normal Heptane, Iso-Octane, Benzene, and Ethyl Ether Flames. Jour. Chem. Phys., vol. 20, no. 5, May 1952, p. 919.
4. Friedman, Raymond: The Quenching of Laminar Oxyhydrogen Flames by Solid Surfaces. Third Symposium on Combustion and Flame and Explosion Phenomena, The Williams & Wilkins Co. (Baltimore), 1949, pp. 110-120.
5. Lewis, Bernard, and von Elbe, Guenther: Combustion, Flames and Explosion of Gases. Academic Press, Inc., 1951.
6. Potter, A. E., Jr., and Berlad, A. L.: The Quenching of Flames of Propane-Oxygen-Argon and Propane-Oxygen-Helium Mixtures. Jour. Chem. Phys., vol. 60, no. 2, 1956, pp. 97-101.
7. Friedman, Raymond, and Johnston, W. C.: The Wall-Quenching of Laminar Propane Flames as a Function of Pressure, Temperature, and Air-Fuel Ratio. Jour. Appl. Phys., vol. 21, no. 8, Aug. 1950, pp. 791-795.
8. Simon, Dorothy M., Belles, Frank E., and Spakowski, Adolph E.: Investigation and Interpretation of the Flammability Region for Some Lean Hydrocarbon-Air Mixtures. Fourth Symposium (International) on Combustion, The Williams & Wilkins Co. (Baltimore), 1953, pp. 126-138.
9. Berlad, Abraham L.: Flame Quenching by a Variable-Width Rectangular-Slot Burner as a Function of Pressure for Various Propane-Oxygen-Nitrogen Mixtures. NACA RM E53K30, 1954. (See also Jour. Phys. Chem., vol. 58, no. 11, Nov. 1954, pp. 1023-1026.)
10. Wohl, Kurt: Quenching, Flash-Back, Blow-Off—Theory and Experiment. Fourth Symposium (International) on Combustion, The Williams & Wilkins Co. (Baltimore), 1953, pp. 68-89.
11. Starkman, E. S., Haxby, L. P., and Cattaneo, A. G.: A Study of Free Flames in Turbulent Streams. Fourth Symposium (International) on Combustion, The Williams & Wilkins Co. (Baltimore), 1953, pp. 670-673.
12. Olsen, H. L., and Gayhart, E. L.: Incipient Flame Propagation in a Turbulent Stream. Jet Prop., vol. 25, no. 6, June 1955, pp. 276-283.
13. Olsen, H. L., and Gayhart, E. L.: Effect of Turbulence on Incipient Flame Propagation. Jour. Chem. Phys., vol. 23, no. 2, Feb. 1955, pp. 402-403.
14. von Elbe, Guenther, and Lewis, Bernard: Theory of Ignition, Quenching and Stabilization of Flames of Nonturbulent Gas Mixtures. Third Symposium on Combustion and Flame and Explosion Phenomena, The Williams & Wilkins Co. (Baltimore), 1949, pp. 68-79.
15. Belles, Frank E., and Berlad, A. L.: Chain Breaking and Branching in the Active-Particle Diffusion Concept of Quenching. NACA TN 3409, 1955.
16. Potter, A. E., Jr., and Berlad, A. L.: A Thermal Equation for Flame Quenching. NACA TN 3398, 1955.
17. Lewis, Bernard, and von Elbe, Guenther: Ignition and Flame Stabilization in Gases. Trans. ASME, vol. 70, no. 4, May 1948, pp. 307-314; discussion, pp. 314-316.
18. Swett, Clyde C., Jr.: Spark Ignition of Flowing Gases. II—Effect of Electrode Parameters on Energy Required to Ignite a Propane-Air Mixture. NACA RM E51J12, 1951.
19. Coward, H. F., and Jones, G. W.: Limits of Flammability of Gases and Vapors. Bull. 503, Bur. Mines, 1952.
20. Spakowski, Adolph E.: Pressure Limits of Flame Propagation of Pure Hydrocarbon-Air Mixtures at Reduced Pressures. NACA RM E52H15, 1952.
21. Barnett, Henry C., and Hibbard, R. R.: Fuel Characteristics Pertinent to the Design of Aircraft Fuel Systems. NACA RM E53A21, 1953.
22. Jones, G. W., et al.: Research on the Flammability Characteristics of Aircraft Fuels. WADC Tech. Rep. 52-35, Wright Air Dev. Center, Wright-Patterson Air Force Base, June 1952. (Contract AF 33 (038) 50-1293E.)
23. Wolfhard, H. G., and Parker, W. G.: Evaporation Processes in a Burning Kerosene Spray. Jour. Inst. Petroleum, vol. 35, no. 302, Feb. 1949, pp. 118-125.
24. Burgoyne, J. H., and Richardson, J. F.: The Inflammability of Oil Mists. Fuel, vol. XXVIII, no. 1, Jan. 1949, pp. 2-6.
25. Sullivan, M. V., Wolfe, J. K., and Zisman, W. A.: Flammability of the Higher Boiling Liquids and Their Mists. Ind. and Eng. Chem., vol. 39, no. 12, Dec. 1947, pp. 1607-1614.

26. Burgoyne, J. H., and Cohen, L.: The Effect of Drop Size on Flame Propagation in Liquid Aerosols. *Proc. Roy. Soc. (London)*, ser. A, vol. 225, no. 1162, Sept. 14, 1954, pp. 375-392.
27. Moran, H. E., Jr., and Bertschy, A. W.: Flammability Limits for Mixtures of Hydrocarbon Fuels, Air, and Halogen Compounds. Rep. No. NRL 4121, Naval Res. Lab., Wash. (D. C.), Feb. 25, 1953.
28. Fryburg, George: Review of Literature Pertinent to Fire-Extinguishing Agents and to Basic Mechanisms Involved in Their Action. NACA TN 2102, 1950.
29. Belles, Frank E.: Chemical Action of Halogenated Agents in Fire Extinguishing. NACA TN 3565, 1955.
30. Burgoyne, J. H., and Williams-Leir, G.: The Influence of Incombustible Vapours on the Limits of Inflammability of Gases and Vapors in Air. *Proc. Roy. Soc. (London)*, ser. A, vol. 193, July 21, 1948, pp. 525-539.
31. Belles, Frank E.: A Preliminary Investigation on Wall Effects of Pressure-Inflammability Limits of Propane-Air Mixtures. NACA RM E50J10a, 1950.
32. Karlovitz, Béla: Open Turbulent Flames. Fourth Symposium (International) on Combustion, The Williams & Wilkins Co. (Baltimore), 1953, pp. 60-67.
33. Damon, Glenn H.: Monthly Report on Contract AF-18(600)151: Flammability Characteristics of Aircraft Fuels. U. S. Dept. Interior, Bur. Mines, Pittsburgh (Pa.), May 6, 1952.
34. DiPiazza, James T., Gerstein, Melvin, and Weast, Robert C.: Flammability Limits of Hydrocarbon-Air Mixtures. Reduced Pressures. *Ind. and Eng. Chem.*, vol. 43, no. 12, Dec. 1951, pp. 2721-2725.
35. Egerton, Alfred, and Powling, J.: The Limits of Flame Propagation at Atmospheric Pressure. I. The Influence of "Promoters." *Proc. Roy. Soc. (London)*, ser. A, vol. 193, May 27, 1948, pp. 172-190.
36. Zeldovich, Y. B.: Theory of Combustion and Detonation of Gases. Tech. Rep. No. F-TS-1226-IA (GDAM A9-T-45), Air Materiel Command, 1949. (Trans. by Brown Univ.)
37. Moore, Harold: Spontaneous Ignition Temperatures of Liquid Fuels for Internal Combustion Engines. *Jour. Soc. Chem. Ind.*, vol. XXXVI, no. 3, Feb. 15, 1917, pp. 109-112.
38. Anon.: The Spontaneous Ignition Temperatures of Liquid Fuels. *Engineering*, vol. CIX, Jan. 30, 1920, pp. 151-152.
39. Setchkin, Nicholas P.: Self-Ignition Temperatures of Combustible Liquids. *Jour. Res. Nat. Bur. Standards*, vol. 53, no. 1, 1954, pp. 49-66.
40. Dixon, H. B., and Higgins, W. F.: On the Ignition-Point of Gases at Different Pressures. *Memoirs and Proc. Manchester Literary and Phil. Soc. (Manchester Memoirs)*, vol. LXX, 1925-26, pp. 29-36.
41. Tizard, H. T., and Pye, D. R.: Experiments on the Ignition of Gases by Sudden Compression. *Phil. Mag. and Jour. Sci.*, vol. XLIV, no. 259, July 1922, pp. 79-121.
42. Mason, Walter, and Wheeler, Richard Vernon: The Ignition of Gases. Pt. IV. Ignition by a Heated Surface. Mixtures of the Paraffins with Air. *Jour. Chem. Soc. Trans. (London)*, pt. II, vol. CXXV, 1924, pp. 1869-1875.
43. Guest, P. G.: Ignition of Natural Gas-Air Mixtures by Heated Surfaces. Tech. Paper 475, Bur. Mines, 1930.
44. Glendinning, W. G.: Possible Cause of Aircraft Fires on Crash. R. & M. No. 1375, British A. R. C., Jan. 1930.
45. Dykstra, F. J., and Edgar, Graham: Spontaneous Ignition Temperature of Liquid Hydrocarbons at Atmospheric Pressure. *Ind. and Eng. Chem.*, vol. 26, no. 5, May 1934, pp. 509-510.
46. Sortman, Charles W., Beatty, Harold A., and Heron, S. D.: Spontaneous Ignition of Hydrocarbons. Zones of Nonignition. *Ind. and Eng. Chem.*, vol. 33, no. 3, Mar. 1941, pp. 357-360.
47. Townsend, D. T. A.: The Present Era in Combustion. *Chem. and Ind. (London)*, no. 44, Nov. 10, 1945, pp. 346-351.
48. Moore, Harold: Spontaneous Ignition-Temperatures of Liquid Fuels. *The Auto. Eng.*, vol. X, no. 138, May 1920, pp. 199-204.
49. Silver, Robert S.: The Ignition of Gaseous Mixtures by Hot Particles. *Phil. Mag. and Jour. Sci.*, ser. 7, vol. 23, no. 156, Apr. 1937, suppl., pp. 633-657.
50. Mullen, James W., II, Fenn, John B., and Irby, Moreland R.: The Ignition of High Velocity Streams of Combustible Gases by Heated Cylindrical Rods. Third Symposium on Combustion and Flame and Explosion Phenomena, The Williams & Wilkins Co. (Baltimore), 1949, pp. 317-329.
51. Masson, Henry James, and Hamilton, William F.: A Study of Auto-Ignition Temperatures. III—(a) Mixtures of Pure Substances, (b) Gasolines. *Ind. and Eng. Chem.*, vol. 21, no. 6, June 1929, pp. 544-549.
52. Frank, Charles E., and Blackham, Angus U.: Spontaneous Ignition of Organic Compounds. *Ind. and Eng. Chem.*, vol. 44, no. 4, Apr. 1952, pp. 862-867.
53. Thompson, Norman J.: Auto-Ignition Temperatures of Flammable Liquids. *Ind. and Eng. Chem.*, vol. 21, no. 2, Feb. 1929, pp. 134-139.
54. Couriot, et Meunier, Jean: Action d'un conducteur électrique incandescent sur les gaz qui lentourent. *Comptes Rendus*, T. 145, Dec. 9, 1907, pp. 1161-1163.
55. The Associated Factory Mutual Fire Insurance Cos.: Properties of Flammable Liquids, Gases, and Solids. *Ind. and Eng. Chem.*, vol. 32, no. 6, June 1940, pp. 880-884.
56. Jackson, Joseph L.: Spontaneous Ignition Temperatures of Pure Hydrocarbons and Commercial Fluids. NACA RM E50J10, 1950. (See also *Ind. and Eng. Chem.*, vol. 43, no. 12, Dec. 1951, p. 2869.)
57. Heron, S. D., and Beatty, Harold A.: Aviation Fuels—Present and Future Developments. *Proc. Ninth Mid-Year meeting Am. Petroleum Inst.*, sec. 111, vol. 20M(III), pub. by A. P. I. (New York), 1939.
58. Edgar, Graham: Ignition Temperatures of Aircraft Combustible Liquids. *SAE Jour. (Trans.)*, vol. 45, no. 1, July 1939, p. 294.
59. Tausz, J., and Schulte, F.: Determination of Ignition Points of Liquid Fuels Under Pressure. NACA TM 299, 1925.
60. Morgan, J. D.: Principles of Ignition. Isaac Pitman & Sons, Ltd. (London), 1942.
61. Jackson, Joseph L., and Brokaw, Richard S.: Variation of Spontaneous Ignition Delays with Temperature and Composition for Propane-Oxygen-Nitrogen Mixtures at Atmospheric Pressure. NACA RM E54B19, 1954.
62. Brokaw, Richard S., and Jackson, Joseph L.: Effect of Temperature, Pressure, and Composition on Ignition Delays for Propane Flames. Fifth Symposium (International) on Combustion, Rheinhold Pub. Corp., 1955, pp. 563-569.
63. Mullins, B. P.: Studies on the Spontaneous Ignition of Fuels Injected into a Hot-Air Stream: General Introduction and Pt. I—The Development of a Combustion Test Rig for Measuring the Ignition Delay of Fuels. Rep. No. R. 89, British N.G.T.E., Aug. 1951.
64. Mullins, B. P.: Studies on the Spontaneous Ignition of Fuels Injected into a Hot-Air Stream: Pt. II—The Effect of Physical Factors Upon the Ignition Delay of Kerosine-Air Mixtures. Rep. No. R. 90, British N.G.T.E., Sept. 1951.
65. Mullins, B. P.: Studies on the Spontaneous Ignition of Fuels Injected into a Hot-Air Stream: Pt. IV—Ignition Delay Measurements on Some Gaseous Fuels at Atmospheric and Reduced Static Pressures. Rep. No. R. 96, British N.G.T.E., Oct. 1951.
66. Barr, J., and Mullins, B. P.: Concerning Combustion in Vitiated Atmospheres. Rep. No. R. 44, British N. G. T. E., June 1949.
67. Evans, Marjorie W.: Current Theoretical Concepts of Steady-State Flame Propagation. *Chem. Rev.*, vol. 51, no. 3, 1952, pp. 363-429.
68. Shepherd, W. C. F.: The Ignition of Gas Mixtures by Impulsive Pressures. Third Symposium on Combustion and Flame and Explosion Phenomena, The Williams & Wilkins Co. (Baltimore), 1949, pp. 301-316.

69. Fay, James A.: Some Experiments on the Initiation of Detonation in $2H_2-O_2$ Mixtures by Uniform Shock Waves. Fourth Symposium (International) on Combustion, The Williams & Wilkins Co. (Baltimore), 1953, pp. 501-507.
70. Steinberg, M., and Kaskan, W. E.: The Ignition of Combustible Mixtures by Shock Waves. Fifth Symposium (International) on Combustion, Reinhold Pub. Corp., 1955, pp. 664-672.
71. Rand, Frank F., Jr.: The Shock Ignition Engine. *Aero. Eng. Rev.*, vol. 11, no. 10, Oct. 1952, pp. 22-27; 62.
72. Hazard, Herbert R.: A Review of Research on Spark Ignition. Tech. Rep. No. 15037-1, Battelle Memorial Inst., Mar. 13, 1952. (Contract AF 33(038)-12656, E. O. No. 460-35 S. R.-8)
73. Guest, P. G.: Apparatus for Determining Minimum Energies for Electric Spark Ignition of Flammable Gases and Vapors. R. I. 3753, Bur. Mines, May 1944.
74. Blanc, M. V., Guest, P. G., von Elbe, Guenther, and Lewis Bernard: Ignition of Explosive Gas Mixtures by Electric Sparks. Pt. III. Minimum Ignition Energies and Quenching Distances of Mixtures of Hydrocarbons and Ether with Oxygen and Inert Gases. Third Symposium on Combustion and Flame and Explosion Phenomena, The Williams & Wilkins Co. (Baltimore), 1949, pp. 363-367.
75. Swett, Clyde C., Jr.: Spark Ignition of Flowing Gases. I—Energies to Ignite Propane-Air Mixtures in Pressure Range of 2 to 4 Inches Mercury Absolute. NACA RM E9E17, 1949.
76. Calcote, H. F., Gregory, C. A., Jr., Barnett, C. M., and Gilmer, Ruth B.: Spark Ignition—Effect of Molecular Structure. *Ind. and Eng. Chem.*, vol. 44, no. 11, Nov. 1952, pp. 2656-2660; discussion, pp. 2660-2662.
77. Boyle, A. R., and Llewellyn, F. J.: The Electrostatic Ignitability of Various Solvent Vapour-Air Mixtures. *Jour. Soc. Chem. Ind.*, vol. 66, no. 3, Mar. 1947, pp. 99-102.
78. Blanc, M. V., Guest, P. G., von Elbe, Guenther, and Lewis, Bernard: Ignition of Explosive Gas Mixture by Electric Sparks. I. Minimum Ignition Energies and Quenching Distances of Mixtures of Methane, Oxygen, and Inert Gases. *Jour. Chem. Phys.*, vol. 15, no. 11, Nov. 1947, pp. 798-802.
79. Jost, Wilhelm: Explosion and Combustion Processes in Gases. First ed., McGraw-Hill Book Co., Inc., 1946.
80. Finch, G. I., and Thompson, H. H.: The Effect of Frequency on the Condensed Discharge Ignition of Carbonic Oxide-Air Detonating Gas. *Proc. Roy. Soc. (London)*, vol. CXXXVI, no. A823, Nov. 3, 1931, pp. 343-348; discussion, pp. 349-351.
81. Paterson, Clifford C., and Campbell, Norman: Some Characteristics of the Spark Discharge and Its Effect in Igniting Explosive Mixtures. *Proc. Phys. Soc. (London)*, vol. XXXI, Dec. 1918-Aug. 1919, pp. 168-227; discussion, pp. 227-228.
82. Swett, Clyde C., Jr., and Donlon, Richard H.: Spark Ignition of Flowing Gases. III—Effect of Turbulence Promoter on Energy Required to Ignite a Propane-Air Mixture. NACA RM E52J28, 1953.
83. Swett, Clyde C., Jr.: Spark Ignition of Flowing Gases. IV. Theory of Ignition in Nonturbulent and Turbulent Flow Using Long-Duration Discharges. NACA RM E54F29a, 1954.
84. Lakin, W. P., Thwaites, H. L., Skarstrom, C. W., and Baum, A. W.: Fourth Annual Rep. on Fundamental Studies of Combustion. Rep. No. RL-5M-48(69), Esso Labs. Res. Div. (Standard Oil Dev. Co.), Nov. 30, 1948. (Contract N6-ori-109.)
85. Lewis, Bernard: Monthly Report on Contract AF-18(600) 151: Flammability Characteristics of Aircraft Fuels. U. S. Dept. Interior, Bur. Mines, Feb. 10, 1953.
86. Fenn, J. B.: Lean Flammability Limit and Minimum Spark Ignition Energy. *Ind. and Eng. Chem.*, vol. 43, no. 12, Dec. 1951, pp. 2865-2868.
87. Swett, Clyde C., Jr.: Spark Ignition of Flowing Gases. V—Application of Fuel-Air-Ratio and Initial-Temperature Data to Ignition Theory. NACA RM E55I16, 1955.
88. Scull, Wilfred E.: Relation Between Inflammables and Ignition Sources in Aircraft Environments. NACA Rep. 1019, 1951. (Supersedes NACA TN 2227.)
89. Wheeler, Richard Vernon: The Ignition of Gases. Pt. III. Ignition by the Impulsive Electrical Discharge. Mixtures of the Paraffins with Air. *Jour. Chem. Soc. Trans. (London)*, vol. CXXV, pt. II, 1924, pp. 1858-1867.
90. Wheeler, Richard Vernon: The Ignition of Gases. Pt. I. Ignition by the Impulsive Electrical Discharge. Mixtures of Methane and Air. *Jour. Chem. Soc. Trans. (London)*, vol. CXVII, pt. II, 1920, pp. 903-917.
91. Thornton, W. M.: The Reaction Between Gas and Pole in the Electrical Ignition of Gaseous Mixtures. *Proc. Roy. Soc. (London)*, ser. A, vol. XCII, no. A634, Oct. 1, 1915, pp. 9-22.
92. Morgan, John David: The Ignition of Explosive Gases by Electric Sparks. *Jour. Chem. Soc. Trans. (London)*, vol. CXV, 1919, pp. 94-104.
93. Morgan, J. D.: The Thermal Theory of Gas Ignition by Electric Sparks. *Phil. Mag. and Jour. Sci.*, ser. 6, vol. 49, no. 290, Feb. 1925, pp. 323-336.
94. Wheeler, R. V.: The Electric Ignition of Firedamp: Alternating and Continuing Currents Compared. Paper No. 20, Safety in Mines Res. Board (London), 1926.
95. Allsop, G., and Guénault, E. M.: The Incendivity of Electric Sparks in Relation to the Characteristics of the Circuit. Third Symposium on Combustion and Flame and Explosion Phenomena, The Williams & Wilkins Co. (Baltimore), 1949, pp. 341-353.

CHAPTER IV

LAMINAR FLAME PROPAGATION

By GORDON L. DUGGER, DOROTHY M. SIMON, and MELVIN GERSTEIN

INTRODUCTION

The ultimate goal of fundamental studies in laminar flame propagation is a complete knowledge of the chemical kinetics of the flame reactions. With a knowledge of the kinetics, the effects of variables on the propagation rate could be predicted and the problems of combustion-chamber design could be approached with greater confidence. Unfortunately, however, the experimental problems involved in the study of kinetics at high temperatures are yet to be solved. Consequently, current studies of the combustion process are necessarily conducted in terms of the laminar flame velocity, minimum ignition energy, flammability limits, and quenching distance. Theoretical interrelations that are in accord with the experimental results indicate these to be fundamental properties of the mixture when properly measured. Correlations between some of these properties and engine performance parameters show that the results of such studies may be of considerable practical value in the aircraft propulsion field.

Available information on laminar flame propagation is summarized in this chapter. Characteristics of laminar flames—the structure of the combustion wave and the relation of direct, schlieren, and shadow photography to that structure—are considered. Also discussed are methods of measuring flame velocity, along with effects of physical and chemical variables on flame velocity. A brief survey of the theory of laminar flame propagation is presented, with particular emphasis on the Semenov (thermal mechanism) and Tanford-Pease (active-particle-diffusion mechanism) equations for flame velocity. The more significant experimental evidence in the controversy concerning thermal against diffusional mechanisms is also discussed. Finally, experimental data and methods of predicting flame velocity are summarized with respect to their significance and application to practical problems of combustion.

SYMBOLS

The following symbols are used in this chapter:

A	cross-sectional area
\mathcal{A}	Avogadro number, 6.025×10^{23} molecules/g-mole
a	exponent
B, B'	dimensionless quantities
b_c	height of luminous cone
C	flame velocity coefficient
\mathcal{C}	concentration, molecules/cm ³
c	exponent
c_p	specific heat at constant pressure
D	diffusion coefficient, cm ² /sec

d	diameter
d_{col}	collision diameter, cm
E_{act}	activation energy, cal/mole
\mathcal{E}	expansion ratio of gas mixture
\mathcal{F}	function
G	mass-flow rate per unit area, g/(cm ²) (sec)
H	total enthalpy, cal/g
I	rate of production by chemical reaction
\mathcal{K}	constant
k	specific rate constant
k_H	empirical proportionality factor
\bar{k}_Σ	average proportionality constant
l	length of curve
dl	length of flame boundary
M	molecular weight
m	ratio of moles of reactants to moles of products
N	number of C-H bonds
\mathcal{P}	steric factor
p	pressure
Q_{re}	heat of reaction, cal/molecule of reactant
q	amount of heat extracted
R	universal gas constant, 1.987 cal/(°K) (mole)
r	radial distance
dr	distance between flow lines
S	surface area
s	slant height
T	temperature
\mathcal{T}_{re}	reaction-zone thickness, cm
t	time
U	velocity
V_{fl}	volume flow rate
X	mole fraction
x	distance
Z	collision number, number of molecular collisions per (cm ³)(sec) when concentration is 1 molecule of each type per cm ³
α	angle between direction of approach flow and burning surface
γ	ratio of specific heats
Θ	$c_p(T - T_o)/Q_{re}$
κ	thermal conductivity, cal/(cm ²)(sec)(°K/cm)
μ	absolute viscosity, poise
ξ	probability of occurrence of chain-branching reaction
ξ'	probability of occurrence of chain-breaking reaction
ρ	density
φ	equivalence ratio
ψ	molar ratio, O ₂ /(O ₂ + N ₂)
ω	reaction rate, (molecules of reactant)/(cm ³)(sec)

Subscripts:

<i>am</i>	ambient
<i>av</i>	average
<i>b</i>	bomb
<i>cir</i>	circumscribed
<i>d</i>	diffusion
<i>eff</i>	effective
<i>eq</i>	equilibrium
<i>F</i>	flame
<i>f</i>	fuel
<i>fin</i>	final
<i>g</i>	gas
<i>i</i>	<i>i</i> th species
<i>ig</i>	ignition
<i>ins</i>	inscribed
<i>j</i>	<i>j</i> th species
<i>l</i>	lower
<i>lin</i>	linear
<i>m</i>	mean
<i>max</i>	maximum
<i>O</i>	oxygen atom
<i>O₂</i>	oxygen molecule
<i>o</i>	initial conditions
<i>p</i>	potential
<i>rel</i>	relative
<i>rt</i>	reactant
<i>st</i>	stoichiometric
<i>t</i>	total
<i>tube</i>	tube
<i>u</i>	upper
<i>w</i>	weighted
3	inflection point

CHARACTERISTICS OF LAMINAR FLAMES

A flame is a rapid, self-sustaining chemical reaction occurring in a discrete reaction zone. Reactants may be introduced into this reaction zone; or the reaction zone may move into the reactants, depending on whether the unburned-gas velocity is greater or less than the flame velocity. The flame velocity, which is also called burning velocity or normal combustion velocity, is the velocity at which unburned gas moves through the combustion wave in the direction normal to the wave surface. This definition refers to the velocity of unburned gas relative to the flame front as determined at some point beyond the influence of the flame; that is, at a point where the gas velocity has not yet been altered by either heat conduction from the flame or the pressure field set up as a result of the thrust pressure of the flame. It is obvious that different types of flame photography and different methods of measurement and computation from flame photographs would give different results, depending on how closely the photographs and measurements approximate the true relation between the reference gas velocity and the flame front.

The preheating of the gas by heat conduction from the flame reaction zone is best understood by considering the temperature profile for a laminar flame and the relation of each type of photography to some point in the temperature profile as determined by theoretical considerations and ex-

perimental evidence. The bending of unburned-gas flow lines due to the pressure field receives less attention than the preheating effect in this chapter, since its effect on flame velocity measurements is generally less important.

TEMPERATURE PROFILE

Three experimental techniques have been used recently to determine temperature profiles:

- (1) Traversing with fine thermocouple (refs. 1 and 2)
- (2) Traversing with very fine slit of light and determining flame temperature from refractive index (ref. 3)
- (3) Tracing curved path of stroboscopically illuminated dust particle and computing temperature from measurements of its direction and velocity (refs. 4 and 5)

Friedman (ref. 2) used a ceramic-coated thermocouple made by gas-welding 0.0012-centimeter platinum and platinum-10-percent-rhodium wires to traverse a very lean propane-air flame (flat flame on 25-cm burner; mass air-propane ratio, 29.2; flame thickness, ≈ 2 cm; pressure, 0.0594 atm). The resulting temperature profile had a shape similar to that of figure 127. The significance of such a temperature profile is as follows: At the point x_o , the temperature of the unburned gas has just begun to increase because of the heat conducted from the flame reaction. The temperature rises rapidly until the equilibrium flame temperature T_F is reached at a point x_F . These boundaries are not defined exactly, since the limiting values T_o and T_F are approached asymptotically; but the convergence is very rapid, so that the boundaries can be defined within narrow limits of T .

Consider first the part of the profile in which the temperature rises from T_o to a temperature T_3 , which marks the inflection point of the T, x curve. This portion of the curve is convex toward the x -axis ($\frac{\partial^2 T}{\partial x^2} > 0$), which means that a mass element in this region gains heat by conduction from the hotter elements downstream faster than it loses heat to the cooler elements upstream. There is little chemical reaction in this region; hence, little heat is evolved. Calculations of reference 6 show that 14 percent of the heat

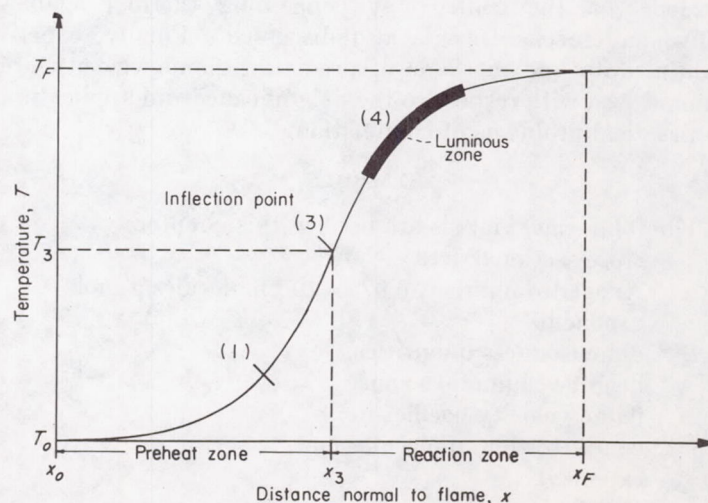


FIGURE 127.—Qualitative temperature-distance diagram for stationary flame.

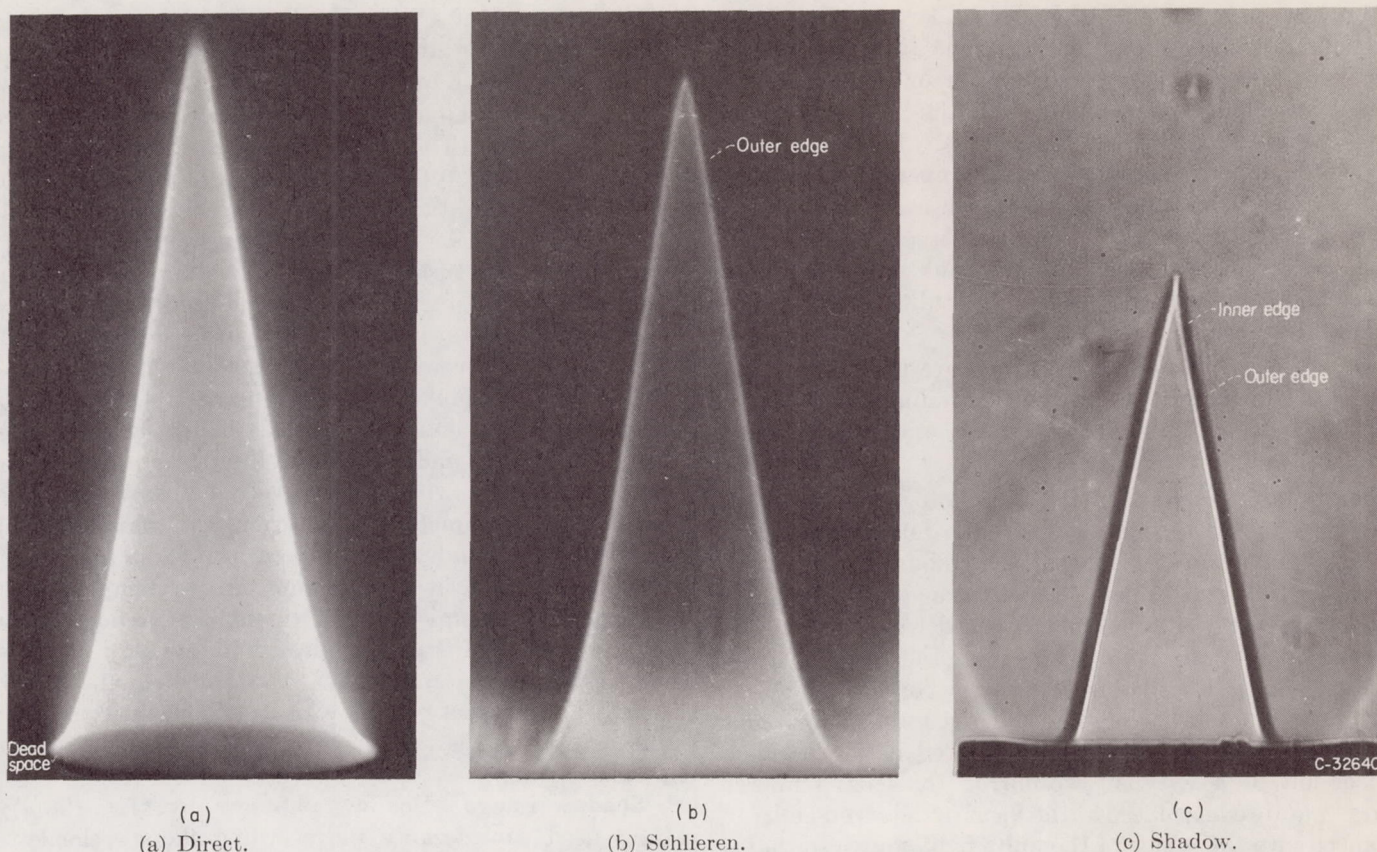


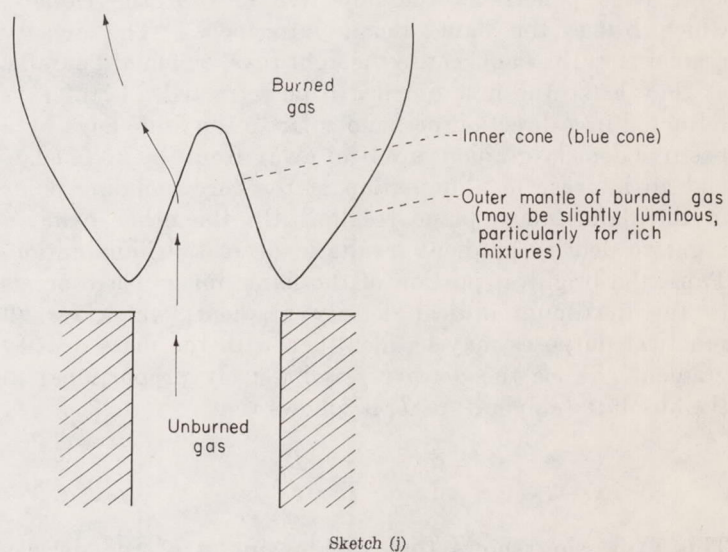
FIGURE 128.—Typical photographs of laminar Bunsen flames.

release occurs before the luminous zone is reached. This zone is considered to begin at some point beyond (T_3, x_3) . Consequently, this region may be called the preheat zone. The mass element expands in volume, causing an acceleration of the unburned gas. On passing T_3 , the mass element changes from a heat sink to a heat source, and the curve is concave toward the x -axis ($\frac{\partial^2 T}{\partial x^2} < 0$). The temperature of

the element continues to rise because of the heat evolution from the chemical reaction, and this region between T_3 and T_F may therefore be called the reaction zone.

The inflection point T_3 may be called the ignition temperature, but it is distinguished from the spontaneous-ignition temperature determined in a static system (see ch. III and the appendix), where the ignition-delay time may be 10^3 to 10^6 times the period required for the element to traverse the preheat zone of a stationary flame. The temperature T_3 may be calculated by numerical integration of theoretical equations for simple decomposition flames such as the ethylene oxide flame (ref. 7) or determined approximately by careful temperature traverse of the reaction zone by one of the methods mentioned previously.

The relation of direct, shadow, and schlieren images to the temperature profile is discussed in the following sections. While differences in the flame areas determined by these three types of flame photographs are pertinent to any method for measuring flame velocity, most of the discussion is given in terms of the inner cone of a Bunsen burner flame illustrated in the following sketch:



RELATION OF VARIOUS IMAGES TO TEMPERATURE PROFILE

Luminous zone.—Direct photography, or direct observation, reveals the luminous zones of the flame. Flame velocity measurements from direct photographs (fig. 128(a)) are based on the zone of most intense illumination, which in the case of Bunsen flames is the bright inner cone, sometimes called the blue cone (see sketch (j)). Early workers in the combustion field (see reviews in refs. 8 and 9) presumed that the width of this luminous zone represented the distance between the initiation of combustion and its completion and that flame velocity measurements were properly

based on the inner edge of this zone. It has since been established that the entire luminous zone (inner cone) lies at a temperature very near the maximum, or flame temperature, as represented by the region (4) adjacent to inflection point (3) in figure 127 (refs. 1, 10, and 11). Before reaching this zone of high heat release but small temperature gradient, the gases experience preheating that causes expansion and bending of the flow lines. As a result, a flame surface chosen at any point in the luminous zone is too large for flame velocity measurements, which are traditionally referred to the unburned-gas flow.

Therefore, direct photographs, which are the easiest type to obtain if the flame is sufficiently luminous, produce a surface larger than the cold gas surface and may indicate erroneously low flame velocities.

Schlieren image.—When schlieren photography (refs. 1, 4, 8, and 10 to 13) is used, a surface is found that has a temperature much nearer that of the unburned gas. The schlieren method also has the advantage of a sharply defined surface (fig. 128(b)) as compared with the less distinct inner edge of the luminous zone or the comparatively fuzzy outer edge of the shadow cast by the cone (fig. 128(c)). In the most common use of the schlieren method for flame velocity measurements, the flame is placed in the parallel-beam section of a Z-type, two-mirror (or lens) schlieren system. A knife edge, placed at the focus of the second mirror, is advanced into the image of the finite light source so that it cuts out approximately half the light. The light passing the knife edge penetrates the objective lens of the camera, which brings the flame image into focus. The density gradients in the flame cause the light rays, which are parallel as they leave the first mirror, to be refracted. Light rays refracted in a direction perpendicular to the knife edge by a positive density gradient are bent away from the knife edge, and an increase in illumination at the corresponding point in the flame-image plane results. On the other hand, a negative density gradient results in decreased illumination. Thus, the brightest portion of the flame image corresponds to the maximum optical density gradient, which for all practical purposes may be identified with the mass density gradient. Since the density ρ is inversely proportional to the absolute temperature T , it follows that

$$\frac{d\rho}{dx} \approx -\frac{1}{T^2} \frac{dT}{dx}$$

This expression shows that the maximum of the density gradient (flame cone edge given by schlieren image) does not coincide with the maximum of the temperature gradient represented by inflection point (3) in figure 127, but occurs at a considerably lower temperature represented by point (1).

Experimental verification of the applicability of the schlieren surface for measuring flame velocity, insofar as the bending of flow lines due to temperature is concerned, has been obtained in several ways. Broeze (ref. 11) investigated the temperature gradient near the schlieren boundary by introducing smoke into the unburned gas. Ammonium chloride, which decomposes at 320° C, and zinc oxide, which

sublimes at 1800° C, were used. The ammonium chloride track disappeared about 1 millimeter before it reached the luminous zone in a butane-air flame at atmospheric pressure. The point of disappearance coincided with the edge of the schlieren image. The zinc oxide smoke showed a sharp drop in density about 0.1 millimeter beyond the schlieren edge. Thus, the temperature gradient is very steep in this vicinity. Lewis and von Elbe (ref. 8, p. 254) similarly found the preheat zone of a natural gas flame to be approximately 1 millimeter thick by using stannic chloride hydrate smoke, which disappears by dissociation of the hydrate beginning at about 83° C and reappears as stannic acid after passing the reaction zone. Klaukens and Wolfhard (ref. 1) studied the reaction zone of flat acetylene-air flames at low pressures using luminous and schlieren photographs and thermocouple traverses, with qualitatively similar results. For a flame at 15 millimeters of mercury, the maximum density gradient corresponded to a temperature of 200° C, whereas the maximum luminosity corresponded to a temperature near the maximum temperature. Reference 4, reporting studies of the tracks of stroboscopically illuminated particles of magnesium oxide, and reference 13 added further confirmation. The majority of investigators believe that schlieren photography gives the image best suited for flame velocity measurements.

Shadow image.—Shadow photography (fig. 128(c)) has been used considerably in recording flame velocity data. The optical setup for a shadow system is simpler than that for a schlieren system. In the simplest form, a point source of light is placed on one side of the flame and the film is placed on the other side. Shadow photographs are also obtained by the parallel-beam method, in which case the camera is focused on a plane between the flame and the second mirror (real shadow image of the flame).

Formerly, many investigators based their flame velocity measurements on the inside edge of the shadow cast by the cone, but it has since been demonstrated that the outside edge of the shadow should be used. In reference 14, calculations were made of refractions of parallel rays for a simple flame model in which the flame surface of the inner cone was considered as a discontinuity between the cold unburned gas and the hot burned gas within the outer mantle. Constant refractive indices of 1.0003 for the unburned gas and the external atmosphere and 1.00004 for the burned gas were assumed. The calculations showed that the flame deflected the rays in such a way that a caustic curve of high light intensity was formed. The distance of the caustic (represented by the sharp demarcation between black and white at the inner edge of the shadow in fig. 128(c)) from the flame axis decreased with increasing distance of the shadowgraph object plane from the flame in a manner similar to that observed experimentally; whereas, the outer edge of the shadow corresponded closely to the position of the discontinuity in refractive index represented by the flame cone. Hence, flame velocities based on the inner edge of the shadow are erroneously high, but the error decreases as the distance between the flame and the shadow object plane decreases and approaches zero at zero distance.

Reference 14 states that the schlieren image of a flame is exactly coincident with the outer edge of the shadow cone obtained with parallel light; therefore, the two methods should give the same values for flame velocity. However, the outer edge of the shadow is not clearly defined, whereas the inner edge is very sharply defined. The desirability of using this sharply defined surface has led some investigators to take shadowgraphs at several distances from the flame and extrapolate back to zero distance (refs. 14 and 15), while others have computed correction factors for fixed positions (refs. 14 and 16).

In summary, it may be said that the schlieren image represents a surface near the start of the preheat zone, whereas the luminous zone represents a region in the reaction zone at temperatures just below the flame temperature.

FLAME VELOCITY

METHODS OF MEASURING

Stationary flame or burner.—The first attempt to measure flame velocity was made by Bunsen (see ref. 17, p. 66), who determined the flow velocity through a burner at which the flame would just flash back, so that the flame velocity was equal to the flow velocity. This method is accurate only for a flat flame, which in turn is obtained only when the stream velocity is constant over the burner-mouth cross section. Flat-flame burners have been developed (refs. 18 and 19) but can be used only for flame velocities less than 15 or 20 centimeters per second. Therefore, these burners are of little interest for most flame velocity studies, although the flat flame is ideal for studying flame structure, and the method may be useful in defining lean flammability limits.

The majority of the burner methods employ the inner flame cone (fig. 128) obtained above vertical tubes or convergent nozzles, which give a more nearly conical inner cone and give the same results as cylindrical tubes when comparable methods of measurement are used (refs. 4 and 10). Tubes employed in such studies are of the order of 1 centimeter in diameter and are more than 40 diameters in length to ensure laminar flow. It is generally found that the mean approach-stream velocity does not affect the results as long as the flow is laminar and that burner diameter has no effect until the quenching diameter is approached (e. g., refs. 8, p. 459, and 16 and 20; for contrary results, see ref. 21).

The methods of measurement of burner flames are variations or modifications of either the total-area method (ref. 22) or the angle method (ref. 23). In the former, an average flame velocity for the entire cone U_F is obtained by dividing the volumetric flow rate of the unburned gas V_{fl} by the surface area of the cone S_F :

$$U_F = \frac{V_{fl}}{S_F} = \frac{U_{o,m} A_{tube}}{S_F} \quad (1)$$

where the space mean velocity of the approach flow in the tube $U_{o,m}$ and the flame velocity U_F are in centimeters per second, V_{fl} is in cubic centimeters per second, and S_F and A_{tube} are in square centimeters. The area S_F is usually

computed by assuming the flame cone to be a right cone. In the early studies, S_F was often computed from the height of the luminous cone b_c and the radius of either the burner tube or the actual flame base r_{tube} by the equation

$$S_F = \pi r_{tube} \sqrt{r_{tube}^2 + b_c^2} \quad (2a)$$

One simple method of computing S_F avoids the necessity of choosing between the burner diameter and the actual flame diameter, which varies with both method of photography and approach-flow conditions (ref. 24):

$$S_F = \frac{\pi A_F l}{b_c} \quad (2b)$$

where

A_F area of projected image of flame measured by planimeter, cm^2

l length of curve that generates S_F when rotated about tube axis (corresponds to slant height of right cone), cm

When the assumption of a right conical shape becomes poor, graphical methods may be used (e. g., ref. 25).

In the angle method, a local flame velocity is computed from the local approach velocity U_o and the angle α between the direction of the approach flow and the burning surface:

$$U_F = U_o \sin \alpha \quad (3)$$

The approach velocity U_o is usually computed for a given position along the flame by assuming that the approach-velocity distribution follows the Poiseuille equation (ref. 8, p. 248)

$$U_o = \frac{2V_{fl}(r_{tube}^2 - r^2)}{\pi r_{tube}^4} = \frac{2U_{o,m}(r_{tube}^2 - r^2)}{r_{tube}^2} \quad (4)$$

where r_{tube} is the tube radius (cm), and r is the radial distance from the tube axis to the flame surface (cm). In some instances where convergent nozzles have been used, apparent flame velocities have been computed on the assumption that the approach velocity U_o was constant over the entire cone and equal to $U_{o,m}$ (e. g., ref. 24). Such an assumption could result in significant errors, since local velocities over the central portion of a nozzle may be as much as 20 percent higher than $U_{o,m}$ because of the boundary-layer effect (ref. 16).

The chief advantage of burner methods is that the equipment is simple, flexible, relatively inexpensive, and easily adapted for measurements at varying temperatures and pressures and with imposed flow disturbances (ref. 26). Burner methods have also been adapted for convenient use with normally liquid fuels (ref. 27). Furthermore, there are obvious advantages in having a readily observed stationary flame. One disadvantage of burner methods is that diffusional interchange with the surrounding atmosphere alters the fuel-oxidant ratio, so that the flame velocity observed may not represent the measured fuel-air ratio. Diffusion may also lead to instability, evidenced by a fluted or polyhedral flame (refs. 28 and 29). This instability might be remedied in some

cases by using a split-flame (Smithells separator) burner, which allows the gases of the outer mantle to burn on an outer concentric tube (ref. 30); however, such a modification complicates the photography. Other problems result from the complex flame shape, which directly complicates the area method and indirectly affects the angle method.

The main objections to the area method are as follows:

(1) The flame velocity near the base of the cone is reduced by the quenching action of the burner rim, and the flame velocity in the region of the tip is increased by accelerated heat and active-particle transfer that results from the small radius of curvature. Hence, the average flame velocity may not be equal to the flame velocity for a plane flame.

(2) Some small amount of gas may escape through the dead space (fig. 128(a)) between the flame base and the burner rim, tending to make the measured U_F too large.

(3) The method makes the choice of the proper surface (inside visible, outside shadow, or schlieren) to be used for computation very important, particularly for small flames.

The errors due to (1) are minimized if the method is restricted to gas mixtures and flow rates that yield nearly conical flame shapes and to burner tube diameters above approximately 1 centimeter (refs. 10 and 20). The error due to (2) is probably small, as evidenced by the lack of a discernible separation between flame base and burner rim in most schlieren photographs. These errors may be reduced somewhat but not eliminated by using only a frustum area from the middle portion of the cone (ref. 8, p. 464). The volumetric flow passing through this portion of the flame is computed by assuming Poiseuille flow (eq. (4)) up to the chosen flame surface. The flame velocity is therefore computed by

$$U_F = \frac{2U_{o,m}(r_l - r_u) \left(1 - \frac{r_l^2 - r_u^2}{2r_{tube}^2} \right)}{s} \quad (5)$$

where r_u and r_l are the radii of the upper and lower bases of the frustum (cm), and s is the slant height of the frustum (cm).

The frustum-area method still requires the choice of the proper surface in order to eliminate flow-line bending due to temperature rise. In addition, since only a part of the cone is considered, it may be even more important to consider the redistribution of unburned-gas flow due to the pressure field set up by the flame (refs. 8, p. 257, and 31 and 32). The volumetric flow computed by equation (4) does not correspond to the surface computed. Even disallowing the differences of (1) and (2), the result is different from that obtained if the total area is used. Further refinement may be made by using a rectangular burner in which the larger dimension is at least three times the smaller dimension, thus reducing the effect of flame curvature when the flame is viewed parallel to the larger dimension (ref. 33).

In the angle method, the bendings of the flow lines due to (1) the temperature rise and (2) the pressure field are again the main problems, whether the more common cylindrical tubes or rectangular tubes are used. The temperature-rise problem is again solved by choosing the proper surface corresponding to a low temperature. The pressure-field

problem might be solved by using the particle-track method. The latter method is a good solution, if the approach-flow conditions are measured far enough upstream to avoid pressure-field effects and are then properly related to a point on the flame surface. Inertia effects connected with the particles must also be taken into account. Investigators who have used the particle-track method apparently did not take full advantage of its possibilities with respect to the pressure-field effects. Although reference 8 (pp. 254-257) presents photographs showing the bending of flow lines due to the pressure effect, dr and $U'_{o,m}$ were probably not measured far enough upstream when flame velocities were computed from the equation

$$U_F = U'_m \frac{dr}{dl} \quad (6)$$

where

U'_m mean velocity for stream tube bounded by the two flow lines considered, computed for Poiseuille flow at plane where dr is measured, cm/sec

dr distance between flow lines at a point far enough upstream to avoid distortion due to pressure, cm

dl length of flame boundary between flow lines, cm

In reference 4, the angle between the direction of the particle track ahead of the preheat zone and the surface of the luminous zone was determined at the point where the track intersects the luminous zone, but measurements probably were not made far enough upstream to determine the direction of the particle track.

A stationary flame method that is of interest by analogy to flames supported on a flameholder is the inverted flame or V-flame method (ref. 8, p. 268 and refs. 34 to 36). In this method, the flame burns above the end of an axially mounted wire in the form of an inverted cone or above a horizontal wire or rod over the tube port in the form of a two-dimensional V. An apparent flame velocity may be determined by measuring the flame angle near the flameholder and relating it to a local velocity within the tube at that distance from the axis (ref. 35 used eqs. (3) and (4)). The velocities obtained in such a manner are far from true flame velocities, because the flame thrust causes a strong outward deflection of the flow lines in the unconfined unburned gas approaching the flame. Better values for flame velocity could be determined from inverted-cone or V-flames by the particle-track methods described previously.

Gross (ref. 36) used the V-flame in connection with a stationary flame method that employs an entirely different approach. Flame pressures were measured by traverses of the flame front of a V-flame with a total-pressure tube connected to a micromanometer. Flame temperatures were measured with a platinum and platinum-10-percent-rhodium thermocouple. Flame velocities were then computed by combining the equation for conservation of momentum across a plane, steady-state combustion wave

$$p_o - p_F = \rho_o U_F^2 \left(\frac{\rho_o}{\rho_F} - 1 \right) \quad (7)$$

and the total pressure for incompressible, inviscid flow

$$p_t = p + \left(\frac{\rho U^2}{2} \right) \quad (8)$$

to obtain the equation for flame velocity

$$U_F = \frac{\rho_F}{\rho_o - \rho_F} \sqrt{\frac{2}{\rho_o} \left[-\left(\frac{\rho_o}{\rho_F} - 1 \right) (p_{t,o} - p_o) - \frac{\rho_o}{\rho_F} (p_{t,F} - p_{t,o}) \right]} \quad (9)$$

where p is the static pressure (dynes/cm²), p_t is the total (stagnation) pressure (dynes/cm²), and ρ is the density (g/cm³). The disadvantages of the method arise from the effects of the total-pressure tube on the flow and the flame, the corrections that must be applied to total-pressure measurements at low velocities, and the difficulties in calibrating, operating, and maintaining an ultrasensitive pressure meter.

Others (refs. 8 and 37) have computed flame velocities from equation (7) by assuming p_F to be equal to the ambient pressure in the room. Vasilescu (ref. 37) points out, however, that p_F is in reality smaller than p_{am} and that corrections must be added to the measured value of $p_o - p_{am}$ (the correction may be several times the magnitude of the measured $p_o - p_{am}$). Thus, agreement between values computed from equation (2a) and from equation (7) for $p_F = p_{am}$ that were reported by von Elbe and Mentser for acetylene flames (ref. 8, p. 266) may be a fortuitous result of the choice of the method of equation (2a) for the calculation of flame velocities.

All things considered, the total-area method with schlieren photography is the most easily executed and reproduced burner method and is probably as accurate as the more complicated methods.

Transparent tube.—If a horizontal transparent tube having an inside diameter greater than the quenching diameter and a length of the order of 1 meter is filled with a homogeneous combustible gas mixture, which is then ignited (preferably by another small flame) at one end of the tube, a flame will travel through the tube. By placing suitable orifices at both ends of the tube to reduce reflected pressure waves, a uniform linear flame movement over a good portion of the tube and a flame of constant shape for that portion may be obtained (ref. 38). The linear velocity of uniform movement is determined either by timing the passage of the flame between two detectors such as photocells or ionization gaps or by photographing it with a rotating drum or movie camera. The flame velocity is calculated by a total-area method from the equation

$$U_F = (U_{lin} - U_g) \frac{A_{tube}}{S_F} \quad (10)$$

where

U_{lin} linear velocity of uniform flame movement, cm/sec
 U_g velocity of unburned gas ahead of flame (determined by allowing gas pushed out of tube to blow a soap bubble, ref. 38), cm/sec

The setup required for the tube method is simple and inexpensive, with the possible exception of the timing devices; the method requires very small quantities of fuel compared with burner methods. The method is inferior to the burner

method for absolute flame velocities because of the greater difficulty in determining S_F from the more complex flame shapes, which, partly because of the necessity of using direct photography, are rather arbitrarily defined. Wall effects are also unknown or difficult to ascertain. Since the measurements are made in a quiescent mixture in a transparent tube, the method is less readily adapted for measurements at pressures or temperatures other than room conditions than is the burner method.

The tube method shares with the bomb and soap-bubble methods the advantage that the flame is not exposed to an external atmosphere, and as a result determinations may be made over a slightly wider range of compositions (ref. 39). It is believed that relative flame velocities or trends indicated by the method are as good as those obtained by other methods when a consistent and reasonable means of determining S_F is used by a single investigator (provided that wall effects, particularly chemical effects, may be neglected). To this end, a simplified equation for determining S_F for the flames, which usually take the shape of semiellipsoids, was presented in reference 40:

$$S_F = \frac{2\pi(r_{cir}r_{ins} + r_{ins}r_{tube} + r_{cir}r_{tube})}{3} \quad (11)$$

where r_{cir} is the radius of the circumscribed circle about the projected flame image (cm), and r_{ins} is the radius of the inscribed circle (cm).

Soap-bubble or constant-pressure bomb.—In the soap-bubble method (refs. 41 to 43), a homogeneous combustible mixture is used to blow a soap bubble around a pair of spark electrodes. The mixture is spark-ignited, and the growth of both the sphere of flame and the soap bubble is recorded by a rotating drum or movie camera. The flame velocity is calculated from

$$U_F = \frac{U_{lin}}{C} = \frac{U_{lin}r_o^3}{r_{fin}^3} \quad (12)$$

where r_o is the initial radius of the soap bubble (cm), and r_{fin} is the final radius of the sphere of burned gas (cm).

The method is simple in principle and offers (ideally, at least) the desirable feature of a spherical flame shape. Since the final flame diameter is rather large (10 to 20 cm), the type of photography used to define the flame surface is less important than with burner or tube methods. On the other hand, the experimental difficulty in determining r_{fin} is considerable because of afterburning and the possibility of nonspherical flame growth due to (1) gravity effects when slow-burning mixtures such as paraffin hydrocarbons and air are used or (2) nonisotropic propagation (wrinkled surface) when very fast-burning mixtures such as hydrocarbons and oxygen are used (ref. 43). The spark-ignition system should be investigated to avoid effects of spatial velocity (ref. 43). Water soap bubbles cannot be used where water has an appreciable effect on the flame velocity; in this case special glycerin solutions may be used for the bubble (refs. 42 and 43). In either case, diffusion through the confining film and the effects of the components of the film on the burning process must be considered. A recent improvement of the method is the use of an inert atmosphere around the

bubble to eliminate afterburning (ref. 42). The method may be used at various pressures by placing the soap-bubble equipment within a large pressure-controlled chamber.

Constant-volume bomb.—In the constant-volume bomb method (refs. 8, 44, and 45), the combustible mixture is ignited in the center of a rigid spherical vessel of the order of 30 centimeters in diameter. Photographs of the growing sphere of flame and one or more continuous pressure records are obtained simultaneously. As the flame progresses, the expansion of the burned gas causes both the pressure and temperature of the unburned gas to increase because of adiabatic compression. The temperature increase causes the flame velocity to increase continuously from the center toward the walls.

The flame velocity may be calculated by two methods. In the first, for any instantaneous flame diameter observed from the photographs, the volume occupied by the burned gas before combustion is calculated with the aid of the pressure record. The equation for U_F derived from the differential equation for adiabatic compression is (ref. 44)

$$U_F = \left(1 - \frac{r_b^3 - r_F^3}{3p\gamma r_F^2} \frac{dp}{dr_F} \right) \frac{dr_F}{dt} \quad (13)$$

where

- r_b bomb radius, cm
- r_F flame radius at time t from photograph, cm
- p static pressure at time t , dynes/cm²
- γ ratio of specific heats in unburned gas at instantaneous conditions T and p

In this method, two differential quotients are required, and U_F is obtained as a difference of quantities of comparable magnitude, so that errors in these differential quotients and other data are magnified. A 10- to 15-percent scatter in data may result (ref. 8, p. 476).

The second method uses only the pressure record, from which r_F is calculated, and may be verified by the observed r_F :

$$U_F = \frac{dr_o}{dt} \left(\frac{r_o}{r_F} \right)^2 \left(\frac{p_o}{p} \right)^{\frac{1}{\gamma}} \quad (14)$$

where

$$r_o = r_b \left(\frac{p - p_o}{p_{eq} - p_o} \right)^{\frac{1}{\gamma}} \quad (15)$$

and

$$r_F = r_b \left[1 - \left(\frac{p_o}{p} \right)^{\frac{1}{\gamma}} \left(\frac{p_{eq} - p}{p_{eq} - p_o} \right) \right]^{\frac{1}{\gamma}} \quad (15a)$$

where p_o is the initial static pressure before ignition (dynes/cm²), and p_{eq} is the final equilibrium pressure after the gas has burned (dynes/cm²).

Lewis and von Elbe (ref. 8, p. 499) present an example of a CO-O₂-H₂O flame for which the calculated r_F is consistently about 1 percent higher than that observed. They state that even this small difference is partly due to the error in observed r_F , which results from the use of direct photography to locate the flame front.

The experimental advantages of the bomb method are that it allows good control over the initial temperature, pressure,

TABLE X.—COMPARISON OF MAXIMUM FLAME VELOCITIES DETERMINED BY VARIOUS METHODS

[Propane-air at 25° C and 1 atm.]

Method	Type of photography	Tube diam., d_{tube} , cm	Equivalence ratio for $U_{F,max}$, ϕ_{max}	Max. flame velocity, $U_{F,max}$, cm/sec	Reference
Burner:					
Total area (eq. (2b))	Schlieren	1.26	1.06	{ 43.0 40.7 }	49
Angle, r/r_{tube} in const. velocity range.	Schlieren	1.358	1.08	^a 43.2	118
Total area	Shadow, outer edge	1.57	1.12	40.2	16
Total area	Shadow, inner edge with extrapolation to flame axis.	1.27 (tube or nozzle)	1.03	^a 45.5	4, 15
Total area	Shadow, inner edge	1.57	1.12	45.4	16
Frustum area including cone tip.	Shadow, inner edge		(1.05)	46.7	47
Frustum area, rectangular burner.	Direct, inner luminous edge	0.65 × 2.55	^b 1.0	^a 41.2	-----
Frustum area	Direct	1.36	1.07	^a 41.5	119
Frustum area	Direct	0.94	1.05	^a 46.3	8
Total area (eq. (2b))	Direct, center of luminous zone	1.57	1.1	38	16
Angle, at 0.36 to 0.51 r/r_{tube}	Direct	1.36	1.06	^a 43.3	119
Angle, at common point	Combination of direct and shadow			^a 48.5	-----
Particle track	Stroboscopic direct	1.27 (nozzle)	1.05	^a 45.0	4, 15
Tube:					
Total area	Direct	2.5	1.14	^a 39.0	38
Bomb:					
Pressure record	None	} 15-cm sphere	^b 1.0	40.6	45
Flame record	Direct		^b 1.0	40.4	45

^a Exact temperature not specified but assumed to be $\approx 25^\circ$ C.

^b These determinations for stoichiometric mixtures do not represent maximums, but are probably lower than the maximums by no more than 2 cm/sec.

and humidity of the unburned gas and it requires only small amounts of gases. Its disadvantages are that the apparatus is complex, the calculations are lengthy and depend on very rapid and accurate pressure measurements, and the flame velocity varies continuously during a run. The spark-gap width and energy must be properly matched to obtain spherical flames (ref. 45). While the pressure-record method largely eliminates errors due to convection currents for slow-moving flames, there is still difficulty with nonisotropic propagation with very fast flames or in mixtures that show diffusion instability (tendency of flame front to break into cells because of concentration gradients set up by preferential diffusion of the lighter components of the mixture).

The bomb method, using only the pressure record, may prove to be the most accurate method for determining flame velocities; as such it could be used to establish absolute values of flame velocities, which could in turn be used to appraise the accuracy of simpler burner methods.

Evaluation of methods.—Since there are large differences in flame velocities reported by various investigators for the same fuel-oxidant mixture at the same conditions (table X), those who wish to compare data from various sources must use caution. For a given experimental method, particularly the various burner methods, measurements that are made from schlieren photographs are probably nearer the true flame velocity than measurements based on direct or shadow photographs. Of the methods for measuring flame velocity, the constant-volume bomb method (using the pressure record only) may prove to be most precise (≈ 1 percent). In general, Bunsen burner methods are the simplest, cheapest, most versatile, and most productive. Of the various burner methods, the total-area method is probably the simplest, has a precision at least as good as the other methods, and has an accuracy comparable with most of them. The tube, soap-bubble, and bomb methods are particularly good under conditions where their disadvantages are unimportant for very small quantities of gases. Unless otherwise stated, a precision of ± 5 percent is about the average to be

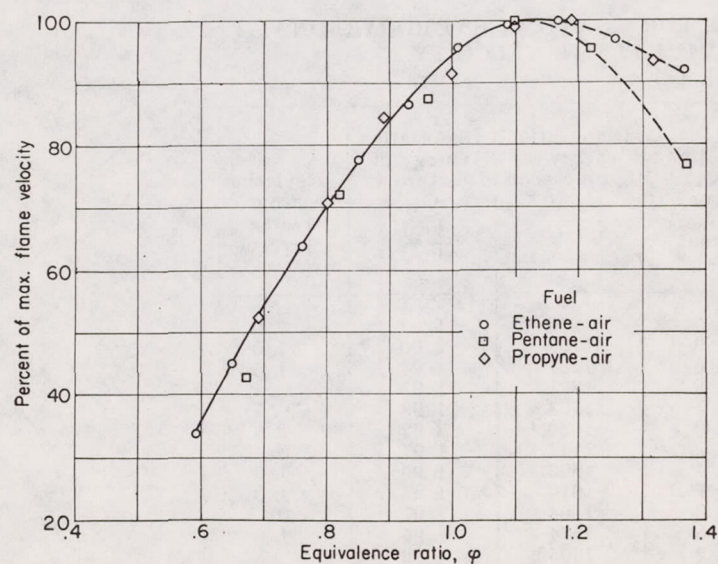


FIGURE 129.—Change in relative flame velocity with equivalence ratio at 25° C and 1 atmosphere (ref. 39).

expected when a single method is used by a single investigator; this fact should be kept in mind when considering relative changes in flame velocities or comparisons for various fuels such as those given in the appendix.

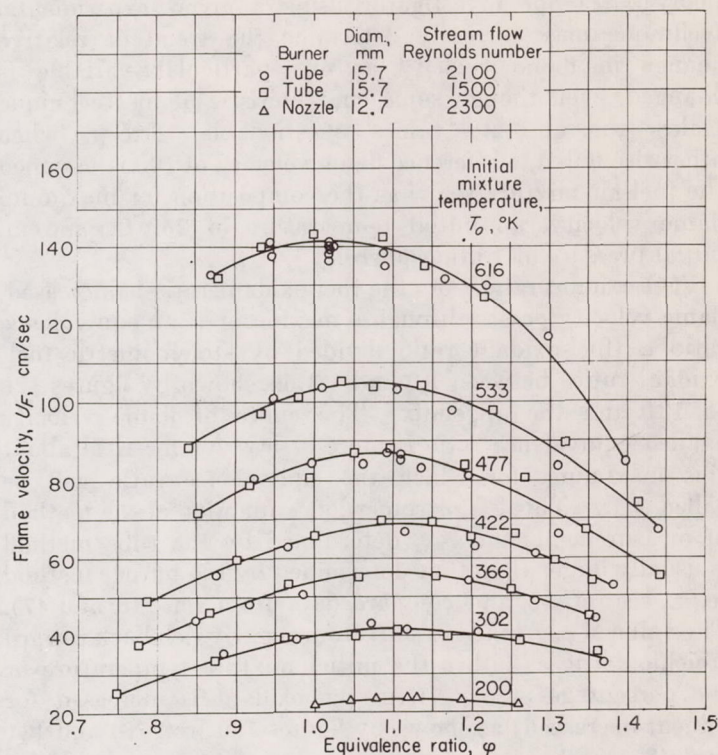


FIGURE 130.—Flame velocity as function of equivalence ratio at various initial mixture temperatures for propane-air flames at 1 atmosphere, measured by outer-shadow-edge total-area burner method (ref. 16).

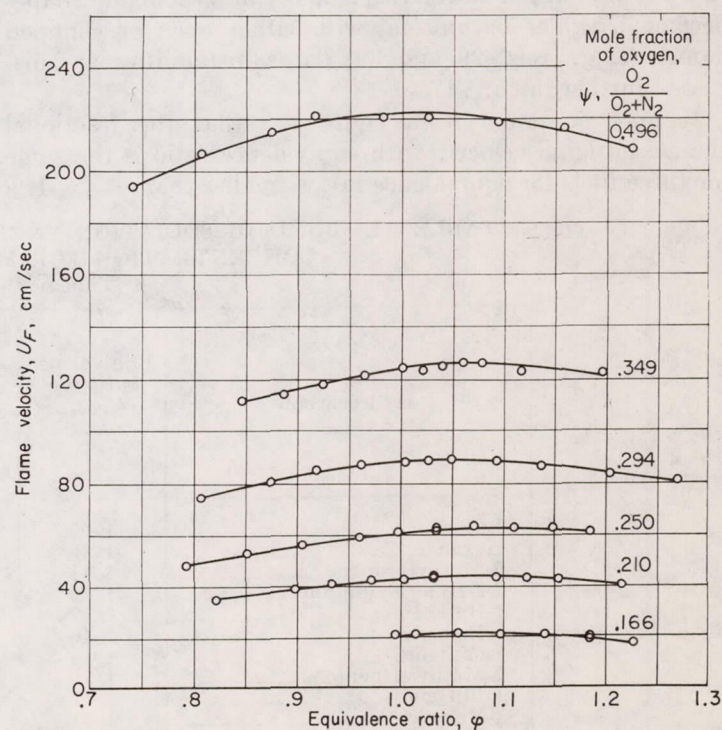


FIGURE 131.—Flame velocity as function of equivalence ratio over range of oxygen concentrations for propane-oxygen-nitrogen mixtures at 311° K, measured by schlieren total-area burner method (ref. 48).

EFFECTS OF CHEMICAL VARIABLES

In the present survey, flame velocities are reported as relative values referred to some standard fuel-oxidant mixture or condition. This is done in the belief that in many cases one investigator using a given experimental technique may correctly determine the trend or relative change in flame velocity as one particular variable is changed, even though some characteristic of his technique makes the absolute values questionable. Except when otherwise noted, a reference flame velocity of 100 is assigned the fuel-air mixture that has the composition for maximum flame velocity, an initial temperature of 25° C, and an initial pressure of 1 atmosphere.

Fuel-oxidant ratio.—As the fuel-oxidant ratio is increased, flame velocity passes through a maximum at an equivalence ratio ϕ (fuel-oxidant ratio divided by stoichiometric fuel-oxidant ratio) between 1.0 and 1.3, as shown by figures 129 to 131 and the appendix. The curve of flame velocity against equivalence ratio is more or less symmetrical about this maximum, for which the equivalence ratio will be called ϕ_{max} . This ϕ_{max} is somewhat a function of the method of measurement; the ϕ_{max} determined by the tube method is usually larger than that determined by the burner method (e. g., see ref. 12, and compare data from refs. 46 and 47). The value of ϕ_{max} tends to shift from slightly rich back toward stoichiometric as either the initial mixture temperature or the percentage of oxygen in the oxidant is increased (or diluent decreased) as shown by figures 130 (ref. 16) and 131 (ref. 48).

The flame velocity near the lean flammability limit ($\phi \approx 0.5$ to 0.6) is of the order of $\frac{1}{4}$ to $\frac{1}{3}$ the maximum (refs. 18 and 39). Flame velocity determinations with hydrocarbons are limited on the rich side because the flame shapes become irregular or unusual with either open or confined flames (e. g., refs. 29 and 39; flame instabilities are discussed further in ch. VI).

It may be noted from figure 129 that the fractional change in flame velocity with equivalence ratio is the same for three fuels for equivalence ratios smaller than ϕ_{max} . If a

logarithmic scale were used for ϕ , it would be seen that a linear relation between U_F and $\log \phi$ exists for $\phi < 1$:

$$\frac{U_F}{U_{F,max}} = 2.6 \log \phi + 0.94 \quad (16)$$

An interesting variation of the preceding relation is the plot of the logarithm of the total bond dissociation energy of the fuel per unit volume of mixture against flame velocity illustrated by figure 132 (ref. 49). The correlations are

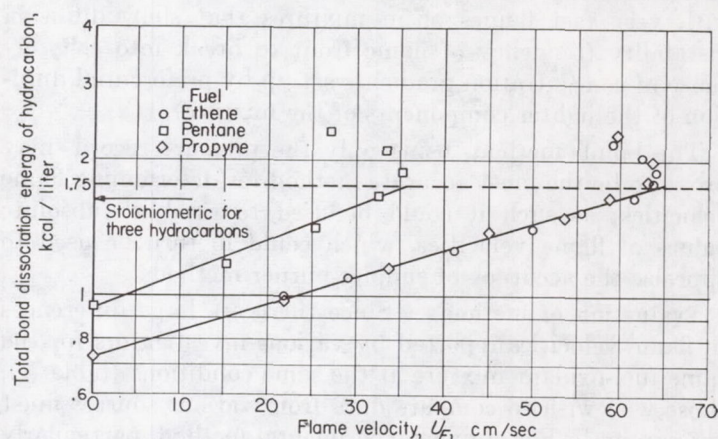


FIGURE 132.—Empirical correlation for equivalence-ratio data. Tube method (ref. 49).

linear for lean mixtures and the lines extrapolate to the lean limit of flame propagation (zero flame velocity) in a 1-inch flame tube. The advantage in using the total bond dissociation energy rather than simple ϕ is that the maximum flame velocities of all three fuels may be estimated by extrapolating the linear portions of their curves to a common value of the total bond dissociation energy, 1.75 kilocalories per liter. However, both the slopes of the lines and the energy for $U_{F,max}$ depend somewhat on the method of measurement of U_F ; the data presented were obtained by the tube method.

A correlation was also observed between the equivalence ratio for maximum flame velocity and the total bond dis-

TABLE XI.—BOND DISSOCIATION ENERGIES FOR C₄ AND C₆ HYDROCARBONS AT CONCENTRATION FOR MAXIMUM FLAME VELOCITY
[Tube method, ref. 49.]

Hydrocarbon	Equivalence ratio for $U_{F,max}$, ϕ_{max}	Deviation of ϕ_{max} from $\phi_{max,av}$, percent	Dissociation energy of hydrocarbon, kcal/g-mole	Dissociation energy of mixture at ϕ_{max} , kcal/liter	Deviation from average, percent
Butane.....	1.09	5.5	1250	1.93	2.0
Hexane.....	1.16	.9	1791	2.00	1.5
2-Methylpropane.....	1.11	3.6	1257	1.94	1.5
2,2-Dimethylbutane.....	1.12	2.5	1821	1.97
1-Butene.....	1.17	1.7	1133	1.98	.5
1-Hexene.....	1.16	.9	1680	2.02	2.5
Isobutene.....	1.14	.9	1147	1.97
2-Methyl-1-pentene.....	1.19	3.4	1603	1.99	1.0
1-Butyne.....	1.17	1.7	1016	1.95	1.0
1-Hexyne.....	1.21	5.0	1564	1.97	0
4-Methylpentyne.....	1.18	2.5	1574	1.95	1.0
Benzene.....	1.34	14.2	1305	1.96	.5
Average.....	1.15	3.29	-----	1.96	0.9

sociation energy of the fuel. Table XI (ref. 49) shows that, for the C_4 and C_6 hydrocarbons tested, the total bond dissociation energy per unit volume of the hydrocarbon-air mixture corresponding to the mixture giving the maximum flame velocity (tube method) is nearly constant, with an average deviation of only 0.9 percent from the average value. This deviation is less than $\frac{1}{3}$ of that obtained by simply assuming that the maximum will occur at an average equivalence ratio of 1.15. It may be noted that the average total bond dissociation energy of 1.96 (kcal/liter) for φ_{max} is different from the 1.75 that gave maximum flame velocities from the linear extrapolation in figure 132, because the data in that figure began to deviate from the straight line before φ_{max} was reached.

An avenue of experimental study that may clarify the reaction kinetics of flames is the determination of flame velocities for fuel-oxygen-nitrogen systems in which the concentrations are varied in such a way that constant flame temperatures are maintained. If the effective mean reaction-zone temperature is also constant and the reaction mechanism does not change with composition, the true effects of fuel and oxygen concentrations on flame velocity and hence on the over-all reaction rate might be expressed by

$$U_F^2 \propto \mathcal{F} \left(\frac{dX_f}{dt} \right) \propto X_f^a X_{O_2}^c \quad (17)$$

where

X_f mole fraction of fuel in unburned gas

X_{O_2} mole fraction of oxygen in unburned gas

a, c empirical exponents expressing reaction order of fuel and oxygen, respectively

The exponent a is determined by studying mixtures for which $\varphi \geq 1$, and the exponent c is determined when $\varphi \leq 1$. In the former case, X_{O_2} is practically constant; whereas, in the latter case, X_f is practically constant.

In reference 50, flame velocities were determined at constant calculated adiabatic flame temperatures for hydrogen-, carbon monoxide-, and methane-oxygen-nitrogen systems. The empirical equation for H_2 - O_2 - N_2 for X_{O_2}/X_f between 0.8 and 8 at 2000° K is

$$U_F = 7650 X_f^2 X_{O_2} + 54 \quad (18)$$

This equation has the form of equation (17) except for the constant 54. An equation of a different form was reported for methane-oxygen-nitrogen for X_{O_2}/X_f between 0.3 and 0.7 at 2000° K:

$$U_F = 13.3 \ln \left(\frac{X_{O_2}}{X_f} \right) + 14.9 \quad (19)$$

No empirical equations were reported for H_2 - O_2 - N_2 at 2250° K or for CO - O_2 - N_2 at 2000° K.

Zeldovich (ref. 51) reports experiments with lean CO - O_2 - N_2 mixtures in which the carbon monoxide concentration was held constant and the O_2 - N_2 ratio was varied so that the flame temperatures were essentially constant. The flame velocity, and hence the reaction rate, was found to vary by less than a factor of 1.5 when X_{O_2} was varied from 0.20 to 0.72. Similar experiments with lean mixtures show that flame velocity is proportional to the square root of the carbon monoxide concentration in the reaction zone.

In summary, the flame velocity passes through a maximum $U_{F,max}$ at a fuel-oxidant ratio slightly richer than stoichiometric. For lean hydrocarbon-air mixtures, flame velocity and equivalence ratio may be related by an equation such as

$$\frac{U_F}{U_{F,max}} = 2.6 \log \varphi + 0.94 \quad (16)$$

The logarithm of the total bond dissociation energy of the fuel per unit volume of mixture correlates both the flame velocities of lean mixtures of a given fuel with air and the equivalence ratios for maximum flame velocities of various fuels. Studies of the effects of fuel and oxygen concentra-

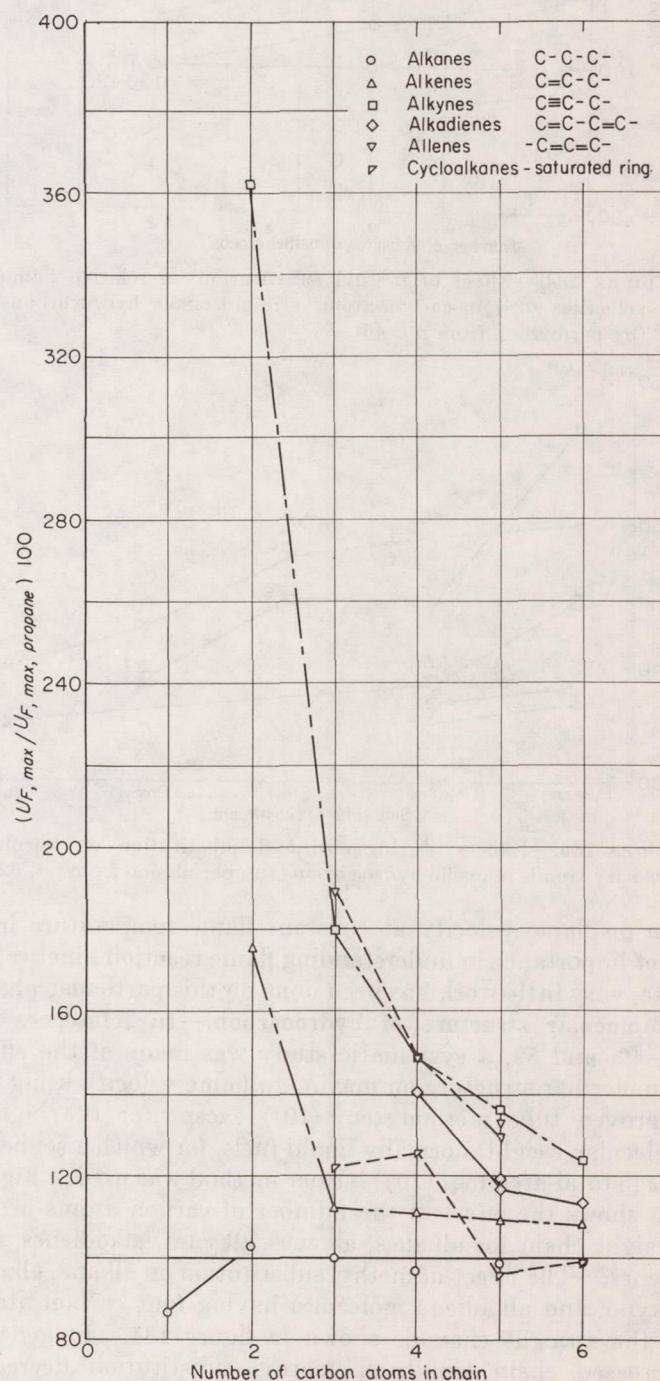


FIGURE 133.—Effect of chain length and saturation on relative flame velocities of straight-chain (or non-substituted-ring) hydrocarbons at 25° C and 1 atmosphere (by permission from refs. 38, 40, and 46).

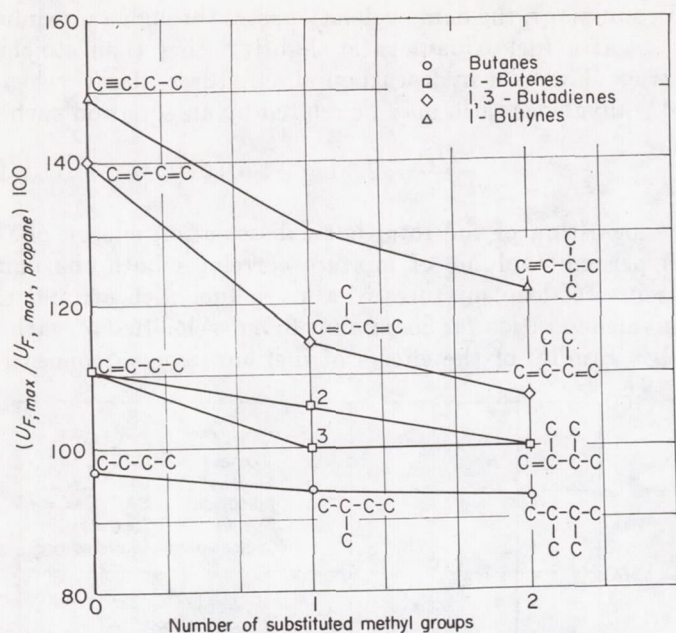


FIGURE 134.—Effect of methyl substitution on relative flame velocities of four-carbon-atom, straight-chain hydrocarbons (by permission from ref. 46).

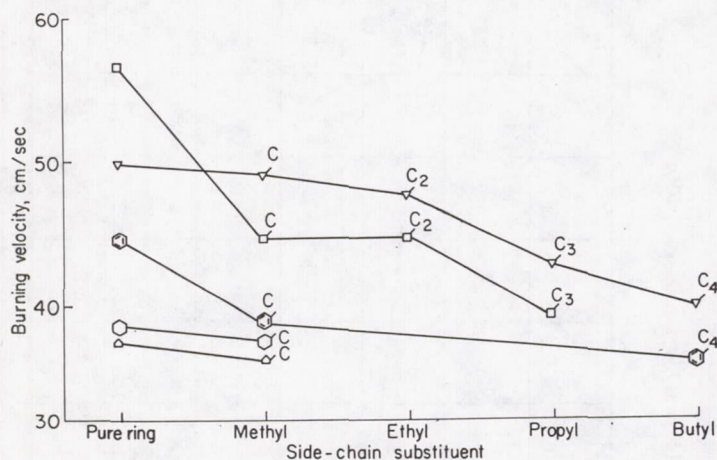


FIGURE 135.—Effects of ring size and substitution on burning-velocity trends in cyclic hydrocarbons (by permission from ref. 52).

tion on flame velocity at constant flame temperature may be of importance in understanding flame reaction kinetics; to date, very little work has been done on this particular phase.

Molecular structure of hydrocarbon.—In references 38, 40, 46, and 52, a systematic study was made of the effect of molecular structure on maximum flame velocity using the improved tube method (eq. (10)) except for the higher-molecular-weight, normally liquid fuels, for which a schlieren image total-area (eq. (2b)) burner method was used. Figure 133 shows the effect of the number of carbon atoms in the straight chain for alkanes, alkenes, alkynes, alkadienes, and allenes. The effect of methyl substitution on alkane, alkene, alkyne, and alkadiene molecules having four carbon atoms in the straight chain is shown in figure 134. In general, increased chain length or methyl substitution decreases flame velocity, except for the alkanes, which are not appreciably affected by either. These two figures also emphasize the effect of unsaturation: The flame velocity increases in the order alkanes < alkenes < alkadienes (for

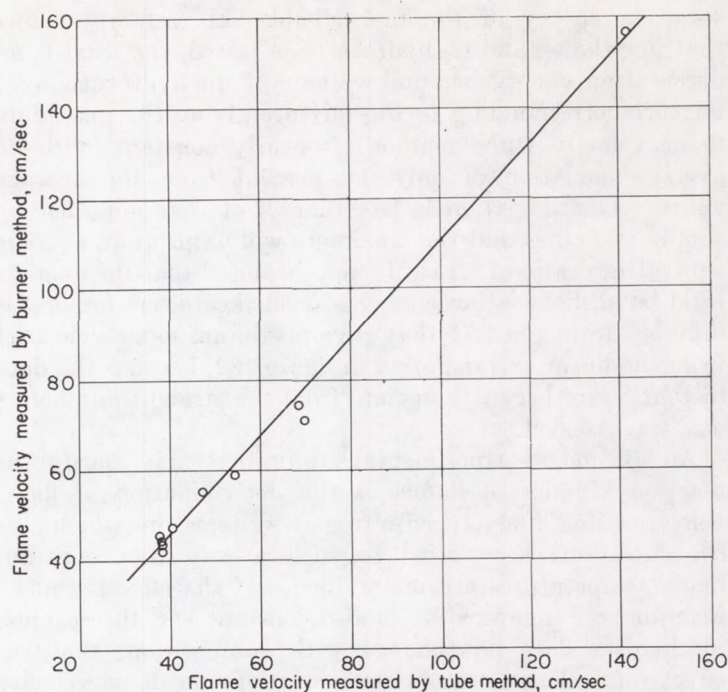


FIGURE 136.—Comparison of flame velocities measured by inner-shadow-edge burner method (ref. 47) with values measured by tube method (ref. 40).

which isolated < conjugated < cumulated double bonds) < alkynes.

The effects of cycloalkane ring size and of side-chain substituent size in a given cycloalkane are shown in figure 135, and the effects of alkyl substitution in a benzene ring are shown by data in the appendix. The fact that the three- and four-membered cycloalkanes have flame velocities greater than the corresponding alkanes, whereas the five- and six-membered rings have flame velocities near the corresponding alkanes, is in keeping with the general chemical behavior associated with ring compounds. Small, saturated rings generally exhibit some double-bond character, but large ones do not. Cyclopropane has a flame velocity 13 percent higher than its isomer, propene; and spiropentane (two three-membered rings joined together by one C-C bond) has a flame velocity (see appendix) 13 percent higher than the fastest isomeric pentadiene flame; this indicates that three-membered rings are somewhat more effective than double bonds. The addition of alkyl groups to aromatic rings shows no definite trend, sometimes reducing flame velocity, sometimes not affecting it.

Some effects of type of oxygen linkage in oxygen-containing compounds are also suggested, but not well established, by data in the appendix. It appears that flame velocity increases with the type of linkage in the order esters < ethers < alcohols < aldehydes and ketones < alkyl oxides. This suggested order is based primarily on data from reference 52, with the position of alcohols and esters suggested by the data of reference 47. Other measurements from reference 47 are in conflict with the suggested order. The measurements were based on the inner edge of the shadow cast by the Bunsen cone, using only the upper part of the cone. In general, the agreement between relative values given by references 40 and 47 is good, as shown by figure 136. The

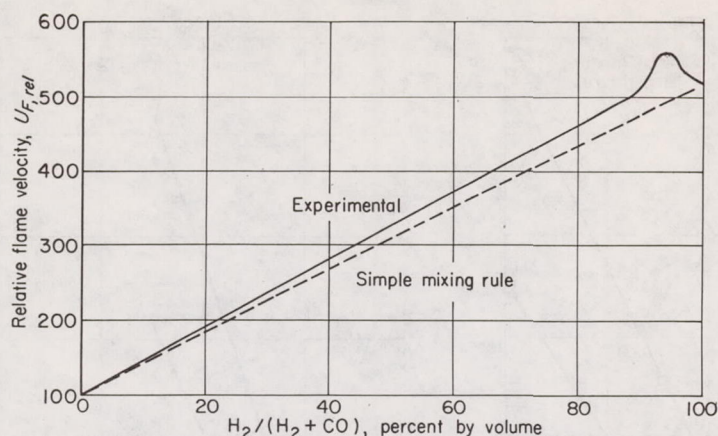


FIGURE 137.—Comparison of experimental data with simple mixing rule for flame velocities of mixtures of hydrogen and carbon monoxide (ref. 59).

maximum flame velocities determined for fuels other than those of references 38, 40, 46, and 52 have been put on a relative basis and are included in the appendix.

In reference 53, an empirical correlation is obtained in which the maximum flame velocity of a hydrocarbon burning with air is calculated from the sum of the contributions of the various H-C bonds in the fuel molecule according to

$$U_F = N_A C_A + N_B C_B + N_C C_C + \dots \quad (20)$$

where N_A , N_B , N_C , N_D , N_E , N_F , N_G , and N_H are the numbers of methane, primary, secondary, tertiary, alkene, cyclohexyl, and aromatic C-H bonds, respectively, per unit volume of hydrocarbon-air mixtures; and C_A , C_B , C_C , . . . are the flame velocity coefficients of these bonds. For the special cases of C-H bonds on carbon atoms placed alpha to (next to) the alkyne C≡C bond, a factor equal to 0.96 was introduced into terms representing these alpha bonds. Flame velocity coefficients established from 34 hydrocarbons gave an average deviation in predicted flame velocity of 1.9 percent. In the evaluation of these coefficients, ethene was excluded, since its coefficient deviated by more than 5 times the average. These coefficients, based on an experimental reference flame velocity of 100 for propane, are given in table XII. Since the coefficients are averaged for 34 hydrocarbons, the computed value for propane is 97.7 compared with the experimental reference velocity of 100.

The general effects of molecular structure may be summarized as follows: Increased straight-chain length, chain

TABLE XII.—EMPIRICAL COEFFICIENTS FOR CALCULATING MAXIMUM FLAME VELOCITY FROM HYDROCARBON STRUCTURE (Ref. 53)

Type C-H bond	Coefficient, ^a cm/(sec) (bond/cm ³)
Methane.....	$C_A = 90 \times 10^{-19}$
Primary.....	$C_B = 109$
Secondary.....	$C_C = 122$
Tertiary.....	$C_D = 116$
Cyclohexyl.....	$C_E = 129$
Alkene.....	$C_F = 207$
Aromatic.....	$C_H = 216$
Alkyne.....	$C_I = 574$

^a Relative to propane.

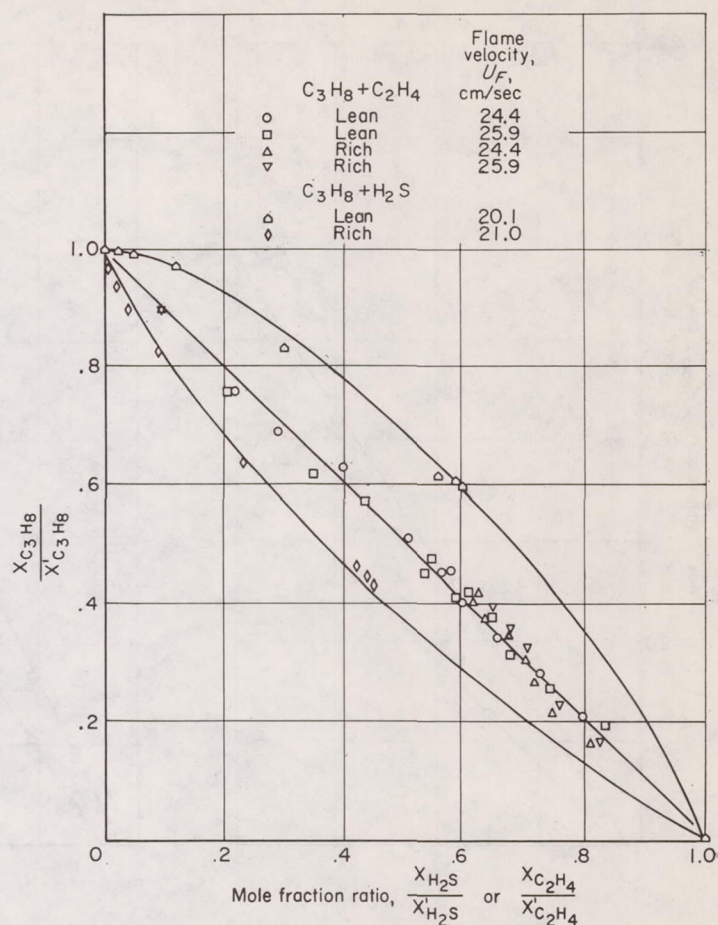


FIGURE 138.—Relation between $X_{C_3H_8}/X'_{C_3H_8}$ and X_{H_2S}/X'_{H_2S} and between $X_{C_2H_4}/X'_{C_2H_4}$ for lean and rich binary fuel mixtures at constant flame velocity levels (reprinted by permission from ref. 62).

branching, side-chain substitution, or ring size of cycloalkanes (except for cyclopropane-cyclobutane reversal) tends to decrease flame velocity; whereas unsaturation tends to increase flame velocity; all these effects become smaller as the size of the molecule is increased. The flame velocities of oxygen-containing compounds are believed to follow the order esters < ethers < alcohols < aldehydes and ketones < alkyl oxides.

Additives, antiknocks, and fuel blending.—Reference 54 reports the effects on flame velocity of small additions (<3 percent) of other fuels to rich mixtures of city gas and air. The compounds studied as additives (acetone, acetaldehyde, benzaldehyde, diethyl ether, benzene, and carbon disulfide) were chosen from those which displayed oxidation phenomena in low-temperature oxidation and hence were expected to decrease the induction period and increase flame velocity. Despite apparent differences in oxidation properties, all compounds changed the flame velocity (luminous-cone total-area method, using skirted burner) in exactly the same way that dilution with excess fuel would change it, on the basis of oxygen requirement. There was no phenomenon equivalent to the effect of aldehyde on reaction rate in the low-temperature oxidation of hydrocarbons.

In propane-air-additive (isooctane, benzene, acetone, methylethyl ketone, carbon monoxide, acetaldehyde, diethyl

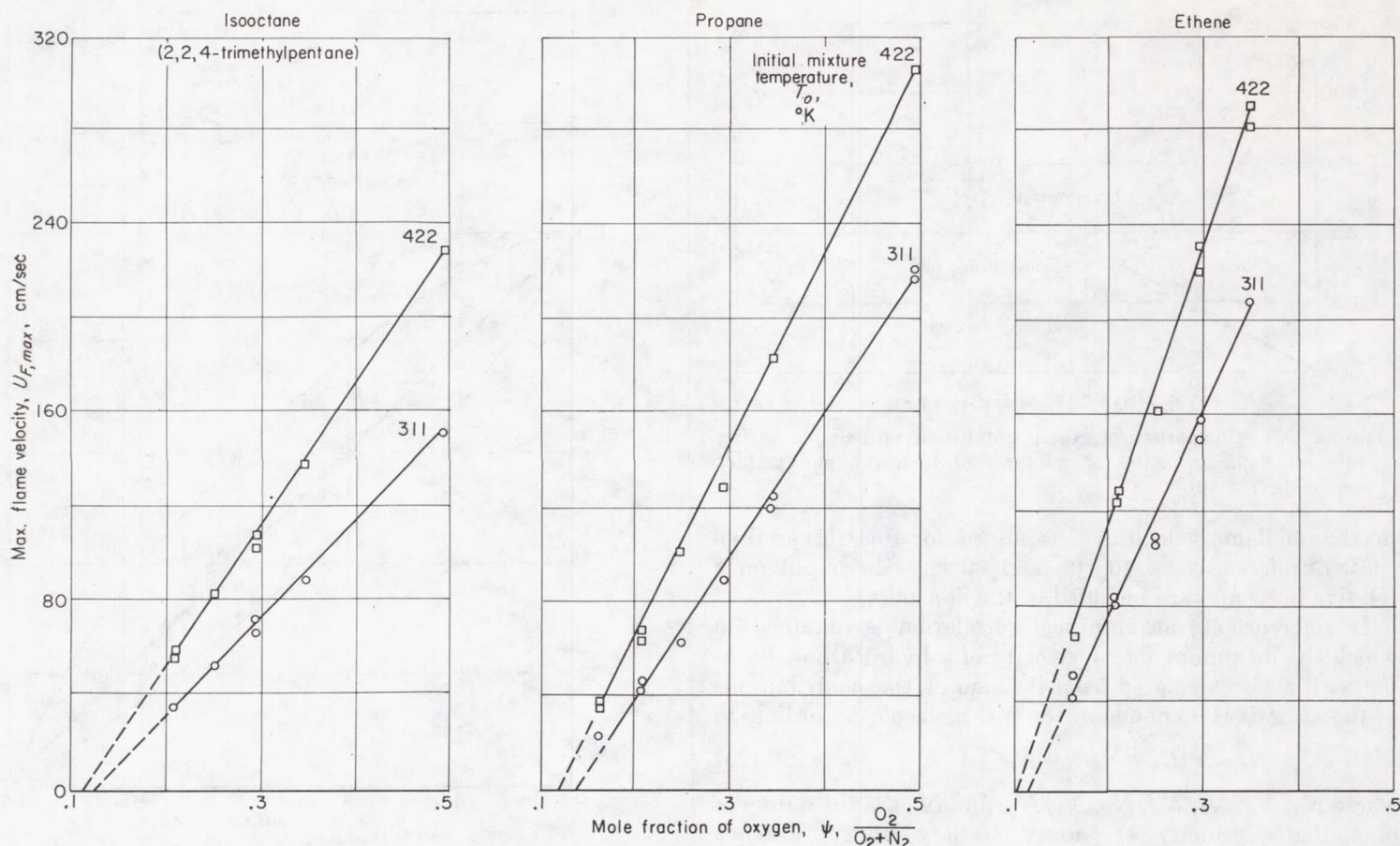


FIGURE 139.—Effect of oxygen concentration on maximum flame velocities; schlieren total-area method (ref. 66).

ether, oxygen, hydrogen, and nitrogen) mixtures, however, reference 55 states that the small but distinct changes in flame velocity were not strictly additive. Additive concentrations amounting to 5 to 30 percent of the total fuel were used; in many cases, the flame velocity of the binary mixture was greater than that of either component. The reference also states that the change in theoretical flame temperature does not sufficiently explain the results, but that a nearly linear correlation with $(6.5X_H + X_{OH} + X_O)_F$ was obtained.

Studies with moist carbon monoxide (ref. 8, p. 463, and ref. 17, p. 121) show that its flame velocity is raised appreciably by the addition of small amounts of hydrogen or hydrogen-containing fuels (or water vapor, see later discussion). For example, the replacement of 1.5 percent of the carbon monoxide by hydrogen raised the flame velocity of a moist carbon monoxide-air flame by 40 percent or a moist carbon monoxide-oxygen flame by 45 percent; in both cases, this increase was considerably greater than that expected by a simple mixing rule. Even fuels with flame velocities smaller than the moist carbon monoxide caused a marked increase; for example, 1 percent of hexane

increased the flame velocity 29.5 percent. On the other hand, carbon disulfide, which contains no hydrogen, had the opposite effect.

It might be expected that common antiknock additives would especially decrease flame velocity, but such is not the case in constant-pressure combustion. Tetraethyl lead had no effect on the flame velocities (measured approximately by a ballistic impulse meter) of isooctane-air mixtures at temperatures up to 500° C, or on *n*-butane up to 300° C (ref. 56). Above 300° C, the flame velocity of *n*-butane was markedly diminished by preflame oxidation, which in turn was suppressed by the addition of tetraethyl lead. The conclusion was that the antiknock effect of tetraethyl lead must not be ascribed to a decreased flame velocity. However, in an internal-combustion engine it is believed (ref. 57) that, toward the end of the piston travel when the pressure is rising rapidly, the inhibiting effect of tetraethyl lead is very great. The addition of 0.36 percent tetraethyl lead or 5 percent ethyl nitrate had no effect on the flame velocities (cone height, burner method) of 20 fuels of various types at room temperature (ref. 58). Likewise, iron pentacarbonyl did not appreciably decrease the flame velocities of ether-carbon monoxide flames (ref. 17, p. 122).

When two fuels A and B are blended in various proportions, the maximum flame velocity of the blend is generally greater than that which would be computed from the maximum flame velocities of the individual fuels by a simple mixing rule:

$$U_{F,blend} = X_A U_{F,A} + X_B U_{F,B} \quad (21)$$

where X_A and X_B are the mole fractions of A and B in the fuel blend. Reference 59 found that flame velocities of various binary mixtures of any two of the fuels methane, ethene, acetylene, carbon monoxide, and hydrogen were greater than those obtained by the simple mixing rule. As an example, figure 137 for hydrogen plus carbon monoxide is presented. In reference 60, a similar result was found for propane plus carbon monoxide; the maximum flame velocity occurred with a fuel mixture of 96 percent dry carbon monoxide and 4 percent propane (35 percent total fuel mixed with air) and was 63 percent greater than the value obtained from equation (21).

For the correlation of flame velocities of mixed fuels, reference 61 presents an equation which is simplified in reference 62 to the form

$$\sum_j \frac{X_{f,j}}{X'_{f,j}} = 1 \quad (j=1,2,3, \dots n) \quad (22)$$

where

$X_{f,j}$ mole fraction of j^{th} fuel in multifuel mixture with air that has flame velocity U_F

$X'_{f,j}$ mole fraction of j^{th} fuel in its binary mixture with air that has same flame velocity U_F as multifuel mixture

Thus, for a mixture of two fuels and air, a plot of $(X_{f,1}/X'_{f,1})$ against $(X_{f,2}/X'_{f,2})$ should give a straight line with intercepts (1,0) and (0,1). Reference 62 presents studies of ternary mixtures of propane, air, and either ethene or hydrogen sulfide. Equation (22) was found to be valid for propane plus ethene but invalid for propane plus hydrogen sulfide, as shown by figure 138. According to reference 62, the data represented by figure 138 show that hydrogen sulfide is an effective flame velocity inhibitor; such a statement is misleading, since the addition of similar quantities of nitrogen to propane-air mixtures causes comparable decreases in flame velocity, as can be computed from the data of reference 48.

Water vapor: The pronounced promoting effect of water vapor on the flame velocity of carbon monoxide has been observed by many investigators. For 45 percent carbon monoxide in air, the flame velocity passes through a maximum after approximately 5 volume percent water has been added, at which point the flame velocity is 2.1 times the value for 0.7 percent water (ref. 17, p. 121, and ref. 63). Heavy water (deuterium oxide) increases the flame velocity of carbon monoxide by a smaller amount than the same percentage of ordinary water (ref. 64). This effect is discussed later in connection with studies of deuterated acetylene.

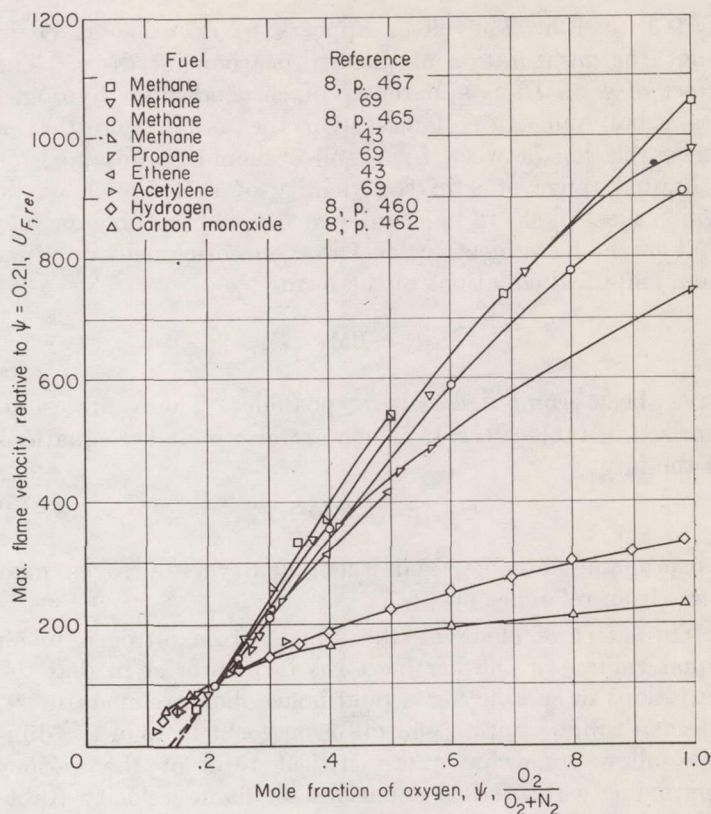


FIGURE 140.—Effect of oxygen concentration on relative flame velocities of various fuel-oxygen-nitrogen systems at room temperature and atmospheric pressure.

With hydrocarbons, water vapor has a slight inhibiting effect; for a butane-air mixture containing 2.8 volume percent water, the flame velocity is approximately 8 to 10 percent lower than that for a similar mixture containing 0.08 percent water (ref. 65).

Inert diluents: A decrease in the percentage of nitrogen in the primary air with which a fuel burns causes a marked increase in flame velocity for a given equivalence ratio. For example, the effect of increasing the molar ratio $O_2/(O_2+N_2)$, hereinafter called ψ , is shown in figure 131, from reference 48. Reference 66 reports that, for flame velocities of propane-, ethene-, and isooctane-oxygen-nitrogen mixtures measured by a schlieren total-area method, the maximum flame velocity is a linear function of ψ for the ranges studied. These data are presented in figure 139. Additional data on maximum flame velocities of fuel-oxygen-nitrogen systems are reported in references 8 (pp. 460–467) and 43 and are plotted in figure 140 as relative flame velocity, referred to the value with air for which $\psi=0.21$, against ψ .

Figure 140 shows that the relative flame velocity of hydrocarbon-oxygen-nitrogen mixtures continues to increase markedly as ψ is increased to 1.0, but that there is some tendency for the rate of increase to diminish in the region

$\psi=0.5$ to 1.0. The effect appears to decrease as chain length or unsaturation of the hydrocarbon increases. The effect of ψ on U_F is apparently much smaller for hydrogen or carbon monoxide flames. On the assumption that a linear relation between $U_{F,rel}$ and ψ should be obtained for a limited range of ψ in the vicinity of 0.21, which is the region most likely to be of interest for air-breathing engines that might be subject to local oxygen enrichment or vitiation, empirical equations of the form

$$U_{F,rel} = B(\psi - \mathcal{H}) \quad (23)$$

have been computed where possible. These are summarized in table XIII, in which are also included equations of the form

$$U_{F,rel} = B'T_o^c(\psi - \mathcal{H}_{av}) \quad (24)$$

for propane-, ethene-, and isooctane-oxygen-nitrogen mixtures from reference 66.

The effect of changing the diluent from nitrogen to an equal volume of another inert gas is of interest in that the variations in specific heats (and hence flame temperatures), thermal conductivities, and diffusion coefficients of the diluents allow somewhat more critical tests of the various approximate theoretical equations for flame velocity (table XIV). Table XV shows maximum flame velocities, relative to an arbitrary value of 100 with nitrogen as the inert gas,

for several fuels burning with primary air in which the nitrogen has been replaced by an equal volume of argon, helium, or carbon dioxide (refs. 8, 17, and 67 to 73). In all cases the flame velocity increases as the diluent is changed from carbon dioxide to nitrogen to argon to helium. As the ratio $O_2/(O_2 + \text{inert})$ increases, the effect of changing the diluent is smaller, because the common value of 100 for $O_2/(O_2 + \text{inert})=1$ is approached.

EFFECTS OF PHYSICAL VARIABLES

Pressure.—From the contradictory data reported in the literature, it appears that the accurate measurement of the pressure-dependence of flame velocity is very difficult and that at present all reported pressure effects must be questioned. Some recent measurements (table XVI, from ref. 74) indicate that the flame velocities of stoichiometric methane-, propane-, and ethene-air mixtures are independent of pressure, whether measured by the constant-volume bomb method or the slot-burner (luminous) method. Reference 75 reports the flame velocities of acetylene burning with oxygen, oxygen and argon, and air (pressures >10 mm Hg) to be independent of pressure. The flame velocities were measured by a luminous-cone angle method, and the burner diameter was increased in proportion to the pressure decrease. Reference 76 confirms that flame velocity is independent of pressure by using the soap-bubble method. It is believed (ref. 76) that earlier results obtained by a burner method, which showed a pressure effect, were probably less reliable.

TABLE XIII.—VALUES OF EMPIRICAL EQUATIONS^a FOR EFFECT OF ψ ON RELATIVE MAXIMUM FLAME VELOCITY^b
[Pressure, 1 atm.]

Fuel	T_o , °K	Range of ψ , $\frac{O_2}{(O_2 + N_2)}$	B	\mathcal{H}	B'	c	\mathcal{H}_{av}	Method and reference ^c
Methane-----	Room	0.21-0.50 .18-.50 .21-.50 .20-.50	1290 1550 1520 1420	0.135 .144 .143 .140	----- ----- ----- -----	----- ----- ----- -----	----- ----- ----- -----	1 2 3 4
Propane-----	311 422 Room	0.17-0.50 .17-.50 .21-.42	1420 1195 1290	0.140 .126 .135	} 1.79 -----	1.16 -----	0.133 -----	5 4
Isooctane-----	311 422	0.21-0.50 .21-.50	1172 1056	0.125 .115				5
Ethene-----	311 422 Room	0.17-0.35 .17-.35 .21-.50	1085 981 1100	0.118 .108 .12	} 1.23 -----	1.18 -----	0.113 -----	5 3
Acetylene-----	Room	0.11-0.24	770	0.08	-----	-----	-----	4
Hydrogen-----	Room	0.13-0.25	620	0.05	-----	-----	-----	1
Carbon monoxide-----	Room	0.13-0.25	600	0.04	-----	-----	-----	1

^a $U_{F,rel} = B(\psi - \mathcal{H})$; $U_{F,rel} = B'T_o^c(\psi - \mathcal{H}_{av})$.

^b $U_{F,rel}$ is maximum flame velocity (with respect to equivalence ratio) relative to arbitrary value of 100 for $\psi=0.21$ and $T=298^\circ$ K.

^c Methods and references:

1. Cone-height, total-area method of eq. (2a); ref. 8, pp. 459-466.
2. Luminous-cone, frustum-area method of eq. (5); ref. 8, p. 467.
3. Soap-bubble method; ref. 39.
4. Schlieren-image (line of maximum intensity obtained with horizontal knife edge) special angle method with nozzle burner; ref. 69.
5. Schlieren-image (outer edge of image obtained with horizontal knife edge), total-area method of eq. (26); ref. 66.

TABLE XIV.—SUMMARY OF BURNING-VELOCITY CORRELATIONS

Type of data	Combustion system	Correlations with diffusion theories				Correlations with thermal theories	
		U_F vs. active-particle concentrations	Reference	Equation	Reference	Equations and properties	Reference
Range of mixture concentrations	CO-O ₂ -N ₂ plus H ₂ O or H ₂	U_F vs. p_H , nonlinear.....	102.....	Tanford-Pease.....	103, 107	U_F vs. $\left(\frac{T_F - T_o}{T_{ig} - T_o}\right)$	115
	C ₂ N ₂ -O ₂ -A plus H ₂ O or D ₂ O	U_F^2 vs. p_{OH} , linear.....	116.....	Tanford-Pease.....	116		
	H ₂ -O ₂ -N ₂			Tanford-Pease.....	103		
	CH ₄ -O ₂ -N ₂			Tanford-Pease.....	103		
	C ₂ H ₄ -O ₂ -N ₂	U_F vs. $6.5 p_H + p_O + p_{OH}$, nonlinear	66, 100, 39 (fig. 149).....	Tanford-Pease.....	49	U_F vs. $\left(\frac{T_F - T_o}{T_{ig} - T_o}\right)$	100
				Manson.....	49	Semenov eq.	49
	C ₃ H ₈ -O ₂ -N ₂	U_F vs. $6.5 p_H + p_O + p_{OH}$, nonlinear	66 (fig. 148).....	Tanford-Pease.....		Semenov eq.	49
		U_F vs. $\sqrt{6.5 p_H + p_O + p_{OH}}$, nonlinear	66.....	Manson.....	49		
	C ₃ H ₄ -O ₂ -N ₂	U_F vs. $6.5 p_H + p_O + p_{OH}$, nonlinear	39 (fig. 149).....	Tanford-Pease.....	39	Semenov eq.	Unpub.
	C ₆ H ₁₂ -O ₂ -N ₂ (pentane)	U_F vs. $6.5 p_H + p_O + p_{OH}$, nonlinear	39 (fig. 149).....	Tanford-Pease.....	39	Semenov eq.	Unpub.
	C ₈ H ₁₈ -O ₂ -N ₂ (2,2,4-trimethylpentane)	U_F vs. $6.5 p_H + p_O + p_{OH}$, nonlinear	66.....	Tanford-Pease.....	49	Semenov eq.	49
		U_F vs. $\sqrt{6.5 p_H + p_O + p_{OH}}$, nonlinear	66.....	Manson.....	49		
Series of compounds at maximum burning velocity	Paraffins, olefins, diolefins, acetylenes, and benzene in air	U_F vs. p_H	120, 121, 122.....	Tanford-Pease.....	111	U_F vs. T_F	111, 120, 122
		U_F vs. $6.5 p_H + p_O + p_{OH}$, nonlinear	111, 123.....	Manson.....	49	Semenov eq.	112, 124
	Nonhydrocarbons in air	U_F vs. $6.5 p_H + p_O + p_{OH}$	111.....				
Different initial temperatures	CH ₄ -O ₂ -N ₂	U_F vs. p_H , linear.....	16 (fig. 147).....	Tanford-Pease.....	49	Semenov eq.	49
		U_F vs. $6.5 p_H + p_O + p_{OH}$, linear	16.....	Manson.....	49		
	C ₂ H ₄ -O ₂ -N ₂	U_F vs. p_H , linear.....	16 (fig. 147).....	Tanford-Pease.....	49	Semenov eq.	49
				Manson.....	49		
	C ₃ H ₈ -O ₂ -N ₂	U_F vs. p_H , linear.....	16 (fig. 147).....	Tanford-Pease.....	49, 16	Semenov eq.	49
		U_F vs. $6.5 p_H + p_O + p_{OH}$, linear	16.....	Manson.....	49		
Additives.....	C ₃ H ₈ -O ₂ -N ₂ plus various compounds ^a	U_F vs. $6.5 p_H + p_O + p_{OH}$, nearly linear	55.....				
Pressure-dependence of burning velocity	Various hydrocarbons in air or oxygen			Tanford-Pease.....	102	Semenov eq.	
				Gaydon-Wolfhard.....	105, 125		
				Manson.....	126		
Isotope substitution.....	C ₂ H ₂ or C ₂ D ₂			Tanford-Pease.....	6	Damköhler eq.	6
Change of diluent.....	CO-O ₂ -A or He.....		Table XXI.....	Ratio of \sqrt{D} calculated	113, 127	Ratio of $\sqrt{\kappa}$ calculated	113, 127
	H ₂ -O ₂ -A or He.....		Table XXI.....	Ratio of \sqrt{D} calculated	119, 113, 127	Ratio of $\sqrt{\kappa}$ calculated	119, 113, 127
	CH ₄ -O ₂ -A or He.....		Table XXI.....	Tanford-Pease.....	67	Ratio of $\sqrt{\kappa}$ calculated	49
				Ratio of \sqrt{D} calculated	49		
	C ₂ H ₂ -O ₂ -A or He.....		Table XXI.....	Ratio of \sqrt{D} calculated	113, 127	Ratio of $\sqrt{\kappa}$ calculated	113, 127
	CH ₄ -O ₂ -N ₂ or A.....			Tanford-Pease.....	67		
	Butadiene-O ₂ -N ₂ or He			Tanford-Pease.....	71		
				Manson.....	128		

^a Isooctane, benzene, acetone, methylethyl ketone, carbon monoxide, acetaldehyde, diethyl ether, oxygen, hydrogen, and nitrogen.

TABLE XV.—MAXIMUM FLAME VELOCITIES

[Relative to arbitrary value of 100 for nitrogen with primary air in which nitrogen was replaced by indicated inert gas.]

Fuel	Reference	Method	$\frac{O_2}{O_2 + \text{inert}}$	$U_{F,rel}$ with inert gas		
				Argon	Helium	CO ₂
Methane-----	69-----	Shadow total-area-----	0. 21	231	327	-----
	17, p. 2-----	Spatial velocity in tube-----	. 21	270	320	-----
	68-----	Tube, area-----	. 21	^a 231	^a 321	-----
	67 for A, He-----	Schlieren total-area-----	0. 21	185	300	-----
			. 30	155	260	24
			. 40	140	200	26
	8, p. 465 for CO ₂ ----	Cone-height total-area-----	0. 60	115	150	54
			. 80	105	115	76
Propane-----	67-----	Schlieren total-area-----	0. 21	180	280	-----
			. 32	140	235	-----
			. 42	120	160	-----
			. 57	110	150	-----
Ethene-----	70-----	Soap-bubble-----	0. 21	151	217	-----
Butadiene-----	71-----	-----	0. 21	-----	332	-----
Acetylene-----	70-----	Soap-bubble-----	0. 21	146	225	26
	73-----	Schlieren total-area-----	0. 11	190	340	-----
			. 21	145	215	-----
Hydrogen-----	68-----	Spatial velocity in tube-----	0. 21	135	^b 135	-----
	72-----	Cone-height total-area-----	. 12	^c 115	^c 275	-----
	8, p. 460-----	Cone-height total-area-----	0. 21	-----	-----	50
			. 30	-----	-----	68
			. 50	-----	-----	85
			. 80	-----	-----	96
Carbon monoxide contain- ing 1.5 percent H ₂ , 1.35 percent H ₂ O.	8, p. 462-----	Cone-height total-area-----	0. 21	-----	-----	52
			. 40	-----	-----	70
			. 60	-----	-----	86
			. 80	-----	-----	94

^a No nitrogen value was given; these are based on relative value for argon from ref. 69.^b Same value was also given for neon; results seem questionable in view of ref. 72.^c No nitrogen value was given for this inert concentration; relative values are based on interpolated nitrogen value from ref. 8, p. 460.

TABLE XVI.—FLAME-VELOCITY MEASUREMENTS OF STOICHIOMETRIC HYDROCARBON-AIR MIXTURES

[Constant-volume bomb and rectangular-burner, inner-luminous-edge, frustum-area methods; ref. 74.]

Fuel	Pressure, mm Hg	Flame velocity, cm/sec		
		Bomb method		Burner method
		Pressure record	Flame record	
Methane-----	253	-----	-----	38. 1
	380	-----	-----	37. 8
	532	36. 0	36. 3	-----
	760	36. 6	36. 4	37. 0
Propane-----	253	-----	-----	39. 9
	523	40. 2	40. 5	-----
	760	40. 6	40. 4	41. 2
Ethene-----	38	62. 5	63. 0	-----
	76	62. 7	62. 9	-----
	152	63. 0	63. 5	-----
	380	62. 8	63. 3	-----
	760	63. 1	63. 0	-----
	1140	62. 3	62. 5	-----

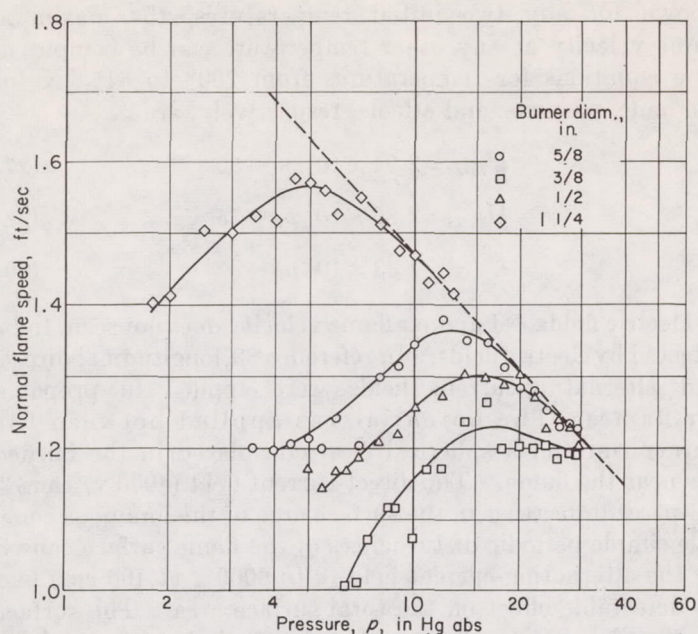


FIGURE 141.—Variation of normal flame speed with pressure for propane-air Bunsen flames. Fuel-air ratio, 0.067 (ref. 77).

On the other hand, reference 77 reports that, even though the burner diameters were varied, there was a pressure effect such that the flame velocities of propane-air and ethene-air mixtures were inversely proportional to the logarithm of pressure in the range $\frac{1}{3}$ to 1 atmosphere. The propane-air curves of reference 77 are reproduced in figure 141 and, for various tube diameters, approach a common upper envelope.

Many other investigators also report pressure effects. In general, the majority find flame velocity to be inversely proportional to pressure raised to a power between 0.1 and 0.5. The pressure-dependences indicated by some of the more recent studies (refs. 19 and 74 to 81) are summarized in table XVII. However, until the effect of apparatus on the measurement of the pressure-dependence of flame velocity is more clearly resolved, it is assumed that flame velocity is independent of pressure in the range of interest for jet-engine combustion chambers.

Temperature.—The initial temperature of the unburned gas mixture has an appreciable effect on flame velocity. As an example, data for propane-air obtained by a shadowgraph total-area method are presented in figure 130. The relative effects of initial temperature on the maximum flame velocity

TABLE XVII.—EFFECT OF PRESSURE ON FLAME VELOCITY

System	Equivalence ratio, ϕ	Pressure range, atm	Approximate pressure-dependence	Method and reference ^a
Methane-air	1.00	0.7–1.0	None	1
	1.00	.33–1.0	None	2
	1.00 or ϕ_{max}	.25–1.0	$p^{-0.24}$	3
	1.46	1.0–6.3	$p^{-0.45}$	3
	.60–.65	.25–6.3	$p^{-0.5}$	3
		.26–.66	$p^{-0.49}$	4
Propane-air	1.00	0.7–1.0	None	1
	1.00	.33–1.0	None	2
	1.00		$\log p$	5
	.56	.26–.66	$p^{-0.30}$	4
	ϕ_{max}	1–5	None	6
Butane-air	ϕ_{max}	0.25–1.0	$p^{0.17}$	3
<i>n</i> -Heptane-air	1.00	0.53–0.99	$p^{-0.36}$	7
Isooctane-air	1.00	0.53–0.92	$p^{-0.39}$	7
Ethene-air	1.00	0.33–1.0	$\log p$	5
	1.00	.05–1.5	None	1
	1.08–1.24	.30–.80	None	8
	1.4	.35–1.0	$p^{-0.39}$	9
	.46	.26–.66	$p^{-0.31}$	4
Acetylene-air	ϕ_{max}	0.01–1.0	None	10
	0.33	.26–.66	$p^{-0.47}$	4
Acetylene-O ₂	ϕ_{max}	0.01–1.0	None	10
Benzene-air	1.00	0.40–0.92	$p^{-0.31}$	7

^a Methods and references:

1. Constant-volume bomb, pressure record or flame record; ref. 74.
2. Rectangular burner, luminous cone, frustum-area; ref. 74.
3. Burner, inner edge of luminous zone, total area; no effect of tube diameter from 1 to 2 cm; ref. 78.
4. Flat-flame burner, luminous zone, total area; ref. 19.
5. Burner, luminous cone, angle; ref. 77.
6. Spatial velocity in tube (drum camera); ref. 79.
7. Ref. 80.
8. Soap-bubble; ref. 76.
9. Burner; ref. 81.
10. Burner, luminous cone, angle; ref. 75.

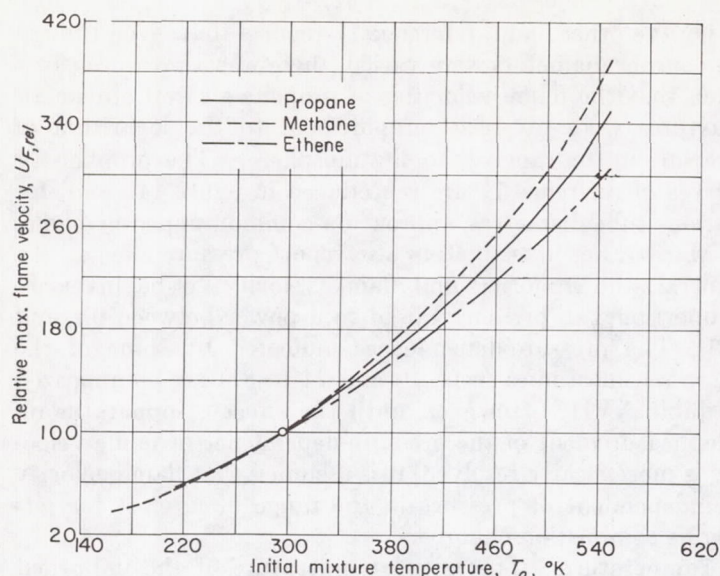


FIGURE 142.—Variation of relative maximum flame velocity referred to maximum flame velocity at 25° C with initial mixture temperature (ref. 16).

of methane-, propane-, and ethene-air flames are shown in figure 142. References 16, 37, 52, 54, 66, 73, and 82 to 88 present extensive studies of the temperature effect. A summary of these effects is given in table XVIII. The only references that are purposely omitted from table XVIII are those covering too small a temperature range to be significant, investigating nonhydrocarbon fuels not likely to be of interest, or containing results that are questionable or contradictory to the more extensive studies. Where possible, an empirical equation of the form

$$U_{F,rel} = B + \mathcal{K} T_0^c \quad (25)$$

is given. The relative flame velocities computed from these equations are referred to an arbitrary value of 100 at 25° C. The flame velocity is a function of T_0 raised to a power between 1.4 and 2.1; the exponent varies with the temperature range covered and with the fuel. Since propane is a fairly representative paraffin hydrocarbon, most blends containing a preponderance of paraffin hydrocarbons would be reasonably well represented by the equation

$$U_{F,rel} = 25 + 0.00085 T_0^2 \quad (26)$$

for the temperature range 200° to 615° K. For the smaller temperature range 290° to 420° K (or 520° to 760° R), it might be assumed that $U_F \propto T_0^{1.4}$. Alternatively, the percentage change of maximum flame velocity could be determined from the propane curve (fig. 142).

A method of empirical prediction for ethene, as well as methane and propane, and hence useful for both paraffinic and olefinic fuels, is demonstrated in reference 16. A very good linear correlation between computed adiabatic equilibrium hydrogen atom concentration p_H and flame velocity exists for each of the three fuels. These correlations indicate that, for any similar fuel, if maximum flame velocities are

known for any two initial temperatures, the maximum flame velocity at any other temperature can be computed. The equations for temperatures from 200° to 615° K for methane, propane, and ethene, respectively, are

$$U_{F,rel} = 2.91 \times 10^5 p_H - 50 \quad (27)$$

$$U_{F,rel} = 2.89 \times 10^5 p_H - 75 \quad (28)$$

$$U_{F,rel} = 1.33 \times 10^5 p_H - 97 \quad (29)$$

Electric fields.—Laminar flame velocity does not seem to be affected by electric fields. In reference 89, longitudinal direct- and alternating-current fields were applied to propane-air flames. The potential was applied between the burner rim and a spherical electrode placed in the burned gas near the flame. The direct-current field (4000 v) caused a 5-percent decrease in the surface area of the luminous cone. The simple periodic disturbances of the flame surface caused by the alternating-current field (0 to 6000 v at 400 cps) had no detectable effect on the total surface area. The surface area, and hence the flame velocity, was independent of the amplitude and phase of the disturbance.

Reference 90 presents measured velocities of burner flames of butane and air in transverse electric fields (electrodes on either side of the flame; 0 to 15,000-v potential). The flame cone was deflected toward the negative electrode. Local flame velocities were computed from the particle-track method of equation (6); the flame velocity increased on the side of the cone near the positive electrode and decreased on the negative side by as much as 50 percent of the original value. The average flame velocity (total-area method) was probably not changed appreciably. The observed variations in local flame velocity were in the direction to be expected if positive ions played an active role in flame propagation.

Acoustical and mechanical disturbances.—The effect of sound on propane-air burner flames was also studied in reference 89. No change in flame surface area, and hence no change in flame velocity, was observed. Reference 91 likewise reports no effect of sound (12.7 kc and known intensity) on the surface area of propane-air flames. In reference 25, however, flame velocity was increased by 7 or 8 percent, and sound of medium intensity was most effective.

Reference 92 reports investigation of vibrating flames of methane, city gas, propane, or ethene that traveled through transparent tubes of various lengths and diameters against gas velocities slightly smaller than the flame velocities. With carefully selected compositions and flow rates, flames were obtained that, after traveling partway down the tube, became saucer-shaped so that they were flat over the major portion of the cross section. Consideration of (1) the circulation of unburned gas ahead of the flame indicated by the curling and uncurling of the flame edges toward the unburned gas, (2) the lack of vibration at the point where coupling of an oscillatory heat source and a vibrating gas column should have been optimum, and (3) photographic evidence that waves in the unburned gas receded from the flame front at an essentially constant rate, led to the conclusion that variations

in flame velocity were small.

Reference 26 states that disadvantages in the methods used in generating electrical and acoustical disturbances in reference 89 were (1) no allowance for a measurement of the initial amplitude of the flow disturbance introduced into the flame, and (2) complication of acoustical disturbances by resonance effects. A mechanical disturbance, which could be applied

locally to the flame and the amplitude of which could be measured accurately, was obtained with a wire that touched the flame and vibrated perpendicular to the flame front surface. The resulting distortion of the flame surface was similar to that obtained with the alternating-current field or the sound. The surface area of the periodically disturbed flames, and hence the flame velocity, was unaffected.

TABLE XVIII.—EFFECT OF INITIAL MIXTURE TEMPERATURE ON LAMINAR FLAME VELOCITY

[Empirical equations for flame velocity relative to arbitrary value of 100 at 25° C; pressure, 1 atm. Calculations can only be made when B , \mathcal{K} , and c are given.]

Fuel	Oxidant	T_0 range, °K	$U_{F,rel} = B + \mathcal{K} T_0^c$			Method and reference ^a
			B	\mathcal{K}	c	
Methane-----	Air-----	293-703	-----	-----	1.70	1
		293-973	-----	-----	2.00	2
		141-615	24	0.47×10^{-3}	2.11	3
	Oxygen-----	273-1273	30	-----	^b ≈ 1.70	4
Ethane-----	Oxygen-----	273-773	23	-----	^b 2.00	4
Propane-----	Air ^d -----	322-411	(^e)	38.0×10^{-3}	1.38	5
		307-615	(^e)	5.32	1.72	6
		200-617	25	.85	2.00	3
		307-867	-----	-----	-----	7
	Oxygen-----	273-773	32	-----	^b 2.00	4
Isooctane-----	Air ^d -----	311-422	-----	11.9×10^{-3}	1.40	5
Decane-----	Air-----	367-411	(^e)	7.39×10^{-3}	1.67	8
1-Decene-----	Air-----	367-411	(^e)	1.99×10^{-3}	1.90	8
Benzene-----	Air-----	311-395	(^e)	3.95×10^{-3}	1.78	8
Toluene-----	Air-----	318-422	(^e)	28.90×10^{-3}	1.43	8
Ethene-----	Air-----	293-773	-----	-----	2.00	2
		322-411	(^e)	23.4×10^{-3}	1.47	5
		307-615	(^e)	12.8×10^{-3}	1.565	6
		200-617	16	4.05	1.74	3
Acetylene-----	Air-----	417-590	-----	-----	^f 1.80	9
Hydrogen-----	Air-----	293-700	-----	-----	2.00	2
Carbon monoxide-----	Air (dry)-----	293-733	-----	-----	2.00	1
		291-873	0	4.8×10^{-3}	1.75	10
		293-723	-----	-----	2.00	2
	Air (moist)-----	293-823	-----	-----	2.00	2
Natural gas-----	Air-----	332-756	-----	-----	2.00	9
City gas-----	Air-----	293-973	-----	-----	-----	2
		293-773	-----	-----	^g 1.74	11
Coke-oven gas-----	Air-----	283-673	-----	-----	1.64	12

^a Methods and references:

1. Luminous-cone-height total-area by eq. (2a); ref. 83.
2. Luminous-cone-height total-area by eq. (2a); ref. 84.
3. Inner or outer edge of cone shadow, total-area by eq. (2b); ref. 16.
4. Luminous-cone-height total-area by eq. (2a); ref. 86.
5. Outer edge of schlieren cone (horizontal knife edge advanced downward), total-area by eq. (2b); ref. 66.
6. Inner or outer edge of cone shadow, total-area by eq. (2b); ref. 85.
7. Outer edge of schlieren cone (horizontal knife edge advanced downward), total-area by eq. (2b); ref. 87.
8. Luminous-cone angle at $0.5 r_c$; ref. 52.
9. Schlieren; ref. 73.
10. Luminous-cone total-area; ref. 88.
11. Luminous-cone total-area; ref. 37.
12. Luminous-cone-height total-area by eq. (2b); ref. 37.

^b These constants based on authors' belief that Sachse had not corrected his flame velocities for expansion due to preheating. All Sachse's curves are for lean fuel-oxygen mixtures.

^d Same relation successfully used empirically for $O_2/(O_2+N_2)=0.25$ to 0.50 ; ref. 54.

^e Deliberately equated to zero to simplify expression for engine application.

^f Range of data too limited and/or data scatter too great to rely on results.

^g Preheated only air.

THEORIES OF LAMINAR FLAME PROPAGATION

The phenomenon of laminar flame propagation can be described by the use of the basic equations of fluid dynamics, modified to account for the liberation and conduction of heat and for changes in chemical species within the reaction zone. (An excellent review of the theoretical concepts of laminar flame propagation as of 1951 is given by ref. 8, pp. 337–351; see also ref. 9.) The formulation of the problem requires equations of continuity for each chemical component, of state, and of conservation of energy, momentum, and total mass. In order to solve these equations for a unique flame velocity (eigenvalue), the following simplifying assumptions are made:

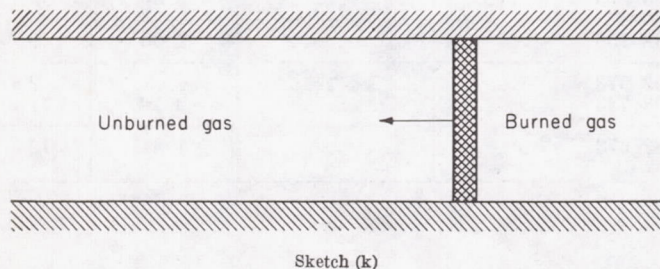
- (1) The flame is one-dimensional.
- (2) The flame is steady with respect to time.
- (3) Velocity gradients may be neglected; hence, viscosity terms in the momentum and energy equations may be ignored.
- (4) Pressure is essentially constant across the flame front, so that the equation for conservation of momentum may be ignored.
- (5) The effect of gravity is negligible.
- (6) The loss of energy by radiation is negligible.

In order to solve the mass and energy equations, boundary conditions must be selected. The hot boundary for the flame reaction zone is assumed to be the condition of thermodynamic equilibrium at the adiabatic flame temperature $T = T_F$ at $x = x_\infty$. The selection of a cold boundary with respect to the chemical reaction involved in these equations requires some justification, because the reaction rate never falls to zero if it follows an Arrhenius type relation

$$\omega \propto \exp\left(\frac{-E_{act}}{RT}\right) \quad (30)$$

However, some reasonable approximation for a cold-boundary condition must be found. The choice of this cold-boundary condition is intimately related to the question of whether or not a unique flame velocity exists in an essentially adiabatic system.

Consider a tube of infinite extent, adiabatically isolated from the surroundings and without heat-absorbing walls, filled with combustible mixture as follows:

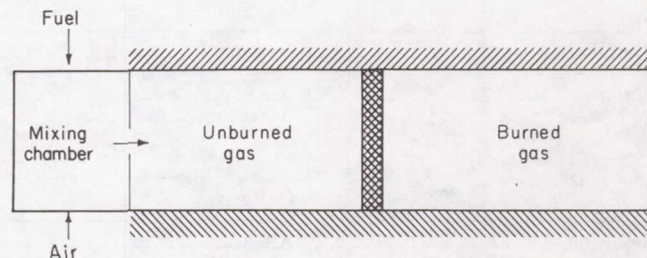


Sketch (k)

A flat flame is shown moving into the unburned gas. Since the pipe is of infinite length, the unburned gas far from the flame will be changing in composition and temperature because of the finite (albeit extremely slow) rate of exo-

thermic reaction, even at T_0 . Only if the increase in temperature and change in composition exactly compensate with respect to flame velocity effects would a constant flame velocity be possible. Zeldovich (ref. 51) has shown, and it may be seen by comparison of the effect of initial temperature with the effect of dilution on flame velocity (see previous data sections), that such compensation does not occur for carbon monoxide flames. This suggests that in an infinite, adiabatic system a unique flame velocity does not exist. However, the reactions at T_0 are very slow, and there is, therefore, a very long period of flame travel before a measurable change in flame velocity would occur. If the equations for flame propagation including a time-dependence were set up and solved for short periods of time, the ignition temperature as a boundary condition should not be required. If a steady state is assumed, as is usually done, an ignition temperature is required in the infinite system.

Suppose, however, that there is a mixing chamber a short distance from the flame, as follows:



Sketch (l)

The problem of slow reaction at an infinite time is thus eliminated, but the presence of the mixing chamber in the neighborhood of (even several meters from) the flame means that a small but finite transfer of heat to the mixing chamber and a small but finite back-diffusion of products must occur. Hirschfelder (ref. 93), whose comprehensive equations are presented hereinafter, has indicated that the temperature drop to the mixing chamber need only be 10^{-6} °K but that the heat transfer is required to describe a steady-state flame with a unique flame velocity. This kind of cold-boundary condition closely approximates the conditions under which experimental observations are made, and accounts, at least in part, for the apparent existence of a steady-state flame when theoretically such a flame does not exist.

When the temperature profile for a laminar flame (fig. 127) was discussed, it was pointed out that there is a temperature T_3 at which the chemical reaction becomes appreciable to the extent that a mass element of gas changes from a heat sink to a heat source. As will be shown in the following sections, most of the simplified equations for flame velocity are obtained by assuming the temperature T_3 to be the cold boundary for the reaction zone. With this assumption, the energy equation can be integrated for the preheat zone (T_0 to T_3) and the reaction zone (T_3 to T_F) and solved for flame velocity by equating the two integrals at the T_3 boundary, where dT/dx must be the same for both zones.

COMPREHENSIVE EQUATIONS

The following equations are formulated in reference 94 to describe the steady-state, one-dimensional flame:

Continuity equations:

For each component:

$$\frac{d}{dx} \left[\frac{\mathcal{C}_i(U+U_{a,i})}{\mathcal{A}} \right] = I_i \quad (i=1,2,3, \dots j) \quad (31)$$

For the total:

$$\left(\sum_i \frac{\mathcal{C}_i M_i}{\mathcal{A}} \right) U = \rho U = \rho_o U_F = G = \text{constant} \quad (32)$$

Energy equation:

$$\frac{d}{dx} \left(\kappa \frac{dT}{dx} \right) - \frac{d}{dx} \left[\sum_i \frac{\mathcal{C}_i M_i H_i (U+U_{a,i})}{\mathcal{A}} \right] = 0 \quad (33)$$

Equation of state:

$$\mathcal{C} = \sum_i \mathcal{C}_i = \frac{\mathcal{A} p}{RT} \quad (34)$$

where I_i is the rate of production by chemical reaction of i^{th} species (g-mole/(cm³)(sec)).

It is assumed that the cold boundary is terminated by a flameholder that has two properties: It prevents back-diffusion of product molecules into the gases outside the cold boundary of the flame front, and it extracts an amount of heat q_o from the flame:

$$q_o = -\kappa \left(\frac{dT}{dx} \right)_o \quad (35)$$

Since equations (31) to (34) are formulated in terms of individual chemical species, it is necessary to identify each chemical species occurring during the combustion reaction and to know the enthalpy, molecular weight, and other properties of the species. It is also necessary to know the specific rates of chemical production for a sufficient number of species so that the rest may be calculated from the chemical equations relating the various species. In order to determine these chemical kinetic factors, the scheme of reaction occurring in the flame and the rate constants for each independent step in the scheme must be established. But this information is completely lacking for hydrocarbon-air flames; indeed, few homogeneous, low-temperature chemical reactions have been incontrovertibly established. The comprehensive equations of Hirschfelder and Curtiss have been solved by approximate methods for only a few of the simplest flames—for example, the azomethane (ref. 94) and ethylene oxide (ref. 7) decomposition flames and the ozone flame (ref. 93).

Although the comprehensive theory of laminar flames is necessary for an understanding of flame propagation, it is currently impossible to use it to predict flame velocities of hydrocarbons or the effects of changes in experimental variables without making further simplifying assumptions. It is desirable to develop simpler equations for these pur-

poses, even if some of the theoretical exactness is lost. Some of the approximate equations, which usually emphasize only one process of the total mechanism such as the heat-conduction process or the active-particle diffusion process, have proven quite satisfactory for the prediction of flame velocity.

APPROXIMATE EQUATIONS

Thermal mechanism.—Both the early flame velocity equations of Mallard and LeChatelier, Nusselt, Jouguet and Crussard, Daniell, and Damköhler and the equations more recently reported by Bechert, Bartholomé and Emmons, Harr, and Strong are based on thermal concepts (ref. 9). The original, frequently quoted Mallard-LeChatelier equation was obtained simply by equating the sensible heat gain in the preheat zone to the heat conducted from the reaction zone at the T_3 boundary:

$$\bar{c}_p(\rho_o U_F)(T_3 - T_o) = \kappa \left(\frac{dT}{dx} \right)_3 \quad (36)$$

where it was assumed that

$$\left(\frac{dT}{dx} \right)_3 \simeq \frac{T_F - T_3}{x_F - x_3} \quad (37)$$

hence,

$$U_F = \frac{\kappa}{\bar{c}_p \rho_o (x_F - x_3)} \frac{T_F - T_3}{T_3 - T_o} \quad (38)$$

where \bar{c}_p is the mean specific heat from T_o to T_3 (cal/(g)(°K)). Assumption (37) regards the T, x curve as linear in the reaction zone with a slope equal to that at x_3 as determined by approaching x_3 through the preheat zone. It involves the chemical reaction rate only indirectly through the reaction-zone thickness ($x_F - x_3$). All authors since Mallard and LeChatelier have included some consideration of the reaction rate. The early equations included an ignition temperature; however, it is not easy to determine the proper ignition temperature to use in such equations (see previous discussion of T_3 and fig. 127).

Zeldovich and Frank-Kamenetsky have derived an equation for flame velocity for which the beginning basic equations were quite comprehensive. In its final simplified and approximate form, it includes diffusion of molecules but not free radicals and atoms. As a result, it emphasizes the thermal mechanism. Semenov (ref. 95) has presented the derivation of this equation in detail. Because this equation, hereinafter called the Semenov equation, has been widely used in the correlation of experimental flame velocities of hydrocarbons, its derivation is discussed briefly.

In the Semenov derivation, an ignition temperature is used only as a mathematical device for approximate computation. Semenov assumes that this ignition temperature, above which nearly all the reaction occurs, is near the flame temperature, because the chemical reaction rate is an exponential function of the temperature according to equation (30). By approximations, the ignition temperature is entirely eliminated from the final equation, thus making the equation more useful than the previous ones. The

following assumptions, in addition to that regarding ignition temperature and those stated heretofore for the comprehensive theory, are used:

- (1) Diffusion is important only as it affects energy balance.
- (2) Flame velocity may be described in terms of an over-all chemical reaction; equations are set up in terms of zero-order, first-order (monomolecular), or second-order (bimolecular) reactions.
- (3) Specific heat c_p and thermal conductivity κ are constant.
- (4) Thermal diffusivity $\kappa/c_p\rho$ is equal to molecular diffusivity D .
- (5) Total number of molecules is constant.

The basic equations, which may be compared with the corresponding exact equations (32) to (34), are as follows: Continuity equation:

$$D\rho = \frac{d^2\mathcal{C}'}{dx^2} - G \frac{d\mathcal{C}'}{dx} + \omega = 0 \quad (32a)$$

$$\mathcal{C}' = \mathcal{C}_{rt,o}\rho_o - \frac{\mathcal{C}_{rt}}{\rho}$$

Energy equation:

$$\frac{\kappa}{c_p} \frac{d^2T}{dx^2} - G \frac{dT}{dx} + \omega \frac{Q_{re}}{c_p} = 0 \quad (33a)$$

$$G = \rho U = \rho_o U_F$$

Equation of state:

$$\frac{\rho}{\rho_o} = \frac{T_o}{T} \quad (34a)$$

The energy equation consists of three terms, the first representing the heat gained by a mass element through conduction from a hotter element downstream, the second the loss of heat through mass transfer, and the third the heat evolved by the chemical reaction. In the preheat zone x_o to x_3 , it is assumed that no chemical reaction occurs; and in the reaction zone x_3 to x_F , it is assumed that the net energy loss due to mass transfer may be neglected in comparison with the chemical-reaction and heat-conduction terms. With these assumptions, the equation is solved for U_F by integrating over the preheat and reaction zones separately and establishing the condition of continuity by equating dT/dx at $x=x_3$ for the two zones. The result is

$$U_F = \sqrt{\frac{2\kappa}{\mathcal{C}_{rt,o}\rho_o c_p (T_F - T_o)} \int_0^{T_F} \omega dT} \quad (39)$$

In order to evaluate the reaction-rate integral in equation (39), an Arrhenius type temperature relation is assumed. It is generally assumed that the over-all reaction is bimolecular and second-order with respect to fuel and oxygen. Following the Semenov derivation, the rate integral is evaluated as follows:

$$\int_0^{T_F} \omega dT = \int_0^{T_F} \mathcal{C}_f \mathcal{C}_{O_2} \mathcal{P} Z \exp\left(\frac{-E_{act}}{RT}\right) \quad (40a)$$

$$\cong \mathcal{C}_{f,eff} \mathcal{C}_{O_2,eff} \mathcal{P} Z \frac{RT_F^2}{E_{act}} \exp\left(\frac{-E_{act}}{RT_F}\right) \quad (40b)$$

where $\mathcal{C}_{f,eff}$ and $\mathcal{C}_{O_2,eff}$ are the effective mean concentrations of fuel and oxygen in the reaction zone (molecules/cm³). Semenov states that the approximation for the exponential term obtained from equations (40a) and (40b) is satisfactory for $RT_F/E_{act} \leq 0.1$.

Approximate solutions must be obtained for the effective concentration terms. The relation between concentration and temperature is first established for a zero-order reaction as follows: A new variable, $\Theta = c_p(T - T_o)/Q_{re}$, is introduced into the energy equation to give

$$\frac{\kappa}{c_p} \frac{d^2\Theta}{dx^2} - G \frac{d\Theta}{dx} + \omega = 0 \quad (41)$$

which is formally identical with the continuity equation (32a), because, by assumption (4), $\kappa/c_p = D\rho$. It can be shown that the boundary conditions of these equations coincide at x_o and x_F . If $\mathcal{C}' = \Theta$ for the entire interval, a relation between concentration and temperature is obtained:

$$c_p T + \mathcal{C}_{rt} Q_{re} = c_p T_o + \mathcal{C}_{rt,o} Q_{re} = c_p T_F \quad (42)$$

Equation (42) means that the sum of chemical and thermal energies is constant throughout the flame (a condition that holds only where assumption (4) is valid). Following the approximation technique used by Semenov, this relation is modified for $\mathcal{C}_{f,eff}$ and $\mathcal{C}_{O_2,eff}$ for the bimolecular reaction as follows:

For rich mixtures, $\varphi > 1$:

$$\left. \begin{aligned} \mathcal{C}_{f,eff} &= \mathcal{C}_{f,o} \frac{T_o}{T_F} \left(1 - \frac{1-\beta}{\varphi}\right) \\ \mathcal{C}_{O_2,eff} &= \mathcal{C}_{O_2,o} \frac{T_o}{T_F} \beta \end{aligned} \right\} \quad (43)$$

For lean mixtures, $\varphi < 1$:

$$\left. \begin{aligned} \mathcal{C}_{f,eff} &= \mathcal{C}_{f,o} \frac{T_o}{T_F} \beta \\ \mathcal{C}_{O_2,eff} &= \mathcal{C}_{O_2,o} \frac{T_o}{T_F} \left[1 - \varphi(1-\beta)\right] \end{aligned} \right\} \quad (44)$$

where

$$\beta = \frac{RT_F^2}{E_{act}(T_F - T_o)} \quad (45)$$

and

$$\mathcal{C}_{O_2,o} = \frac{\mathcal{C}_{f,o}}{\varphi} \left(\frac{\mathcal{C}_{f,o}}{\mathcal{C}_{O_2,o}}\right)_{st} \quad (46)$$

where $(\mathcal{C}_{f,o}/\mathcal{C}_{O_2,o})_{st}$ is the stoichiometric fuel-oxygen ratio.

Corrections may now be applied to some of the assumptions as follows: Assumption (3) is corrected by the use of a mean value of κ/c_p for the preheat zone, and it is assumed that physical properties in the reaction zone may be represented by their values at T_F . For the bimolecular reaction, assumptions (4) and (5) are corrected by inserting the factors $(\kappa/c_p\rho D)_F^2$ and m^2 , respectively, under the square root sign in equation (39) (m is the ratio of moles of reactants to moles of products in the stoichiometric reaction). These correction factors and equations (34a), (40b), (43) or (44), and

(45) are substituted into the flame velocity equation (39). After collecting terms, the resulting equation for rich mixtures is:

$$U_F = \frac{\mathcal{H}\beta}{c_p F D_F} \sqrt{\frac{2\kappa_F^3 \mathcal{P} Z \mathcal{C}_{f,o} \left(1 - \frac{1-\beta}{\varphi}\right)}{\rho_o^3 c_p \varphi \left(\frac{\mathcal{C}_{f,o}}{\mathcal{C}_{O_2,o}}\right)_{st}}} \exp\left(\frac{-E_{act}}{RT_F}\right) \quad (47)$$

For lean mixtures, the term $[1 - (1-\beta)/\varphi]$ is replaced by $[1 - \varphi(1-\beta)]$, and for stoichiometric mixtures it becomes simply β .

All the factors in equation (47) except \mathcal{P} and E_{act} can be estimated by extrapolation of thermodynamic tables (refs. 96 and 97) and by use of the following equations:

$$c_p = \sum_i c_{p,i} x_i \quad (48)$$

$$\kappa = \left(c_p' + \frac{5}{4R}\right) \frac{\mu}{M} \quad (49)$$

$$D = 1.336 \frac{\mu}{\rho} \quad (50)$$

$$Z = \left(\frac{d_{col,f} + d_{col,O_2}}{2}\right) \sqrt{8\pi \frac{R}{\mathcal{A}} T \left(\frac{M_f + M_{O_2}}{M_f M_{O_2}}\right)} \quad (51)$$

where c_p' is the molar heat capacity (cal/(g-mole)(°K)). The values of μ for combustion-product mixtures were determined by the additive volume rule analogous to equation (47) and were within 1 percent of values calculated by the method of reference 98.

For lack of better knowledge, low-temperature activation energies reported in the literature for the appropriate hydrocarbon oxidation may be substituted for E_{act} . For example,

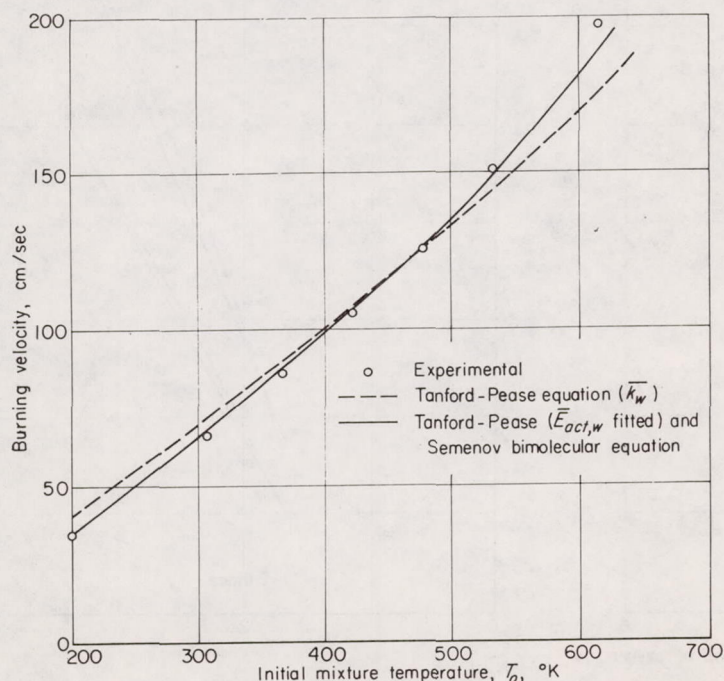


FIGURE 143.—Comparison of measured and calculated burning velocities for ethene-air mixtures at different initial temperatures (data of ref. 16 and calculations of ref. 49).

the following activation energies (kcal/g-mole) were used for burning-velocity predictions in references 49 and 16: methane, 51 (ref. 99); propane, 38 (ref. 17); and ethene, 40 (ref. 100). In reference 49, the steric factor \mathcal{P} was calculated from each experimental flame velocity. These values of \mathcal{P} were then averaged to give $\bar{\mathcal{P}}$ for the group of data under consideration. The ratio of predicted to experimental flame velocity was calculated as $(\bar{\mathcal{P}}/\mathcal{P})^{1/2}$ for each point.

Figures 143 and 144 illustrate the agreement between experimental flame velocities and the relative values obtained by multiplying the experimental values by $(\bar{\mathcal{P}}/\mathcal{P})^{1/2}$. The relative predictions are satisfactory for these three- to sevenfold increases in flame velocity that result from changes in initial temperature or O_2/N_2 ratio. The accuracies of these and other predictions for methane, propane, and ethene are indicated in table XIX by the average percent deviation of $(\bar{\mathcal{P}}/\mathcal{P})^{1/2}$ from unity for each of the data ranges studied.

Equation (47) may be further simplified for particular purposes by making additional assumptions. For example, in order to predict the effect of initial mixture temperature on flame velocity, the non-temperature-dependent terms may be eliminated to give (ref. 16)

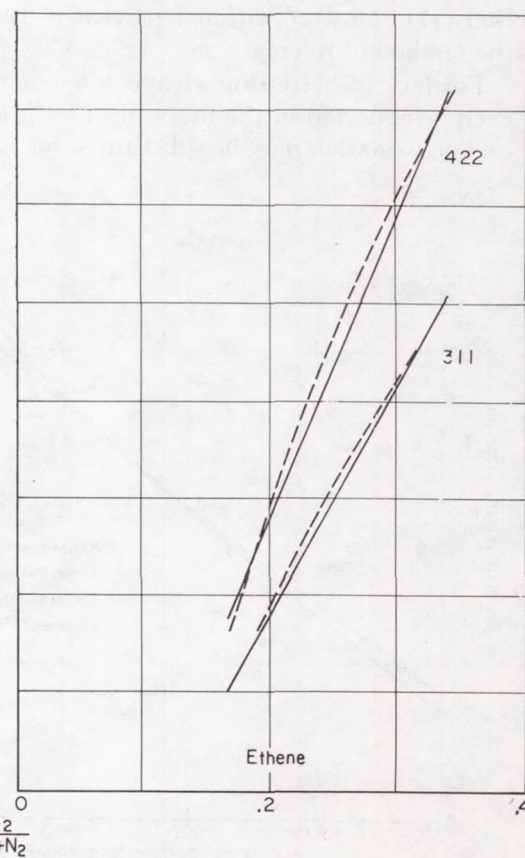
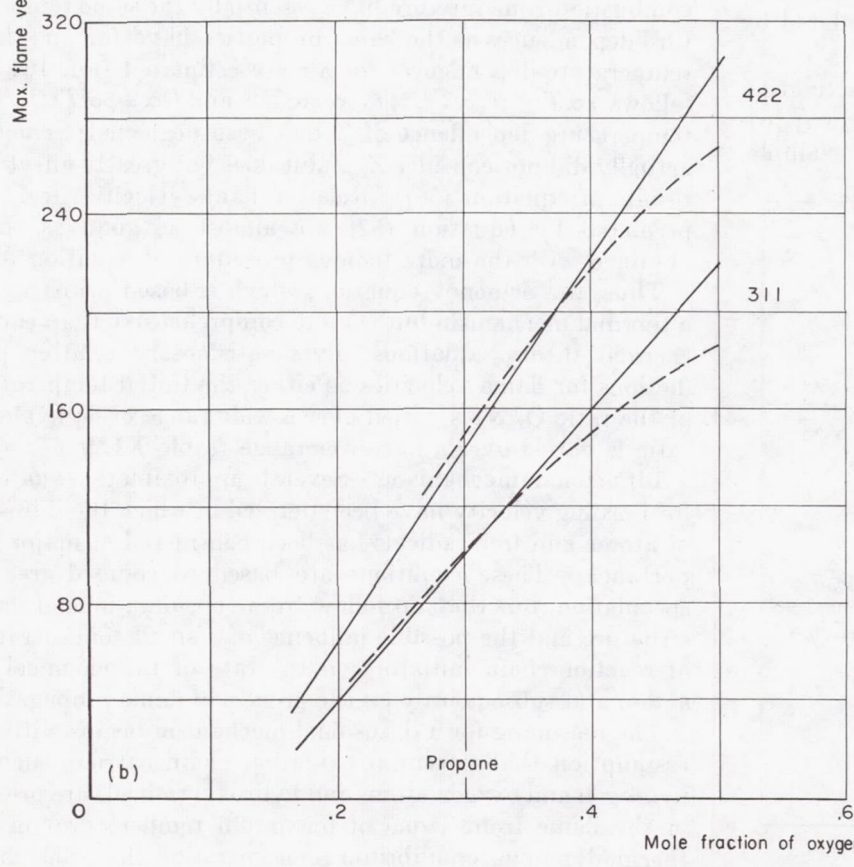
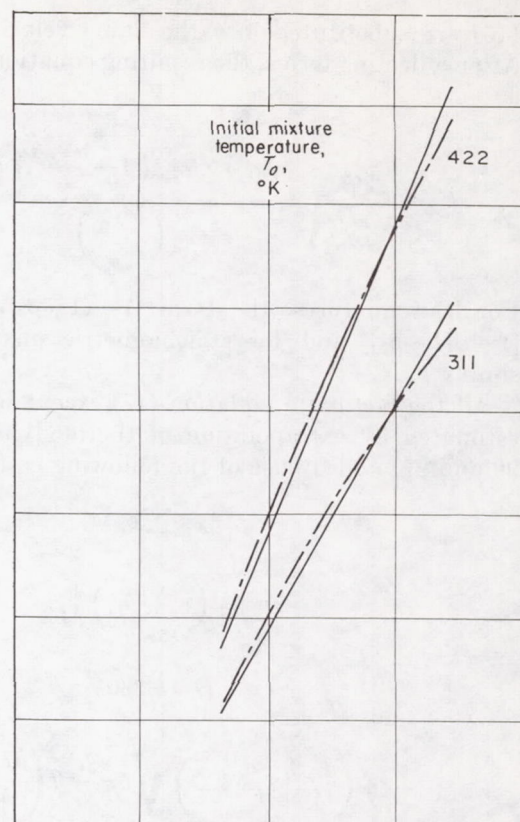
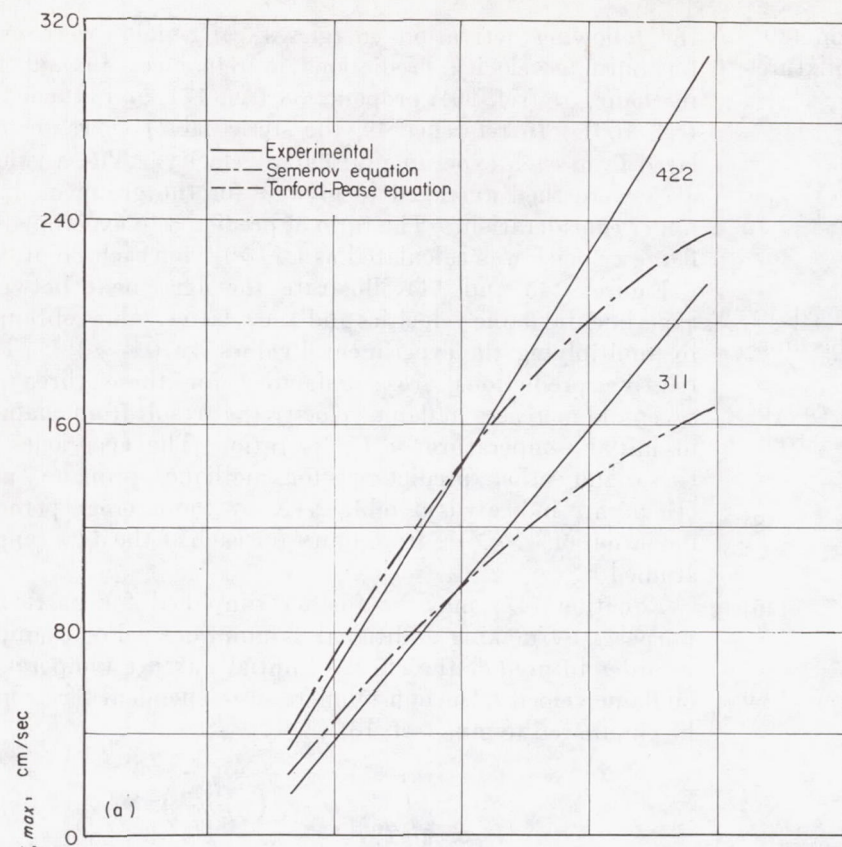
$$U_F \propto \sqrt{\frac{T_o^2 T_F^{4.9}}{(T_F - T_o)^3}} \exp\left(\frac{-E_{act}}{RT_F}\right) \quad (52)$$

Here it is assumed that the physical properties of the combustion-zone mixture have essentially the same temperature-dependences as the same properties have for air; these temperature-dependences for air are estimated (ref. 101) as follows: $\kappa \propto T^{0.84}$; $c_p \propto T^{0.09}$; $\mathcal{C}_{f,o} \propto \rho \propto T^{-1}$; and $D \propto \mu/\rho \propto T^{1.67}$. The temperature-dependence of Z has been neglected; Semenov actually did not consider Z , and it does not greatly affect the results of equation (52). Relative flame velocities (ref. 49) predicted by equation (52) are almost as good as those obtained with the more tedious procedure of equation (47).

Thus, the Semenov equation, which is based primarily on a thermal mechanism but is more comprehensive than earlier thermal theory equations, gives satisfactory relative predictions for flame velocities as either the initial temperature or the ratio O_2/N_2 is varied over a wide range or equivalence ratio is varied over a narrower range (table XIX).

Diffusional mechanism.—Several approximate equations for burning velocity have been derived in which the diffusion of atoms and free radicals has been considered of major importance. These equations are based to some degree on speculation, but they do follow from considerations of flame structure and the possible influence of a small concentration of reaction-chain initiators on the rate of the chemical reaction and subsequently on the process of flame propagation.

The reasoning for a diffusional mechanism begins with the assumption that potential oxidation chain carriers such as hydrogen and oxygen atoms and hydroxyl radicals are present in the flame front (zone of maximum temperature) in the thermodynamic equilibrium concentration for the flame temperature (ref. 102). Because some of these particles, especially hydrogen atoms, diffuse rapidly, it is further assumed that the concentration of chain carriers in the colder



(a) Semenov bimolecular equation.

(b) Tanford-Pease equation.

FIGURE 144.—Comparison of predicted and experimental flame velocities (ref. 66).

TABLE XIX.—PERCENT AVERAGE DEVIATION IN RATIO OF PREDICTED TO MEASURED FLAME VELOCITY

Hydrocarbon	Equivalence ratio, φ	$\frac{\text{O}_2}{\text{O}_2 + \text{N}_2}$ mole fraction	Initial temperature, °K	Burning-velocity range, cm/sec	Average deviation, percent ^a				
					Semenov equation (bimolecular) using \mathcal{P}	Tanford-Pease equation		Manson equation	
						\bar{k}_w	$\bar{E}_{act,w}$ from T_o data	Using \bar{k}_H	Using \bar{k}_Z
Methane	Stoichiometric ± 0.20	0.21	307	25–36	7.4	5.7	7.0	23.6	1.8
	Max. burning velocity	.21	200–615	19–133	2.7	7.8	.8	10.3	10.1
Propane	Stoichiometric ± 0.20	0.21	302	25–40	4.0	0.6	----	15.1	1.2
	Max. burning velocity	0.21	200–615	23–141	2.1	6.1	----	10.0	13.0
		.17–.50	422	33–305	12.4	5.2	----	12.7	13.0
Ethene	Stoichiometric ± 0.20	0.21	298	58–65	5.0	3.7	3.3	10.1	1.8
	Max. burning velocity	0.21	200–615	35–196	1.8	5.8	1.8	12.0	13.8
		.17–.35	422	69–287	3.0	4.6	----	6.8	5.3

^a Average deviation from unity of $(\bar{\mathcal{K}}/\mathcal{K})^{1/2}$ where \mathcal{K} is remaining "constant" unknown quantity in flame-velocity equation. For example, for the Semenov equation, \mathcal{K} is steric

factor \mathcal{P} , and percent average deviation is calculated by $\frac{\sum_{i=1}^n \left| (\bar{\mathcal{P}}/\mathcal{P})^{1/2} - 1 \right|}{n} \times 100$, where n is number of data points.

unburned gas ahead of the flame front is increased by diffusion to a value far greater than the thermodynamic equilibrium concentration for that region (e. g., table XX, from ref. 103). A concentration profile similar to that shown in figure 145 is obtained. Even in the cold gas these active particles react rapidly, because chemical reactions involving atoms and free radicals generally have low energies of activation; that is, the reaction rate is not very dependent on the temperature. Therefore, these active particles could serve as initiators of the oxidation reaction. Since the concentration of active particles reaching the unburned gas by diffusion must be related to the maximum concentration in the flame front, the conclusion is that flame velocity should be related to the equilibrium concentrations at the adiabatic flame temperature.

It is difficult to measure the concentration of hydrogen atoms in a flame zone, but hydroxyl radicals [OH] may be observed spectroscopically. By use of this method, it was found in reference 104 that the relative concentration of hydroxyl radicals remained high in the unburned gas ahead of the visible flame zone (fig. 146). Reference 105 shows

TABLE XX.—HYDROGEN ATOM CONCENTRATION IN COMBUSTION ZONE OF MOIST CARBON MONOXIDE—OXYGEN FLAMES (Ref. 103)

x , cm	Local mixture temperature, °K	H atom, mole fraction	
		Local equilibrium	Diffusion (eq. (54))
0	2930	2.4×10^{-3}	2.40×10^{-3}
.002	2630	8.5×10^{-4}	2.37×10^{-3}
.004	2330	2.3×10^{-4}	2.34×10^{-3}
.006	2030	4.0×10^{-5}	2.32×10^{-3}
.008	1740	4.4×10^{-6}	2.29×10^{-3}
.010	1460	2.2×10^{-7}	2.26×10^{-3}

that the width of the reaction zone for several hydrocarbon-air and -oxygen flames as determined from the temperature profiles of the flames is roughly equal to the limit of diffusion of hydrogen atoms from the flame front into the unburned gas. Measurements and calculations such as those of table XX substantiate the assumption that the concentrations of active particles that diffuse ahead of the flame may be large enough to be important.

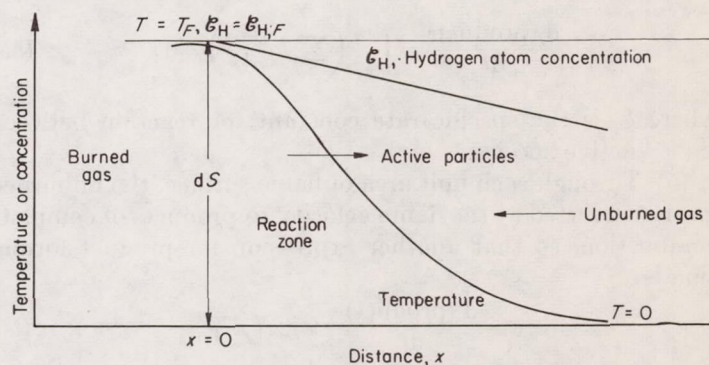


FIGURE 145.—Model of structure of flame front (ref. 103).

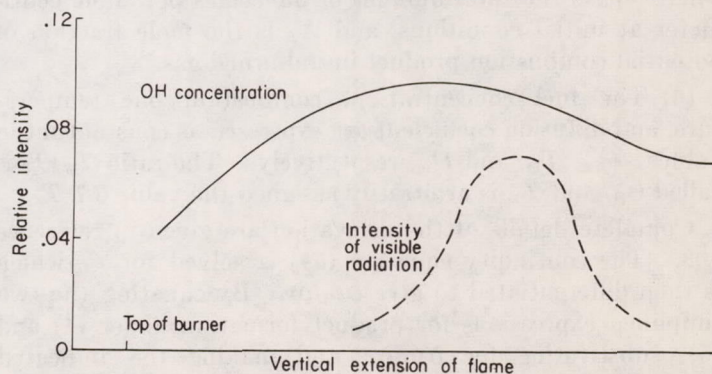
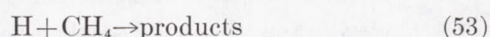


FIGURE 146.—Measured hydroxyl radical concentration in acetylene-air flame. Pressure, 66 millimeters of mercury (ref. 104).

From studies of the slow oxidation of hydrocarbons (ref. 8, pp. 94–202), it seems probable that the chemical reaction in the flame follows a chain mechanism. As previously stated, the activation energies of reactions between fuel molecules and chain carriers are low (usually 10 kcal or less, ref. 106). Hence, the assumption that the introduction of a few chain carriers into relatively cool gas could initiate the flame reaction may also be valid. The diffusion model of flame propagation thus qualitatively follows known features of the structure of the flame and the oxidation reaction. Tanford and Pease (refs. 103, 107, and 108) have derived an approximate equation for flame velocity based on the diffusion model. In addition to the assumptions listed for the comprehensive theory, the following simplifications and assumptions were made:

(1) Chain branching does not occur.

(2) The rate-controlling step (or steps) in the chemical chain reaction is the reaction of an active particle, such as the hydrogen atom, with a fuel molecule; for example,



(3) The number of active particles is calculated from the linear continuity equation

$$D_i \left(\frac{d^2 \mathcal{C}_i}{dx^2} \right) + U_F \left(\frac{d \mathcal{C}_i}{dx} \right) + I_i = 0 \quad (54)$$

where I_i is the rate of production of the active species regardless of the reaction order of process (molecules/(cm³)(sec)).

(4) The rate of formation of combustion products per unit area of flame surface can be written as the integral of a sum of a number of terms, one for each active particle:

$$\frac{d(\text{product})}{dt} = \int_{x_0}^{x_\infty} \left(\sum_i k_i \frac{d \mathcal{C}_i}{dx} \right) \mathcal{C}_i dx \quad (55)$$

where k_i is the specific rate constant for reaction between the i^{th} active species.

(5) Through each unit area of flame surface, the unburned gas is converted at the flame velocity to products of complete combustion, so that another expression for product formation is:

$$\frac{d(\text{product})}{dt} = \mathcal{C}_{t,o} X_p U_F \quad (56)$$

where $\mathcal{C}_{t,o}$ is the total number of molecules per cubic centimeter at initial conditions, and X_p is the mole fraction of potential combustion product in unburned gas.

(6) The fuel concentration, combustion-zone temperature, and diffusion coefficient are expressed as constant mean values, $\mathcal{C}_{f,m}$, T_m , and D_m , respectively. The ratio T_m/T_o is called Θ_m , and T_m is arbitrarily assigned the value $0.7 T_F$.

Complete details of the derivation are given in reference 108. The continuity equation (54) is solved for \mathcal{C}_i , which is then differentiated to give $\partial \mathcal{C}_i / \partial x$. By equating the two simplified expressions for product formation under (4) and (5), substituting for $\partial \mathcal{C}_i / \partial x$, and making the indicated

integration, there is obtained the square-root law for flame velocity:

$$U_F = \left(\frac{\mathcal{C}_{t,m} X_{f,o} \sum_i \frac{k_i X_{i,F} D_{i,m}}{B_i}}{\Theta_m^2 X_p} \right)^{1/2} \quad (57)$$

where

$X_{f,o}$ mole fraction of fuel in unburned gas

$\Theta_m = 0.7 T_F/T_o$

$X_{i,F}$ calculated mole fraction of i^{th} active species at equilibrium flame temperature T_F

$D_{i,m}$ diffusion coefficient for i^{th} species into unburned gas at mean combustion-zone temperature, cm²/sec

B_i dimensionless factor (near unity) that allows for radical recombination

Tanford and Pease have substituted $D_{i,o}$ for $D_{i,m}/\Theta_m^2$, thus assuming that the diffusion coefficient is proportional to the square of absolute temperature.

For predicting relative flame velocities of hydrocarbons, equation (57) has been modified (ref. 49) as follows: The active particles are considered to be H, OH, and O. It is assumed that D_i varies with the 1.67 power of absolute temperature and that $B_O = B_{OH} = 1$. It is further assumed that the specific rate constants k_i of equation (55) can be replaced by a weighted mean specific rate constant k_w representing all three active particles, so that

$$\sum_i \frac{k_i X_{i,F} D_{i,m}}{B_i} \cong k_w \left(\frac{X_{H,F} D_{H,o}}{B_H} + X_{OH,F} D_{OH,o} + X_{O,F} D_{O,o} \right) \Theta_m^{1.67} \quad (58)$$

where the recombination factor B_H is calculated by (ref. 108)

$$B_H = \frac{1}{2} \left[1 + \sqrt{1 + \frac{24,000 (D_{H,o} \Theta_m^{1.67})}{U_F^2 \Theta_m^4} 0.5 X_{O,o} + 3700 X_{H,F}} \right] \quad (59)$$

The required flame temperature and active-particle concentrations are calculated, assuming adiabatic thermal equilibrium, by the method of reference 109. Diffusion coefficients are computed by the Stefan-Maxwell equation (ref. 110) to be 1.78 for H, 0.28 for OH, and 0.4 for O at 298° K. The quantities $\mathcal{C}_{t,m}$, $X_{f,o}$, $X_{O_2,o}$, and X_p are calculated from a knowledge of the over-all oxidation process and the initial fuel and oxygen concentrations.

With these modifications and substitutions, equation (57) has been used in two ways with comparable success. In the first case, k_w was treated as a semiempirical constant independent of temperature; it was calculated for each flame velocity from equation (57). The average k_w for the group of data under consideration was called \bar{k}_w , and the ratio of predicted to measured flame velocity was calculated as $(\bar{k}_w/k_w)^{1/2}$. The mean deviation of this factor from unity is given in table XIX. In the second method, the Arrhenius rate expression

$$k_w = \mathcal{P}_w Z_w e^{-E_{act,w}/RT_m} \quad (60)$$

was substituted. The two unknowns \mathcal{P}_w and $E_{act,w}$ in this expression were calculated simultaneously from the flame velocity data in which the initial temperature was varied.

The resulting $\bar{E}_{act,w}$ was used for the prediction of burning velocities for the same hydrocarbon under other experimental conditions. For each set of experimental data a new $\bar{\mathcal{P}}_w$ was calculated (table XIX).

Fairly satisfactory predictions of maximum burning velocity for hydrocarbon-air mixtures in which the molecular structure (chain length, branching, saturation, etc.) of the hydrocarbon is varied may be made by either the Tanford-Pease equation (first method, \bar{k}_w independent of temperature, ref. 111) using an average empirical rate constant for all compounds except acetylene and ethene, or by a simplified form of the Semenov equation using an average steric factor and a constant activation energy of 40 kilocalories per gram-mole for all compounds except acetylene and ethene (ref. 112). Examples of these predictions are shown in the following table:

Hydrocarbon in air	Burning velocity, cm/sec		
	Measured	Calculated by Tanford-Pease eq. (ref. 111)	Calculated by Semenov eq. (ref. 112)
Methane-----	33.8	33.9	40.2
Propane-----	39.0	37.7	39.0
Hexane-----	38.5	37.3	37.2
2-Methylbutane-----	36.6	37.1	38.8
2,3-Dimethylbutane-----	36.3	37.0	39.1
2,2,3-Trimethylbutane-----	35.9	36.6	37.0
Propene-----	43.8	45.3	48.9
1-Hexene-----	42.1	41.7	42.0
2-Ethyl-1-butene-----	39.3	40.7	41.7
Propyne-----	69.9	61.3	64.9
1-Hexyne-----	48.5	48.6	46.0
Cyclohexane-----	38.7	37.4	38.3
Benzene-----	40.7	40.4	44.5

Miscellaneous approximate equations.—Other equations for burning velocity that are either based on a diffusional mechanism or include a diffusion concentration have been derived by Van Tiggelen, Gaydon and Wolfhard, and Manson. Details of these derivations and references to the original papers are given in reference 9. The final burning velocity equations are as follows:

Van Tiggelen:

$$U_F = \frac{4T_o}{\pi} \sqrt{\frac{2R(\xi - \xi')}{3MT_m}} \quad (61)$$

where M is the molecular weight of active particles, and T_m is the mean temperature of the reaction zone.

Gaydon-Wolfhard:

$$U_F = \frac{D_n T_o}{2\mathcal{F}_e T_m} \quad (62)$$

Manson:

$$U_F = \sqrt{\frac{\rho_F}{\rho_o(\rho_o - \rho_F)} \frac{pX_H T_o}{2T_F}} \quad (63)$$

where p is the pressure (dyne/cm²), and X_H is the mole fraction of hydrogen atoms in burned gas.

The Manson equation is derived from an aerodynamic

model of the combustion process (eq. (7)) and does not include chemical kinetics. The flame chemistry enters only through pX_H , which has been substituted for the flame pressure drop. It is interesting to compare flame velocities predicted by this equation with the Semenov and Tanford-Pease predictions. In reference 49, equation (63) was used to predict flame velocities in two ways: (1) An empirical proportionality factor k_H was evaluated for each set of experimental data (table XIX), or (2) the effects of all types of active particles were considered by substituting

$$X_H + X_{OH} \frac{D_{OH}}{D_H} + X_O \frac{D_O}{D_H} \quad (64)$$

for X_H in equation (63). In this case, again an average proportionality constant designated as \bar{k}_Σ was used for each set of experimental data (see table XIX).

Table XIX and the other work reported in reference 49 show that burning-velocity predictions from either form of the Manson equation are not as consistent as those from the Semenov or the Tanford-Pease equations. The average deviation of the predicted velocities from measured values is about the same for the Semenov equation and for the Tanford-Pease equation (method (2)) using an empirical activation energy.

Neither the Tanford-Pease equation nor the Semenov equation gives as good predictions of burning velocity when the empirical factor determined with one variable is used to predict the effects of other variables. When the empirical factor calculated for ethene flames from equivalence-ratio data was used in the Semenov equation to predict flame velocities over the ranges of initial temperature and oxygen concentration covered experimentally, the predicted velocities differed from the measured velocities by an average of 14 percent. The maximum deviation was 24 percent. Similarly, an average rate constant \bar{k}_w calculated from the ethene-air data over a range of concentrations used with the Tanford-Pease equation gave burning-velocity predictions for ethene-air mixtures at various initial temperatures that deviated from the measured burning velocities by -9 to 13 percent with an average deviation of 6 percent. Predicted flame velocities for various oxygen concentrations with the same \bar{k}_w differed from experimental values by 8 to 22 percent with an average deviation of 12 percent.

In conclusion, if sufficient burning-velocity data are available to evaluate the necessary empirical constants, fairly good predictions of burning velocity can be made by semitheoretical methods for hydrocarbon-oxygen-nitrogen systems in which the following are varied: (1) molecular structure of hydrocarbon, (2) equivalence ratio, (3) initial mixture temperature, or (4) the oxygen concentration in the oxygen-nitrogen part of the mixture.

Evaluation of thermal and diffusional mechanisms.—Correlations of measured burning velocities with values predicted by approximate theoretical equations or with parameters from these equations have been presented from time to time as evidence that either a thermal or a diffusional mechanism of flame propagation is operative. For example, approximate equations based on a thermal mechanism generally indicate a relation between flame velocity and thermal

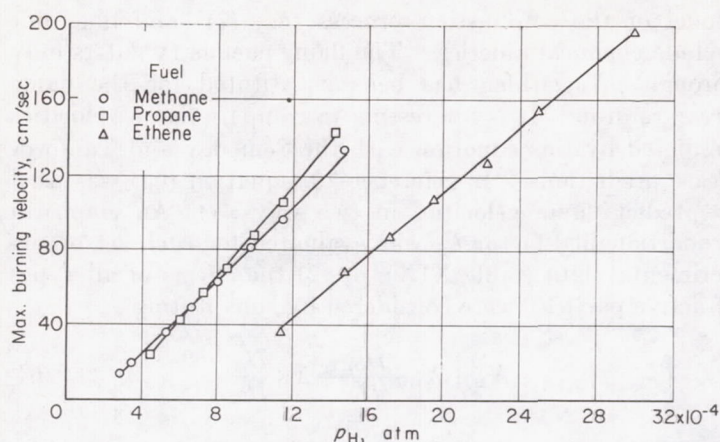


FIGURE 147.—Variation of burning velocity with hydrogen atom concentration for flames of different initial mixture temperature (ref. 16).

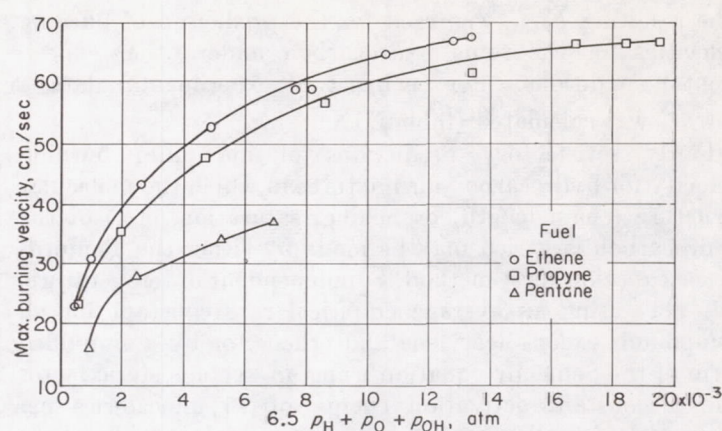


FIGURE 149.—Variation of burning velocity with relative diffusion concentration of active particles for three hydrocarbons in air for range of hydrocarbon concentrations (ref. 39).

conductivity, whereas those based on a diffusional mechanism generally indicate a relation between flame velocity and equilibrium concentrations and diffusion coefficients of the active particles. Many such correlations are reported in the literature. These include studies of the following variables: (1) mixture composition (or equivalence ratio), (2) molecular structure of the fuel, (3) initial mixture temperature, (4) pressure, (5) fuel additives, (6) isotope substitution of deuterium for hydrogen in the fuel, and (7) change of inert diluent. The correlations based on diffusional mechanisms are summarized in table XIV; references to the original papers in which these correlations were given and to figures showing representative examples (figs. 147 to 149) are also given.

The generality of the correlations between flame velocity and active-particle concentrations indicates a need for a critical study of the physical significance of the diffusion concept. Judgment or understanding of the physical significance is difficult for several reasons:

(1) Equations for heat conduction are mathematically similar to those for diffusion, so that burning-velocity equations based on either a thermal or a diffusion mechanism of flame propagation are similar in form.

(2) The calculated equilibrium concentrations of active particles depend strongly on the temperature of the flame. Moreover, these calculated concentrations may not represent the concentrations that exist in the flame.

(3) All the equations that may be used to test the experimental data are based on broad simplifying assumptions, and the validity of many of these assumptions varies for different combustion systems.

(4) The chemical kinetic factors that occur in the equations have not been independently determined (and probably will not be determined for many years).

(5) Thermal and transport properties of mixtures at high temperatures and diffusion coefficients for atoms and free radicals used in the equations are questionable.

(6) The precision of burning-velocity measurement is usually 2 to 5 percent, while the accuracy is probably much less.

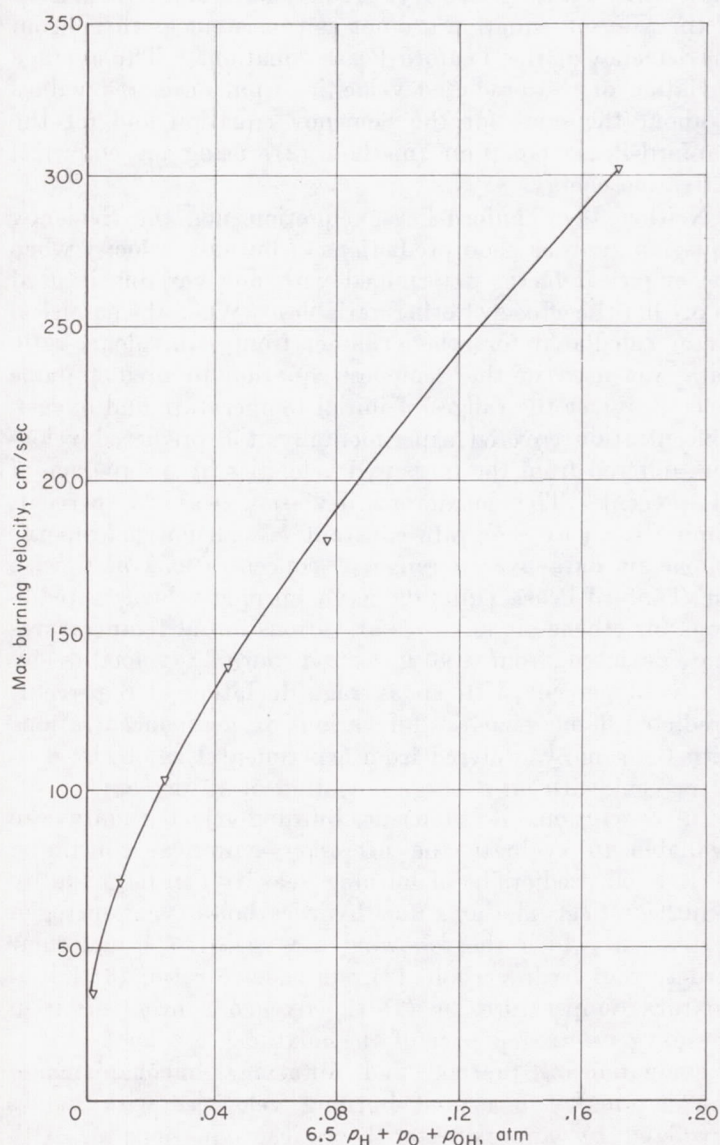


FIGURE 148.—Correlation of maximum burning velocity with relative diffusion concentration of active particles for propane-oxygen-nitrogen mixtures. Variable oxygen concentration of atmosphere (ref. 66).

Many detailed studies of various combustible systems have been published (table XIV), and experiments have been designed with the purpose of distinguishing between the two mechanisms. Two such experiments are studies of the effects on burning velocity of the change in diluent from argon to helium (e. g., ref. 113) and of substitution of a deuterated hydrocarbon for a hydrogenated one (ref. 114). In the former case the flame temperature remains essentially constant, while diffusion coefficients and thermal conductivities change. In the latter case the major change is in the most important type of chain carrier, which is usually the hydrogen atom but which, on the substitution of a deuterated compound, becomes the deuterium atom. Critical examination of all such experiments shows that diffusion effects do not give unique explanations of the experimental data; only two experimental investigations appear to favor one mechanism over the other. Both indicate that diffusion may be more important than heat conduction:

(1) Non-hydrogen-containing combustible systems to which water or hydrogen is added show increased burning velocities, while hydrogen-containing systems are not greatly affected. The increased burning velocity is explicable on the basis of free-radical diffusion. For one of the two non-hydrogen-containing systems studied (CO-O_2), the burning-velocity effect on addition of water (refs. 64 and 115) is also explicable on a conduction-mechanism basis (ref. 115). The other system ($\text{C}_2\text{N}_2\text{-O}_2\text{-A}$, ref. 116) is not so easily explained on a thermal basis.

(2) Changes in burning velocity caused by interchanging argon and helium as diluents are closer to the predictions of diffusion theories than those of thermal theories, as shown by table XXI (ref. 113). In this table, the ratio of flame velocity of a mixture containing helium to that of a mixture containing an equal volume of argon is compared with the ratio of the square roots of the thermal conductivities of these mixtures and with the ratios of the square roots of the diffusion coefficients of various active particles. The ratios of diffusion coefficients are closer to the flame velocity

ratio than is the ratio of thermal conductivity for all the fuels listed except hydrogen.

Neither of these pieces of evidence is very strong, and both are subject to criticism as to the validity of the criteria used to judge which mechanism is operative. It is probable that both heat conduction and the diffusion of atoms and free radicals contribute to the propagation of flame, and that both concepts are needed to explain flame behavior. A better understanding of the mechanism of laminar flame propagation in the future will result from the further development of the comprehensive theory and the investigation of the chemical kinetics of flames.

APPLICATION OF LAMINAR FLAME RESEARCH TO PRACTICAL COMBUSTION PROBLEMS

A high flame velocity contributes to maximum heat release per unit volume and enables an air-breathing engine to operate at high throughput rates without blowout. (It has been suggested, however, that in some cases a high flame velocity may contribute to instability in the region near a flameholder through increased shear; see ch. VI.) The chemical factors that are important in obtaining a high flame velocity are the fuel-oxygen ratio, the molecular structure of the fuel, and the mole fraction of oxygen in the air used. The only physical factor that has an established and appreciable effect on the laminar flame velocity is the initial mixture temperature. (The effects of flow parameters on turbulent flame velocity are discussed in ch. V.) The effects of these factors and of less important factors are summarized in the following paragraphs.

As the fuel-oxygen ratio is increased from the lean flammability limit, the flame velocity increases by a factor of 3 or 4 to a maximum value at a fuel-oxygen ratio that is 1.0 to 1.2 times the stoichiometric ratio and then decreases to give a rather symmetrical pattern about the maximum. This shows the importance of proper mixture preparation, as discussed in chapter I. Between the lean flammability limit and the stoichiometric mixture, the flame velocity may be related to the fraction of stoichiometric fuel-oxygen

TABLE XXI.—COMPARISONS FOR FLAMES WITH ARGON AND HELIUM AS INERT (Ref. 113)

Fuel	Fuel, percent	Inert, percent	<div>Property with He as inert</div> <div>Property with A as inert</div>				
			U_F	$\sqrt{\kappa}$	$\sqrt{D_H}$	$\sqrt{D_{OH}}$	$\sqrt{D_O}$
C_2H_2 -----	8	73	1.61	2.69	1.30	1.39	1.41
	10	71	1.54	2.67	1.28	1.38	1.39
	13	69	1.55	2.64	1.27	1.35	1.37
$\text{CO(H}_2\text{O)}$ -----	50	20	1.09	1.37	1.06	1.07	1.08
	37	40	1.28	1.95	1.13	1.15	1.18
CH_4 -----	10	71	1.39	2.65	1.29	1.39	1.41
H_2 -----	21	68	2.40	1.94	1.32	1.47	1.51
C_2H_4 -----	6	75	1.42	2.71	1.24	1.42	1.44
	7.7	73	1.43	2.70	1.23	1.40	1.43
	10	71	1.46	2.68	1.22	1.38	1.41

ratio by an equation such as

$$\frac{U_F}{U_{F,max}} = 2.6 \log \varphi + 0.94$$

which holds for ethene-, propyne-, and pentane-air mixtures. Empirical methods based on the bond dissociation energy of the fuel are reported by which $U_{F,max}$ and the corresponding φ may be predicted.

The maximum flame velocities of all hydrocarbons with air at 25° C and 1 atmosphere fall in the range 30 to 80 centimeters per second, with the exception of acetylene at 142 centimeters per second. Within this range, the following molecular structural features contribute to high flame velocity: short chain length or small cycloalkane ring size, unsaturation, and minimum chain branching. The effects of unsaturation and branching become smaller as the chain length increases. Aromatic compounds generally have flame velocities equal to or smaller than the saturated hydrocarbons (alkanes, $U_F \approx 40$ cm/sec), and chain branching has less effect on them. Alkyl oxides (e. g., propylene oxide) have higher flame velocities than their parent alkenes; aldehydes and ketones are generally intermediate between alkanes and alkenes; and alcohols and ethers are near the alkanes.

An empirical equation has been developed for the flame velocities of aliphatic hydrocarbons based on the number of various types of carbon-hydrogen bonds. The flame velocity of a mixture of hydrocarbons is related to the individual flame velocities through

$$\sum_j \frac{X_{f,j}}{X'_{f,j}} = 1$$

No additives, including antiknock compounds, have been found that will increase flame velocity beyond the mixing effect given by the preceding equation for constant-pressure combustion. Water decreases the flame velocity of hydrocarbons somewhat, but not as much as an equal quantity of nitrogen.

A factor that could enter the jet combustion picture either through deliberate oxygen enrichment (e. g., for a pilot flame) or through vitiation of the combustion air (as in tailpipe burning) is the oxygen-nitrogen ratio, or more generally, the oxygen-inert ratio. For hydrocarbon-oxygen-nitrogen mixtures, there is a linear increase in maximum flame velocity as the mole ratio $O_2/(O_2 + N_2)$ is increased from 0.15 to 0.35. Empirical equations have been presented for a number of hydrocarbons. If the nitrogen is replaced by an equal volume of carbon dioxide, argon, or helium, the flame velocity of the mixture increases in the order carbon dioxide < nitrogen < argon < helium.

The flame velocity can also be increased several times by increasing the initial mixture temperature, according to a

relation such as that for propane-air in the range 200° to 615° K:

$$U_{F,rel} = 25 + 0.00085 T_o^2$$

This shows the advantage that could be obtained with a fuel injector that would inject hot gaseous fuel into hot primary air. For the smaller temperature range 290° to 420° K (or 520° to 760° R), it appears that $U_F \propto T_o^{1.4}$ would be a reasonable assumption for many hydrocarbons, with the power increasing toward 2.0 as the high end of the temperature range is increased.

At present, it appears that pressure has a negligible effect on flame velocity; at most, $U_F \propto p^{-0.5}$. Electric fields and acoustical and mechanical disturbances also have little or no effect.

Considerable advances have been made in recent years in the theory of the propagation of a one-dimensional steady-state flame. Comprehensive equations have been presented that take into account all the chemical species involved in the flame reactions with the necessary reaction rates and diffusion rates for each species. These comprehensive equations have been solved by numerical integration for the simplest kinds of flames, but the present state of knowledge does not allow their solution for the flame velocities of complex hydrocarbon flames. Instead, various simpler, approximate equations for the laminar flame velocity have been presented. Most of these approximate equations consider flame propagation to occur through a mechanism that is based primarily on either the conduction of heat from the flame to the unburned gas (thermal mechanism) or the diffusion of active reaction centers into the unburned gas (diffusional mechanism). This chapter has shown that both types of equations, as represented by the Semenov and Tanford-Pease equations, can be used to predict, generally within 10 or 20 percent, the relative changes in flame velocity caused by changing the important chemical and physical factors.

The question is repeatedly raised whether heat conduction or active-particle diffusion is more important in laminar flame propagation. Since both types of equations usually give equally good relative predictions of flame velocity for the chemical and physical factors that are of interest to engine applications, the question remains unsolved. There are two experimental investigations, neither of which can be considered final, that appear to favor a diffusional mechanism. One shows that the addition of water or hydrogen to non-hydrogen-containing combustible mixtures increases flame velocities, while hydrogen-containing systems are not greatly affected; the other shows that changes in the flame velocity caused by interchanging argon and helium as inert diluents are closer to the predictions of diffusional equations than to those of thermal equations. It is probable that both heat conduction and active-particle diffusion contribute to the propagation of any flame; both are included in the comprehensive equations.

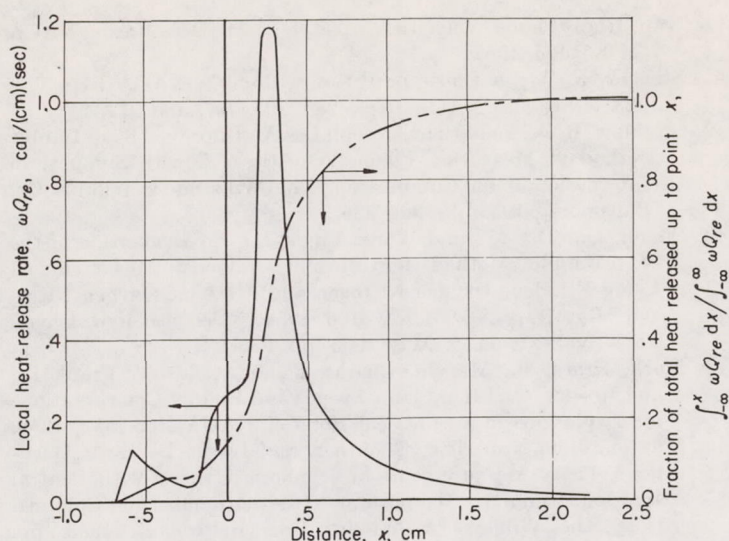


FIGURE 150.—Local and integrated heat-release rates as functions of distance through flame. Beginning of luminous zone designated by $x=0$; mass air-propane ratio, 29.2; absolute pressure, 0.0594 atmosphere; initial temperature, 46°C ; 25-centimeter flat-flame burner (reprinted by permission from ref. 6).

Another use of the equations describing laminar flame propagation and of some of the recent experimental investigations that is of interest in engine applications is the calculation of maximum heat-release rates in laminar flames. Zeldovich (ref. 51) and Avery and Hart (ref. 117) have used thermal equations to calculate heat-release rates of 10^{10} and 10^9 (Btu/(cu ft)(hr)(atm²)) for carbon monoxide and butane flames, respectively. Avery and Hart point out that a heat-release rate of approximately 10^8 (Btu/(cu ft)(hr)) has been achieved at 1 atmosphere in a ramjet engine and that this indicates the possibility that combustion rates under ramjet conditions of maximum heat release may be determined by kinetic factors rather than mixing times. Friedman and Burke (ref. 6) have used an energy equation analogous to equation (35) together with their experimental temperature profile to calculate the heat-release rate as a function of distance through a lean propane-air flame at 0.06 atmosphere, with the results shown in figure 150.

Empirical relations for the effects of such factors as the ratio $\text{O}_2/(\text{O}_2+\text{N}_2)$ and the initial temperature have already found use in correlations of engine performance. These and other correlations for engine combustion efficiency and stability that include terms for the chemical reaction rates are discussed in subsequent chapters.

REFERENCES

1. Klaukens, H., and Wolfhard, H. G.: Measurements in the Reaction Zone of a Bunsen Flame. *Proc. Roy. Soc. (London)*, vol. A193, July 21, 1948, pp. 512-524.
2. Friedman, Raymond: Measurement of the Temperature Profile in a Laminar Flame. Fourth Symposium (International) on

- Combustion, The Williams & Wilkins Co. (Baltimore), 1953, pp. 259-263.
3. Dixon-Lewis, G.: Temperature Distribution in Flame Reaction Zones. Fourth Symposium (International) on Combustion, The Williams & Wilkins Co. (Baltimore), 1953, pp. 263-267.
4. Andersen, J. W., and Fein, R. S.: Measurements of Normal Burning Velocities and Flame Temperatures in Bunsen Flames. *Jour. Chem. Phys.*, vol. 17, no. 12, Dec. 1949, pp. 1268-1273.
5. Fristrom, R. M., Prescott, R., Neumann, R. K., and Avery, W. H.: Temperature Profiles in Propane-Air Flame Fronts. Fourth Symposium (International) on Combustion, The Williams & Wilkins Co. (Baltimore), 1953, pp. 267-274.
6. Friedman, Raymond, and Burke, Edward: Measurement of Temperature Distribution in a Low-Pressure Flat Flame. *Jour. Chem. Phys.*, vol. 22, no. 5, May 1954, pp. 824-830.
7. Gerstein, Melvin, McDonald, Glen E., and Schalla, Rose L.: Decomposition Flame Studies with Ethylene Oxide. Fourth Symposium (International) on Combustion, The Williams & Wilkins Co. (Baltimore), 1953, pp. 375-383.
8. Lewis, Bernard, and von Elbe, Guenther: *Combustion, Flames and Explosions of Gases*. Academic Press, Inc., 1951.
9. Evans, Marjorie W.: Current Theoretical Concepts of Steady-State Flame Propagation. *Chem. Rev.*, vol. 51, no. 3, Dec. 1952, pp. 363-429.
10. Wohl, Kurt, Kapp, N. M., Coon, D. C., Jr., and Fulmer, R. F.: Methods of Determining Burning Velocities and Stability Measurements of Tube and Nozzle Flames. Meteor Rep. UAC-49, Res. Dept., United Aircraft Corp., Dec. 1950. (Proj. Meteor, U. S. Navy BuOrd Contract NOrd 9845 with M. I. T.)
11. Broeze, J. J.: Theories and Phenomena of Flame Propagation. Third Symposium on Combustion and Flame and Explosion Phenomena, The Williams & Wilkins Co. (Baltimore), 1949, pp. 146-155.
12. Linnett, J. W.: Methods of Measuring Burning Velocities. Fourth Symposium (International) on Combustion, The Williams & Wilkins Co. (Baltimore), 1953, pp. 20-35.
13. Guenoche, H.: Note on the Application of Optical Methods to Stationary Flames. *Rev. Inst. Francais Petrole*, vol. 6, no. 2, Feb. 1951, pp. 60-63.
14. Grove, J. R., Hoare, M. F., and Linnett, J. W.: The Shadow Cast by a Bunsen Flame, Its Production and Usefulness. *Trans. Faraday Soc. (London)*, pt. 9, vol. 46, Sept. 1950, pp. 745-755.
15. Andersen, J. W., and Fein, R. S.: Measurement and Correlation of Burning Velocities of Propane-Air Flames. Rep. CM-552, Dept. Chem., Naval Res. Lab., Univ. Wisconsin, July 20, 1949. (BuOrd Contract NOrd 9938, Task WIS-1-G.)
16. Dugger, Gordon, L.: Effect of Initial Mixture Temperature on Flame Speed of Methane-Air, Propane-Air, and Ethylene-Air Mixtures. NACA Rep. 1061, 1952. (Supersedes NACA TN's 2170 and 2374.)
17. Jost, Wilhelm: *Explosion and Combustion Processes in Gases*. McGraw-Hill Book Co., Inc., 1946.
18. Powling, J.: A New Burner Method for the Determination of Low Burning Velocities and Limits of Inflammability. *Fuel*, vol. XXVIII, no. 2, 1949, pp. 25-28.
19. Egerton, Alfred, and Sen, D.: Flame Propagation: The Influence of Pressure on the Burning Velocities of Flat Flames. Fourth Symposium (International) on Combustion, The Williams & Wilkins Co. (Baltimore), 1953, pp. 321-328.
20. Culshaw, G. W., and Garside, J. E.: A Study of Burning Velocity. Third Symposium on Combustion and Flame and Explosion Phenomena, The Williams & Wilkins Co. (Baltimore), 1949, pp. 204-209.

21. Caldwell, Frank R., Broida, Herbert P., and Dover, Jerome J.: Combustion in Bunsen Flames. *Ind. and Eng. Chem.*, vol. 43, no. 12, Dec. 1951, pp. 2731-2739.
22. Gouy, M.: Recherches Photométriques sur les Flammes Colorées. *Ann. de Chim. et de Phys.*, ser. 5, T. XVIII, 1879, pp. 5-101.
23. Smith, Francis A., and Pickering, S. F.: Measurements of Flame Velocity by a Modified Burner Method. *Res. Paper RP900*, Jour. Res. Nat. Bur. Standards, vol. 17, no. 1, July 1936, pp. 7-43.
24. Corsiglia, John: New Method for Determining Ignition Velocity of Air and Gas Mixtures. *Am. Gas Assoc. Monthly*, vol. XIII, no. 10, Oct. 1931, pp. 437-422.
25. Hahnemann, H., and Ehret, L.: Effect of Intense Sound Waves on a Stationary Gas Flame. *NACA TM 1271*, 1950.
26. Markstein, G. H.: Interaction of Flame Propagation and Flow Disturbances. *Third Symposium on Combustion and Flame and Explosion Phenomena*, The Williams & Wilkins Co. (Baltimore), 1949, pp. 162-167.
27. Calcote, Hartwell F.: Accurate Control and Vaporizing System for Small Liquid Flows. *Anal. Chem.*, vol. 22, no. 8, Aug. 1950, pp. 1058-1060.
28. Behrens, H.: Flame Instabilities and Combustion Mechanism. *Fourth Symposium (International) on Combustion*, The Williams & Wilkins Co. (Baltimore), 1953, pp. 538-545.
29. Garside, J. E., and Jackson, B.: The Formation and Some Properties of Polyhedral Burner Flames. *Fourth Symposium (International) on Combustion*, The Williams & Wilkins Co. (Baltimore), 1953, pp. 545-552.
30. Kurz, Philip F.: Flame Stability on Bunsen-Smithells Burners. *Tech. Rep. 15036-17*, Battelle Memorial Inst., Feb. 1953. (Contract AF 33(038)-12656, E.O. No. 460-35, S.R.-8.)
31. Ball, George A.: Combustion Aerodynamics—A Study of a Two-Dimensional Flame. *Dept. Eng. Sci. and Appl. Phys.*, Harvard Univ., July 1951. (Army Ord. Dept. Contract No. W19-020-ORD-6509.)
32. Fabri, J., Siestrunk, R., and Fouré, C.: On the Aerodynamic Field of Stabilized Flames. *Fourth Symposium (International) on Combustion*, The Williams & Wilkins Co. (Baltimore), 1953, pp. 443-450.
33. Singer, J. M.: Burning-Velocity Measurements on Slot Burners; Comparison with Cylindrical Burner Determinations. *Fourth Symposium (International) on Combustion*, The Williams & Wilkins Co. (Baltimore), 1953, pp. 352-358.
34. Morrison, R. B., and Dunlap, R. A.: Measurement of Flame Speeds with the V-Flame. *Rep. UMM-21*, Aero. Res. Center, Eng. Res. Inst., Univ. Mich., May 1948. (AAF Contract W33-038 ac 14222, Proj. MX-794.)
35. Pilcher, J. M., Miesse, C. C., Jensen, R. A., and Terrill, F. B.: Study of Flame Speeds. *Thirty-Sixth Prog. Rep. to Hdq.*, AMC, Battelle Memorial Inst., Mar. 2-May 1, 1950. (Contract AF 33 (038)-2038.)
36. Gross, Robert A.: Aerodynamics of a Two-Dimensional Flame. *Combustion Tunnel Lab. Interim Tech. Rep. No. 2*, Div. Appl. Sci., Harvard Univ., June 1952. (Contract No. DA-19-020-ORD-1029, Army Ord. Dept.)
37. Culshaw, G. W., and Garside, J. E.: Recent Studies of Aerated Burner Flames. *Inst. Gas. Eng. Inst. (London) Gas Res. Fellowship Rep.*, 1946-1947. (Reviews papers from period 1943-1946, including those of Delbourg, Heiligenstaedt, and Vasilescu.)
38. Gerstein, Melvin, Levine, Oscar, and Wong, Edgar L.: Fundamental Flame Velocities of Pure Hydrocarbons. I—Alkanes, Alkenes, Alkynes, Benzene, and Cyclohexane. *NACA RM E50G24*, 1950. (See also *Jour. Am. Chem. Soc.*, vol. 73, no. 1, Jan. 1951, pp. 418-422.)
39. Simon, Dorothy M., and Wong, Edgar L.: Flame Velocities over a Wide Composition Range for Pentane-Air, Ethylene-Air, and Propyne-Air Flames. *NACA RM E51H09*, 1951.
40. Levine, Oscar, and Gerstein, Melvin: Fundamental Flame Velocities of Pure Hydrocarbons. III—Extension of Tube Method to High Flame Velocities—Acetylene-Air Mixtures. *NACA RM E51J05*, 1951.
41. Stevens, F. W.: A Constant Pressure Bomb. *NACA Rep. 176* 1923. (See also *NACA Reps.* 280, 305, 337, and 372.)
42. Strehlow, R. A., and Stuart, Joseph G.: An Improved Soap Bubble Method of Measuring Flame Velocities. *Fourth Symposium (International) on Combustion*, The Williams & Wilkins Co. (Baltimore), 1953, pp. 329-336.
43. Simon, Dorothy M., and Wong, Edgar L.: An Evaluation of the Soap-Bubble Method for Burning Velocity Measurements Using Ethylene-Oxygen-Nitrogen and Methane-Oxygen-Nitrogen Mixtures. *NACA TN 3106*, 1954. (See also *Jour. Chem. Phys.*, vol. 21, no. 5, May 1953, pp. 936-937.)
44. Fiock, Ernest F., Marvin, Charles F., Jr., Caldwell, Frank R., and Roeder, Carl H.: Flame Speeds and Energy Considerations for Explosions in a Spherical Bomb. *NACA Rep. 682*, 1940.
45. Manton, John, von Elbe, Guenther, and Lewis, Bernard: Burning-Velocity Measurements in a Spherical Vessel with Central Ignition. *Fourth Symposium (International) on Combustion*, The Williams & Wilkins Co. (Baltimore), 1953, pp. 358-363.
46. Gerstein, Melvin, Levine, Oscar, and Wong, Edgar L.: Fundamental Flame Velocities of Hydrocarbons. *Ind. and Eng. Chem.*, vol. 43, no. 12, Dec. 1951, pp. 2770-2772.
47. Calcote, Hartwell F., Barnett, Charles M., and Irby, Moreland R.: The Burning Velocity of Various Compounds by the Bunsen Burner Method. Paper presented at meeting Am. Chem. Soc., Atlantic City (N. J.), Sept. 18-23, 1949. (See *Abs. of Papers*, 116th meeting Am. Chem. Soc., p. 38P.)
48. Dugger, Gordon L., and Graab, Dorothy D.: Flame Velocities of Propane- and Ethylene-Oxygen-Nitrogen Mixtures. *NACA RM E52J24*, 1953.
49. Dugger, Gordon L., and Simon, Dorothy M.: Prediction of Flame Velocities of Hydrocarbon Flames. *NACA Rep. 1158*, 1954. (Supersedes *NACA RM E52J13*.) (See also *Fourth Symposium (International) on Combustion*, The Williams & Wilkins Co., 1953, pp. 336-345.)
50. Nicol, D. L., Fedde, P., Katz, S., and Linden, H. R.: Study of Fundamentals of Combustion. *Rep. No. 2*, Inst. Gas Tech. Center (Chicago), Jan. 1951. (Contract N-onr-04100, Office Naval Res., Dept. Navy.) (See also other reps. same series, same title, including: Nicol, D. L., Flanagan, O., and Shomaker, J., *Rep. No. 3*, May 1952; Searight, E. F., Sickafoose, R. D., Nicol, D. L., and Peck, R. E., *Rep. No. 5*, Mar. 1952.)
51. Zeldovich, Y. B.: Theory of Combustion and Detonation of Gases. *Tech. Rep. F-TS-1226-IA* (GDAM A9-T-45), Air Materiel Command, 1949. (Trans. by Brown Univ.)
52. Wagner, Paul, and Dugger, Gordon L.: Flame Propagation. V. Structural Influences on Burning Velocity. Comparison of Measured and Calculated Burning Velocity. *Jour. Am. Chem. Soc.*, vol. 77, no. 1, Jan. 5, 1955, pp. 227-231.
53. Hibbard, R. R., and Pinkel, B.: Flame Propagation. IV. Correlation of Maximum Fundamental Flame Velocity with Hydrocarbon Structure. *Jour. Am. Chem. Soc.*, vol. 73, no. 4, Apr. 1951, pp. 1622-1625.
54. Leason, D. B.: The Effect of Organic Additions on Ignition Velocity. Pt. I—Review of Previous Work and the Effect on Rich Town Gas-Air Mixtures. *Rep. E. 62*, Div. Aero., Australian Council Sci. and Ind. Res. (Melbourne), Nov. 1948.
55. Leason, D. B.: The Effect of Gaseous Additions on the Burning Velocity of Propane-Air Mixtures. *Fourth Symposium (International) on Combustion*, The Williams & Wilkins Co. (Baltimore), 1953, pp. 369-375.
56. Smittenberg, J., and Kooijman, P. L.: Tentative Investigation into the Influence of Tetra-Ethyl-Lead on the Flame Velocity in Hydrocarbon-Air Mixtures, Ignited by Electric Sparks. *Rec. des Travaux Chim. des Pays-Bas*, T. 59, 1940, pp. 591-600.
57. Egerton, A. C.: General Statement as to Existing Knowledge on Knocking and Its Prevention. *The Sci. of Petroleum*, Oxford Univ. Press, 1938, p. 2924.

58. Sachsse, H., und Bartholome, E : Beiträge zur Frage der Flammgeschwindigkeit. *Zs. f. Elektrochemie*, Bd. 53, Heft 4, Aug. 1949, pp. 183-190.
59. Ubbelohde, L., und Hofsass, M : Über die Entzündungsgeschwindigkeit im Innenkegel der Bunsenflamme. *Jour. Gasbel.*, Jahrg. 56, Nr. 51, Dec. 20, 1913, pp. 1253-1262.
60. Walker, P. L., Jr., and Wright, C. C : Stability and Burning Velocity of Bunsen Flames with Propane-Carbon Monoxide Mixtures. *Fuel*, vol. XXXI, no. 1, Jan. 1952, pp. 45-49.
61. Payman, W : The Propagation of Flame in Complex Gaseous Mixtures. *Jour. Chem. Soc.*, vol. 115, Dec. 1919, pp. 1436-1462.
62. Kurz, Philip F : Influence of Hydrogen Sulfide on Flame Speed of Propane-Air Mixtures. *Ind. and Eng. Chem.*, vol. 45, no. 10, Oct. 1953, pp. 2361-2366.
63. Fiock, Ernest F., and King, H. Kendall: The Effect of Water Vapor on Flame Velocity in Equivalent CO-O₂ Mixtures. *NACA Rep.* 531, 1935.
64. McDonald, Glen E : Measurement of Uniform Flame Movement in Carbon Monoxide-Air Mixtures Containing Either Added D₂O or H₂O. *NACA RM E50C10*, 1950.
65. Kapp, N. M., Snow, B., and Wohl, K : The Effect of Water Vapor on the Normal Burning Velocity and on the Stability of Butane-Air Flames Burning Above Tubes in Free Air. *Meteor Rep. UAC-30*, Res. Dept., United Aircraft Corp., Nov. 1948. (U. S. Navy, Bur. Ord. Contract NOrd 9845 with M. I. T.)
66. Dugger, Gordon L., and Grabb, Dorothy D.: Flame Velocities of Hydrocarbon-Oxygen-Nitrogen Mixtures. Fourth Symposium (International) on Combustion, The Williams & Wilkins Co. (Baltimore), 1953, pp. 302-310. (See also NACA TN 2680 and NACA RM E52J24.)
67. Clingman, William H., Brokaw, Richard S., and Pease, Robert N.: Burning Velocities of Methane with Nitrogen-Oxygen, Argon-Oxygen, and Helium-Oxygen Mixtures. Fourth Symposium (International) on Combustion, The Williams & Wilkins Co. (Baltimore), 1953, pp. 310-313.
68. Coward, H. F., and Payman, W : Problems in Flame Propagation. *Chem. Rev.*, vol. 21, no. 3, Dec. 1937, pp. 359-366.
69. Caldwell, F. R., Ruegg, F. W., and Olsen, L. O : Seventy-Second Report of Progress on the Combustion Chamber Research Program for the Quarter ending Dec. 31, 1951. *Rep. 1B111*, U. S. Dept. Commerce, Nat. Bur. Standards, Jan. 30, 1952.
70. Mellish, C. E., and Linnett, J. W.: The Influence of Inert Gases on Some Flame Phenomena. Fourth Symposium (International) on Combustion, The Williams & Wilkins Co. (Baltimore), 1953, pp. 407-420.
71. Badin, Elmer J., Stuart, Joseph G., and Pease, Robert N : Burning Velocities of Butadiene-1,3 with Nitrogen-Oxygen and Helium-Oxygen Mixtures. *Jour. Chem. Phys.*, vol. 17, no. 3, Mar. 1949, pp. 314-316.
72. Friedman, Raymond: The Quenching of Laminar Oxyhydrogen Flames by Solid Surfaces. Third Symposium on Combustion and Flame and Explosion Phenomena, The Williams & Wilkins Co. (Baltimore), 1949, pp. 110-120.
73. Johnston, W. C : Measured Flame Velocity of Fuels at Low Pressures. *SAE Jour.*, vol. 55, no. 12, Dec. 1947, pp. 62-65.
74. Lewis, Bernard, et al : Research of Flame and Ignition Phenomena. Semi-Annual Prog. Rep., James Forrestal Res. Center, Princeton Univ., Apr. 1, 1953, pp. 81-91. (Office Naval Res. Contract N6-ori-105, Task Order 111, NR-098-038.)
75. Wolfhard, H. G.: Die Eigenschaften stationärer Flammen im Unterdruck. *Zs. f. Tech. Phys.*, Nr. 9, 1943, pp. 206-211.
76. Pickering, H. S., and Linnett, J. W : Burning Velocity Determinations. VII—The Burning Velocities of Some Ethylene+Oxygen+Nitrogen Mixtures. *Trans. Faraday Soc.*, vol. 47, pt. 10, Oct. 1951, pp. 1101-1103; discussion, pp. 1104-1106.
77. Cullen, R. E : A Non-Dimensional Correlation of Flame Propagation at Subatmospheric Pressures. *Trans. ASME*, vol. 75, no. 1, Jan. 1953, pp. 43-49.
78. Wohl, Kurt, and Kapp, Numer M : Flame Stability at Variable Pressures. *Meteor Rep. UAC-42*, Res. Dept., United Aircraft Corp., Oct. 1949. (Proj. METEOR, Bur. Ord. Contract NOrd 9845 with M. I. T.)
79. Ribaud, G., and Gaudry, H : Effect of Pressure on the Speed of Propagation of Flame at Constant Speed and under Constant Pressure in Various Combustible Gas Mixtures (Propane, Benzene, and City Gas). *Tech. Phys., USSR*, vol. 3, no. 11, 1936, pp. 18-23.
80. Garner, F. H., Ashforth, G. K., and Long, R : The Effect of Pressure on Burning Velocities of Benzene-Air, *n*-Heptane-Air and 2,2,4-Trimethylpentane-Air Mixtures. *Fuel*, vol. XXX, no. 1, Jan. 1951, pp. 17-19.
81. Linnett, J. W., and Wheatley, P. T : Effect of Pressure on Velocity of Burning. *Nature*, vol. 164, no. 4166, Sept. 3, 1949, pp. 403-404.
82. Albright, R. E., Heath, D. P., and Thena, R. H.: Flame Velocities of Liquid Hydrocarbons. *Ind. and Eng. Chem.*, vol. 44, no. 10, Oct. 1952, pp. 2490-2496.
83. Ubbelohde, L., und Dommer, O : Zur Kenntnis der Verbrennung im Innenkegel der Bunsenflamme. *Jour. Gasbel*, Jahrg. 57, Nr. 31, Aug. 1914, pp. 757-765; 781-787; 805-810.
84. Passauer, H. Eisenstein: Verbrennungsgeschwindigkeit und Verbrennungstemperatur bei Vorwärmung von Gas und Luft. *Das Gas- und Wasserfach*, Jahrg. 73, Heft 17, Apr. 26, 1930, pp. 393-397.
85. Dugger, Gordon L : Effect of Initial Mixture Temperature on Flame Speed of Methane-Air, Propane-Air, and Ethylene-Air Mixtures. *NACA Rep.* 1061, 1952. (Supersedes NACA TN's 2170 and 2374.)
86. Sachsse, Hans: Über die Temperaturabhängigkeit der Flammgeschwindigkeit und das Temperaturgefälle in der Flammenfront. *Zs. f. Phys. Chem.*, Bd. 180, Heft 4, Abt. A, Oct. 1935, pp. 305-313.
87. Dugger, Gordon L., Weast, Robert C., and Heimel, Sheldon: Flame Velocity and Preflame Reaction in Heated Propane-Air Mixtures. *Ind. and Eng. Chem.*, vol. 47, no. 1, Jan. 1955, pp. 114-116.
88. Tamman, G., and Thiele, H : Speeds of Combustion in Gas Mixtures. *Zs. anorg. all gem. Chem.*, vol. 192, 1930, pp. 65-89.
89. Polanyi, M. L., and Markstein, G. H.: Phenomena in Electrically and Acoustically Disturbed Bunsen Burner Flames. *Tech. Rep. No. 5*, Proj. Squid, Aero Lab., Cornell Univ., Sept. 15, 1947.
90. Calcote, Hartwell F : Electrical Properties of Flames. Burner Flames in Transverse Electric Fields. Third Symposium on Combustion and Flame and Explosion Phenomena, The Williams & Wilkins Co. (Baltimore), 1949, pp. 245-253.
91. Loshaek, Sam, Fein, R. S., and Olsen, H. L : The Effect of Sound on the Normal Velocity and Stability Limits of Laminar Propane-Air Flames. *Rep. CM-553*, Dept. Chem., Naval Res. Lab., Univ. Wisconsin, July 9, 1949. (Navy BuOrd Contract NOrd 9938.)
92. Kaskan, W. E : An Investigation of Vibrating Flames. Fourth Symposium (International) on Combustion, The Williams & Wilkins Co. (Baltimore), 1953, pp. 575-591.
93. Hirschfelder, J. O., Curtiss, C. F., and Campbell, Dorothy E.: The Theory of Flames and Detonations. Fourth Symposium (International) on Combustion, The Williams & Wilkins Co. (Baltimore), 1953, pp. 190-211.
94. Hirschfelder, J. O., and Curtiss, C. F : Theory of Propagation of Flames. Pt. 1—General Equations. Third Symposium on Combustion and Flame and Explosion Phenomena, The Williams & Wilkins Co. (Baltimore), 1949, pp. 121-127.
95. Semenov, N. N : Thermal Theory of Combustion and Explosion. III—Theory of Normal Flame Propagation. *NACA TM* 1026, 1942.
96. Hirschfelder, J. O., Bird, R. B., and Spotz, Ellen L : Viscosity and Other Physical Properties of Gases and Gas Mixtures. *Trans. ASME*, vol. 21, no. 8, Nov. 1949, pp. 921-937.

97. Rossini, Frederick D., et al: Selected Values of Properties of Hydrocarbons. Circular 461, Nat. Bur. Standards, Nov. 1947.
98. Bromley, L. A., and Wilke, C. R.: Viscosity Behavior of Gases. *Ind. and Eng. Chem.*, vol. 43, no. 7, July 1951, pp. 1641-1648.
99. Chamberlain, G. H. N., et Walsh, A. D.: L'oxydation lente de l'éther diisopropylique dans l'intervalle de températures 360°-460° C. *Revue de L'Institut Français du Pétrole et Annales des Combustibles Liquides*, T. IV, Nr. 7, July 1949, pp. 301-313; discussion, pp. 314-318.
100. Linnett, J. W., and Hoare, M. F.: Burning Velocities in Ethylene-Air-Nitrogen Mixtures. Third Symposium on Combustion and Flame and Explosion Phenomena, The Williams & Wilkins Co. (Baltimore), 1949, pp. 195-204.
101. McAdams, William H.: Heat Transmission. Second ed., McGraw-Hill Book Co., Inc., 1942, pp. 391-411.
102. Tanford, Charles, and Pease, Robert N.: Equilibrium Atom and Free Radical Concentrations in Carbon Monoxide Flames and Correlation with Burning Velocities. *Jour. Chem. Phys.*, vol. 15, no. 7, July 1947, pp. 431-433.
103. Tanford, Charles: The Role of Free Atoms and Radicals in Burner Flames. Third Symposium on Combustion and Flame and Explosion Phenomena, The Williams & Wilkins Co. (Baltimore), 1949, pp. 140-146.
104. Gaydon, A. G., and Wolfhard, H. G.: Spectroscopic Studies of Low Pressure Flames; Temperature Measurements in Acetylene Flames. *Proc. Roy. Soc. (London)*, ser. A, vol. 194, no. A1037, Aug. 12, 1948, pp. 169-184.
105. Gaydon, A. G., and Wolfhard, H. G.: The Influence of Diffusion on Flame Propagation. *Proc. Roy. Soc. (London)*, ser. A, vol. 196, 1949, pp. 105-113.
106. Steacie, E. W. R.: Atomic and Free Radical Reactions. Reinhold Pub. Co., 1946.
107. Tanford, Charles, and Pease, Robert N.: Theory of Burning Velocity. II—The Square Root Law for Burning Velocity. *Jour. Chem. Phys.*, vol. 15, no. 12, Dec. 1947, pp. 861-865.
108. Tanford, Charles: Theory of Burning Velocity. I—Temperature and Free Radical Concentrations Near the Flame Front, Relative Importance of Heat Conduction and Diffusion. *Jour. Chem. Phys.*, vol. 15, no. 7, July 1947, pp. 433-439.
109. Huff, Vearl N., Gordon, Sanford, and Morrell, Virginia E.: General Method and Thermodynamic Tables for Computation of Equilibrium Composition and Temperature of Chemical Reactions. NACA Rep. 1037, 1951. (Supersedes NACA TN's 2113 and 2161.)
110. Jeans, James: An Introduction to the Kinetic Theory of Gases. Cambridge Univ. Press (London), 1940, p. 207.
111. Simon, Dorothy Martin: Flame Propagation—Active Particle Diffusion Theory. *Ind. and Eng. Chem.*, vol. 43, no. 12, Dec. 1951, pp. 2718-2721.
112. Walker, P. L., Jr., and Wright, C. C.: Hydrocarbon Burning Velocities Predicted by Thermal Versus Diffusional Mechanisms. *Jour. Am. Chem. Soc.*, vol. 74, no. 15, Aug. 5, 1952, pp. 3769-3771.
113. Mellish, C. E., and Linnett, J. W.: The Influence of Inert Gases on Some Flame Phenomena. Fourth Symposium (International) on Combustion, The Williams & Wilkins Co. (Baltimore), 1953, pp. 407-420.
114. Friedman, Raymond, and Burke, Edward: Burning Velocities—Acetylene and Dideuteroacetylene with Air. *Ind. and Eng. Chem.*, vol. 43, no. 12, Dec. 1951, pp. 2772-2776.
115. Hoare, M. F., and Linnett, J. W.: The Mechanism of Flame Propagation. *Jour. Chem. Phys.*, vol. 16, no. 8, Aug. 1948, pp. 747-749.
116. Brokaw, Richard S., and Pease, Robert N.: The Effect of Water on the Burning Velocities of Cyanogen-Oxygen-Argon Mixtures. *Jour. Am. Chem. Soc.*, vol. 75, no. 6, Mar. 20, 1953, pp. 1454-1457.
117. Avery, W. H., and Hart, R. W.: Combustor Performance with Instantaneous Mixing. *Ind. and Eng. Chem.*, vol. 45, no. 8, Aug. 1953, pp. 1634-1637.
118. Harris, Margaret E., Grumer, Joseph, von Elbe, Guenther, and Lewis, Bernard: Burning Velocities, Quenching, and Stability Data on Nonturbulent Flames of Methane and Propane with Oxygen and Nitrogen—Applications of Theory of Ignition, Quenching, and Stabilization to Flames of Propane and Air. Third Symposium on Combustion and Flame and Explosion Phenomena, The Williams & Wilkins Co. (Baltimore), 1949, pp. 80-89.
119. Linnett, J. W.: Methods of Measuring Burning Velocities. Fourth Symposium (International) on Combustion, The Williams & Wilkins Co. (Baltimore), 1953, pp. 20-35.
120. Bartholomé, E.: Die Flammengeschwindigkeit in stationär brennenden Flammen. *Die Naturwissenschaften*, Jahrg. 36, Heft 6, 1949, pp. 171-175.
121. Bartholomé, E.: Die Flammengeschwindigkeit in sehr heißen Flammen. *Zs. f. Elektrochemie*, Bd. 54, Heft 3, 1950, p. 169.
122. Sachsse, H., und Bartholomé, E.: Beiträge zur Frage der Flammengeschwindigkeit. *Zs. f. Elektrochemie*, Bd. 53, Heft 4, 1949, pp. 183-190.
123. Simon, Dorothy Martin: Flame Propagation. III. Theoretical Consideration of the Burning Velocities of Hydrocarbons. *Jour. Am. Chem. Soc.*, vol. 73, no. 1, Jan. 1951, pp. 422-425.
124. Walker, P. L., Jr., and Wright, C. C.: Prediction of Hydrocarbon Burning Velocities by Modified Semenov Equation. *Jour. Am. Chem. Soc.*, vol. 75, no. 5, Feb. 5, 1953, pp. 750-751.
125. Gaydon, A. G., and Wolfhard, H. G.: Low-Pressure Flames and Flame Propagation. *Fuel*, vol. XXIX, no. 1, Jan. 1950, pp. 15-19.
126. Manson, N.: Effect of Pressure on the Fundamental Burning Velocity in Gaseous Mixtures. *Fuel*, vol. XXXII, 1953, pp. 186-195.
127. Wheatley, P. J., and Linnett, J. W.: Burning Velocity Determinations. Pt. 8 — Some Acetylene + Oxygen + Inert Gas Mixtures. *Trans. Faraday Soc.*, vol. 48, 1952, pp. 338-345.
128. Manson, N.: On the Theory of Burning Velocities in Gas Mixtures. *Jour. Chem. Phys.*, vol. 17, no. 9, Sept. 1949, pp. 837-838.

CHAPTER V

TURBULENT FLAMES

By MELVIN GERSTEIN and GORDON L. DUGGER

INTRODUCTION

The previous chapter is concerned with laminar flames in which a smooth, discrete flame zone exists. Such smooth flames (e. g., fig. 128) occur when the unburned-gas flow is laminar and undisturbed (ref. 1). Small flow disturbances may distort the flame surface (ref. 2) and influence the rate of flame propagation somewhat, but the discrete reaction zone remains. If, however, the unburned-gas flow is made turbulent, a diffuse, brushy flame results, and the rate at which the combustible mixture is consumed increases greatly. The turbulent flame, unlike the laminar one, is often accompanied by noise and rapid fluctuations of the flame envelope.

For the laminar flame, it is possible to define a flame velocity that, within reasonable limits, is independent of the experimental apparatus. It would be equally desirable to define a propagation velocity for turbulent flames that would be independent of the experimental apparatus and depend only on the fuel-air mixture and some easily identified properties of the flow. This is not yet possible, however, and the numerical values of turbulent propagation velocities depend not only on the experimental technique but also on the concept of turbulent flames assumed by the investigator. Similarly, the theoretical concepts of turbulent flames are not so well defined as laminar flame theories. These points should be kept in mind during consideration of this chapter, in which the current status of knowledge in the field of turbulent flame propagation is discussed.

SYMBOLS

The following symbols are used in this chapter:

A	cross-sectional area
a	constant
B	constant
b	height
c_p	specific heat at constant pressure
d	diameter
E	energy
\mathcal{F}	function
$\Delta H_{f,a}$	heating value per unit volume of fuel-air mixture
K	constant
\mathcal{K}	constant
\mathcal{L}	scale of turbulence
p	pressure
ΔQ_{sp}	space heating rate
Re	Reynolds number
\mathcal{R}	correlation factor

r	radius
S	surface area
T	temperature
\mathcal{T}_F	flame thickness
t	time
U	velocity
$U'_{F,T}$	turbulent component of turbulent flame velocity
u_x	fluctuating velocity in x -direction
$\sqrt{\overline{u_x^2}}$	intensity of turbulence
u_y	fluctuating velocity in y -direction
V	volume
V_{fl}	volume flow rate
\mathcal{V}	$V_{fl,o}/V_F$
$W_{dt/2}$	duct half-width
$W_{F/2}$	flame half-width
w	mass-flow rate
x	longitudinal distance
\bar{Y}	mean displacement
y	distance perpendicular to x
ϵ	eddy diffusivity
ι	fraction of fuel
κ	thermal conductivity
ν	kinematic viscosity
ρ	density
φ	equivalence ratio
ω	chemical reaction rate

Subscripts:

av	average
bg	burned gas
c	cone
Eu	Eulerian
F	flame
L	laminar
La	Lagrangian
m	mean
max	maximum
o	initial conditions
P	perturbation
p	port
re	reaction
T	turbulent
t	total
$tube$	tube
un	unburned gas
y	perpendicular to x -direction
ϵ	eddy
3	inflection point

CHARACTERISTICS OF TURBULENT FLAMES

The nature of turbulent flames has been studied by the photographic techniques developed for laminar flames (ch. IV). Unlike the laminar flame, however, the flame surface is very complex, and it is difficult to locate the various surfaces that are used to characterize laminar flames. The characteristics of some turbulent flames are described briefly in the following sections.

BUNSEN FLAMES

The turbulent Bunsen flame has probably received the most attention. Laminar and turbulent Bunsen flames are shown in figure 151, which compares time exposures of the luminous zones of a laminar and a turbulent flame. The diffuse appearance of the time exposure of the luminous turbulent flame zone is due to the rapid oscillations of a wrinkled flame front, which can be seen in instantaneous schlieren photographs (ref. 1). Superposition of the schlieren photograph on the luminous photograph shows that the random fluctuations of the instantaneous flame front are contained within the luminous envelope (ref. 1, p. 481).

Flame height.—As long as the approach flow of unburned gas toward an open flame remains laminar, an increase in the average stream velocity is maintained according to equation (1) of chapter IV. The cone height increases correspondingly, and for a perfectly conical flame the relation between cone height and average stream velocity is given

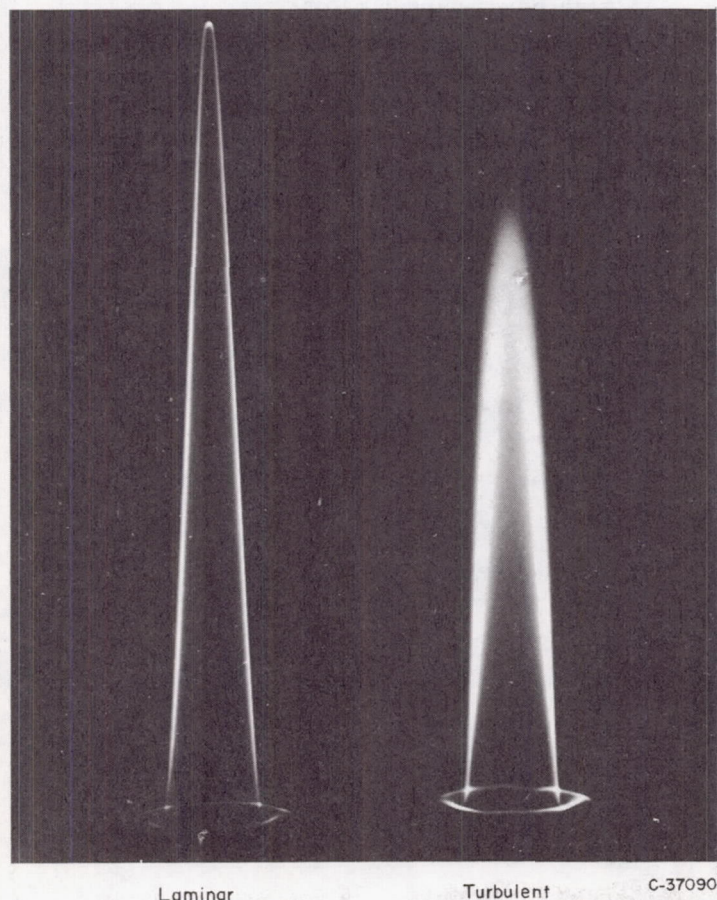


FIGURE 151.—Comparison of direct photographs of laminar and turbulent flames at same flow rate, fuel-air ratio, and burner size.

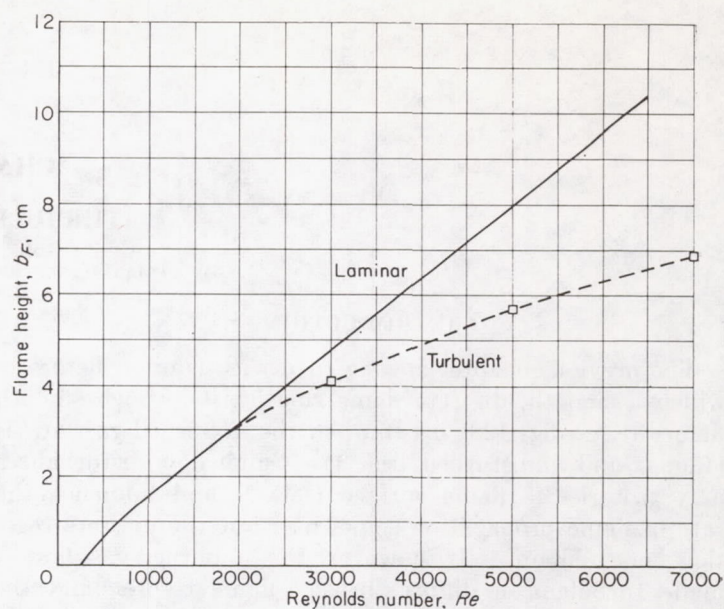


FIGURE 152.—Effect of Reynolds number of approach flow on cone heights of laminar and turbulent flames.

by the solid line in figure 152. When the flow becomes turbulent, however, the flame becomes turbulent and the mean flame height (fig. 153) no longer increases in the same manner; greater quantities of fuel-air mixture are consumed in a turbulent flame than would be consumed in a laminar flame of the same height. The dashed curve in figure 152 represents the mean flame heights measured (ref. 3) for turbulent flames burning under conditions comparable with those used to calculate the laminar curve except for the nature of the flow. The variation of the mean flame height with flow velocity and tube diameter for three fuels (propane, ethene, and acetylene) is shown in figure 154 (from ref. 3).

Shore (ref. 4) has measured the height of butane-air flames on a 1-inch burner. The variation of flame height with velocity is as follows:

Velocity, U_o , cm/sec	Flame height, b_F , cm	
	$\phi = 1.00$	$\phi = 1.26$
540-----	8.7	7.5
1500-----	16.8	13.4

The flame heights for an equivalence ratio ϕ of 1.26, which is near ϕ for maximum flame velocity, agree well with the data in figure 154 for propane. For a given velocity, the effect of intensity of turbulence $\sqrt{u_z^2}$ on flame height is as follows (ref. 4):

Velocity, U_o , cm/sec	$\sqrt{u_z^2}/U_o$	$\sqrt{u_z^2}$	Flame height, b_F , cm	
			$\phi = 1.00$	$\phi = 1.26$
540-----	0.008	4.32	14.7	11.2
	^a 0.04	21.6	8.7	7.5
	.075	40.5	7.5	5.9
1500-----	^a 0.04	60.0	16.8	13.4

^a From ref. 5.

For a given burner diameter, the flame height increases with velocity; at a given velocity the flame height decreases as intensity of turbulence increases. At higher velocities a greater mass of fuel is consumed. The ratio b_F/U_o , then, is proportional to the flame height per unit mass flow for a given burner. A plot of b_F/U_o against $\sqrt{u_x^2}$ (fig. 155) shows that the height per unit mass flow decreases regularly with increase in the intensity of turbulence. In other words, more heat is released in a given length as the intensity of turbulence is increased.

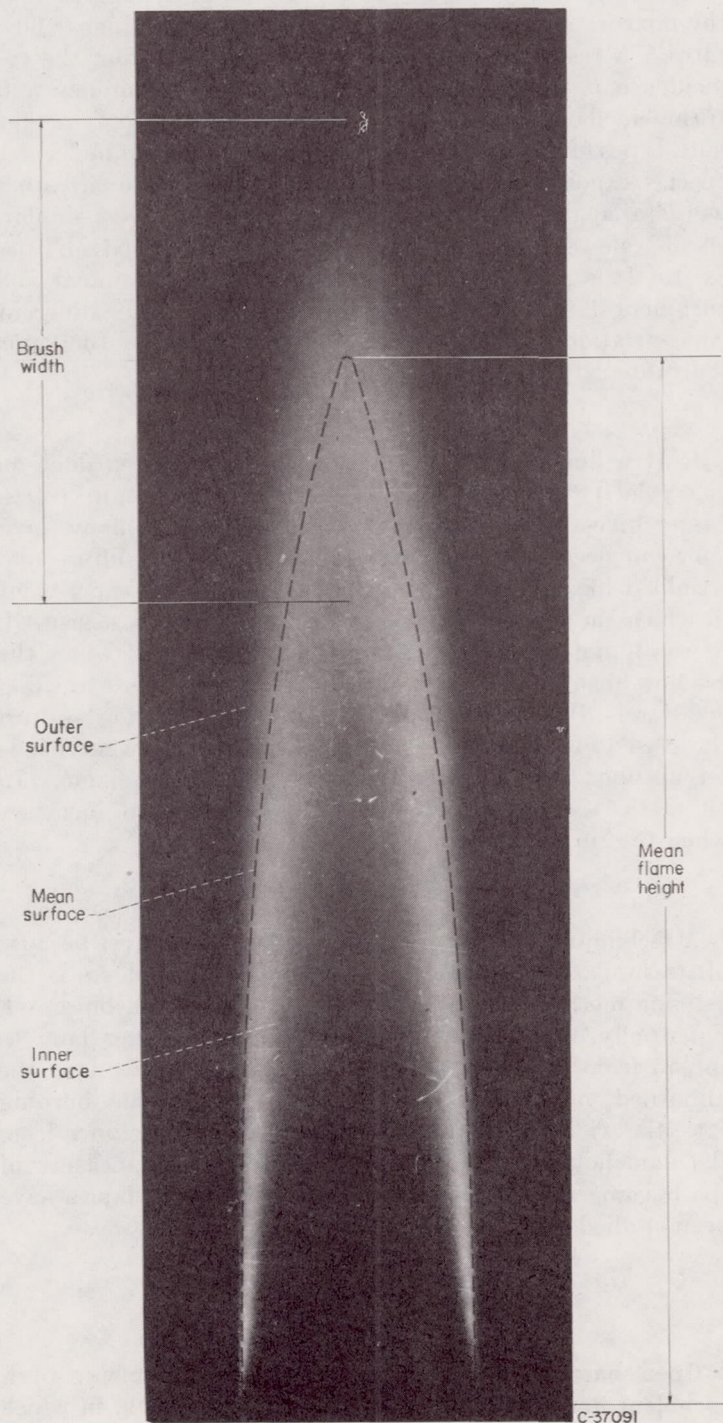


FIGURE 153.—Time exposure of luminous turbulent flame showing boundaries of flame brush and mean surface about which instantaneous flame front oscillates (ref. 3).

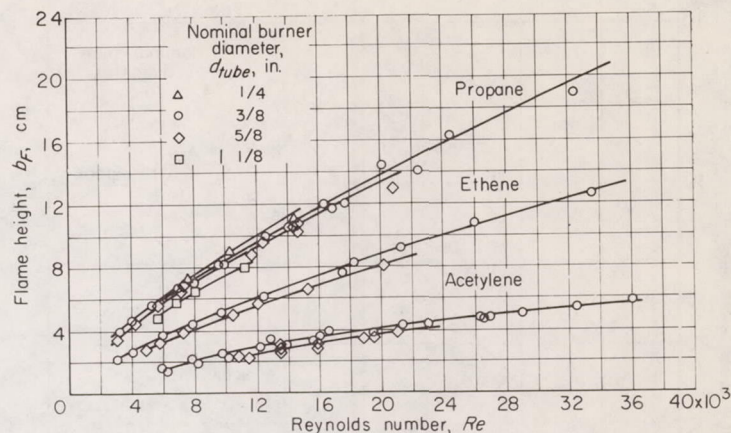


FIGURE 154.—Variation of mean flame height with Reynolds number for hydrocarbon-air flames. Constant density and viscosity (ref. 3).

The mean flame height determined from the point of maximum light intensity also falls within a few millimeters of the point of maximum rate of decrease in oxygen concentration or the point of maximum reaction rate (ref. 6). The mean height of the flame and the width of the burner port can be used to estimate a lower limit to the flame volume required under a particular set of conditions. Any reduction in available space should lead to inefficient burning.

Brush width.—A time exposure of the turbulent flame surface appears as a brush of increasing width from base to tip, as shown in figure 153. The distance between the inner and outer boundaries of the flame brush at the tip of the flame has been called the brush width. In reference 3, the brush width was measured as a function of flow velocity and tube diameter for propane and acetylene flames. The data are plotted against Reynolds number in figure 156. At low Reynolds numbers (below 2000) where the flow and flame become laminar, the distance between the inner and outer boundaries should approach the thickness of the luminous zone of a laminar flame, of the order of 0.1 millimeter (ref. 1, pp. 238, 254). Only flow velocity and tube diameter were varied in this study, density and viscosity remaining roughly constant.

Flame radiation.—A flame emits radiation of various frequencies and intensities, depending on the molecular species present and the temperature to which the molecules are exposed. Several studies have been made to determine the radiating species in laminar flames (see ch. IV). Clark and

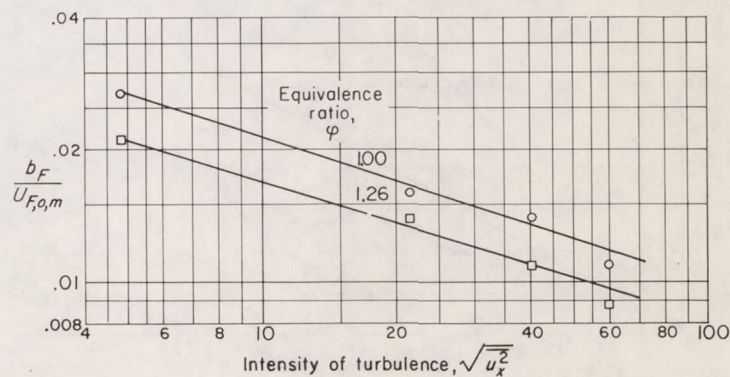


FIGURE 155.—Variation of ratio $b_F/U_{F,o,m}$ with intensity of turbulence.

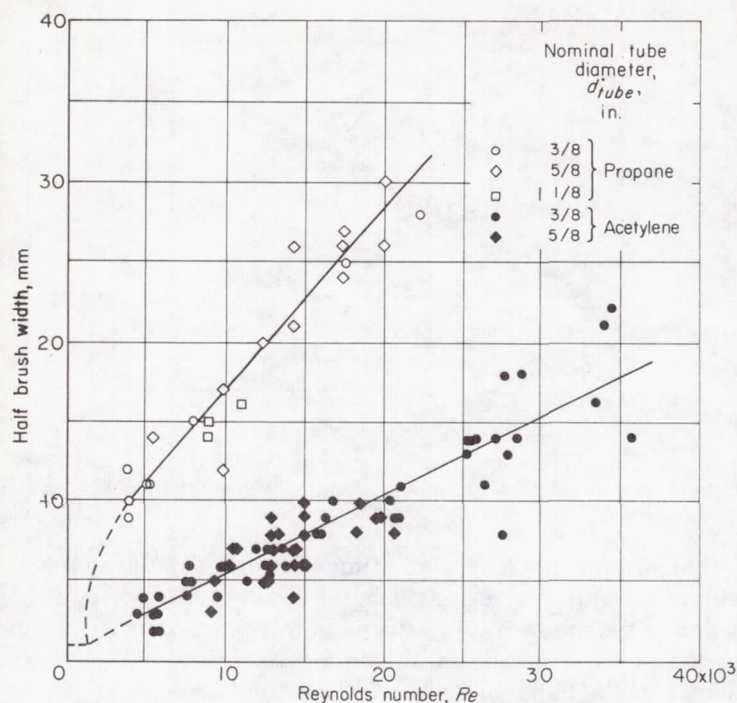


FIGURE 156.—Variation of half brush width with Reynolds number. Constant density and viscosity (ref. 3).

Bittker (ref. 7) have compared the light intensity emitted by laminar and turbulent propane-air flames under similar conditions of flow rate and fuel-air ratio. Port diameters were varied to obtain laminar and turbulent flames. A photocell was used to measure the intensity of the light passing through either a yellow filter (principally C_2 radiation) or a blue filter (principally CH radiation). As shown in figure 157, the radiation intensity for both the laminar and turbulent flames coincides at equal mixture flow rates. The data

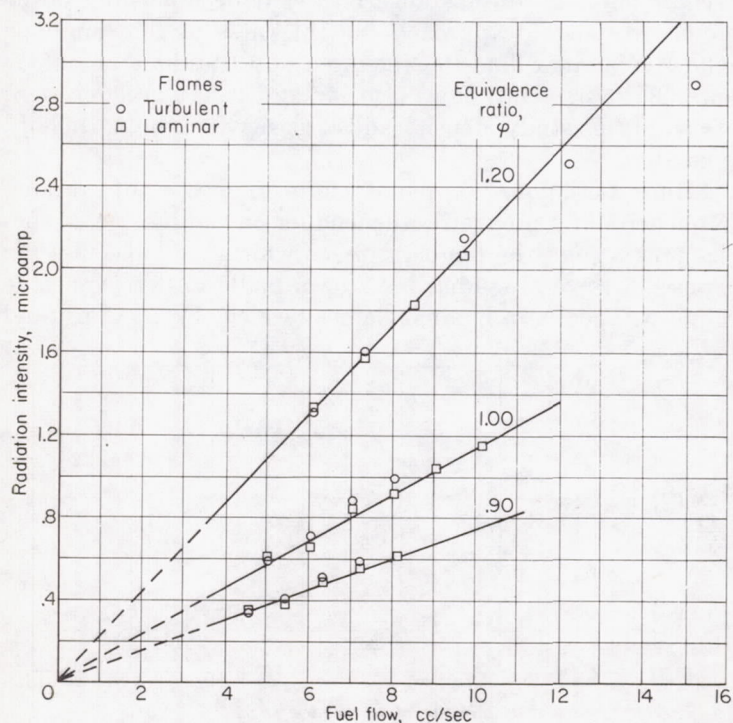


FIGURE 157.—Variation of laminar and turbulent flame intensities with fuel flow. Yellow filter; burner diameter, 0.536 centimeter.

shown were obtained with the yellow filter; similar results were found with the blue filter.

The ratio of intensities measured with the blue and yellow filters was found to be a function of equivalence ratio for the laminar flames. Examination of this ratio for turbulent flames showed that the fuel-air ratio obtained from the intensities agreed well with the measured fuel-air ratio except for the points at an equivalence ratio at 1.20 above a fuel flow of 10 cubic centimeters per second. These points showed a leaner fuel-air ratio based on the intensity ratio than the metered fuel-air ratio. The results suggest that the mixture is diluted with secondary air at the higher flow rates. A reasonable conclusion can be drawn from the coincidence of the intensity measurements for laminar and turbulent flames where dilution is not suspected. It is that both types of flames have similar concentrations of molecular species exposed to a similar temperature profile; in other words, that the laminar and turbulent flames have a similar, small-scale structure. Unfortunately, other possibilities exist. It is possible that the structures of the laminar and turbulent flames differ but that the net result of the different concentration and temperature profiles produces the same light intensity through a given filter.

FLAMES IN TUBES

Only a limited amount of basic work has been done on the velocity and structure of turbulent flames in tubes. Many investigators have noted that a laminar flame in a tube can become oscillatory and finally become diffuse and wrinkled like a turbulent burner flame. In an experiment in which the gas velocity ahead of the flame was measured, it was found that the turbulent flame appeared when the gas flow ahead of the flame had a Reynolds number exceeding 2000 (ref. 8). In the case of flames propagating toward the closed end of a tube, a turbulent circulatory motion is set up ahead of the flame, creating a turbulent flame. In all cases, the spatial rate of flame propagation increases when the turbulent flame appears.

FLAMES SUPPORTED ON RODS (V-FLAMES)

A technique that has created considerable interest because of its similarity to flames supported on flameholders is the V-flame method, in which the flame is supported on a rod. Essentially, the V-flame measures the ability of the flame to spread from the sheltered zone near the stabilizer into the unburned gas flowing past it. The greater the burning rate, the wider the flame will grow at a given distance from the flameholder. The flame width, then, is a measure of the burning rate. Both laminar and turbulent flames have been studied with this technique.

TURBULENT FLAME VELOCITY

MEASUREMENT

Open burner flames.—The earliest measurements of a turbulent flame velocity were those of reference 9, in which it was assumed that the inner boundary of the turbulent flame represented a zone of maximum burning rate or the turbulent flame velocity, while the outer boundary represented the zone of slowest burning rate or the laminar

flame velocity. The surface areas corresponding to these zones were measured, and flame velocities were calculated by a total-area method using equation (1) of chapter IV. The flame velocity calculated from the inner surface is a maximum value and corresponds to the hypothetical condition that at any instant all the flame exists along this surface. As is evident from instantaneous schlieren photographs of turbulent flames, only part of the flame exists at the inner surface at any instant.

In considering the fluctuating nature of a turbulent flame, a line, such as the dashed line in figure 153, might be drawn somewhere between the inner and outer boundaries to indicate a mean flame surface about which the instantaneous flame front oscillates. It might be considered the most probable position of any given increment of flame front. In reference 3, the line was drawn midway between the inner and outer boundaries; such a surface does not give a mean surface area. In reference 10, the locus of maximum light intensity determined from densitometer measurements on the time exposure was used. Since the extreme boundaries of a turbulent flame are quite diffuse, this method of determining a mean boundary is more precise and more readily reproduced. More recently, it has been shown (ref. 4) that the surface of maximum light intensity corresponds closely to the surface of maximum rate of oxygen consumption. The flame velocity obtained from densitometer traces is intermediate between the minimum and the maximum of reference 9; there is no simple relation between the maximum flame velocity of reference 9 and the turbulent flame velocity of reference 10, because the dimensions of the flame brush change as flow conditions change (fig. 156).

References 3 and 9 report flame velocities computed by a total-area method based on surface-of-revolution formulas (ch. IV, eq. (2b)); whereas, in reference 10, an angle method was used (ch. IV, eq. (3)). It is important to note, however, that none of these methods of computing turbulent flame velocity corresponds to that for computing the laminar flame velocity, which is defined as the flow velocity of unburned gas perpendicular to the instantaneous flame surface. The calculated turbulent flame velocity corresponds to the flow velocity of unburned gas perpendicular to a time-averaged position of the flame, and the instantaneous flame surface area does not enter the calculation. No precise measurements have been made of the velocity normal to the actual flame surface, although the laminar flame velocity does enter many of the proposed theoretical relations discussed in this chapter.

An examination of many turbulent flames has shown that the mean flame surface is approximately a paraboloid of revolution about the burner axis (ref. 5). With this assumption, it is possible to calculate the mean flame surface area $S_{F,T}$ from the mean height b_F and port radius r_p by the equation

$$S_{F,T} = \frac{2\pi}{3} \left(\frac{r_p^2}{2b_F} \right)^{1/2} \left[\left(2b_F + \frac{r_p^2}{2b_F} \right)^{3/2} - \left(\frac{r_p^2}{2b_F} \right)^{3/2} \right] \quad (1)$$

When $\frac{r_p^2}{2b_F} \ll 2b_F$, the equation reduces to

$$S_{F,T} = \frac{4\pi}{3} r_p b_F \quad (1a)$$

In practice, it was found that a 2-percent error resulted when $b_F = 2r_p$ (ref. 5) using equation (1a).

In reference 11, an attempt was made to estimate the total area of the wrinkled flame surface from the height and diameter of the wrinkles visible on a spark photograph. The area was computed by assuming that each wrinkle was a cone. Examination of the surface showed that the diameters of the wrinkles d_P were related to the scale of turbulence \mathcal{L} by

$$d_P = 5.0 d_\epsilon \quad (2)$$

where d_ϵ is the eddy diameter obtained from the turbulence scale (d_ϵ at $\mathcal{R}_\nu = 0.5$). The height of the wrinkles b_P was related to the intensity of turbulence $\sqrt{u_x^2}$ by

$$b_P = \frac{0.266 \sqrt{u_x^2}}{U_{F,L}} \quad (3)$$

Another proposed method for determining the total surface area of a turbulent flame uses the radiation intensities discussed earlier. Figure 157 shows that the radiation intensity through a given filter is a linear function of fuel-flow rate. At a given fuel-air ratio, the light intensity is a linear function of the total flow of fuel and air. Since the surface area of laminar flames can be measured as a function of flow rate, it is possible to replace the flow rate by flame area. The light intensity may then be used as a measure of flame area for turbulent flames once a calibration curve has been obtained with laminar flames. The use of this method, however, depends heavily on the assumption that the radiation is uniform over the entire flame surface and that the laminar and turbulent flames have similar structures.

Flames in tubes.—In reference 12, spatial velocities of turbulent flames in tubes were measured. The ratio of turbulent to laminar spatial velocity in a tube is equivalent to the ratio obtained with a Bunsen burner with the additional assumption that the mean flame boundary has the same meaning in both cases.

Spherical flames.—Analogous to the use of the soap-bubble or constant-volume bomb method for laminar flame velocities, spherical flames have been used to study turbulent flame velocity. In reference 13, a single spark was used to ignite a turbulent mixture flowing through a 4- by 4-inch duct, thus creating a sphere of flame that expanded into the flowing unburned-gas mixture. As in the soap-bubble method, the spatial rate of propagation of the mean spherical surface multiplied by an expansion ratio resulted in a flame velocity. In the soap-bubble and constant-volume bomb experiments, the required expansion ratios could be measured, but in the free-stream method used in reference 13 a theoretical expansion ratio was used that was based on the equilibrium flame temperature. The ratio of turbulent to laminar spatial velocities, assuming the same expansion ratio applies for both cases, should then be equivalent to the flame velocity ratio obtained in tube and Bunsen flames.

Flames supported on rods (V-flames).—The turbulent V-flame may be used to determine the flame velocity in a manner analogous to the laminar V-flame (ch. IV). Consider the sketch in figure 158 (ref. 14). The total length of burning surface of one side of the V-flame is \overline{OS} , the approach-stream velocity is U_o , and the duct half-width is $W_{dt/2}$. Consider the flame segment $\overline{OS'}$, which extends from the flameholder to the point where the flame half-width is $W_{F/2}$. The unburned gas that enters segment $\overline{OS'}$ originally had a stream-tube half-width $W_{F/2,o}$ and velocity U_o in the approach stream. In this two-dimensional system, $W_{F/2}$, $W_{F/2,o}$, and $\overline{OS'}$ are representative of areas; and, since the pressure drop due to combustion is small, the density of the unburned gas may be assumed constant. Hence, the product $W_{F/2}U$ is constant for conservation of mass. By analogy to equation (1) of chapter IV, the average turbulent flame velocity for the segment is

$$U_{F,T} = \frac{W_{F/2,o}U_o}{\overline{OS'}} \quad (4)$$

The fraction of fuel ι burned in segment $W_{F/2}$ is

$$\iota = \frac{W_{F/2,o}U_o}{W_{dt/2}U_o} = \frac{W_{F/2,o}}{W_{dt/2}} \quad (5)$$

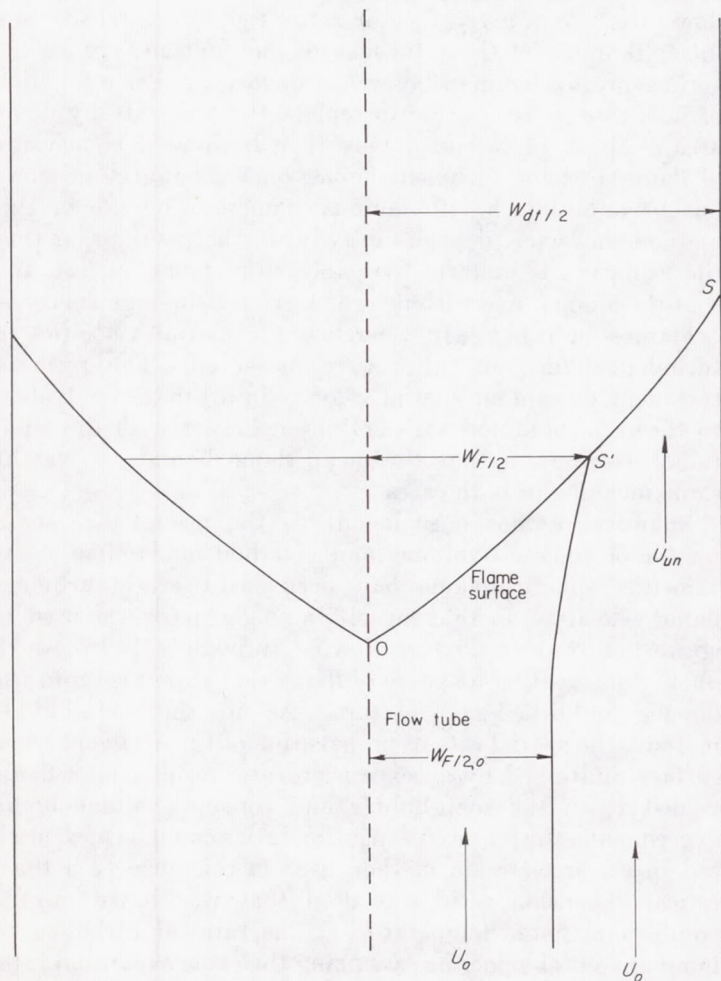


FIGURE 158.—Sketch of V-flame showing quantities used in calculating flame velocity (ref. 14).

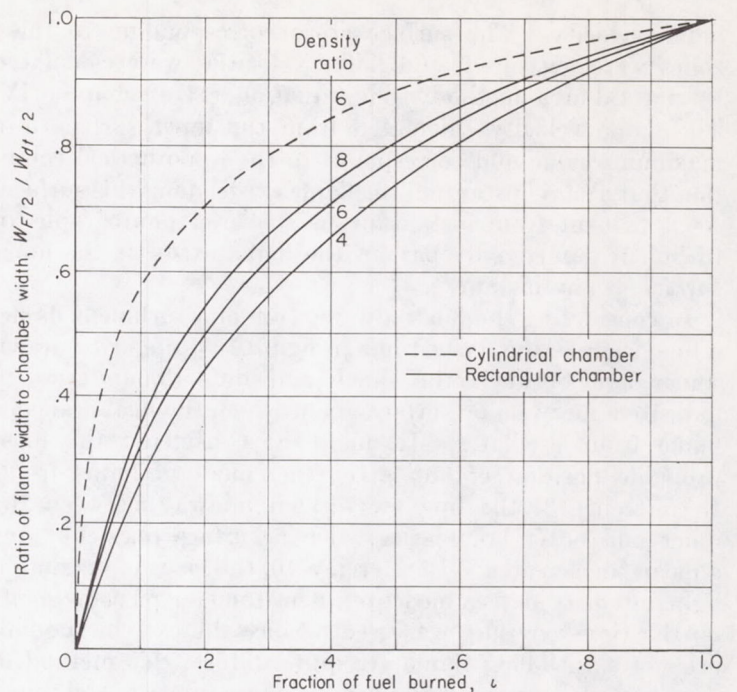


FIGURE 159.—Calculated variation of ratio of flame width to chamber width with fraction of fuel burned up to point of measurement of flame width (ref. 14).

Therefore,

$$U_{F,T} = \iota W_{dt/2} \frac{U_o}{\overline{OS}}, \quad (6)$$

The flame half-width $W_{F/2}$ was considered a differential width $dW_{F/2}$ with corresponding increments in pressure and unburned- and burned-gas velocities in reference 14; this concept was used in writing the differential equations for the over-all mass balance, over-all force balance, and force balances on the burned and unburned gases. These equations were solved by a stepwise method for finite increments in order to obtain curves of $W_{F/2}/W_{dt/2}$ against ι (fig. 159). Flame widths $W_{F/2}$ were measured from the outer edge of the luminous flame zone from a time exposure of the turbulent V-flame. The values of ι were then read from figure 159, and the average turbulent flame velocities were calculated by equation (6).

Dependence of flame velocity on location of measurement.—As with the laminar flame (ch. IV), the turbulent flame velocity may vary from point to point. Figure 160 shows the ratio of turbulent to laminar flame velocity $U_{F,T}/U_{F,L}$ plotted against the fraction of the tube radius r/r_{tube} . The flame velocity ratio increases from unity at the tube rim ($r/r_{tube}=1$) to the order of 4 at $r/r_{tube}=0.7$. These changes are considered further in the discussion of flame-induced turbulence. The effects of chemical and physical variables on $U_{F,T}$ discussed hereinafter apply to average velocities determined by total-area methods.

EFFECTS OF CHEMICAL VARIABLES

Fuel concentration.—Reference 9 reports measurements of the effect of fuel concentration on the turbulent flame velocities of propane-oxygen mixtures. The results are

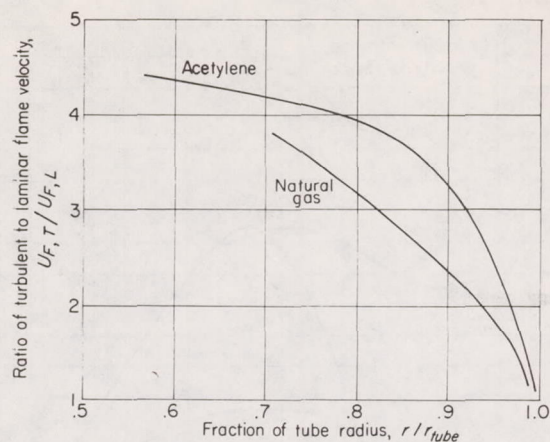


FIGURE 160.—Variation of ratio of turbulent to laminar flame velocity with fraction of radial distance from tube axis to rim, for stoichiometric acetylene-air and natural-gas-air flames. Reynolds number, 25,000 (ref. 10).

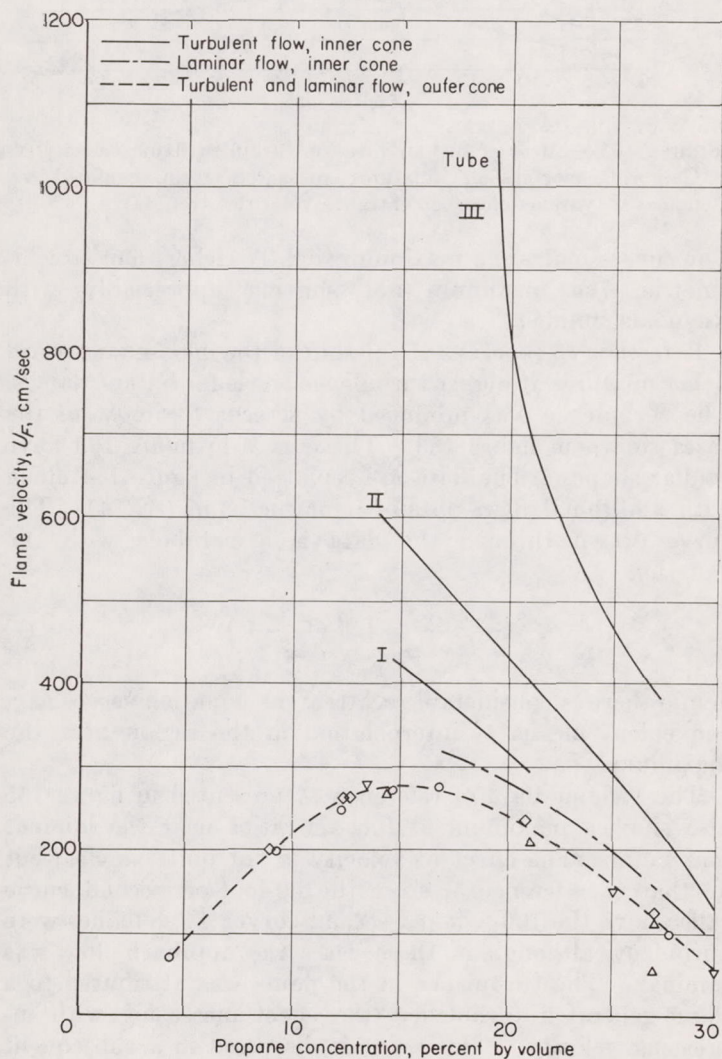


FIGURE 161.—Effect of fuel concentration on laminar and turbulent flame velocities of propane-oxygen mixtures (ref. 9).

shown in figure 161, where the dashed curve represents measurements based on the outer boundary of the flame brush and the solid curves are based on the inner boundary. According to reference 9, these velocities represent laminar and turbulent flame velocities, respectively. The dashed curve shows laminar flame velocities measured from the outer boundary of the luminous zone of a laminar flame. As would be expected, if the outer boundary of the turbulent flame brush does represent a laminar flame velocity, all the points computed from it, irrespective of tube size or flow characteristics, fall on a single curve. The dot-dashed curve, representing laminar flame velocity based on the inner boundary of the luminous zone, might be expected to fall above the dashed curve because of the finite thickness of the luminous zone. The turbulent flames show a rapidly increasing velocity from rich mixtures toward stoichiometric. Unfortunately, leaner flames were unstable and could not be studied. It should be noted that the higher flame velocities in figure 161 were measured with higher flow velocities, so that the increase in flame velocity was not due to changes in fuel-oxidant ratio alone; and, as will be evident in the discussion of the effect of flow velocity on turbulent flame velocity, the increases in flame velocity from rich to stoichiometric mixtures were greater than would be expected from the effect of fuel-oxidant ratio alone.

In reference 3, a more complete study was made of the effect of fuel concentration of ethene-air flames on a $\frac{3}{8}$ -inch burner using flow velocity (expressed in terms of Reynolds number) as a parameter. The data are shown in figure 162.

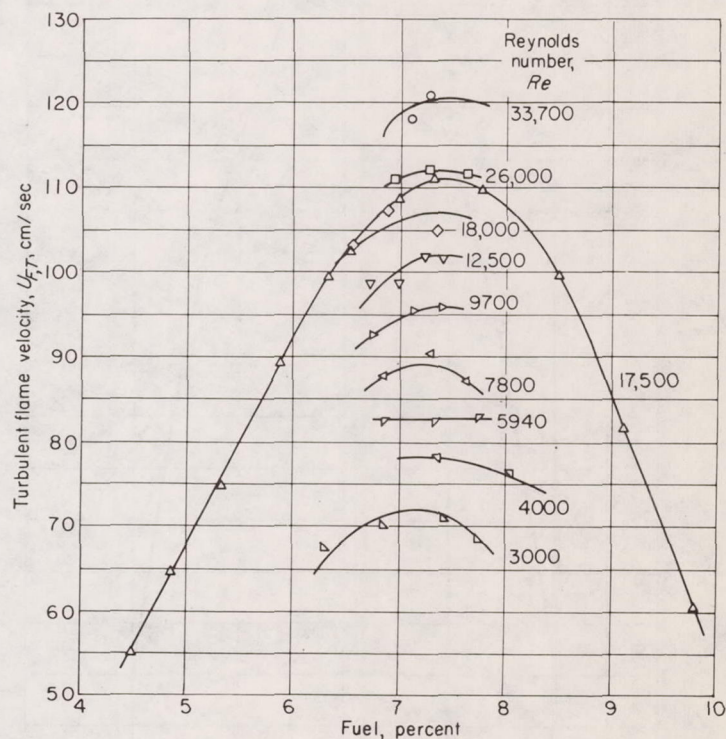


FIGURE 162.—Effect of fuel concentration on turbulent flame velocity of ethene-air mixtures at various Reynolds numbers. Constant density and viscosity; $\frac{3}{8}$ -inch burner (ref. 3).

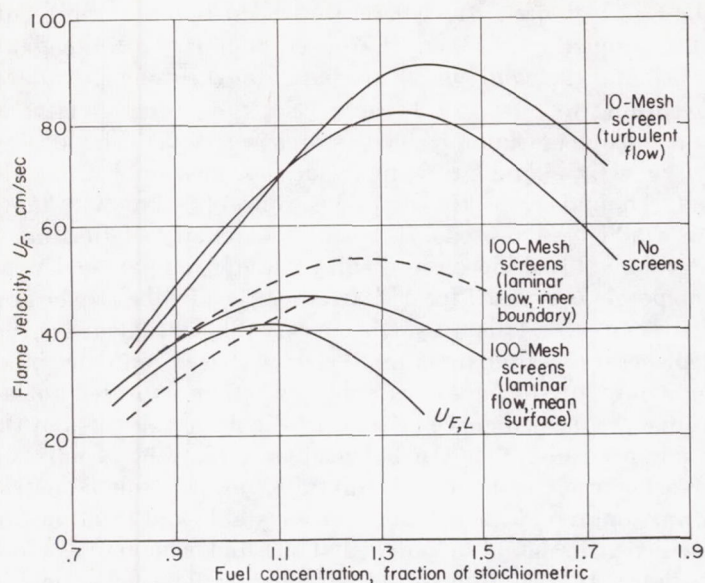


FIGURE 163.—Variation of flame velocity of butane-air mixtures with volume fraction of stoichiometric fuel concentration for various degrees of turbulence. Turbulent flames held by pilot flame on 2.55-centimeter burner at 540 centimeters per second; Reynolds number, 8800 (ref. 15).

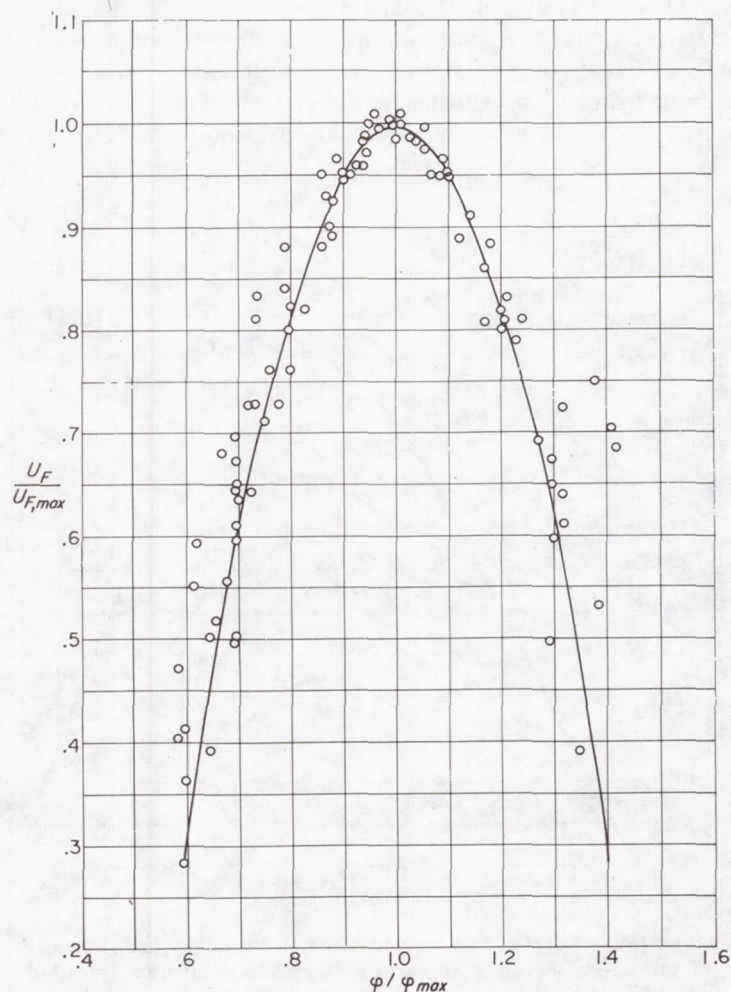


FIGURE 164.—Variation of ratio $U_F/U_{F,max}$ with ϕ/ϕ_{max} for laminar and turbulent flames of methane and butane.

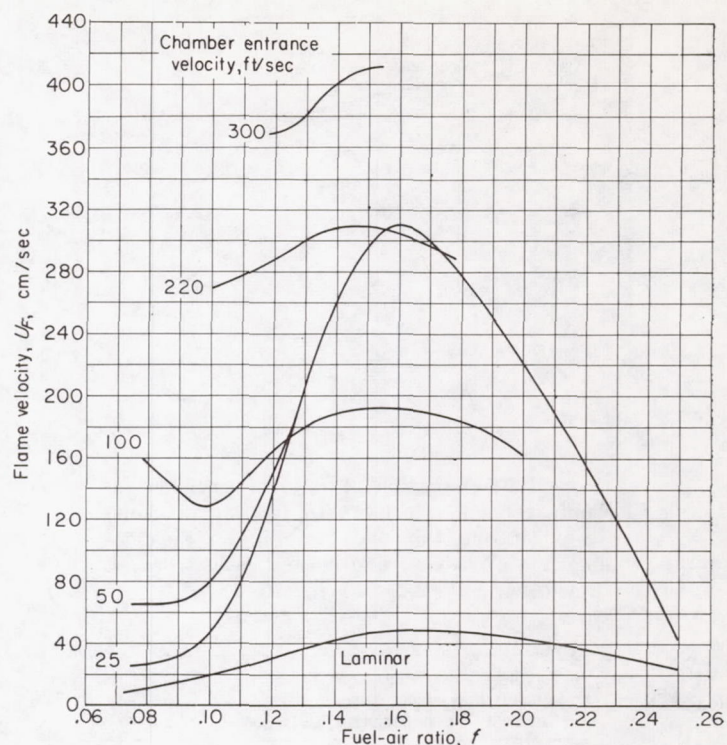


FIGURE 165.—Effect of fuel-air ratio on turbulent flame velocity of Cambridge-city-gas-air mixtures measured from confined V-flames at various chamber entrance velocities (ref. 14).

The curves indicate a maximum slightly richer than stoichiometric, the maximum not shifting appreciably with Reynolds number.

Reference 15 reports a slight shift of the maximum toward richer mixtures at higher turbulence levels for butane flames. The turbulence was produced by screens for most of the cases shown in figure 163. The curves in figure 163 have similar shapes. The data are replotted in figure 164 along with additional data obtained for methane (ref. 4). The curve drawn through the data is a parabola with the equation

$$1 - \frac{U_F}{U_{F,max}} = 4.5 \left(\frac{\phi}{\phi_{max}} - 1 \right)^2 \quad (7)$$

While there is considerable scatter, the equation serves as a convenient means of interpolation in the region near the maximum.

The V-flame data of reference 14 presented in figure 165 also show a maximum at fuel-air ratios near the laminar maximum. The effect of velocity is not quite as clear-cut as that of reference 3, since the 50-foot-per-second curve falls above the 100-foot-per-second curve. The flames were turbulent, although in these cases the approach flow was laminar. The turbulence in the flame was attributed to a flame-generated turbulence, the effect increasing with increasing velocity. This point is discussed in a subsequent section in this chapter. The results are relatively independent of stabilizer size and shape and are insensitive to the introduction of turbulence-producing screens just ahead of the stabilizer.

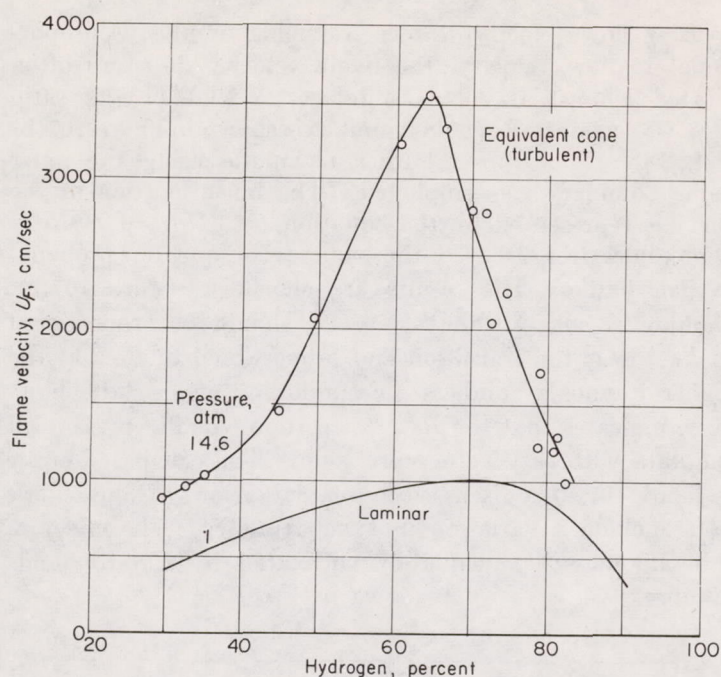


FIGURE 166.—Comparison of equivalent cone flame velocity with laminar flame velocity. Hydrogen-oxygen flames on 0.3-millimeter burner (ref. 17).

Fuel type.—Reference 3 shows that the turbulent flame velocities for propane-, ethene-, and acetylene-air flames are empirically correlated by the expression showing a direct proportionality to laminar flame velocity (table XXII). Thus, turbulent flame velocity, under the conditions studied, might be expected to vary with hydrocarbon structure in the same way that laminar flame velocity varies. This is also in agreement with the theoretical treatments of references 10, 14, and 16.

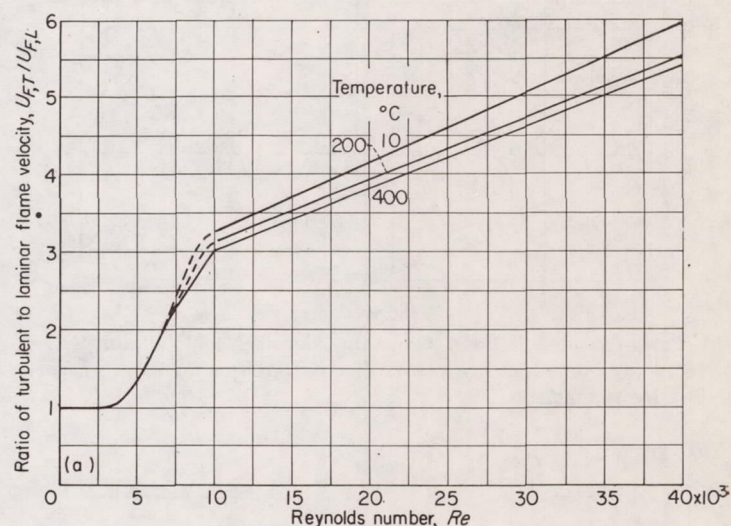
EFFECTS OF PHYSICAL VARIABLES

Pressure.—There is no adequate information on the effects of pressure on turbulent flame velocity. However, the problem is considered in reference 17, in which turbulent hydrogen-oxygen flames at a pressure of 14.6 atmospheres were studied. The burner diameter and the height of the equivalent cone defined by the angle of the turbulent flame near the burner rim in equation (2a) of chapter IV were used

to obtain an equivalent cone area. An equivalent flame velocity for the turbulent flame was then computed from this area by equation (1) of chapter IV. Since $U_{F,T}/U_{F,L}$ approaches 1 near the rim (fig. 160), these flame velocities would be near the laminar flame velocities.

A comparison of these computed velocities at a pressure of 14.6 atmospheres with laminar flame velocities at 1 atmosphere is shown in figure 166. The effect of pressure is difficult to discuss quantitatively, since the flames were small and the measurements are necessarily less reliable than those obtained for slower flames.

Temperature.—The effect of initial air temperature on turbulent flame velocity of coke-oven-gas-air mixtures was measured by Heiligenstaedt (ref. 18), whose curves are replotted in terms of $U_{F,T}/U_{F,L}$ in figure 167(a). The inner flame surface was used and assumed to be a right circular cone. Although three distinct curves for the three temperatures appear in the figure, indicating a small negative temperature dependence of $U_{F,T}/U_{F,L}$, Reynolds number correlates the data to within 10 percent over the range 10° to 400° C. Heiligenstaedt reported the turbulent flame



(a) Coke-oven-gas-air flames (ref. 18).

FIGURE 167.—Effect of Reynolds number on ratio of turbulent to laminar flame velocity.

TABLE XXII.—EXPERIMENTAL RELATIONS BETWEEN TURBULENT FLAME VELOCITY AND REYNOLDS NUMBER

Mixture	Reynolds number range	Relation	Reference
Propane-oxygen -----	2, 000–5, 000	$U_{F,T} \propto Re^{0.5}$	9
	5, 000–40, 000	$U_{F,T} = \mathcal{K}_1 + \mathcal{K}_2 Re$	
Town gas-air -----	2, 000–40, 000	$U_{F,T} \propto U_{F,L} Re^{0.4}$	16
Propane-air ^a ----- Ethene-air ^a ----- Acetylene-air ^a -----	3, 000–40, 000	$U_{F,T} = U_{F,L} (0.18 d_{turb}^{0.25} Re^{0.24})$	3

^a Fuel-oxidant ratio for maximum turbulent flame velocity.

velocity to increase approximately as the 1.6 power of the absolute initial temperature:

$$U_{F,T} \propto T_o^{1.6} \quad (8)$$

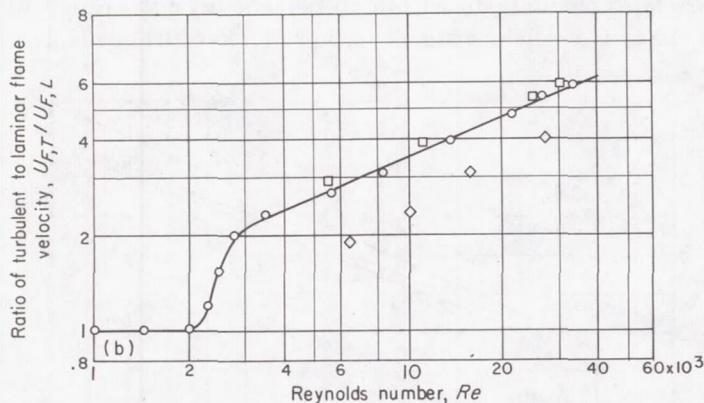
According to Delbourg (ref. 18), for town-gas-air flames,

$$\frac{U_{F,T}}{U_{F,L}} \propto \frac{T_o^{1.65}}{T_o^{1.74}} \propto T_o^{-0.09} \quad (9)$$

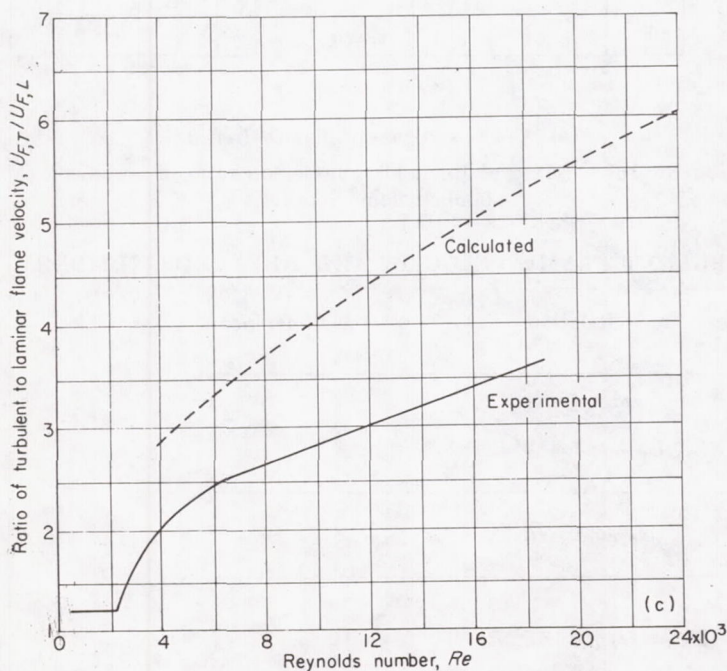
Thus, for both of these examples the ratio of turbulent to laminar flame velocity is practically independent of initial temperature.

Velocity and turbulence promotion.—Several investigators have studied the effect of flow velocity and turbulence promoters on turbulent flame velocity. Tube diameter was also varied in most of these investigations. Chapter IV pointed out that the laminar flame velocity is independent of flow velocity. At a Reynolds number of about 2000, however, the flow becomes turbulent and flame velocity rises rapidly. The turbulent flame velocity increases with in-

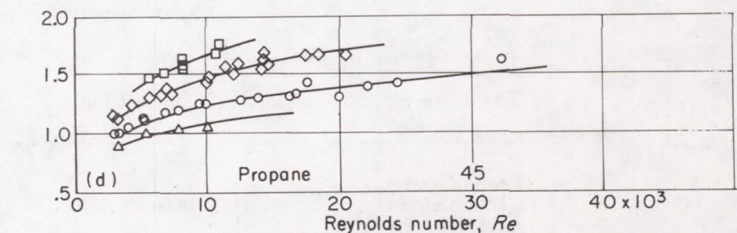
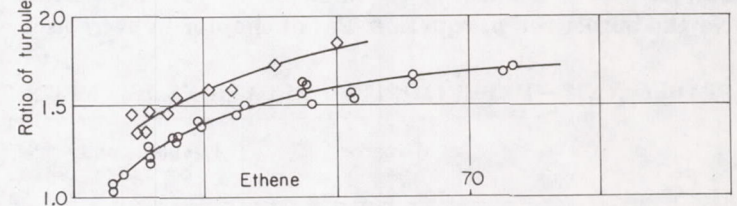
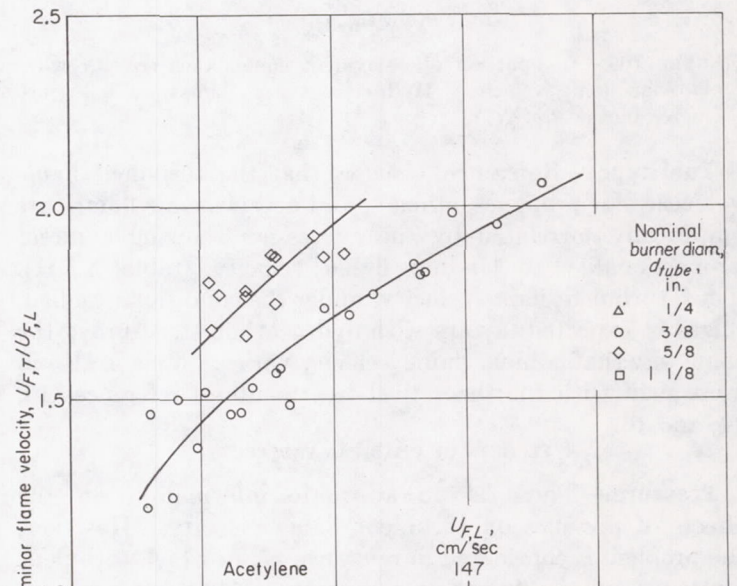
creasing flow velocity. Since Reynolds number is proportional to flow velocity, the flame velocity data are often plotted against Reynolds number. A plot of the ratio $U_{F,T}/U_{F,L}$ against Reynolds number is shown in figure 167(b) (ref. 18). The Bunsen-burner technique using the inner flame boundary was employed. The linear portion of the curve is represented by the equation $U_{F,T}/U_{F,L} = 0.088 Re^{0.4}$. Damköhler (ref. 9) used the same technique for propane-oxygen flames. His results are shown in figure 167(c). Damköhler suggests that $U_{F,T}/U_{F,L}$ should be proportional to $Re^{0.5}$ near the transition and proportional to $Re^{1.0}$ at the higher Reynolds numbers. Examination of his data, however, indicates that the $Re^{0.4}$ correlation would represent all the data with satisfactory precision. The calculated curve in figure 167(c) is discussed in a later section. Damköhler's data include a variation in tube diameter. The effect of tube diameter is adequately correlated by the Reynolds number.



(b) Town-gas-air flames. Constant density and viscosity (ref. 18). (Symbols indicate points of constant fuel-air ratio unspecified by reference.)



(c) Propane-oxygen flames. Constant density and viscosity (ref. 9).



(d) Hydrocarbon-air flames. Constant density and viscosity (ref. 3).

FIGURE 167.—Concluded. Effect of Reynolds number on ratio of turbulent to laminar flame velocity.

The variation of the ratio of turbulent to laminar flame velocity for acetylene-, ethene-, and propane-air flames is shown in figure 167(d) (ref. 3). These data were obtained from the mean surface of a turbulent Bunsen flame. Empirical equations for the curves are given in table XXII. In general, the flame velocity ratio varies with $Re^{0.24}$, but separate lines are found for different tube diameters. Wohl (ref. 6) has also studied the effect of flow velocity on flame velocity. He finds a linear relation between flame velocity and flow velocity. Examination of a log-log plot of Wohl's data, however, shows that a line of approximately 0.25 slope would fit reasonably well.

While Reynolds number has been used as a correlating parameter for the effects of flow velocity and tube diameter on the ratio of turbulent to laminar flame velocity in the previous discussion, the other parameters involved in the Reynolds number have not been varied appreciably. Wagner (ref. 5) has studied the effect of kinematic-viscosity changes on the ratio of turbulent to laminar flame velocity by the use of argon and helium instead of nitrogen as the inert gas in the oxidant. The proportion of each diluent to oxygen was maintained the same as the nitrogen-oxygen ratio in air. The following results were obtained:

- (1) For propane-oxygen-nitrogen:

$$\frac{U_{F,T}}{U_{F,L}} \propto Re^{0.25}$$

- (2) For propane-oxygen-helium:

$$\frac{U_{F,T}}{U_{F,L}} \propto Re^{0.20}$$

- (3) For propane-oxygen-argon:

$$\frac{U_{F,T}}{U_{F,L}} \propto Re^{0.44}$$

These equations include data obtained with tubes of various

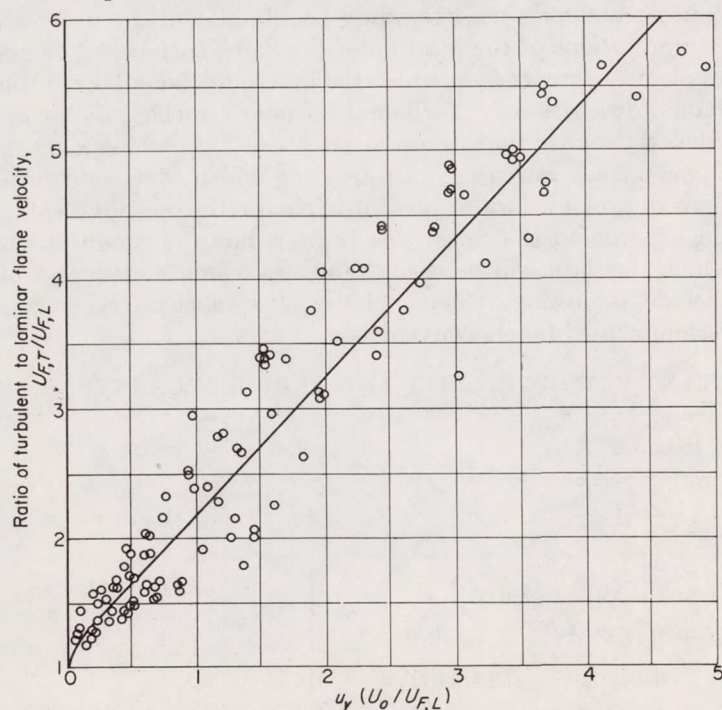


FIGURE 168.—Variation of ratio of turbulent to laminar flame velocity with parameter $u_y (U_o/U_{F,L})$. Propane-air flames on various rectangular nozzles at various fuel-air ratios and velocities (ref. 19).

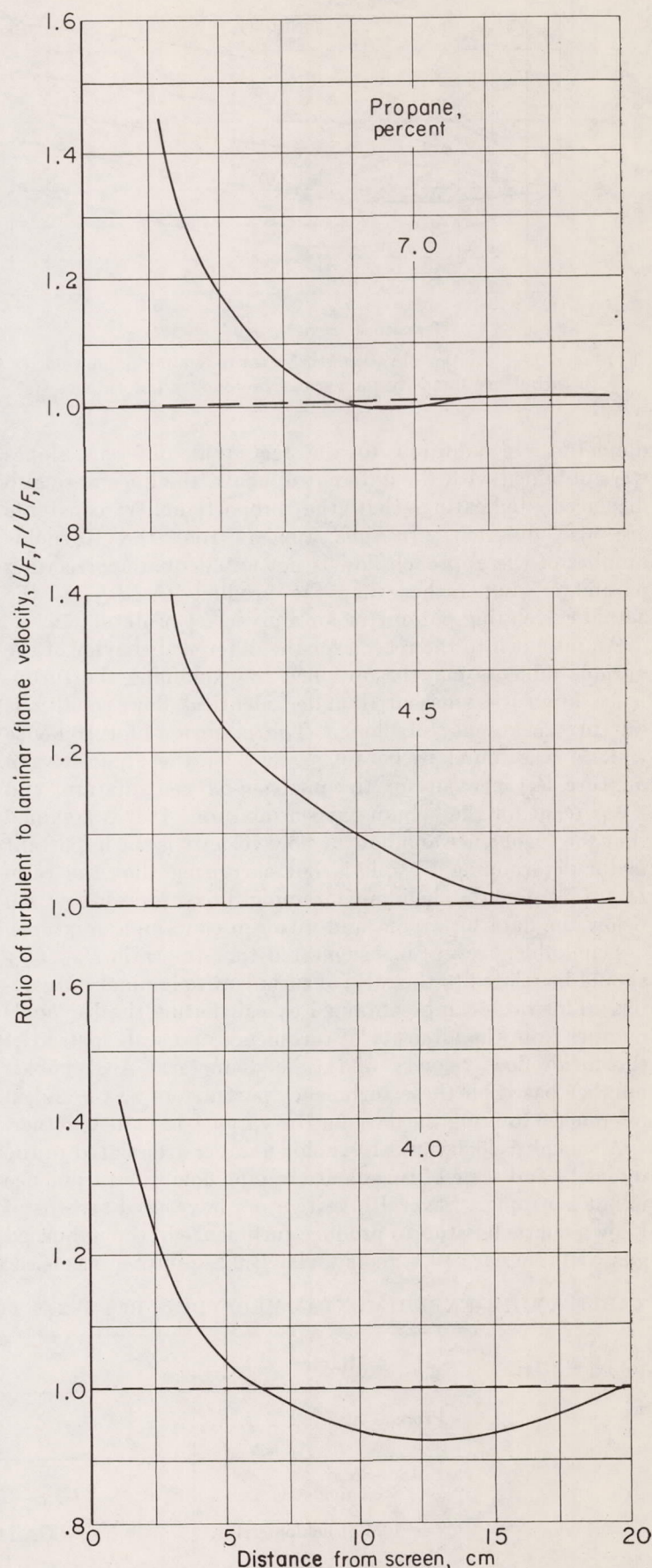


FIGURE 169.—Variation of ratio of turbulent to laminar flame velocity with distance from screen of 6.0-millimeter mesh and 1.5-millimeter wire diameter. Propane-air flames inside 5.4-centimeter tube moving against flow velocity of 58.8 centimeters per second (ref. 12).

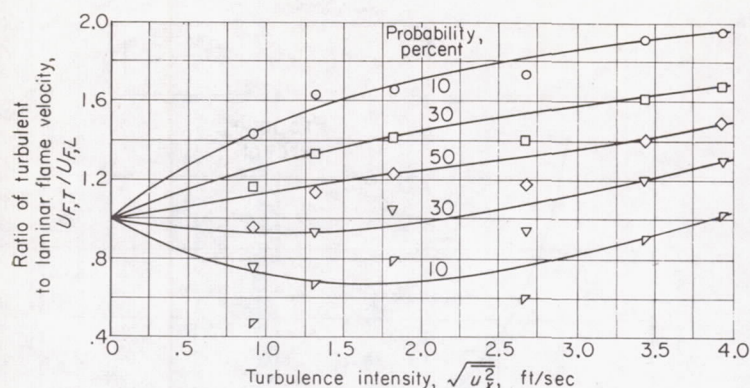


FIGURE 170.—Variation of ratio of turbulent to laminar flame velocity with turbulence intensity for various probability percentages (ref. 13).

diameter. In addition to the fact that different slopes were obtained with the different diluents, the lines were also displaced, indicating that the proportionality constants are also different. It thus appears that the Reynolds number of the approach flow is not an adequate correlating parameter, but rather that the product $U_{o,m}d_{tube}$ is the actual correlating parameter for a given set of data.

An insight into the reason for the different behavior of the various diluents may be obtained by examining the turbulence intensities measured under identical flow conditions but in the absence of flame. The intensity of turbulence (ref. 5) was found to be 4.9 percent for the argon-oxygen mixture, 4.1 percent for the nitrogen-oxygen mixture, and 2.0 percent for the helium-oxygen mixture. If it is assumed that the turbulence and not the flow velocity is the important factor determining $U_{F,T}$, it is not surprising that the ratio $U_{F,T}/U_{F,L}$ for the helium-containing mixtures always fell below the data for argon- and nitrogen-containing mixtures.

Damköhler (ref. 9) has suggested that the ratio $U_{F,T}/U_{F,L}$ should be related to the ratio of turbulent to laminar diffusivity. This ratio can be obtained by calculating the Reynolds number from the intensity of turbulence and scale instead of the mean flow velocity and tube diameter. A Reynolds number based on these turbulence parameters was found in reference 9 to bring the data for the various diluents together.

Although velocity and Reynolds number are related to the intensity and scale of turbulence in pipe flow, the turbulence is not isotropic. Several investigators have used screens of known characteristics to produce turbulence in the unburned gas. In reference 19, a rectangular Bunsen burner was used;

the ratio of turbulent to laminar flame velocity and the intensity of turbulence in the narrow dimension of the burner were correlated. The results are shown in figure 168. In reference 20, a similar technique was used with a symmetrical burner; the results correlated with the turbulence intensity along the direction of flow. A tube method was used in reference 12; the spatial velocity as a function of distance from the turbulence-producing screen was measured. Since the intensity of turbulence varies with distance from the screen, the results (fig. 169) show the variation of flame speed with intensity of turbulence. In reference 13, the expanding spherical flame was used, with screens to create turbulence; a variation was obtained, as shown in figure 170. The author found a very low laminar flame velocity of only 0.59 foot per second, which is unexplained as yet. A distribution of flame velocities was obtained that the author associated with the random nature of turbulence. The curves illustrate the data obtained as a function of the fraction of the measurements giving a certain flame velocity. It should be noted that in all these experiments the turbulence level was based on measured or calculated intensities in the absence of flame. Except for the experiments of reference 12, in which the intensity was considered at each point in the tube, the measurements were made at the initiation point of the flame (the lip of the burner for Bunsen flames or the ignition point for spherical flames), and hence the flame propagated into regions of varying turbulence.

The empirical equations for the variations of turbulent flame velocity with turbulence intensity in the approach stream are given in table XXIII. Since Reynolds number can be related to intensity by the equation $Re \propto \sqrt{u_x^2}$ (ref. 9), the data of references 3, 9, and 16 (table XXII) can also be compared. The comparison of turbulent burning velocities by different investigators is difficult, however, because of the varied techniques used to study the flame and the different interpretations of the location of the flame surface. For example, in reference 9, in which the innermost boundary of the flame brush was used, turbulent burning velocities were considerably higher than those of reference 3, in which a mean flame surface was used. In deciding which of several relations to use, it is best at present to choose the one obtained in the experiment that most closely resembles the condition for which the data will be used. For approximate estimates of turbulent burning velocity, the expression of reference 3 is recommended for its convenience.

TABLE XXIII.—EXPERIMENTAL RELATIONS BETWEEN TURBULENT FLAME VELOCITY AND TURBULENCE INTENSITY

Mixture	Relation	Reference
Propane-air-----	$U_{F,T} \propto u_y U_o$	19
Butane-air Stoichiometric-----	$U_{F,T} = U_{F,L} [1 + 0.02 U_o (\sqrt{u_x^2}/U_o + 0.04)]$	20
1.25 Stoichiometric---	$U_{F,T} = U_{F,L} [1 + (24 + 0.0147 U_o) (\sqrt{u_x^2}/U_o + 0.01)]$	
1.50 Stoichiometric---	$U_{F,T} = U_{F,L} [1 + (77 + 0.0406 U_o) (\sqrt{u_x^2}/U_o + 0.01)]$	
Propane-air, stoichiometric.	$U_{F,T} = U_{F,L} [1 + 26.2 (\sqrt{u_x^2}/U_o) + 1.40 (U_o/24)^{1.12}]$	15

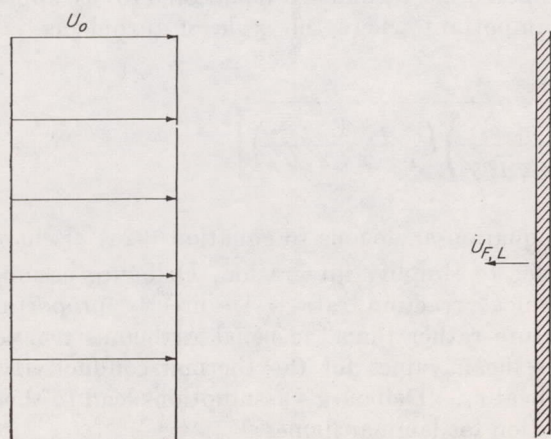
THEORIES OF TURBULENT FLAME VELOCITY

The increased rate of burning of a fuel-air mixture in a turbulent flame compared with a laminar flame may be due to any one or a combination of three processes: (1) The turbulent flow may distort the flame so that the surface area is markedly increased, while the normal component of the burning velocity remains the laminar flame velocity. (2) Turbulence may increase the rate of transport of heat and active species, thus increasing the actual burning velocity normal to the flame surface. (3) Turbulence may rapidly mix the burned and unburned gas in such a way that the flame becomes essentially a homogeneous reaction, the rate depending on the ratio of burned to unburned gas produced in the mixing process. The first two processes have received the major emphasis in the consideration of turbulent Bunsen burner, tube, and V-flames, while the third process has been considered for some combustor systems and is discussed in the section on SPACE HEATING RATES.

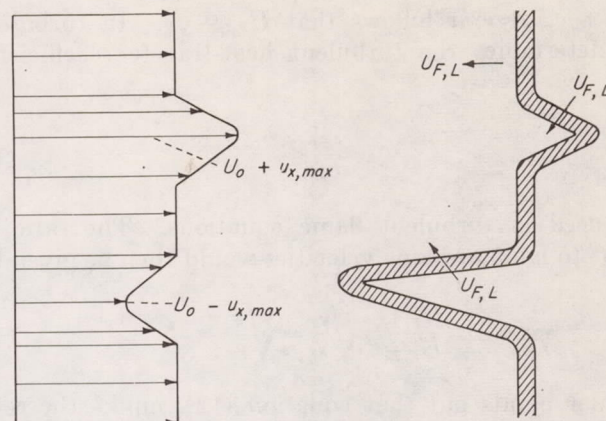
TURBULENT FLAMES

Damköhler theory.—Damköhler (ref. 9) pioneered in theoretical considerations of turbulent flames. He considered separately the cases of large-scale (greater than the flame thickness \mathcal{F}), small-intensity turbulence, and small-scale ($< \mathcal{F}$), large-intensity turbulence. He readily admitted that both situations existed in most flames, the large-scale turbulence being of greater importance in combustor applications. Damköhler points out that the eddy diffusivity ϵ alone may not be sufficient to describe the effects of turbulence on flames, since $\epsilon = \mathcal{L} \sqrt{u_x^2}$ and both \mathcal{L} and $\sqrt{u_x^2}$ may have different influences on flame propagation. It is necessary, therefore, to know the influence of both the scale and intensity of turbulence.

In the case of large-scale, low-intensity turbulence, Damköhler suggests that the flame will be wrinkled but that the laminar transport processes will remain virtually unaffected. This is not unreasonable if large-scale turbulence is considered to consist of large eddies, within which the molecular processes of heat transfer and diffusion take place independently of the movement of the eddy as a whole. Damköhler suggests the following picture:



Sketch (m)



Sketch (n)

In the case of a laminar flat flame with constant $U_o = U_{F,L}$ the situation in (m) is obtained. If velocity fluctuations u_x are introduced, however, the velocity at some points will be $U_o + u_x$, and a conical Bunsen-like flame retaining a normal flame velocity $U_{F,L}$ will be obtained (sketch (n)). Where $U_o - u_x$ exists, a local flashback will occur. In the case of flashback, the flame surface area continues to increase so that the spatial rate of flame movement increases with time, and hence the distortion is greater where the velocity fluctuation is negative. In order to reverse the flashback, the flow velocity must exceed $U_o + u_x$. The velocity fluctuations thus produce a wrinkled flame.

Equation (1) of chapter IV shows that for a constant $U_{F,L}$ the flame area will be proportional to the flow velocity; hence, the mean flow through the turbulent flame $U_{F,T} \propto \sqrt{u_x^2}$; or, if \mathcal{L} is constant as is true for tube flow, $U_{F,T} \propto \epsilon$. Since $\epsilon \propto Re$, it follows, according to Damköhler, that $U_{F,T} \propto Re$ for large-scale, low-intensity turbulence. Because of the complex nature of the wrinkling, Damköhler concludes that the exact relation between Reynolds number and $U_{F,T}$ cannot be written, but only the proportionality. As is evident from figure 167(c), the turbulent flame velocity measured by Damköhler using the inner luminous surface is linear with Reynolds number at the higher Reynolds numbers. Since the higher Reynolds numbers were produced in tubes of large diameter, they do represent large-scale turbulence in which \mathcal{L}/\mathcal{F} varies from 2.7 to 2.1. Actually, the equation representing the straight portion is of the form $U_{F,T} = aRe + \mathcal{B}$, and Damköhler attributed the term \mathcal{B} to small-scale turbulence. For a different interpretation of the same data, see the discussion of Delbourg's theory.

In order to explain the influence of small-scale turbulence on flame velocity, Damköhler investigated the change in diffusion and heat transfer with Reynolds number, since the small-scale turbulence is assumed to produce no roughening of the flame surface. In thermal mechanisms of flame propagation, the flame velocity is related to transport properties by the following relation from equation (39) of chapter IV:

$$U_{F,L} \propto \sqrt{\frac{\kappa_L}{c_p \rho_o}} \quad (10)$$

Since $\kappa_L/c_p\rho_0 \approx \nu$, it follows that $U_{F,L} \propto \sqrt{\nu}$. In turbulent flow, ϵ determines the turbulent heat-transfer coefficient, so that

$$\epsilon = \frac{\kappa_T}{c_p\rho_0} \quad (11)$$

can be used in turbulent flame equations. The ratio of turbulent to laminar flame velocities would then be given by

$$\frac{U_{F,T}}{U_{F,L}} = \sqrt{\frac{\kappa_T}{\kappa_L}} = \sqrt{\frac{\epsilon}{\nu}} \quad (12)$$

Damköhler points out that equation (12), unlike the relations for large-scale turbulence, shows the direct dependence of the flame velocity ratio and not merely proportionality. It should be remembered, however, that this is true only if the remaining terms in equation (39) of chapter IV are not influenced by turbulence. Note that the right side of equation (12) is related to the Reynolds number based on turbulence parameters used by Wagner (ref. 5).

Equation (12) would permit the calculation of turbulent flame velocities for small-scale turbulence. Since the value of ϵ changes across the burner diameter, however, and only a mean flame velocity was measured by Damköhler, a direct comparison was not possible. Damköhler constructed a hypothetical inner flame cone using equation (12) and an equation for the radius and height for laminar flames. He then calculated a mean turbulent flame velocity from the constructed flame shape. The dashed line in figure 167(c) indicates reasonable agreement between his calculations and experimental results.

Shelkin theory.—Shelkin (ref. 21) expanded Damköhler's model of turbulent flame propagation but, in general, came to similar conclusions. He assumed from the early thermal theories that the flame velocity could be represented by

$$U_{F,L} = \sqrt{\frac{\kappa_L}{t_{re}}} \quad (13)$$

In the turbulent case, molecular and turbulent heat transfer would be combined so that

$$U_{F,T} = \sqrt{\frac{\kappa_L + \kappa_T}{t_{re}}} \quad (14)$$

which assumes that t_{re} is unchanged in small-scale, high-intensity turbulence. Rearranging,

$$U_{F,T} = \sqrt{\frac{\kappa_L}{t_{re}}} \left(1 + \frac{\kappa_T}{\kappa_L}\right) = U_{F,L} \sqrt{1 + \frac{\kappa_T}{\kappa_L}} \quad (15)$$

may be written. If it is assumed that $\kappa_L + \kappa_T = c_p\rho_0\epsilon$, Damköhler's equation is obtained.

For large-scale turbulence, Shelkin also assumes that only the flame area changes. He assumes that the flame breaks into cones and that the ratio of turbulent to laminar flame velocity will be equal to the ratio of the surface area of the average cone to the area of its base. The height of the cone is taken to be proportional to the intensity of turbulence $\sqrt{u_x^2}$ (see fig. 152 for the variation of cone height with velocity) and is given by $\mathcal{L}\sqrt{u_x^2}/U_{F,L}$. The surface area of the cone is then

$$S_c = \frac{1}{2} \pi \mathcal{L} \sqrt{\left(\frac{\mathcal{L}}{2}\right)^2 + \left(\frac{\mathcal{L}\sqrt{u_x^2}}{U_{F,L}}\right)^2} \quad (16)$$

while the area of the base is $A = \pi(\mathcal{L}/2)^2$. Hence, the ratio becomes, after rearranging,

$$\frac{U_{F,T}}{U_{F,L}} = \frac{S_c}{A} = \sqrt{1 + \left(\frac{\mathcal{B}\sqrt{u_x^2}}{U_{F,L}}\right)^2} \quad (17)$$

($\mathcal{B}=2$ for a cone, but Shelkin prefers the arbitrary constant \mathcal{B} .) This reduces to Damköhler's equation when $(\mathcal{B}\sqrt{u_x^2}/U_{F,L})^2 \gg 1$ or when $\sqrt{u_x^2} > U_{F,L}$; hence, Shelkin concludes that Damköhler's equation applies for large-scale, high-intensity turbulence. For very large intensities, Shelkin suggests that the flame breaks up into two small islands and that the rate of burning depends only on the rate of mixing, so that $U_{F,T} \propto \sqrt{u_x^2}$ and is completely independent of $U_{F,L}$. While this is evidently not the case for burner flames (see fig. 167(d)), it is reasonable that some combustor conditions may exist where mixing processes control the burning rate.

Scurlock (ref. 14) combines both of Shelkin's equations so that for small-scale turbulence equation (15) is approached, for large-scale turbulence equation (17) is approached, and both are important where the scale of turbulence is of the order of the flame thickness. Scurlock's equation is

$$\frac{U_{F,T}}{U_{F,L}} = \sqrt{\left[1 + \left(\frac{2\sqrt{u_x^2}}{U_{F,L}}\right)^2 \left(\frac{\mathcal{L}/\mathcal{T}_F}{\mathcal{K}_1 + \mathcal{L}/\mathcal{T}_F}\right)\right] \left[1 + \left(\frac{\kappa/c_p\rho_0}{\mathcal{K}\sqrt{u_x^2}\mathcal{L}}\right) \left(\frac{1}{1 + \mathcal{L}/\mathcal{K}_2\mathcal{T}_F}\right)\right]} \quad (18)$$

Delbourg theory.—Delbourg (ref. 16) investigated in greater detail the regime that Damköhler and Shelkin attributed to small-scale turbulence where the flame speed changes because of changes in the transport properties. Delbourg, like Shelkin, introduces an over-all thermal conductivity $\kappa = \kappa_L + \kappa_T$ composed of laminar and turbulent components. Delbourg uses essentially a thermal approach to calculate turbulent flame velocity. He writes an energy equation analogous to the integrated form of the energy equation (33a) of chapter IV for laminar flames, and a con-

tinuity equation analogous to equation (32a) of chapter IV.

In order to simplify integration, Delbourg assumes that the chemical reaction rate ω is directly proportional to temperature rather than the usual Arrhenius reaction rate and uses mean values for the thermal conductivity κ and specific heat c_p . Delbourg's assumptions lead to the following equation for laminar flames:

$$U_{F,L} = \frac{\mathcal{K}_L T_o}{\rho_o c_p} \kappa_L \frac{T_F - T_3}{T_3 - T_o} \quad (19)$$

By analogy, he writes for turbulent flames

$$U_{F,T} = \frac{\mathcal{K}_1 T_0}{\rho_0 c_p} \kappa \frac{T_F - T_3}{T_3 - T_0} \quad (20)$$

where \mathcal{K}_1 represents the non-temperature-dependent terms in the turbulent reaction rate, and, like κ , may be considered to be composed of a turbulent and a laminar component:

$$\mathcal{K}_1 = \mathcal{K}_T + \mathcal{K}_L \quad (21)$$

Some changes in the equations are necessary to obtain a solution in terms of measurable quantities. From equation (11), the turbulent component of thermal conductivity is proportional to the eddy diffusivity:

$$\kappa_T \propto \epsilon \quad (22)$$

and, for tube flow,

$$\epsilon = \mathcal{F} \left(\frac{W_{F/2}}{r} \right) Re^{1/2} \quad (23)$$

Since κ_T is therefore a function of radius, it is difficult to relate the calculations to the measured average flame velocity. A turbulent flame velocity based on an average across the tube may be defined:

$$\bar{U}_{F,T} = \bar{U}_0 \frac{A_{tub}}{S_F} \quad (24)$$

By numerical integration of the differential equations relating the surface area of the turbulent flame to measurable quantities, Delbourg gets

$$\frac{\bar{U}_{F,T}}{\bar{U}_{F,L}} = 0.0128 Re^{0.4} \quad (25)$$

which is in reasonable agreement with his experimental relation

$$\frac{U_{F,T}}{U_{F,L}} = 0.088 Re^{0.4} \quad (26)$$

As shown in figure 171, Delbourg points out that Damköhler's data are in agreement, since they may be represented by an equation

$$\frac{U_{F,T}}{U_{F,L}} = 0.07 Re^{0.4} \quad (27)$$

Delbourg states that the ratio $U_{F,T}/U_{F,L}$ is relatively independent of the fuel-air mixture.

Karlovitz theory.—Karlovitz and coworkers (ref. 10) studied a model much like Damköhler's for large-scale turbulence. They considered the effect produced as an eddy passes through a laminar flame front. The time of contact between the eddy and the flame is given by $t = \mathcal{L}/U_{F,L}$. During this contact period the flame is distorted, since the element of flame in contact with the eddy is advanced a distance $\sqrt{x^2}$ in the time t because of the con-

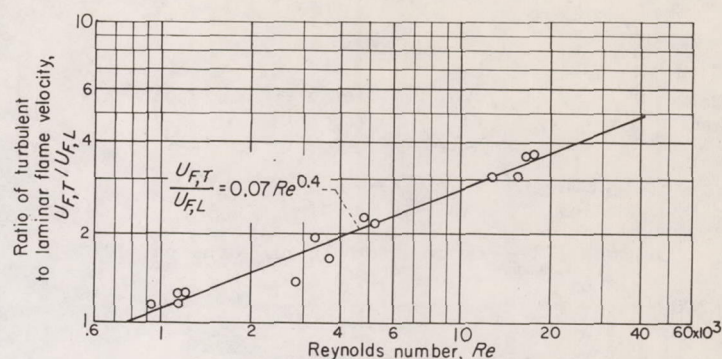


FIGURE 171.—Variation of ratio of turbulent to laminar flame velocity with Reynolds number. Data of reference 9; equation of reference 16.

tact with the eddy. The turbulent movement velocity is then

$$U'_{F,T} = \frac{\sqrt{x^2}}{t} \quad (28)$$

The value of $\sqrt{x^2}$ is determined from the equation

$$\sqrt{x^2} = \{2\bar{u}_x^2 t_0 [t - t_0(1 - e^{-t/t_0})]\}^{1/2} \quad (29)$$

where $t_0 = \mathcal{L}/\sqrt{u_x^2}$.

Substituting these relations in equation (28), there results the general equation

$$(U'_{F,T})^2 = 2U_{F,L}\sqrt{u_x^2} \left[1 - \frac{U_{F,L}}{\sqrt{u_x^2}} \left(1 - e^{-\sqrt{u_x^2}/U_{F,L}} \right) \right] \quad (30)$$

which, for $t/t_0 \ll 1$ (low-intensity turbulence), reduces to

$$U'_{F,T} = \sqrt{u_x^2} \quad (30a)$$

and, for $t/t_0 \gg 1$ (high intensity), reduces to

$$U'_{F,T} = (2U_{F,L}\sqrt{u_x^2})^{1/2} \quad (30b)$$

or

$$\frac{U'_{F,T}}{U_{F,L}} = \left(2\frac{\sqrt{u_x^2}}{U_{F,L}} \right)^{1/2} \quad (30c)$$

Karlovitz found that equation (30c) represents the general equation (30) over most of the range. If it is assumed that $\sqrt{u_x^2} \propto Re$, then Karlovitz's results are in qualitative agreement with Delbourg's Re variation, but Karlovitz shows a dependence of the ratio on laminar flame velocity.

Equations (30) give only a part of the turbulent flame movement, however. Karlovitz suggests that the turbulent motion described by $U'_{F,T}$ proceeds forward and backward with equal velocity but produces no net movement of the entire flame. There must be added to the turbulent movement the one-directional flame movement that results from laminar flame propagation, so that the turbulent flame velocity is

$$U_{F,T} = U'_{F,T} + U_{F,L} \quad (31)$$

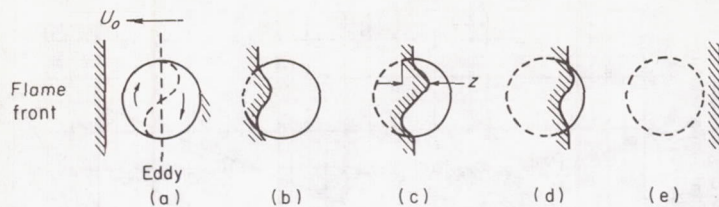


FIGURE 172.—Passage of eddy through flame (ref. 12).

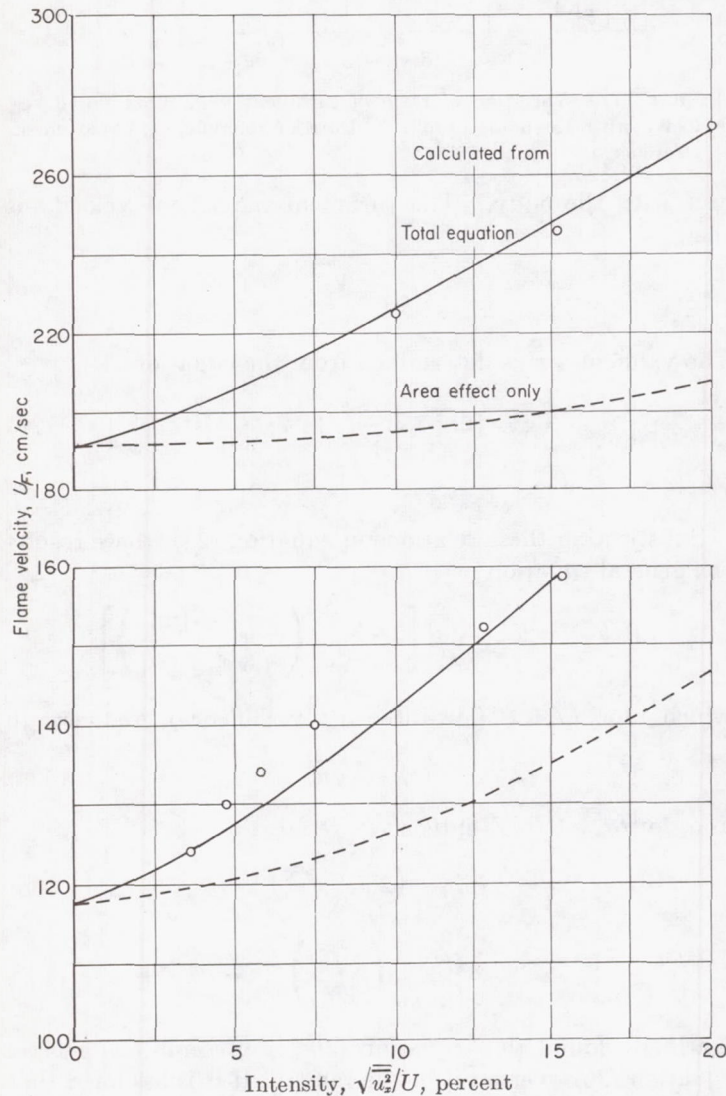


FIGURE 173.—Comparison of theoretical curves with experimental data (ref. 12).

The equations for turbulent flame velocity thus become:
General equation:

$$\frac{U_{F,T}}{U_{F,L}} = 1 + \left\{ \left(\frac{2\sqrt{u_z^2}}{U_{F,L}} \right) \left[1 - \left(1 - e^{-\sqrt{u_z^2}/U_{F,L}} \right) \frac{U_{F,L}}{\sqrt{u_z^2}} \right] \right\}^{1/2} \quad (32)$$

For $t/t_0 \ll 1$:

$$\frac{U_{F,T}}{U_{F,L}} = 1 + \frac{\sqrt{u_z^2}}{U_{F,L}} \quad (33)$$

For $t/t_0 \gg 1$:

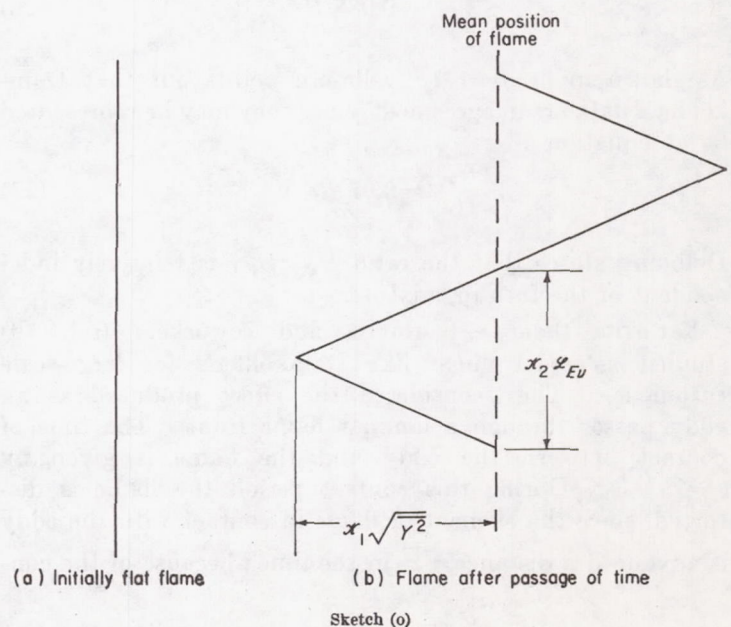
$$\frac{U_{F,T}}{U_{F,L}} = 1 + \left(\frac{2\sqrt{u_z^2}}{U_{F,L}} \right)^{1/2} \quad (34)$$

Leason theory.—Leason (ref. 12) also considers the effect produced when an eddy passes through a flame. The physical picture, which is based on an eddy containing a sinusoidal velocity profile, is illustrated in figure 172. Leason obtains from the geometric consideration alone the relation

$$\frac{U_{F,T}}{U_{F,L}} = \left[1 + \left(\frac{2\sqrt{u_z^2}}{U_0} \right)^2 \right]^{1/2} \quad (35)$$

which would be the same as Shelkin's relation for a cone (eq. (17), $B=2$) if the U_0 in the brackets were replaced by $U_{F,L}$. Leason found that the area extension alone did not account for all of the flame velocity increase with turbulence. Therefore, he added a diffusivity factor similar to Damköhler's, except that it takes into account the statistical property of the turbulent flow. The use of the entire spectrum of turbulence intensities, of course, greatly complicates the equations, but the good agreement obtained by Leason between his modified equation and his experiments is shown in figure 173. Since Leason does not give the complete development of his equations, it is difficult to evaluate the results.

Scurlock and Grover theory.—Scurlock and Grover (ref. 22) developed in detail the processes that can produce wrinkling of the flame surface in turbulent flow. Only large-scale turbulence is considered, and it is assumed that the laminar flame velocity within the wrinkled flame remains unchanged. In the manner of Shelkin (ref. 21) and Leason (ref. 12), Scurlock and Grover assume that the passage of an eddy through the undisturbed flame front produces the wrinkling. The assumed wrinkled flame shape after the passage of a certain time is given in sketch (o):



Note the similarity to figure 172 from Leason's model. It is assumed that the average height of the wrinkles is proportional to the root-mean-square displacement $\sqrt{\bar{Y}^2}$ of a flame element from the mean flame front position and that the average base width of these wrinkles is proportional to the Eulerian scale \mathcal{L}_{Eu} . Considering the wrinkle either as an infinitely long prism with the cross section corresponding to one of the wrinkles in the sketch, or as a cone with height and base diameter as shown, would give the ratio of wrinkled area (turbulent flame) to base area (laminar flame):

$$\frac{A_T}{A_L} = \frac{U_{F,T}}{U_{F,L}} = \left[1 + \mathcal{K}_3 \left(\frac{\bar{Y}^2}{\mathcal{L}_{Eu}^2} \right) \right]^{1/2} \quad (36)$$

where $\mathcal{K}_3 = 4\mathcal{K}_1^2/\mathcal{K}_2^2$. This has the same form as Shelkin's equation (see eq. (17)), but the root-mean-square displacement and Eulerian scale are used instead of the turbulence intensity and laminar flame velocity.

According to the preceding picture of a turbulent flame, the ratio of the turbulent to laminar flame velocities will depend on both \bar{Y}^2 and \mathcal{L}_{Eu} . Scurlock and Grover describe three effects believed to be important in determining \bar{Y}^2 :

- (1) Eddy diffusion associated with turbulence in the unburned gases, which tends to increase \bar{Y}^2
- (2) Propagation of the flame into the unburned gases, which tends to reduce \bar{Y}^2
- (3) Flame-generated instability and shear and eddy diffusion, which are associated with the density decrease across a flame and which tend to increase \bar{Y}^2

The process of eddy diffusion resulting from turbulence in the approach flow can be considered alone if $U_{F,L}$ is assumed small, so that $U_{F,L}/\sqrt{u_x^2}$ approaches zero, and if the density change across the flame is ignored. Under these conditions, the mean displacement at any time t can be calculated from the equation

$$\frac{d(\bar{Y}^2)}{dt} = 2\bar{u}_x^2 \int_0^t \mathcal{R}_t dt \quad (37)$$

(See ch. II for a more detailed discussion of calculations of the mean displacement.) In the actual flame, however, the flame has moved a distance $y = U_{F,L}t$, so that the simple displacement previously calculated does not apply. Consideration must also be given to the change of flame position. Scurlock and Grover accomplish this by means of a mixed (time and position) correlation factor \mathcal{R}_{ty} , such that

$$\frac{d(\bar{Y}^2)}{dt} = 2\bar{u}_x^2 \int_0^t \mathcal{R}_{ty} dt = 2\bar{u}_x^2 \int_0^t \mathcal{R}_t \mathcal{R}_y dt \quad (38)$$

For very short diffusion times, $\mathcal{R}_t \mathcal{R}_y \approx 1$, and equation (38) reduces to

$$\frac{d\bar{Y}^2}{dt} \approx 2\bar{u}_x^2 t \quad (39)$$

or

$$\bar{Y}^2 = \bar{u}_x^2 t^2 \quad (40)$$

For long diffusion times,

$$\bar{Y}^2 = 2\sqrt{\bar{u}_x^2} \mathcal{L}'_{La} t \quad (41)$$

where

$$\mathcal{L}'_{La} = \sqrt{\bar{u}_x^2} \int_0^\infty \mathcal{R}_t \mathcal{R}_y dt = \sqrt{\bar{u}_x^2} T_o \quad (42)$$

It is much more difficult to evaluate the equation for intermediate times. Scurlock and Grover derive the equation

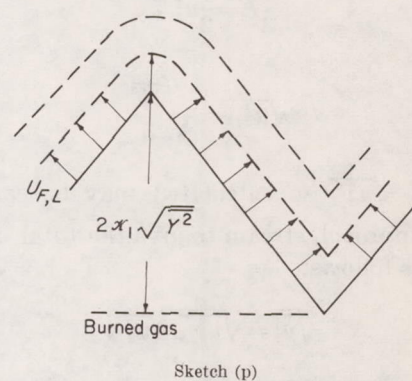
$$\bar{Y}^2 = 2\sqrt{\bar{u}_x^2} \mathcal{L}'_{La} t \left[1 - \frac{\mathcal{L}'_{La}}{\sqrt{\bar{u}_x^2} t} \left(1 - e^{-\sqrt{\bar{u}_x^2} t / \mathcal{L}'_{La}} \right) \right] \quad (43)$$

and suggest that \mathcal{L}'_{La} can be calculated from the equation

$$\mathcal{L}'_{La} = \frac{\mathcal{L}_{La}}{1 + \frac{U_{F,L}}{2\sqrt{\bar{u}_x^2}}} = \frac{\mathcal{L}_{Eu}}{2 + \frac{U_{F,L}}{\sqrt{\bar{u}_x^2}}} \quad (44)$$

It should be noted that the consideration of eddy diffusion alone predicts that the area increases rapidly and reaches no limiting value with increasing time. The rate of area increase is reduced by decreasing $\sqrt{\bar{u}_x^2}$, by increasing $U_{F,L}$, and by increasing \mathcal{L}_{Eu} .

The tendency for a flame to flatten and decrease the flame surface was treated by Karlovitz and coworkers (ref. 10). Scurlock uses an essentially similar treatment. Consider a single wrinkle in the flame and the effect of laminar flame propagation:



As illustrated, the presence of a constant velocity tends to flatten the flame, thus reducing the area ratio A_T/A_L . If the mean depth of the wrinkle is $\mathcal{K}_1\sqrt{\bar{Y}^2}$, the distance between the heads of two wrinkles, one facing toward the unburned gas and the other toward the burned gas, is $2\mathcal{K}_1\sqrt{\bar{Y}^2}$. The rate of change of this quantity with time consists of two terms, a positive term representing the rate of movement of the apex into the unburned gas and equal to $U_{F,L}$, and a negative term representing a decrease in the protrusion of the negative apex into the burned gas and given by $-U_{F,L}(1 + \mathcal{K}_2\bar{Y}^2/\mathcal{L}_{Eu}^2)^{1/2}$.

The change in displacement due to flame propagation may thus be obtained from

$$\frac{d\sqrt{\bar{Y}^2}}{dt} = -\mathcal{K}_3 U_{F,L} \left\{ \left[1 + \mathcal{K}_2 \left(\frac{\bar{Y}^2}{\mathcal{L}_{Eu}^2} \right) \right]^{\frac{1}{2}} - 1 \right\} \quad (45)$$

The negative sign indicates the reduction in \bar{Y}^2 due to the flame propagation.

The last effect considered by Scurlock and Grover is the increased displacement due to flame-generated disturbance resulting from the decreased density of the burned gas compared with the unburned gas. A sketch is presented in figure 174 showing the shear regions that generate turbulence in a rod-stabilized flame. In region 1, the unburned-gas velocity exceeds the velocities in the sheltered eddy region behind the stabilizer. In region 2, the unburned gases, which have been accelerated, still have lower velocities than the burned gases. Finally, the burned gases are completely mixed and a uniform velocity results. Scurlock and Grover write momentum balances between the unburned gases and the gases exiting in nonuniform flow from the combustion zone (shear region 2 in fig. 174), and between the unburned gases and the gases exiting in uniform flow after complete mixing (burned gases of region 3 in fig. 174). From these two momentum balances they solve for half the difference in the squares of the velocities of unmixed and mixed burned gases; this quantity represents the maximum kinetic energy that would be available for the turbulence generation from this source. Assuming that this energy is equally divided among the three directions to produce an isotropic turbulence intensity $\sqrt{u_{x,F}^2}$,

$$\frac{1}{3}E = \frac{1}{2}u_{x,F}^2 \quad (46)$$

or

$$\sqrt{u_{x,F}^2} = \sqrt{\frac{2E}{3}} \quad (47)$$

The value of $\sqrt{u_{x,F}^2}$ so calculated may be combined with $\sqrt{u_{x,o}^2}$ of the approach stream to give the total intensity $\sqrt{u_x^2}$ in the flame as follows:

$$\sqrt{u_x^2} = \sqrt{u_{x,o}^2 + u_{x,F}^2} \quad (48)$$

The combined displacement for the three effects can then be calculated from the sum of equations (43) and (45) wherein $\sqrt{u_x^2}$ is calculated by equation (48).

A comparison of the shape and thickness of turbulent flames resulting from a consideration of the three processes influencing \bar{Y}^2 is shown in figure 175. The curves of $U_{F,T}/U_{F,L}$ against initial velocity calculated from a combination of the three effects agree well in shape with the data of reference 3, although the theory does not predict the strong effect of scale (as indicated by the dependence of $U_{F,T}/U_{F,L}$ on the tube diameter) found in reference 3. Scurlock and Grover suggest that the discrepancy may be in the fraction of the kinetic energy of the burned gases, which is converted into turbulence having a scale-dependence.

The theories of turbulent flame velocity consider small-scale turbulence as a means of increasing the heat-transfer

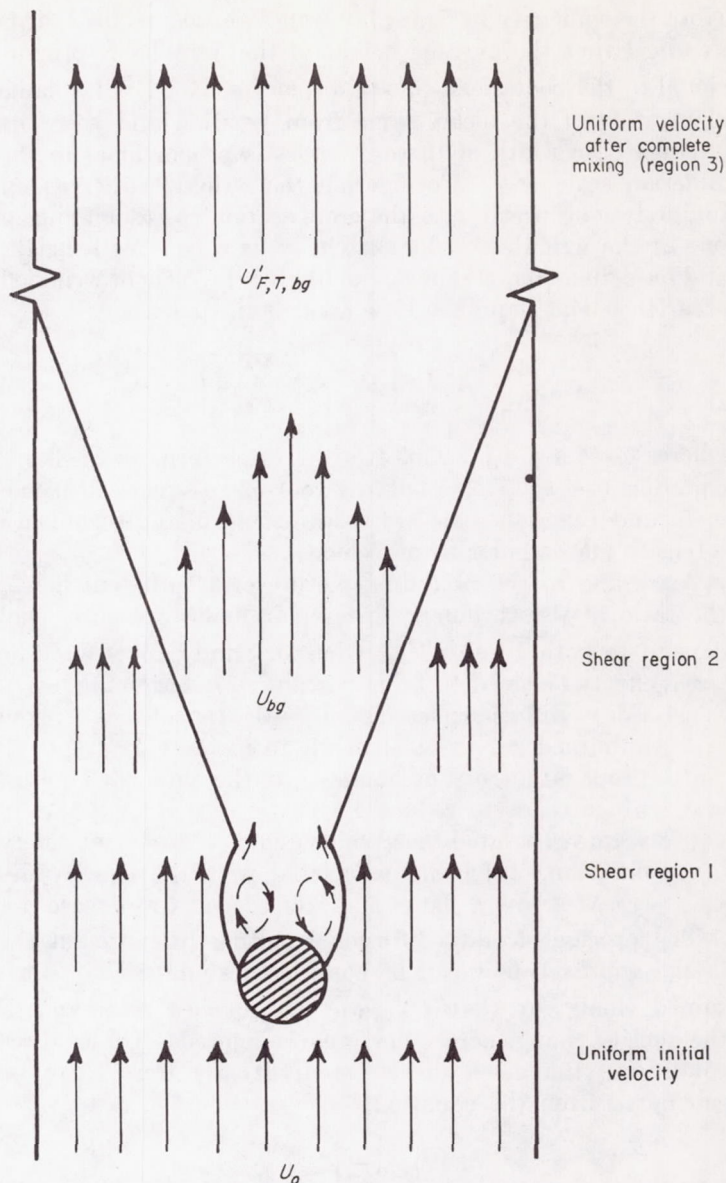


FIGURE 174.—Shear regions generating turbulence in a rod-stabilized flame (ref. 14).

and diffusion characteristics of the system, while large-scale turbulence increases the surface area of the flame. The latter condition is probably of the most interest in practical applications. The theories are not yet sufficiently advanced to be of great value in predicting turbulent flame velocities. It appears, at this time, that more reliable estimates may be made with the empirical relations listed in tables XXII and XXIII.

FLAME-INDUCED TURBULENCE

The theoretical studies presented attempt to relate the turbulent flame velocity to the intensity and scale of the approach-stream turbulence. While Damköhler, Delbourg, and Leason met with some success in this regard, some of the observations by Scurlock and Karlovitz require additional explanations.

If the turbulent flame velocity is strongly dependent on the approach-stream turbulence, it would be expected that changes in the intensity of turbulence should be reflected in

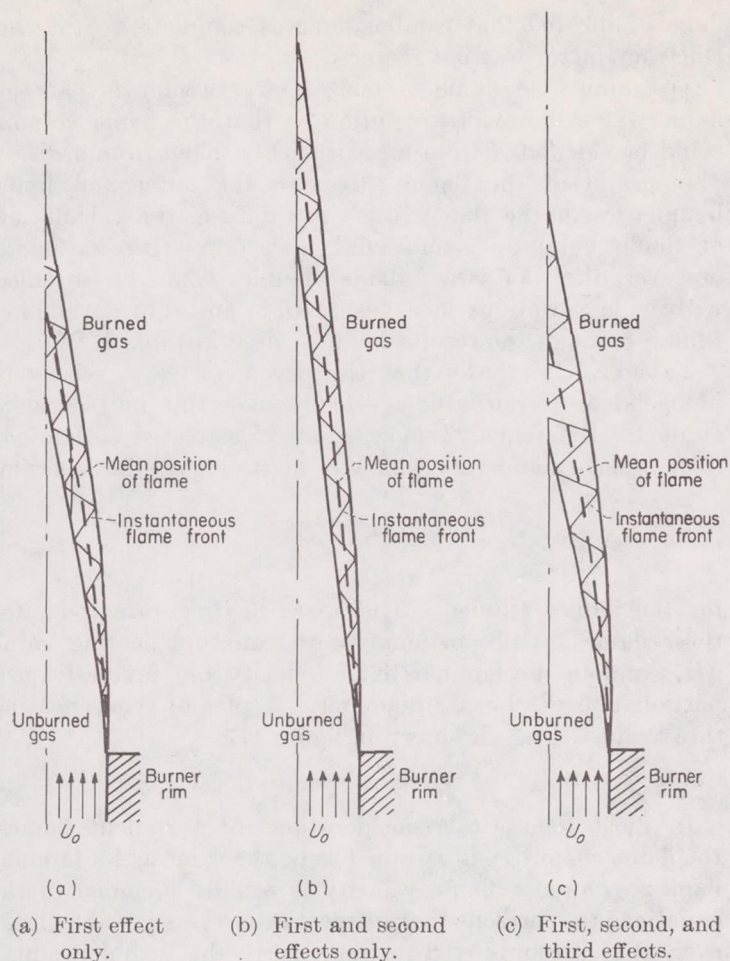


FIGURE 175.—Schematic diagrams of stabilized unconfined flames disturbed by turbulence, assuming 100-percent conversion of available energy to turbulence (ref. 14).

the flame velocity. Scurlock (ref. 14) found in his V-flame experiments that the insertion of screens in the approach flow had a negligible effect on the measured flame velocity. He explains this phenomenon by suggesting a model in which the approach-stream turbulence merely is added to a much stronger turbulence produced by the flame itself. As burning begins at the stabilizer, as shown in figure 174, the unburned gas around it must either expand or accelerate. Since the gas flow is enclosed in a tunnel, the unburned gases accelerate, producing shear forces between the burned and unburned gas and creating a highly turbulent flow. If the shear forces become sufficiently great, as may occur at very high velocities, the flame may not be able to transfer heat and active particles at a sufficient rate to propagate. This suggests that too much turbulence can be detrimental to flame propagation and is consistent with experimental observations of flame stability (ch. VI).

Karlovitz (ref. 10) subsequently found it necessary to consider flame-induced turbulence for open flames as well. Since he used an angle method to determine turbulent flame velocity, he was able to measure flame velocity as a function of the distance from the tube edge. Using equation (32) to calculate turbulence intensities from his measured turbulent flame velocities, Karlovitz found that the calculated $\sqrt{u_x^2}$ agreed with the $\sqrt{u_x^2}$ measured by a hot-wire anemometer

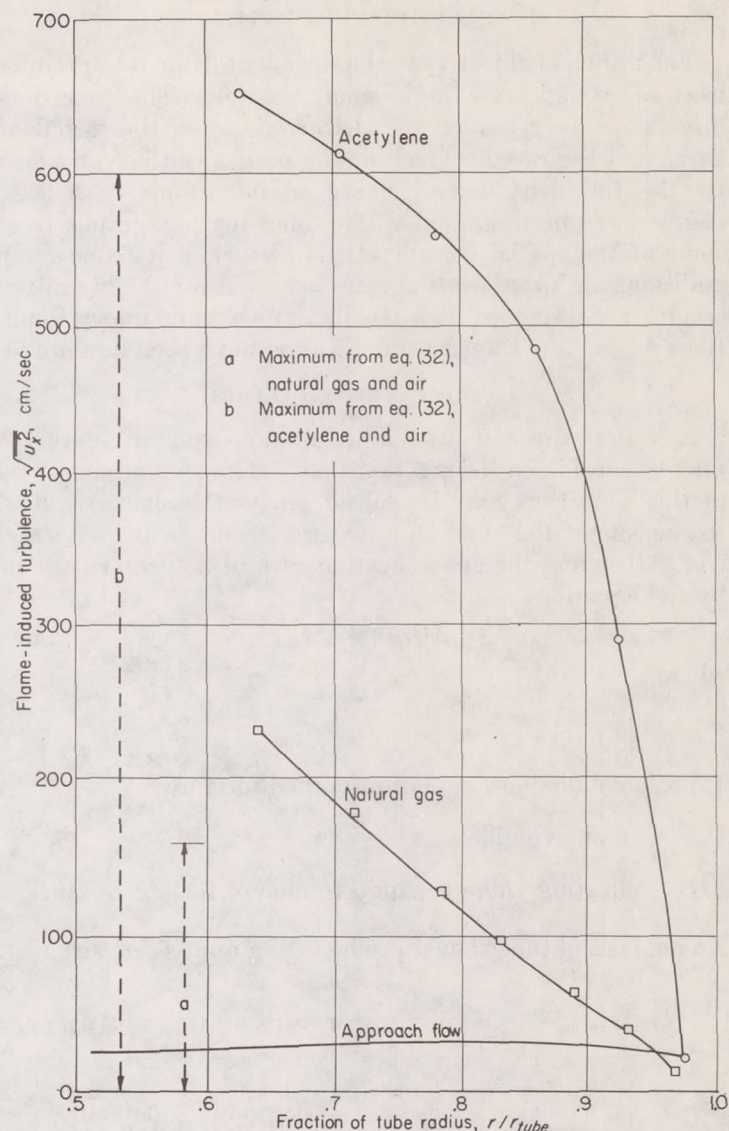


FIGURE 176.—Variation of flame-induced turbulence with fraction of tube radius as calculated from experimental flame velocities (ref. 10).

only at the burner rim, and, as shown in figure 176, the calculated $\sqrt{u_x^2}$ is considerably greater than the measured intensity at other points. It was mentioned previously that the expansion of the burned gas may either accelerate the unburned gas or cause it to expand. In the closed pipe, a velocity increase was suggested. With the open flame, Karlovitz suggests that the expansion of the burned gas from the flame, which is oriented at random angles, produces random fluctuations in the unburned gas, thus increasing the turbulence intensity. The turbulence intensity increases as the burning proceeds from the base to the tip of the flame. Karlovitz computes the maximum flame-generated turbulence from an equation based on the expansion ratio, where

$$\sqrt{u_x^2} = \left(\frac{1}{\sqrt{3}} \right) \left(\frac{\rho_{un}}{\rho_{bg}} = 1 \right) U_{F,L} \quad (49)$$

The calculated flame-generated turbulence is shown in figure 176, and it is evident that this could account for the discrepancy between calculated and measured turbulence intensities.

SPACE HEATING RATES

The principal objective of the turbulent flame is to produce heat at a high rate in a small volume. The preceding discussions have treated the characteristics of the turbulent flame and the rate at which unburned gas can be consumed by the turbulent flame. Space considerations to a large degree have been ignored. The following paragraphs treat some of the spatial considerations of turbulent flames. In addition, the space heating rates achieved in a highly mixed reactor are discussed as a possible upper limit under conditions where heat transfer and diffusion have been minimized.

TURBULENT BUNSEN FLAMES

As a first approximation, the luminous zone in figure 153 may be considered the reaction zone. The volume contained in this zone thus may be considered as the space required to consume the fuel-air mixture. Simon and Wagner (ref. 23) define the space heating rate of a turbulent flame by the equation

$$\Delta Q_{sp} = \mathcal{V} \Delta H_{f,a} \quad (50)$$

where

$$\mathcal{V} = V_{fl,o} / V_F$$

$V_{fl,o}$ volume flow rate of unburned mixture

V_F flame volume

$\Delta H_{f,a}$ heating value per unit volume of fuel-air mixture

An analysis of the exhaust products of a number of turbulent

flames indicated that combustion was complete, so that an efficiency factor was not required.

To obtain the flame volume, it was assumed that the flame was a figure of revolution so that the flame volume could be calculated from measurements taken from a direct photograph of the flame. Because the outer and inner boundaries of the flame brush are diffuse, the calculation of flame volume is somewhat uncertain. It was found, however, that consistent flame volumes could be obtained with wide variations in exposure time and film developing time. Some of the results are presented in table XXIV.

Table XXIV shows that the parameter \mathcal{V} is relatively independent of linear flow velocity over the limited range studied. Reference 23 shows that \mathcal{V} is related to laminar flame velocity and tube diameter according to the equation

$$\mathcal{V} = 6.1 \frac{U_{F,L}}{d_{tube}}$$

for the flames studied. The space heating rate then, for these flames, is proportional to the mixture heating value $\Delta H_{f,a}$ and to the laminar flame velocity but inversely proportional to the burner diameter. A plot of space heating rate against $1/d_{tube}$ is shown in figure 177.

SPHERICAL REACTOR

In most theoretical considerations of turbulent flames, the flame chemistry is assumed to be the same as for laminar flames. Laminar flame velocity is usually included in the equations to represent the chemical rate. It is possible, however, that the improved mixing due to the turbulence may

TABLE XXIV.—SPACE HEATING RATES OF TURBULENT BUNSEN FLAMES (Ref. 23)

Laminar burning velocity, $U_{F,L}$, cm/sec	Burner diam., d_{tube} , cm	Linear flow rate, $U_{o,m}$, cm/sec	Volume flow rate, $V_{fl,o}$, cc/sec	Flame volume, V_F , cc	\mathcal{V} , sec ⁻¹	\mathcal{V}_{av} , sec ⁻¹	Space heating values	
							cal/(sec) (cc)	Btu/(hr) (cu ft)
35.5	0.639	1648	528	1.49	354	344	2.88×10^2	1.17×10^8
		2000	640	1.92	334			
	1.016	800	647	2.74	236	222	1.86×10^2	7.55×10^7
		1173	951	4.61	206			
		1605	1301	6.23	209			
		2030	1644	7.62	216			
		2410	1957	9.01	217			
		2780	2257	9.07	249			
	1.459	782	1301	7.36	177	191	1.81×10^2	6.50×10^7
		984	1644	8.58	192			
		1194	1982	9.76	203			
	1.890	239	670	4.65	144	138	1.16×10^2	4.69×10^7
		661	1894	14.29	133			
71	1.016	1301	1054	2.12	498	462	-----	-----
		1837	1489	3.36	443			
		2114	1713	3.83	445			
	1.459	630	1054	3.42	308	327	-----	-----
		890	1489	4.52	329			
		1152	1927	5.61	344			
	1.890	530	1489	7.20	208	236	-----	-----
		610	1713	6.94	247			
		765	2150	8.50	253			

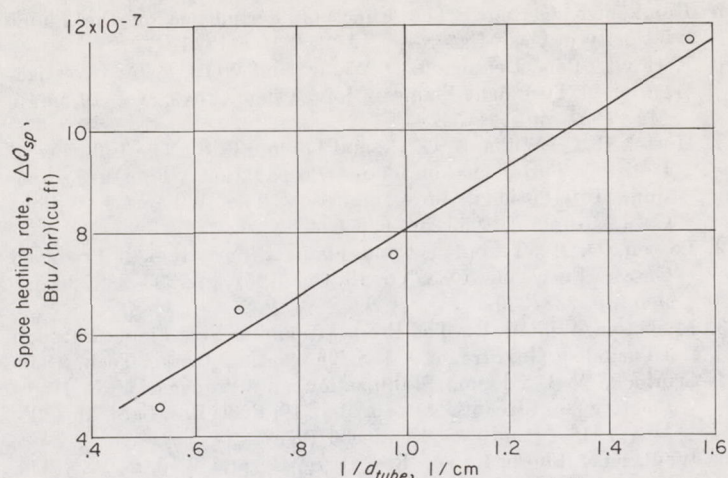


FIGURE 177.—Space heating rates for propane-air flames.

alter the environment in the reaction zone so that the rate of reaction is no longer properly represented by laminar flame velocity. In the extreme, the mixing processes may be so efficient that an essentially homogeneous reaction occurs. Longwell and Weiss (ref. 24) have constructed a spherical reactor in which high-velocity jets of fuel-air mixture are used to create a highly stirred reaction system. The homogeneity of the system during reaction was assessed by removing gas samples at various locations within the sphere. It was found for the time-averaged samples taken that the composition was uniform through more than 90 percent of the reaction volume.

In general, the conditions of mass flow, pressure, or fuel-air ratio were altered until blowout was achieved; thus, the maximum burning rate could be determined for each set of inlet conditions. It was found that the blowout data were a function of fuel-air ratio such that

$$\frac{w}{V_{re} p^{1.8}} = \mathcal{F}(\phi)$$

In a perfectly stirred reactor, the blowout condition is related to the rate of the chemical reaction. As the unburned fuel-air mixture feed rate is increased, for example, the reaction temperature decreases but the concentration of reactants increases. A condition is ultimately reached at which the decrease of reaction rate due to the lowering of temperature exceeds the increase in reaction rate due to the increased reactant concentration. At this condition the reaction stops. Longwell and Weiss used two somewhat differing equations for their fuel-lean and fuel-rich blowout data. For the lean case, the pre-exponential term was $1.67 \times 10^{10} (\text{liters})^{0.8} (^\circ\text{K})^{0.5} (\text{g-mole})^{0.8}$, and for the rich case this constant was 1.11×10^{11} in the same units. An activation energy of 42,000 calories per mole was used for both conditions. From the data obtained, the limiting space heat-release rate for a stoichiometric mixture at atmospheric pressure and 400° K inlet temperature was 3×10^8 Btu/(cu ft)(hr).

COMPARISON OF SPACE HEAT-RELEASE RATES

It is now of interest to compare the space heating rates for various systems. Table XXV is taken from reference 23, where such a comparison is made. It should be kept in mind that the choice of the reaction volume is somewhat arbitrary in some of the systems quoted, so that variations in the heat-release values may exist. From the table it appears that the reaction zone of the laminar flame exhibits the highest heat-release rate, with the reactor of Longwell and Weiss (ref. 24) approaching a similar value. The turbulent Bunsen flame has a somewhat lower heat-release rate, while a turbulent diffusion flame and most turbojet combustors have less than 1/100 the heat-release rate of the laminar flame or spherical reactor.

One may infer from the table that considerable improvement is possible for practical combustors, but it must be remembered that the highest heat-release rates have been obtained without regard to some of the practical considerations that are partly responsible for the lower rates found in combustors.

TABLE XXV.—HEATING VALUES FOR VARIOUS TYPES OF COMBUSTION (Ref. 23)

Combustion system	Space heating rate, ΔQ_{sp} , Btu/(hr) (cu ft of flame or reactor at atm. pressure)	Reference
Laminar flame, stoichiometric propane-air	4×10^8	(*)
Laminar flame, 0.9 stoichiometric propane-air at 3200° F, ¼ atm	6×10^8	25
Homogeneous reactor, stirred stoichiometric propane-air	3×10^8	24
Turbulent premixed stoichiometric propane-air	$5-11 \times 10^7$	23
Turbulent diffusion flame, city gas	1.2×10^6	26
Combustors	Order of 10^6	---

* Calculated from $U_{FL}=35.5$ cm/sec and $\mathcal{F}=0.03$ cm.

APPLICABILITY OF TURBULENT FLAME STUDIES TO JET-ENGINE COMBUSTION

One of the characteristics that the turbulent flames considered in this chapter have in common is the apparent existence of a continuous flame surface. While islands of flame may be broken away from the main body of flame under high flow conditions, such flames have not received much study. The flames existing in practical combustors may or may not have a continuous surface. It appears reasonable that a flame burning from a flameholder, at least under conditions of moderate flow velocity, should resemble the V-flames discussed herein. There is no analogy, however, between these flames and the highly broken-up flame in a turbojet combustor. Nevertheless, if these islands of flame behave as individual burning spheres, each such sphere may retain the burning characteristics of the turbulent flames discussed in this chapter.

Despite the uncertainty in the prediction of turbulent burning velocity, the flame dimensions included herein may be used to compute the space requirements for combustion under a given flow condition. It may be assumed, for example, that the envelope of a turbulent Bunsen flame represents the minimum volume necessary for complete combustion of the mixture flowing into the flame. Correlations based on this and analogous concepts are presented in subsequent chapters.

REFERENCES

1. Lewis, Bernard, and von Elbe, Guenther: Combustion, Flames and Explosions of Gases. Academic Press, Inc., 1951.
2. Kaskan, W. E.: An Investigation of Vibrating Flames. Fourth Symposium (International) on Combustion, The Williams & Wilkins Co. (Baltimore), 1953, pp. 575-591.
3. Bollinger, Lowell M., and Williams, David T.: Effect of Reynolds Number in Turbulent-Flow Range on Flame Speeds of Bunsen Burner Flames. NACA Rep. 932, 1949. (Supersedes NACA TN 1707.)
4. Shore, Leon B.: A Study of the Characteristics of Open Turbulent Flames Burning from Tubes. Ph. D. Thesis, Univ. of Delaware, 1953.
5. Wagner, Paul: Burning Velocities of Various Premixed Turbulent Propane Flames on Open Burners. NACA TN 3575, 1955.
6. Wohl, Kurt: Burning Velocity of Unconfined Turbulent Flames—Theory of Turbulent Burning Velocity. Ind. and Eng. Chem., vol. 47, no. 4, Apr. 1955, pp. 825-827.
7. Clark, Thomas P., and Bittker, David A.: A Study of the Radiation from Laminar and Turbulent Open Propane-Air Flames as a Function of Flame Area, Equivalence Ratio, and Fuel Flow Rate. NACA RM E54F29, 1954.
8. Levine, Oscar, and Gerstein, Melvin: Fundamental Flame Velocities of Pure Hydrocarbons. III—Extension of Tube Method to High Flame Velocities—Acetylene-Air Mixtures. NACA RM E51J05, 1951.
9. Damköhler, Gerhard: The Effect of Turbulence on the Flame Velocity in Gas Mixtures. NACA TM 1112, 1947.
10. Karlovitz, Béla, Denniston, D. W., Jr., and Wells, F. E.: Investigation of Turbulent Flames. Jour. Chem. Phys., vol. 19, no. 5, May 1951, pp. 541-547.
11. Hottel, H. C., Williams, G. C., and Levine, R. S.: The Influence of Isotropic Turbulence on Flame Propagation. Fourth Symposium (International) on Combustion, The Williams & Wilkins Co. (Baltimore), 1953, pp. 636-644.
12. Leason, D. B.: Turbulence and Flame Propagation in Premixed Gases. Fuel, vol. XXX, no. 10, Oct. 1951, pp. 233-238; discussion, pp. 238-239.
13. Mickelsen, William R.: The Propagation of a Free Flame Through a Turbulent Gas Stream. M. S. Thesis, Case Inst. of Tech., 1953.
14. Scurlock, A. C.: Flame Stabilization and Propagation in High-Velocity Gas Streams. Meteor Rep. 19, Fuels Res. Lab., M. I. T., May 1948. (Contract NORD 9661.)
15. Wohl, Kurt, Shore, L., von Rosenberg, H., and Weil, C. W.: The Burning Velocity of Turbulent Flames. Fourth Symposium (International) on Combustion, The Williams & Wilkins Co. (Baltimore), 1953, pp. 620-635.
16. Delbourg, M. P. (C. C. Graves, trans.): Influence of the Turbulence on the Mechanism of the Reactions of Combustion in the Gaseous Phase. Trans. from Revue de L'Institut Francaise de Petrole et annales des combustibles liquides, vol. 4, Sept. 1949, pp. 530-538.
17. Edse, Rudolph: Studies on Burner Flames of Hydrogen-Oxygen Mixtures at High Pressures. Tech. Rep. 52-59, Flight Res. Lab., Wright Air Dev. Center, Wright-Patterson Air Force Base, Apr. 1952. (RDO No. R-467-1.)
18. Culshaw, G. W., and Garside, J. E.: Recent Studies of Aerated Burner Flames. Inst. Gas Eng. (London), Inst. Gas Res. Fellowship Rep. 1946-1947. (Reviews papers from period 1943-1946, including those of Delbourg, Heiligenstaedt, and Vasilescu.)
19. Wright, F. H.: Measurements of Flame Speed and Turbulence in a Small Burner. Prog. Rep. No. 3-21, C. I. T., June 6, 1950.
20. Wohl, K., et al.: Investigation of the Basic Problems Associated with Gaseous Combustion. Proj. Squid Semi-Annual Prog. Rep., James Forrestal Res. Center, Princeton Univ., Apr. 1, 1953, pp. 61-73. (Office Naval Res. Contract N6-ori-105, Task Order III, NR-098-038.)
21. Shelkin, K. I.: On Combustion in a Turbulent Flow. NACA TM 1110, 1947.
22. Scurlock, A. C., and Grover, J. H.: Propagation of Turbulent Flames. Fourth Symposium (International) on Combustion, The Williams & Wilkins Co. (Baltimore), 1953, pp. 645-658.
23. Simon, Dorothy M., and Wagner, Paul: Characterization of Turbulent Combustion by Flame Space and Space Heating Rates. Ind. and Eng. Chem., vol. 48, no. 1, Jan. 1956, pp. 129-133.
24. Longwell, John P., and Weiss, Malcolm A.: Heat Release Rates in Hydrocarbon Combustion. Sec. 4: Internal-Combustion Engines. The Inst. Mech. Eng. (London), and ASME Joint Conf. on Combustion, 1955.
25. Avery, W. H.: Space Heating Rates and High Temperature Kinetics. Fifth Symposium (International) on Combustion, Reinhold Pub. Corp., 1955, pp. 86-91.
26. Scurlock, A. C., and Grover, J. H.: Experimental Studies on Turbulent Flames. AGARD Selected Combustion Problems, Butterworths Sci. Pub., 1954, pp. 215-247.

CHAPTER VI

FLAME STABILIZATION

By GORDON L. DUGGER and MELVIN GERSTEIN

INTRODUCTION

The discussion of flame stabilization presented in this chapter is limited to studies of open flames burning from the ends of cylindrical tubes or nozzles and of confined flames burning from single flameholders in small, ramjet-type combustion chambers. The description, definition, and significance of critical boundary velocity gradients, penetration distances, and eddy stabilization are given. Also included are experimental data and correlations of the effects of various flow parameters and chemical factors on flame stability. Some instability phenomena connected with the propagation of nonturbulent flames are discussed. Finally, theoretical treatments for the prediction of critical boundary velocity gradients and for stabilization in the recirculation zone behind bluff bodies (eddy stabilization) are considered.

SYMBOLS

The following symbols are used in this chapter:

A	cross-sectional area
a	constant
b	exponent
C_D	drag coefficient
\mathcal{C}	concentration
c	exponent
c_p	specific heat at constant pressure
D	diffusion coefficient
\mathcal{D}	ratio of rod diameter to tube diameter
d	diameter
d_{fh}^*	characteristic dimension of flameholder
E_{act}	activation energy
F_{fr}	friction factor
\mathcal{F}	function
f	fuel-air ratio
g	boundary velocity gradient
K	property of multifuel mixture
k	constant
M	molecular weight
m	exponent
p	pressure
Q	heat-supply rate
R	universal gas constant
Re	Reynolds number
r	radius
s	percent of stoichiometric oxidant
T	temperature
T_3	ignition temperature

\mathcal{T}_{re}	reaction-zone thickness
U	velocity
V	volume
w	mass-flow rate
X	mole fraction
x	distance
Z	collision factor
ι_{in}	fraction of entering fuel
ι_{st}	fraction of stoichiometric fuel concentration
κ	thermal conductivity
μ	absolute viscosity
ν	kinematic viscosity
ρ	density
φ	equivalence ratio
ψ	volumetric ratio

Subscripts:

a	air
av	average
bo	blowoff
c	cell
cr	critical
cyl	cylinder
dt	duct
F	flame
f	fuel
fb	flashback
i	i^{th} fuel
j	j^{th} fuel
L	laminar
mx	mixture
o	initial conditions
pen	penetration
r	rod
req	required
sh	sheltered zone
st	stoichiometric
$tube$	tube

STABILITY DIAGRAMS: VELOCITY-CONCENTRATION LIMITS

OPEN FLAMES WITH SECONDARY AIR

The velocity-concentration regions for the various stability phenomena typical of open burner flames with secondary (ambient) air, which have been studied by a number of investigators (e. g., refs. 1 to 3), are schematically illustrated in figure 178. When the approach velocity to a seated open flame is decreased until the flame velocity exceeds the approach velocity over some portion of the burner

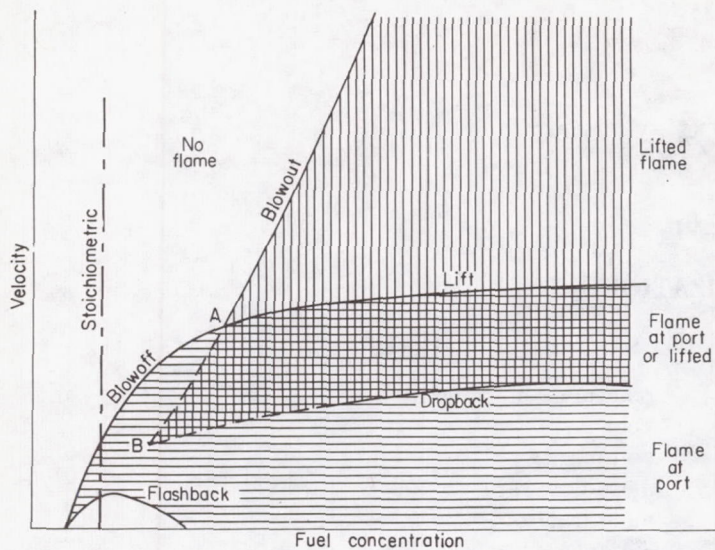


FIGURE 178.—Characteristic stability diagram for open flames (ref. 1).

port, the flame flashes back into the burner. This flashback always occurs in the unshaded area under the flashback curve in figure 178. If, on the other hand, the approach velocity is increased until it exceeds the flame velocity at every point, the flame will either be extinguished completely when the conditions fall in the unshaded region to the left of the blowoff curve or, for fuel-rich mixtures, it will be lifted above the burner until a new stable position in the gas

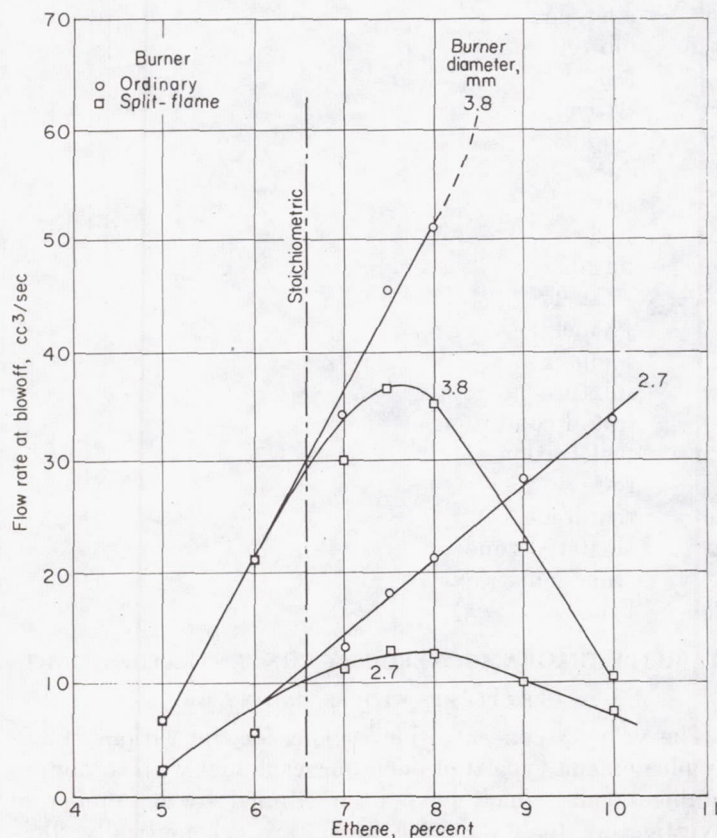


FIGURE 179.—Comparison of blowoff curves obtained with split-flame (Smithells) burners with those obtained on ordinary single-tube burners. Ethene-air mixtures saturated with water vapor at 20° C (ref. 5).

stream above the port is reached as a result of turbulent mixing with and dilution by secondary air. The lift curve is a continuation of the blowoff curve beyond a critical percentage of the fuel gas at point A. The blowout curve corresponds to the gas velocity required to extinguish a lifted flame. Once the flame has been lifted above the port, the approach velocity must be decreased to well below the lift velocity before the flame will drop back and be reseat on the burner rim. Between fuel concentrations A and B, the blowout of the lifted flame occurs at a lower velocity than the flame blowoff from the port. Such a lifted flame, at constant composition, can be produced only by ignition from above the port.

FLAMES DEPRIVED OF SECONDARY AIR

Burner flames may be deprived of secondary air either by surrounding the flame with an annular flow of an inert gas (ref. 4) or by splitting the flame (Smithells separator-type burner) so that the outer mantle burns above an outer concentric tube, thus depriving the inner cone of access to the secondary air (ref. 5). In either case, blowoff curves pass through a maximum near the stoichiometric concentration (fig. 179) and therefore are similar in shape to flame velocity curves (e. g., fig. 129). The decrease in blowoff velocity with increasing concentration on the rich side is not observed with open flames having access to secondary air, because, as a rich mixture is diluted by secondary air through molecular and eddy diffusion, the flame velocity is kept high and the blowoff velocity continues to increase. For the same reason, lifted flames do not occur in the absence of secondary air. Flashback is, of course, unaffected

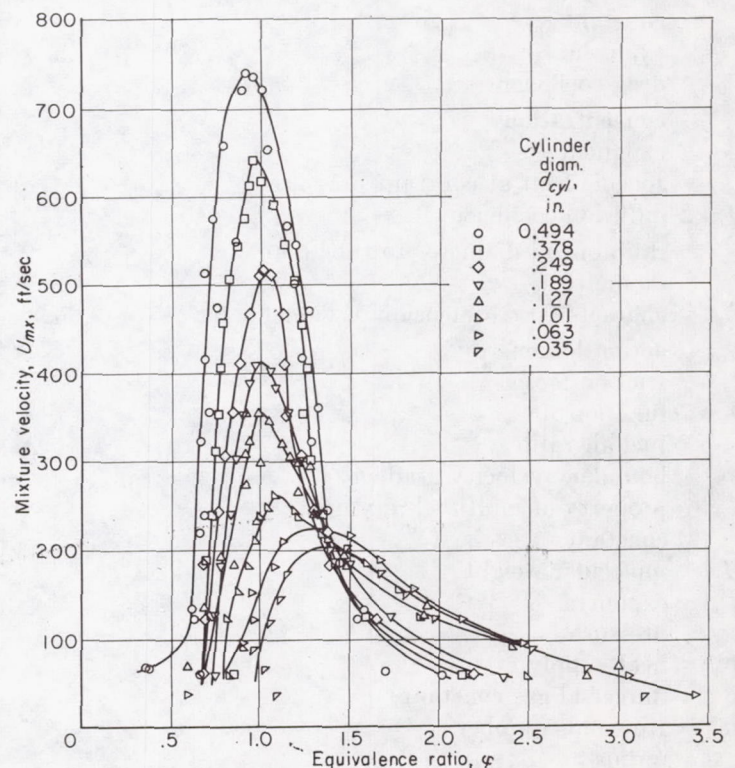


FIGURE 180.—Flame blowoff limits for cylinder sizes from 0.035 to 0.494 inch in diameter. Fuel, hydrocarbon blend (commercial paint thinner); mixture stagnation temperature, 150° F; static pressure, approximately 1 atmosphere (ref. 6).

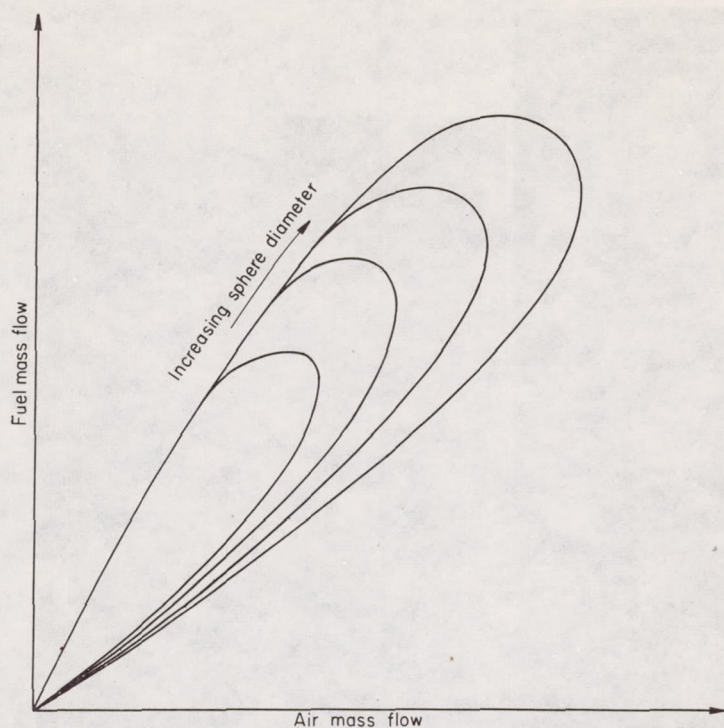


FIGURE 181.—Blowoff from spherical flameholders in 1-inch free jet at atmospheric pressure (ref. 7).

by secondary air. The blowoff behavior of confined flames burning from flameholders is similar, as illustrated by figure 180 for a hydrocarbon fuel burning from flameholders of various diameters (ref. 6). These flameholders were mounted across the 1-inch dimension of a 1- by 4- by 12-inch combustion chamber.

Another type of stability diagram that eliminated the effect of flameholder diameter for rich blowoff from spherical flameholders in a 1-inch free jet at atmospheric pressure is demonstrated in reference 7. Fuel mass flow was plotted

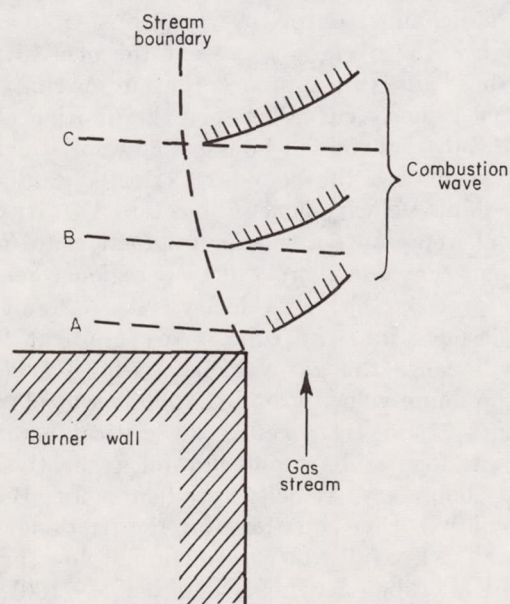
against air mass flow, as shown in figure 181, in which the rich curves form a common envelope.

MECHANISMS OF FLAME STABILIZATION

CRITICAL BOUNDARY VELOCITY GRADIENT

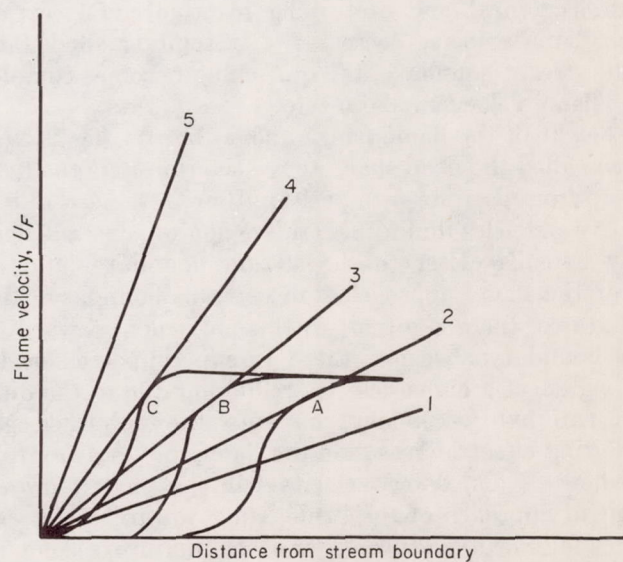
Flames stabilized on burner.—The conditions for stability may be described in terms of laminar flow, regardless of whether the flow in the tube is laminar or turbulent, because in either case there is a laminar sublayer at the stream boundary (ref. 1). Any point of equality between flow velocity and flame velocity must lie within the laminar sublayer, because the gas velocity at the boundary between the sublayer and the turbulent core is greater than the flame velocity. The velocity gradient in this region near the stream boundary where stabilization must occur may be assumed constant if the width of the region is small compared with the tube diameter. In reference 3 (p. 282), curves for flashback of natural-gas flames indicate that this assumption is satisfactory for correlating flashback data obtained with tube diameters larger than the flame-quenching diameter. The critical boundary velocity gradients for flashback and blowoff have been used quite successfully both to correlate flashback or blowoff data obtained with burners of various sizes and shapes (ref. 3, pp. 282-302, and ref. 8) and to correlate turbulent with laminar blowoff data (e. g., refs. 2 and 9).

The interaction of the flame velocity and the critical boundary velocity gradient for a Bunsen flame can be understood by reference to figure 182. Figure 182(a) illustrates how the flame position shifts with increasing gas flow, the flow increasing from flame position A to C. As the flame moves away from the burner port, the fringe of the flame moves closer to the stream boundary. The reason for this can be seen by considering also curves A, B, and C of figure 182(b), which represent the variation of flame velocity with



(a)

(a) Location of flame with respect to burner at various distances above port.



(b)

(b) Relation between flame and stream velocity as function of distance from stream boundary.

FIGURE 182.—Interaction of flame velocity and critical boundary velocity gradient. Bunsen flame (ref. 3, p. 244).

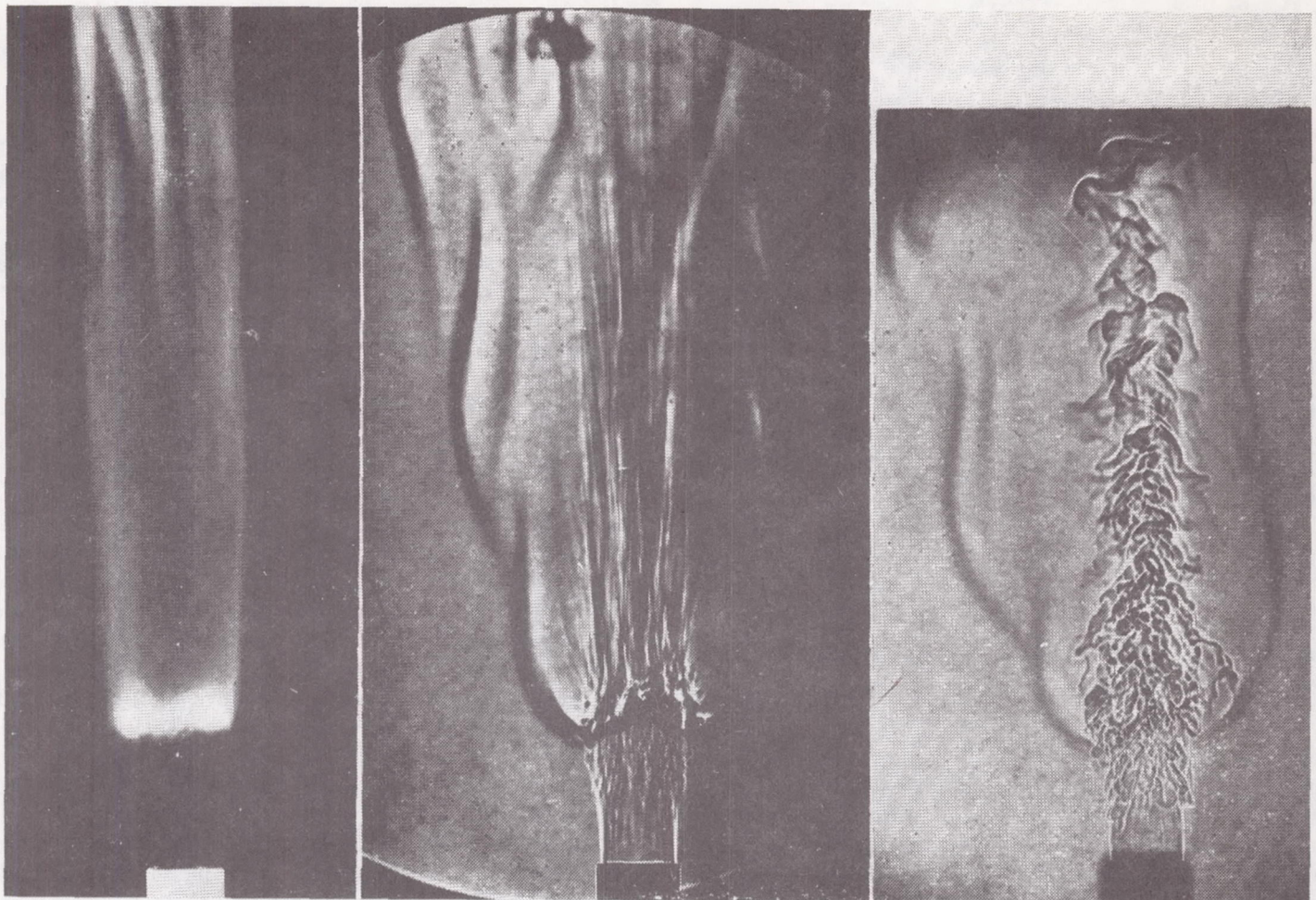


FIGURE 183.—Lifted turbulent burner flame (ref. 3).

distance from the stream boundary for flame positions A, B, and C. In all these curves, the flame velocity is constant far from the stream boundary, but at smaller distances the solid burner rim exerts a quenching effect on the flame by extracting heat and destroying reactive chain carriers, and the flame velocity decreases. At some small distance from the stream boundary, the quenching becomes complete and the flame velocity falls to zero.

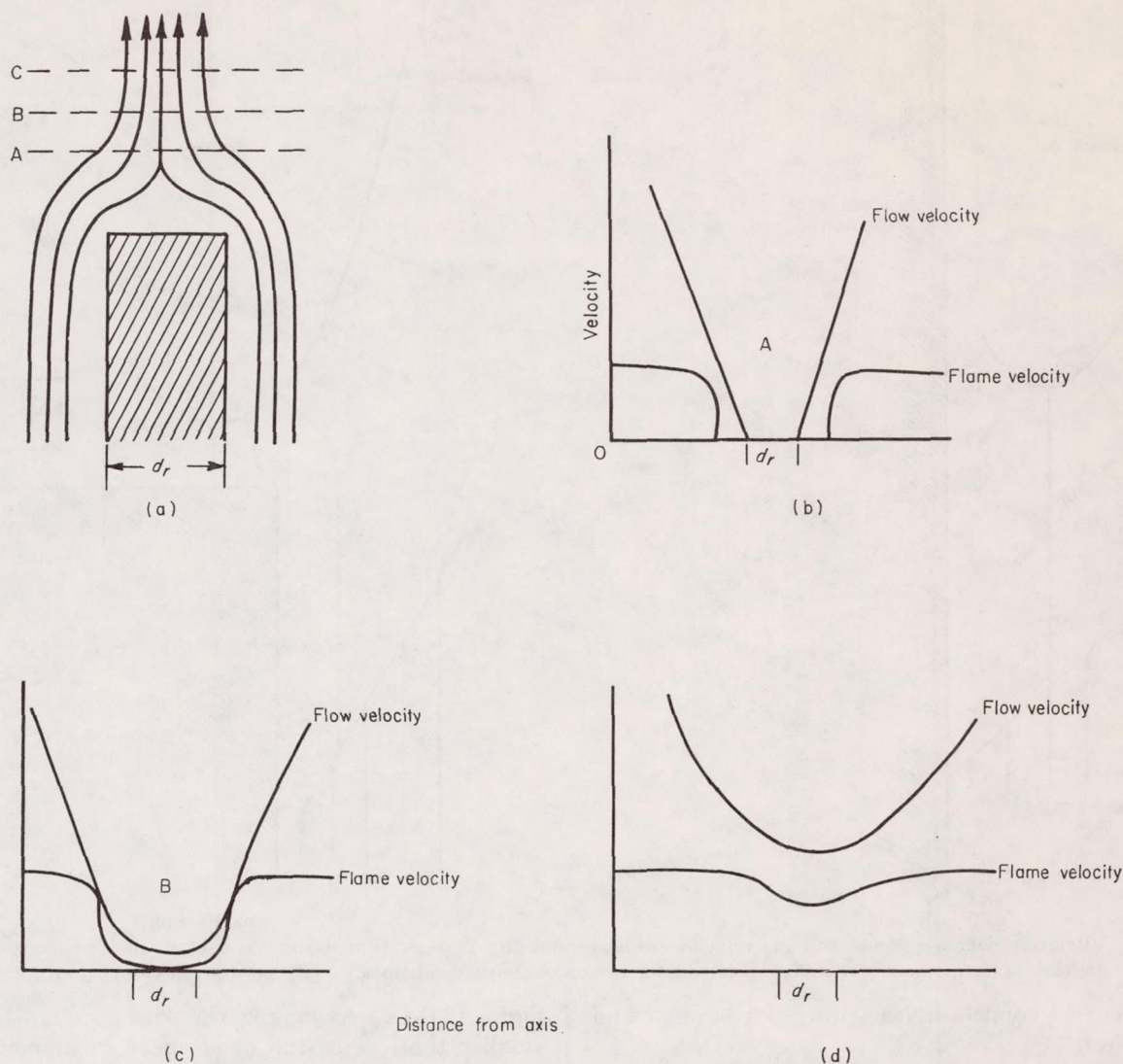
The height of the flame fringe above the rim (fig. 182(a)) has been called the dead space above the rim. As the flame moves up from position A to position B or C, the loss of heat and active particles diminishes, the region of constant flame velocity extends closer to the stream boundary, and the fringe of the flame approaches the stream boundary. For lean mixtures, there is a limit to this movement toward the stream boundary, because there is superimposed on the quenching effect a flame velocity reduction due to the diffusion of external (secondary) air into the unburned gas. This diluting effect increases as the flame moves away from the burner. Thus, flame velocity curve C may represent the limit of approach of the flame fringe toward the stream boundary for a lean mixture. For a rich mixture, secondary-air dilution may increase the flame velocity; for a very rich mixture, a stable lifted flame may be obtained several tube diameters above the port (fig. 183; note that the base of the flame is at the point of turbulent breakup of the laminar jet

issuing from the port; the turbulent eddy diffusion is required to mix sufficient secondary air with the very rich mixture so that a nearly stoichiometric mixture results). Conversely, curve A of figure 182(b) may represent the nearest point to which a stable flame can approach the burner rim.

For any flame velocity curve between the limiting curves A and C (fig. 182(b)), there will be a gas flow for which the straight line representing the boundary velocity gradient is tangent to the flame velocity curve (lines 2 to 4). Any line such as 1, which represents a smaller gradient than line 2, will intersect curve A, and there will be a region where the flame velocity exceeds the gas velocity. As a result, the flame will flash back into the tube. Any gradient larger than line 4 will cause the gas velocity to be everywhere greater than the flame velocity, and the flame will blow off. Hence, gradients 2 and 4 are called the critical boundary velocity gradients for flashback and blowoff, respectively.

The critical boundary velocity gradients for Bunsen flames are calculated from equations for the frictional drag imposed by a wall. For fully developed laminar flow through a long cylindrical tube (Reynolds number < 2100), the critical boundary velocity gradient g may be found by differentiating the Poiseuille equation (ref. 3, p. 279), which gives

$$g = \frac{8U_{av}}{d_{tube}} \quad (1)$$



(a) Flow lines around rod.
 (c) Burning and flow velocity in plane B.

(b) Burning and flow velocity in plane A.
 (d) Burning and flow velocity in plane C.

FIGURE 184.—Stabilization of combustion wave by rod (ref. 3, p. 246).

The more general equation, which holds for either laminar or turbulent flow, is

$$g = \frac{F_{fr} \rho U_{av}^2}{2\mu} = \frac{F_{fr} U_{av} Re}{2d_{tube}} \quad (2)$$

where F_{fr} is the friction factor from the empirical Fanning equation (ref. 9). For the laminar-flow condition through long cylinders considered in equation (1), $F_{fr} = 16/Re$. The following expressions are given in reference 8 for the friction factor in laminar flow through various types of burners:

Short circular port (orifice):

$$F_{fr} = \frac{8.5}{Re^{0.85}} \quad (3)$$

Long square channel:

$$F_{fr} = \frac{18.9}{Re^{1.11}} \quad (4)$$

Long rectangular channel:

$$F_{fr} = \frac{40.2}{Re^{1.27}} \quad (5)$$

Long triangular channel:

$$F_{fr} = \frac{29.8}{Re^{1.29}} \quad (6)$$

In all these cases, the diameter used in computing Re is the hydraulic diameter (i. e., twice the cross-sectional area of the channel divided by the perimeter).

For turbulent flow in long, smooth, cylindrical tubes, several equations have appeared in the literature. The empirical equation of Blasius (see ref. 9) is used in references 2 and 8 to 10. For $3000 < Re < 100,000$, this equation gives

$$F_{fr} = \frac{0.080}{Re^{0.25}} \quad (7)$$

Others (e. g., ref. 1) have used the empirical equation of Koo (see ref. 11), which, for the range $5000 < Re < 200,000$, gives

$$F_{fr} = \frac{0.046}{Re^{0.2}} \quad (8)$$

For flow in the transition region between laminar and turbulent flow ($2100 < Re < 3000$ to 5000), there is no available equation for F_{fr} . Some estimate of F_{fr} is obtained

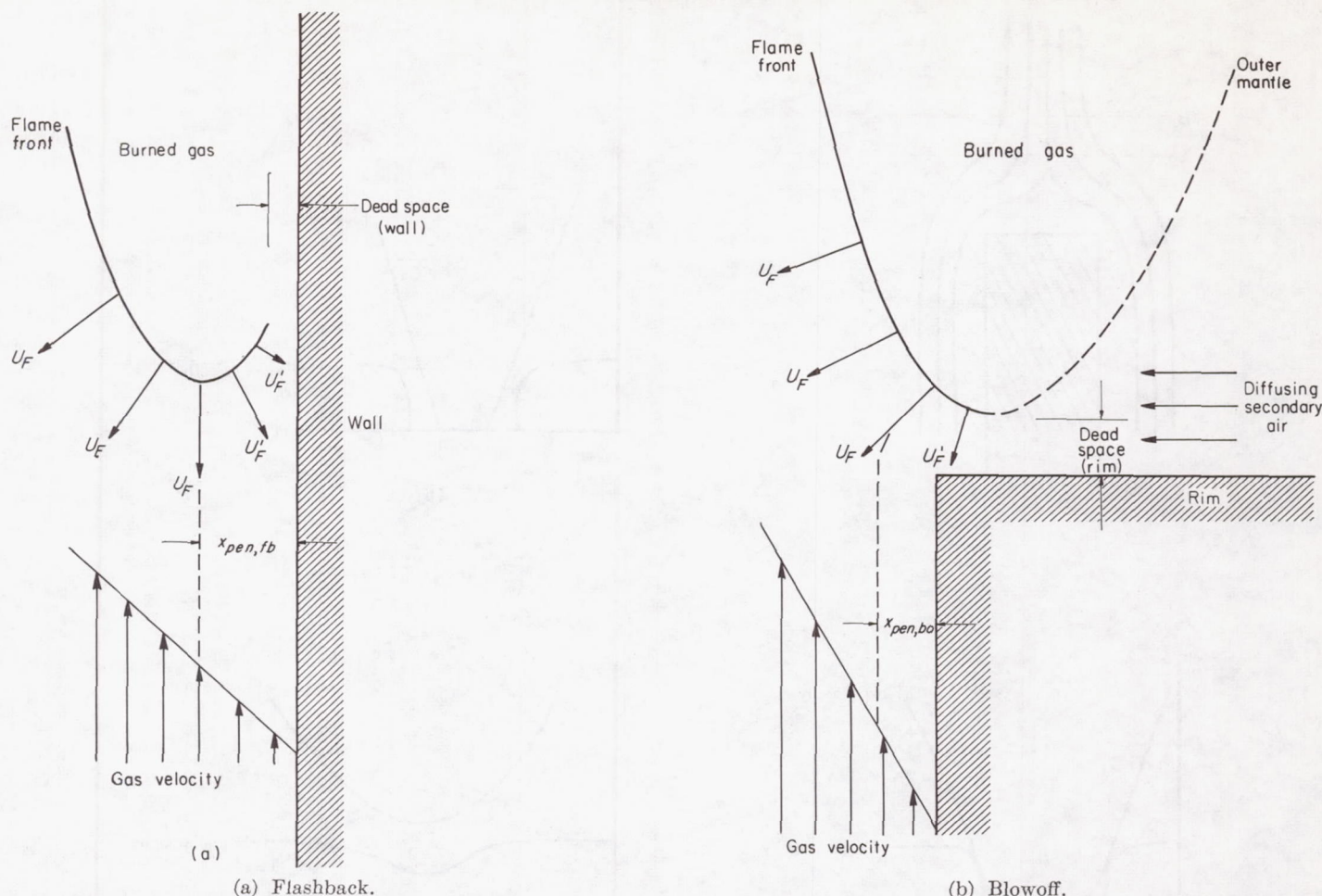


FIGURE 185.—Relation between flame- and gas-velocity curves at stability limits. (For flashback, tube diameter is considered to be at least twice quenching distance; primes refer to nonadiabatic conditions.) (By permission from ref. 10.)

from arbitrary curves connecting the curves for laminar and turbulent flow (ref. 11).

Flames supported on wires or rods.—A mechanism similar to that for burner flames can be applied with some success to flames supported on wires or rods, but the correlations are not as good as those for burner flames, and other mechanisms have been proposed. Nevertheless, it is of interest to examine this theory for supported flames. Lewis and von Elbe (ref. 3, p. 245) visualize the stabilization as shown in figure 184. In figure 184(a), the concept of the flow around a wire located coaxially with the flow is shown. Just above the wire, there is a region of zero flow velocity followed by a gradient to the stream flow. At position A above the wire, the condition shown in figure 184(b) exists, in which the flame velocity is everywhere lower than the flow velocity and a stable flame cannot exist. The flame would thus be forced upward, away from the wire. At a position more remote from the wire, such as position B, both the flow velocity and the flame velocity in this region increase, the flame velocity increasing more rapidly than the flow velocity, so that ultimately a point of tangency exists as shown in figure 184(c), which corresponds to the condition of stability. The increase in flame velocity is limited, however, since it presumably will approach laminar flame velocity when the quenching action of the wire is reduced; but the flow velocity can be increased so that ultimately the flow velocity exceeds the flame velocity at all points and the flame blows off, as shown by the curves of

figure 184(d). As long as the wire does not heat up and is smaller than twice the dead space in diameter, Lewis and von Elbe predict that the velocity gradient for blowoff is independent of wire diameter. However, larger wires produce a large sheltered region, so that a higher flow velocity and a higher boundary velocity gradient are reached before blowoff occurs.

The critical boundary velocity gradients for flames anchored at the end of an axially mounted wire or rod may be calculated by differentiating the equation for flow through an annular space, which gives (ref. 3, p. 289)

$$g_{bo} = \frac{2U_{av}}{r_{tube}} \mathcal{D} \left[\frac{1 - \frac{1}{\mathcal{D}^2}}{-2 + \frac{\ln \mathcal{D}}{\mathcal{D}^2 - 1}} \right] \quad (9)$$

Penetration distance.—An arbitrarily defined quantity that has been used to illustrate the effects of wall quenching and secondary-air dilution (e. g., refs. 1, 3 (p. 285), 9, 10, and 12) is the penetration distance x_{pen} :

$$x_{pen} \equiv \frac{U_F}{g_{fb}} \quad (10)$$

This ratio of fundamental flame velocity to critical boundary velocity gradient represents the distance from the burner wall at which the local stream velocity is equal to the fundamental flame velocity (fig. 185). The penetration distance

is to be distinguished from the small dead space at the wall (fig. 185(a)) or the dead space above the rim (fig. 185(b)) where quenching is complete and the luminous zone assumes a position parallel to the gas-flow lines. For flashback, this distance approximates the depth of penetration of the quenching effect of a single wall; that is, the distance from the wall at which the local flame velocity becomes smaller than the fundamental flame velocity of the mixture as a result of quenching. For blowoff, secondary-air dilution also affects the penetration distance; for a lean mixture, secondary-air dilution would tend to decrease the flame velocity and thus decrease the penetration distance, whereas it would have the opposite effect for very rich mixtures. (The maximum flame velocity generally occurs with a mixture slightly richer than stoichiometric.) The subject of penetration distance is discussed further in the theoretical section of this chapter.

STABILIZATION BY EDDIES

While the mechanism of Lewis and von Elbe is reasonable for supported flames as well as for burner flames, some of the characteristics of supported flames are not so well described as is desirable. Supported flames do not always blow off as the theory suggests, but often a small residual flame remains in the wake of the support. Lewis and von Elbe have, in fact, shown that this region is not characterized by a linear velocity gradient but that eddies are formed just after the support. These are shown schematically in figure 186, in which the eddies are apparently stabilized by the flame, since for a given flow the eddy is smaller with ignition than without. Reference 13 suggests that these eddies act as a source of heat and active radicals and thus provide a constant ignition source to stabilize the flame. The nature

of these eddies and of the flow around them determines when blowoff occurs, because an equilibrium is set up between the production of heat in the eddies, its transfer to the surrounding flow, and the ignition requirements. This subject is also discussed later in this chapter.

EFFECT OF VARIABLES ON STABILITY LIMITS

FLOW VARIABLES AT CONSTANT PRESSURE AND TEMPERATURE

Characteristic dimension of burner or flameholder.—A number of investigators have found that flashback and blowoff limits of open flames burning from tubes or nozzles at room conditions are independent of tube diameter when plotted as fuel concentration (or equivalence ratio) against the critical boundary velocity gradient. Lewis and von Elbe (ref. 3, pp. 282–300) plotted flashback-limit data for natural-gas-air, hydrogen-air, hydrogen-oxygen, acetylene-oxygen, methane-oxygen-nitrogen, and propane-oxygen-nitrogen flames in this manner. They found the critical boundary velocity gradients for flashback g_{fb} to be independent of tube diameter as long as the diameter was somewhat larger than the quenching diameter but not so large that flashback was preceded by a severe tilting of the flame, in which case the limit was not clearly distinguished.

The critical boundary velocity gradients for blowoff g_{bo} of natural-gas-air mixtures in the laminar-flow region were also independent of diameter both for ordinary Bunsen flames and for some inverted flames stabilized at the ends of wires mounted in the axes of the tubes. Successful correlations were obtained with g_{bo} for several other fuel-oxygen-nitrogen mixtures in laminar flow. Reference 2 presents a correlation extending from the laminar-flow range well into the turbulent-flow range on a continuous curve for propane-air flames for a range of tube diameters as shown in figure 187. This figure shows that the curves for the small tubes deviate toward higher velocity gradients only above a propane mole fraction of 0.15. Reference 1 also presents continuous curves from laminar into turbulent flow for butane-air flames. Furthermore, the hydrogen-air data of reference 3 (pp. 292–293) when properly calculated give a similar smooth curve extending into the turbulent region.

For blowoff limits of simple, single flameholders in small combustion chambers, various investigators have found correlations with a parameter

$$\frac{U_{av,bo}}{d_{fh}^{*b}} = \mathcal{F}(\varphi) \quad (11)$$

plotted against fuel concentration, where d_{fh}^{*} is the characteristic dimension of the flameholder and b is an empirical exponent (table XXVI). For example, in reference 13, a correlation was obtained for $b=0.45$ with rods varying in diameter from 0.016 to 0.498 inch (some of which were downstream of turbulence-producing screens) for city-gas-air flames in a two-dimensional combustion chamber 1 by 3 inches in cross section (fig. 188). Reference 6 reports the data of figure 180 to be correlated with $b=0.5$ for equivalence ratios below 1.5. However, reference 14 found that $b=0.18$ gave the best correlation for new data on rod-stabilized city-gas-air flames, and that, for lean hydrogen-air flames and for propane and city-gas flames in certain ranges of velocity and concentration, b is negative.

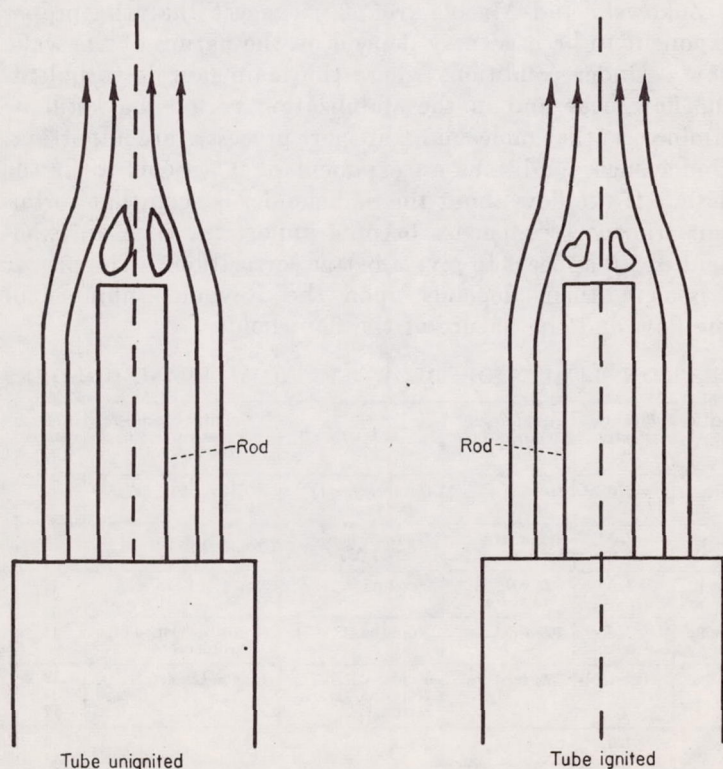


FIGURE 186.—Flow lines around axially placed rod with and without flame (ref. 3, p. 269).

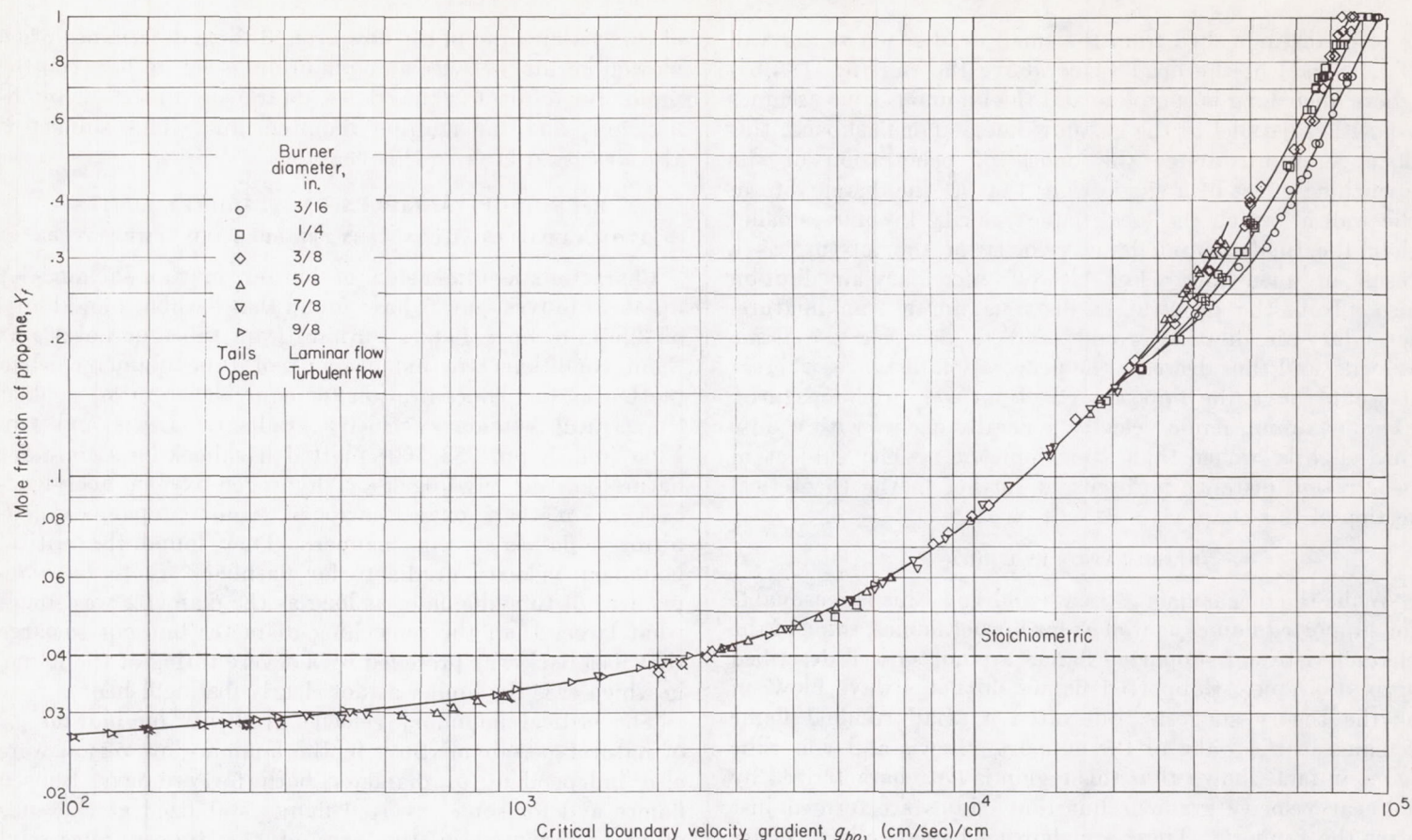


FIGURE 187.—Variation of fuel-air ratio with velocity gradient at tube wall for blowoff of seated propane-air flames (ref. 2).

Axially mounted cylinders and cones in high-velocity streams (200 to 900 ft/sec) near the open end of a 6-inch pipe were used in reference 15, in which a correlation was observed with diameter for $b=1.0$, when a high-boiling mixture of paraffins and naphthenes was used. DeZubay (refs. 16 and 17) used disks mounted with the diameter normal to the flow in a cylindrical duct. He obtained a correlation with $b=1.0$ for naphtha, 0.85 for propane, and 0.74 for hydrogen. DeZubay pointed out that, in the case of reference 13 (and the same comment would apply to refs. 6 and 18), the projected flameholder area was proportional to the characteristic dimension d_{fh}^* , because in all cases the flameholder extended across a duct of fixed width. On the other hand, for DeZubay's data (or those of ref. 15), the projected area is proportional to the diameter squared. Hence, all the

correlations except those recently reported in reference 14 are close to $U_{av, bo}/A^{0.5}$. These and other empirical correlations (refs. 6, 7, 13, and 15 to 19) involving the characteristic dimension d_{fh}^* are summarized in table XXVI.

Zukowski and Marble (ref. 20) suggest that the proper exponent to be used may depend on the nature of the wake flow. Under conditions where the main flow is turbulent, the flow near and in the stabilization region may still be laminar, so that molecular transport processes are important. Under such conditions an exponent of 0.5 seems to fit the data. If the flow about the flameholder is such that turbulent transport properties become important, then an exponent of 1.0 appears to give a better correlation. The proper exponent, then, depends upon the Reynolds number of the flow and the nature of the flameholder.

TABLE XXVI.—CORRELATING PARAMETERS FOR CONCENTRATION LIMITS OF BLOWOFF FROM FLAMEHOLDERS

Flameholder mounted in chamber	Correlating parameter	Flameholder	Characteristic dimension, d_{fh}^* , in.	Mixture velocity, U_{mz} , ft/sec	Pressure, p , atm	Approach temperature, T_{oi} , °R	Fuel	Calming-chamber screens and contraction ratio	Reference
Transverse, in 1" by 3"	$U/d^{0.45}$	Uncooled rods or gutters	0.016-0.498	60-300 approach	1.0	520-600; mixture	Cambridge city gas; propane	200-Mesh; 20:1 ($\mu/U=0.004$)	13
Transverse, in 1" by 4"	$U/d^{0.3}$ $U/T_{oi}^{1.2}$	Cooled cylinders	0.035-0.494 .127	60-740 approach	1.0	610; mixture	Hydrocarbon blend (C ₆ -C ₈)	150-Mesh; 28:1	6
Transverse, in 1 1/2" by 3"	$U/d^{0.5} T_{oi}^{1.2}$			60-600 approach	1.0	606-970			
Transverse, in 1 1/2" by 3"	$U/d^{0.5} T_{oi}^{1.2}$	Cooled or uncooled rods	0.187-0.375	120-850 approach	1.0	660, 860; mixture	Gasoline		18
Axial, in 6" pipe	U/d	Uncooled rods, cones, annuli, or gutters	0.75-3.5	200-950 past baffle	1.0	760; inlet air	Naphtha (C ₆ -C ₈)	(Fully developed pipe turbulence)	15
Axial, in 4" pipe	$U/d^{0.55} p^{0.55}$ U/d $U/d^{0.74}$	Disks	0.25-2.0	40-550 past baffle	0.2-1.0	550; mixture	Propane	Fine mesh; 4:1	16
		Spheres					Naphtha		17
Axial	$U/d^{0.5}$	Disks			1.0				19
	U/d	Spheres			1.0				19
Axial, above 3/8" to 1 1/4" nozzle	U/p (given d)	Spheres	0.0625-0.189	65-350 approach		100; inlet air	Propane	100-Mesh; 576:1	7

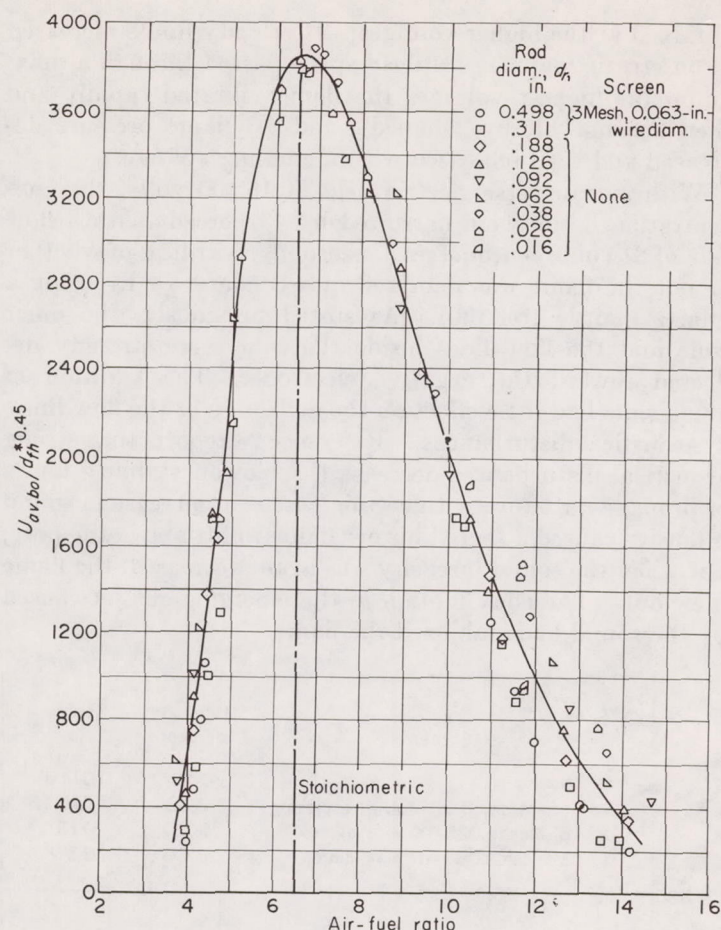


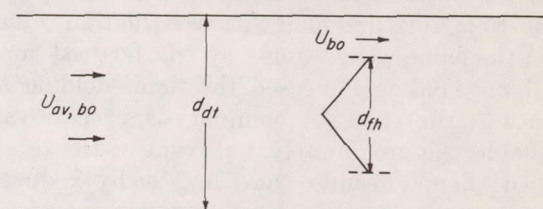
FIGURE 188.—Correlation of rod stabilizer blowoff-limit data. Fuel, city gas; stabilizers 9 inches from chamber entrance (ref. 13).

On the other hand, Barrère and Mestre (ref. 21) showed a lack of correlation with characteristic dimension, because, for a cylinder, a 90° gutter, and a flat plate, each having a projected width of 5 millimeters, three different sets of velocity-concentration curves were obtained. Gerstein (ref. 21) suggests that for greater generality the correlating parameter should account for differences in flow about obstacles of different shapes. The dimension sought may be, for example, the lateral width of the vortex formed behind the obstacle. In cold flow, a cylinder with a projected width of 0.75 inch has a vortex width of 1.09 inches, whereas a flat plate of the same projected width produces a vortex 1.30 inches wide under the same flow conditions (ref. 22). The use of these relative vortex widths would bring the data of reference 21 for the cylinder and the flat plate together. Unfortunately, such agreement based on cold-flow vortex widths may be fortuitous, because the flame does influence the flow (ref. 23).

More recently Mestre (ref. 24) has shown that the drag coefficient of the flameholder, measured during combustion, serves to improve the correlation between flameholders of various shapes. His correlating parameter becomes $U_{av,bo}/d_{fh}^* C_D$, where C_D is the drag coefficient.

Reference 13 reports that the stability limits for a given size flameholder are unaffected by chamber width for ratios of chamber width to stabilizer critical dimensions from 10 to 79. In practice it is often desirable to determine the

optimum size of flameholder in a duct of given size. Presumably, it is the velocity past the flameholder that is the important factor in blowoff. If the ratio of duct diameter to flameholder diameter d_{dt}/d_{fh}^* is large, then the average velocity of flow in the duct is very close to that past the flameholder. If the flameholder size is increased, then, according to equation (11), a higher velocity should be required for blowoff. Increasing the flameholder diameter, however, causes the flow near the flameholder to accelerate and thus limits the increase in average flow in the duct. If the simple system in sketch (q) is assumed



Sketch (q)

then the optimum ratio of flameholder diameter to duct diameter becomes

$$\left(\frac{d_{fh}^*}{d_{dt}}\right)^{b+1} = \frac{1}{b+2} \quad (12)$$

where b is the exponent in equation (11). For $b=0.5$ a blocked area of about 30 percent is found to be the optimum, while for $b=1$ a blocked area of about 35 percent is optimum.

In general, then, the velocity-concentration limits for open burner flames, or for open flames supported at the end of axially mounted wires, may be correlated by the critical boundary velocity gradient. For confined flames supported on flameholders, an empirical correlation of the type

$$\frac{U_{av,bo}}{A^c} = \mathcal{F}(\varphi) \quad (13)$$

may be applicable, where c is of the order of 0.5; for greater generality, a function of some length or area associated with the flow about the obstacle might be used in place of $A^{0.5}$.

Turbulence.—It has already been noted that blowoff data for open flames on tubes of various diameters are correlated by a single curve of critical boundary velocity gradient against fuel concentration for both laminar and turbulent flow. Turbulent flashback is not ordinarily encountered in laboratory experiments; but, with very high velocity flames (e. g., H_2-O_2 flames, ref. 25) in large-diameter tubes, or at increased pressure, it may occur (ref. 12). The g_{fb} for turbulent flames is always greater than that for laminar flames of the same mixture, because the laminar boundary layer at the wall within which stabilization must occur becomes smaller.

Scurlock (ref. 13) produced known turbulence in the approach stream of confined flames by means of screens. As the intensity of turbulence was increased, blowoff velocities decreased (fig. 189). The effect of turbulence of given scale and intensity decreased with increase in the ratio of flameholder diameter to turbulence scale. Contradictory results are reported in reference 19, which states that placing a flameholder farther from the source of turbulence (closer to the combustion-chamber exit), where the intensity and frequency of turbulence are smaller, decreased the stability limits.

Boundary-layer thickness.—In reference 26, the thickness of the boundary layer on a flameholder was varied by removing part of the layer by suction through grooves in the flameholder. The data of reference 26 and other data show no effect on blowoff velocity as long as both the approach flow and the boundary layer are laminar. If the approach stream is turbulent, a thin boundary layer may be penetrated to favor blowoff. When the boundary layer itself is turbulent, blowoff is accelerated in the same manner as it is promoted by upstream turbulence, but the effect may be more severe because of the absence of the laminar buffer layer between the combustible mixture and the recirculation zone. An increase in the flame-wedge angle at the farthest upstream point of flame holding increased the flame-holding ability. In reference 7, the effect of boundary-layer removal from the flameholder (approximately 1 percent of the total flow) was studied; flame heights were drastically reduced and blowoff velocities were halved.

Reference 27 reports that, for stream velocities of 80 to 180 feet per second, the theoretically complete removal of the boundary layer markedly decreased the blowoff velocity of a fuel-lean flame and slightly decreased the blowoff velocity of a fuel-rich flame. It was also observed that blowing air into the boundary layer decreased the stability of lean flames and increased the stability of rich flames. A stable pilot was obtained by blowing propane into the boundary layer, even when the mainstream fuel concentration was zero.

In summary, boundary-layer removal has no effect when both the approach flow and the boundary layer are laminar; when the laminar boundary layer becomes very thin because of approach-stream turbulence, or when the boundary layer itself becomes turbulent, its removal reduces stability. Lean flames are affected more than rich flames.

Electric fields.—Reference 28 reports that longitudinal electric fields, either alternating current at 400 cps or direct current with the positive electrode in the burned gas, approximately doubled the blowoff velocity of a given propane-air burner flame as the voltage was increased from zero to 2000 volts. The rate of increase of the blowoff limits decreased rapidly after 2000 volts.

Reference 29 confirms the preceding longitudinal direct-current field results in a study with butane-air flames. In the apparatus of reference 29, the downstream electrode was a platinum ring around the outer tube or skirt of a split-flame burner, and therefore the blowoff curves obtained were typical of confined flames. The inner flame cone was subjected to a direct-current field of 0 to 18,000 volts, which caused a current through the flame of 0 to 100 microamperes. Further results obtained for a positive field (positive downstream electrode) were as follows: (1) Concentration limits could be widened 200 percent, (2) dead space could be reduced 70 percent, and (3) flame pressure could be more than doubled. When the downstream electrode was made negative and the direct-current voltage was increased, it was found that (1) concentration limits narrowed at low voltages, but the same widening obtained with positive fields was

obtained at the higher voltages; (2) velocity limits increased in an erratic manner; (3) dead space passed through a maximum (at highest voltages the flame vibrated rapidly and then became "derby" shaped); and (4) flame pressure decreased and then increased with increasing voltage.

With a transverse electric field of 15,000 volts, the concentration limits were narrowed by 43 percent with a flow rate of 61 cubic centimeters per second, regardless of whether or not the flame was deprived of secondary air by using a quartz mantle (ref. 30). As stated previously, the inner cone and the flow lines inside the cone were strongly deflected toward the negative electrode. The addition of alkali salts had little effect on the deflection of the flow lines.

Acoustical disturbances.—Reference 28 reports that strong acoustical disturbances decrease the blowoff stability limits of propane-air flames. In certain cases, an increase in sound intensity caused a seated burner flame to lift above the port; but when the sound intensity was again decreased, the flame blew out. The eddy motion in the emerging gas jet caused by the sound had stabilized the flame.

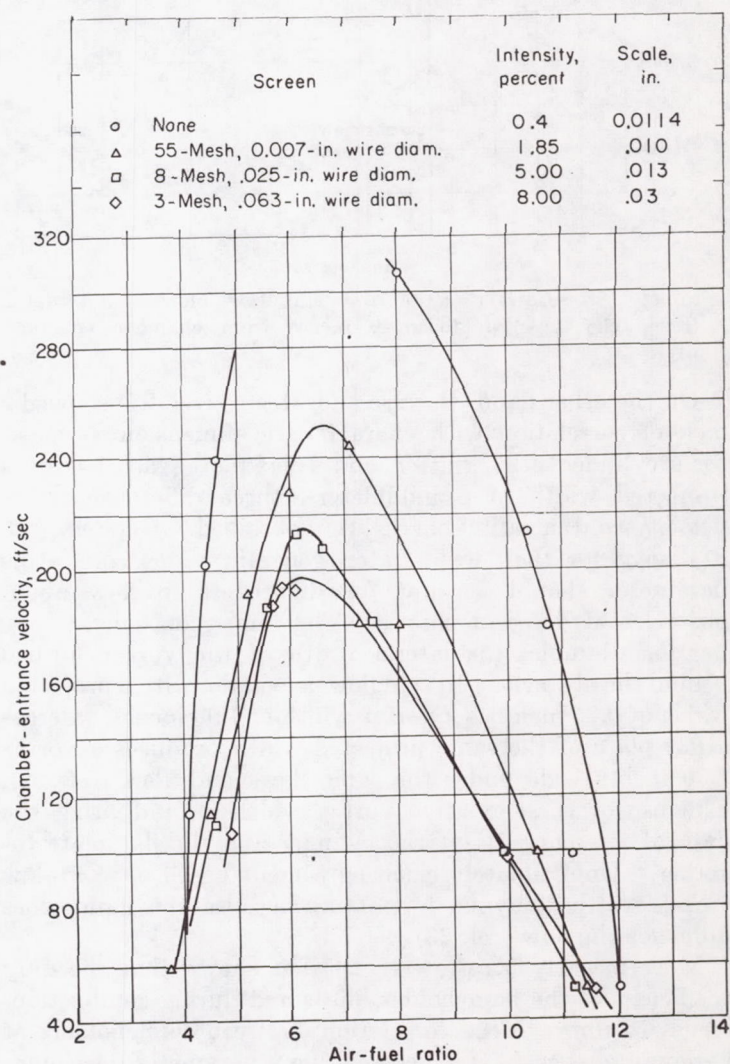


FIGURE 189.—Effect of approach-stream turbulence on rod stabilizer blowoff limits of Cambridge-city-gas-air flames. Screens 2 inches upstream of 0.038-inch rod in 1- by 3-inch chamber (ref. 13).

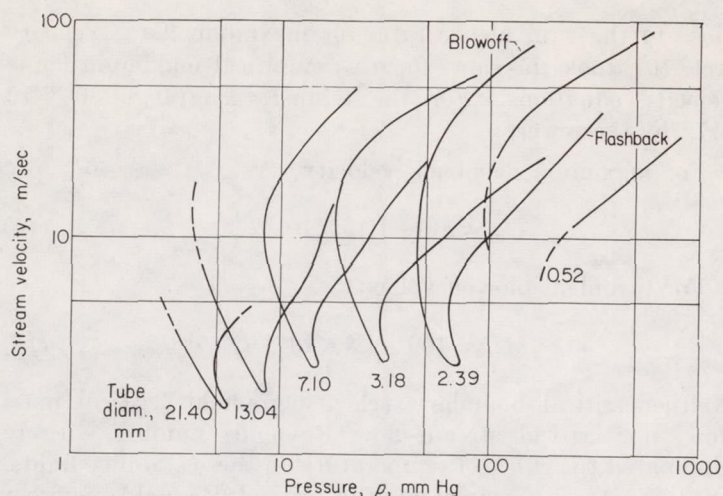


FIGURE 190.—Effect of pressure and burner-nozzle diameter on stability limits of stoichiometric acetylene-air flames at room temperature (ref. 31).

PRESSURE AND TEMPERATURE VARIATION

Pressure.—Stability diagrams are presented in reference 31 for acetylene-argon-oxygen and acetylene-air flames. The data are actually presented on what might be considered velocity-pressure limits for these mixtures in various tubes. For a given mixture, a different velocity-pressure curve for each burner-nozzle diameter was obtained as shown in figure 190 for acetylene-air flames. Each of these curves consists of a blowoff branch to the upper left and a flashback branch to the right. The lower part of each curve, which has a negative slope and connects the blowoff and flashback portions, represents the extinction limit where the flame dies out because of its inability to supply enough heat or active radicals to a sufficient volume of gas to continue the propagation.

The curves of figure 190 were obtained by varying pressure along a constant volumetric flow line until either flashback, blowoff, or extinction occurred. The narrowing of the flashback extinction neck in the curves at lower velocities was pronounced for these acetylene-air flames. In this neck region, flat flames were obtained, and the computed flame velocity dropped below the non-pressure-dependent value obtained when this region was avoided. The minimum of each curve represents a minimum propagation velocity for the mixture, which apparently is not greatly affected by pressure or tube diameter. The limiting pressure for combustion of a given mixture at a given velocity was inversely proportional to tube diameter. In other words, the blowoff extinction curves of figure 190 may be brought together by plotting critical velocity against the product pd_{tube} (see also ref. 12). This is analogous to the use of the correlating parameter U/pd_{tube} for blowoff from spherical or disk-shaped flameholders (table XXVI).

Reference 32 presents the extinction curve for stoichiometric propane-air flames burning from Bunsen tubes or from round-end rods mounted axially in tubes. The extinction velocity was proportional to p^{-2} . The length of the extinction curve was increased by means of longitudinal electric fields, which displace blowoff curves toward higher velocities as discussed previously. Reference 33 reports that the critical velocity gradient for flashback g_{fb} increased pressure for methane-air from $\frac{1}{4}$ to 1 atmosphere, or $g_{fb} \propto p^{0.6 \text{ to } 0.8}$. Since the data of reference 33 showed flame velocity $U_F \propto p^{-0.24}$ for methane, the penetration distance was approximately inversely proportional to pressure. The critical velocity gradient for blowoff g_{bo} also increased with pressure (ref. 33). While the blowoff data were more erratic than the flashback data for methane, g_{bo} was approximately proportional to pressure for both methane and butane in the range $\frac{1}{4}$ to 1 atmosphere.

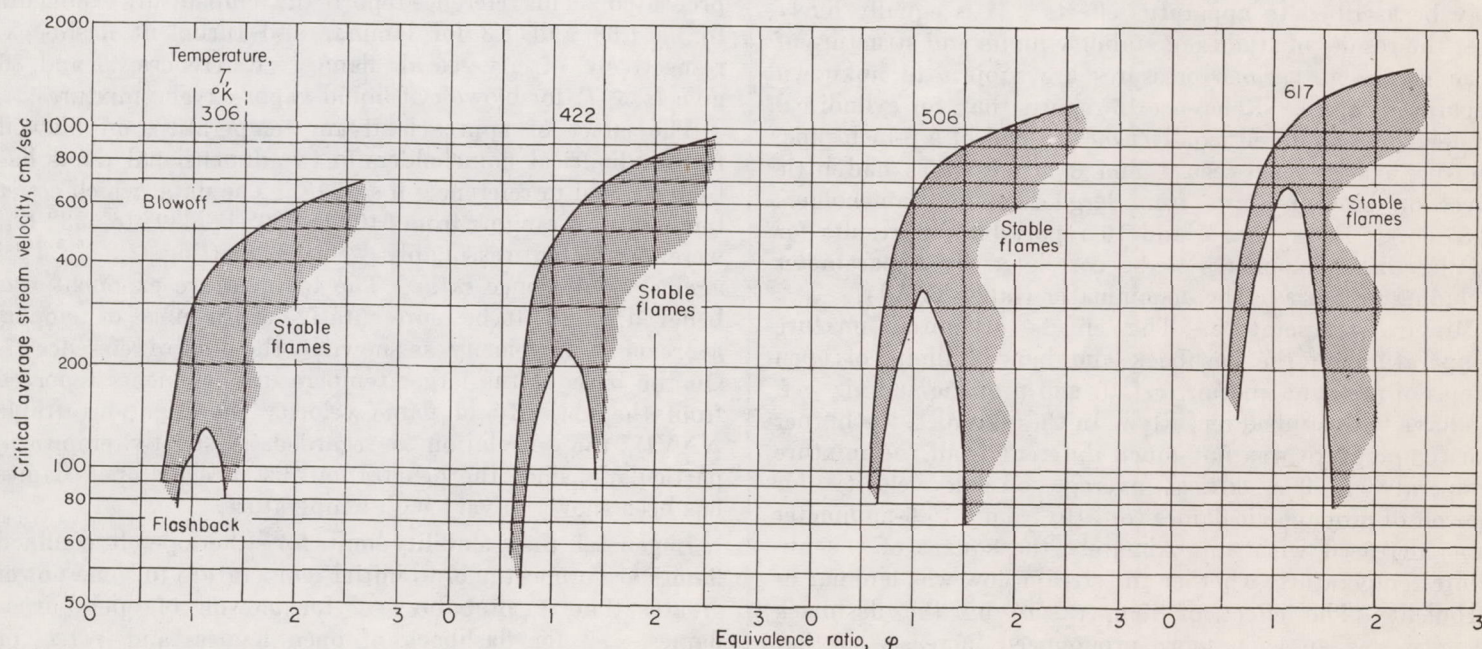


FIGURE 191.—Effect of initial mixture temperature on stable flame region for propane-air flames on 15.6-millimeter burner at atmospheric pressure (by permission from ref. 10).

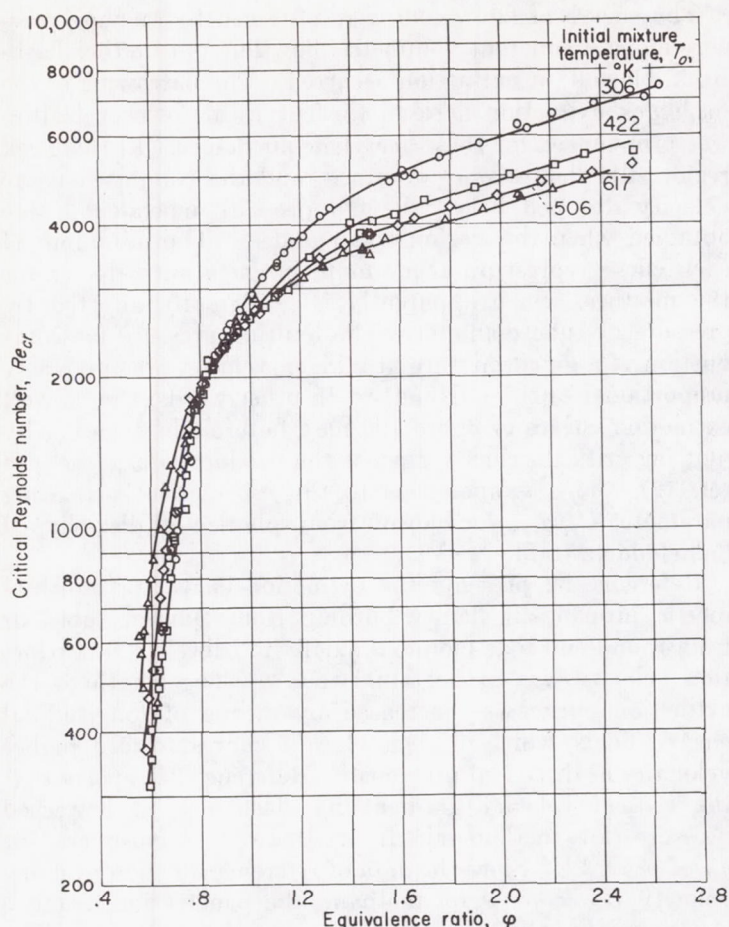


FIGURE 192.—Effect of initial mixture temperature on critical Reynolds number for blowoff (by permission from ref. 10).

It has already been stated that the contradictory reports on the effect of pressure on flame velocity may very probably be ascribed to apparatus effects. It is equally likely that the results of studies of stability limits and structure of open flames at various pressures are subject to unknown apparatus effects. Reference 15 reports that, for cylindrical flameholders mounted axially near the end of a 6-inch pipe, pressure changes between 1 and 3 atmospheres had little effect on blowoff limits from large-diameter flameholders (2.87 in.). References 7 and 16 report blowoff results for smaller disks or spheres to be correlated by a parameter including pressure in the denominator (table XXVI).

Mixture temperature.—The effects of initial mixture temperature on the flashback and blowoff limits of open flames of methane and air (ref. 9) and propane and air (ref. 10) have been studied recently. In these studies, the burner rim temperature was not much different from the mixture temperature. The critical average stream velocity for blowoff of propane-air flames (ref. 10) from a 15.6-millimeter tube increased with approximately the square of the absolute temperature, whether the stream flow was laminar or turbulent. The effect of temperature on the flashback velocity was an even more pronounced increase, so that there was a relative decrease in the flow range for stable flames, as shown by figure 191. Empirical equations for maximum flashback velocity and for turbulent blowoff velocity at the same equivalence ratio, 1.12, which was also

close to the equivalence ratio for maximum flame velocity (ref. 10), took the same form as empirical maximum flame velocity equations. For the temperature range 306° to 617° K, these were:

For maximum flashback velocity,

$$U_{av} = 100 + 1.15 \times 10^{-9} T_o^{4.2} \quad (14)$$

For turbulent blowoff velocity,

$$U_{av} = 100 + 4.5 \times 10^{-3} T_o^{1.9} \quad (15)$$

Neither critical boundary velocity gradient, critical mass flow, nor critical stream flow Reynolds number entirely eliminated the effect of temperature on these stability limits. Of these three parameters, the critical Reynolds number (using only one tube diameter) most nearly eliminated the temperature effect, particularly for blowoff limit, as shown in figure 192. The penetration distance decreased with temperature for flashback and increased for blowoff. A comparison of twice the penetration distance x_{pen} with reported values of the quenching distance between parallel plates $x_{||}$ showed the ratio $2x_{pen}/x_{||}$ to be 0.6 to 0.7. The suggestion was made that this ratio was less than 1 because a minimum space was required for the occupancy of the flame itself in traveling through a tube or between parallel plates. Approximately the same value of $2x_{pen}/x_{||}$ was observed in reference 3 (p. 285) for natural-gas-air flames at room conditions. The prediction of the effect of initial mixture temperature on critical boundary velocity gradients is discussed in the theoretical section hereinafter.

Other investigations have also reported critical average velocities to be proportional to T_o to a power equal to or greater than 1. It was found in reference 34 that $U_{av} \propto T_o$ for flashback of coke-oven gas flames when only the air was preheated. This reference reports the temperature exponents to be 1.63 and 1.3 for laminar and turbulent flashback, respectively, of city-gas-air flames. References 35 and 36 give $U_{av} \propto T_o$ for blowoff of liquid-vapor-oxygen mixtures.

The effect of approach-stream temperature on blowoff from cylindrical flameholders in two-dimensional ducts has been studied in references 6 and 18. The data, which cover temperatures ranging from 610° to 960° R (339° to 533° K), were correlated reasonably well by plotting $U_{av}/d_{tube}^{0.5} T_o^{1.2}$ against equivalence ratio. The temperature exponent was believed (ref. 6) to be representative of the effect of temperature on flame velocity, as shown by the data of reference 37. On the basis of the larger temperature exponents reported from the majority of flame velocity investigations (table XXVI), the correlation is regarded as strictly empirical, particularly since the penetration distance for open flames has been shown to vary with temperature.

In general, then, stability limits for either open or confined flames are proportional to initial temperature to some power greater than 1, probably ≈ 2 for blowoff of open-burner flames, > 2 for flashback of open flames, and ≈ 1.2 for blowoff of rod-stabilized confined flames. Undoubtedly, the exponents vary with concentration and fuel type and are influenced by such factors as wall temperature and water vapor.

Liquid fuel.—In references 35 and 36, the blowoff, flashback, and lift curves of open flames were determined for a variety of liquid fuels burning with air or oxygen at initial mixture temperatures ranging from 125° to 535° F. Insufficient heat was added to completely vaporize the fuel. The stability curves were quite similar to those for completely gaseous systems, except for low T_o and high concentrations when a large part of the fuel remained in the liquid state. For a given lean mixture and given burner geometry, the blowoff velocity was proportional to T_o . Both ordinary burners (diam. approx. 0.1 to 0.2 in.) and skirted (split-flame) burners (skirt diam. of order of 1 in.) were studied. With very rich mixtures, lifted flames were stabilized near the skirt exit by a vortex flow of secondary air when the skirt length beyond the burner exit was approximately 3 inches; with longer skirts, the hot skirt itself stabilized the flame.

Reference 38 reports studies of the stability of rod-stabilized flames using liquid fuel. It was found that flames could be supported in much leaner mixtures for sprays than for gaseous mixtures. This was attributed to the fuel-concentrating action of the stabilizer. Increasing the volatility of the fuel and decreasing the drop size in the spray tended to shift the stability curves toward the rich side, these changes tending to approach more closely the conditions for gaseous mixtures.

Vapor-fuel concentration in the eddy region near the stabilizer may be higher than that in the free stream when liquid spray injection is used. The vapor concentration in the eddy depends on the collection efficiency of drops from the free stream onto the stabilizer and the heat transfer between the flame, the stabilizer, and the liquid. Increased air velocity moved the lean and rich blowout limits toward the lean side for sprays, as contrasted to gaseous systems where the lean blowout limit moves to the rich side as velocity is increased and the rich blowout moves toward leaner fuel-air ratios. Stable combustion of sprays was possible at much leaner fuel-air ratios than was possible with gaseous fuels. It was suggested (ref. 38) that flame extinction occurs in two ways: As the spray fuel-air ratio becomes rich because of increasing the fuel flow, more of the liquid fuel reaching the flameholder sloughs off without burning. The sensible heat carried by the liquid fuel cools the flameholder and reduces the vapor concentration to a point where flame can no longer be stabilized. As the spray fuel-air ratio becomes lean, less fuel impinges on the flameholder and the flameholder temperature rises. Ultimately, the flameholder becomes dry and the flameholder temperature rises sharply. At this point, an insulating film of fuel vapor surrounds the flameholder and reduces the heat transfer to the surrounding spray. Again, the rate of vaporization decreases and the flame blows out.

Flameholder temperature.—Reference 13 reports stability limits to be widened considerably as flameholder temperature is increased. This was confirmed in reference 39, in which, for lean mixtures, the mass air-fuel ratio at blowoff was linearly related to flameholder temperature for velocities of 30 feet per second or greater, but was independent of flameholder temperature at velocities below 20 feet per second. On the other hand, little change was ob-

served (ref. 6) in the limits for a flameholder that was allowed to seek its equilibrium temperature (various mixture temperatures and velocities to 600 ft/sec) as compared with a water-cooled flameholder. Flashback and blowoff velocities for burner flames may also be increased by heating the burner lip, thus decreasing the thermal gradient associated with the penetration distance.

Increasing flameholder temperature may have a deleterious effect on the stabilization of flames supported by fuel sprays (ref. 38). In fact, the flame may actually be extinguished by adding sufficient heat to the flameholder. While the addition of heat to the stabilizer may assist vaporization for small heat additions, ultimately, sufficient heat may be added to produce either a too-rich region near the stabilizer or a film of vapor fuel which, as for lean blowout, reduces heat transfer from the stabilizer to the liquid fuel.

CHEMICAL VARIABLES

Fuel type.—It was observed in reference 1 that curves of critical boundary velocity gradients g_{bo} against percent of stoichiometric oxidant concentration were nearly the same for propane, butane, and Pittsburgh natural gas (largely methane). However, gases with higher flame velocities—Newark city gas, hydrogen, and acetylene-oxygen—showed much higher values of g_{bo} , and therefore penetration distances were smaller; for example, hydrogen had a penetration distance of 0.00033 centimeter compared with 0.076 centimeter for propane, both fuels burning with 130 percent of stoichiometric air. In other words, the quenching effect of the wall is much smaller for the higher-velocity flames. Since the g_{bo} curves on semilog paper were nearly linear, reference 1 suggests the empirical equation

$$g_{bo} = a \frac{10^{-ks}}{100} \quad (16)$$

where s is percent of stoichiometric oxidant (volume basis) and a and k are constants that must be determined for each fuel gas. A similar effect for flames held on disks in a circular duct was pointed out by DeZubay (ref. 17). He noted that the exponent b in the blowoff parameter U/a_{fh}^{*b} decreased as molecular weight decreased from naphtha to propane to hydrogen, but this is also the order of increasing flame velocity.

Additives and fuel blending.—Reference 40 reports studies of the stability of mixed fuels with vortex burners having (1) radial fuel injection from the axis, or (2) radial fuel injection from the periphery. In each type, the mixing of fuel and air occurred in the burner with tangential air admission. Mixing was rapid and uniform. The flame was seated in a divergent nozzle at the open end of the burner (pressure-recovery section). These vortex burners are reported to be useful for studying flame stability of both slow- and fast-burning mixtures with a single burner. The following mixing equation was found to apply for a common blowoff velocity (to be exact, a hold velocity, which is one flow increment less than the blowoff velocity) as well as for a common flame velocity for all studies of binary hydrocarbon mixtures (e. g., propane-propene and propane-

ethane):

$$\sum_j \frac{X_j}{X_j^*} = 1 \quad (17)$$

where

X_j mole fraction of j^{th} fuel in multifuel mixture with air that has a given blowoff limit

X_j^* mole fraction of j^{th} fuel in binary mixture of j with air that has the same blowoff limit

It was concluded that the combustion mechanisms for the various hydrocarbons must therefore be compatible and that all hydrocarbons burn according to the same mechanism for the initial, rate-determining steps.

Propane-hydrogen (refs. 40 and 41) and methane-hydrogen (ref. 42) were also investigated. A simple linear mixing rule such as

$$K = \sum_j X_j K_j \quad (18)$$

cannot be used to determine stability limits of these binary mixtures of hydrocarbons with hydrogen, but equation (17) can be used to determine blowoff limits for lean hydrocarbon-hydrogen mixtures (ref. 40). A significant result of the studies is that a small addition of hydrogen to a hydrocarbon, particularly for rich over-all mixtures, widens the stability range, because the blowoff velocity increases much faster than the flashback velocity (refs. 41 and 42).

References 42 to 44 also report studies of mixtures of methane, propane, or hydrogen with carbon monoxide. For the hydrocarbon-carbon monoxide mixtures, the critical velocities or velocity gradients for flashback or blowoff pass through a maximum for low hydrocarbon-carbon monoxide ratios for a given over-all equivalence ratio. It appears that these ratios for maximum limits are such that the equivalence ratio with respect to the hydrocarbon is of the same order as that with respect to carbon monoxide. With hydrogen-carbon monoxide or hydrocarbon-hydrogen mixtures, such maximums do not occur. While the simple linear mixing rule (eq. (18)) does not apply for averaging critical boundary velocity gradients of single gases to obtain critical gradients of binary mixtures, it does work reasonably well when binary mixtures such as $\text{CO} + \text{CH}_4$ and $\text{H}_2 + \text{CH}_4$ are combined to determine the critical boundary velocity gradient of the ternary mixture $\text{CO} + \text{H}_2 + \text{CH}_4$.

Hydrogen sulfide decreases the flame stability of hydrocarbons just as it decreases the flame velocity, the extent of the decrease becoming greater as the over-all equivalence ratio is increased. However, lean mixtures of H_2 - H_2S follow equation (17) (ref. 40). Equation (17) was also tested for isobutane-ethene mixtures deprived of secondary air (ref. 4). It was found to apply for lean mixtures, but the indicated summation was less than 1 for rich mixtures.

Water vapor.—The addition of 2.5 percent water vapor to the primary air decreased the blowoff, lift, and dropback limits of butane flames (ref. 45). The blowoff velocities of rich mixtures decreased approximately 5 percent and the blowoff velocities for lean mixtures decreased by 10 to 30 percent. The addition of water vapor to the secondary air had less effect, although some decrease was noted at higher concentrations and velocities. Similarly, the addition of water vapor to the primary air decreased the flashback and

blowoff velocities of methane flames, but the water content of the secondary air had little effect (ref. 43). For carbon monoxide flames, water in either the primary or the secondary air increased the blowoff velocity, but the flashback velocity gradient was not affected by water in the secondary air, as would be expected (ref. 43).

Diluent concentration.—The effect of diluent concentration is presented in terms of the volumetric ratio $\psi = \text{O}_2/(\text{O}_2 + \text{N}_2)$ by Lewis and von Elbe (ref. 3, pp. 299–302) for methane- and propane-oxygen-nitrogen mixtures. As ψ increases from 0.21 (air) to 1.0 for CH_4 - O_2 - N_2 mixtures, both flashback and blowoff velocity gradients increase approximately a hundredfold for concentrations near stoichiometric and a thousandfold for lean flames. The values of g_{bo} increase somewhat more than those of g_{fb} , so that a slight widening of the stability range results. It might be noted that the corresponding increase in maximum flame velocity is only of the order of 10 (fig. 139), so that penetration distance near stoichiometric decreases by a factor of the order of 10.

THERMAL THEORIES OF FLAME STABILIZATION

BURNER FLAMES—CRITICAL BOUNDARY VELOCITY GRADIENTS

Lewis and von Elbe (ref. 3, pp. 379–390 and 425–429) have obtained approximate theoretical equations by which g_{fb} and g_{bo} may be calculated if flame velocities and minimum ignition energies are known. These equations were obtained by considering the flow line for which the stream velocity and flame velocity are equal and integrating the energy equation for a plane combustion wave. To accomplish the integration for the reaction zone, this zone was subdivided into an adiabatic and an isothermal zone, and it was assumed that $dT/dx = (T_F - T_3)/(x_F - x_3)$ for the adiabatic zone. Ignition-energy data were used to determine the inflection-point temperature T_3 . Agreement between calculated and experimental g_{bo} curves for methane-air at room conditions was satisfactory with regard to the curve shape, but calculated values were low by a factor of 2 to 10. Calculated flashback and quenching limits for propane-air did not even show the correct trends in all cases.

More recently, satisfactory relative predictions of critical boundary velocity gradients at various initial mixture temperatures T_o were obtained for methane-air flames by solving equation (10) for g (ref. 9):

$$g = \frac{U_F}{x_{pen}} \quad (19)$$

It was assumed that

$$U_F \propto \frac{T_F - T_3}{T_F - T_o} \quad (20)$$

from the Mallard-LeChatelier equation (see ch. IV, eq. (38)), where T_F is the calculated adiabatic flame temperature and T_3 is the ignition temperature for the flame reaction zone. (In ch. IV, the factor $\kappa/c_p \mathcal{F}_e$ was assumed to be independent of temperature.) It was further assumed that, for flashback,

$$x_{pen, fb} \propto T_3 - T_o \quad (21)$$

and, for blowoff,

$$x_{pen, bo} \propto \sqrt{D_o} \propto T_o^{3/4} \quad (22)$$

where D_o is the diffusion coefficient for secondary air diffusing into unburned gas at T_o . Assuming T_3 to be independent of T_o , the value of T_3 was calculated for every pair of experimentally determined gradients for a given fuel-air mixture at two temperatures by

$$\frac{g_1}{g_2} = \frac{\mathcal{F}(U_F)_1 \cdot \mathcal{F}(x_{pen})_1}{\mathcal{F}(U_F)_2 \cdot \mathcal{F}(x_{pen})_2} \quad (23)$$

and equations (20) and (21) or (22). This procedure gave an equation for T_3 that was cubic for flashback or quadratic for blowoff. The values of T_3 (largest of the real roots) from various pairs of gradients were averaged, and the average value was used to compute gradients for the temperature range studied.

An approach that avoids the necessity of determining T_3 and that takes into account approximately the variations in thermal properties and reaction rate (which in turn is related to the reaction-zone thickness \mathcal{T}_{re}) is suggested in reference 10. This approach employs the modified form of the Semenov equation (bimolecular reaction) for flame velocity (ch. IV):

$$U_F \propto \sqrt{T_o^2 T_F^{4.9} \frac{\exp(-E_{act}/RT_F)}{(T_F - T_o)^3}} \quad (24)$$

For flashback it is assumed that

$$x_{pen,fb} \propto (T_F - T_o) \quad (25)$$

The latter assumption is in keeping with the Semenov approach for flame velocity, because Semenov assumed that T_3 was always near T_F and varied with T_F because of the exponential variation of the reaction rate with temperature. Equations (24) and (25) can be substituted for U_F and $x_{pen,fb}$ in equation (23) by using activation energies from low-temperature oxidation studies in the literature. This substitution permits direct solution for the ratio of any two values of g_{fb} . It might be argued that the use of activation energies from low-temperature oxidation studies is subject to question, but such activation energies have been used successfully for flame velocity predictions (ch. IV) and must suffice until more appropriate values are measured.

Critical boundary velocity gradients for flashback (referred to the gradient at 306° K) have been calculated from the data of reference 10 using 38 kilocalories per mole for E_{act} for propane and adiabatic flame temperatures as follows:

Initial temperature, T_o , °K	Critical boundary velocity gradient for flashback, g_{fb} , sec ⁻¹	
	Calculated	Measured
306-----	-----	680
422-----	1200	1190
506-----	1720	1710
617-----	2620	3500

Equation (22) for the penetration distance for blowoff may be oversimplified even for fuel-lean flames, because it neglects the role of wall-quenching and assumes that secondary-air diffusion occurs at T_o only. Actually, the secondary air

must either travel through the dead space, where the temperature varies from T_o to some value near T_F , or through the burned gas (fig. 185(b)). Since T_F , for many fuel-air mixtures, increases approximately $\frac{1}{2}^\circ$ for each $^\circ$ K that T_o is increased, it follows that any temperature between T_o and T_F increases less rapidly than T_o , so that it might be more reasonable to assume that the square root of the diffusion coefficient varies with $T_o^{1/4}$. Hence, taking the effect of wall quenching into account in the same manner as flashback,

$$x_{pen,bo} \propto T_o^{1/4} (T_F - T_o) \quad (26)$$

In spite of these arguments, however, equation (22) gave somewhat better results for propane-air at an equivalence ratio of 1.12 (ref. 10), as can be seen from the following table:

Initial temperature, T_o , °K	Critical boundary velocity gradient for blowoff, g_{bo} , sec ⁻¹		
	Eqs. (22) to (24)	Eqs. (23), (24), and (26)	Measured
306-----	-----	-----	4,000
422-----	5,400	6,500	5,300
506-----	6,600	8,900	7,300
617-----	8,400	13,000	10,400

In summary, either the method of reference 9 or the method suggested in reference 10 appears to give satisfactory predictions of the effect of temperature on critical boundary velocity gradients, but the latter method is less tedious and somewhat more desirable theoretically because it uses the Semenov approach with regard to ignition temperature.

FLAMES SUPPORTED ON FLAMEHOLDERS—EDDY STABILIZATION

Reference 13 suggests that, on a thermal basis alone, the quantity of energy required from the stabilizer would be increased by (1) increasing the approach-stream velocity U_o , (2) increasing the difference between the ignition temperature and the approach-stream temperature $T_3 - T_o$, (3) increasing the thickness of the preignition zone, or (4) increasing the heat capacity per unit volume. If, as in the early thermal theories, the thickness of the preignition zone is assumed proportional to the thermal diffusivity $\kappa/\rho c_p$ divided by the laminar flame velocity, then the required heat-supply rate can be written as

$$Q_{req} \propto \frac{U_o \kappa}{U_{F,L}} (T_3 - T_o) \quad (27)$$

At blowoff, the heat required is infinitesimally greater than the heat supplied from the sheltered zone, which is given by

$$Q_{sh} \propto \left[\left(\frac{dU_o}{\nu} \right)^c \frac{\kappa}{d_r} \right] d_r (T_F - T_o) \quad (28)$$

where c is a constant and where the bracketed term includes the factors affecting the heat-transfer coefficient from heated cylinders. In the two-dimensional duct, the area for heat transfer is proportional to the rod diameter d_r . Equating

Q_{reg} and Q_{sh} , a relation of the form

$$\frac{U_{bo}}{d^b} = \mathcal{F}(\varphi) \quad (29)$$

is obtained, where the new exponent b on the rod diameter replaces $c/(1-c)$. This type of correlation is demonstrated in table XXVI.

In reference 46, a quantitative relation was obtained by considering the recirculation zone behind a flameholder to be a steady-state reactor of volume V . If a homogeneous unburned-gas mixture of fuel-air mass ratio f enters this volume at a rate such that the air mass-flow rate is w_a (in g/sec), and a fraction ι_{in} of the entering fuel is burned within the volume, then the fuel burned is $w_a f \iota_{in}$. This quantity must be equal to the fuel consumed by chemical reaction. Reference 46 states that a second-order reaction is required to account for the observed effect of pressure (stability correlates with p^{-1} , table XXVI). The actual rate-limiting reactions are unknown, but their concentrations can be assumed proportional to the mass air and fuel concentrations \mathcal{C}_a and \mathcal{C}_f , respectively. The collision factor Z combines the collision number, the steric factor, and the concentration proportionality constants. Thus, the material balance can be written

$$w_a f = V \mathcal{C}_a \mathcal{C}_f Z \exp\left(\frac{-E_{act}}{RT}\right) \quad (30)$$

Now \mathcal{C}_a and \mathcal{C}_f can be related to the initial fuel concentration and the initial temperature through f and ι_{in} ; with the appropriate substitutions, equation (30) can be written as

$$\frac{w_a}{V p^2} = \frac{Z \exp\left(\frac{-E_{act}}{RT}\right)}{T_F^2} \frac{(1 - \iota_{in})(1 - \iota_{in} \iota_{st})}{\iota_{in} \psi} \quad (31)$$

where

- T_F adiabatic flame temperature corresponding to fraction burned
- ι_{st} fraction of stoichiometric fuel concentration if mixture is lean, unity if mixture is rich
- ψ $(Rf/M + R/29)^2$
- M molecular weight of fuel

If w_a/Vp^2 from equation (31) is plotted against ι_{in} , curves such as those sketched in figure 193 are obtained for various concentrations using a given activation energy. (The equation is actually triple-valued in part, but only the values indicated by the solid curves are of practical interest.) A blowout curve of w_a/Vp^2 against concentration can be obtained by cross-plotting the maximums of such curves against concentration; the maximums could be obtained directly by setting the derivative of equation (31) equal to zero, solving for ι_{in} by trial and error, and substituting values of ι_{in} and T_F into equation (31) to obtain values of w_a/Vp^2 .

The air mass flow w_a into the recirculation zone is proportional to the velocity U , to the stream density, which in turn is proportional to the static pressure p , and to some function

of the diameter d . The zone volume V depends almost entirely on some function of d . Hence,

$$\frac{w_a}{V p^2} \propto \frac{U}{d^b p} \quad (32)$$

which has the same form as the correlating factor used by DeZubay and others if $b=0.85$ or some such value (table XXVI). From DeZubay's data, \dot{Z} was estimated to be 4×10^{12} cubic centimeters per gram mole (ref. 16) for E_{act} of 40 kilocalories per gram mole. These values are reasonable and are comparable with those obtained from classical kinetics. For a stoichiometric mixture, these values give a maximum value of w_a/Vp^2 of 40 g/(sec)(cc)(atm²), which

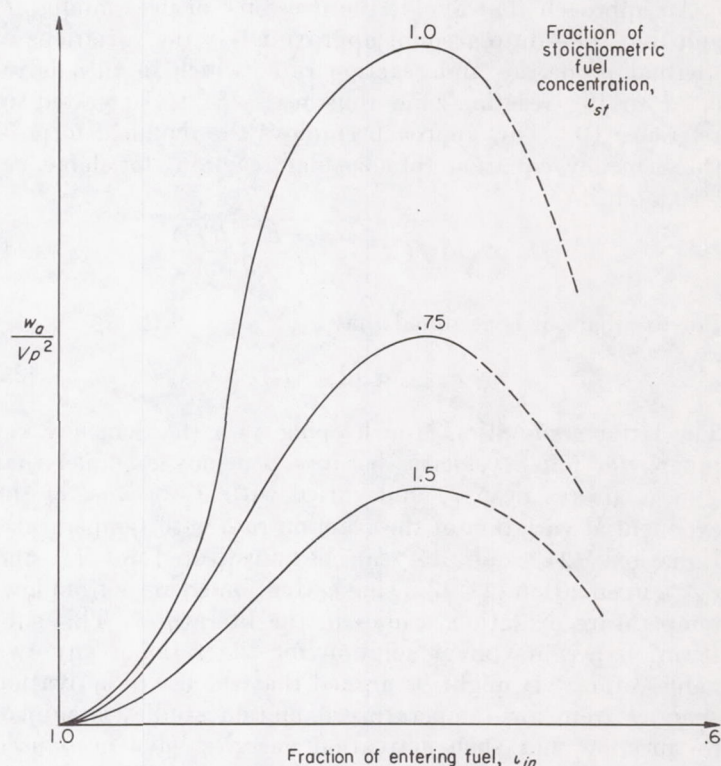


FIGURE 193.—Variation of w_a/Vp^2 with ι_{in} .

corresponds to $\iota_{in}=0.72$ and a heat-release rate of 190 calories per cubic centimeter per second, or 77 million Btu per cubic foot per hour. These data are used in reference 15 to calculate a flame-front thickness of 0.022 centimeter. It is stated that, since a reported value of the flame-front thickness of a propane flame is 0.05 centimeter, or more than twice as great as the calculated value of reference 15, the flame fronts in the recirculation zone must overlap. Thus, a state of homogeneity would be approached, or, in other words, the calculated results are not inconsistent with the original assumption of homogeneity. The general conclusion is that under certain conditions combustion appears to proceed homogeneously as a second-order chemical reaction. The gross features of flame stabilization behind flameholders in high-velocity airstreams are explained by this hypothesis.

More recent data (ref. 47) lead to the suggestion that the nature of the recirculation zone with regard to temperature and composition may not change appreciably as blowout is approached. The blowout condition could occur because of insufficient heat and free-radical transport from the recirculation zone to the main stream when a critical velocity gradient is reached in the region of the flameholder. Measurements of recirculation-zone size, temperature, and composition tend to support this view. This different concept of flameholder stabilization is of considerable interest, and further study is required before a choice can be made between the two mechanisms.

In all the mechanisms of flame holding by rods discussed herein it has been assumed that the recirculation zone behind the flameholder is an important part of the flameholding process. Schaffer and Cambel (ref. 48) have generated the reverse flow necessary for stabilization by an opposing jet, thus eliminating the need of a physical flameholder. Generally, a flame could be anchored initially more easily with the air jet than with a physical flameholder. The dilution effect of the air, however, usually meant that richer mixtures were required. A comparison of the blowout curves with a physical flameholder, an air jet,

occurs in the jet-stabilized flame because of entrainment of the burned gases along the boundary of the free jet.

The performance curves indicate that, for the flameholders tested, the recirculation is greater for the air jet than for the physical flameholder. The presence of the recirculation zone in both cases was confirmed by schlieren photographs. It has thus been demonstrated that stabilization can be achieved without a physical flameholder if an adequate recirculation can be achieved by an alternative method. Failure of the authors (ref. 48) to obtain flame holding with an opposing nitrogen jet indicates that the recirculation zone must be an active source of heat and chemically active species. In agreement with this, an oxygen jet was found to give superior stabilization to an air jet. This suggests that augmentation of the recirculation can improve flame stabilization. Addition of oxygen behind a bluff body and the use of pilot flames are practical methods of improving flame stabilization.

NONISOTROPIC FLAMES

Stationary open flames were long considered evidence that the laminar combustion wave is dynamically stable. Analyses of flame propagation (ch. IV) customarily start with the assumption of a steady-state, one-dimensional flame front. Many investigators have occasionally observed nonisotropic flames, usually in the form of polyhedral open flames, in which the ordinarily smooth cone breaks up into several (usually three to eight) petal-like sides, convex toward the unburned gas and separated by dark ridges. These polyhedrons could be made to remain stationary or to rotate at variable speeds, depending on composition and flow rate. However, the appearance of such flames was generally considered an abnormal phenomenon. The reasons and conditions for such instabilities received little attention before the recent studies of cellular or filamented flames in tubes (refs. 49 to 51) and studies of polyhedral open flames (refs. 34 and 49 to 54). Nonisotropic propagation has also been observed with spherical flames (ref. 55).

CELL FORMATION AND SURFACE BREAKUP OF OPEN FLAMES

Reference 52 reports that very lean hydrogen-air or H_2 - O_2 - CO_2 flames burning on a 1.36-centimeter nozzle separated into several filaments that rose from the burner rim and failed to combine into a closed cone tip. The number of filaments increased (or conversely, the size of the filaments decreased) with O_2/CO_2 ratio, with fraction of stoichiometric volume-percent fuel (between 0.05 and 0.28, depending on the absence or presence of CO_2), and with flow rate (fig. 195). The use of a 3.08-centimeter glass filter (sintered glass) as a burner enabled smaller, more clearly defined, paraboloid-shaped filaments to be obtained, which were evenly distributed over the filter surface. No effect of filter porosity was observed. Nonisotropic structure was also observed in lean methane-plus-hydrogen flames and in rich flames of various hydrocarbons. The manner of soot formation in rich, polyhedral flames of hydrocarbon-air mixtures was particularly noted: With benzene, carbon issued from the flame exclu-

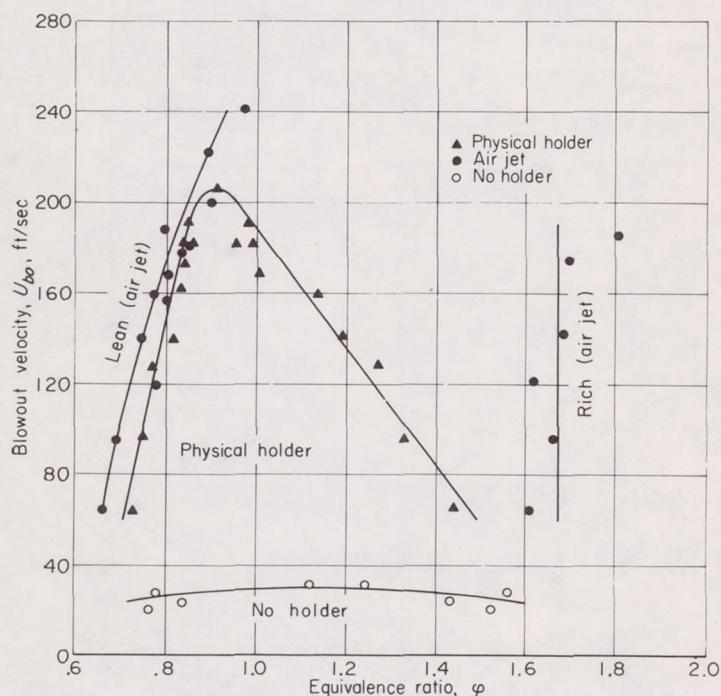


FIGURE 194.—Blowout curves for physical holder, opposing air jet, and no holder.

and no flameholder are shown in figure 194 (ref. 48). The air jet and physical flameholder give similar lean blowout limits, but the air jet gives a much richer limit. Of course, the air added by the jet is responsible for the broadening of the limit, since only the approach-flow fuel-air ratio is considered in the abscissa. The air jet also gives a higher peak blowout velocity, the actual maximum not being attainable in the tests. The authors suggest that the recirculation

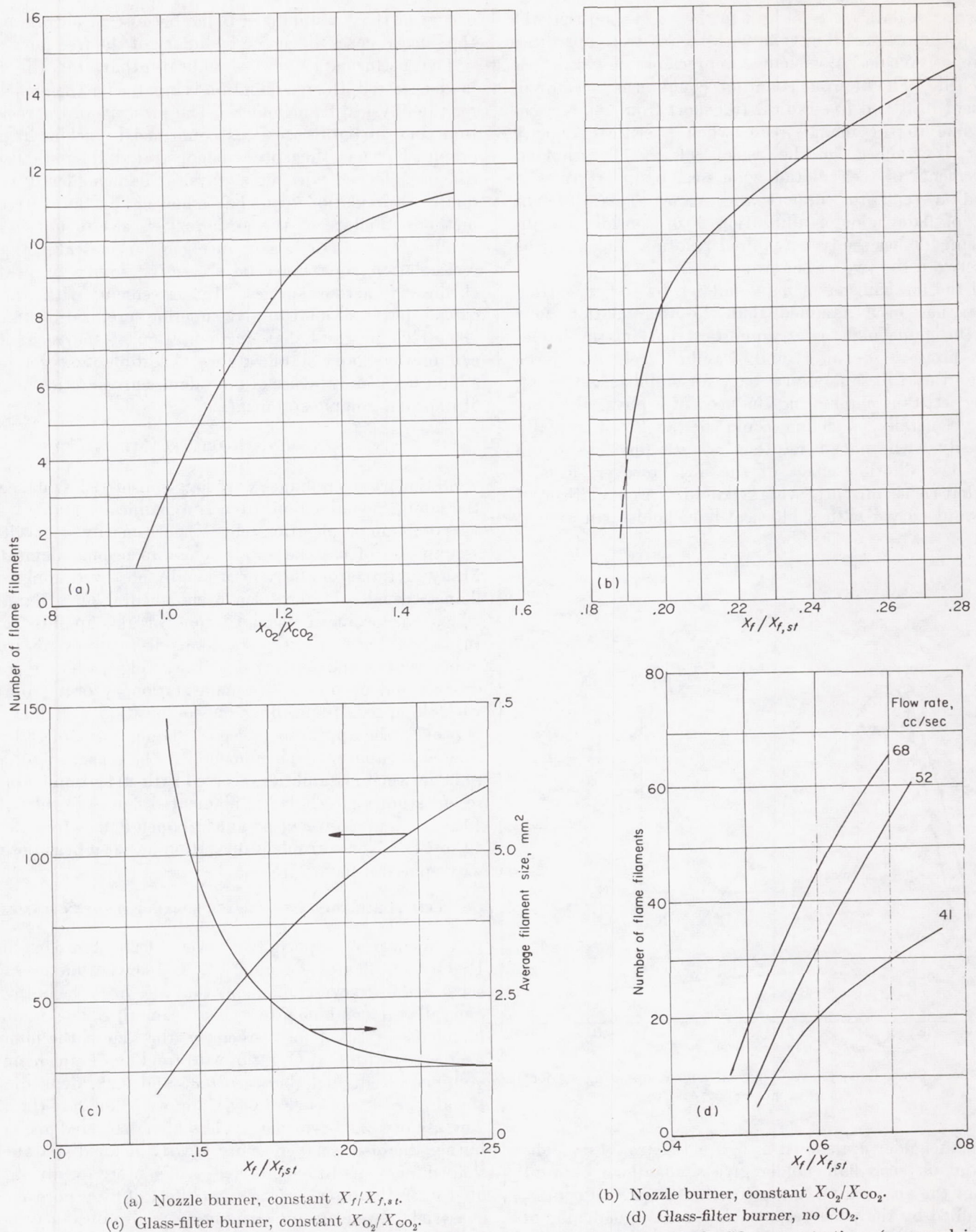


FIGURE 195.—Number of flame filaments for lean hydrogen burner flames at various H_2 - O_2 - CO_2 concentrations (expressed in mole fractions), on 1.36-centimeter nozzle or 3.08-millimeter sintered glass filter (ref. 52).

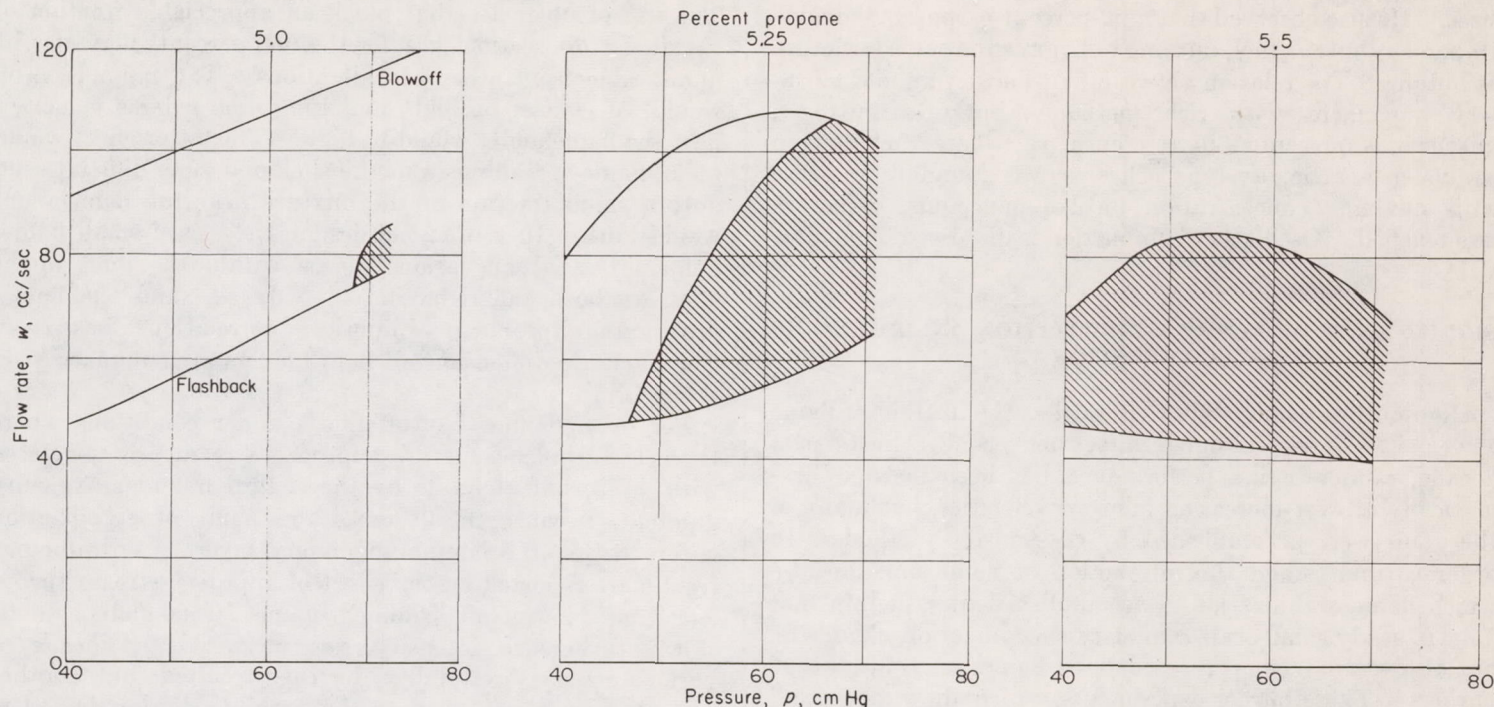


FIGURE 196.—Regions of polyhedral flames (shaded areas) of propane-air mixtures at reduced pressure. Split-flame burner (ref. 54).

sively as a narrow stream at the tip; whereas, with acetylene, it appeared in a luminous region that surrounded the cone uniformly, except for a dark region at the tip and a cup-shaped region of increased luminosity rising from the rim. Rich, polyhedral flames of other hydrocarbons (e. g., butane, heptane) exhibited intermediate behavior; oxygen-enrichment shifted the behavior of some of these toward the benzene type.

In reference 54, regions of polyhedral flames were mapped on flow-rate-pressure diagrams for various rich propane- and butane-air mixtures and lean hydrogen-air mixtures. A typical diagram for a propane-air mixture is shown in figure 196. At constant pressure and composition within the region for polyhedral flames, the number of polyhedron sides increased with increasing flow rate. Upon the addition of 1 to 7 percent hydrogen, which by itself only exhibits instabilities in lean mixtures, to rich propane-air mixtures, the over-all equivalence ratios at which polyhedral flames occur were reduced, other conditions being fixed. Adding hydrogen to rich carbon monoxide-air mixtures, which would otherwise exhibit no polyhedral flames at any composition, also produced polyhedral flames.

The most generally accepted explanation of nonisotropic structure in rich open flames of hydrocarbons and of soot formation at the tip is the preferential diffusion of the oxygen molecules, which are lighter than the fuel molecules, to the valleys, where the propagation is faster. In lean hydrogen or hydrogen-methane flames, the fuel becomes the lighter component and diffuses preferentially. In either case, it is the diffusion of combustion products into the unburned gas that sets up the concentration gradients leading to this preferential diffusion. Some investigators also

believe in the necessity of the presence of hydrogen (refs. 52 and 54), and Behrens (ref. 52) points to the role of thermal diffusion in producing the observed soot filaments. Markstein (ref. 49) uses a different attack—an aerodynamic treatment into which he incorporates the assumption that all transport phenomena can be described to a first approximation by a linear relation between flame velocity and reciprocal radius of curvature of the flame front. This aerodynamic treatment includes the effect of gravity. It appears that the question of diffusion kinetics against aerodynamic instability is yet unresolved.

CELLULAR FLAMES IN TUBES

Nonisotropic structure of flame propagating through tubes is particularly evident in flammability-limit studies (ref. 45 and ch. III). Markstein (refs. 49 to 51) has made more definitive studies insofar as cell diameter d_c , molecular weight of fuel M_f , and pressure effects are concerned by studying near-stoichiometric flames traveling downward through larger tubes (10-cm diam.) at low velocities. The low spatial velocities were obtained by reducing the flame velocity through the addition of nitrogen and letting the flame travel against a small unburned-gas flow. For hydrocarbons in the molecular-weight range 42 to 114, $d_c \propto M_f^{-1/2}$. For *n*-butane-air-nitrogen mixtures at pressures from $\frac{1}{2}$ to 1 atmosphere, $d_c \propto M_f^{-3/4}$. Both of these effects were determined for equivalence ratios between 1.2 and 1.4.

Contrary to the results of reference 54, Markstein found that the addition of hydrogen to rich mixtures of higher hydrocarbons suppressed cell structure, whereas addition to lean mixtures gave nonisotropic structure with small cell

sizes. He also observed that a 90-percent carbon monoxide–10-percent butane fuel, burning rich, gave the same structure as butane. The relation between flame structure and vibratory movement with rich methane-*n*-butane-air-nitrogen mixtures is presented in reference 51, where, for a given equivalence ratio, average cell size was found to increase with methane concentration until a noncellular structure was reached. Oscillatory combustion is discussed in chapter VIII.

SIGNIFICANCE OF FLAME STABILIZATION IN JET-ENGINE COMBUSTION

High-output combustors require the stabilization of flame at velocities of several hundred feet per second. In the past decade, ramjet-engine performance has been boosted dramatically at ever-increasing inlet-air velocities, but many of the gains were accomplished by cut-and-try methods. In order to understand the interaction of flame and flow by which flame stabilization is accomplished, it is helpful not only to study small-scale ramjet-type combustion chambers, but also to analyze open or confined flames on Bunsen-type burners. These burner experiments, which allow more rigid control and separation of operating variables, add to the basic understanding of such factors as wall quenching and secondary-air dilution. The experimental results reviewed in this chapter, together with some of the major theoretical concepts emphasized in recent years, are summarized in the following paragraphs.

For open flames burning above channels of simple geometric shape, including cylindrical tubes containing axially mounted rods, blowoff or flashback limits for various lengths of the characteristic dimension of a given type of channel are correlated by means of the critical boundary velocity gradient, that is, the linear velocity gradient near the flameholding solid surface or the stream boundary. For confined flames supported on flameholders, the stabilization process depends on a recirculation zone behind the flameholder; and, since the size of the recirculation zone is related to a characteristic dimension of the flameholder, the concentration-velocity limits are also related to flameholder dimensions. From experimental results in the literature (and from theoretical considerations mentioned hereinafter), it appears that a quantity such as $U_{av,bo}/A^c$ against a concentration parameter may correlate blowoff-limit data, where A is the projected area of the flameholder and c is an exponent of the order of $\frac{1}{2}$. For greater generality, a more direct function of the recirculation-zone size should be used instead of A^c , because obstacles of different shapes are known to produce vortices of different sizes.

The use of the vortex size rather than the obstacle size may also correct for effects that occur when the size of the obstacles is no longer small compared with the duct size. As the size of the obstacle is increased, a point is reached at which the vortex size begins to decrease; as the obstacle size approaches the duct size, the vortex may be considerably smaller than the obstacle, and reduced stability may result. Thus, the previous expression applies only for small stabilizers in large ducts as long as A refers to obstacle dimensions.

The use of obstacles that block an appreciable fraction of the duct cross section (greater than 60 percent) may also be undesirable from other considerations. The pressure drop would, of course, be high, and the unburned-gas velocities past the flameholder would be high. The latter effect would make flame-spreading from the sheltered zone difficult, and only a small fraction of the mixture near the flameholder would burn. In a practical design, the use of small flameholders located at various places within the duct might alleviate both the reduction in eddy size and the flame-propagation problem. Empirical correlations based on characteristic dimensions of flameholders are summarized in table XXVI.

For open flames, blowoff limits under conditions where there is turbulence in the approach stream are correlated with nonturbulent limits by the critical boundary velocity gradient, because in all cases the point of stabilization occurs within the laminar boundary layer. Contradictory results are reported on the effect of approach-stream turbulence on blowoff of confined flames from flameholders. When turbulence intensity was increased by means of various screens, a stability decrease resulted, but another investigation reported that the stability limits decreased when turbulence intensity was decreased by moving the flameholder downstream. Partial removal of a laminar boundary layer has little effect on blowoff from flameholders, unless the approach flow is so turbulent that the laminar sublayer is very thin. Lean flames are affected by boundary-layer removal more than rich flames. Blowing a gaseous fuel into the boundary layer through slots in a flameholder may provide good pilot flames.

A 2000-volt axial electric field, either alternating current at 400 cps or direct current with the positive electrode in the burned gas, can double the blowoff velocity and triple the stable concentration range for burner flames. On the other hand, a transverse direct-current field of 15,000 volts decreased concentration limits of butane flames by 43 percent. Strong acoustical disturbances decrease stability (see also ch. VIII).

For burner flames, the effect of pressure is related to tube diameter d_{tube} ; that is, $U_{av,bo}/pd_{tube}$ is a function of concentration. An analogous situation is encountered with confined, supported flames; for example, for disk-shaped flameholders of diameter d , $U_{av,bo}/p^{0.95}d^{0.85}$ was related to fuel-air ratio for propane flames. This type of correlation is substantiated by theoretical considerations. Scurlock arrived at the generality $U_{av,bo}/d^b = \mathcal{F}(\mathcal{C})$ by considering the heat transferred between the eddy region behind the flameholder and the main stream. In reference 15, $w_a/Vp^2 \propto U_{av,bo}/d^b p = \mathcal{F}(\mathcal{C})$ was obtained, where w_a is the air mass flow entering the recirculation zone behind the flameholder, and V is the volume of that zone, which is considered to be a homogeneous, second-order reaction zone. The $\mathcal{F}(\mathcal{C})$ results from considering the second-order reaction and a certain fraction of the fuel within the zone being burned to produce a certain adiabatic reaction temperature. (The initial mixture temperature could also be included through its effect on this reaction-zone temperature.)

The blowoff velocity of open flames increases with approximately the square of the absolute initial mixture temperature; the exact exponent varies with concentration and fuel type and may be influenced by such factors as wall temperature and water vapor. The flashback velocity is even more temperature-dependent, so that a decrease in relative stability range occurs as temperature is increased. The relative effect of temperature on critical boundary velocity gradients may be predicted by considering the effects of temperature on flame velocity and penetration distance (wall quenching and/or secondary-air dilution effect) on a thermal basis. Empirical correlations indicate that blowoff from flameholders may depend on a lower power of the initial mixture temperature; the parameter $U_{av,bo}/d^{1/2}T_o^{1.2}$ correlated data for a hydrocarbon blend. At this point, it might be noted that the effects of flameholder area, pressure, and temperature might be combined in a correlating parameter such as $U_{av,bo}/A^c p T_o^m$, where c and m may be of the order of 0.5 and 1.2, respectively.

Liquid-vapor-air mixtures obtained by partial vaporization of liquid fuels generally gave Bunsen-burner stability curves similar to those for gaseous systems. Blowoff limits can be increased appreciably by heating the flameholder; blowoff and flashback velocities of burner flames are also increased by heating the burner rim. Therefore, a heated flameholder, which might, in turn, be used to preheat fuel, would be advantageous in a high-speed engine.

The effect of fuel type on flame velocity was discussed in chapter IV; as might be expected, the blowoff and flashback velocity gradients are greater for fuels with high flame velocities. Disk-stabilized, confined flames became less dependent on the disk diameter for fuels of higher flame velocity. Blowoff velocities of mixed fuels generally follow the relation of equation (17) herein.

Added water vapor decreases stability velocities; 2.5 percent water in the primary air reduced the blowoff velocities of butane flames by approximately 5 percent for lean mixtures and up to 30 percent for rich mixtures. Decreasing the diluent concentration in a combustible mixture greatly increases blowoff and flashback velocities; for example, the critical boundary velocity gradients for methane-oxygen mixtures are two to three orders of magnitude greater than those for methane-air mixtures. This indicates that oxygen-enrichment of the inlet air is another method of obtaining very stable flames or pilot flames.

Also reviewed in this chapter were certain instability phenomena observed in bench-scale equipment and, for the most part, with laminar flames. The breakup of open laminar flames into cells or polyhedral shapes is believed by some investigators to be a diffusion-kinetics process, while others treat it primarily as an aerodynamic instability.

In final summary, most of the experimental results for the stability of burner flames can be explained on the basis of the interaction between flame velocity and flow velocity in terms of the critical boundary velocity gradient. For confined flames, stabilization occurs through the recirculation zone behind a flameholder that is bluff or nonstreamlined on its downstream end. All the gross features of this latter

type of stabilization appear to be explained by an assumption that the recirculation zone behaves as a volume of homogeneous, second-order reaction.

REFERENCES

1. Wohl, Kurt, Kapp, Numer M., and Gazley, Carl: The Stability of Open Flames. Third Symposium on Combustion and Flame and Explosion Phenomena, The Williams & Wilkins Co. (Baltimore), 1949, pp. 3-21.
2. Bollinger, Lowell M., and Williams, David T.: Experiments on Stability of Bunsen-Burner Flames for Turbulent Flow. NACA Rep. 913, 1948. (Supersedes NACA TN 1234.)
3. Lewis, Bernard, and von Elbe, Guenther: Combustion, Flames and Explosion of Gases. Academic Press, Inc., 1951.
4. Garside, J. E., Hall, A. R., and Townend, D. T. A.: The Stability of Aerated Burner Flames. Trans. Inst. Gas Eng., vol. 91, 1941-1942, pp. 81-110.
5. Kurz, Philip F.: The Stability of Isobutane-Ethylene Flames on a Bunsen Burner Shielded to Exclude Ambient Air. Rep. No. 15036-18, Battelle Memorial Inst., Feb. 27, 1953. (Contract AF 33 (038)-12653, E. O. No. 460-35, S. R.-8.)
6. Haddock, Gordon W.: Flame-Blowoff Studies of Cylindrical Flame Holders in Channeled Flow. Prog. Rep. No. 3-24, Jet Prop. Lab., C.I.T., May 14, 1951.
7. Weir, Alexander, Jr., Rogers, Donald E., and Cullen, Robert E.: Blowoff Velocities of Spherical Flameholders. Rep. UMM 74, Willow Run Res. Center, Eng. Res. Inst., Univ. Mich., Sept. 1950. (USAF Contract W33-038-ac-21100, Proj. MX-772.)
8. Grumer, Joseph, Harris, Margaret E., and Schultz, Harold: Flame Stabilization on Burners with Short Ports or Non-circular Ports. Fourth Symposium (International) on Combustion, The Williams & Wilkins Co. (Baltimore), 1953, pp. 695-701.
9. Grumer, Joseph, and Harris, Margaret E.: Flame-Stability Limits of Methane, Hydrogen, and Carbon Monoxide Mixtures. Ind. and Eng. Chem., vol. 44, no. 7, July 1952, pp. 1547-1559.
10. Dugger, Gordon L.: Flame Stability of Preheated Propane-Air Mixtures. Ind. and Eng. Chem., vol. 47, no. 1, Jan. 1955, pp. 109-114.
11. McAdams, William H.: Heat Transmission. Second ed., McGraw-Hill Book Co., Inc., 1942, pp. 117-120.
12. Wohl, Kurt: Quenching, Flash-Back, Blow-Off—Theory and Experiment. Fourth Symposium (International) on Combustion, The Williams & Wilkins Co. (Baltimore), 1953, pp. 68-89.
13. Scurlock, A. C.: Flame Stabilization and Propagation in High-Velocity Gas Streams. METEOR Rep. 19, Fuels Res. Lab., M.I.T., May 1948. (Contract NOrd 9661.)
14. Scurlock, A. C., Grover, J. H., and Barnes, W. P.: Turbulent Flames, Flame Stability, and Rough Burning. Semi-Annual Prog. Rep., Proj. Squid, James Forrestal Res. Center, Princeton Univ., Apr. 1, 1953, pp. 127-131. (Office Naval Res. Contract N7-ori-105, Task Order III, NR-098-038.)
15. Longwell, J. P., Chenevey, J. E., Clark, W. W., and Frost, E. E.: Flame Stabilization by Baffles in a High Velocity Gas Stream. Third Symposium on Combustion and Flame and Explosion Phenomena, The Williams & Wilkins Co. (Baltimore), 1949, pp. 40-44.
16. DeZubay, E. A.: Characteristics of Disk-Controlled Flame. Aero. Digest, vol. 61, no. 1, July 1950, pp. 54-56; 102-104.
17. Longwell, J. P.: Flame Stabilization by Bluff Bodies and Turbulent Flames in Ducts. Fourth Symposium (International) on Combustion, The Williams & Wilkins Co. (Baltimore), 1953, pp. 90-97.
18. Caldwell, F. R., Ruegg, F. W., and Olsen, L. O.: Seventy-First Report on Progress on the Combustion Chamber Research Program for the Quarter Ending Sept. 30, 1951. Rep. 1B106, U. S. Dept. Commerce, Nat. Bur. Standards, Oct. 29, 1951. (NAer Order 01183.)

19. Williams, Glenn C., and Shipman, C. W.: Some Properties of Rod-Stabilized Flames of Homogeneous Gas Mixtures. Fourth Symposium (International) on Combustion, The Williams & Wilkins Co. (Baltimore), 1953, pp. 733-742.
20. Zukoski, Edward E., and Marble, Frank E.: The Role of Wake Transition in the Process of Flame Stabilization on Bluff Bodies. Combustion Res. and Rev., Butterworths Sci. Pub. (London), 1955, pp. 167-180.
21. Barrère, M., et Mestre, A.: Stabilisation des Flammes par des Obstacles. Selected Combustion Problems—Fundamentals and Aeronautical Applications, Butterworths Sci. Pub. (London), 1954, pp. 426-446. (Comments by Melvin Gerstein, p. 524.)
22. Younger, George G., Gabriel, David S., and Mickelsen, William R.: Experimental Study of Isothermal Wake-Flow Characteristics of Various Flame-Holder Shapes. NACA RM E51K07, 1952.
23. Nickolson, H. M., and Field, J. P.: Some Experimental Techniques for the Investigation of the Mechanism of Flame Stabilization in the Wakes of Bluff Bodies. Third Symposium on Combustion and Flame and Explosion Phenomena, The Williams & Wilkins Co. (Baltimore), 1949, pp. 44-68.
24. Mestre, André: Étude des Limites de Stabilité en Relation avec la Résistance des Obstacles à l'Écoulement. Combustion Res. and Rev., Butterworths Sci. Pub. (London), 1955, pp. 72-86.
25. Edse, Rudolph: Studies on Burner Flames of Hydrogen-Oxygen Mixtures at High Pressures. Tech. Rep. 52-59, Flight Res. Lab., Wright Air Dev. Center, Wright-Patterson Air Force Base, Apr. 1952. (RDO No. R-467-1.)
26. Putnam, Abbott A., and Landry, Bertrand A.: The Effect of Boundary-Layer Thickness on Flame Stability. Tech. Rep. 15033-1, Battelle Memorial Inst., Dec. 15, 1952. (Contract No. AF 33(038)-12656, E. O. No. 460-35, S. R.-8.)
27. Hottel, Hoyt C., et al.: High Output Combustion. Semi-Annual Prog. Rep., Proj. Squid, James Forrestal Res. Center, Princeton Univ., Oct. 1, 1953, pp. 97-125. (Office Naval Res. Contract N7-ori-105, Task Order III, NR-098-038.)
28. Polanyi, M. L., and Markstein, G. H.: Phenomena in Electrically and Acoustically Disturbed Bunsen Burner Flames. Tech. Rep. No. 5, Proj. Squid, Cornell Aero. Lab., Sept. 15, 1947.
29. Calcote, Hartwell F., and Pease, Robert N.: Electrical Properties of Flames—Burner Flames in Longitudinal Electric Fields. Ind. and Eng. Chem., vol. 43, no. 12, Dec. 1951, pp. 2726-2731.
30. Calcote, Hartwell F.: Electrical Properties of Flames—Burner Flames in Transverse Electric Fields. Third Symposium on Combustion and Flame and Explosion Phenomena, The Williams & Wilkins Co. (Baltimore), 1949, pp. 245-253.
31. Wolfhard, H. G.: Die Eigenschaften stationärer Flammen im Unterdruck. Zs. f. Tech. Phys., Nr. 9, 1943, pp. 206-211.
32. Putnam, Abbott A., and Smith, Robert L.: On the Extinction Limit of Laminar Flames. Fourth Symposium (International) on Combustion, The Williams & Wilkins Co. (Baltimore), 1953, pp. 708-714.
33. Wohl, Kurt, and Kapp, Numer M.: Flame Stability at Variable Pressures. Meteor Rep. UAC-42, Res. Dept., United Aircraft Corp., Oct. 1949. (Proj. METEOR, Bur. Ord. Contract NOrd 9845 with M.I.T.)
34. Culshaw, G. W., and Garside, J. E.: Recent Studies of Aerated Burner Flames. Inst. Gas. Eng. Inst. (London), Gas. Res. Fellowship Rep. 1946-1947. (Reviews papers from period 1943-1946, including those of Delbourgh, Heiligenstaedt, and Vasileseo.)
35. Browning, James A., and Thorpe, Merle L.: Flame Stability of Liquid-Vapor Oxygen Mixtures. Tech. Memo. Dart-1, Proj. Squid, Thayer School of Eng., Dartmouth College, Feb. 11, 1952. (Contract N-onr-438, Task Order 1, NR 090172.)
36. Browning, James A., and Thorpe, Merle L.: Flame Stability of Liquid-Vapor Air Mixtures. Tech. Memo. Dart-2, Proj. Squid, Dartmouth College, Oct. 1, 1952. (Contract N6-ori-105, T. O. III, NR-098-038.)
37. Sachsse, Hans: Über die Temperaturabhängigkeit der Flammgeschwindigkeit und das Temperaturgefälle in der Flammenfront. Zs. f. Phys. Chem., Bd. 180, Heft 4, Abt. A, Oct. 1935, pp. 305-313.
38. May, Walter G., and Maddocks, Frank E., Jr.: Flame Stabilization in Air/Fuel-Spray Mixtures at High Velocity. Meteor Rep. No. 54, Fuels Res. Lab., M.I.T., Apr. 1950.
39. Russi, M. J., Cornet, I., and Cornog, R.: The Influence of Flame Holder Temperature on Flame Stabilization. Fourth Symposium (International) on Combustion, The Williams & Wilkins Co. (Baltimore), 1953, pp. 743-748.
40. Kurz, Philip F.: Flame-Stability Studies with Mixed Fuels. Ind. and Eng. Chem., vol. 45, no. 9, Sept. 1953, pp. 2072-2078.
41. Reiter, S. H., and Wright, C. C.: Stability of Burner Flames with Propane-Hydrogen Mixtures. Ind. and Eng. Chem., vol. 42, no. 4, Apr. 1950, pp. 691-694.
42. Grumer, Joseph, and Harris, Margaret E.: Flame-Stability Limits of Methane, Hydrogen, and Carbon Monoxide Mixtures. Ind. and Eng. Chem., vol. 44, no. 7, July 1952, pp. 1547-1559.
43. Walker, P. L., Jr., and Wright, C. C.: Stability of Burner Flames for Binary and Tertiary Mixtures of Methane, Carbon Monoxide and Water Vapour. Fuel, vol. XXI, no. 1, Jan. 1951, pp. 37-44.
44. Walker, P. L., Jr., and Wright, C. C.: Stability and Burning Velocity of Bunsen Flames with Propane-Carbon Monoxide Mixtures. Fuel, vol. XXXI, no. 1, Jan. 1952, pp. 45-49.
45. Kapp, N. M., Snow, B., and Wohl, K.: The Effect of Water Vapor on the Normal Burning Velocity and on the Stability of Butane-Air Flames Burning Above Tubes in Free Air. Meteor Rep. UAC-30, United Aircraft Corp., Nov. 1948. (U. S. Navy Bur. Ord. Contract NOrd 9845 with M.I.T.)
46. Longwell, John P., Frost, Edward E., and Weiss, Malcom A.: Flame Stability in Bluff Body Recirculation Zones. Ind. and Eng. Chem., vol. 45, no. 8, Aug. 1953, pp. 1629-1633.
47. Zukoski, Edward E., and Marble, Frank E.: Experiments Concerning the Mechanism of Flame Blowoff from Bluff Bodies. Proc. Aerothermochem. Gas Dynamics Symposium, Northwestern Univ., 1956, pp. 205-210.
48. Schaffer, Allan, and Cambel, Ali Bulent: The Effect of an Opposing Jet on Flame Stability. Jet Prop., vol. 25, no. 6, June 1955, pp. 284-287.
49. Markstein, George H.: Instability Phenomena in Combustion Waves. Fourth Symposium (International) on Combustion, The Williams & Wilkins Co. (Baltimore), 1953, pp. 44-59.
50. Markstein, George H.: Experimental and Theoretical Studies of Flame-Front Stability. Jour. Aero. Sci., vol. 18, no. 3, Mar. 1951, pp. 199-209.
51. Markstein, G. H., and Somers, L. M.: Cellular Flame Structure and Vibratory Flame Movement in N-Butane-Methane Mixtures. Fourth Symposium (International) on Combustion, The Williams & Wilkins Co. (Baltimore), 1953, pp. 527-535.
52. Behrens, Hans: Untersuchung über Aussehen und Gestalt von Brennerflammen. Zs. Phys. Chem., Bd. 196, Sept. 1950, pp. 78-101.
53. Garside, J. E., and Jackson, B.: The Formation and Some Properties of Polyhedral Burner Flames. Fourth Symposium (International) on Combustion, The Williams & Wilkins Co. (Baltimore), 1953, pp. 545-552.
54. Jost, W., Krug, Joachim, and Sieg, L.: Observations on Disturbed Flames. Fourth Symposium (International) on Combustion, The Williams & Wilkins Co. (Baltimore), 1953, pp. 535-537.
55. Simon, Dorothy M., and Wong, Edgar L.: Burning Velocity Measurement. Jour. Chem. Phys., vol. 21, no. 5, May 1953, pp. 936-937.

CHAPTER VII

DIFFUSION FLAMES

By RICHARD S. BROKAW and MELVIN GERSTEIN

INTRODUCTION

The previous chapters consider combustion occurring in systems in which the fuel and air are homogeneously distributed. Chapter II discusses the preparation of such mixtures. If the mixing occurs rapidly compared with the combustion reactions, or well ahead of the flame zone, burning may be considered solely in terms of homogeneous processes. There are systems, however, in which mixing is slow compared with the reaction rates, so that the mixing time controls the burning rate. This is true for so-called diffusion flames, in which the fuel and oxidant come together in a reaction zone through molecular and turbulent diffusion. The fuel may be in the form of a gaseous jet or a liquid surface. The distinctive characteristic of a diffusion flame is that the burning rate is determined by the rate at which the fuel and oxidant are brought together in proper proportions for reaction. Between the extremes in which the chemical reaction rate on the one hand and the mixing rate on the other control the burning rate, there is the region in which the chemistry and mixing have similar rates and must be considered together. This middle region has received very little attention in fundamental studies because of its complexity, but is considered in some of the practical systems discussed in subsequent chapters.

SYMBOLS

The following symbols are used in this chapter:

A	constant
B	constant
\mathcal{B}	transfer number
b_F	flame height
b_p	height of plate
\mathcal{C}	concentration
c_p	specific heat at constant pressure
D	diffusion coefficient
\mathcal{D}	distribution constant
d	diameter
\mathcal{F}	function
f	fuel-air ratio
G	mass-flow rate per unit area
g	acceleration due to gravity, 32.17 ft/sec ²
H	heat-transfer coefficient
h	specific enthalpy
i	stoichiometric number of moles of oxygen per mole of fuel
J_0, J_1	Bessel functions of the first kind
K	constant
\mathcal{K}	evaporation constant

k	constant
\mathcal{L}_{La}	Lagrangian scale of turbulence
M	molecular weight
m	mass
P	absolute total pressure
Pr	Prandtl number
p	partial pressure
R	universal gas constant
Re	Reynolds number
r	radial distance
T	temperature
$\mathcal{T}_{1/2}$	half-thickness of port
t	time
U	velocity
$\sqrt{u_x^2}$	intensity of turbulence
V_{fl}	volume flow rate
W_{st}	stoichiometric weight of oxygen per unit weight of fuel
w	total mass flow
X	mole fraction
x	longitudinal distance
y	distance from drop center
α	concentration parameter
ϵ	eddy diffusivity
ι_{dr}	drop distribution parameter
κ	thermal conductivity
Λ	size constant
μ	absolute viscosity
Ξ	time parameter
ρ	density
τ	concentration parameter
Subscripts:	
A	drop surface
a	air
B	burning
C	surrounding atmosphere
c	combustion
dr	drop
F	flame
f	fuel
j	jet
L	laminar
l	liquid
o	initial conditions
P	products
s	secondary flow
st	stoichiometric
T	turbulent
$tube$	tube
v	vaporization

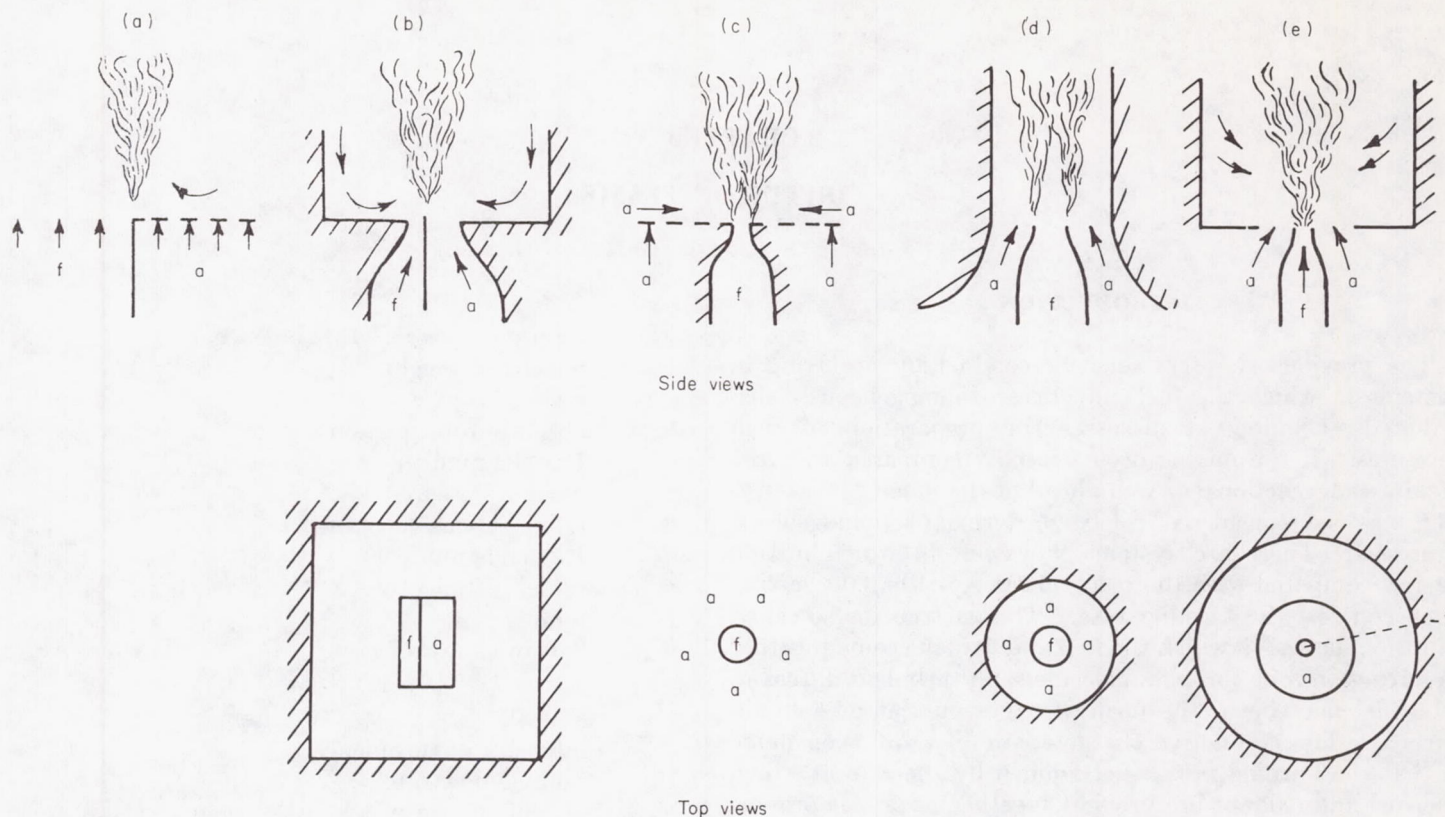


FIGURE 197.—Various configurations used to obtain gaseous diffusion flames (ref. 1).

GASEOUS DIFFUSION FLAMES

Gaseous diffusion flames occur upon ignition of a jet of fuel entering either quiescent air or an airstream. The resulting flame emits heat and light and appears to have a discrete reaction zone, the appearance of which depends on the conditions of burning. Gaseous diffusion flames are most commonly encountered in simple home and industrial burners but may exist in any system where fuel and air are admitted separately and where the mixing processes are slow compared with chemical reaction rates. Typical ways in which the fuel and oxidant are caused to interact are shown in figure 197 (ref. 1, p. 99). Most of the basic work on diffusion flames has been done with the concentric-tube arrangement (197(c)), since it has the simplest geometry. Arrangement (a) has been used for some spectroscopic studies of flames, which are discussed herein.

APPEARANCE

The shape of a laminar flame burning from a jet of fuel depends on the relative quantity of air supplied. If excess air is present, the flame is a closed, elongated figure. Such flames occur when a jet of fuel is admitted into a large volume of quiescent air or when two laminar coaxial jets are used, the inner containing fuel and the outer containing an excess of air. If the air supply in the outer tube is reduced below the stoichiometric proportions, a fan-shaped, underventilated flame is produced.

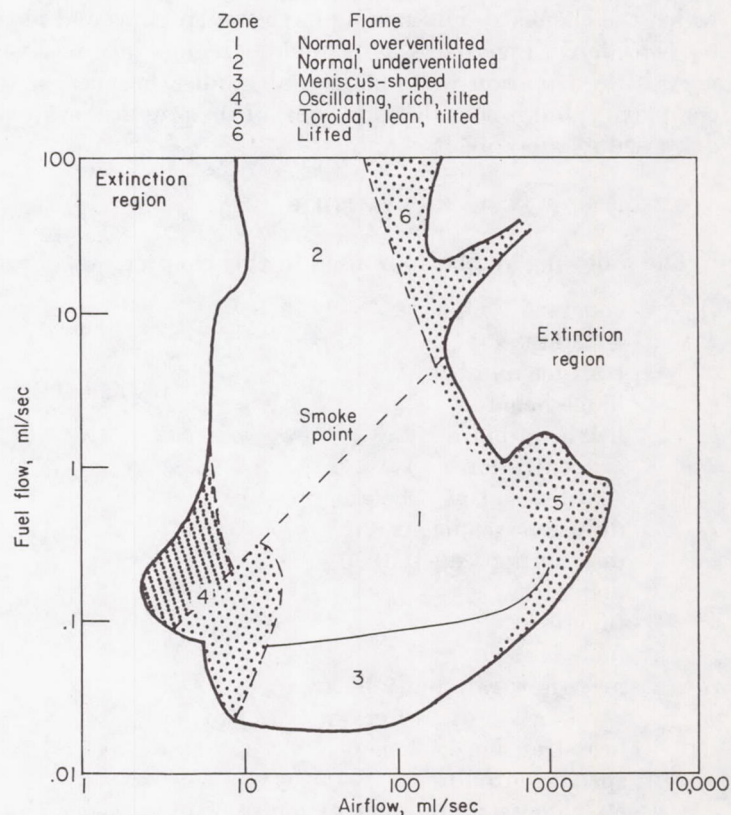


FIGURE 198.—Flame zones for gaseous diffusion flames (ref. 2, p. 766).

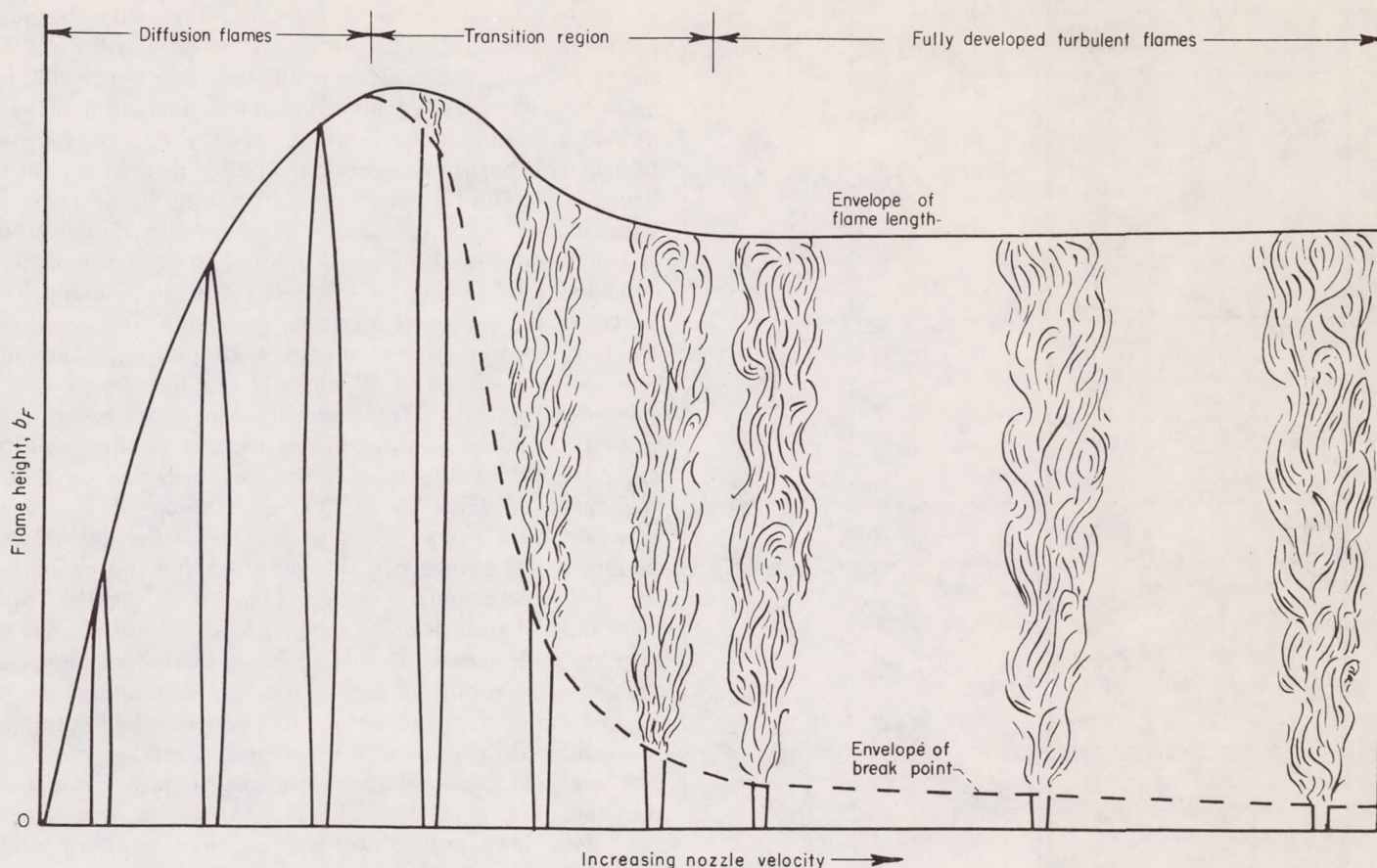


FIGURE 199.—Progressive change in flame type with increase in nozzle velocity (ref. 4).

Under certain limiting flow conditions, the flame can assume a more complex structure. Flame shapes obtained in concentric-tube hydrocarbon diffusion flames (fig. 197(c)) for various fuel flows and airflows are classified in reference 2. These flame zones are illustrated in figure 198. Zone 1 indicates a normal, over-ventilated diffusion flame, and zone 2 indicates the underventilated flame. The dashed line separating zones 1 and 2 denotes the smoke point, smoke appearing as the fuel flow is increased (see ch. IX). Zone 3 illustrates overventilated flames having a meniscus shape without the yellow glow usually associated with diffusion flames. The shaded areas are essentially zones of unstable flames. In the lower part of zone 4 there appear flames that oscillate from side to side, called lambent flames in reference 2; and in the upper part of zone 4 rich, tilted flames appear. In the lower part of zone 5 are found toroidal-shaped flames, called vortex flames; and in the upper part of zone 5 are lean, tilted flames. The flame in zone 6 has begun to move away from the burner base and corresponds to the lifted flames discussed in chapter VI.

If either the fuel flow or the airflow is made turbulent, a brushy, rough flame results. At flows near the critical transition from laminar to turbulent, only the upper portion of the flame is turbulent, the flame near the burner port retaining the appearance of a laminar flame. Typical changes in the appearance of a gaseous diffusion flame as the fuel-flow velocity is increased are shown in figure 199. The line separating the laminar portion of the flame from the turbulent

portion is called the break point. When the break point closely approaches the nozzle, further increases in velocity have very little effect on either the total flame height (measured from the burner port) or the break point, although the noise intensity increases. The quantitative variation of flame height with flow velocity is treated in a subsequent section.

STRUCTURE

Unlike the flame of premixed gases, which has a very narrow reaction zone, the diffusion flame has a wide region over which the composition of the gas changes. These

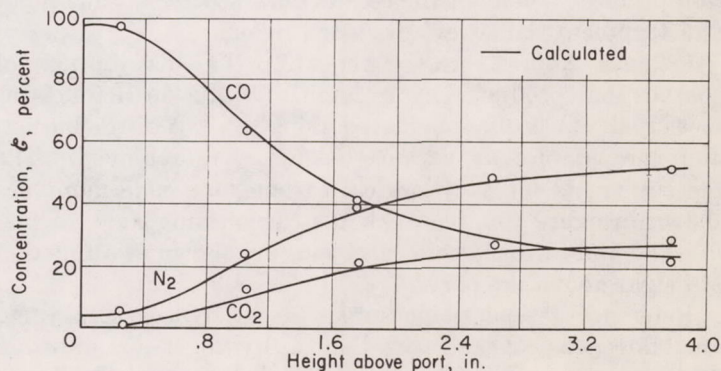


FIGURE 200.—Concentrations of carbon monoxide, nitrogen, and carbon dioxide on axis of cylindrical carbon monoxide flame (by permission from ref. 3).

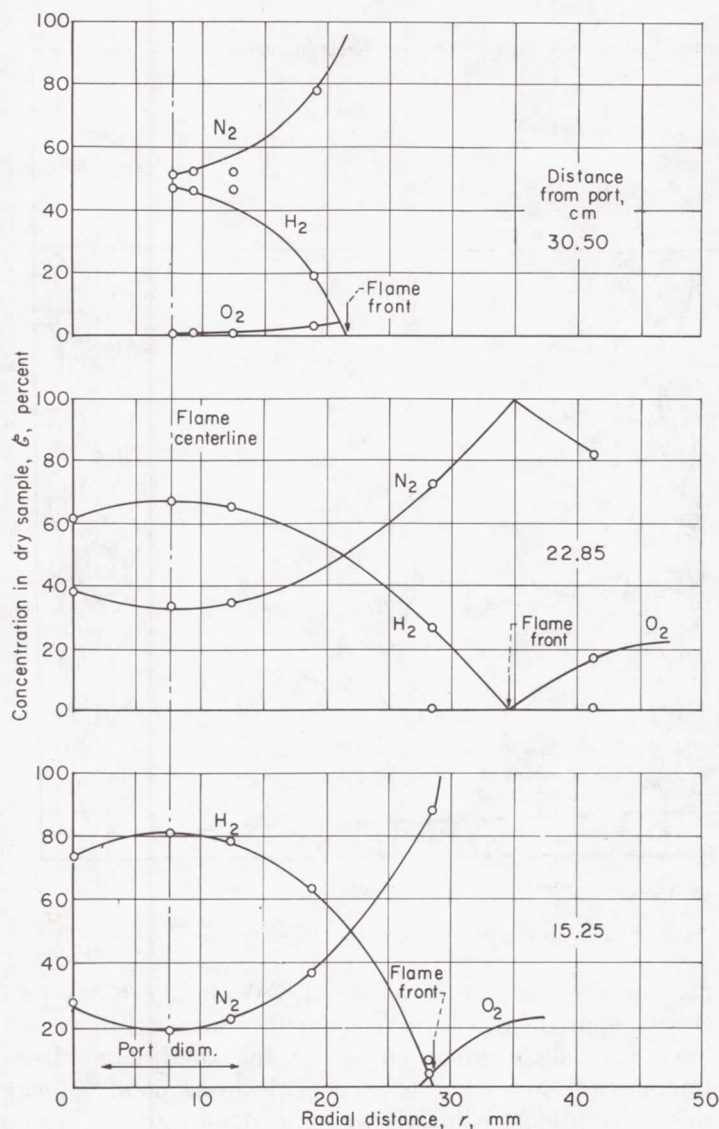


FIGURE 201.—Composition of hydrogen diffusion flame. Nozzle diameter, $\frac{1}{4}$ inch; nozzle velocity, 108 feet per second (ref. 4).

changes are principally due to the interdiffusion of reactants and products, since the actual reaction apparently takes place rapidly in a narrow zone. The diffusion flame is thus better suited for studies of the temperatures and concentration profiles. Some of the results obtained for both laminar and turbulent flames are discussed herein.

Laminar flames.—In reference 3, the distribution of combustion products in a laminar diffusion flame was measured. A probe was placed along the axis of the burner, and gas samples at various heights were removed. The measurements for a cylindrical carbon monoxide flame are shown in figure 200, in which the carbon monoxide, carbon dioxide, and nitrogen concentrations are shown as a function of height above the port.

Reference 4 reports measurements of hydrogen, oxygen, and nitrogen concentrations in a hydrogen-air diffusion flame at various heights and radial distances in the flame. The results are shown in figure 201. The measurable O_2 concentration shown in the fuel side of the flame front is

attributed to air entering the sampling tube because of flame movement. The structure of the diffusion flame suggested from the analysis is illustrated in figure 202, which may be considered generally typical for laminar gaseous diffusion flames. The figure shows the fuel-gas concentration at the burner centerline dropping to zero at the flame front, while the O_2 rises from zero at the flame front to its value in the ambient stream. The concentration of products is a maximum at the flame front. The oxygen and fuel are considered to reach the flame front in stoichiometric proportions and to react to form products instantaneously. In most theoretical treatments, a simplified picture of the reaction is assumed in which only one diffusing gas is considered. Instead of treating both fuel and oxygen varying from their initial concentrations to zero at the flame front, the fuel, for example, is treated as negative oxygen. In the reaction $2H_2 + O_2 \rightarrow 2H_2O$, each mole of hydrogen is equivalent to $\frac{1}{2}$ mole of oxygen. One of the dashed curves in figure 202 represents the reflected fuel curve corrected for the stoichiometric ratio. Thus, it is possible to consider only the diffusion of oxygen from its initial concentration through zero at the flame front to the proper negative value in the unburned fuel. In a similar manner, the other dashed curve illustrates the condition in which the oxygen is considered in terms of its fuel equivalent.

The actual flame is not as simple as the previous discussion may suggest, since, in addition to the molecular species that have been studied by conventional sampling and gas

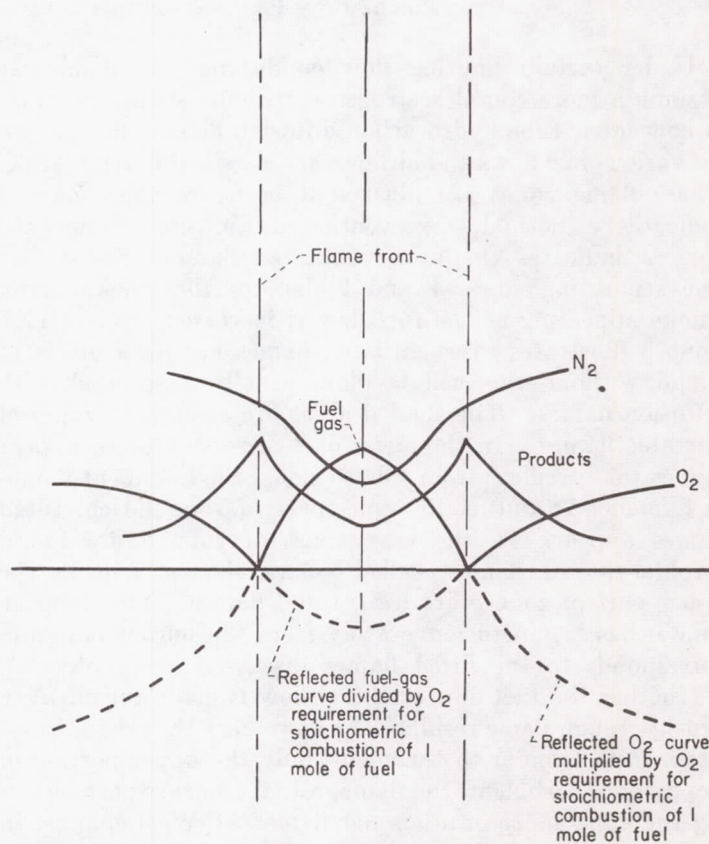


FIGURE 202.—Simplified diagram of concentration profiles in typical laminar diffusion flame (ref. 4).

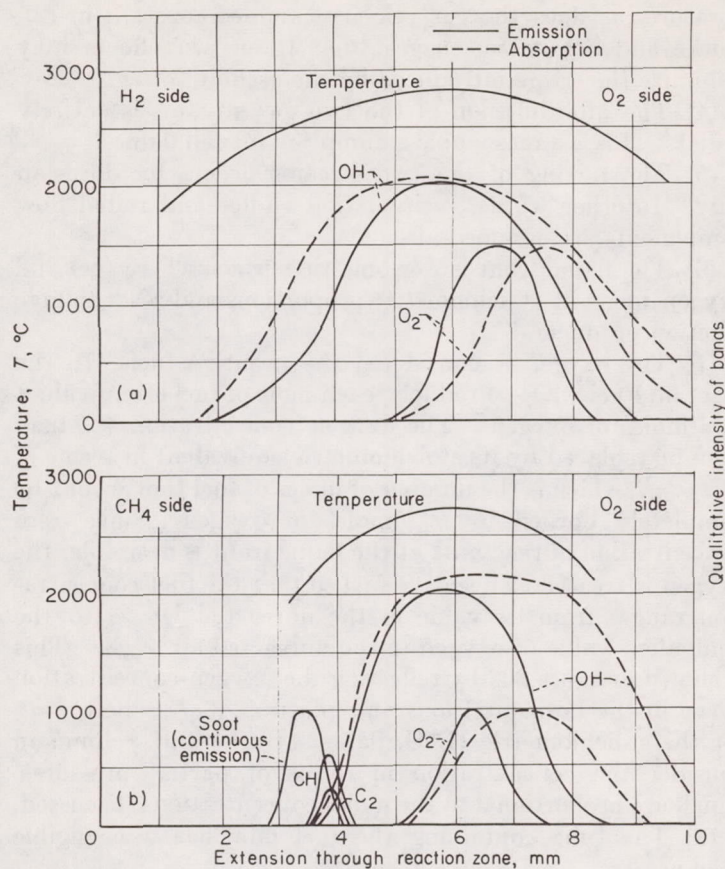
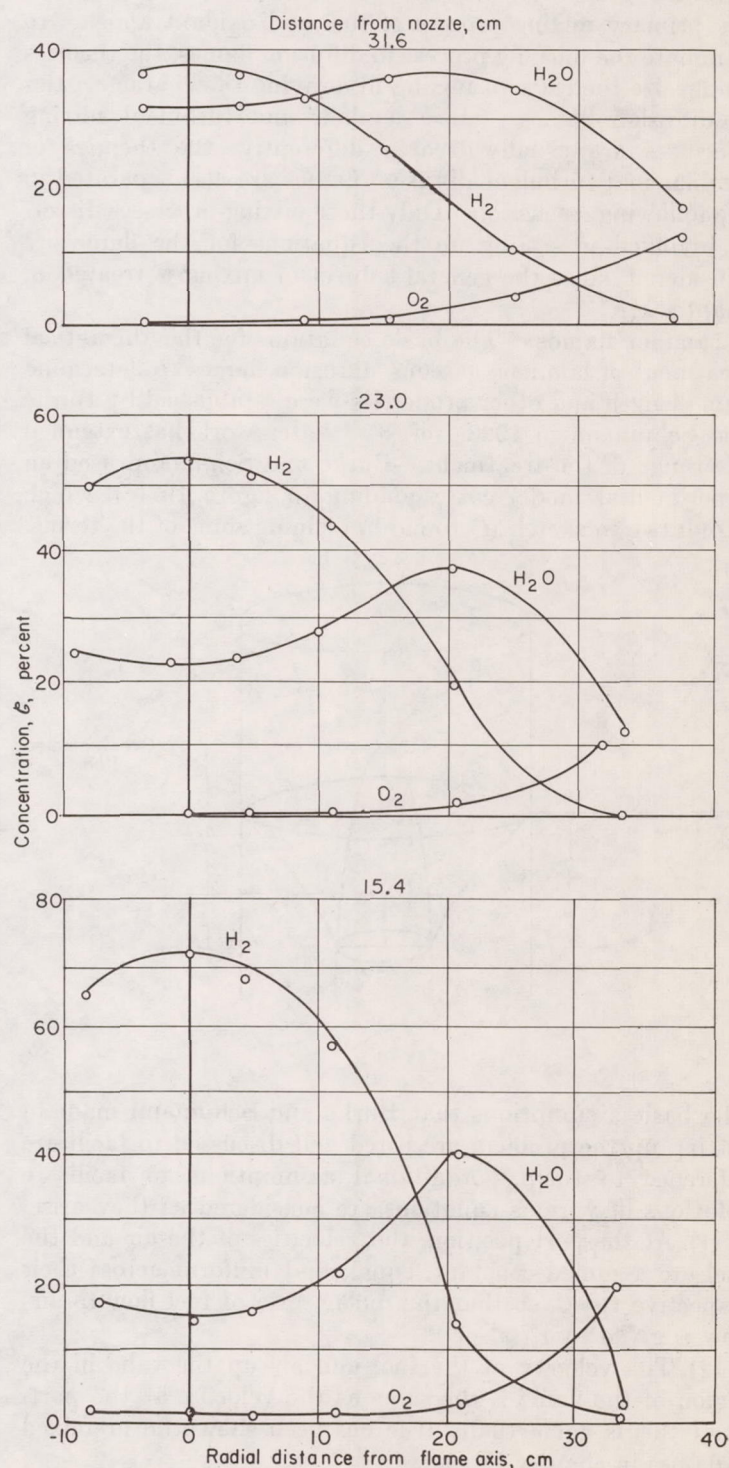
(a) Distribution of OH and O_2 in H_2 - O_2 flame.(b) Distribution of OH, O_2 , CH, C_2 , and soot in CH_4 - O_2 flame.

FIGURE 203.—Temperature profiles and distributions of various species in flat diffusion flames (ref. 5).

analysis, free atoms and radicals are present. A flat flame in an apparatus similar to that shown in figure 197(a) was used in reference 5, in which the distribution of various species in the flame was studied by a spectroscopic method. In addition, a sodium line reversal method was employed to measure flame temperature. The results are given for a H_2 - O_2 flame in figure 203(a). The temperature profile is shown, in addition to a qualitative intensity distribution for OH and O_2 as determined by both emission and absorption spectroscopy. The relatively flat temperature profile has a maximum of about 2800 $^{\circ}\text{C}$, which agrees closely with calculated adiabatic flame temperatures for the stoichiometric reaction. A similar set of curves for CH_4 - O_2 flames is shown in figure 203(b). In addition to OH and O_2 , the C_2 , CH, and continuous emission are shown. Similar curves are shown for NH_3 - O_2 flames in reference 5, while additional curves for H_2 - O_2 and NH_3 - O_2 along with C_2H_4 - O_2 and CO - O_2 are given in reference 6. The general characteristics are similar.

Turbulent flames.—The distribution of reactants and products in a turbulent diffusion flame of hydrogen and air is studied in reference 7. The situation is somewhat more complex than in the laminar flame. Unfortunately, the results are influenced by the confining duct, so that the curves can be applied only qualitatively to open flames. The data are shown in figure 204 for various heights and radial positions. The O_2 and H_2 concentrations were meas-

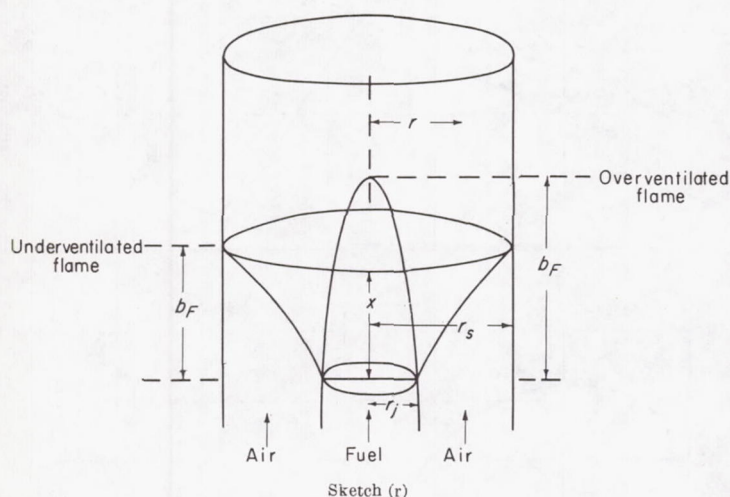
ured, while the H_2O concentration was calculated. The general appearance of the H_2 and O_2 curves resembles that of a laminar flame, although there is considerably more overlapping of the H_2 and O_2 in the vicinity of the flame front. This result is consistent, however, with the oscillating nature of the turbulent flame, which results in the apparent thickening of the reaction zone when a time-average, rather than an instantaneous, position is considered.

FIGURE 204.—Concentration profiles in hydrogen-air flame. Nozzle diameter, $\frac{3}{16}$ inch; no primary air; flow velocity, 162 feet per second (ref. 7).

THEORY

The theories of the burning of premixed fuel-oxidant systems discussed in chapters IV and V consist essentially in analyses of the factors such as diffusion, heat transfer, and reaction mechanisms as they affect the rate of the homogeneous reaction taking place. "Homogeneous" is used in the sense that fuel and oxidant molecules are intimately mixed in the unburned gas, although concentration and temperature gradients exist in the reaction zone. Because the primary mixing process of fuel and oxidant appears to dominate the burning process in diffusion flames, the theories emphasize the rates of mixing in deriving the characteristics of diffusion flames. Since laminar and turbulent mixing processes are usually treated differently, the theories of laminar and turbulent diffusion flames are also separated in the following discussion. Only those mixing processes directly involved in setting up the equations for the flame are considered, since the general subject of mixing is treated in chapter II.

Laminar flames.—The basic equations for the theoretical treatment of laminar, gaseous diffusion flames to determine flame length and other properties were established by Burke and Schumann in 1928 (ref. 3). Later work has extended the range of the treatment. Burke and Schumann used an experimental model corresponding to figure 197(c), which is redrawn in sketch (r) to aid in defining some of the terms:



The basic assumptions that Burke and Schumann made in setting up the problem are listed and discussed to facilitate reference to them. Additional assumptions to facilitate solutions of various equations are considered as they arise.

(1) At the port position, the velocities of the air and the fuel are assumed constant, equal, and uniform across their respective tubes, so that the molar ratio of fuel flow to air flow is given by $r_f^2/(r_s^2 - r_f^2)$.

(2) The velocity of the fuel and air up the tube in the region of the flame is the same as the velocity at the port. That this is not actually true has been shown for premixed V-flames in chapter IV.

(3) The coefficient of interdiffusion of the two gas streams is constant. Since diffusion coefficient increases with tem-

perature, as does the gas velocity assumed constant in (2), Burke and Schumann suggest that these two effects may minimize the errors introduced by the assumptions.

(4) The interdiffusion of the two gas streams is entirely radial. This is a reasonable assumption for tall flames.

(5) The mixing of the two streams occurs by diffusion only. In other words, recirculation eddies and radial flow components are assumed absent.

(6) The flame front is a geometric surface where fuel and oxygen meet in stoichiometric proportions and react to give reaction products.

(7) The oxygen is considered the negative fuel. In the reaction $\text{Fuel} + i\text{O}_2 \rightarrow \text{Products}$, each mole of fuel is equivalent to i moles of oxygen. The oxygen concentration \mathcal{C}_{O_2} may then be replaced by its stoichiometric equivalent in terms of fuel $\mathcal{C}_{\text{O}_2}/i$, which is the number of moles of fuel that would be completely burned by \mathcal{C}_{O_2} moles of oxygen. Since zero concentration of reactants at the flame front is desirable, the oxygen is treated as negative fuel so that the fuel concentration ranges from its value in the unreacted jet \mathcal{C}_f to the equivalent value of oxygen in the unreacted air $\mathcal{C}_{\text{O}_2}/i$. This is shown in figure 202 by reflecting the oxygen-concentration curve in the horizontal axis and plotting $\mathcal{C}_{\text{O}_2}/i$, where $i = \frac{1}{2}$ for the stoichiometric $\text{H}_2\text{-O}_2$ flame. Burke and Schumann consider the concentration in terms of partial pressures, which are proportional to the molal concentrations discussed.

(8) The tube containing the fuel flow has a negligible thickness.

These assumptions reduce the problem to one of diffusion of a single gas having a certain initial distribution and subject to certain boundary conditions. In cylindrical coordinates, Fick's law of diffusion gives the equation describing the concentration as a function of time and coordinates:

$$\frac{\partial p}{\partial t} = D \left(\frac{\partial^2 p}{\partial r^2} + \frac{1}{r} \frac{\partial p}{\partial r} \right) \quad (1)$$

From assumptions (1) and (2), t can be replaced by vertical distance, since

$$t = \frac{x}{U_j} \quad (2)$$

and there results

$$\frac{\partial \mathcal{C}}{\partial x} = \frac{D}{U_j} \left(\frac{\partial^2 \mathcal{C}}{\partial r^2} + \frac{1}{r} \frac{\partial \mathcal{C}}{\partial r} \right) \quad \frac{\partial p}{\partial x} = \frac{D}{U_j} \left(\frac{\partial^2 p}{\partial r^2} + \frac{1}{r} \frac{\partial p}{\partial r} \right) \quad (3)$$

which now contains the height and radius. The boundary conditions can be stated on the basis of the burner port at $x=0$. At this point,

$x=0$	$p = p_f$	$0 \leq r \leq r_j - \mathcal{F}_{1/2}$
	$p = \frac{p_{\text{O}_2}}{i}$	$r_j + \mathcal{F}_{1/2} \leq r \leq r_s$

(4)

The half-thickness of the port $\mathcal{T}_{3/2}$ is assumed negligibly small. Also,

$$\frac{\partial p}{\partial r} = 0 \begin{cases} r=0 \\ r=r_s \end{cases} \quad (5)$$

The solution of equation (3) with the boundary conditions (4) and (5) is

$$p = P \frac{r_j^2}{r_s^2} - \frac{p_{O_2}}{i} + \frac{2r_j P}{r_s^2} \sum \frac{1}{k} \frac{J_1(kr_j) J_0(kr_s)}{[J_0(kr_s)]^2} e^{-\frac{Dk^2 x}{U_i}} \quad (6)$$

where

k constant that assumes all positive roots of the equation $J_1(kr_s) = 0$
 $P = p_f + (p_{O_2}/i)$

For further discussion of the solution of equation (3), see reference 8. General methods of solution of equations of this type are discussed in reference 9.

The equation for the flame front is obtained by setting $p=0$ at $r=r_F$, so that equation (6) becomes at the flame front

$$\sum \frac{l}{k} \frac{J_1(kr_j) J_0(kr_F)}{[J_0(kr_s)]^2} e^{-\frac{Dk^2 x}{U_i}} = \frac{r_s^2 p_{O_2}}{2r_s i P} - \frac{r_j}{2} \quad (7)$$

The shape of the flame front can be obtained by plotting the values of r_F and x that satisfy equation (7). The height of the flame b_F is given by the value of x when $r_F=0$ for an overventilated flame and $r_F=r_s$ for an underventilated flame. The results of a typical calculation are illustrated in figure 205 for an overventilated and an underventilated flame for which it was assumed $r_j = \frac{1}{2}$ inch, $r_s = 1$ inch, $D = 0.0763$ square inch per second, and $U_j = 0.610$ inch per second, which correspond to a fuel flow of 1 cubic foot per hour. The calculated shapes agree well with the observed flame shapes. A similar treatment was used (ref. 3) to calculate the flame shape for a flat diffusion flame on a burner resembling that of figure 197(a).

The properties of diffusion flames are also calculated in reference 8, in which the analysis was begun with equation (1) and essentially the same assumptions except assumption (1) were used. The fuel and air velocities were not required to be equal, although it was required that the air velocity be constant over the annulus and the fuel velocity over the inner tube, and that no momentum transfer occur during diffusion (assumption (2)). Solution of the equation of reference 8 gives

$$\sum \frac{l}{k} \frac{J_1(kr_j) J_0(kr_F)}{[J_0(kr_s)]^2} e^{-\frac{Dk^2 x}{U_i}} + \frac{iU_j}{p_{O_2} U_s} e^{-\frac{Dk^2 x}{U_i}} = \frac{r_s^2 - r_j^2}{2r_j} - \frac{iU_j}{p_{O_2} U_s} \frac{r_j}{2} \quad (8)$$

Comparison of equations (7) and (8) shows the similarity. The principal difference is the addition of two terms containing the ratio U_j/U_s , which was assumed equal to 1 by Burke and Schumann.

The analysis was also begun with equation (1) in reference

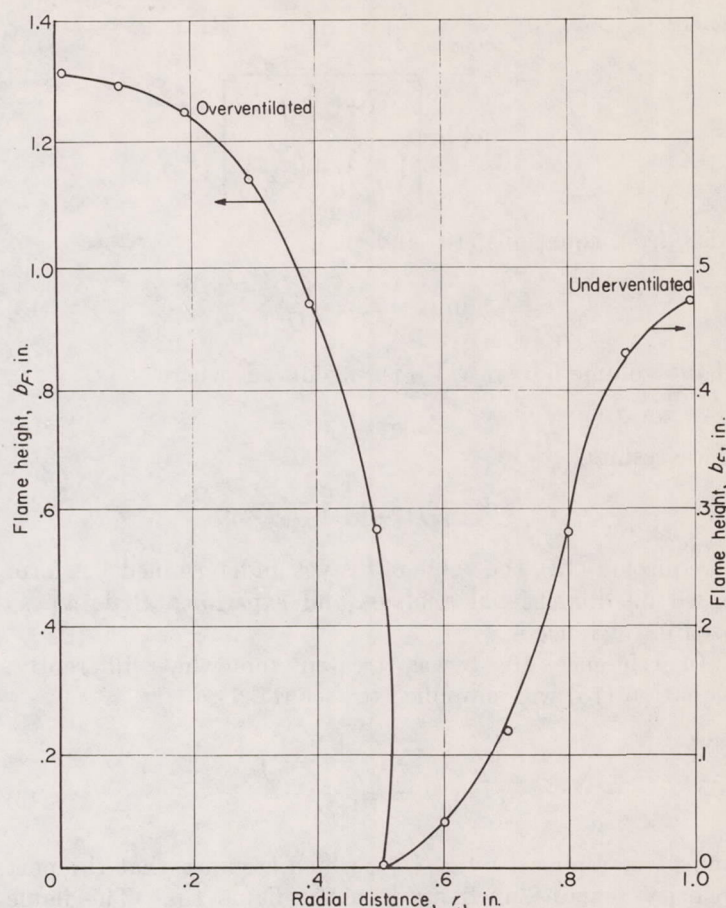


FIGURE 205.—Calculated flame shape using equation (6) for underventilated and overventilated flame (by permission from ref. 3).

4, in which the characteristics of the flame burning on a jet of fuel discharging into still air were computed. Essentially the same assumptions as those of reference 3 were used, except assumptions (1) and (2), which no longer apply. Unlike the assumption of reference 3, in which the oxygen is considered negative fuel, the analogous position that fuel is negative oxygen is taken in reference 4. The oxygen-concentration curve would then follow the dashed line in figure 202 on the fuel side of the flame front, where the fuel concentration is replaced by $-ip_f$. The oxygen partial pressure varies in an air flame from 0.21 to $-ip_f$. The solution of reference 4 was obtained in terms of a generalized dimensionless concentration \mathcal{C}_m , defined as

$$\mathcal{C}_{m,F} = \frac{1 + \left(\frac{\mathcal{C}_a}{\mathcal{C}_f}\right)_j}{1 + \left(\frac{\mathcal{C}_a}{\mathcal{C}_f}\right)_{st}} \quad (9)$$

and a dimensionless time parameter Ξ defined by the equation

$$\Xi = \frac{4Dt}{8r_j^2} \quad (10)$$

The solution of equation (7) is (ref. 4)

$$\mathcal{C}_{m,F} = 1 - e^{-\frac{1}{4\Xi r}} \quad (11)$$

where

$$\Xi_F = \frac{1}{4 \ln \left[\frac{1 + \left(\frac{\mathcal{C}_a}{\mathcal{C}_f} \right)_{st}}{\left(\frac{\mathcal{C}_a}{\mathcal{C}_f} \right)_{st} + \left(\frac{\mathcal{C}_a}{\mathcal{C}_f} \right)_j} \right]} \quad (12)$$

Also, from equations (10) and (11),

$$\ln(1 - \mathcal{C}_m) = \frac{r_j^2}{2Dt} \quad (13)$$

If the volume flow rate V_{fi} is introduced, where

$$V_{fi} = \pi U_j r_j^2 \quad (14)$$

there results

$$U_j t = \frac{V_{fi}}{4\pi D [-\ln(1 - \mathcal{C}_{m,F})]} \quad (15)$$

In equation (15), the value of t is yet undetermined. A form based on dimensional analysis and experimental data was used in reference 4.

In reference 10, t was treated somewhat differently. Equation (15) was simplified to (see ref. 1)

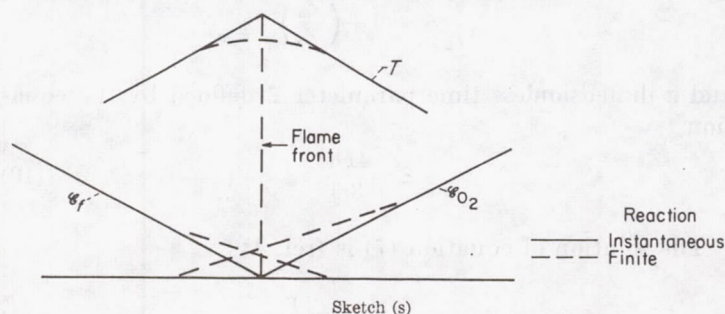
$$U_j t \approx \frac{V_{fi} \left(\frac{1}{\mathcal{C}_{m,F}} - \frac{1}{2} \right)}{4\pi D} \quad (16)$$

and t was replaced by $b_F/U_{o,j}$, which assumes that the port velocity remains unchanged to the flame tip. The flame height is then given by

$$b_{F,L} = \frac{V_{fi} \left(\frac{1}{\mathcal{C}_{m,F}} - \frac{1}{2} \right)}{4\pi D} = \frac{V_{fi} \Xi_F}{\pi D} \quad (17)$$

which is in agreement with the result of reference 3.

While the laminar diffusion flame theories discussed in the previous paragraphs consider the general characteristics of the flame, they do not consider the detailed phenomena occurring in the flame region. These theories consider the flame as a discontinuity, while in the actual case the flame has a thickness that depends on the relative rates of chemical reaction and mixing. The details of flame structure are considered in reference 11, in which an Arrhenius type of reaction-rate expression is used. At remote points from the reaction zone, the curves of concentration and temperature are not appreciably altered, but the sharp break assumed by the earlier theories at the instantaneous reaction zone becomes a rounded curve for a finite reaction time:



Under the usual condition of burning in a laminar diffusion flame, the simplified flame diagram used by Burke and Schumann and others is adequate. If the flow conditions are altered so that the flame zone becomes thin compared with its length, the diffusion processes may be sufficiently rapid that the chemical reaction rate becomes important, and the more complicated treatment of reference 11 is necessary. Such may well be the case near the extinction limits. Equation (8) may be used for calculating the dimensions and concentration gradients in a diffusion flame, while the simpler equation (17) is useful for estimating relative flame heights.

Turbulent flames.—The theoretical treatment of turbulent diffusion flames is less advanced than that of laminar diffusion flames because of the much more complicated mixing process involved. There have been essentially two approaches to the problem: The first uses the laminar diffusion flame equations but replaces the molecular diffusion coefficient by an eddy diffusivity, and the second uses equations based on the mixing of turbulent jets and derives a new set of equations. Since the first treatment follows directly from the previous discussions, it is discussed first.

The eddy diffusivity ϵ that will replace the molecular diffusion coefficient is given by

$$\epsilon = \mathcal{L}_{La} \sqrt{u_x^2} \quad (18)$$

For fully developed turbulent flow inside the burner tube, \mathcal{L}_{La} is proportional to the tube diameter, and the intensity of turbulence is approximately proportional to the mean flow velocity at the axis, so that

$$\epsilon \propto U_o r_j \quad (19)$$

can now be inserted into equation (17), for example, to give

$$b_{F,T} = \frac{V_{fi} \Xi_F}{\pi \epsilon} \propto \frac{V_{fi} \Xi_F}{\pi U_j r_j} \quad (20)$$

Substituting V_{fi} from equation (14), there results

$$\frac{b_{F,T}}{r_j} \propto \Xi_F \quad (21)$$

which indicates that $b_{F,T}/r_j$ is nearly constant in the turbulent region. A similar result is shown in reference 12 for flat flames (fig. 197(a)).

In reference 7, the diffusion flame is described by use of the cold-jet mixing process. The details of this mixing process are discussed in chapter II. In this section, only the application of turbulent mixing to diffusion flames is considered. Therefore, only the distance required to produce a stoichiometric mixture is of concern here, for, as in the laminar flame, this equiconcentration surface is considered to be the flame front. For simple turbulent mixing, the axial distance at which a given concentration is reached (e. g., stoichiometric) is found to depend only on diameter and not on velocity. Thus, $b_{F,T}/r_j$ would be a constant, in agreement with the results obtained previously. A consideration of the actual mixing process

in the presence of buoyancy due to density differences and in the presence of chemical reaction is quite complex. The problem is treated in reference 7, in which the following equation is obtained:

$$\frac{b_{F,T}}{r_j} = \frac{10.6}{\tau} \sqrt{\frac{T_F}{\alpha T_j} \left[\tau + (1-\tau) \frac{M_s}{M_j} \right]} \quad (22)$$

where

$$\tau = \left[\frac{(\mathcal{C}_f + \mathcal{C}_a)_j}{(\mathcal{C}_f + \mathcal{C}_a)_j + \mathcal{C}_{a,s}} \right]_{st}$$

and

$$\alpha = \left[\frac{(\mathcal{C}_f + \mathcal{C}_a)_j + \mathcal{C}_{a,s}}{\mathcal{C}_p} \right]_{st}$$

As with the previous treatments, the ratio $b_{F,T}/r_j$ depends only on the stoichiometry and thermodynamics of the system and is independent of velocity and diameter. Although obtained by a less rigorous treatment than the equations for laminar diffusion flames, equation (22) reflects the same type of controlling process and is one of the most readily used equations for predicting the relative flame heights of turbulent gaseous diffusion flames.

EFFECT OF VARIABLES ON FLAME HEIGHT

Laminar flames.—Within the region designated normal flames (zones 1 and 2 of fig. 198), the flame height varies with changes in fuel flow. For a given fuel flow, the shorter flame indicates a greater burning rate per unit volume of space than the higher flame, so that flame height is often used in diffusion flames as a measure of burning rate. A study was made of the effect of various factors that can influence the flame height of diffusion flames containing some premixed primary air (ref. 13). The apparatus was essentially that of figure 197(c), except that the secondary air was supplied by natural rather than forced convection. The effects of port velocity, port diameter, and ratio of primary air to gas on the flame height were investigated. While a discussion of the addition of primary air overlaps previous discussions (chs. IV and V), it should be recalled that even so-called premixed flames with primary gases richer in fuel than stoichiometric have an outer flame zone that is a diffusion flame. Reference 13 found that flame height increased with increasing port diameter and primary gas velocity; the results for Cambridge city gas are represented by the equation

$$b_{F,L} = K_1 \log U_j + K_2 \log r_j + K_3 \quad (23)$$

where K_1 , K_2 , and K_3 are constants that depend on the ratio of primary air to gas. The quantity of secondary gas supplied to the flame had little effect on the flame height, provided there was sufficient secondary air for combustion of 75 percent of the fuel (ref. 13).

The results of Gaunce quoted in reference 4 for Cambridge city-gas flames with no primary air, burning on a 0.125-inch port, are shown in figure 206. Reference 4 found that the data of reference 13, the laminar portion of the data of Gaunce for Cambridge city gas, and the data of reference 4 for carbon monoxide could be empirically correlated,

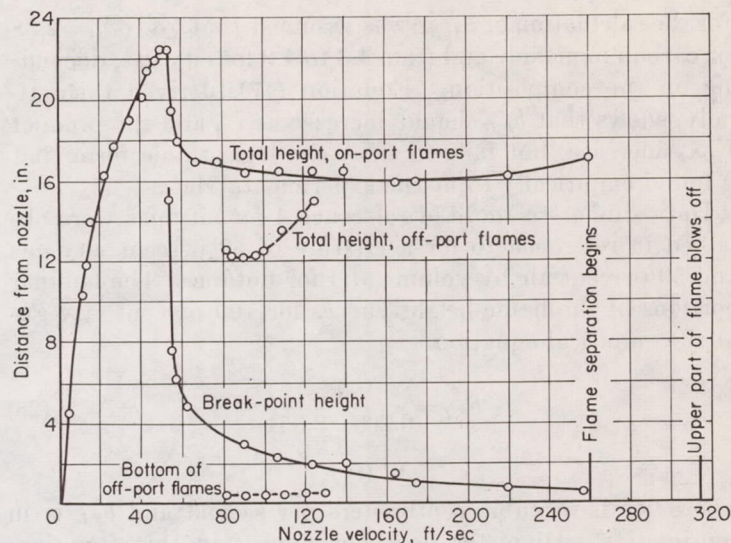


FIGURE 206.—Effect of nozzle velocity on flame height of city-gas flames. Molecular weight, 19.7; no primary air; air requirement, approximately 4.5; nozzle diameter, $\frac{1}{8}$ inch (ref. 4).

using only two empirical constants depending on fuel type and air-gas ratio. The equation is

$$b_{F,L} = K_1 \log V_{fL} \mathcal{E}_f + K_2 \quad (24)$$

The values of K_1 and K_2 used are given in the following table, and the effectiveness of the correlation is shown in figure 207, where straight lines are obtained when $\log V_{fL} \mathcal{E}_f$ is plotted against flame height:

Fuel	$\mathcal{C}_a/\mathcal{C}_f$	K_1	K_2
City gas	0	1.39	5.09
City gas	1.29	1.87	5.93
CO	0	1.39	4.91

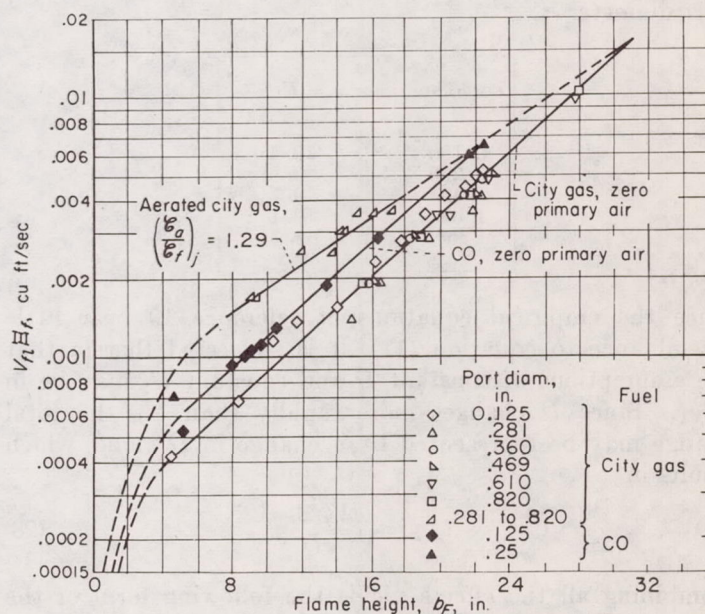


FIGURE 207 — Correlation of data on height of diffusion flames (ref. 4).

For the calculation of Ξ_f , it was assumed that $(\mathcal{C}_a/\mathcal{C}_f)_{st}=2.38$ for carbon monoxide and from 4.3 to 4.8 for city gas, depending on the composition. Equation (17), derived theoretically, shows that $b_{F,L}$ should increase as U_j and the product $V_{fL}\Xi_F$ increase, but fails to show the logarithmic form that is found empirically to fit the experimental data.

Data similar to those of reference 4 for city gas were obtained in reference 10 for a mixture of 50 percent city gas and 50 percent air by volume and for butane. The laminar portions of the flame-height curves for 100 percent city gas fit the empirical equation

$$b_{F,L} = \frac{1}{\frac{0.206}{\sqrt{V_{fL}}} + \frac{0.354}{V_{fL}}} \quad (25)$$

where V_{fL} is in cubic centimeters per second and $b_{F,L}$ is in centimeters. Diameter does not appear in this equation, since flame height was independent of port diameter at the low flows necessary for laminar flow. Actually, the experimental curves do show a slight effect of tube diameter. A larger diameter effect is found when a mixture of 50 percent city gas and 50 percent air is used. These data fit the empirical equation

$$\frac{b_{F,L}}{r_j} = \frac{2}{\frac{0.275}{\sqrt{U_j}} + \frac{2.47}{U_j}} \quad (26)$$

where U is in centimeters per second. It was found (ref. 10) that 100 percent butane and butane-primary-air flames follow a very simple relation with flow rate for tubes:

$$b_{F,L} = \frac{K_1}{\sqrt{V_{fL}X_f}} \quad (27)$$

where X_f is the mole fraction of fuel in the jet. The data are shown in figure 208 for a 0.4-inch-diameter port. The empirical coefficient decreases slightly for large changes in port diameter:

Port diam., in.	K_1
0.180	10.4
.290	9.9
.40	9.7
1.03	9.1
1.99	8.3

Since the empirical equations of reference 10 bear little resemblance to equation (17), it is suggested therein that the assumptions of constant D and constant U_j may be in error. Since D changes more rapidly than U_j , the total change may be represented by a change in D alone, which results in

$$b_{F,L} \approx \sqrt{\frac{V_{fL}\Xi_F}{\pi D}} \quad (28)$$

Combining all the effects yields the following form of the theoretical equation:

$$b_{F,L} = \frac{1}{\sqrt{\frac{1}{2} \frac{\pi k}{V_{fL}\Xi_F} + \frac{1}{2} \frac{\pi D}{V_{fL}\Xi_F}}} \quad (29)$$

which has the same form as equation (25). In general, the measurements and correlations that have been presented were determined for flames that ranged initially from 4 to 6 inches up to about 25 inches.

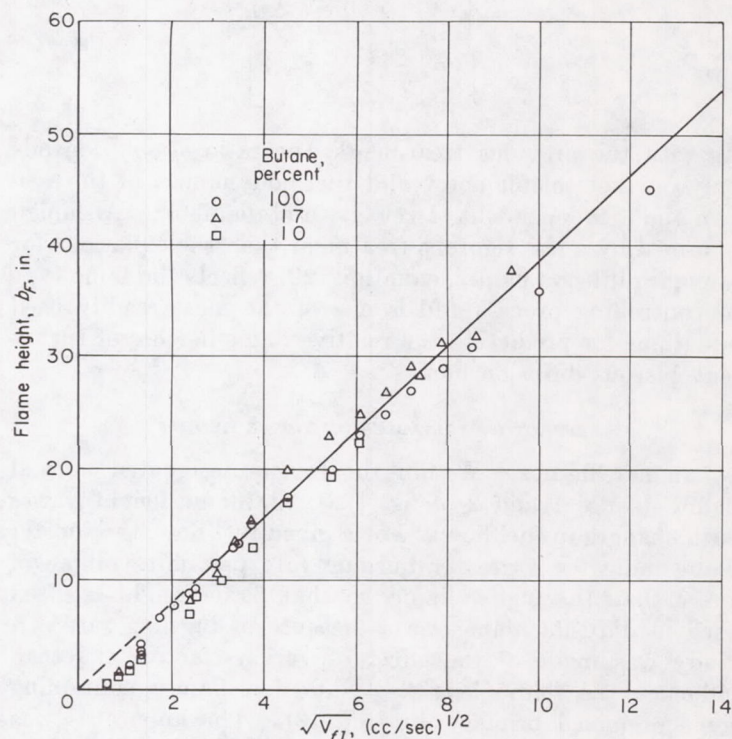


FIGURE 208.—Heights of butane-air flames in free air. Burner-tube inside diameter, 0.4 inch (ref. 10). Reynolds number, 2300.

Reference 8 presents some measurements of flames from 0.2 to about 1.5 inches in length. The effect of fuel velocity on flame height is shown in figure 209(a). In the region of low fuel velocities the flame heights are independent of the air velocity, in agreement with the data of reference 13; but at higher fuel velocities the points for the lower air flows of 0.9 and 1.74 inches per second rise above the other data. The lines in the figure were calculated from equation (8), and reasonably good agreement is obtained for the higher air velocities. The proper trend in flame height is predicted for the airflows of 0.9 and 1.74 inches per second, but the theory predicts a greater separation of the 3.45- and 5.13-inch-per-second data than was found experimentally. Equation (8) contains the parameters $b_{F,L}/U_j$ and U_j/U_s , which suggests that these quantities may be useful in correlating the experimental data. The first of these has the dimension of time, while the second is proportional to the fuel-air ratio. A plot of $b_{F,L}/U_j$ against fuel-air ratio is shown in figure 209(b) along with the line obtained theoretically from equation (8). Reasonably good correlation and agreement with theory are obtained.

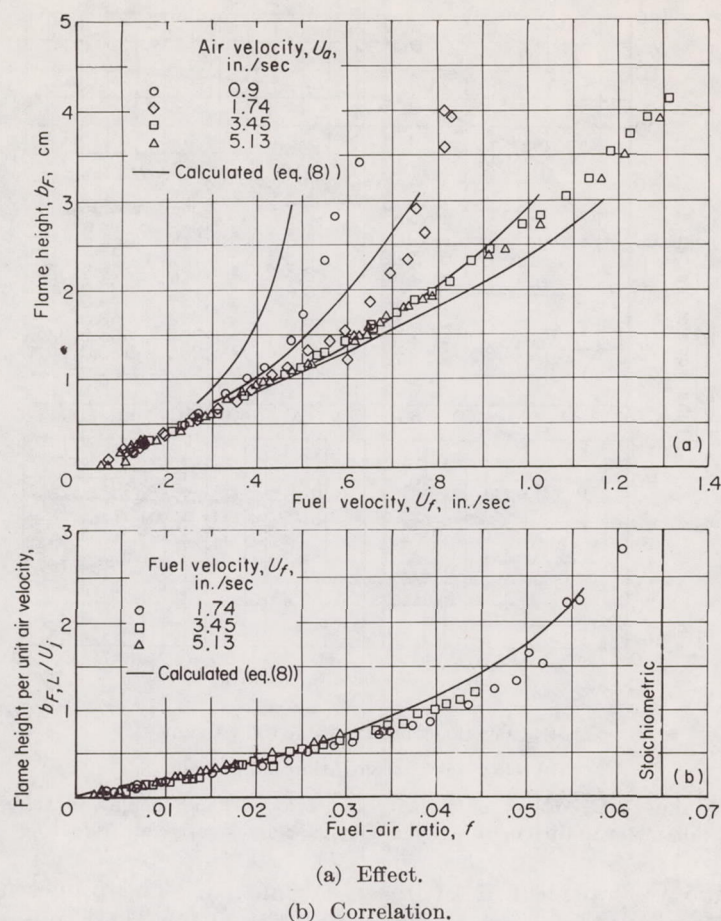


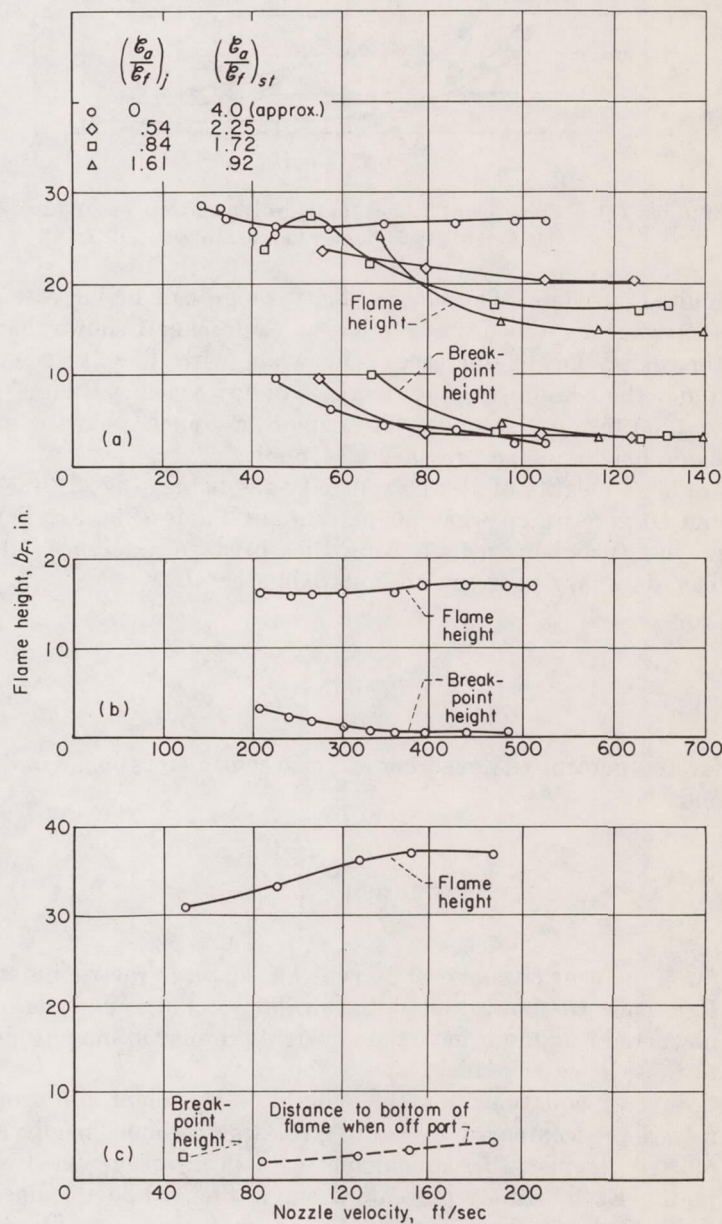
FIGURE 209.—Effect of fuel and air velocity on flame height (ref. 8).

The change in flame height with flow velocity and tube diameter represents the principal studies on laminar diffusion flames. Only a little work has been done on the effect of pressure on flame height. It was found in reference 8 that pressure changes of 10 to 1 atmospheres had practically no effect on flame height. The theory (eq. (8)) predicts that flame height should be independent of pressure. Reference 3 also found flame height to be insensitive to temperature and pressure. Theoretically, this independence of flame height results from the fact that pressure and temperature affect the flow velocity and diffusion coefficient in opposite directions, thus canceling their effects.

The rather simple form of equation (24) and its success in correlating the data for different systems make it appear the most useful for calculating laminar flame heights where the empirical constants are known. The difficulty of applying the theoretical equations and the uncertainty of some of the assumptions limit their use in predicting absolute flame heights.

Turbulent flames.—Figure 206 shows that, at certain critical flows, the tip of the flame becomes turbulent and the turbulent portion increases with increasing flow rate. The break points of city gas, hydrogen, and propane flames were measured in reference 7. The total flame heights, which are relatively constant, were also measured and are shown along with the break points in figure 210. It is evident that both the total flame heights and break-point heights are relatively

insensitive to flow rate in the fully developed turbulent flame, which agrees with equation (22). The break points for two gases of differing diffusion coefficients are shown in figure 211, where the ratio of break-point height to port diameter is plotted against the product of diffusion coefficient and flow velocity. Again, there is a drop in break-point height with flow velocity until a critical velocity occurs, after which there is little change. Break points for unignited and ignited ethene systems were studied in reference 14, which revealed that the break point was higher for the



(a) City gas; molecular weight, 16.2; 1/4-inch nozzle.
 (b) Hydrogen; molecular weight, 2; 1/8-inch nozzle; $(C_a/C_f)_i$, 0; $(C_a/C_f)_{st}$, 2.38.
 (c) Propane; molecular weight, 43.2; 1/8-inch nozzle; $(C_a/C_f)_i$, 0; $(C_a/C_f)_{st}$, 2.38.

FIGURE 210.—Visible flame-height characteristics. Unconfined flames; rounded nozzles (ref. 7).

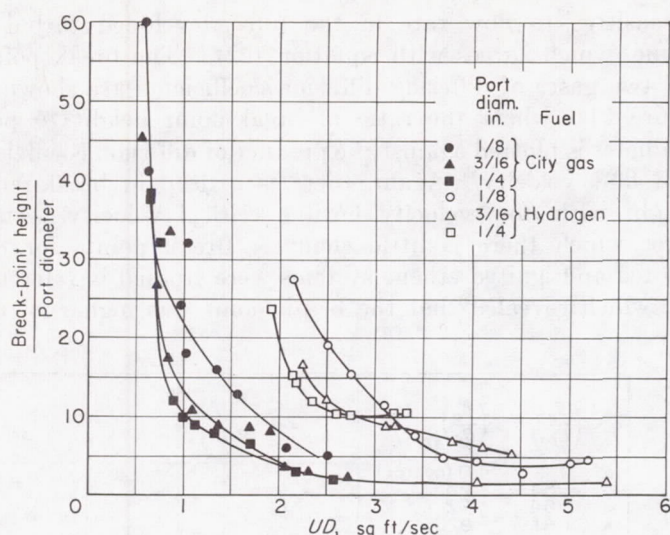


FIGURE 211.—Break-point heights for hydrogen and city gas (molecular weight, 19.7) flames (nonpremixed) (ref. 7).

ignited stream. The flow-velocity range can be increased somewhat by the use of a pilot, and reference 1 shows that the flame height increases somewhat with flow velocity under these conditions; an increase of flow velocity from 200 to 1200 feet per second causes about a 5-inch increase in flame height in the presence of a pilot.

Flame heights of 100 percent city-gas flames (fig. 212(a)) and 50 percent city gas–50 percent air flames (fig. 212(b)) in the turbulent regime were measured in reference 10. The data are represented approximately by

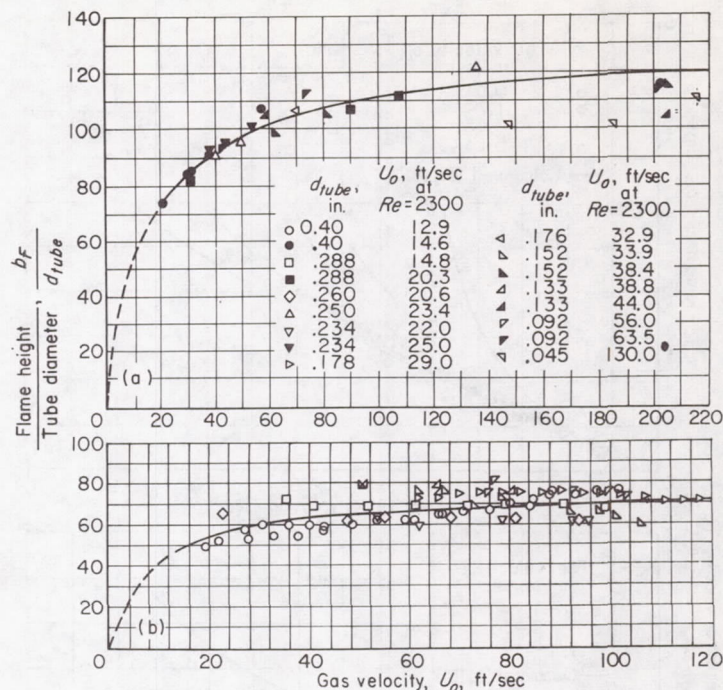
$$\frac{b_{F,T}}{r_j} = \frac{2}{0.00775 + \frac{3.80}{U_o}} \quad (30)$$

for 100 percent city gas where U_o is in centimeters per second; and

$$\frac{b_{F,T}}{r_j} = \frac{2}{0.0132 + \frac{3.23}{U_o}} \quad (31)$$

for 50 percent city gas–50 percent air, again in metric units. Reference 15 shows that diffusion flames containing jets of powdered coal in air have flame heights similar in magnitude to those of gaseous fuels.

Several equations for the length of turbulent diffusion flames are compared in figure 213, where flame height is plotted against the stoichiometric concentration for five fuels. Each point represents a single fuel, while the lines are calculated from the equations shown in the figure. Wohl's equation is shown as a dashed line; a curve derived in reference 15 in which $x \propto \log \tau$ is shown as a dot-dash line; and the equation of reference 1 is represented as a family of solid lines for various molecular-weight ratios. Black dots on these lines indicate the range of $C_{m,F}$ of interest. It is apparent that, for fuels of widely differing molecular weight, the molecular-weight ratio is necessary, although Wohl's equation can be made to agree with equation (22) to within



(a) City-gas concentration, 100 percent.

(b) City-gas concentration, 50 percent.

FIGURE 212.—Effect of velocity on ratio of flame height to tube diameter in turbulent region of city-gas flames in free air (ref. 10).

about 30 percent if hydrogen is omitted. The proposed function of reference 15 cannot fit different fuel types unless a different empirical constant is used for each fuel.

STABILITY

The diffusion flame, like the premixed flame, has certain regions of stability beyond which burning cannot occur.

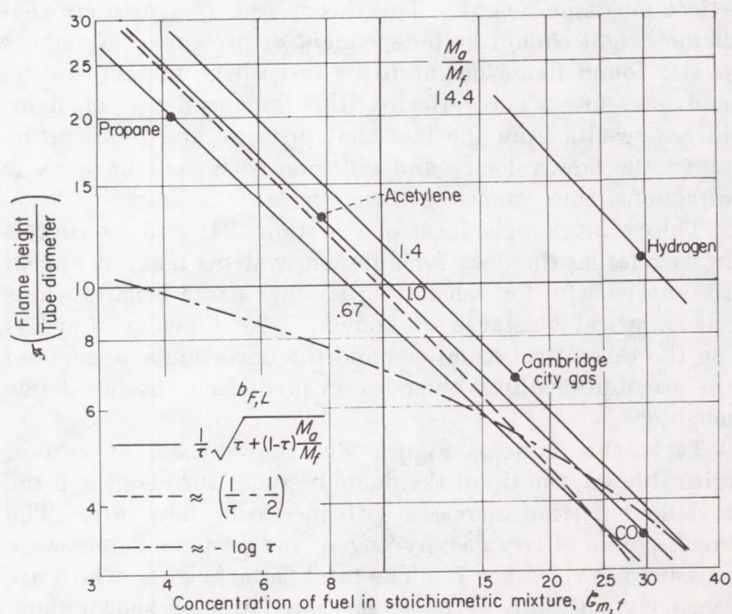


FIGURE 213.—Comparison of calculated curves and experimental data for five fuels (ref. 1).

These have already been indicated in figure 198 by the boundary separating the various flame zones from the extinction region. While the phenomenon of flashback is, of course, not possible for diffusion flames, the extinction curve does not extend to either zero fuel flow or zero airflow. As the fuel flow is decreased, the flame becomes smaller and smaller until the quenching action of the nozzle wall is sufficient to prevent propagation. Thus, a lower boundary is set to the fuel flow. As the fuel flow is increased, the flame length increases. At critical fuel flows, however, the processes of flame lift and blowoff occur entirely analogously to the Bunsen flame. In fact, the blowoff of rich Bunsen flames (see ch. VI) may well depend on the characteristics of the outer-mantle diffusion flame. Some typical data on the lifting and ultimate blowoff of a butane diffusion flame (ref. 2) are illustrated by figure 214. The solid line shows the location of the flame base as the flow velocity is increased and lift occurs. The dashed line, on which typical flames are shown, illustrates the path of the flame bases as the butane flow velocity is reduced and the flame resettles. This type of hysteresis in the lift curves also occurs with premixed gases (see ch. VI). The ultimate point, at a flow velocity of about 300 milliliters per second, corresponds to complete blowoff. The data of reference 2 are for rather short laminar flames, but the phenomenon of lift is illustrated for turbulent flames by the dashed curves of figure 206, which show the location of the bottom of lifted flames and their corresponding total flame height.

The stability range of diffusion flames of ethene issuing from carburetor-type jets into still air is reported in reference 14. The results showing the stability region as a function of jet diameter and Reynolds number may be seen in figure 215. The range of gas flow over which the flame is stable increases only slightly with increasing jet diameter. Above a certain diameter, the range over which the lifted flame persists widens rapidly as the jet size increases, because of

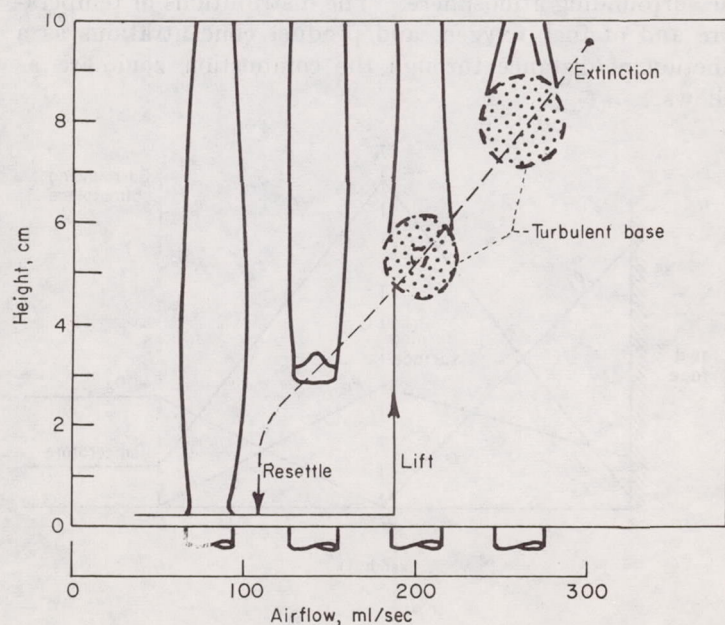


FIGURE 214.—Flame lifting. Butane flow, 10 millimeters per second (ref. 2).

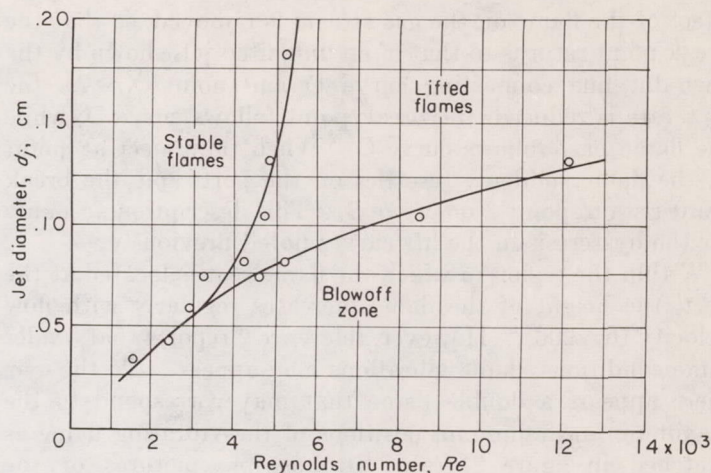


FIGURE 215.—Stability ranges of diffusion flames on carburetor-type jets (ref. 14).

the rapid decrease in blowoff tendency on larger jets. On small jets, the lift and blowoff limits coincide. The phenomenon of lift is explained in reference 14 by a comparison of the break points of ignited and unignited streams and the height of the base of the lifted flame. In figure 216, the height to turbulence or the break point or the height to the base of a lifted flame is plotted against Reynolds number—essentially flow velocity. Curves A and B connect the data for the height to turbulence in the unignited and ignited streams, respectively. Note that the height to turbulence occurs at higher Reynolds numbers for the ignited gas stream. The stabilization was attributed in reference 14 to heat addition from the flame. Curve C represents the height between the top of the burner and the base of the lifted flame. Curve D represents the height to turbulence in the fuel jet of a lifted flame. At a flow rate immediately before lift, the break point in the gas stream lies well within the flame envelope. At the actual lift point, the flame is stabilized by eddies formed at the break point, and the base of the flame is at the same height as the height to turbulence (point X in fig. 216). After the flame has lifted, the heating

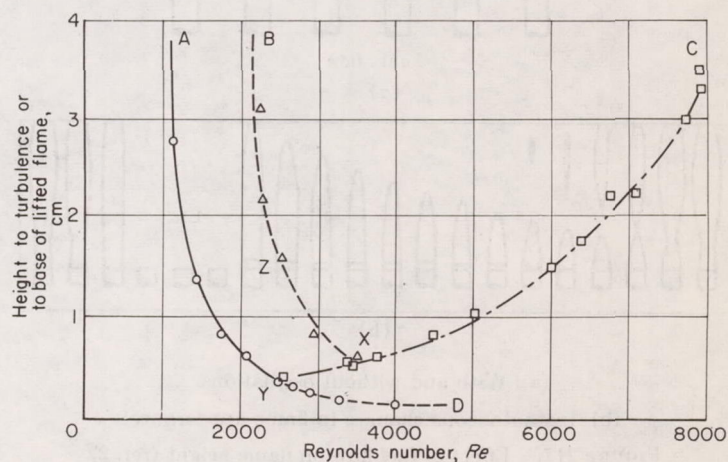


FIGURE 216.—Diffusion-flame stability diagram showing: A, height to turbulence in unignited jet; B, height to turbulence in presence of seated flame; C, height to flame base of lifted flame; and D, height to turbulence in presence of lifted flame (ref. 14).

effect of the flame on the gas stream is removed, so that the break point returns to that of an unignited jet, shown by the dash-dot line connecting curve D and point X. As the flow rate is reduced, the break point follows curve D, while the flame base follows curve C. When they meet at point Y, the flame suddenly resettles on the port, and the break point rises to point Z on curve B. This description accounts for the hysteresis in the lift curves noted previously.

Within the region in which the flame seat is located at the port, the height of the flame increases regularly with flow velocity (fig. 206). However, reference 2 reports that, under some conditions, flame vibrations may appear. To the eye, there appears a double flame that may correspond to the maximum and minimum positions of the vibrating flame as sketched in figure 217(a). Stroboscopic pictures of the

flame (fig. 217(b)) show that the vibration consists of a progressive necking of the flame; this can lead to the formation of an island of flame which, separated from the seated flame, burns itself out. The butane flame vibrations have a frequency of about 8 cps that is relatively independent of the flow. Modifications of the fuel supply system change the vibration frequency so that frequencies from 3 to 20 cps have been measured. Hydrogen gives a frequency of about 200 cps; in a few cases, the butane frequency can be equally high. Similar frequencies were found (ref. 16) for the rate of flicker of diffusion flames; hence, it appears that the phenomena are related. In reference 2, the vibrations are related to the phase lag Δt between the occurrence of maximum fuel flow in the oscillating flow and the appearance of maximum flame height. If the phase lag is small compared with the half-period of the vibration ($\Delta t \ll t_{1/2}$), the flame flickers; if $\Delta t = t_{1/2}$, the flame height rises to a maximum and suddenly drops to its initial value; if $\Delta t > t_{1/2}$, flame necking and ultimate breaking off of islands of flame can occur.

LIQUID DIFFUSION FLAMES

SINGLE-DROP COMBUSTION

When a single drop of liquid fuel burns, it is surrounded by a diffusion flame, as illustrated in figure 218. Fuel is evaporated from the liquid interface and diffuses to the flame front, while oxygen moves from the outside air to the burning surface. The rate at which the drop evaporates and burns is determined by the rate of heat transfer from the flame front to the liquid surface. As in the case of gaseous diffusion flames, chemical processes are assumed to occur so rapidly that burning rates are determined solely by mass- and heat-transfer rates.

Theory.—Flame structure: Spalding (refs. 17 and 18) and Graves (ref. 19) consider a double-film model for combustion of a liquid fuel. One film separates the drop surface from the flame front; a second separates the flame front from the surrounding atmosphere. The distributions of temperature and of fuel, oxygen, and product concentrations as a function of distance through the combustion zone are as follows:

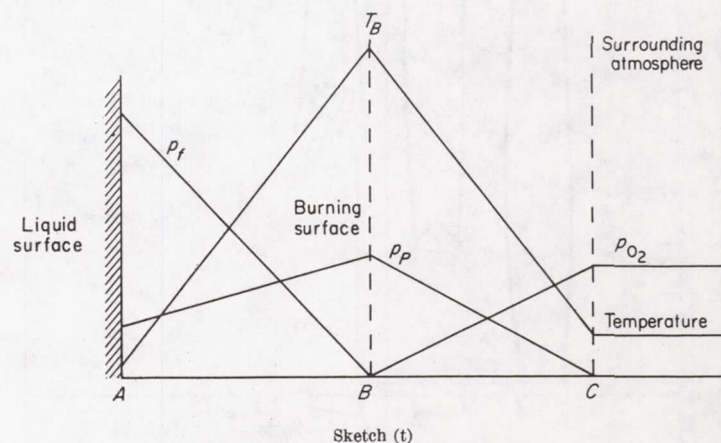


FIGURE 217.—Effect of fuel flow on flame height (ref. 2).

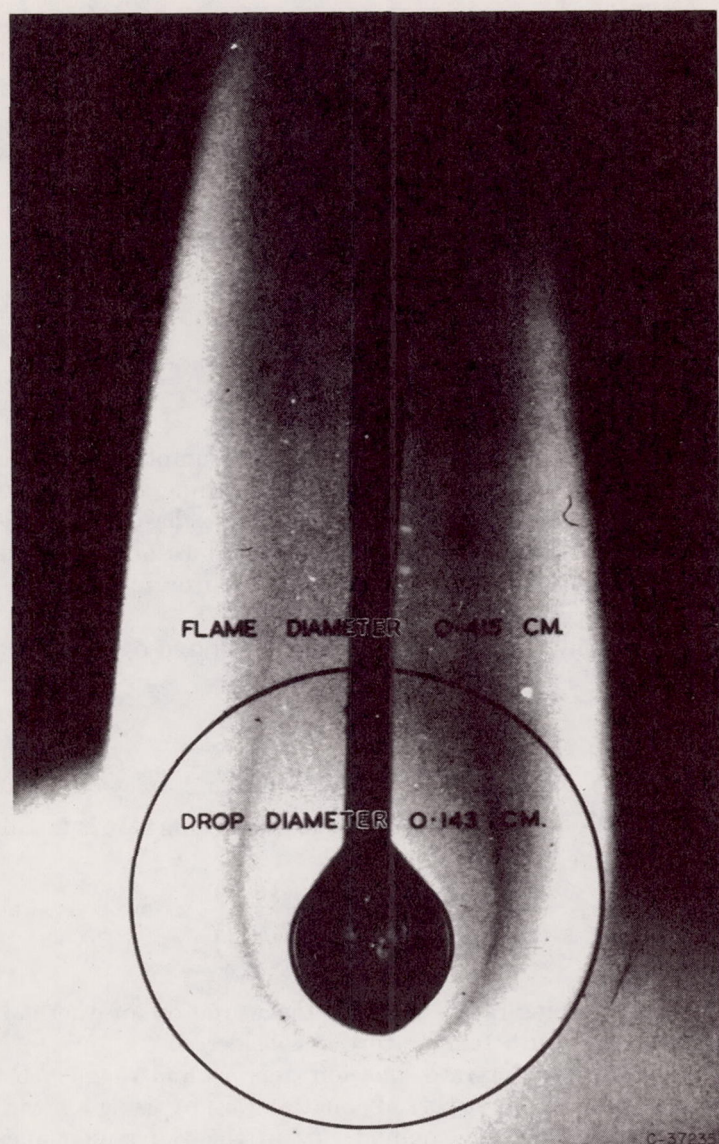


FIGURE 218.—Burning benzene drop (ref. 29).

In steady-state combustion, the liquid surface is assumed to be at a temperature a few degrees below the normal boiling point of the fuel, as surveys of the temperature fields in burning liquids indicate (ref. 20). In the *AB* region, fuel evaporates at the drop surface and diffuses to the flame front, where it is consumed. Heat conducted from the flame front serves to vaporize the fuel and heat it to the burning temperature T_B . (It is assumed that there is no chemical reaction of the fuel before it reaches the flame front.) In the *BC* region, oxygen diffuses to the flame front, and combustion products and heat are transported to the surrounding atmosphere. The position of the *C* surface is determined by convection (natural or forced).

Burning temperature: By equating fuel flow to oxygen diffusion and heat conduction in the *BC* region, the burning

temperature may be determined. For oxygen diffusion, with the fuel and oxygen flowing in opposite directions,

$$G_f = \frac{w_f}{4\pi y^2} = -\frac{w_{O_2}}{4\pi y^2 W_{st}} = \frac{DP}{W_{st} RT} \frac{M_{O_2}}{P + \left(\frac{X_P}{X_{O_2}} - 1\right) p_{O_2}} \frac{dp_{O_2}}{dy} \quad (32)$$

where

W_{st} weight of oxygen consumed in combustion of unit weight of fuel (stoichiometric relation)
 X_P/X_{O_2} number of moles of products formed per mole of oxygen consumed

The term $(X_P/X_{O_2} - 1)$ takes some account of the fact that there will be a net gas motion if $X_P/X_{O_2} \neq 1$. The expression is applicable to the steady-state diffusion of both components of a binary mixture (ref. 21) and neglects the presence of a stagnant inert gas. For heat flow in region *BC*,

$$\frac{w_f}{4\pi y^2} [h_c - (h_P - h_{P,C}) + (h_{O_2} - h_{O_2,C})] = -\kappa_{BC} \frac{dT}{dy} \quad (33)$$

where

h_c specific lower heat of combustion of liquid fuel at temperature of surrounding atmosphere
 h_P specific enthalpy of products referred to unit quantity of fuel
 h_{O_2} specific enthalpy of oxygen referred to unit quantity of fuel

The term in the brackets is the heat that must be transported to the point *y* in the combustion of unit quantity of fuel. Eliminating the fuel flow from equations (32) and (33) and integrating give

$$\begin{aligned} \frac{\kappa_{BC} W_{st}}{D \rho_{O_2}} \int_{T_C}^{T_B} \frac{dT}{h_c - (h_P - h_{P,C}) + (h_{O_2} - h_{O_2,C})} \\ = \frac{1}{\frac{X_P}{X_{O_2}} - 1} \ln \left[1 + \frac{p_{O_2,C}}{P} \left(\frac{X_P}{X_{O_2}} - 1 \right) \right] \cong \frac{p_{O_2,C}}{P} \quad (34) \end{aligned}$$

if $p_{O_2,C}$ is small and $X_P/X_{O_2} \approx 1$. The factor $\kappa_{BC} W_{st}/D \rho_{O_2}$ is considered independent of temperature.

Integrating the left side of equation (34) by introducing mean specific heat c_p for products and oxygen results in

$$\begin{aligned} \frac{\kappa_{BC} W_{st}}{D \rho_{O_2} (c_{p,P} - c_{p,O_2})} \ln \left[1 - \frac{(c_{p,P} - c_{p,O_2})(T_B - T_C)}{h_c} \right] \\ \cong \frac{\kappa_{BC} W_{st}}{D \rho_{O_2}} \frac{T_B - T_C}{h_c} \cong \frac{p_{O_2,C}}{P} \end{aligned}$$

or

$$T_B - T_C \cong \frac{D \rho_{O_2}}{\kappa_{BC}} \frac{h_c}{W_{st}} \frac{p_{O_2,C}}{P} \quad (34a)$$

Unfortunately, the error introduced by expansion of the logarithm is in the opposite direction from the expansion of equation (34), and predicted burning temperatures are too high. Nonetheless, equation (34a) is useful for showing qualitatively the factors that influence the burning temperatures.

Equation (34) permits a more reliable calculation of the burning temperature. It has been used (ref. 18) to obtain burning temperatures for kerosene drops in atmospheres of varying temperature and oxygen concentration, with carbon dioxide and water assumed to be the sole combustion products. Preferential diffusion of water with respect to carbon dioxide was also neglected. The calculations of reference 19 for isooctane burning in atmospheres of various oxygen concentrations neglected preferential product diffusion and employed the simplified form of equation (34) valid for low oxygen partial pressure or $X_P/X_{O_2} \approx 1$; however, equilibrium dissociation of products was taken into consideration. In figure 219, burning temperatures of references 18 and 19 are compared for similar conditions. Burning temperatures for isooctane calculated from equation (34a) are

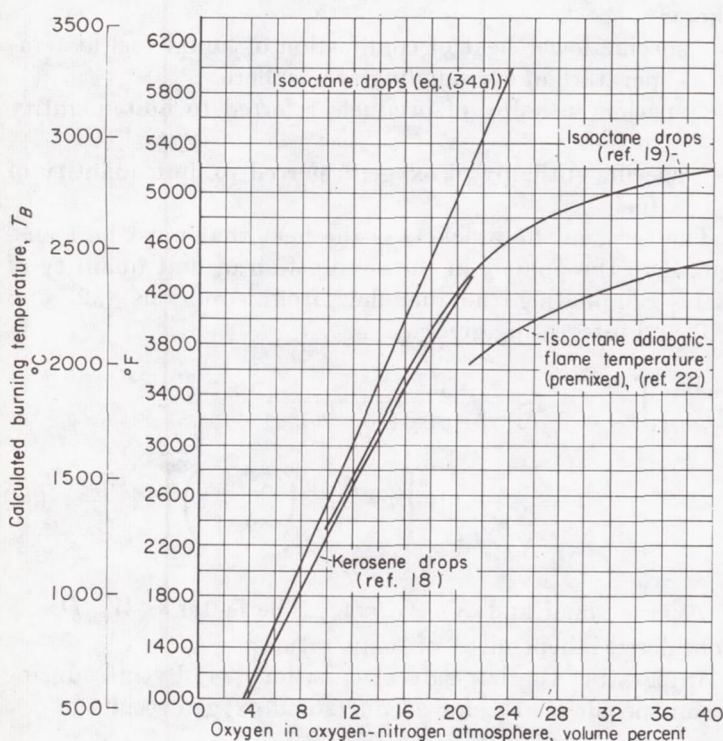


FIGURE 219.—Calculated burning temperatures. Initial temperature, 77° F.

also shown. It is to be noted that these temperatures are higher than the adiabatic flame temperatures for corresponding isooctane vapor-oxygen-nitrogen mixtures (ref. 22). Drop burning temperatures may be greater because there is no net flow of inert gas (nitrogen) through the burning zone and because the oxygen is preheated to the combustion temperature by the hot reaction products. The fact that the reaction zone must have a finite thickness will give rise to lower burning temperatures than those calculated from equation (34).

Burning rate: For the AB region, heat and fuel flow may

be equated analogously to equation (33) (directions of fuel and heat flow are opposite):

$$\frac{w_f}{4\pi y^2} = \frac{\kappa_{AB}}{h_v + h_i + h_f - h_{f,A}} \frac{dT}{dy} \quad (35)$$

where

h_i heat necessary to raise unit mass of fuel to vaporization temperature

h_f specific enthalpy of fuel vapor

Integrating over the AB region gives

$$\frac{w_f}{4\pi} \left(\frac{1}{y_A} - \frac{1}{y_B} \right) = \int_{T_A}^{T_B} \frac{\kappa_{AB} dT}{h_v + h_i + h_f - h_{f,A}} = A \quad (36)$$

The term h_i is included because of the assumption that the bulk of the drop remains at the initial temperature during combustion. If the entire drop rapidly reaches the surface temperature during the first stages of combustion, h_i should be omitted. The factors determining the drop interior temperature are discussed in reference 23.

If equation (33) is rearranged and integrated over the BC region,

$$\frac{w_f}{4\pi} \left(\frac{1}{y_B} - \frac{1}{y_C} \right) = \int_{T_C}^{T_B} \frac{\kappa_{BC} dT}{h_c - (h_P - h_{P,C}) + (h_{O_2} - h_{O_2,C})} = B \quad (37)$$

From equations (36) and (37), the mass burning rate is found to be

$$w_f = \frac{4\pi A}{\left(\frac{1}{y_A} - \frac{1}{y_B} \right)} = \frac{4\pi(A+B)}{\left(\frac{1}{y_A} - \frac{1}{y_C} \right)} \quad (38)$$

In the burning-rate equation, the variation of thermal conductivities with temperature is considered.

Godsave's burning-rate equation (refs. 24 and 25) may be obtained from the first part of equation (38) by using a mean value for the thermal conductivity in the AB region and letting $h_f - h_{f,A} = c_{p,f}(T - T_A)$:

$$w_f = \frac{4\pi A}{\left(\frac{1}{y_A} - \frac{1}{y_B} \right)} = \frac{4\pi \kappa_{AB}}{c_{p,f}} \ln \frac{1 + \frac{c_{p,f}(T_B - T_A)}{h_i + h_v}}{\left(\frac{1}{y_A} - \frac{1}{y_B} \right)} \quad (38a)$$

For a liquid sphere, the relation

$$\frac{dm}{dt} = -w_f = 4\pi \rho_l y_A^2 \frac{dy_A}{dt} \quad (39)$$

gives the mass burning rate in terms of the change of radius with time.

Experimentally (refs. 19 and 25 to 28), mass burning rates of single fuel drops are found to be proportional to the drop radius. Variation of drop diameter with time is given by

$$d_{dr}^2 = d_{dr,0}^2 - \mathcal{K}t \quad (40)$$

where $d_{dr,0}$ is the initial drop diameter, $d_{dr} = 2y_A$ is the diameter at any subsequent time, and \mathcal{K} is the evaporation constant. The rate of change of radius with time may be obtained from equation (40):

$$\frac{dy_A}{dt} = -\frac{\mathcal{K}}{8y_A} \quad (41)$$

From equations (38), (39), and (41), it follows that

$$\mathcal{K} = \frac{2w_f}{\pi \rho_i y_A} = \frac{8(A+B)}{\rho_i \left(1 - \frac{y_A}{y_c}\right)} \quad (42)$$

Note that \mathcal{K} will be constant if y_A/y_c is constant or if $y_c = \infty$ (drop burning in the absence of convection). Equation (42) has been successfully used to predict evaporation constants for the combustion of single fuel drops.

Combustion in quiescent air.—Evaporation constants of single drops (initial diam. 1000 to 1500 microns) of various liquid fuels burning in quiescent air have been obtained by Godsave (refs. 25 and 26) with a motion-picture technique. By the same method, Graves (ref. 19) has studied the combustion of isooctane drops in various oxygen-nitrogen atmospheres. Plots of square of drop diameter against time were found to be linear (see eq. (40)). Figure 220 shows a typical plot for isooctane burning in an atmosphere

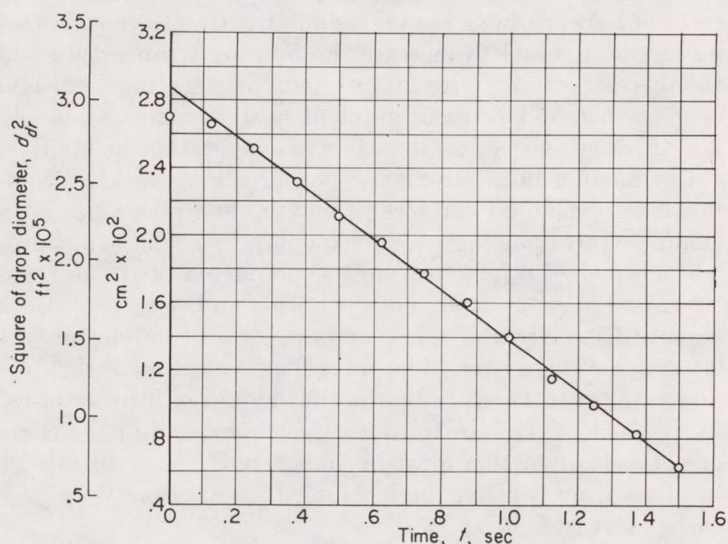


FIGURE 220.—Time variation in diameter for drop of isooctane burning in oxygen-nitrogen atmosphere containing 34.9 percent oxygen (ref. 19).

containing 34.9 percent oxygen. In table XXVII, experimental and calculated (ref. 29) values of evaporation constants for combustion in air determined by Godsave are presented. Although values for jet fuels were not determined, evaporation constants of about 10×10^{-6} square foot per second (similar to kerosene) are to be expected. Evaporation constants from reference 19 for isooctane are presented in table XXVIII.

The combustion of suspended single droplets of decane, tetralin, furfuryl alcohol, and amyl acetate was studied in reference 28, and drop lifetimes were measured at pressures between 1 and 20 atmospheres. Lifetimes were found to be very nearly proportional to the square of the initial drop diameter for a given pressure and fuel, in agreement with equation (40). Evaporation constants were not determined as such, but droplet lifetimes were consistent with evaporation constants of the order of 10×10^{-6} square foot per second (similar to those of tables XXVII and XXVIII). With increasing pressure, volumetric burning rates increased approximately with the fourth root of the pressure.

TABLE XXVII.—EVAPORATION CONSTANTS FOR VARIOUS FUELS BURNING IN AIR

Fuel	Evaporation constant, \mathcal{K} , ft^2/sec		
	Experimental (refs. 25 and 26)	Calculated (ref. 29)	Calculated ^a
Petroleum ether (100° to 120° C)---	10.6×10^{-6}	-----	-----
Kerosene-----	10.3	-----	-----
Diesel fuel-----	8.5	-----	-----
Ethyl alcohol-----	8.7	-----	8.6×10^{-6}
Benzene-----	10.4	10.6×10^{-6}	9.6
Toluene-----	^b 7.1	-----	9.6
Ethylbenzene-----	9.3	-----	9.2
<i>o</i> -Xylene-----	8.5	-----	8.9
<i>p</i> -Xylene-----	8.3	-----	9.1
Isopropylbenzene-----	8.4	-----	8.7
Pseudocumene-----	^c 9.4	-----	8.4
<i>n</i> -Butylbenzene-----	^c 9.3	-----	8.2
<i>tert</i> -Butylbenzene-----	8.3	10.3	8.3
<i>tert</i> -Amylbenzene-----	8.4	-----	7.8
<i>n</i> -Heptane-----	10.4	11.6	10.4
Isooctane-----	10.2	-----	10.1

^aCalculated using equation (38a) and a correction factor of 0.79.

^bExperimental value believed to be too low.

^cExperimental value believed to be too high.

TABLE XXVIII.—EVAPORATION CONSTANTS FOR ISOOCTANE IN VARIOUS OXYGEN-NITROGEN ATMOSPHERES (Ref. 19)

Oxygen in atmosphere, %	Evaporation constant, \mathcal{K} , ft^2/sec
17.0	11.5×10^{-6}
20.9 (air)	12.3
24.9	13.5
34.9	15.4

(The effect on mass burning rates may be somewhat less, since the density of the fuel drop may be lower at higher pressures because of higher drop surface temperatures.) It was observed that at the higher pressures the distance between flame front and drop surface decreased, which might be expected with a higher burning rate (see eq. (38a)). This is probably a result of a decrease in film thickness under natural convection at high pressure, as suggested by reference 30. In contrast, vaporization rates in the absence of combustion decrease when pressure is raised (ref. 31).

In addition, reference 28 reports investigations of the burning of free droplets (150 to 700 microns initial diam.) in air at 1310° F and atmospheric pressure. In these experiments, drops of uniform size produced by feeding liquid fuel onto the center of a rotating disk were projected into a furnace, and droplet lifetimes were recorded by means of a drum camera. In this regime also, lifetimes were found to be proportional to the square of the initial drop diameter; it is not surprising that burning rates were somewhat faster at the higher temperature.

Equation (38a) has been used (ref. 29) to calculate evaporation constants for benzene, *tert*-butylbenzene, and *n*-heptane combustion. The diameter of the burning surface was evaluated from photographs, and allowance was made for

estimated heat transfer by radiation. The assumed burning temperature of 3100° F seems too low; calculations (refs. 18 and 19, see fig. 219) would suggest 4300° F as a more reasonable estimate. Results of Godsave's calculations (ref. 29) are shown in the third column of table XXVII; and, while the agreement may in part be due to fortuitous choice of T_B , $c_{p,f}$, and κ_{AB} , the values are of the correct order of magnitude and suggest that Godsave's equation (38a) is useful for estimating hydrocarbon burning rates. Accordingly, equation (38a) has been used to calculate variations in evaporation constants for the series of compounds investigated by Godsave. Burning temperatures were estimated by employing equation (34a) to convert variations in h_c/W_{st} into equivalent variations in oxygen concentrations; burning temperatures could then be estimated from the isooctane curve of reference 19. Mean heat capacities and thermal conductivities were taken at 2200° F; the latter was taken as the mean of the thermal conductivities of air and the fuel. The position of the burning surface with respect to the drop was taken from Godsave's determinations (ref. 29). (For isooctane and ethyl alcohol, the value of n -heptane was employed, since no measurements were made.)

Evaporation constants so calculated were found to be, on the average, 26 percent higher than experimental values; therefore, they have been reduced by this amount and tabulated in the last column of table XXVII. Reference 26 suggests that, unless otherwise indicated, the experimental evaporation constants are precise to 10 percent; reduced calculated values agree with the reliable values to within this margin. Accuracy of this type of experiment may be poor. Since the isooctane-air value of reference 19 is some 20 percent higher than that of reference 26, the 26-percent correction factor does not prove that the calculations are in error by this amount.

Evaporation constants for isooctane combustion in the absence of convection ($y_c = \infty$) were calculated in reference 19. The transport properties of air were assumed in the BC region, and preferential diffusion among combustion products was neglected. Figure 221 shows three curves calculated with the following assumptions:

- (1) Thermal conductivity of isooctane in region between drop and burning surfaces; dissociation of products (middle curve)
- (2) Thermal conductivity of isooctane; no dissociation (top curve)
- (3) Thermal conductivity of air; no dissociation (bottom curve)

The experimental determinations of reference 19 are also plotted.

It must be noted that these calculations are for no convection. Equations (36) and (37) may be employed to calculate the position of the burning surface with respect to the drop. The result is

$$\frac{y_B}{y_A} = \frac{A+B}{A\left(\frac{y_A}{y_C}\right)+B} \quad (43)$$

For an isooctane drop burning in air in the absence of convection, values of the integrals A and B (ref. 19) predict $y_B/y_A = 18.5$. On the other hand, for n -heptane, the meas-

urement (ref. 29) shows that $y_B/y_A \approx 3$. (Because of convection, the burning surface is highly distorted from a spherical shape; the value of ref. 29 must be regarded as a minimum, see fig. 218.) With the same value assumed for isooctane, $y_A/y_C \approx 0.3$ (from eq. (43)). Observed evaporation constants should be diminished by 30 percent to yield values applicable in the absence of convection (eq. (43)). Measured values so reduced are also plotted in figure 221 to indicate the range for experimental constants in the absence of convection.

It appears, therefore, that the essential features governing the rate of combustion for single drops in quiescent air are well understood. Uncertainties in the proper selection of transport properties for the calculation, as well as experimental uncertainties, cause difficulties in drawing conclusions from figure 221 on the relative merits of the various assumptions of reference 19. However, the calculation that considers product dissociation seems preferable, since it presents a more realistic picture of the state of combustion products, particularly at higher temperatures. In general, burning rates of hydrocarbons are very similar. Rates are increased by factors tending to increase the burning temperature and the thermal conductivity in the region between the flame and drop surfaces. Decreases in latent heat of vaporization and film thickness also cause increases in evaporation constant.

Combustion in airstreams.—The principal work on combustion from liquid surfaces in moving airstreams has been conducted by Spalding (refs. 32 and 33), with spill-type burners in which the fuel (for most experiments, kerosene) was circulated over the surface of the burner and collected. Both vertical flat-plate and spherical burners were employed (the latter simulates a drop of liquid fuel). Variation of the fuel-flow rate permitted variation in the amount of heat absorbed by the fuel. The burners were of such a size that the effect of natural convection must be considered. Experiments on burning from spheres under forced convection were also carried out (ref. 33).

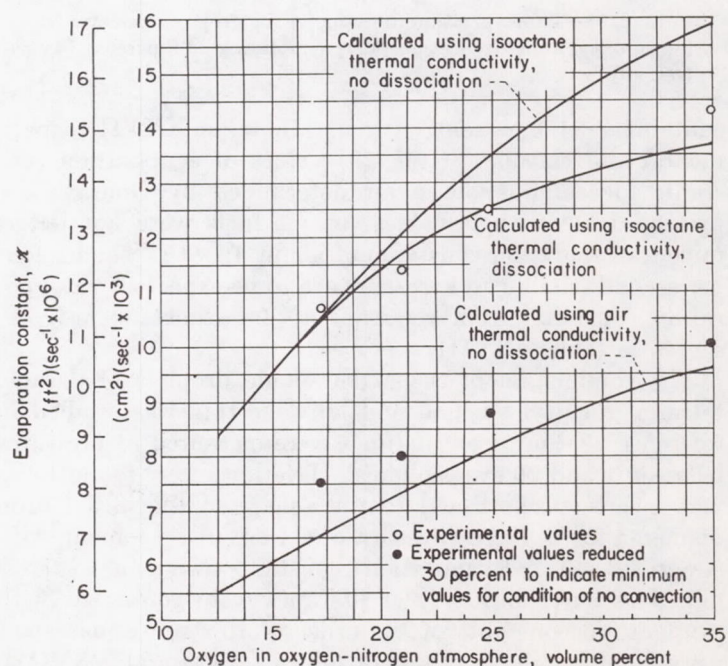


FIGURE 221.—Comparison of calculated and experimental evaporation constants for isooctane drops (ref. 19).

Spalding (refs. 33 and 34) presents without complete derivation the following equation in terms of dimensionless groups for combustion from a vertical flat plate under laminar natural convection:

$$\frac{G_f b_p c_p}{\kappa} = \mathcal{F}_1(\mathcal{B}, Pr) \left(\frac{g b_p^3 c_p^2 \rho^2}{\kappa^2} \right)^{1/4} = \mathcal{F}_1(\mathcal{B}, Pr) \left[Pr^2 \left(\frac{g b_p^3 \rho^2}{\mu^2} \right) \right]^{1/4} \quad (44)$$

where

$$\mathcal{B} = \frac{m_{O_2} h_c}{W_{st}} + c_p (T_c - T_A)$$

$$h_i + h_v$$

and m_{O_2} is the weight of oxygen per unit weight of gas mixture in the atmosphere.

Values of specific heat, density, thermal conductivity, and viscosity to be employed are not specified; however, for his calculations, Spalding used the room-temperature properties of air. It might be noted that the group $g b_p^3 \rho^2 / \mu^2$ is a part of the Grashof number. The function $\mathcal{F}_1(\mathcal{B}, Pr)$ is approximated by $0.769 \ln(1 + \mathcal{B})$ when $Pr = 0.71$ (air).

For forced convection from a flat plate in a longitudinal laminar gas stream, the following formula is given:

$$\frac{G_f b_p}{\mu} = \mathcal{F}_2(\mathcal{B}, Pr) Re^{1/2} \quad (45)$$

For $Pr = 0.71$, the function $\mathcal{F}_2(\mathcal{B}, Pr)$ is approximated by $0.646 \ln(1 + \mathcal{B})$.

It is stated that, in general, mass-transfer rates (burning rates) can be predicted approximately from existing heat-transfer data by the relation

$$G_f = \left(\frac{H}{c_p} \right) \ln(1 + \mathcal{B}) \quad (46)$$

where H is the heat-transfer coefficient determined in an experiment without combustion or mass transport.

Equation (46) is similar to equation (38a), which, when based on a burning rate per unit area, yields

$$G_f = \frac{w_f}{4\pi y_A^2} = \frac{1}{c_{p,f} y_A (y_B - y_A)} \ln \left[1 + \frac{c_{p,f} (T_B + T_A)}{h_v + h_i} \right] \quad (47)$$

The term $(y_B/y_A) [\kappa_{AB}/(y_B - y_A)]$ might be replaced by a heat-transfer coefficient.

By introducing the burning temperature from equation (34a),

$$\frac{c_{p,f} (T_B - T_A)}{h_v + h_i} = \frac{\left[\frac{c_{p,f} \rho_{O_2} D h_c}{\kappa_{BC} W_{st}} \frac{p_{O_2, c}}{P} + c_{p,f} (T_c - T_A) \right]}{h_v + h_i}$$

$$\cong \frac{\left[\frac{h_c}{W_{st}} \frac{p_{O_2, c}}{P} + c_{p,f} (T_c - T_A) \right]}{h_v + h_i} \cong \mathcal{B} \quad (48)$$

since $c_p \rho D / \kappa \approx 1$, and for air $p_{O_2, c} / P \approx m_{O_2}$. Thus, the relation between equations (46) and (47) may be seen.

Natural convection: Spalding's experiments on combustion

in natural convection employed a flat-plate burner 2.5 inches high and 2.08 inches wide and a 1.5-inch-diameter spherical burner. Upon variation of the fuel-flow rate over the burner, the heat absorbed by the liquid could be as high as 4000 Btu per pound of fuel burned. This permitted a much wider variation of $h_v + h_i$ than could be obtained by burning single drops of fuels of different heats of vaporization and boiling points.

Data for both the plate and spherical burners were well correlated by equation (44). For combustion from a sphere, the diameter was used as the characteristic dimension in place of the plate height. Spalding justifies this procedure with the statement that heat-transfer data by natural convection from plates, spheres, or cylinders are well correlated by a single relation, so that the same might be expected to hold true for combustion results. Most of the experiments were on kerosene combustion, but data on gas oil, gasoline, and heavy naphtha were predicted equally well by equation (44). Equations (44) and (46) are considered equally good for estimating burning rates by natural convection.

Forced convection: For most of his experiments on forced convection, Spalding employed a 1-inch-diameter spherical burner, with kerosene, gasoline, ethyl alcohol, and benzene as fuels. Experimental burning rates were 10 to 15 percent higher than theoretical for a flat-plate burner according to equation (45), but were an equal amount lower than the predictions of equation (46). Data were not as reproducible as results on natural convection. A calculation based on equation (46) gives an estimate of 5 milliseconds as the lifetime of a 100-micron jet-fuel droplet burning in a 400° F airstream when the velocity of the drop relative to the airstream is 50 feet per second. In the absence of convection, the lifetime would be 12 milliseconds.

A more exact treatment of combustion from a flat plate in forced convection is reported in reference 35, in which a Prandtl number of 1 is assumed. The results of this calculation appear to agree with experiment somewhat better than equation (45) or (46).

During experiments on combustion from spheres in airstreams, it was observed that at a critical air velocity the leading half of the envelope flame surrounding the sphere was extinguished. Spalding attributes this extinction phenomenon to chemical limitations on the combustion rate. As the air velocity is increased, the boundary layer becomes thinner, and mass transport to the flame front is increased. Since chemical reaction rates at the burning surface are finite, the reaction zone thickens and its temperature falls. Eventually, a point is reached at which the chemical reaction rate can no longer keep pace with the rate at which fuel and oxygen are supplied to the burning zone, and the flame is extinguished. Spalding conducted extinction experiments under forced convection on spheres of varying diameter (0.275 to 1.025 in.). It was predicted that at extinction the air velocity (expressed in diam/sec) and the distance of the flame from the sphere surface on the upstream side should be constant for spheres of varying diameter. This was found to be true, within 10 percent, for the 3.7-fold variation in sphere diameter studied.

Another method of studying combustion by convection is that employed in reference 36, in which fuel droplets (about 300 to 600 microns initial diam.) fall through a heated furnace at their terminal velocities. Quantitative data on evaporation in high-temperature atmospheres were obtained by this technique, but only a few qualitative observations on residues from burning residual fuel-oil droplets are presented.

In general, Spalding's equations appear to predict well experimental burning rates under natural and forced convection. However, drop sizes encountered in fuel sprays are 3 or more orders of magnitude smaller than the spherical burners used by Spalding, and no other quantitative data on burning under convection are available. Therefore, it is difficult to assess the value of his equations for application to the combustion of small droplets.

FUEL SPRAYS AND MISTS

The mode of combustion of the droplets in a burning fuel spray might be considered in terms of two extremes. In the first instance, the droplet may burn as a diffusion flame in the local atmosphere surrounding it. In this event, its combustion will be governed by the factors considered in the preceding section. On the other hand, the droplet might evaporate and mix by diffusion with the air in the preheat zone of an established flame front. The burning of the spray would in this case be determined by the same considerations that apply to the combustion of gaseous fuel-air mixtures.

Theory of combustion.—The evaporation or burning of liquid fuel sprays is examined theoretically in reference 37. It is assumed there that the evaporation or burning rates of individual drops are proportional to the drop diameters (as observed experimentally), that the evaporation constant is the same for all drops, and that all drops have the same available time for burning. The fuel spray drop-size distribution is represented by the Rosin-Rammler relation

$$\frac{v_{dr}}{v} = e^{-\left(\frac{d_{dr}}{\Lambda}\right)^{\mathcal{D}}} \quad (49)$$

where v_{dr} is the volume or weight fraction of the spray composed of drops greater in diameter than d_{dr} . The constants Λ and \mathcal{D} are known as the size and distribution constants, respectively. The more uniform the drop size, the higher the value of \mathcal{D} ; if all drops were of the same size, \mathcal{D} would be infinite. In practice, it has been found that atomizing nozzles give sprays having values of \mathcal{D} between 2 and 4. Mean diameters that determine the evaporation rate of the injected spray and of the spray in steady-state burning (where injection and evaporation rates are equal) have been evaluated. The specific volume in steady burning, which is the volume of unevaporated fuel divided by the volume of fuel introduced per second, has also been calculated.

Incomplete evaporation of the spray for limited evaporative time was considered. The results are shown in figure 222, where the fraction of the spray unevaporated is plotted against $\pi t/\Lambda^2$ for sprays in which the distribution constant is 2, 3, or 4. The dashed line illustrates the behavior of a single fuel droplet, or a spray in which all drops are the same size ($\mathcal{D} = \infty$). Note that in the early stages sprays of low distribution constant \mathcal{D} evaporate most rapidly (since more

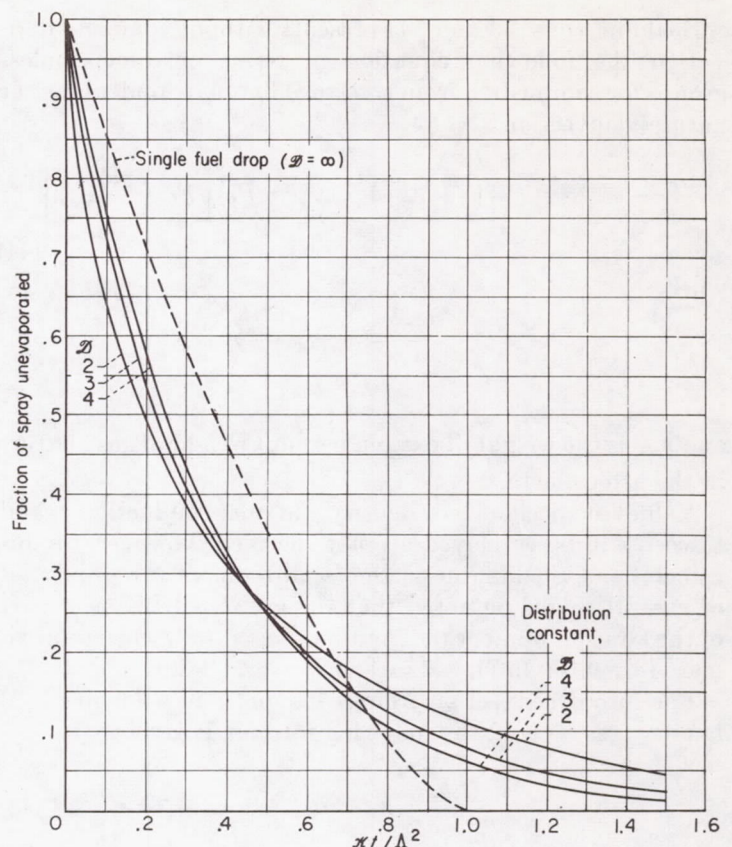


FIGURE 222.—Evaporation of fuel spray (ref. 37).

small droplets are present). Later, however, sprays of uniform size distribution (large \mathcal{D}) are favored, since they have fewer large drops (which evaporate more slowly). In general, it was concluded (ref. 37) that the size constant Λ is the most important factor in determining the evaporation or burning rate of sprays. The distribution constant has a much smaller effect, although a large value of \mathcal{D} favors more complete evaporation, despite the fact that the initial evaporation rate of the injected spray will be lower. In appendix C of reference 19, the relations of reference 37 were applied to a fuel spray burning in a duct where heat release changes the average velocity along the duct. In this manner, the author calculated what the effect of evaporation rate on combustion efficiency should be.

The foregoing considerations are applicable if the burning of a fuel spray may be represented as an integration of the burning of single drops.

Experimental observation.—The observations of reference 38 on a kerosene spray burning in still air give some information as to the manner in which the fuel droplets are consumed. It was observed that a flame front was established about 1 inch from the spray nozzle. As indicated in calculations, at this point small drops (size of the order of 10 microns) were at rest with respect to the airstream, which was moving with a velocity of about 0.7 to 1.0 foot per second (compatible with normal burning velocities). It was concluded that, in the period of about 0.1 second that the small drops spent in transit from the nozzle to the flame front (for larger drops, this time was even shorter), very little evaporation was possible. With the preheat zone of the kerosene flame

assumed to be approximately 0.1 inch thick, calculations on heat transfer to small drops indicated that this thickness was sufficient to allow evaporation and mixing with air in the preheat zone. Larger drops (size of the order of 100 microns) could pass through the flame front without being completely vaporized.

Some confirmation for this analysis was provided by observations on kerosene droplets in the approach streams of premixed Bunsen flames. For a butane-air flame, droplets (sizes 9 to 30 microns) disappeared before reaching the luminous inner cone of the flame. However, when an acetylene-air flame was used, conditions for vaporization were not as favorable, because of a narrower preheat zone and higher gas-stream velocity. Some droplets escaped evaporation in the preheat zone; large droplets (of the order of 80 microns) completed evaporation definitely above the inner cone.

Limits of flammability: Flammability limits for mists and sprays have been discussed in chapter III. Fine fuel mists behave like fuel-vapor-air mixtures. Thus, when drop sizes are of the order of 10 microns or less, lean limits for mists occur at the same fuel-air ratios as vapors. Likewise, the minimum oxygen concentration necessary for combustion in an oxygen-nitrogen atmosphere is approximately 12 percent for both vapors and fine mists.

As drop sizes are increased, lean limits and minimum oxygen requirements decrease, according to reference 39 (aerosols of tetralin with drop sizes in the range of 7 to 55 microns). The appearance of the flames also varies with drop size (ref. 39). Fine mists give blue flames similar to vapor-air mixtures. For larger drops, diffusion flames surround the individual droplets. These results are in agreement with the observations of reference 38.

Rate of flame propagation: Spatial flame speeds were determined (ref. 40) for condensed mists and the equivalent vapor mixtures, and the results are presented in table XXIX. Although flame speeds for vapors were higher, the experiments on vapors were conducted at higher temperatures. Therefore, mist flame speeds were increased to values that might be anticipated at the vapor experiment temperature, with the flame speed assumed to increase as the 1.4 power of the absolute temperature, as for isooctane (ref. 22). These corrected mist flame speeds (table XXIX) have in most instances the same values as vapor. It should be noted that some of the spatial flame speeds are quite large, suggesting that the propagating flames were not laminar. Presumably, conditions were the same in both mist

and vapor mixtures, so that the comparison is still permissible.

Burning velocities of kerosene mists (average drop diam. 0.5 to 1 micron) are similar to those of propane-air mixtures, according to reference 41. This again suggests that, for fine mists, drops evaporate and mix with air in the preheat zone of the flame. Blowoff curves for mists showed wider and richer stability limits than those for propane flames (see ch. VI, fig. 180). Presumably this is due to the fact that in order to stabilize a Bunsen flame a combustible vapor-air mixture must be present just above the burner rim. For lean mixtures, propane can more readily supply the necessary fuel vapor to this zone. On the other hand, at rich blowoff, fuel vapor is in excess. Accordingly, mists are stable at richer fuel concentrations, since some of the excess fuel is not vaporized; gas-phase fuel-air ratios are correspondingly lower.

Data of reference 39 yield clues as to the effect of drop size on burning velocity. Measurements for large drop sizes were rather uncertain, but it seems that burning velocity increases with increasing drop size.

In conclusion, flammability limits and flame velocities for mists and sprays (drop diam. of 10 microns or less) correspond closely to those of vaporized fuel-air mixtures. This result is compatible with the idea that small droplets can vaporize and mix with air in the preheat zone of an established flame front. Both lean and rich blowoff limits for mists occur at higher fuel concentrations than for fuel vapor-air mixtures.

Larger drops burn surrounded by diffusion flames. Lean limits decrease and apparent flame velocities increase with increasing drop size in the range of 10 to 50 microns. Flames appear to propagate in a particulate fashion; that is, the flame surrounding a burning drop ignites an adjacent drop and in this manner progresses from burning into unburned mixture.

APPLICABILITY OF RESEARCH DATA ON DIFFUSION FLAMES TO JET-ENGINE COMBUSTOR DESIGN

In this chapter, the present status of knowledge of the burning of gaseous and liquid fuels as diffusion flames is reviewed. For simple systems (simple fuel jets or single drops of liquid fuels), combustion properties may be quite successfully predicted from mixing rates; chemical reaction rates are not considered. Mixing rates are, in turn, determined by mass- and heat-transport processes. Current understanding of the burning of complex gas jets and fuel

TABLE XXIX.—SPATIAL FLAME SPEEDS OF MIST AND VAPOR (Ref. 40)

Fuel	Mist				Vapor		Mist flame speed corrected to temperature of vapor experiment, ft/sec
	Fuel-air ratio	Fuel as vapor, percent	Temperature, °F	Flame speed, ft/sec	Temperature, °F	Flame speed, ft/sec	
Petroleum (180° to 220° C) -----	0.044	34	75	3.6	140	4.3	4.2
	.061	30	93	16	140	18	18
	.072	33	99	19	140	22	21
Tetralin -----	0.040	^a 6	84	2.3	212	2.6	3.1
	.080	^a 3	113	3.6	212	6.2	4.5

^a Calculated from estimated fuel vapor pressure.

sprays is far less complete. Fine fuel sprays and mists appear to be similar to premixed fuel-air systems, while for coarser sprays behavior intermediate between that of diffusion and premixed flames might be expected. The application of the data of this chapter to combustor performance is therefore somewhat limited. Another limitation exists because of the high heat-release rates required by aircraft combustion systems. The high velocities may result in conditions that more nearly approach the extinction regions of the flames where chemical reaction rates appear to be important. The extinction of diffusion flames has received somewhat less attention than normal burning and appears to be a fruitful area for research.

REFERENCES

- Hottel, H. C.: Burning in Laminar and Turbulent Fuel Jets. Fourth Symposium (International) on Combustion, The Williams & Wilkins Co. (Baltimore), 1953, pp. 97-113.
- Barr, John: Diffusion Flames. Fourth Symposium (International) on Combustion, The Williams & Wilkins Co. (Baltimore), 1953, pp. 765-771.
- Burke, S. P., and Schumann, T. E. W.: Diffusion Flames. *Ind. and Eng. Chem.*, vol. 20, no. 10, Oct. 1928, pp. 998-1004.
- Hottel, H. C., and Hawthorne, W. R.: Diffusion in Laminar Flame Jets. Third Symposium on Combustion and Flame and Explosion Phenomena, The Williams & Wilkins Co. (Baltimore), 1949, pp. 254-266.
- Wolfhard, H. G., and Parker, W. G.: A New Technique for the Spectroscopic Examination of Flames at Normal Pressures. *Proc. Phys. Soc., sec. A*, vol. 62, Nov. 1949, pp. 722-730.
- Wolfhard, H. G., and Parker, W. G.: A Spectroscopic Investigation into the Structure of Diffusion Flames. *Proc. Phys. Soc., sec. A*, vol. 65, Jan. 1952, pp. 2-19.
- Hawthorne, W. R., Weddell, D. S., and Hottel, H. C.: Mixing and Combustion in Turbulent Gas Jets. Third Symposium on Combustion and Flame and Explosion Phenomena, The Williams & Wilkins Co. (Baltimore), 1949, pp. 266-288.
- Barr, J., and Mullins, B. P.: Concerning Combustion in Vitiating Atmospheres. Rep. No. R.44, British N.G.T.E., June 1949.
- Gray, Andrew, Mathews, G. B., and MacRobert, T. M.: A Treatise on Bessel Functions and Their Application to Physics. Second ed., MacMillan and Co. (London), 1931, p. 78.
- Wohl, Kurt, Gazley, Carl, and Kapp, Numer.: Diffusion in Flames. Third Symposium on Combustion and Flame and Explosion Phenomena, The Williams & Wilkins Co. (Baltimore), 1949, pp. 288-300.
- Zeldovich, Y. B.: On the Theory of Combustion of Initially Unmixed Gases. NACA TM 1296, 1951.
- Sawai, Ikutaro, Kurugi, Masanga, and Jinno, Hircshi: Turbulent Diffusion Flames. Fourth Symposium (International) on Combustion, The Williams & Wilkins Co. (Baltimore), 1953, pp. 806-814.
- Rembert, E. W., and Haslam, R. T.: Factors Influencing Length of a Gas Flame Burning in Secondary Air. *Ind. and Eng. Chem.*, vol. 17, no. 12, Dec. 1925, pp. 1236-1238.
- Scholefield, D. A., and Garside, J. E.: The Structure and Stability of Diffusion Flames. Third Symposium on Combustion and Flame and Explosion Phenomena, The Williams & Wilkins Co. (Baltimore), 1949, pp. 102-110.
- Yagi, Sakae, and Saji, Kenjiro: Problems of Turbulent Diffusion and Flame Jet. Fourth Symposium (International) on Combustion, The Williams & Wilkins Co. (Baltimore), 1953, pp. 771-781.
- Chamberlin, D. S., and Rose, A.: Flicker of Luminous Flames. *Ind. and Eng. Chem.*, vol. 20, no. 10, Oct. 1928, pp. 1013-1016.
- Spalding, D. B.: Combustion of Liquid Fuel in a Gas Stream, Pt. I. *Fuel*, vol. XXIX, no. 1, Jan. 1950, pp. 2-7.
- Spalding, D. B.: Combustion of Fuel Particles. *Fuel*, vol. XXX, no. 6, June 1951, pp. 121-130.
- Graves, Charles C.: Burning Rates of Single Fuel Drops and Their Application to Turbojet Combustion Process. NACA RM E53E22, 1953.
- Khudyakov, G. N.: Distribution of Temperature within a Liquid Burning from a Free Surface, and Description of the Flame Formed. RAE Lib. Trans. No. 422, Feb. 1953.
- Sherwood, Thomas K.: Absorption and Extraction. McGraw-Hill Book Co., Inc., 1937, p. 9.
- Dugger, Gordon L., and Graab, Dorothy D.: Flame Speeds of 2,2,4-Trimethylpentane-Oxygen-Nitrogen Mixtures. NACA TN 2680, 1952.
- Godsave, G. A. E.: The Burning of Single Drops of Fuel. Pt. IV. The Flow of Heat and Carbon Residue Formation in Drops of Fuel. Rep. No. R.125, British N.G.T.E., Oct. 1952.
- Godsave, G. A. E.: The Burning of Single Drops of Fuel. Pt. I. Temperature Distribution and Heat Transfer in the Pre-Flame Region. Rep. No. R.66, British N.G.T.E., Mar. 1950.
- Godsave, G. A. E.: Studies of the Combustion of Drops in a Fuel Spray—The Burning of Single Drops of Fuel. Fourth Symposium (International) on Combustion, The Williams & Wilkins Co. (Baltimore), 1953, pp. 819-830.
- Godsave, G. A. E.: The Burning of Single Drops of Fuel. Pt. II. Experimental Results. Rep. No. R.87, British N.G.T.E., Apr. 1951.
- Kumagai, Seiichiro, and Isoda, Hircshi: Combustion of Fuel Droplets. *Nature*, vol. 166, no. 4235, Dec. 30, 1950, p. 1111.
- Hall, A. R., and Diederichsen, J.: An Experimental Study of the Burning of Single Drops of Fuel in Air at Pressures up to Twenty Atmospheres. Fourth Symposium (International) on Combustion, The Williams & Wilkins Co. (Baltimore), 1953, pp. 837-846.
- Godsave, G. A. E.: The Burning of Single Drops of Fuel. Pt. III. Comparison of Experimental and Theoretical Burning Rates and Discussion of the Mechanism of the Combustion Process. Rep. No. R.88, British N.G.T.E., Aug. 1952.
- Spalding, D. B.: Combustion of a Single Droplet and of a Fuel Spray. AGARD Selected Combustion Problems—Fundamentals and Aeronautical Applications, Butterworths Sci. Pub. (London), 1954, pp. 340-351.
- Ingebo, Robert D.: Study of Pressure Effects on Vaporization Rate of Drops in Gas Streams. NACA TN 2850, 1953.
- Spalding, D. B.: Experiments on the Burning and Extinction of Liquid Fuel Spheres. *Fuel*, vol. XXXII, no. 2, Apr. 1953, pp. 169-185.
- Spalding, D. B.: Combustion of Liquid Fuel in a Gas Stream, Pt. II. *Fuel*, vol. XXIX, no. 2, Feb. 1950, pp. 25-32.
- Spalding, D. B.: The Combustion of Liquid Fuels. Fourth Symposium (International) on Combustion, The Williams & Wilkins Co. (Baltimore), 1953, pp. 847-864.
- Emmons, Howard W.: The Film Combustion of Liquid Fuel. Interim. Tech. Rep. No. 6, Combustion Aero. Lab., Harvard Univ., June 1953. (Contract No. DA-19-020-ORD-1029, Army Ord. Dept.)
- Topps, J. E. C.: An Experimental Study of the Evaporation and Combustion of Falling Droplets. N.G.T.E. Memo. No. M.105, British M.O.S., Feb. 1951 (See also *Jour. Inst. Petroleum*, vol. 37, no. 333, Sept. 1951, pp. 535-553.)
- Probert, R. P.: The Influence of Spray Particle Size and Distribution in the Combustion of Oil Droplets. *Phil. Mag.*, ser. 7, vol. XXXVII, no. 265, Feb. 1946, pp. 94-105.
- Wolfhard, H. G., and Parker, W. G.: Combustion Processes in Flames. Pt. II. Evaporation Process in a Burning Kerosene Spray. *Jour. Inst. Petroleum*, vol. 35, no. 302, Feb. 1949, pp. 112-125.
- Burgoyne, J. H., and Cohen, L.: The Effect of Drop Size on Flame Propagation in Liquid Aerosols. *Proc. Roy. Soc. (London)*, ser. A, vol. 225, 1954, pp. 375-392.
- Haber, F., und Wolff, H.: Über Nebelexlosionen. *Zs. Angew. Chem.*, Jahrg. 36, Nr. 55, July 18, 1923, pp. 373-377.
- Browning, J. A., and Krall, W. G.: Effect of Fuel Droplets on Flame Stability, Flame Velocity, and Inflammability Limits. Fifth Symposium (International) on Combustion, Reinhold Pub. Corp., 1955, pp. 159-163.

CHAPTER VIII

OSCILLATIONS IN COMBUSTORS

By PERRY L. BLACKSHEAR, JR., and WARREN D. RAYLE

INTRODUCTION

High-performance jet-engine combustors designed for steady-flow operations frequently and sometimes unexpectedly exhibit periodic flow oscillations, which are usually audible. The frequencies of these sounds range from the 20- to 30-cps buzz of a ramjet engine to the 1000- to 3000-cps screech of a high-performance afterburner. Some type of combustion oscillation may occur at any point within the engine operating range. These combustion oscillations are accompanied by excursions in pressure and velocity within the combustion chamber. Some observers report beneficial effects due to these velocity and pressure excursions evidenced by a noticeable increase in the combustion efficiency within the combustor. Still more observers report deleterious effects, such as a restricted range of operating conditions or the actual destruction of combustor component parts.

Some modes of combustor oscillation exhibit pressure and velocity perturbations that can be described by solutions of the wave equation for an idealized, homogeneous, stationary medium in an enclosure having the dimensions of the combustor. Other oscillations, where the implied wavelength is long compared with the dimension of the enclosure, can better be described by use of a lumped-constant analysis, analogous to the treatment given the Helmholtz resonator. In these analyses, the wave and the enclosure are the primary elements; the flame and the flow processes are given cursory treatment. There are types of combustor oscillation, however, where such treatment does not adequately describe the phenomena, but where the combustor components must be considered. Examples of such oscillations might include those involving aeolian tones, modulation of fuel flow or fuel distribution, and recurrent detonation.

Regardless of the system employed to describe the pressure and velocity distribution within the engine, a few general remarks may be made concerning the importance of the flame and the flowing stream in maintaining the oscillation. Any oscillation, whatever its nature, requires a source of energy for its continued existence. Two sources of energy are available in the combustor: (1) the kinetic energy in the flowing gas, and (2) the chemical energy released in the combustion process. Of these two sources, the chemical energy is far greater. However, this energy can only be made available to drive the oscillation through a time-varying work cycle, while the kinetic energy is immediately available for driving the oscillation by means of any of a number of thermodynamic or aerodynamic processes that alternately store and release this energy.

The interaction of the combustion and flow processes within the oscillatory system is complex. The flame zone is not anchored spatially but can move with and be disturbed by the oscillating gas. Meanwhile, the local reaction rates within this mobile zone vary in some manner with the time-varying pressures and temperatures. These local rate variations act as sources of acoustic waves whose combined effect is to drive the oscillation.

In this chapter, the analyses that have been found useful in identifying modes of combustor oscillation are summarized. The manner in which departure from the assumed ideal condition affects mode identification is discussed, and methods whereby an identified mode may be controlled or eliminated are suggested. An effort is made to formulate a coherent picture of the interaction between the oscillation and the combustion and flow processes in an engine on the basis of the little that is known about such interactions.

SYMBOLS

The following symbols are used in this chapter:

A	cross-sectional area, sq ft
a	sonic velocity, ft/sec
d_r	rod diameter, ft
\mathcal{F}	function of viscosity, distance, and initial stream momentum
f	fuel-air ratio
ℓ	frequency, cps or sec ⁻¹
J_ζ	Bessel function of first kind of order ζ
K_0, K_1, K_2, K_3	constants
k	constant of integration
l	length, ft
M	flow Mach number
$m_{g,B}$	mass of gas in combustion chamber, slugs
$m_{g,d}$	mass of oscillating gas in diffuser, slugs
n, n_z	indices
p	pressure
Q	mean heat-release rate
q	perturbation heat-release rate
r	radius or radial distance, ft
$T_{g,m}$	mean temperature of gas entering combustor
ΔT_B	temperature rise across combustor
t	time, sec
U	velocity, ft/sec
U_i	velocity of signal in loop segment, ft/sec
U_m	mean velocity approaching flameholder, ft/sec
u	perturbation velocity, ft/sec
W_{dt}	duct width, ft

w	total mass flow (mean), slugs/sec
w_{out}	mass-flow rate (mean) of gas through oscillatory area at diffuser outlet, slugs/sec
x	distance from igniter to injector, ft
y	distance perpendicular to direction of flow
z	axial distance, ft
$\alpha_{\zeta,n}$	constant (see table XXX)
γ	ratio of specific heats
ζ	index
θ	tangential distance, radians
ρ_c, ρ_h	densities of gas before and after combustion
Φ	function of viscosity, distance, and initial stream momentum
ϕ_1, ϕ_2	constants
ω	frequency, radians/sec
Subscripts:	
B	combustor, combustion chamber
e	enclosure
i	loop segment
in	diffuser inlet
m	mean
max	maximum
out	diffuser outlet
P	perturbation
s	stream
t	total

MODES OF OSCILLATION

THE BURNER AS A RESONANT ROOM

In almost every case of burner resonance encountered in practice, a portion of the engine containing the fuel in reaction can be assumed separated from the rest of the universe by some acoustic barrier. The resulting enclosure can be treated as a resonant room having certain peculiar acoustic properties. For example, the space between the compressor and the turbine in a turbojet constitutes such a room. In a similar manner, the space between the inlet diffuser and the exhaust nozzle of a ramjet constitutes such a room. The theoretical treatment delineating the modes of resonance possible in a room of a given geometry is available in a number of standard acoustic texts (refs. 1, 2, and others). The rather concise breakdown of the application of these acoustic treatments to a rocket engine given in reference 3 serves as a basis for the following discussion.

The general solution to the wave equation for a cylindrical room closed at both ends with rigid, nondissipative walls is

$$p_P = \sum_{\zeta,n,n_z} J_{\zeta} \left(\frac{\pi \alpha_{\zeta,n} r}{r_e} \right) \cos \left(\frac{n_z \pi z}{l_e} \right) \left[K_1 \cos (\zeta \theta + \omega t - \phi_1) + K_2 \cos (\zeta \theta - \omega t - \phi_2) \right] \quad (1)$$

A mode of oscillation then can be obtained by giving the constants ζ , n , and n_z integral values. Since the wave equation is linear, a combination of different modes may exist simultaneously. The frequency (cps) for any mode of oscillation in the cylindrical room is given by the formula

$$f = \frac{a}{2} \sqrt{\frac{n_z^2}{l_e^2} + \frac{\alpha_{\zeta,n}^2}{r_e^2}} \quad (2)$$

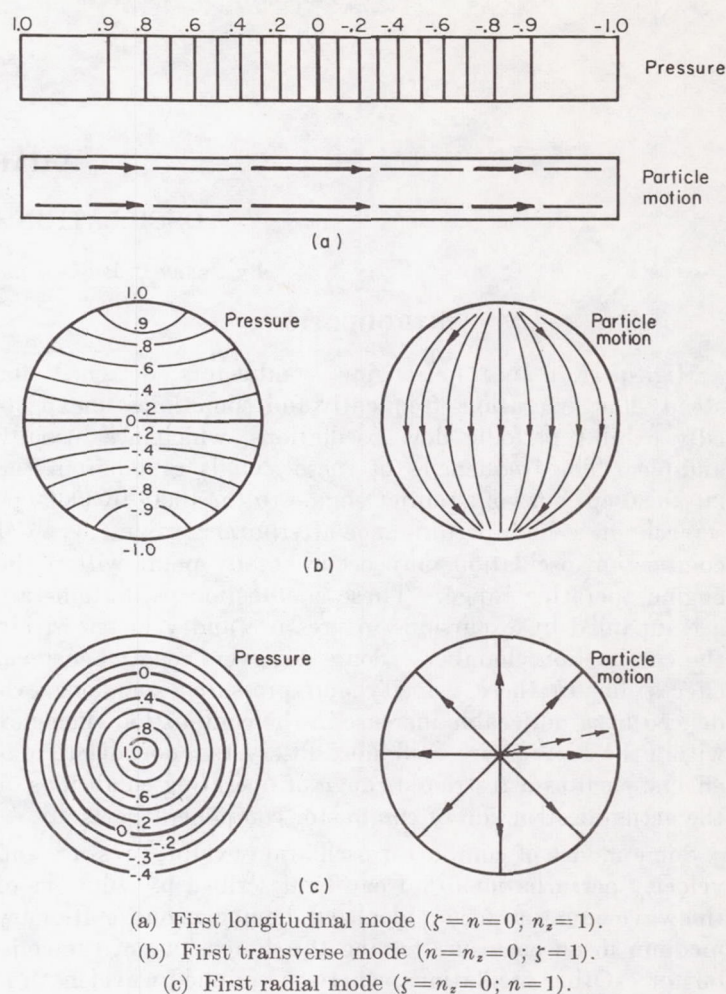


FIGURE 223.—Pressure contours and particle motions for fundamental modes of cylindrical duct (ref. 6).

It is of interest to consider three of the simplest modes possible in the cylindrical room. If $\zeta=n=0$, the mode is the purely longitudinal organ-pipe type of oscillation. For $\zeta=n_z=0$, the mode of oscillation is purely radial with the gas oscillating back and forth from wall to center of the cylinder uniformly along the length of the cylindrical room. For $n=n_z=0$, the mode is a purely transverse oscillation where for $\zeta=1$ the gas sloshes back and forth across a diameter, again uniformly along the length of the cylindrical room. Sketches of the pressure distribution and particle motion for these three simplest cases are given in figure 223. The higher modes of oscillation possible can be computed from equations (1) and (2) with the help of the values of $\alpha_{\zeta,n}$ given in table XXX for the first several modes of trans-

TABLE XXX.—VALUES OF $\alpha_{\zeta,n}$ FOR THE LOWER RADIAL, TRANSVERSE, AND COMPOUND MODES

ζ	Values of α for n of				
	0	1	2	3	4
0	0.0000	1.2197	2.2331	3.2383	4.2411
1	.5861	1.6970	2.7140	3.7261	4.7312
2	.9722	2.1346	3.1734	4.1923	5.2036
3	1.3373	2.5513	3.6115	4.6428	5.6624
4	1.6926	2.9547	4.0368	5.0815	6.1103

verse and radial oscillations for which n_z may or may not be equal to zero.

A similar treatment may be given the annular room (ref. 3) and the rectangular room (refs. 1 and 2). Reference 3 points out the fact, usually omitted by standard acoustic texts, that the transverse mode of oscillation may occur as a traveling wave as well as a standing wave. The pressure distribution for the traveling wave is obtained from equation (1) by taking $K_1=0$, $K_2 \neq 0$; or $K_1 \neq 0$, $K_2=0$. Figure 224 gives a comparison of the pressure and particle-motion distribution of standing and traveling waves for the first transverse mode.

On the basis of the preceding discussion, it is now of interest to consider the methods whereby such modes of oscillation may be experimentally identified. If the modes actually correspond to the simple solutions of the cylindrical-wave equation as discussed herein, for a purely transverse mode, the pressure would undergo a maximum excursion near the wall and go through zero excursion at the centerline of the duct. The pressure on opposite sides of the burner would be out of phase for odd transverse modes and in phase for even transverse modes.

If the transverse mode were a standing wave, the oscillatory pressure about a circumference would reach a maximum at the nodal point, vanish at an antinodal point, and so forth. On either side of the antinodal line, the pressure oscillation would everywhere be in phase. If the transverse mode were a traveling wave, the amplitude about the circumference would be everywhere the same, and the phase difference between two points of circumference would be an integral multiple of their angular displacement. A radial wave would have the pressure distribution shown in figure 223(c). The phasing would be such that the pressure at the center of the duct would be 180° out of phase with the pressure at the wall for odd modes and in phase for even modes.

In both the transverse and radial modes, there would be no change in pressure and phase along the axis of the cylindrical room. In the purely longitudinal mode, however, there should be no change in amplitude or phase across the diameter or around the periphery, whereas there would be a change in amplitude along the axis and a 180° shift in phase every time an antinodal plane was crossed. In selecting a reliable characteristic for the identification of a mode, the effects of departure from the assumed ideal homogeneous stationary medium should be considered.

The presence of steady flow through the burner would probably have its greatest effect on the longitudinal resonance. Strong velocity gradients might occur in a radial direction. These would tend to diffract longitudinal waves and concentrate their energy in the region of low effective sound speed.

Temperature gradients would tend to affect almost all the modes of oscillation. For example, reference 4 gives a theoretical effect of an assumed temperature distribution upon the first transverse mode of oscillation in a cylindrical duct. Reference 5 discusses the effect of a sharp temperature discontinuity upon longitudinal oscillation. Reference 6 gives an experimental demonstration of the effect of sharp

temperature gradients on the first transverse mode of oscillation in a cylindrical duct. The discussions in references 4 and 6 indicate that, where the gas in one section of a cylindrical duct is executing a uniformly transverse motion, at a temperature gradient there will be phase shifts and a propagation of the oscillatory motion in the longitudinal direction. Therefore, although the wave-equation solution for a transverse standing wave may adequately describe the transverse gas motion, there will be a longitudinal component of the gas motion in the pressure-propagation direction. Thus, it would seem that the only possible confusion that could be caused by neglect of velocity and temperature gradients would lie in the identification of a longitudinal mode by a longitudinal pressure survey. Usually, consideration of the frequency alone leads to a rather wide choice of possible modes of oscillation, since sound speed is rarely known accurately.

In burner oscillations, amplitudes are reached that far exceed the values commonly referred to as infinitesimal, for which the wave equation in its linear form applies. Reference 6 shows that for these high-amplitude waves almost any wave form tends toward the saw-tooth wave form because of the differing acoustic velocity in the compressed and rarefied gas. This tendency toward saw-tooth form would not necessarily change the frequency of oscillation, since, even for waves of as much as 2 atmospheres peak-to-peak amplitude, the apparent propagation rate of a train of waves does not differ appreciably from sound speed. There would be an effect, however, in that the waves constituting either a standing- or traveling-wave oscillation would be asymmetrical. A very simple way of demonstrating this effect is by considering equation (1) for the case where $\zeta=n=0$. Since a sum of solutions of the form thus obtained is also a solution of the wave equation, an equation describing a standing-wave system composed of saw-tooth waves may be derived:

$$p = \sum_{n_z=1}^{\infty} (-)^{n_z+1} \frac{K_0}{n_z} \cos \frac{n_z \pi z}{l_e} \cos \frac{n_z \pi a t}{l_e} \quad (3)$$

The rather unusual properties exhibited by this standing-wave system include an amplitude at the antinode of half the value at the node; the frequency of the oscillation measured at this point appears to be doubled. Similarly, the phase obtained by measuring the time between pressure peaks will differ from point to point in the region between a node and antinode when the wave is saw-toothed and will vanish when the wave is sinusoidal.

This same treatment cannot be applied directly to the transverse modes, since higher harmonics are not multiples of the fundamentals. In reference 4 both transverse and plane waves of finite amplitude were investigated by retaining second-order terms in the wave equation. As in reference 2, plane waves of finite amplitude were found to be nonpermanent; that is, the effect of finite amplitude is to encourage a distortion that changes with time. In contrast, the spinning transverse mode in a cylindrical duct was found to possess a permanent wave form that included harmonic distortion. Pairs of such spinning waves could yield a pressure distribution about the circumference similar

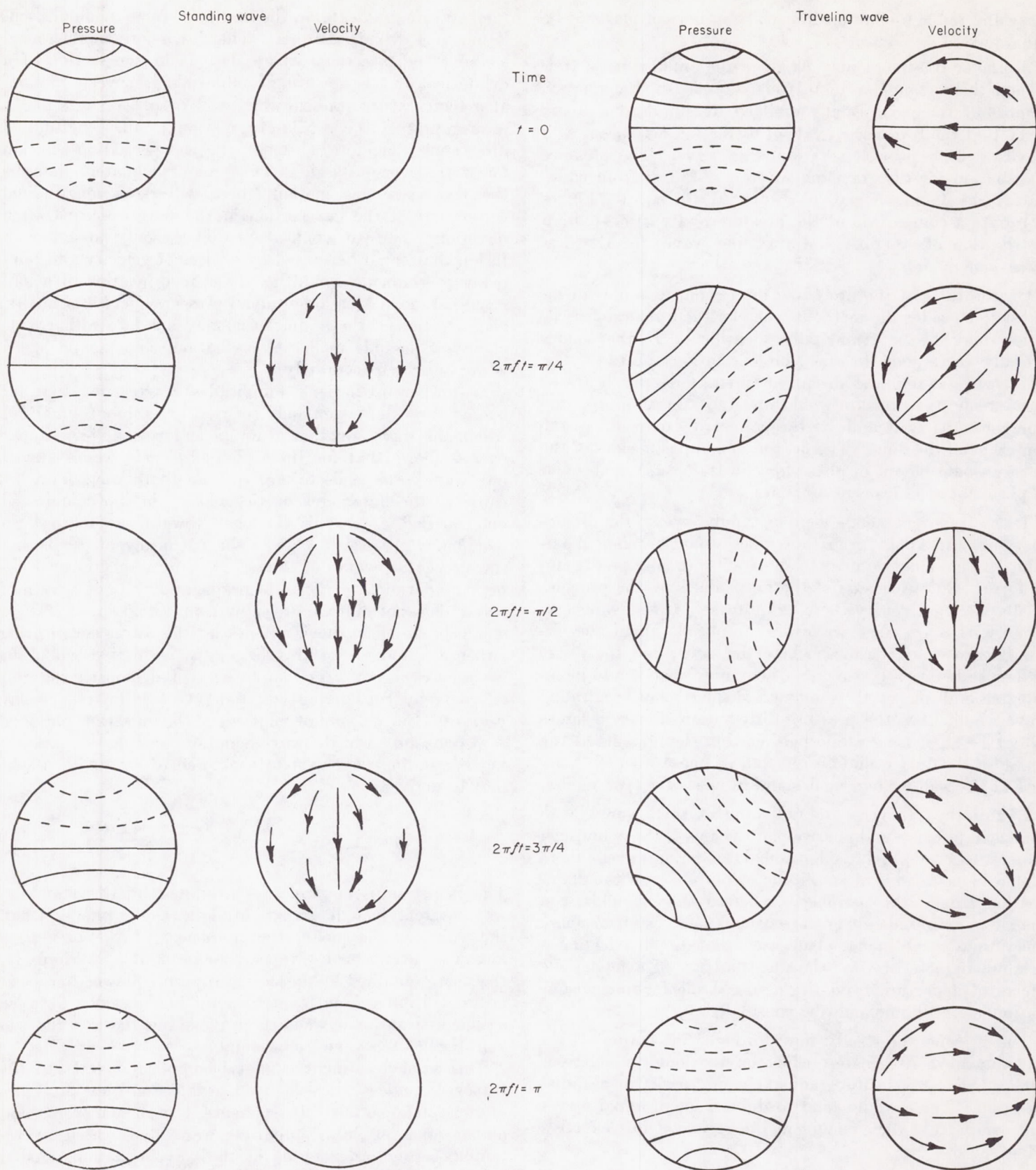


FIGURE 224.—Distribution of pressure and velocity for standing and traveling transverse waves through half a cycle.

to the pressure distribution along the axis for the plane case previously mentioned. In both cases a mode could be identified readily by measuring the intensity distribution of the fundamental about the walls of the duct.

In practice, a rather careful study must be made to ascertain amplitude and frequency distribution about a circumference in order to distinguish between standing and traveling transverse waves. However, the primary aim of mode

identification is to give a clue to the best manner in which damping may be applied; therefore, a rigorous determination as to whether a transverse mode is traveling or standing is not important, since the damping of both waves would be the same.

THE BURNER AS A HELMHOLTZ RESONATOR

Both ramjet engines and turbojet afterburners ordinarily include a subsonic diffuser of smaller cross section than the combustion chamber. This geometry is analogous to that of the Helmholtz resonator. A mode of resonance should then be possible wherein the gas in the diffuser oscillates back and forth and that in the combustion chamber undergoes pressure fluctuations. Such a mode of resonance would be less probable in the afterburner, since the pressure drop across the turbine ensures a nearly constant flow of gas into the afterburner.

Like any other form of oscillation, the Helmholtz type requires that energy be available to sustain it. In the ramjet engine, there are three mechanisms by which the available energy may be applied. The most obvious one is that depending on a time-varying heat-release rate within the combustor. Another relies on a variable pressure recovery of the supersonic diffuser, thus using the kinetic energy of the incoming air to drive the oscillation. Still a third might employ a time-varying temperature or temperature profile at the exhaust nozzle; this would not necessarily imply a varying heat-release rate for the whole combustor.

The effectiveness of varying heat release as a driving mechanism can be easily analyzed. Assume first that the diffuser is of constant area and has a pressure recovery independent of mass flow. Let the temperature rise across the combustion zone be constant; the heat-release variation is produced by variation of mass flow through the (non-stationary) combustion zone. Assume a choked exhaust nozzle and neglect the pressure drop in the combustion chamber. Then, if the density of the hot gas is

$$\rho_h = \rho_c \frac{T_{g,m}}{T_{g,m} + \Delta T_B} \quad (4)$$

the linear differential equation for the gas motion is found to contain the damping term:

$$\left[\frac{\gamma-1}{2} (2\Delta T_B + T_{g,m}) + \Delta T_B - \left(\frac{q}{Q} \right) \left(\frac{p_{B,m}}{p_{P,B}} \right) \gamma \Delta T_B \right] \frac{du}{dt} \quad (5)$$

For maximum instability, q is assumed to be in phase with $p_{P,B}$. Instability results, then, only if

$$\frac{qp_{B,m}}{Qp_{P,B}} > \frac{1}{2\gamma} \left[(\gamma-1) \left(2 + \frac{T_{g,m}}{\Delta T_B} \right) + 2 \right] \quad (6)$$

It is readily seen that, for realistic values of ΔT_B , the criterion becomes nearly

$$\frac{qp_{B,m}}{Qp_{P,B}} > 1 \quad (7)$$

The case of Helmholtz oscillation driven by a variable diffuser pressure recovery is treated by reference 7. For

isothermal flow, a differential equation is derived to describe the gas motion. It may be written as

$$K_1 \frac{d^2 u}{dt^2} + K_2 \frac{du}{dt} + K_3 u = 0 \quad (8)$$

where

$$K_1 = \frac{m_{g,B} m_{g,d}}{w_{out} \gamma p_{t,B} A_{in}} \quad (8a)$$

$$K_2 = \frac{m_{g,B}}{\gamma p_{t,B} A_{out} M_{out}} \left(\frac{\gamma-1}{2} \frac{m_{g,d}}{m_{g,B}} \frac{w}{w_{out}} \frac{a_{out}}{A_{in}} M_{out} - \frac{dp_{t,B}}{dw_{out}} \right) \quad (8b)$$

$$K_3 = \frac{1}{a_{out} M_{out}} \left(1 - \frac{\gamma+1}{2\gamma} \frac{w}{p_{t,B}} \frac{dp_{t,B}}{dw_{out}} \right) \quad (8c)$$

The frequency of oscillation (sec^{-1}) may then be expressed as

$$f = \frac{1}{2\pi} \left[\frac{K_3}{K_1} - \left(\frac{K_2}{K_1} \right)^2 \right]^{1/2} \quad (9)$$

where $p_{t,B}$ is in pounds per square foot absolute. The system is seen to be oscillatory if the quantity K_2 is less than zero. The theoretical frequencies and stability regions are reported in reference 7 to agree reasonably well with experimental values.

When heat is added in the combustion chamber, the analysis becomes more complex. In this case, reference 7 assumes a constant rate of heat release. This part of the investigation, then, includes oscillations driven by a time-varying temperature profile at the exhaust nozzle and by a variable diffuser pressure recovery. The effect of heat addition is to further reduce the region of stable operation for a given configuration. A typical result is presented in figure 225 (ref. 7). This figure shows stability regions computed for isothermal as well as combustion conditions. The oscillation frequencies predicted were found in reference 7 to be considerably lower than those observed. The observed frequencies were sufficiently high that the possibility of standing-wave resonance should be considered.

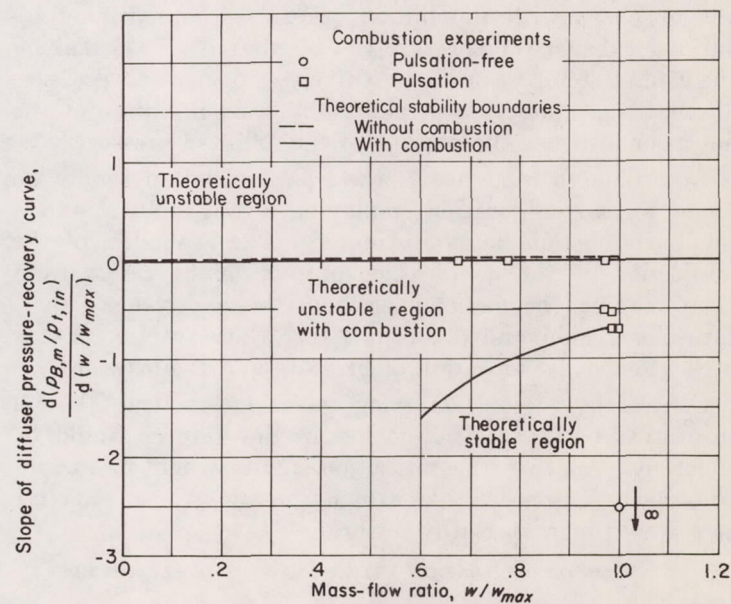


FIGURE 225.—Theoretical and experimental stability conditions of 16-inch ramjet using gasoline as fuel. Free-stream Mach number, 1.77 (ref. 7).

The third factor by which a Helmholtz oscillation may be driven is a variable exhaust temperature. Since the exhaust is usually choked, an increase in gas temperature produces a decrease in mass flow. The analysis of reference 7 does not deal with this effect alone. However, since the heat-release rate is assumed constant, the variation in exhaust temperature with mass flow can be considered to account for the decreased stability accompanying combustion (fig. 225).

In the actual engine, the stability depends on all three factors. Potential instability with respect to one may be overcome by the effects of the others. The analyses available are necessarily simplified, a mathematically rigorous treatment being impossible for a real engine. The stability criteria should nevertheless be indicative.

Departures from the idealized condition affect both the actual stability region and the actual frequencies. The effect of through-flow is included in the analyses; the effects of finite sound level, spatial temperature gradients, and non-linear performance of exhaust and diffuser have not been completely discussed. With respect to the stability criteria, the ultimate amplitude of the oscillation is probably not important. The criteria merely state that under certain conditions infinitesimal disturbances will be amplified. It is possible that additional instability will result from finite disturbances, or triggers; the effect of flow disturbance on heat release cannot be expected to remain linear at high amplitude.

To prevent the Helmholtz-type oscillation, the driving forces must be reduced or opposed. The driving force due to varying diffuser pressure recovery can be reversed by using a diffuser with an appropriate characteristic, that is, a diffuser whose pressure recovery decreases as the mass flow increases. The driving due to varying heat release can be reduced or reversed by (1) reducing the sensitivity of the combustion process to velocity or pressure fluctuations, and (2) bringing any residual perturbations as far as possible out of phase with the burner pressure. The driving by varying exhaust temperature can be altered by (1) making the exhaust temperature insensitive to velocity and pressure fluctuations, and (2) controlling the residence time of the hot gas and hence the phasing of the reflected pressure.

According to reference 7, the least oscillation should be found for a configuration employing a long diffuser and a small combustion-chamber volume. The reduction of the sensitivity of the combustion process might result from (1) removing the flameholder from the high-velocity perturbation region, and (2) using a fuel whose reaction rate is little affected by variation of pressure and temperature.

Control by viscous damping seems impractical, though theoretically a large friction loss in the diffuser would be effective. Another theoretical possibility would be to contrive a pressure-sensitive exhaust nozzle whose effective area would increase with pressure.

SYSTEMS OF OSCILLATION WITH NONACOUSTIC ELEMENTS

Two types of oscillations that occur in burners and can be amplified in a burner cavity are discussed in reference 8. The first is vortex shedding from cylindrical rods. The

frequency of vortex shedding from a cylindrical rod is given as

$$f = 0.185 \frac{U_s}{d_r} \quad (10)$$

Reference 8 found that the vortex shedding occurred with or without a residual flame burning in the rod wake, the frequency in both cases being quite close to the value calculated by equation (10).

Reference 9 shows that it is possible to excite vortex shedding where the flame is an attached fully developed V-flame in the wake of the flameholder, although the frequency in this case is about twice that given by equation (10).

When the frequency of vortex shedding coincides with the frequency of the supported cylindrical rod, the ensuing vibration is greatly amplified. This is the source of the musical note in the aeolian harp and is given a rather general investigation by Strouhal (discussed in ref. 2).

The second type of periodic disturbance due to unstable flows cited in reference 8 is an oscillation with a frequency allied with the flow velocity but not dependent upon flameholder dimension or duct length. This form of disturbance is probably due to the unstable shear region generated by a flame in a duct (ref. 10). In reference 9, a stability analysis of Scurlock's flow (ref. 10) was made, and it was found that the frequency (sec^{-1}) a flame would amplify most was

$$f = \frac{U_m}{W_{at}} \quad (11a)$$

In an experimental check on this result, reference 9 shows an anchored V-flame to be most sensitive to an imposed disturbance with frequency

$$f = \frac{2U_m}{W_{at}} \quad (11b)$$

The results of reference 8 give frequency more nearly equal to

$$f = \frac{3U_m}{W_{at}} \quad (11c)$$

The main point in all of this is to show that a frequency sensitivity exists for a flame anchored in a duct that could, when tuned to a resonant frequency of the burner cavity, excite a high-amplitude oscillation.

Another form of oscillation involving nonacoustic elements is discussed in reference 11. A flow disturbance in the combustion chamber created a pressure pulse that traveled upstream and modulated the rate of fuel flow from a fuel injector. The modulated fuel-air mixture then traveled downstream at stream velocity, arrived at the combustion chamber, caused a change in pressure in the combustion chamber, and sent a corresponding pressure pulse upstream to repeat the cycle. The frequency of oscillation for this type of nonacoustic vibration is given as

$$f = \left[2 \left(\frac{x}{U_s} + \frac{x}{a - U_s} \right) \right]^{-1} \quad (12)$$

where a is 1280 feet per second. Also discussed in reference

11 is a type of oscillation involving recurrent detonation originating in the boundary layer of a duct filled with a combustible mixture. The frequency of this type of oscillation can be determined from equations (1) and (2) of reference 11.

All these types of oscillations would be affected by the acoustic damping discussed previously; however, special treatment may be given these types of oscillations. For example, the physical structure of the offending strut can be modified either in its rigidity or in its size and location so that its natural frequencies differ from the excitable frequencies of the burner enclosure. For the second type of oscillation, the injection pressure can be increased to render the fuel-injection system relatively insensitive to small fluctuations in the combustor pressure. The oscillation involving recurrent detonation was controlled in reference 11 by the injection of chain-breaking additives in the boundary layer of the combustion chamber immediately downstream of the flameholder.

Reference 12 uses a quasi-one-dimensional plane-wave theory to express pressure-time relations in a buzzing ramjet. This isothermal pulsation is assumed to be triggered by flow separation in the diffuser. The consequent momentary reduction in mass flow is accompanied by a shift in the location of the normal shock and by pressure and rarefaction waves that propagate into the combustor. These waves are reflected back and forth between the exhaust and the diffuser as the engine pressure slowly regains its original value. Then the cycle repeats.

The characteristic of this type of instability is the non-sinusoidal nature of the perturbation of the inlet mass flow. For as much as 70 percent of the cycle this flow is constant. At any station in the combustion chamber, the pressure first undergoes a sharp decrease, then climbs slowly back to its original value, at the same time being modulated by the reechoing pressure-rarefaction couplets. Various predicted pressure-time curves are shown by reference 12 to correspond amazingly well with experimental ones (fig. 226).

This type of pulsation is not combustion-driven. It is of interest as a representative of nonsinusoidal vibration systems, analogous to the electronic relaxation oscillator. These systems differ from the sinusoidal oscillators in that not even an infinitesimal disturbance is needed to start the cycle.

INTERACTIONS

ELEMENTS DISTURBED BY VELOCITY AND PRESSURE OSCILLATIONS

The nature of steady flow through diffusers, around obstructions, through perforated liners, and particularly through the flame zone is poorly understood. Any attempt to describe processes that occur when pressure and velocity oscillations are superimposed on the steady flow may appear presumptuous. The fact remains, however, that in the combustor real oscillations do exist. Even though discussing the effects of these oscillations on the processes that take place in a combustor may be considered sheer speculation, it is felt that to speculate is potentially more profitable than to ignore.

There are a number of possible effects that combustor oscillations may have on the boundary layers existing in the various component parts of the burner. Some of the effects

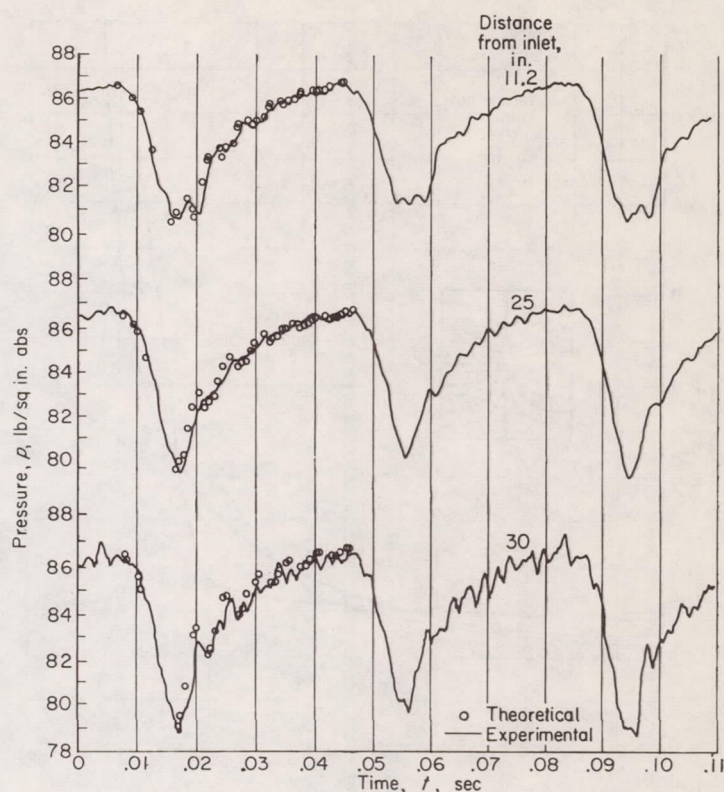


FIGURE 226.—Theoretical and experimental pressure traces for a simulated 34-inch-long ramjet, 3 cycles after onset of diffuser buzz without burning (ref. 12).

can be extremely violent, such as the increase in heat-transfer rate to the outer shell during screeching burning. A possible explanation for this effect is given in reference 3, which states that the velocity of the gas adjacent to the wall is increased during screech by means of the transverse mode of oscillation.

There is no clear-cut demonstration of the effect of oscillations on the over-all buildup and separation of a boundary layer on a straight wall. In some theoretical studies of boundary-layer growth, the amplification of disturbances of a sinusoidal nature has been considered as a possible explanation for the transition from a laminar to a turbulent boundary layer (ref. 13). Since, in most cases, the boundary layer in the combustion chamber will already be turbulent, the possible intermittent separation and attachment of a boundary layer should be considered. The synchronizing of the shedding of a bound vortex on a rod with duct oscillations has already been cited. Reference 10 states that, when a flame is seated on the rod, the vortices no longer shed but become bound and, in most cases, symmetric. The literature is not in unanimous agreement on this point. Reference 14 indicates that, near blowout, vortex shedding with combustion does occur. With combustor oscillations, there certainly seems to be evidence of something resembling vortex shedding in the wake of a flameholder, as can be seen from the excellent schlieren photographs of a simulated ramjet flame during screech in reference 15.

Of general interest regarding the influence of flow fluctuations on a vortex train in the wake of a cylinder with and without combustion is reference 16. Here, the following

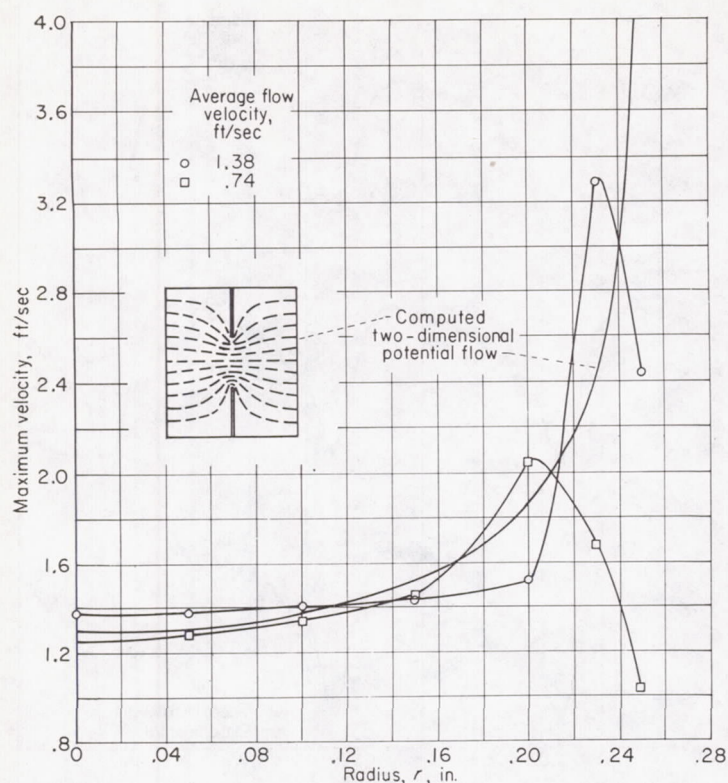


FIGURE 227.—Comparison of measured time-varying flow through flameholder with two-dimensional potential flow (ref. 5).

velocity profile is examined for neutral stability:

$$U = \mathcal{F}k \operatorname{sech}^2(\Phi y) \quad (13)$$

Equation (13) was found (ref. 17) to represent profiles of mixing plane jets and wakes. It was found that the disturbance vortices (for unsymmetric disturbances) formed two trains a distance h apart, alternately alined as in the Kármán vortex street. The relation between h and the distance λ between vortices in a single train is given in reference 16 as

$$\frac{h}{\lambda} = \frac{2}{\pi} \tanh^{-1} \frac{1}{2\Phi k}$$

whereas, for the Kármán street,

$$\frac{h}{\lambda} = \frac{1}{\pi} \tanh^{-1} \frac{1}{\sqrt{2}}$$

or the two agree if

$$\Phi k = \frac{1}{\sqrt{2}} \pm \frac{1}{2}$$

Since vortex occurrence in wakes is possibly connected to the stability of a mean wake profile, the problem can be further simplified by an approximation of the profile with a broken-line V-profile (ref. 9) and a study of the effect of density variations. It is found that the wavelength of the neutral disturbance of the V-profile is the same as for equation (13) when the V is of comparable

width, and that reducing the density of the wake gases has a stabilizing influence, but does not render the profile completely stable, at wavelengths large compared with the profile width. This is in qualitative agreement with the data of reference 10. The interaction, then, is this: Acoustic oscillations supply the initial amplitude to a flow disturbance in a wake, which subsequently grows, decays, or remains unchanged, depending on the wavelength of the disturbance.

In reference 18 the formation of the vortices was considered the key part in the driving of a transverse oscillation. It was argued that the vortex zone represented a zone of unusually intense mixing. The cycle of events was as follows:

- (1) Vortex formation at the flameholder
- (2) Intense mixing of hot exhaust products with combustible gases in the vortex
- (3) An ignition delay
- (4) A rapid burning of the mixed vortex charge phased so as to drive the oscillation.

Although the evidence presented to support the model is far from conclusive, it points to a kind of interaction that might admit to control by chemical and/or physical means.

In reference 5, a study was made of the superimposed steady and time-varying flow through a $\frac{1}{2}$ -inch-diameter thick-plate orifice. The thickness of the time-varying flow boundary layer depended on the Reynolds number of the steady component of the flow. The time-varying flow profile through the orifice was essentially that computable from the potential-flow theory, except for a thin boundary layer that depended on the Reynolds number of the steady flow, as shown in figure 227.

The effects of pressure and velocity oscillations on fuel flow and on mixing rates depend largely on the types of oscillations involved and the location and design of the fuel-injection systems. The pressure pulsations may directly modulate the fuel-flow rate during the oscillation. The major effect on the mixing rate, however, will be that of the time-varying velocity, which will be most strongly felt when the oscillation contains radial or transverse components.

Most studies to establish the fundamental nature of flame-stabilizing elements recognize that flow oscillations greatly affect the performance of flame stabilizers. Reference 10 reports that, when resonance is encountered, blow-out velocity data cannot be reproduced. The possibility of duct resonance in the study reported in reference 10 was removed by placing the flame stabilizer near the exhaust of the test duct so that only a small portion of the stabilized flame remained enclosed in the duct. A number of investigators mention the fact that increasing duct length appears to increase the instability of a burning engine. This trend is illustrated by unpublished NACA data in figure 228, which shows blowoff limits for several different velocities as a function of tailpipe length and fuel-air ratio. The factor affecting both the flame stability and the heat-release rate is the previously mentioned tendency of the time-varying flow to follow potential-flow streamlines. This tendency is shown by the sequence of photographs in figure 229. Thus,

a velocity disturbance at the flameholder, rather than separating at the downstream edge and allowing for a sheltered zone where recirculation may occur, will cause a penetration of this sheltered zone by an amount dependent upon the amplitude of the disturbance. The effect of this potential flow about the flameholder, then, will be (1) to hinder the recirculation in the wake of the flameholder by an inclusion of cold gas and (2) to extend the flame-front area at the flameholder, this extension then flowing downstream at about stream velocity.

It is felt that the wrinkling of a flame front at a flameholder is one of several ways in which the flame area or the heat release may be varied during an oscillation. The sequence of photographs (ref. 5) in figure 229 shows the time history of a wrinkle from its generation at a flameholder to its disappearance at the flame tip.

Reference 19 points out that the stability of a hot-cold interface is markedly affected by the accelerations occurring during acoustic resonance. The effect of acceleration is to destabilize if the acceleration vector has the same direction as the density gradient (refs. 20 and 21).

Data of reference 19 show that a flat flame breaks periodically into cellular flamelets in a resonating tube in phase with the gas acceleration. The phase relation required by the Rayleigh criterion for driving standing waves by heat addition is thus met. The oscillations and the cells occurred in all fuel-air mixtures tested, but amplitudes were greatest in those mixtures in which cells formed spontaneously; that is, in downward-propagating flames that were unstable in spite of the stabilizing effect of gravity.

To treat this problem theoretically, a periodically varying acceleration was substituted for the gravity acceleration in the flame-front stability equations (ref. 19), and remarkably good agreement with experiment was achieved. The same sort of substitution can be made in the stability analyses of references 20 and 21, in which a continuous velocity distribution is assumed parallel to a sequence of discontinuities in densities.

One general conclusion might be drawn from these stability considerations: The flame front can be desensitized if the density gradients are not parallel to probable acceleration vectors.

Some of the oscillations encountered in jet engines reach such violence that it is possible that large reaction-rate changes accompany the oscillations. Whatever the direct cause of the increase in reaction rate, the oscillation is certainly conducive to high performance in some cases. For example, reference 6 showed that during a screech condition the combustion efficiency for a simulated afterburner was 92 to 98 percent, dropping to 65 percent with the cessation of screech. The effects of oscillations on nozzle and diffuser performance are to date unknown.

A few general remarks may be made about the location of the disturbed elements. It has been shown that in some cases a velocity fluctuation causes the sensitive element to be disturbed; whereas, in other cases the pressure fluctua-

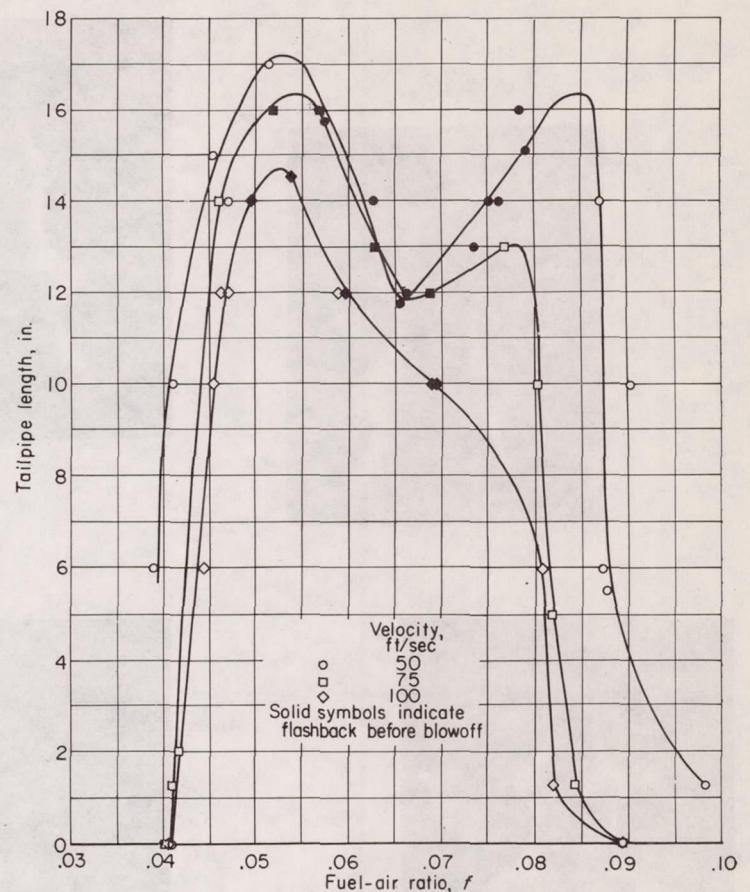


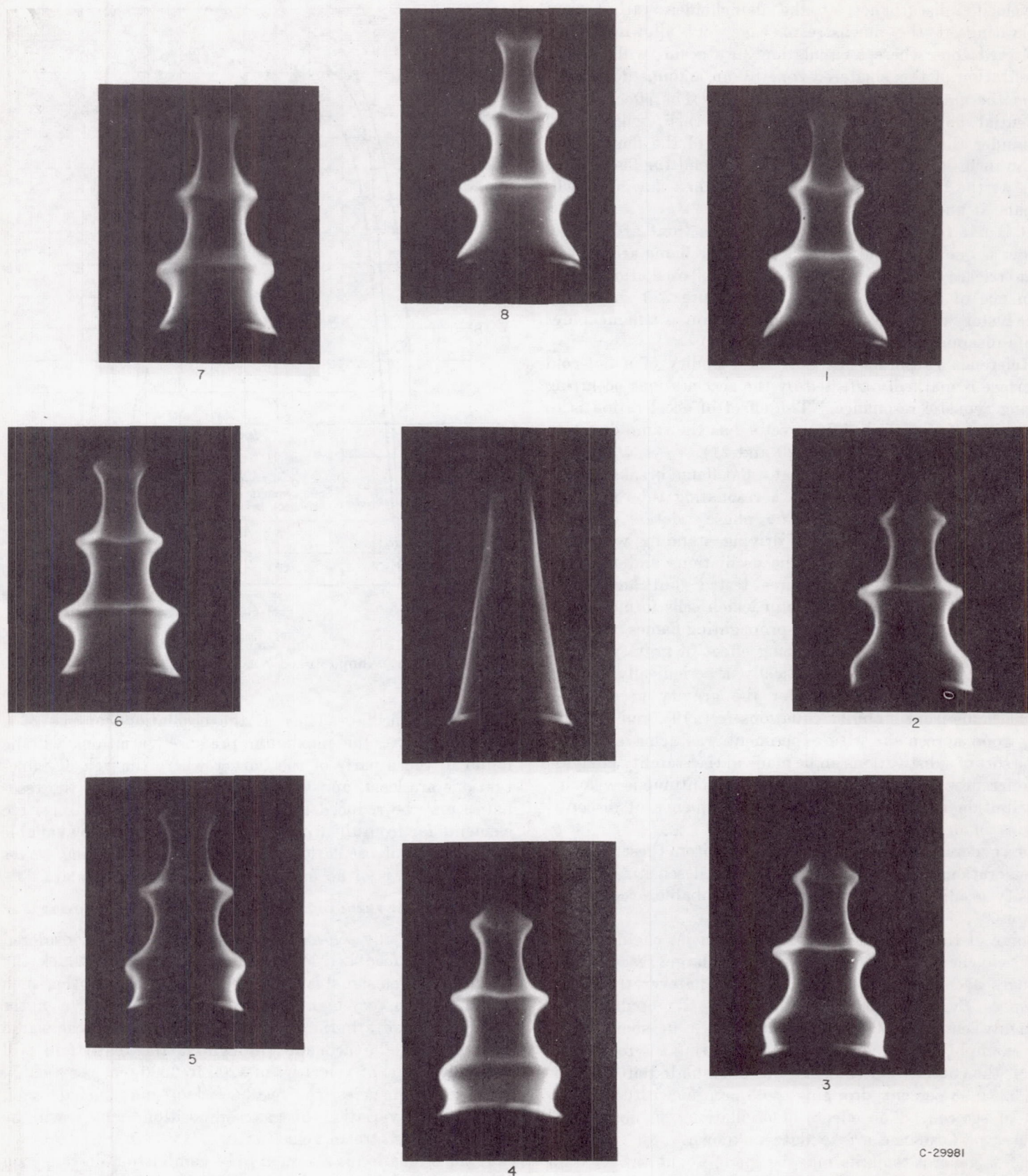
FIGURE 228.—Blowoff limits for 1-inch-diameter ramjet engine (unpublished NACA data).

tion is responsible. Thus, if the oscillation consists of a standing wave, the maximum pressure variations will be found in those parts of the burner where the velocity fluctuations are least, and vice versa. In this case, the resonance may be reduced by judicious location of the sensitive elements far from their exciters. Such a remedy is available if the mode of oscillation is one in which standing waves dominate but is of no use if traveling waves dominate.

EFFECTS OF FEEDBACK LOOPS ON PRESSURE AND VELOCITY

In general, any self-excited oscillation may be considered to involve a feedback loop; that is, a means by which the effect of a given signal is ultimately to generate another such signal. When very high frequency oscillations (wavelengths on the order of a burner diameter) are involved, the signal will probably be acoustic throughout the cycle and will therefore travel at velocities of 1200 to 3000 feet per second. At lower frequencies, the feedback loop may include such elements as variation of gas composition, which will be transported at stream velocities.

If the oscillation is assumed to be combustion-driven, each cycle will include a variation of heat release that may be either local or over-all. This variation will, in turn, produce pressure and velocity waves moving upstream at a



C-29981

FIGURE 229.—Sequence of flame shapes for one cycle at intervals of time. Time increases clockwise; frequency, 329 cps; velocity, 1.378 feet per second; fuel-air ratio, 0.080 (ref. 5).

speed $a_{in}(1-M_{in})$, and downstream at $a_{out}(1+M_{out})$. A composition and a temperature irregularity will also be generated and will move downstream at a velocity $a_{out}(M_{out})$. The problem then becomes one of defining the possible methods whereby these waves can produce subsequent changes in the heat-release rate.

If the gas velocity is sonic at the exhaust, an impinging pressure wave will reflect, and a pressure wave will then propagate upstream. A momentary increase in temperature, on the other hand, will be transformed into a rarefaction wave traveling upstream. These waves may affect the heat release as they pass through the combustion zone by modifying the pressure and temperature therein, or they may have an indirect effect after passing through the combustion zone. In the latter case, the effect of sound waves traveling upstream from the combustion zone may be considered, regardless of whether the waves originate in the time-varying combustion or whether they have already reflected from the exhaust nozzle. Such waves may affect the subsequent heat-release rate in many ways, among which are (1) changing the flame area as the wave passes the flameholder, (2) changing the velocity profile upstream of the flameholder, (3) altering the local fuel-air ratio as the wave passes the fuel injectors, (4) altering the mass-flow rate into the diffuser, and (5) reflection from the inlet diffuser followed by any of the aforementioned interactions.

This summary of possible interactions is intended to be suggestive rather than exhaustive. Additional signal channels such as the shedding of vortices, mechanical vibration, and modulation of fuel spray or fuel evaporation characteristics should be noted.

The fundamental frequency for any loop can be determined as the reciprocal of the time required for the signal to travel the loop:

$$f = \left(\sum U_i l_i \right)^{-1} \quad (14)$$

Although it is impossible to assign a given loop definitely to a known frequency, it is possible to eliminate from consideration those channels requiring unduly long or short intervals. Some caution is necessary; if various channels are simultaneously active, the frequency need not be the fundamental of all and may not be the fundamental of any. It is highly probable that, with the multiplicity of potential feedback loops, many may contribute to any given frequency of oscillation. It is likely that the mode of resonance selected by the burner will be that for which the energy released from the individual feedbacks is greatest.

All the feedback loops considered have one element in common: The signal is carried upstream as an acoustic wave. This suggests the possibility of controlling these oscillations either by damping this wave or by desensitizing the elements it will affect. One method of damping might be to provide channels of varying acoustic length from the flameholder to the region of interest, so that the original wave would be broken down into a series of smaller waves arriving one after another.

The case of oscillation of very high frequency can be considered analogous, except that the signal may be propagating transversely for much of the cycle.

SIGNIFICANCE OF RESONANCE STUDIES IN DESIGN OF JET-ENGINE COMBUSTORS

DESIGN CRITERIA BASED ON MODE OF RESONANCE

The application of results of resonance investigations to the design of jet-engine combustors is somewhat limited because of the opposing requisites for good combustion and less resonance. From acoustic considerations, the features of current combustors are more likely to produce than to reduce resonance. Current designs are symmetrical, smooth, hard, and uniform. On the other hand, less resonance would be anticipated if no two surfaces reflected waves alike, absorbed waves alike, nor had parallel walls. The optimum combustor design must necessarily be a compromise between the two extremes.

In the actual design of the combustor, the simplest rule to apply would be to acoustically soften those parts of the combustor where possible modes of oscillation would have pressure maximums. Thus, for the longitudinal wave, the softened part of the burner should be at the terminations and at the walls near the terminations. For transverse modes of oscillation, the wall surrounding the region where the transverse oscillation might occur would be indicated. If the walls are softened by use of some sound-absorbing material such as filaments of glass or steel wool behind a perforated shell, it might be well to place such sound-absorptive material in a random distribution of patches, random both in size of patch and in location upon the wall.

If the flame is driving the oscillations, and it appears that this is the case in a large number of instances, it is well to keep the flame away from regions where the pressure goes through its maximum excursion. This means that the maximum reaction zone should be kept away from pressure loops in the standing wave, away from the terminating ends of the combustor in the case of longitudinal standing wave, and away from the wall in the case of transverse standing wave. If the combustor is of such a nature that stratification of hot and cold gases is implicit in the design, such hot and cold patches might be sized and spaced to act as sources of wave interference.

After measures to reduce oscillations have been applied, it may be found that a given combustor still oscillates at particular operating conditions. If the mode of this oscillation can be identified, corrective measures specific to that mode may then be applied. Table XXXI gives a summary of corrective measures for specific modes of oscillation.

DESIGN CRITERIA BASED ON SENSITIVITY OF DISTURBED ELEMENTS

If a component part of the combustor such as the flameholder is a sensitive element in the feedback loop causing the self-excited oscillation, at least one design criterion can be employed. If the element is sensitive to velocity or pressure, it can be moved from the locus of maximum velocity

TABLE XXXI.—SUGGESTED METHODS FOR CONTROLLING VARIOUS TYPES OF OSCILLATION

Type of oscillation	Control possibilities
Resonance:	
All modes.....	Use of a fuel whose burning rate is not responsive to pressure and velocity fluctuations.
Longitudinal.....	Absorption by tuned resonators. Absorption of sound at burner terminals. Stratification of flow to give transverse variation of acoustic speed.
Radial.....	Absorption of sound at burner wall or burner center. Diffraction and reflection from temperature variations (transverse).
Transverse.....	Nonreactive layer at wall and center. Absorption of sound at burner walls.
Helmholtz.....	Nonreactive layer near wall. Diffuser design for negative pressure recovery against flow slope. Long diffuser. Small combustion chamber. Controlled residence time.
Nonacoustic feedback:	
Modulated fuel flow....	Increased injection pressure. Increased mixing length.
Modulated fuel-air ratio..	Increased mixing length. Location of fuel injectors away from time-varying velocities.
Vortices shed from upstream obstruction.	Streamlining of obstructions. Location of obstructions farther upstream.
Flow-separation modulation.	Location of obstructions out of line with flameholder. Design to prevent separation. Removal of separation wake from reaction zone.
Relaxation oscillation..	Supercritical operation.
Detonation in boundary.	Nonreactive boundary layer. Addition of chain-breaking substance to boundary.
Temperature distribution reflections (exhaust).	Extra mixing for flat exhaust-temperature profile.

or pressure excursion. Other remedies equally as obvious would be either to desensitize the sensitive element completely or to shift its sensitivity to a frequency range that does not correspond to a possible mode of oscillation in the combustor. Some sensitive elements can be desensitized. For example, a fuel-injection nozzle that can be influenced by pressure pulses could be desensitized by increasing the pressure drop across the injector. A fuel-air mixture could be desensitized by the selection of either a new fuel or a fuel additive that would cause a diminished response of the combustion process to disturbances in pressure and temperature.

THE FUTURE FOR COMBUSTION OSCILLATION

There is an ever-growing group of workers who believe that combustor oscillation has evidenced such impressive advantages that a far more profitable course to follow would be to study the control and use rather than the elimination of oscillation. Measurements indicate that a work cycle over and above the steady-state work cycle is involved in

the oscillatory motion; therefore, there is clearly a large quantity of energy added to the gas in part in the form of additional mixing. Combustors designed to operate at low over-all fuel-air ratios have been shown to perform best if the combustion occurs in mixtures near stoichiometric with the combustion products subsequently diluted with the remainder of the air. The screech cycle might well be used to expedite this mixing. It is not clear how much of this extra energy is directly available for producing thrust.

Reference 6 shows that in the case of screech the maximum pressure amplitude in a transverse oscillation occurred in a very short region relative to the over-all length of the combustor. If the burner were strengthened only in this region to allow for continuous operation without shell failure (ref. 22), the increased combustion efficiencies accompanying screech might be retained without a prohibitive weight penalty.

In reference 9 it was found that oscillations introduced at the flameholder could increase the heat-release rate of an inefficient burner by 30 percent with a sound level in the duct a benign 93 decibels. For such a technique the benefits of screech might be realized without need for increased structural strength. Oscillations in combustors have appeared in many forms since the advent of jet propulsion. It would seem a safe guess that still more and different appearances lie ahead. A great deal of work on momentum and mass transport, combustion, and allied subjects in an unsteady nonhomogeneous flow field is needed before the current and future oscillations in combustors can be intelligently handled.

REFERENCES

1. Morse, Philip M.: *Vibration and Sound*. McGraw-Hill Book Co. Inc., 1936.
2. Rayleigh: *The Theory of Sound*. Vol. II. Dover Pub., 1945.
3. Smith, R. P., and Sprenger, D. F.: *Combustion Instability in Solid-Propellant Rockets*. Fourth Symposium (International) on Combustion, The Williams & Wilkins Co., 1953, pp. 893-906.
4. Moore, Franklin K., and Maslen, Stephen H.: *Transverse Oscillations in a Cylindrical Combustion Chamber*. NACA TN 3152, 1954.
5. Blackshear, Perry L., Jr.: *Driving Standing Waves by Heat Addition*. NACA TN 2772, 1952.
6. Blackshear, Perry L., Jr., Rayle, Warren D., and Tower, Leonard K.: *Study of Screeching Combustion in a 6-Inch Simulated Afterburner*. NACA TN 3567, 1955.
7. Sterbentz, William H., and Evvard, John C.: *Criteria for Prediction and Control of Ram-Jet Flow Pulsations*. NACA TN 3506, 1955.
8. Shonerd, David E.: *Studies of Flame-Front Oscillations*. Rep. No. 3-18, Jet Prop. Lab., C.I.T., June 4, 1952.
9. Blackshear, Perry L., Jr.: *Growth of Disturbances in a Flame-Generated Shear Region*. NACA TN 3830, 1956.
10. Scurlock, A. C.: *Flame Stabilization and Propagation in High-Velocity Gas Streams*. Meteor. Rep. 19, Fuels Res. Lab., M.I.T., May 1948. (Contract NOrd 9661.)
11. Fenn, J. B., Forney, H. B., and Garmon, R. C.: *Burners for Supersonic Ramjets*. Ind. and Eng. Chem., vol. 43, no. 7, July 1951, pp. 1663-1671.
12. Trimpi, Robert L.: *An Analysis of Buzzing in Supersonic Ram Jets by a Modified One-Dimensional Non-Stationary Wave Theory*. NACA RM L52A18, 1952.

13. Shubauer, G. B., and Skramstad, H. K.: Laminar-Boundary-Layer Oscillations and Transition on a Flat Plate. NACA Rep. 909, 1948. (Supersedes NACA WR-8.)
14. Nicholson, H. M., and Field, J. P.: Some Experimental Techniques for the Investigation of the Mechanism of Flame Stabilization in the Wakes of Bluff Bodies. Third Symposium on Combustion and Flame and Explosion Phenomena, The Williams & Wilkins Co., 1949, pp. 44-68.
15. Kaskan, W. E., and Noreen, A. E.: High Frequency Oscillations of a Flame Held by a Bluff Body. Trans. ASME, vol. 77, no. 6, Aug. 1955, pp. 885-891; discussion, pp. 891-895.
16. Savic, P.: On Acoustically Effective Vortex Motion in Gaseous Jets. Phil. Mag., ser. 7, vol. 32, Sept. 1941, pp. 245-252.
17. Bickley, W. G.: The Plane Jet. Phil. Mag., ser. 7, vol. 23, no. 156, Apr. 1937, pp. 727-731.
18. Rogers, Don E., and Marble, Frank E.: A Mechanism for High-Frequency Oscillation in Ramjet Combustors and Afterburners. Jet Prop., vol. 26, no. 6, June 1956, pp. 456-462.
19. Markstein, George H.: Instability Phenomena in Combustion Waves. Fourth Symposium (International) on Combustion, The Williams & Wilkins Co., 1953, pp. 44-59.
20. Taylor, G. I.: Effect of Variation in Density on the Stability of Superposed Streams of Fluid. Proc. Roy. Soc. (London), ser. A, vol. 132, Aug. 1, 1931, pp. 499-524.
21. Goldstein, S.: On the Stability of Superposed Streams of Fluids of Different Densities. Proc. Roy. Soc. (London), ser. A, vol. 132, Aug. 1, 1931, pp. 524-548.
22. Truman, John C., and Newton, Roger T.: Why Do High-Thrust Engines Screech? Aviation Age, vol. 23, no. 5, May 1955, pp. 136-143.

CHAPTER IX

SMOKE AND COKE FORMATION IN THE COMBUSTION OF HYDROCARBON-AIR MIXTURES

By ROSE L. SCHALLA and ROBERT R. HIBBARD

INTRODUCTION

There has been no consistent usage of the terms smoke, soot, carbon, carbon deposits, or coke in referring to the solid products arising from the incomplete combustion of hydrocarbon fuels. In studies of single combustors and engines, the solids discharged with the exhaust gases are usually called smoke, and those deposited in the combustion chamber are usually called carbon, carbon deposits, or coke. Since the so-called carbon and carbon deposits are not chemically pure, the word carbon is restricted herein to the pure element. Therefore, for combustor work, smoke is defined as the solid discharged with the exhaust gases and coke as the material that adheres to the combustor walls.

Deposition of coke and formation of smoke are both undesirable in the operation of turbojet combustors. Of the two factors, coke deposition presents the more serious problem because of its adverse effect on combustor performance and life. Excessive smoke has no effect on the engine but does offer a military tactical problem, in that the presence of a smoke trail facilitates aircraft detection in combat. Under very severe conditions, smoke may hamper landing-field operations or become a nuisance to personnel. The loss in fuel heating value attributable to smoke and coke is unimportant, even under the worst conditions. For example, the heaviest coke deposits found in single-combustor tests in reference 1 amounted to only 26.7 grams for 1240 pounds of fuel, or a loss of heating value of 0.004 percent due to coke deposits. Similar calculations have not been made for the loss due to smoke, but probably there is no loss in combustion efficiency attributable to smoke.

In continuous-combustion engines, the tendency to form coke or smoke varies more among petroleum-derived fuels than does any other combustion property. There is very little difference in the fundamental flame velocity, minimum ignition energy, flammability limits, quenching distance, flame temperature, or heat of combustion for various batches of fuel supplied under a single specification or even for fuels meeting different specifications. However, wide differences may occur in the coking and smoking tendencies of jet fuels.

In addition to coke and smoke considerations, the effect of fuel composition on flame radiation may also be important. Carbon is the only solid that can be formed in the combustion of hydrocarbons; and this solid can, under some burning conditions, greatly affect the amount of radiation emitted by a flame. Radiative heat transfer is an important consideration in engine design and, along with coking and smoking tendencies, becomes increasingly important with high-compression engines.

The control of coke and smoke and of heat-transfer factors in turbojet engines has been accomplished by proper combustor design and by the control of certain fuel properties. However, in this field of combustion research, a fruitful laboratory study of fundamental factors may yield an understanding that would facilitate engine design. Many investigations have been conducted on both the fuel and the flame environmental factors contributing to smoke and coke. The greater part of this work has dealt with burning in the gas phase and therefore with the formation of smoke. From such work, the fuel factors affecting smoking tendency have been fairly well defined. Relatively little has been done on a laboratory scale regarding coke formation because of the difficulties in simulating the engine conditions in which liquid fuel impinges on hot metal in the presence of flame and flowing gases. This chapter summarizes the laboratory phases of smoke and coke formation and describes the properties of these materials, the effect of variables on the formation of smoke and coke, and the chemical mechanisms proposed for their formation.

PHYSICAL AND CHEMICAL NATURE OF SMOKE AND COKE

SMOKE

Luminous hydrocarbon flames, distinct from so-called nonluminous ones, emit a yellow radiation that has a black-body energy-wavelength distribution. This black-body distribution can be emitted only by solids. The only possible solid products from hydrocarbon combustion are either carbon or materials containing very high percentages of carbon. The presence of such materials in luminous flames is confirmed by the deposits formed on a cold probe passed through such a flame. Under some conditions, the solids are released from luminous flames as smoke.

These materials are formed during the combustion of hydrocarbons only when the system is fuel-rich, either over-all or locally. Therefore, the most familiar types of solid-forming combustion processes are the candle or wick-lamp diffusion flames, where fuel alone is released locally and burns after diffusive mixing with oxygen. These hydrocarbon diffusion flames are always luminous at atmospheric pressure and are often smoky. Premixed fuel-oxidant systems, such as the Bunsen burner, are not luminous unless they are operated fuel-rich over-all. For example, in reference 2 premixed benzene-air flames were found to be luminous only when the equivalence ratio exceeded 1.4 and to be smoky only at higher ratios.

The smoke released during smoky combustion is not pure carbon but has been shown by chemical analysis to be a combination of carbon, hydrogen, and oxygen. A typical

analysis (ref. 2) shows 96.2 percent carbon and 0.8 percent hydrogen, with the remainder believed to be oxygen. Similar results have been obtained in the analysis of carbon blacks, which are the products of smoky combustion in diffusion flames.

Hydrocarbon-derived smoke is crystalline on a submicroscopic scale. X-ray diffraction studies show the basic element to be a crystallite with a major edge length of about 20 angstroms (ref. 3). The atomic structure consists of several layers of distorted hexagonal lattices, with the lattice substantially the same as that found in the graphite form of carbon. The distortion is believed to be due to the presence of about 1 atom of hydrogen for every 10 atoms of carbon, and the preceding elemental analysis has approximately this hydrogen-to-carbon atom ratio.

When the same smoke was examined by electron microscopy (ref. 2), these crystallites were shown to be agglomerated into nearly spherical particles of 0.01 to 1.0 micron (100 to 10,000 Å) diameter. These spheres, produced in a burner under a single set of conditions, were quite uniform in diameter and clung together to form an open, lace-like structure.

Although the turbojet combustor operates with an overall fuel-lean mixture, a large amount of the burning reaction takes place in locally fuel-rich regions. These regions are present because all the fuel enters the upstream end of the combustor, whereas the air-entry holes are distributed along the full length of the combustor. Flame in the rich upstream end is highly luminous under many operating conditions, and the environment in this region should be conducive to the formation of large amounts of smoke. Since only small amounts of smoke, if any, are exhausted from most turbojet engines, it appears that much of the smoke probably produced in the upstream end of the combustor is consumed in passage through the burner.

In reference 2, the capacity of laboratory flames in the burning of smoke was studied, and a stream of smoke, freshly produced by a diffusion flame, was easily burned by a secondary Bunsen flame. High concentrations of smoke can be consumed in this manner. This is apparently confirmed by electron micrographs of turbojet combustion smoke, in which the particles look like partially eroded spheres (ref. 2). Their appearance suggests that spherical smoke particles are generated in the engine primary zone and that these particles are largely burned away in passing through the engine.

COKE

The coke found in turbojet combustors varies in nature from soft, fluffy material to hard, brittle deposits. Typical analyses of these types (ref. 4) show the soft coke to contain 80.0 percent carbon and 2.0 percent hydrogen, and the hard coke to contain 92.4 and 1.6 percent of carbon and hydrogen, respectively. The remainder is believed to be mostly oxygen and a small amount of sulfur. Unpublished NACA data show that the sulfur content of combustor cokes varies with the sulfur content of the fuel. For example, coke-deposition tests were run on a fuel containing 0.05 percent sulfur and

on the same fuel to which alkyl disulfides were added to raise the sulfur content to 1.00 percent. The amount of coke formed was substantially the same for both fuels, but the sulfur contents of the cokes were 0.7 and 2.4 percent, respectively. Unpublished NACA data also show that combustor cokes contain 25 to 50 percent of material that is soluble in carbon disulfide. This soluble material contains aromatic rings and a considerable amount of carbonyl oxygen, as indicated by infrared examination of the extract.

X-ray diffraction studies indicate that combustor coke has some of the crystalline character described for smoke. Electron microscopy (ref. 4) indicates that the soft coke consists of nearly spherical particles imbedded in an amorphous matrix. However, the hard coke is a vitreous material with no perceptible microstructure.

EFFECT OF OPERATING VARIABLES ON SMOKING TENDENCY

BURNER GEOMETRY

Diffusion flames.—The two principal types of apparatus used to study the smoking tendency of diffusion flames are the wick lamp and the conical or open-cup burner. Of these two methods, the wick lamp has been used more extensively; however, the exact design of this lamp has varied appreciably from one investigation to another. The Davis factor lamp was one of the earliest wick lamps to be developed (1926). This lamp was later modified (ref. 5) and used for smoking-point determinations as recently as 1953 (ref. 6). In 1935 a test lamp (ref. 7) was standardized by the Institute of Petroleum Technologists (I.P.T.) and has been employed by several investigators (refs. 8 and 9). This I.P.T. lamp is used in the current United States military fuel procurement specifications. The fairly simple lamp shown in figure 230 is a combination of the Davis apparatus and the I.P.T. lamp (used in ref. 10). A comparison of the data obtained with the various wick lamps and accessory equipment indicates that smoking tendencies depend on the geometry of the apparatus and that no simple comparison can be made between smoke-point data obtained with different lamps.

The conical or open-cup lamp is often referred to as the wickless lamp, since the flame burns directly from the top of a pool of liquid fuel contained in a shallow funnel or cup-shaped vessel. Development of the wickless burner is described in reference 11, and similar burners have been used for investigations reported in references 12 and 13.

The main advantage of the wickless lamp is that it can be used for the comparison of less smoky fuels, since flame heights up to 450 millimeters may be measured; whereas, the Davis wick lamp is limited to 102, and the I.P.T. lamp to about 50 millimeters. A comparison of the I.P.T. lamp and the wickless lamp (ref. 9) shows that the smoking points of various fuels measured by the two methods gave a fair correlation, but the correlation appeared logarithmic rather than linear. Reference 9 reports that the wickless lamp is much more difficult to operate than the I.P.T. lamp and recommends that it be used only when the range of the I.P.T. lamp is exceeded.

With all types of diffusion burners, the flame is enclosed by a glass tube that acts as a chimney and keeps the flame erect and stable. The size and position of this chimney greatly influence the smoking point of the flame.

The general procedure in using any of these lamps is to increase the fuel flow until the flame just begins to smoke. The smoke point may be detected visually, or an ice-cooled porcelain surface may be placed above the flame to collect and indicate the presence of smoke. A measure of the smokiness of the fuel may be made in several ways. The technique usually employed is to measure the maximum height to which the flame will burn without smoking; however, in two investigations (refs. 2 and 9), measurements were made of the maximum rate at which fuel can be burned without smoking. A comparison of the two techniques (ref.

9) indicates that the maximum burning rate is readily obtained and is more reproducible than the smoke-height test. It also represents more closely the information desired by the test, namely, the relative amount of fuel that can be burned under standardized conditions before smoke becomes a problem. Only when illumination is concerned does the height of the flame become a significant factor. The smoke-height test, however, is somewhat more convenient to use and therefore has been adopted in the ASTM procedure. Another method (ref. 12) is to pass a light beam through the chimney in which the smoke is issuing from the flame. A photoelectric cell indicates the amount of light absorbed and, consequently, a measure of the smokiness of the fuel. Also, the smoke issuing from various aromatic fuels burning at a given fuel flow has been collected and weighed (ref. 13). The greater the amount of smoke collected, the higher the smoking tendency of the fuel.

As previously stated, the smoke point is generally determined by measuring the maximum height or maximum fuel rate at which the flame will burn without smoking. The higher the flame or the greater the fuel-flow rate, the lower the tendency for that fuel to smoke. Consequently, the smoking tendency is an inverse function of the flame height or fuel flow. Reference 14 defines smoking tendency S as equal to a constant k over the maximum flame height b_F (in millimeters) and assigns the value of 320 to k :

$$S = \frac{k}{b_F}$$

The value of k is unimportant in the following discussion, but the distinction between maximum flame height and the concept of smoking tendency should be noted.

Bunsen flames.—The smoking tendencies of Bunsen flames are reported in references 2, 12, and 15. In reference 15 a continuous-flow apparatus was used in which steady streams of both volatile and nonvolatile fuels could be mixed with air either as vapors or as mist droplets, according to their vapor pressures. The fuel-air mixture was passed up a vertical tube after generation and burned on top in primary air only. The composition of the mixture was determined by analyzing the exhaust gases.

In the investigations reported in references 2 and 12 the fuel was metered from a burette and mixed with metered air. The premixed fuel and air were then burned from a tube surrounded by a glass tube chimney. The effect of varying the burner-tube inside diameter from 6 to 9 millimeters was investigated in reference 2, which showed that the smoking tendency was slightly reduced as the burner-tube diameter was decreased. The influence of chimney length, diameter, and position with respect to the flame was also reported in reference 2. Increasing the chimney length from 120 to 500 millimeters caused a reduction in smoking tendency. Changes in the diameter and position of the chimney gave varied results, depending on the convection in the chimney. In general, all chimney variables that reduced smoke formation did so by generating a flue effect which tended to flow more air around the flame. If the burner tube was ducted so that a controlled secondary-air flow could be passed by the flame, the smoking tendency was reduced as the secondary-air flow was increased.

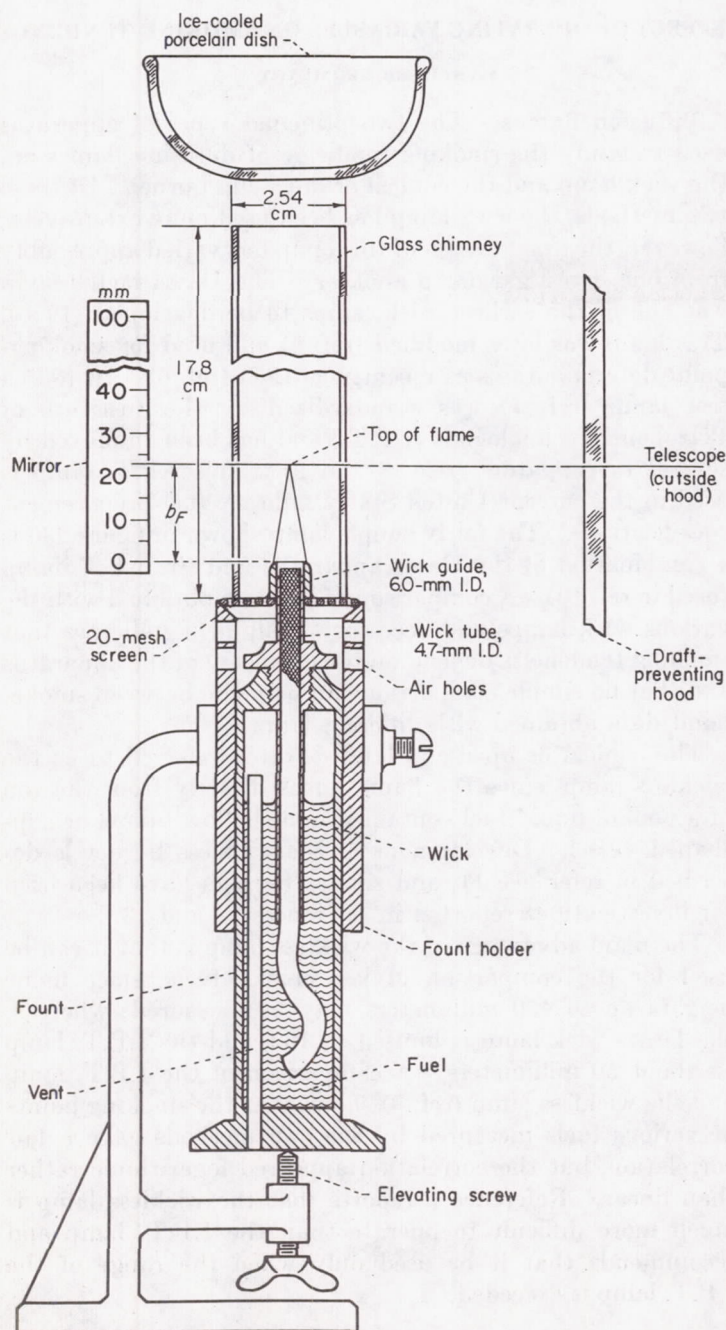


FIGURE 230.—NACA modified Davis factor lamp (ref. 10).

FUEL-AIR RATIO

Diffusion flames.—The effect of over-all fuel-air ratio on the smoking tendency of laminar diffusion flames has been investigated by two different techniques. In reference 13, the air supply past the flame was maintained constant and the smoke issuing from the flame was collected at various increasing fuel flows. A plot of the smoke deposit against the fuel-air ratio is shown in figure 231. Since the airflow was constant, the ordinate is essentially a measure of the fuel flow. As shown in this figure, the initial increase in fuel flow produces a sharp increase in the amount of smoke collected. As higher fuel flows are reached, the amount of smoke produced appears to level off.

In another controlled-air study with diffusion flames (ref. 2), the airflow rate past the flame was increased by gradual steps, and a determination was made of the maximum rate at which the fuel could be burned without smoking at each given airflow. In figure 232, the maximum fuel rate for smoke-free burning is plotted against the airflow rate for eight pure hydrocarbon fuels. With initial increases in airflow, the maximum smoke-free fuel flow increases pro-

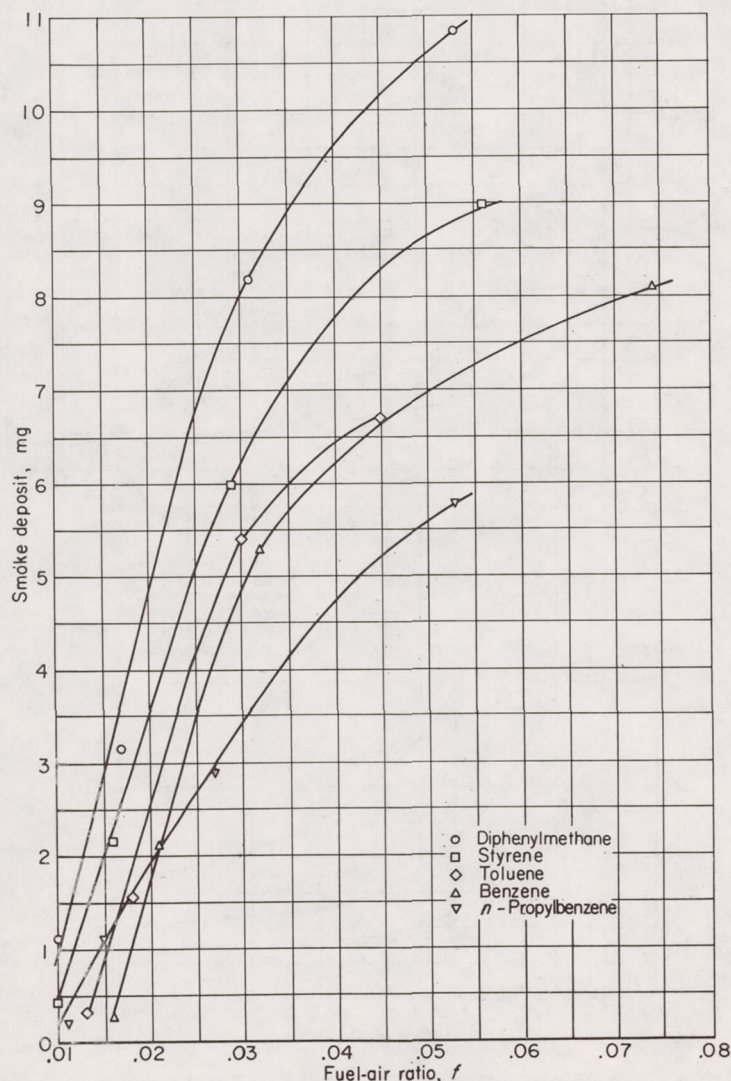


FIGURE 231.—Variation of carbon deposit with fuel-air ratio for several fuels burning as diffusion flames. Airflow past flame, 10 liters per minute (ref. 13).

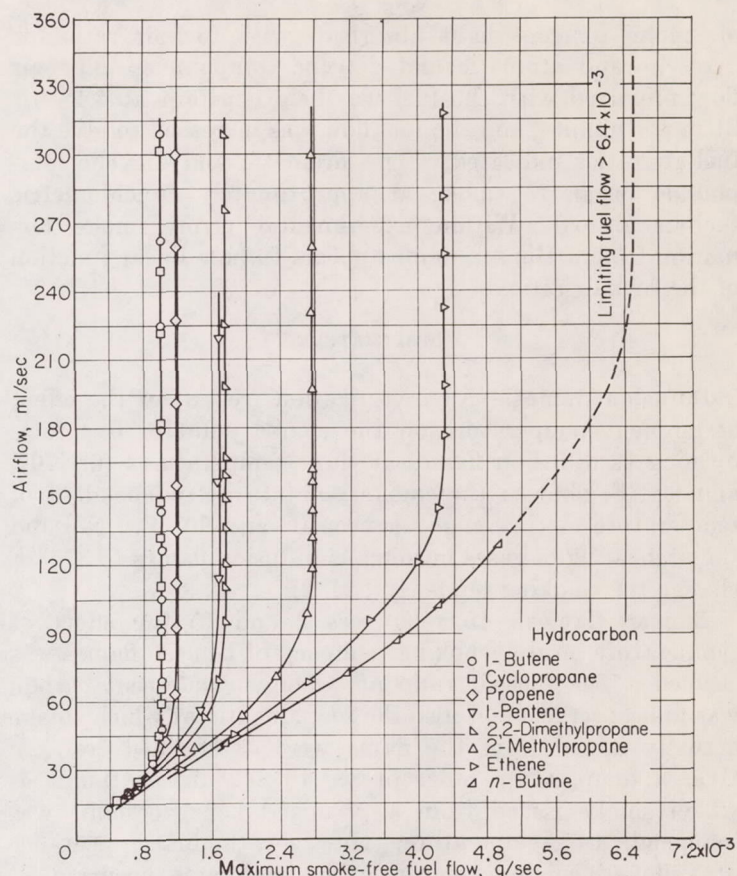


FIGURE 232.—Variation of smoke-free fuel flow with airflow (ref. 2).

portionally, but eventually a limiting fuel flow is reached at which further increases in airflow past the flame do not permit more fuel to burn smoke-free.

Bunsen flames.—The effect of fuel-air ratio on smoke formation from Bunsen flames is reported in reference 12. A measure of the smoke density of the fuel was made by passing a light beam through the chimney in which the smoke was issuing from the flame. A photoelectric cell indicated the amount of light absorbed as a measure of the smoke formation. In this burner, the paraffins, cycloparaffins, and olefins, with the exception of triisobutylene, could not be made to smoke even at the maximum fuel-air ratio that would support combustion. Figure 233 shows the variation

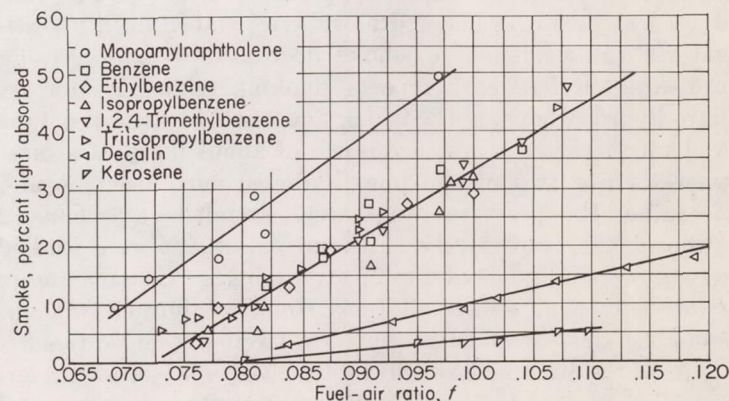


FIGURE 233.—Variation of smoke with fuel-air ratio for several fuels burning as Bunsen flames. Airflow, 4.1 liters per minute (ref. 12).

of smoke (percent light absorbed) with fuel-air ratio for kerosene and aromatic and dicyclic compounds. The air flow premixed with the fuel was held constant at 4.1 ± 0.1 liters per minute, and the fuel flow was increased to give the fuel-air ratios indicated. The aromatic and dicyclic compounds began to smoke at approximately stoichiometric fuel-air ratios. Within experimental error, smoke formation from a Bunsen flame appears to be a linear function of the fuel-air ratio.

TEMPERATURE

Diffusion flames.—An investigation (ref. 8) of the effect of ambient temperature on the smoke point of five fuels burning as diffusion flames at three temperatures (0° , 70° , and 90° F) showed the smoke point to be independent of temperature in the range between 0° and 90° F. Nor did the preheating of gases burning as diffusion flames to 375° F change the smoking tendency (ref. 2).

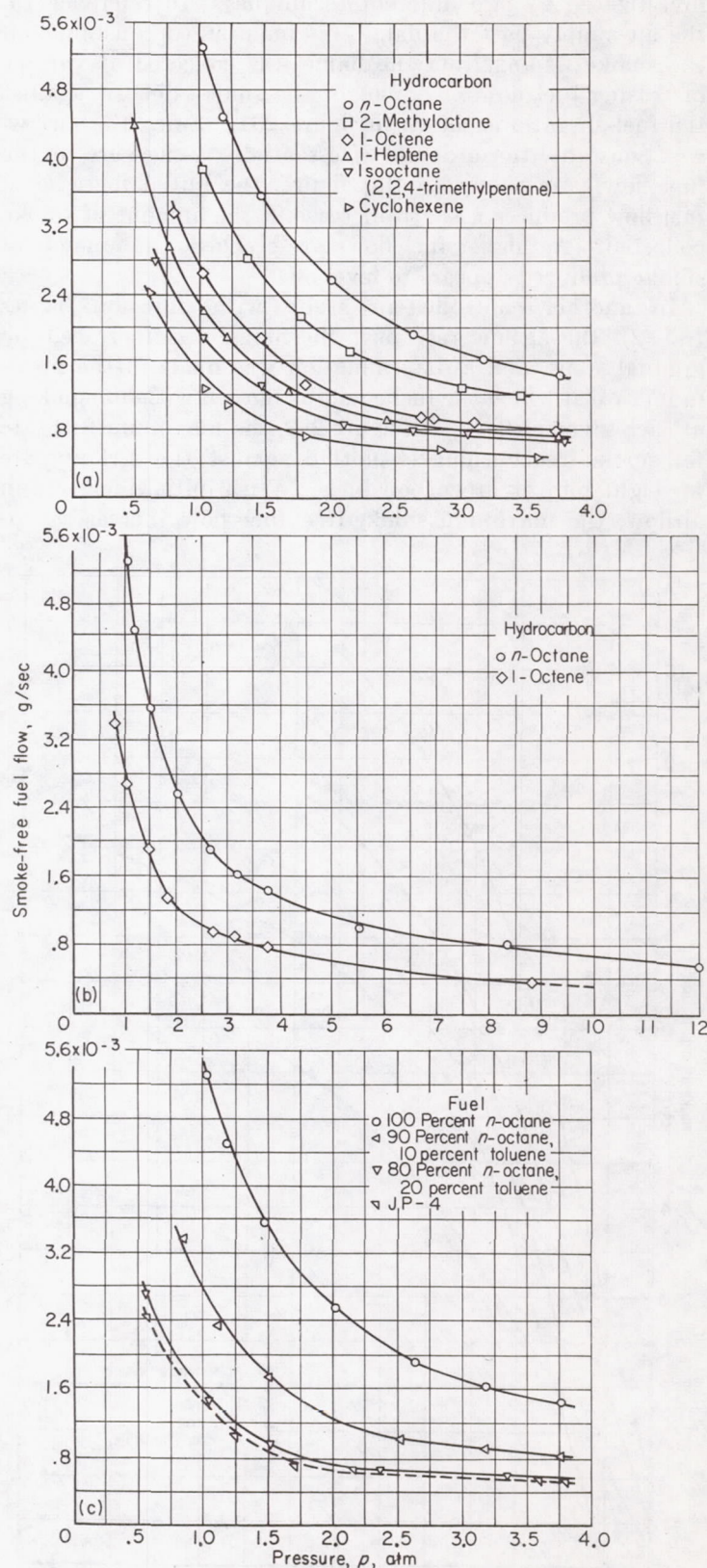
Bunsen flames.—In references 2 and 15 the effect of temperature on the smoking tendency of Bunsen flames was studied. The fuel-air ratio at which incandescent carbon was first observed and also the fuel-air ratio at which smoke actually issued from the flame were determined (ref. 2). Over a temperature range of 82° to 842° F, the point at which smoke issued from a premixed benzene flame was independent of temperature. However, the first appearance of yellow incandescent carbon in the flame occurred at slightly higher fuel-air ratios as the temperature was increased over this range.

In reference 15, only the appearance of yellow incandescent carbon in the flame was used to measure the effect of temperature on propane, propene, benzene, and kerosene flames. Over a temperature range of -40° to 925° F, incandescent carbon in the flame appeared at slightly higher fuel-air ratios as the temperature was increased.

PRESSURE

Diffusion flames.—Studies of the effect of pressure on smoke formation from diffusion flames are reported in references 2, 8, and 16. The investigation of reference 16 was limited to acetylene, and that of reference 8 to petroleum fractions. The work of both references 8 and 16 was conducted at pressures below atmospheric; and in both investigations the tendency to smoke decreased with decreasing pressure. Reference 2 reports smoking tendencies for six pure hydrocarbons, a JP-4 fuel, and two blends of *n*-octane and toluene over a pressure range of about 0.5 to 4 atmospheres. For two of the pure hydrocarbons, 1-octene and *n*-octane, the pressure range was extended to 9 and 12 atmospheres, respectively. Ethane and ethene were studied over a pressure range of 4 to 22 atmospheres. The maximum relative rate at which all fuels could be burned without smoking decreased consistently with increasing pressure. Typical results are shown in figure 234. The data in reference 2 show that the product of the smoke-free fuel flow and the pressure is a constant, or, in other words, that the smoke-free fuel flow is inversely proportional to the pressure. Since diffusion coefficients are also inversely proportional to

the pressure, it was concluded that the rate of diffusion and, consequently, the rate of mixing of fuel and air may account for the variation in smoke formation with pressure.



(a) Six hydrocarbons at pressures to 4 atmospheres.
 (b) Two hydrocarbons at pressures to 12 atmospheres.
 (c) Various fuels and blends at pressures to 4 atmospheres.
 FIGURE 234.—Variation of maximum smoke-free fuel flow with pressure (ref. 2).

Bunsen flames.—In a spectroscopic study of a premixed ethene flame (ref. 17), it was observed that smoke started to form as the pressure was increased. In reference 18 (p. 170), the formation of smoke from an acetylene-oxygen flame at various pressures was studied, and it was concluded that the effect of pressure on smoke formation from Bunsen flames is probably slight. The effects that reference 17 observed were attributed to changes in experimental parameters such as mass flow and the influence of the burner wall. Since the results of the diffusion-flame study (ref. 2) indicate that the increase in smoke formation with pressure results from the decreases in diffusion coefficients with pressure, the smoke formation from a Bunsen flame, which contains all its oxygen, should be independent of pressure if outside diffusion effects are eliminated.

EFFECT OF FUEL VARIABLES ON SMOKING TENDENCY

EFFECT OF HYDROCARBON TYPE ON DIFFUSION FLAMES

One of the first studies to indicate the importance of fuel type on smoke formation is reported in reference 19. The influence of fuel type on smoke has been more extensively investigated, and data have been reported for pure liquid hydrocarbons (refs. 2, 6, 11, 13, and 14) and pure gaseous hydrocarbons (ref. 2). Since each investigator employed a different apparatus, no absolute or standardized values are available; however, certain consistent trends have become apparent. For the pure hydrocarbon compounds, the smoking tendency among the four major homologous series varies as follows: aromatics > alkynes > monoolefins > *n*-paraffins.

The magnitude of the variations in smoking tendency among the aromatic, olefin, and paraffin series is illustrated in the following table:

Reference	Ratio of smoking tendency		
	Aromatic to olefin	Olefin to paraffin	Aromatic to paraffin
11-----	6.2	2.61	16.2
2-----	13.6	2.34	31.8
6-----	15.7	1.51	23.7

The smoking tendency of the average aromatic is reported to be from 6.2 to 15.7 times greater than for the olefins, and 16.2 to 31.8 times greater than for the paraffins. The smoking tendency of the olefins is about twice that of the paraffins. The lack of quantitative agreement becomes readily apparent from examining the values in the table. The variations within the aromatic, alkyne, olefin, and paraffin series are discussed in the following paragraphs.

Aromatics.—As the preceding table indicates, the aromatic compounds have the greatest smoking tendency of the various classes of fuels. With benzene as a reference, the smoking tendency generally increases with the addition of a side chain of one or two carbon atoms; but with a sufficiently long side chain, the smoking tendency is reduced. The total range of flame heights among the aromatic compounds, however, is very small. For example, most investi-

gators report the smoke-point flame height of benzene to be between 5 and 10 millimeters. The aromatics of higher smoking tendency have flame heights ranging down to about 3 millimeters; and those of lesser smoking tendency, up to 12 millimeters. The total range of 3 to 12 millimeters is not very great compared with an average paraffin such as hexane with a flame height of 150 millimeters. The experimental error, percentagewise, in measuring flames as small as 3 to 12 millimeters is very large. Since the aromatics have an essentially uniform smoke point, it is difficult to make a satisfactory differentiation among the various aromatic structures.

Hunt (ref. 6) attempted to overcome this difficulty by studying blends containing 20 percent of various aromatics in *n*-dodecane. This procedure increased the flame height of the benzene blend to 66 millimeters. Blends of about 30 other aromatic and naphthalene compounds were studied in this manner; flame heights ranged from 36 to 81 millimeters. Differences in smoke heights were thus magnified sufficiently to eliminate most experimental errors and permit a definite distinction to be made in smoke points among various aromatic structures. Variations in flame heights for 20 percent blends of 30 aromatic compounds were plotted against the number of carbon atoms in the compound. Most of these are presented in figure 235. Figure 235 emphasizes that substitution on the benzene ring may cause an increase or decrease in the smoke point, depending on the nature of the substituted group. Naphthalene and substituted naphthalene compounds definitely exhibit a greater tendency to smoke than the aromatics.

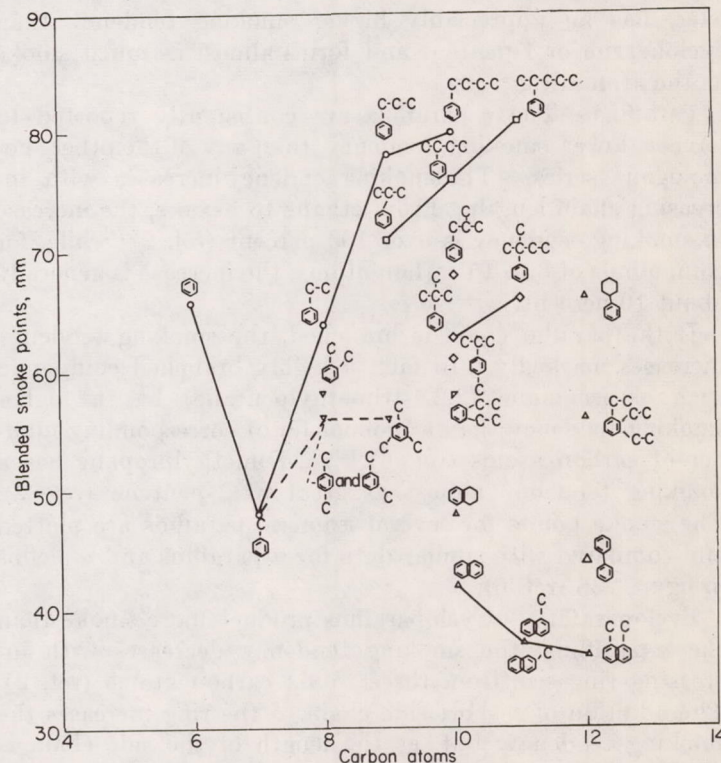


FIGURE 235.—Relation between molecular structure and smoking tendency for aromatics as determined in a modified Davis factor lamp (by permission from ref. 6). (20-Volume-percent blends of aromatic with *n*-dodecane.)

Alkynes.—Smoke-point data for the alkynes are limited. Reference 2 reports the smoking tendency for acetylene, 1-propyne, 1-pentyne, and 1-hexyne. The smoking tendencies decreased slightly with increasing chain length and were of about the same order of magnitude as for the aromatics. Comparison of 1-octyne and 1-dodecyne (ref. 6) showed a decrease in smoking tendency with increasing chain length; however, the smoking tendency for these two alkynes was appreciably less than for the aromatics.

Monoolefins.—All the investigators have reported the monoolefins to be appreciably less smoky than the aromatics but of higher smoking tendency than the *n*-paraffins. From the data of reference 2, the smoking tendency is reported to increase from ethene to butene. References 2, 11, and 14 indicate that, with olefins of five or more carbon atoms, the smoking tendency decreases with increasing chain length. Data from reference 6 indicate that the smoking tendency is essentially constant for all the olefins above five carbon atoms. The effect of the position of the double bond, in the one and two position only, is reported by reference 6, where 2-heptene is shown to have a slightly higher smoking tendency than 1-heptene; however, the difference is less than 6 percent. 1-Octene and 2-octene showed the same smoking tendency (ref. 6).

Diolefins.—Diolefins (refs. 2 and 14) have appreciably higher smoking tendencies than the monoolefins. The smoking tendency of 1,3-butadiene is higher than that of most aromatics (ref. 2). As the chain is lengthened, the smoking tendency decreases.

Cycloolefins.—Cyclohexene has a somewhat higher smoking tendency than 1-hexene (ref. 2). Cyclopentene, however, has an appreciably higher smoking tendency than cyclohexene or 1-pentene and forms almost as much smoke as the aromatics.

Paraffins.—The *n*-paraffins are consistently reported to have a lower smoking tendency than any of the other homologous series. The smoking tendency increases with increasing chain length. From ethane to hexane, the increase in smoking tendency is over 100 percent (ref. 2); while, for compounds of 6 to 15 carbon atoms, the increase is generally about 10 percent.

If the paraffin chain is branched, the smoking tendency increases markedly. In fact, a highly branched compound such as isooctane (2,2,4-trimethylpentane) has a higher smoking tendency than a monoolefin of corresponding number of carbon atoms (ref. 6). 2,2-Dimethylpropane has a smoking tendency almost as great as 1-pentene (ref. 2). The smoke points for several isomeric paraffins are plotted and compared with similar data for *n*-paraffins and *n*-olefins in figure 236 (ref. 6).

Cycloparaffins.—Cycloparaffins produce more smoke than the *n*-paraffins; the smoking tendency decreases with increasing ring size from three to six carbon atoms (ref. 2). The addition of a short side chain to the ring increases the smoking tendency; but, as the length of the side chain is increased, the smoking tendency is reduced slightly. Cyclopentane with a side chain of 10 carbon atoms (decylcyclopentane) has about the same smoking tendency as cyclopentane (ref. 6).

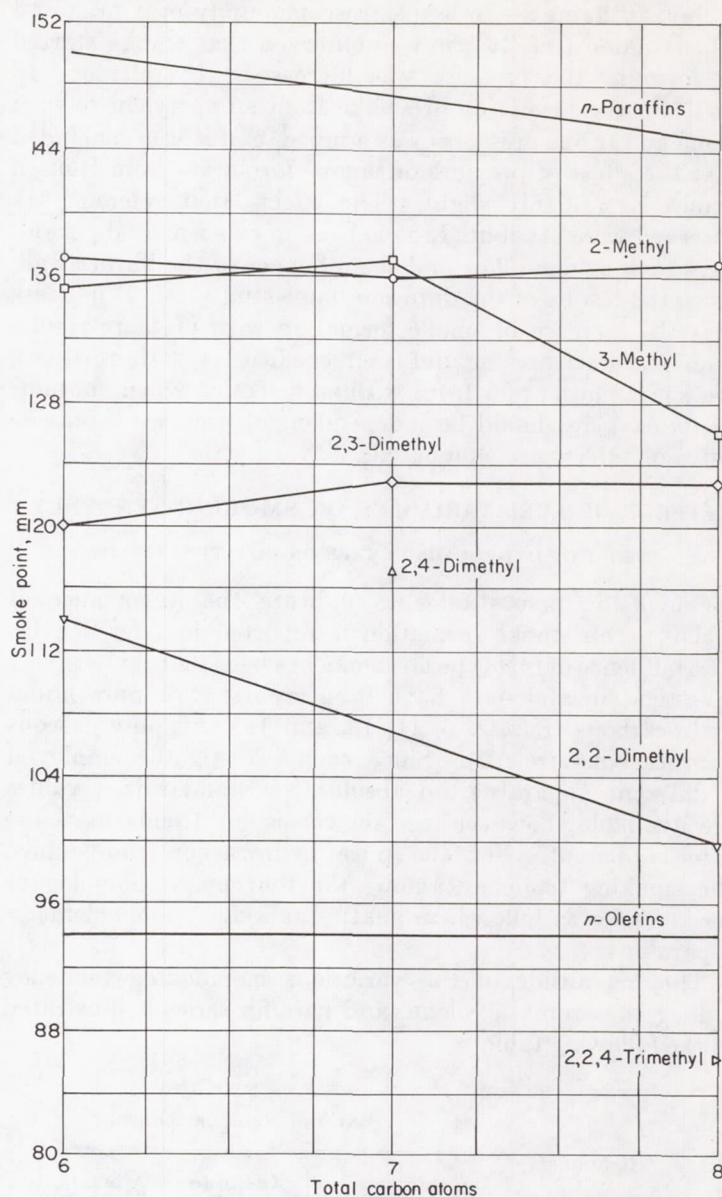


FIGURE 236.—Relation of molecular structure and smoking tendency for paraffins and olefins as determined in a modified Davis factor lamp (by permission from ref. 6).

Summary.—The smoking tendency decreases as follows: aromatics > alkynes > olefins > *n*-paraffins:

(1) All the aromatics have a fairly uniform and extremely high smoking tendency. From an average of three investigations, the aromatics are about 12 times as smoky as the olefins and about 24 times as smoky as the *n*-paraffins.

(2) The alkynes lie between the aromatics and the monoolefins, with the smoking tendency decreasing with increasing chain length.

(3) The smoking tendency of the monoolefins increases from ethene to butene and then decreases with increasing chain length. The olefins are about $\frac{1}{2}$ as smoky as the aromatics, but about twice as smoky as the *n*-paraffins. Branching, ring formation, and additional double bonds increase the smoking tendency.

(4) The *n*-paraffins have a lower smoking tendency than any of the other homologous series. The smoking tendency

increases with increasing chain length, branching, and ring formation.

Hydrocarbon blends and refinery streams.—The smoke points of two component blends of pure hydrocarbons are reported in references 6, 8, and 9. As an example of such blending smoke-point data, figure 237 shows the smoke points for 0 to 100 percent blends of *sec*-butylbenzene and of α -methylnaphthalene in *n*-dodecane (ref. 6). Although the smoke points of the two pure aromatics differ by only 2 millimeters, the blending curves are different. For example, at a 20 percent aromatic concentration, the smoke point of the *sec*-butylbenzene blend is about 74, whereas that of the α -methylnaphthalene blend is only 37. The marked effect of the aromatic on the smoke point of paraffins is also apparent. For example, a 20 percent addition of the aromatic reduces the flame height of *n*-dodecane by about 50 percent or greater. When the concentration of α -methylnaphthalene is 50 percent, the smoke point of the blend is substantially that of the pure aromatic.

Smoking tendencies for various refinery fractions are reported in references 8 to 10, 14, and 19. The early studies were used to evaluate the illumination quality of kerosene-type fuels burning in lamps. The major interest in smoke-point data in the last several years has resulted from the demand for clean-burning jet fuels. The smoking points of 48 jet fuels and the fuel-inspection data for these fuels are reported in reference 8. Reference 10 reports the flame-height smoke point for jet fuels to be about 15 to 30 millimeters, compared with 6 or 7 millimeters for aromatics and 77 millimeters for commercial isoheptane.

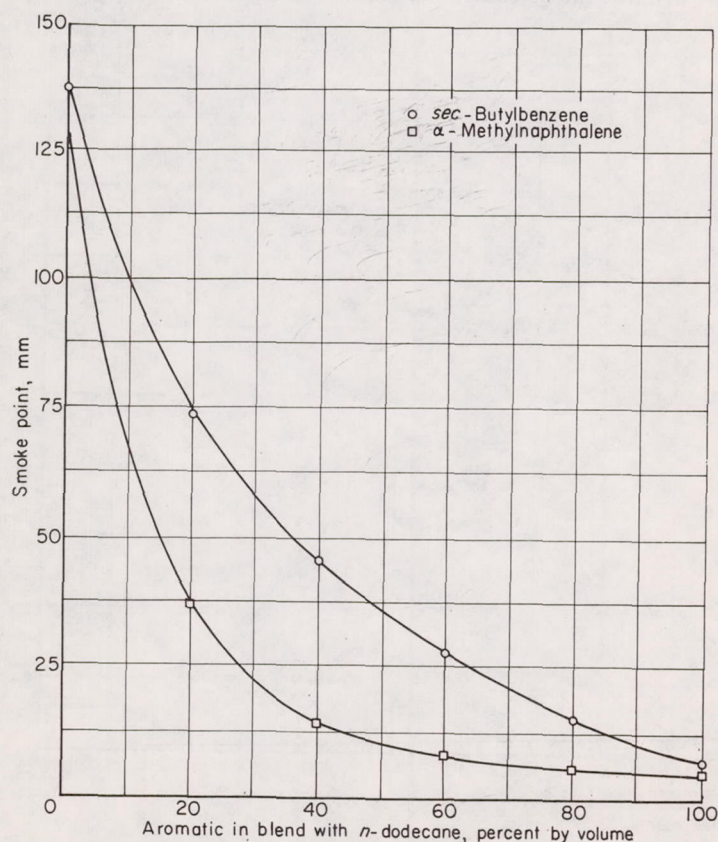


FIGURE 237.—Relation of blend composition and smoking tendency as determined in a modified Davis factor lamp (by permission from ref. 6).

EFFECT OF HYDROCARBON TYPE ON BUNSEN FLAMES

Measurements of variations in smoke formation of various hydrocarbons are reported in references 12 and 15. Since in reference 12 the paraffins, cycloparaffins, and olefins could not be made to smoke even at the maximum fuel-air ratio that would support combustion, these fuels appear to be less smoky than the aromatics and other fuels shown in figure 233. In general, the smoking tendencies of the fuels shown in figure 233 are in the same relation to each other as in diffusion-flame studies. The aromatics show a fairly uniform smoking tendency, as was the case with diffusion flames.

Reference 15 reports determination of the critical fuel-air ratio that would just cause a yellow streak of incandescent carbon to appear in Bunsen flames of various hydrocarbon and oxygenated compounds. The appearance of this yellow streak in the flame, of course, occurs at considerably lower fuel-air ratios than the actual emission of smoke. The results of reference 15 are shown in figure 238, where the critical air-fuel ratio is plotted against the number of carbon atoms in the compound. The higher the position of a fuel on this plot, the greater is its tendency to form an incandescent streak of carbon.

The values for the aromatics, instead of being decidedly worse than the other fuels, are similar to the paraffins, isoparaffins, and olefins. The order of these last three series is the reverse of that observed in diffusion studies. The order of decalin with respect to the substituted naphthalenes and the aromatics differs from the Bunsen work of reference 12 (see fig. 233). The variation with respect to the data in figure 233 may be explained by the fact that the appearance of yellow incandescent carbon in the flame and not the

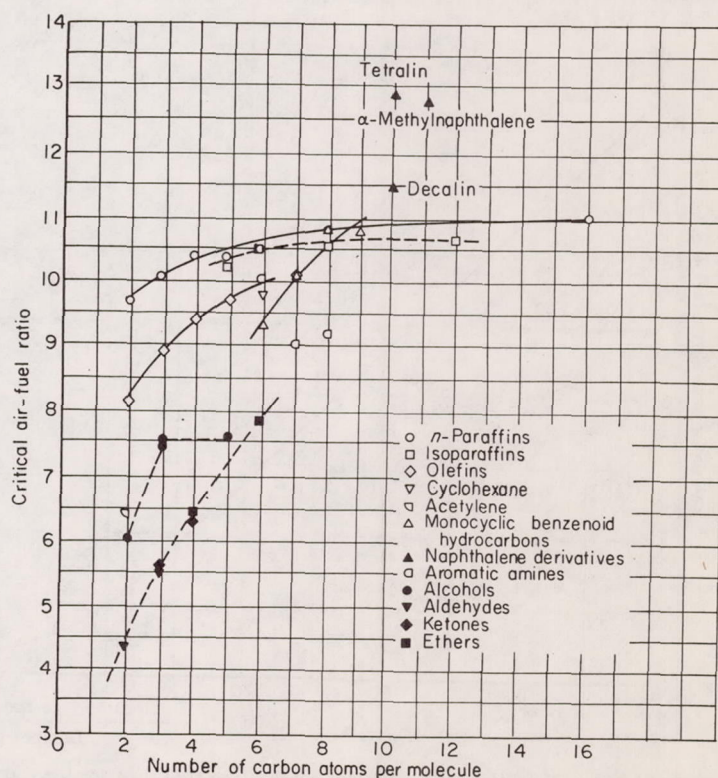


FIGURE 238.—Critical air-fuel ratio for carbon formation as a function of molecular weight and fuel type (ref. 15).

emission of smoke was measured in reference 15. It is probable that these two types of measurements would not be directly proportional. If they are, however, the effect of fuel type on smoke formation as measured by Bunsen and diffusion flames appears appreciably different.

METHODS OF CORRELATING SMOKING TENDENCY WITH HYDROCARBON STRUCTURE IN DIFFUSION FLAMES

Several methods of predicting or explaining the variation of smoking tendency among different fuel types have been proposed. An equation based on the oxygen requirements of diffusion flames was developed in reference 14 to predict the maximum smoke-free flame height b_F (the constants apply only for this particular apparatus):

$$b_F = \frac{(x+3)^2}{36.1xy + 54.9 - 26.65x^2} \quad (1)$$

where

- x molecular volume of combustion products
 y molecular volume of oxygen

While this equation predicts qualitative trends among the various series quite accurately, it does not predict the magnitude by which one series differs from another as reported experimentally. Some of the trends within the series—for example, the effect of branching and ring formation—would not be predicted by the equation. Modification of the equation to fit the apparatus in use may be of some practical value for making qualitative comparisons; but, with respect to theory, the equation does not explain the effect of differences in fuel type such as branching.

The relation between the tendency to smoke and the

carbon-hydrogen ratio of the compound is discussed in reference 11. It is indicated that, in general, compounds of high C-H ratio show a higher smoking tendency than compounds of low C-H ratio. This particular correlation, which gives good qualitative agreement, has been used in predicting combustor coke deposition (ref. 20). Like equation (1), however, it does not explain the differences resulting from such factors as branching and ring formation; consequently, in reference 11 the smokiness of the hydrocarbon molecule is attributed to its compactness.

References 2 and 21 suggest that smoking tendencies may be related to the relative ease of removal of hydrogen atoms compared with the stability of the carbon chain or skeleton of the molecule. A true measure of the stability of the carbon skeleton is difficult to obtain but can be represented to some extent by the carbon-carbon bond strengths. A comparison of the stability as measured by bond strengths is shown in figure 239 and appears to give good qualitative agreement with the smoking tendencies. If all the factors contributing to the stability of the carbon chain could be evaluated and assessed, the agreement might be better.

EFFECT OF NONHYDROCARBON COMPONENTS

Diffusion flames.—Petroleum-derived fuels may contain small quantities of organic sulfur, nitrogen, and oxygen compounds. The maximum amount of sulfur permitted by the current military fuel specifications is 0.2 percent for JP-1, 0.4 percent for JP-3 and JP-4, and 0.5 percent for JP-5. Concentration limits for nitrogen and oxygen are not specified but are not likely to exceed 0.1 and 0.5 percent, respectively.

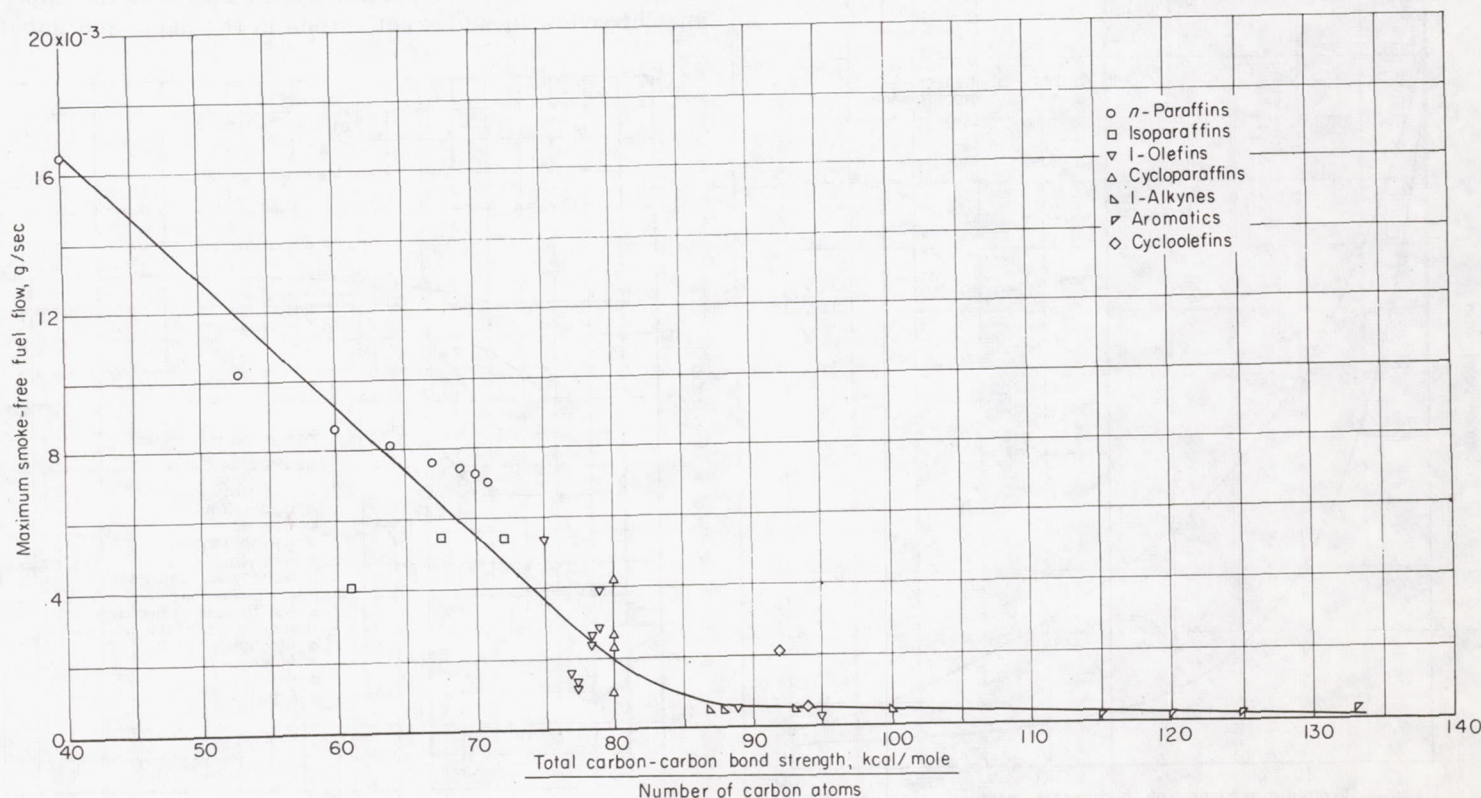


FIGURE 239.—Variation of maximum smoke-free fuel flow with total carbon-carbon bond strength per number of carbon atoms (by permission from ref. 21).

Smoke-point data for some sulfur compounds are reported in reference 6; and for some nitrogen compounds, in references 6 and 11. Both the alkyl-substituted sulfur compounds (mercaptans and disulfides) and the alkyl-substituted nitrogen compounds (amines) have smoking tendencies somewhat higher than their hydrocarbon analogs. The aryl mercaptans and sulfides have smoking tendencies substantially the same as, and the aryl amines appreciably lower than their parent hydrocarbons.

A thorough study of oxygen-containing compounds is reported in reference 11. In general, increasing the oxygen content results in decreasing smoking tendency. Compounds containing high percentages of oxygen, such as methyl acetate, smoke only at very great flame heights. Methyl alcohol cannot be made to smoke at all; and, at equal oxygen concentration, the general order for increasing tendency to smoke is *n*-primary alcohols < *n*-primary nitroparaffins < propionates < acetates < lactates < formates.

In general, the concentrations of sulfur, nitrogen, and oxygen are so low in conventional hydrocarbon fuels that the presence of these impurities should not measurably affect the smoking tendency of the fuel.

Bunsen flames.—Aryl amines and oxygenated compounds were investigated in Bunsen flames in reference 15. The results are shown in figure 238. The values for the aryl amines are not appreciably different from those of their hydrocarbon analogs. The oxygenated compounds show increasing air-fuel ratio with increasing number of carbon atoms in the molecule, the alcohols requiring a higher air-fuel ratio than aldehydes or ketones of a similar number of carbon atoms.

EFFECT OF ADDITIVES

Diffusion flames.—Relatively little information is available on the effect of additives on the smoking characteristics of hydrocarbon flames. This effect may differ between diffusion and Bunsen type flames. Additions of the order of 5 percent of sulfur trioxide are required to measurably reduce the smoking tendency of a diffusion flame (ref. 22), but as little as 0.1 percent of this gas will change a nonluminous Bunsen flame to a luminous one (ref. 18, p. 173). However, the actions of sulfur dioxide and hydrogen sulfide are similar in both type flames; and, with concentrations of the order of 5 percent, slight reductions in smoking tendency of diffusion flames and decreases in the luminosity for Bunsen flames were observed (ref. 18, p. 173). Reference 22 proposes that the oxides of sulfur reduce smoke formation in a diffusion flame by being first converted to S₂ molecules which then react with carbon to form CS.

A few other substances, such as nitric oxide, nitrogen dioxide, diethyl peroxide, and tetraethyl lead, have been tested as additives but have produced no striking effects in regard to smoke formation from diffusion flames (ref. 18, p. 173). One of the most effective additives appears to be dicyclopentadienyliron. Reference 23 shows that the addition of 0.02 weight percent of dicyclopentadienyliron can increase the smoke-free flame height of benzene from 8.4 to 8.9 millimeters, of JP-4 referee from 16.1 to 21.7 millimeters, and of a 100 percent catalytically cracked No. 2 fuel oil from

7.3 to 9.1 millimeters. In studies with a high-pressure atomization-type oil burner, a 75-percent reduction in volume of coke deposits resulted from the use of 0.05 weight percent of dicyclopentadienyliron. In a 2-inch jet burner coke deposits were reduced from a control level of 255 milligrams to 220 milligrams by 0.001 weight percent of dicyclopentadienyliron. With 0.01 weight percent, virtually no coke deposits were formed.

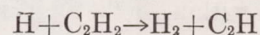
Bunsen flames.—In reference 15, which used the first appearance of incandescent carbon in the flame as a measure of smoking tendency, no additive was found that had any significant effect on the fuel-air ratio in concentrations under 1 percent by weight. Addition in quantities over 10 percent by weight may have an appreciable effect. Halogenated compounds, sulfuric acid, and sulfur trioxide increase the fraction of stoichiometric air required to inhibit carbon formation; nitrogen peroxide, carbon monoxide, tetraethyl lead, methyl alcohol, methylethyl ketone, and amyl nitrate have the opposite effect; sulfur dioxide, carbon dioxide, and water have no effect; carbon disulfide has no effect on kerosene flames but increases the fraction of stoichiometric air required in benzene flames. Sulfur dioxide, though having no effect on the critical air-fuel ratio, appears to reduce the amount of carbon formed in flames of rich mixtures.

THEORIES OF SMOKE AND COKE FORMATION

SMOKE

In the preceding sections it was proposed that the relative ease of removal of hydrogen atoms from the molecule as compared with the breaking of carbon bonds is responsible for the variations in smoking among different fuel types burning as diffusion flames. This proposal suggests that the thermal and oxidative dehydrogenation processes, which occur very early in the burning process, influence the further course of smoke formation. The thermal dehydrogenation probably occurs as soon as the fuel enters a laminar diffusion flame, because the fuel is heated to temperatures of the order of 1500° F or higher before coming in contact with oxygen. Active decomposition particles, then, further promote dehydrogenation processes.

Other investigators who have considered the importance of dehydrogenation reactions tend to support this proposal. For example, the energy requirements for removal of a hydrogen atom from an acetylene molecule by a free hydrogen atom,



were considered in reference 24. This reaction has an activation energy of only 5 kilocalories per mole, which indicates that it could easily occur. Activation energies for the reaction of hydrogen atoms with various other hydrocarbon compounds are of similar magnitude (ref. 25).

It was observed in reference 26 that suppression of the hydrogen-atom concentration in flames accompanies the suppression of smoke formation. Thus, smoke formation could be prevented by reactions that consume hydrogen

atoms or render them ineffective. Reference 27 suggests that smoke formation could be suppressed by carbon monoxide and nitrogen, which serve as nuclei for the recombination and removal of hydrogen atoms. Reference 13 reports that, in addition to hydrogen atoms, other atoms and radicals such as those found in the pyrolysis of halogen compounds also increase smoke formation. All these active species probably promote polymerization reactions leading to smoke by stripping hydrogen from the fuel molecules. Even if halogen atoms react with and remove some of the hydrogen atoms, the concentration of fuel molecules is so much greater than the concentration of the short-lived hydrogen atoms that the dehydrogenation process predominates. It is therefore proposed that the removal of hydrogen atoms from the fuel molecules both by thermal processes and by active atoms is probably the initial process involved in the formation of smoke.

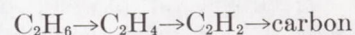
The steps that might occur after total or partial dehydrogenation are controversial. Since aromatics have the greatest smoking tendencies, and since the graphite structure of carbon particles resembles the molecular structure of the multiringed homologs of benzene, the formation of smoke by a buildup of aromatic ring structures has been suggested (ref. 28). This theory is not opposed to the initial step of hydrogen removal, since the fuels would have to lose some hydrogen atoms before a polymerization of the rings might begin. However, absorption spectroscopic examinations of a benzene flame in the ultraviolet region (ref. 16) indicate that benzene is consumed in the lowest portion of the flame and that an appreciable gap exists between the disappearance of benzene and the appearance of smoke particles. No intermediate aromatic products, which should be readily detectable in the ultraviolet, are found in this region. The absence of aromatic intermediates in this gap is evidence against the ring-building theory.

Thorp, Long, and Garner (ref. 29) analyzed the smoke from a flat benzene flame and found diphenyl to be present, thus supporting the aromatic-ring-building theory; but in later work (ref. 30) they did not find diphenyl present in the products of the soots from paraffinic or naphthenic fuels. Consequently, it is unlikely that carbon formation in hydrocarbon diffusion flames occurs through diphenyl, the polyphenyls, or the polycyclic aromatics as intermediate compounds (ref. 30).

Parker and Wolfhard (ref. 16) reject the aromatic-ring-building theory; but they have proposed as mechanisms for smoke formation (1) the formation of large molecules that may graphitize from within, or (2) an increase in the concentration of moderately high molecular weight hydrocarbons until the saturation vapor pressure is reached, at which time condensation occurs to form a mist of droplets that form nuclei and graphitize. Observations on the physical nature of smoke (ref. 31) show that the first mechanism is improbable. Frazee and Anderson (ref. 24) object to both mechanisms, on the basis of prohibitive energy requirements and other considerations. Porter (ref. 32) concludes from considerations based on the time available for polymerization and on the nature of the smoke formed that the droplet-formation mechanism or polymerization mechanisms in gen-

eral do not contribute to smoke formation to any significant extent in ordinary diffusion flames.

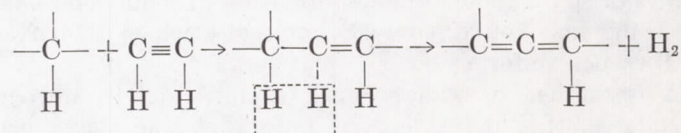
Porter believes, instead, that fuels in combustion waves first decompose to form lower-molecular-weight hydrocarbons such as acetylene as a result of both thermal decomposition and partial oxidation (ref. 32). By rapid adiabatic photolysis he obtained rates of liberation of heat and active particles in a reaction vessel comparable with those which occur in flames. A rapid quenching resulted in the retention of a fraction of all stable intermediates. Complete analysis of the products showed no higher hydrocarbons. Porter therefore proposes a series of reactions:



Previously, Tropsch and Egloff (ref. 33) showed that acetylene is a product of the pyrolysis of pure hydrocarbons. They passed ethane rapidly through a heated tube for various contact times and found that ethene, acetylene, and carbon were formed. This experiment simulates the reactions that might occur in the lowest portion of a diffusion flame where the fuel is heated before coming into contact with oxygen. Similarly, reference 34 studied the pyrolysis products of benzene with a mass spectrometer and showed evidence that the decomposition of benzene to form carbon occurs via acetylene. It was also shown in a study of the autoignition of benzene-air mixtures (ref. 35) that the degradation processes lead to the formation of 2- and 4-carbon acetylenes. Reference 35 concludes that, in light of this evidence, Porter's proposal appears quite plausible for carbon formation from benzene and perhaps other aromatics.

Since acetylene may be the last stable product to appear before smoke formation, the final step in the mechanism of smoke formation would be that leading from acetylene to smoke. If all hydrogen atoms were removed from the C_2H_2 molecule, the mechanism for the final step in the formation of smoke would be the polymerization of C_2 radicals. Such a mechanism was at one time considered a plausible and promising explanation of smoke formation (e. g., ref. 17). However, the theory of smoke formation via C_2 has now been rejected by numerous authors (refs. 16, 24, and 32).

A mechanism based on simultaneous polymerization and dehydrogenation is proposed in reference 32 to account for the steps between acetylene and smoke. The reaction is exemplified by the following equation:



Transient diene structures like those indicated were also deemed important in reference 30.

Analogous to the work of reference 32 is the indication in references 24 and 36 that a mechanism involving free radicals or atoms is important in the formation of smoke and that polymerization and dehydrogenation reactions occur simultaneously rather than in sequence. The activation-energy requirements for some free-radical reactions were

considered, and the following values were reported:

	Energy, kcal/mole
$C_2H + C_2H_2 \rightarrow C_4H_3 \rightarrow C_4H + H_2$	≈ 58
$C_2H + C_2H_2 \rightarrow C_4H_2 + H$	≤ 26
$C_2H_2 + C_2H_2 \rightarrow C_4H_3 + H$	≈ 60

Acetylene was the fuel initially present in these studies. Reference 24 indicates that the first equation is of the type suggested by Porter and proposes that, while the reaction is feasible and may occur to some extent, its activation energy is much higher than that for the reaction shown in the second equation. At particularly high temperatures, more than one reactive radical or hydrogen atom could result from a step such as the second equation, and chain-branching might result. Steps such as these can occur with molecules containing larger and larger numbers of carbon atoms, leading eventually to formation of carbon nuclei and even to growth of a particle. The third equation shows a possibility for the use of the energy of combination in initiating reactions perhaps more effectively than by purely thermal means.

However, an unpublished study of an acetylene-air flame by Ferguson of the National Bureau of Standards indicates that the carbon bonds in the acetylene molecule are broken before smoke formation begins. Ferguson suggests that a buildup of smoke particles initially occurs mainly by the combination of single carbon radicals. It is not known whether the acetylene found in Porter's work was formed by the reaction of single carbon radicals or resulted from dehydrogenation of the original fuel molecule. An understanding of the exact role played by acetylene in smoke formation appears to be very important in the formulation of a final mechanism.

In summary, the general mechanism of smoke formation, based on the information currently available, probably proceeds as follows:

(1) Some hydrogen atoms are removed from the fuel molecule by thermal processes. The hydrogen atoms, in turn, cause further dehydrogenation of the molecule. The more readily the hydrogen atoms are removed as compared with the breaking of carbon bonds, the greater is the probability of smoke formation.

(2) After these initial dehydrogenation steps, the fuel molecules probably continue to decompose to smaller molecules and fragments of molecules. Various authors have shown that a breakdown to smaller products must occur rather than an immediate growth to polymers or aromatic ring structures.

(3) Although a breakdown to small molecules and single carbon radicals takes place, the formation of smoke through polymerization of C_2 radicals has been rejected. It has been proposed that in the final stages the small molecules such as acetylene and perhaps mainly single carbon radicals undergo a simultaneous polymerization and dehydrogenation to form smoke.

COKE

Although the formation of coke may be a more serious problem than that of exhaust smoke, the mechanism of coke formation has received somewhat less attention. Most of the work in this field has involved an analysis of the coke deposits formed in combustors (ref. 4). Reference 4 concludes that hard coke "is largely a petroleum coke resulting from liquid-phase cracking, subsequent pyrolysis, and final coking of the fuel from the spray nozzle as it impinges on the hot liner wall," and that soft combustor coke consists of smoke mixed with the residue from the degradation of fuel in the liquid phase. Reference 37 on the formation and properties of petroleum coke is of interest, since it describes quite fully the later stages in the reactions yielding this product. This reference cites earlier work that proposes the following sequence of reactions: paraffins \rightarrow olefins \rightarrow aromatics with side chains \rightarrow condensed ring systems \rightarrow asphaltenes \rightarrow carboids. The last reaction is then expanded to include the series of: asphalt \rightarrow pitch \rightarrow semipitch \rightarrow asphaltic coke \rightarrow carboid coke (\rightarrow graphite). It is of little importance whether the earlier stages of the over-all coking reaction proceed as indicated, since all commercial jet fuels contain aromatics in sufficient quantity to yield very easily the amount of coke found in combustors. These aromatics would be relatively nonvolatile, and this class of compounds would be concentrated in the liquid residues on combustor walls. The conversion of these residues to the various asphaltic and coke-like products is accomplished at temperatures of the order of 850° to 1475° F, and these products resemble combustor cokes in many ways (ref. 4).

The temperature at which combustor coke is formed cannot be determined by a comparison with the properties of petroleum cokes formed at different temperatures. The hydrogen-to-carbon ratio of hard combustor coke (ref. 3) is about the same as that found in reference 37 for petroleum coke formed at about 1380° F. However, the high concentration in combustor coke of solvent soluble materials suggests a much lower temperature of formation, of the order of 750° to 925° F. Probably this lower temperature range is more nearly the temperature at which the fuel was degraded, and the observed low hydrogen-carbon ratio is the result of the trapping of smoke in the coke deposits. True smoke has a comparatively low hydrogen-carbon ratio and would reduce this ratio to that found in the coke samples (ref. 3).

Combustor coke is produced in the presence of oxygen and flame; petroleum coke results from the decomposition of hydrocarbons alone. Because of these dissimilarities in formation, the determination of the conditions for the production of combustor coke may not be based on those for petroleum coke. The literature on the cracking of hydrocarbons in the presence of small amounts of air or oxygen might be more applicable. The presence of oxygen certainly accelerates the formation of high-molecular-weight asphaltic materials from lower-molecular-weight hydrocarbons. Asphalt is made commercially by blowing residual petroleum fractions with air at temperatures from 425° to 600° F; the liquid hydrocarbon is converted to semisolids by this treatment (ref. 38).

A direct attempt to simulate combustor conditions in the formation of coke with a bench-scale apparatus is reported

in reference 39. In this work, fuel was allowed to drip on a heated metal plate, and the evaporated fuel vapors were ignited by a small pilot flame. The amount of coke deposited was determined by weighing the metal plate before and after the test. Residues similar to combustor coke were formed at plate temperatures of about 600° F, and the amount of deposits decreased to substantially zero at about 1000° F. This test was developed primarily as a fuel evaluation test and has not been used to propose a mechanism for coke formation, although it does indicate that the formation of coke may be minimized with high metal temperatures.

In summary, it appears probable that soft combustor coke is largely formed from gas-phase smoke. The hard, compact deposits probably result from a combination of gas-phase and liquid-phase reactions. The extent to which each type of reaction contributes seems ill-defined at present.

EFFECT OF SOLIDS ON RADIANT HEAT TRANSFER

Information concerning radiant heat transfer from flames is necessary for the evaluation of problems such as combustor-wall cooling, application of flame-immersed fuel vaporizers, and the rate of evaporation of fuel droplets. This section deals with the effect of the solid products of combustion on the radiant power or the emissivity of flames. The solid products that become attached to the combustor walls (coke) may also influence radiant heat transfer to these walls by increasing the surface emissivity. However, this latter effect is not believed to be of much importance, since the emissivity of the usual materials of construction is quite high at high temperatures and would not be greatly increased by coke deposits.

Nonluminous flames emit two types of radiation. These are (1) electronic emission by radicals in the ultraviolet and visible region, and (2) molecular emission by water and carbon dioxide in the infrared. The electronic emission composes a very small fraction of the total radiant power from combustion processes, and its effect on radiant heat transfer can be ignored. Luminous flames yield, in addition to the preceding types of radiation, a black-body radiation that arises from the hot solids present in such flames. A large fraction of this black-body radiation is in the near infrared. A further discussion of the radiation from both types of flames can be found in reference 40.

The radiant power from a combustion zone increases sharply as the flame is changed from a nonluminous to a luminous type. This change may be accomplished by increasing the pressure, the fuel-air ratio, or the smoking tendency of the fuel. As an example of the effect of pressure, a study of the radiation from flames in a turbojet combustor (ref. 41) showed that the radiant power increased rapidly with pressure and to a lesser degree with changes in fuel-air ratio. Pressures ranged from 20 to 95 inches of mercury absolute, and the total radiation from a luminous flame was several times greater than that from a nonluminous flame. Increases in fuel-air ratio that changed nonluminous flames to luminous ones were studied in a laboratory burner (ref. 42) and in a small furnace (ref. 43). A fourfold increase in radiant power was observed with acetylene fuel in the laboratory burner and a two- to three-fold increase with natural

gas in the furnace. In reference 44, the character of the fuel fed to an industrial furnace was varied. The addition of small amounts of fuels of high smoking tendencies, such as benzene or tar, increased the emissivity of the flame from 0.15 to 0.40. In general, the emissivity or radiant power from a flame increases several times as the flame becomes luminous because of the presence of solid products of combustion.

Fairly accurate calculations of the rate of radiant heat transfer can be made for nonluminous flames with the method and charts of reference 45. These require, as input variables, the combustion-chamber geometry, reaction stoichiometry, pressure, and temperature. Similar calculations cannot be made on a theoretical basis alone for luminous flames. These require the experimental measurement of at least two flame properties to determine emissivity. In reference 45, two-color optical pyrometry was used to determine red and green brightness temperatures, which were then used in the calculation of emissivity. In reference 41, a total-radiation pyrometer and a red-filtered optical pyrometer were used to supply the necessary experimental data. Once emissivities are known, the calculation of radiant heat-transfer rates is similar for both luminous and nonluminous flames.

In summary, radiant heat transfer is greatly increased by the presence of solid combustion products. Quantitative determinations of the radiant power from luminous flames require, at present, experimental measurements of the flame in question. However, it is possible that further research plus a backlog of experience on various types of combustors may eventually permit estimates of radiant heat transfer from luminous flames based on theory alone.

SIGNIFICANCE OF BASIC SMOKE AND COKE STUDIES IN DESIGN OF JET-ENGINE COMBUSTORS

The factors relating to the formation of solid carbon during the combustion of hydrocarbons in simple laboratory flames have been reviewed. Some of the major conclusions resulting from the study of laboratory flames that are pertinent to combustor design may be summarized as follows:

1. Smoke is formed only in systems containing a fuel-rich region. Coke and smoke will not result from the combustion of premixed fuel-air systems if the mixture strength is maintained near stoichiometric. Therefore, any combustor design that minimizes or eliminates the presence of local fuel-rich regions should also minimize or eliminate the smoking and coking tendency of the combustor. It is recognized that fuel-lean operation reduces combustor stability and altitude efficiencies. Therefore, compromises must be made in combustor design to obtain satisfactory performance in regard to both burner stability and efficiency and to freedom from coking.

2. Increasing pressure increases the carbon-forming tendency of hydrocarbon flames. Therefore, the problems of smoke and coke and also of radiant heat-transfer effects increase with increasing combustion-chamber pressure.

3. There are pronounced differences in the smoking tendencies of the various hydrocarbon fuels. Of the hydrocarbon types commonly found in petroleum-derived fuels, aromatics have by far the greatest smoking tendencies. However, there are large differences among the various

classes of aromatics. The problems of controlling smoke and coke in turbojet engines can be lessened by limiting the aromatic concentrations in fuels and especially by limiting the concentrations of the more objectionable types of aromatics.

REFERENCES

1. Wear, Jerrold D., and Douglass, Howard W.: Carbon Deposition from AN-F-58 Fuels in a J33 Single Combustor. NACA RM E9D06, 1949.
2. Schalla, Rose L., Clark, Thomas P., and McDonald, Glen E.: Formation and Combustion of Smoke in Laminar Flames. NACA Rep. 1186, 1954. (Supersedes NACA RM's E51E15, E52G24, E52I22, E52I26, E53E05, E53J12, and E54E03.)
3. Biscoe, J., and Warren, B. E.: An X-Ray Study of Carbon Black. Jour. Appl. Phys., vol. 13, no. 6, June 1942, pp. 364-371.
4. Clark, Thomas P.: Examination of Smoke and Carbon from Turbojet-Engine Combustors. NACA RM E52I26, 1952.
5. Terry, John B., and Field, Edward: The Smoke Tendency of Refined Kerosene and Its Determination. Ind. and Eng. Chem. (Anal. ed.), vol. 8, no. 4, July 15, 1936, pp. 293-295.
6. Hunt, Russell A., Jr.: The Relation of Smoke Point to Molecular Structure. Ind. and Eng. Chem., vol. 45, no. 3, Mar. 1953, pp. 602-606.
7. Anon.: Standard Method of Testing Petroleum and Its Products. Third ed., Inst. Petr. Tech. (London), 1935, pp. 133-136.
8. Krynitsky, J. A., Garrett, W. D., and McLean, C. A.: Factors Affecting the Use of a Smoke Lamp for Evaluating Jet Fuels. NRL Rep. 4068, Naval Res. Lab., Oct. 16, 1952.
9. Jezl, J. L.: Smoking Tendencies of Fuels. Rep. No. D-1016, Res. and Dev. Dept., Sun Oil Co., Feb. 14, 1950.
10. Busch, Arthur M.: Correlation of Laboratory Smoke Test with Carbon Deposition in Turbojet Combustors. NACA RM E9K04, 1950.
11. Clarke, A. E., Hunter, T. G., and Garner, F. H.: The Tendency to Smoke of Organic Substances on Burning, Pt. I. Jour. Inst. Petr., vol. 32, no. 274, Oct. 1946, pp. 627-642.
12. Ebersole, Earl R., and Barnett, Henry C.: Smoking Characteristics of Various Fuels as Determined by Open-Cup and Laboratory-Burner Smoke Tests. NACA WR E-190, 1945. (Supersedes NACA MR's E5F20 and E5I12.)
13. Sacks, W., and Ziebell, M. T. I.: Carbon Formation in Flames of Aromatic Hydrocarbons. Lab. Rep. LR-30, Nat. Aero. Est. (Canada), June 25, 1952.
14. Minchin, S. T.: Luminous Stationary Flames: The Quantitative Relationship Between Flame Dimensions at the Sooting Point and Chemical Composition, with Special Reference to Petroleum Hydrocarbons. Jour. Inst. Petr. Tech., vol. 17, 1931, pp. 102-120.
15. Street, J. C., Thomas, A., and Williams, R. A.: Carbon Formation in Pre-Mixed Flames. Rep. K.113, Aero-Eng. Lab., Thornton Res. Center, Sept. 1953. (Contract No. 6/ENGS/4668/CB.11(a).)
16. Parker, W. G., and Wolfhard, H. G.: Carbon Formation in Flames, Pt. III. Jour. Chem. Soc. (London), Aug. 1950, pp. 2038-2044; discussion, pp. 2045-2049.
17. Smith, E. C. W.: The Emission Spectrum of Hydrocarbon Flames. Proc. Roy. Soc. (London), ser. A, vol. 174, no. A956, Jan. 12, 1940, pp. 110-125.
18. Gaydon, A. G., and Wolfhard, H. G.: Flames—Their Structure, Radiation and Temperature. Chapman and Hall (London), 1953.
19. Kewley, J., and Jackson, J. S.: The Burning of Mineral Oils in Wick Fed Lamps. Jour. Inst. Petr. Tech., vol. 13, 1927, pp. 364-397.
20. Jonash, Edmund R., Wear, Jerrold D., and Hibbard, Robert R.: Relation Between Fuel Properties and Combustion Carbon Deposition. NACA RM E52B14, 1952.
21. Schalla, Rose L., and McDonald, Glen E.: Variation in Smoking Tendency Among Hydrocarbons of Low Molecular Weight. Ind. and Eng. Chem., vol. 45, no. 7, July 1953, pp. 1497-1500.
22. Wolfhard, H. G., and Parker, W. G.: Influence of Sulfur on Carbon Formation in Diffusion Flames. Fuel, vol. 29, no. 10, Oct. 1950, pp. 235-240.
23. Arimoto, F. S., Corzilius, M. W., Lamb, J. A., and Melby, A. O.: Dicyclopentadienyliron and Its Effects on Combustion Phenomena. Abs. of papers presented at meeting Am. Chem. Soc., Cincinnati (Ohio), Mar. 29-Apr. 7, 1955, p. 17P.
24. Frazee, J. D., and Anderson, Robbin C.: Carbon Formation and Reaction in Flames in Acetylene. Abs. of papers presented at meeting of Am. Chem. Soc., Chicago (Ill.), Sept. 6-11, 1953.
25. Steacie, E. W. R.: Atomic and Free Radical Reactions. Reinhold Pub. Corp., 1946.
26. Arthur, J. R.: Some Reactions of Atomic Hydrogen in Flames. Nature, vol. 165, no. 4197, Apr. 8, 1950, pp. 557-558.
27. Iyengar, M. S., Vaidyeswaran, R., and Datar, D. S.: Studies on Carbon Formation in Flames. Pt. I—Suppression of Carbon Deposit Formation in Flames of Some Organic Compounds by Carbon Dioxide and Nitrogen. Jour. Sci. Ind. Res. (India), vol. 11B, 1952, pp. 455-457.
28. Rummel, Kurt, and Veh, Paul O.: Radiation of Luminous Flames. I—Literature, Working Hypotheses and Preliminary Tests. Arch. Eisenhüttenw., vol. 14, 1941, pp. 489-499.
29. Thorp, N., Long, R., and Garner, F. H.: Carbon Formation in Benzene-Oxygen Diffusion Flames. Fuel, vol. 30, no. 11, Nov. 1951, p. 266.
30. Garner, F. H., Long, R., and Thorp, N.: Carbon Formation in Hydrocarbon Diffusion Flames. Fuel, vol. 32, 1953, pp. 116-117.
31. Grisdale, R. O.: The Formation of Carbon Black. Jour. Appl. Phys., vol. 24, no. 9, Sept. 1953, pp. 1082-1091.
32. Porter, George: Carbon Formation in the Combustion Wave. Fourth Symposium (International) on Combustion, The Williams & Wilkins Co., 1953, pp. 248-252.
33. Tropsh, Hans, and Egloff, Gustav: High-Temperature Pyrolysis of Gaseous Paraffin Hydrocarbons. Ind. and Eng. Chem., vol. 27, no. 9, Sept. 1935, pp. 1063-1067.
34. Ingold, K. V., and Lossing, F. P.: Free Radicals by Mass Spectrometry. III—Radicals in the Thermal Decomposition of Some Benzene Derivatives. Canadian Jour. Chem., vol. 31, Jan. 1953, pp. 30-41.
35. Beckers, A., and Levedahl, W. J.: Mechanism of Autoignition in Benzene-Air Mixtures. Abs. of papers presented at Am. Chem. Soc. meeting Cincinnati (Ohio), Mar. 29-Apr. 7, 1955, p. 16P.
36. Westbrook, E. A., Hellwig, Katherine, and Anderson, Robbin C.: Self-Combustion of Acetylene. II. Reactions in Flame Propagation. Fifth Symposium on Combustion, Reinhold Pub. Co., 1955, pp. 631-637.
37. Berry, A. G. V., and Edgeworth-Johnstone, R.: Petroleum Coke Formation and Properties. Ind. and Eng. Chem., vol. 36, no. 12, Dec. 1944, pp. 1140-1144.
38. Puller, H. B., et al.: Blown Asphalt, Vol. IV. Sci. of Petr., Oxford Univ. Press, 1938, pp. 2700-2705.
39. Rogers, J. D., and Jones, D. R.: Combustion Characteristics of Gas Turbine Fuels. Prog. Rep. No. 27, Calif. Res. Corp., Dec. 31, 1949. (Air Force Contract W-33-038ac-9083, AMC Proj. MX-587.)
40. Berlad, A. L., and Hibbard, R. R.: Effect of Radiant Energy on Vaporization and Combustion of Liquid Fuels. NACA RM E52I09, 1952.
41. Topper, Leonard: Radiant Heat Transfer From Flames in a Single Tubular Turbojet Combustor. NACA RM E52F23, 1952.
42. Haslam, R. T., and Boyer, M. W.: Radiation from Luminous Flames. Ind. and Eng. Chem., vol. 19, no. 1, Jan. 1927, pp. 4-6.
43. Sherman, Ralph A.: Radiation from Luminous and Non-Luminous Natural-Gas Flames. Trans. ASME, vol. 56, no. 3, Mar. 1934, pp. 177-185.
44. Ribaud, G.: Heat Transmission by Radiation in Industrial Furnaces. Chem. Abs., vol. 42, no. 7, Apr. 10, 1948, p. 2145d. (Abs. from Energie, vol. 31, 1947, pp. 57-67; 92-94.)
45. Hottel, Hoyt C.: Section on Heat Transfer. Chemical Engineers' Handbook, Third ed., John H. Perry, ed., McGraw-Hill Book Co., Inc., 1950, pp. 483-498.

APPENDIX—PHYSICAL AND COMBUSTION PROPERTIES OF SELECTED FUELS

Data according to various investigators have been compiled and are presented in table XXXII. Column headings are explained as follows:

Specific gravities were obtained from reference 1, except as noted. Values from reference 1 are 60°/60° F, while those from reference 2 are generally 20°/4° C.

Normal boiling points at 1 atmosphere were taken from reference 1, except as noted.

Heats of vaporization ΔH_v were obtained from reference 1, except as noted.

Heats of combustion ΔH_B of gaseous fuel to give gaseous products are from reference 1.

Stoichiometric mixtures are given as mole fraction of fuel (volume percent/100) and as fuel-air ratio by weight.

Flammability limits in percent of stoichiometric fuel-air ratio, in most cases obtained with upward propagation in a 2-inch tube closed at both ends, are from reference 3, except as noted.

Spontaneous-ignition temperatures were determined by the modified ASTM drop test in reference 4, except as noted. Minus signs following values indicate that slightly lower values have been reported.

Fuel concentrations \mathcal{C} in percent stoichiometric fuel-air ratio for maximum burning velocity $U_{F,max}$ were determined at 77° F and atmospheric pressure (ref. 5).

Maximum burning velocities $U_{F,max}$ relative to propane, which are arbitrarily rated 100 for each experimental method (see table XXXIII for absolute values for propane for each method), were obtained from reference 5. Burning velocities were, in most cases, measured by the NACA tube method (see ref. 6).

Adiabatic flame temperatures T_F were calculated at the fuel-air ratio f for maximum burning velocity according to the method of reference 7. Values were obtained from reference 5.

Minimum ignition energies at stoichiometric fuel-air ratios and the absolute minimum ignition energies that occur at some richer concentration were obtained from reference 8, except as noted. In most cases, 1/8-inch-rod electrodes (unflanged) and capacitance sparks were used; pressure was 1 atmosphere.

Quenching distances between parallel plates at stoichiometric fuel-air ratios and absolute quenching distances through which no flame will pass regardless of concentration were estimated from log-log correlations between ignition energy and quenching distance (based on data from refs. 9 and 10 and information received from Experiment, Inc.) and minimum ignition energies included herein, except when taken from references 9 and 10.

TABLE XXXIII.—EXPERIMENTAL BURNING VELOCITIES OF PROPANE-AIR MIXTURES

Method	Maximum burning velocity, $U_{F,max}$, ft/sec	Concentra- tion for $U_{F,max}$, % stoichiomet- ric	Reference
Tube.....	1. 28	113	23
Bunsen-burner schlieren.....	1. 41	106	24
Bunsen-burner shadowgraph.....	1. 53	110	14

TABLE XXXII.—PHYSICAL AND COMBUSTION PROPERTIES OF FUELS*

[Numbered superscripts indicate references.]

Fuel	Molecular weight	Specific gravity	Boiling point, °F	ΔH_v , Btu/lb	ΔH_B , gas-gas, Btu/lb	Stoichiometric mixture		Flammability limit, % stoichiometric		Spontaneous ignition temp., °F	C for $U_{F, max}$, % stoichiometric	Relative $U_{F, max}$	T_F at f for $U_{F, max}$, °R	Min. ignition energy, 10 ⁻³ joule		Quenching distance, in.	
						% by volume	f	Lean	Rich					Stoich.	Abs. min.	Stoich.	Abs. min.
Acetaldehyde	44.1	0.783 ²	-70 ²	245 ²	---	0.0772	0.1280	---	---	---	---	---	---	37.6	---	0.09	---
Acetone	58.1	0.792 ²	134 ²	224 ²	---	0.0497	0.1054	a 59 ¹¹	a 233 ¹¹	1042 ¹²	131	117 ¹³	3820	115	---	.15	---
Acetylene	26.0	0.621 ²	b 119	---	20,734	0.0772	0.0755	a 31 ¹¹	a 48 ¹¹	581 ¹²	133	362 ²	---	e 3	---	.03	---
Acrolein	56.1	0.841 ²	127 ²	---	---	0.0564	0.1163	a 48 ¹¹	a 752 ¹¹	532 ¹²	100	144 ¹⁴	---	e 17.5	---	.06	---
Acrylonitrile	53.1	0.797 ²	173 ²	---	---	0.0528	0.1028	a 87 ¹¹	---	898 ¹²	105	109 ¹³	4430	e 36	d 16 ¹⁵	.09	0.06
Allene (propadiene)	40.1	---	-30	19,921	---	0.0497	0.0728	---	---	---	121	189 ¹³	4430	---	---	---	---
Ammonia	17.0	e 817	-28 ²	590 ²	---	0.2181	0.1645	---	---	1204 ¹²	---	---	---	---	---	---	---
Aniline	93.1	1.022 ²	364 ²	187 ¹⁶	---	0.0263	0.0872	---	---	1100	---	---	---	---	---	---	---
Benzene	78.1	0.885	176	169	17,446	0.0271	0.0755	43	336	1097	108	f 104 ¹³	4150	55	d 22.5 ¹⁷	.11	.07
<i>n</i> -butyl-	134.2	0.865	362	---	17,984	0.0153	0.0721	---	---	821	108	f 84 ¹³	4185	---	---	---	---
<i>sec</i> -butyl-	134.2	0.866	344	---	---	0.0153	0.0721	---	---	836	---	---	---	---	---	---	---
<i>tert</i> -butyl-	134.2	0.871	336	---	---	0.0153	0.0721	---	---	891	105	f 85 ¹³	4175	---	---	---	---
1,2-diethyl-	134.2	0.884	362	---	---	0.0153	0.0721	---	---	759	---	---	---	---	---	---	---
1,3-diethyl-	134.2	0.868	358	---	---	0.0153	0.0721	---	---	851	---	---	---	---	---	---	---
1,4-diethyl-	134.2	0.866	363	---	---	0.0153	0.0721	---	---	844	---	---	---	---	---	---	---
1,2-dimethyl- (<i>o</i> -xylene)	106.2	0.885	292	149	17,723	0.0195	0.0734	---	---	934	108	f 80 ¹³	4205	---	---	---	---
1,3-dimethyl- (<i>m</i> -xylene)	106.2	0.869	282	147	17,716	0.0195	0.0734	45	307	1045	---	---	---	---	---	---	---
1,4-dimethyl- (<i>p</i> -xylene)	106.2	0.866	281	146	17,719	0.0195	0.0734	---	---	1048	---	---	---	---	---	---	---
ethyl-	106.2	0.872	277	146	17,767	0.0195	0.0734	a 50 ¹¹	---	860	---	---	---	---	---	---	---
isobutyl-	134.2	0.858	343	---	---	0.0153	0.0721	---	---	853	---	---	---	---	---	---	---
isopropyl- (cumene)	120.2	0.866	306	134	17,873	0.0171	0.0727	52	352	873	---	---	---	---	---	---	---
1-methyl-2-ethyl-	120.2	0.885	329	139	17,864	0.0171	0.0727	---	---	836	---	---	---	---	---	---	---
1-methyl-3-ethyl-	120.2	0.869	322	138	17,853	0.0171	0.0727	---	---	905	---	---	---	---	---	---	---
1-methyl-4-ethyl-	120.2	0.866	324	137	17,848	0.0171	0.0727	---	---	902	---	---	---	---	---	---	---
1-methyl-3,5-diethyl-	148.2	0.867	393	---	---	0.0138	0.0717	---	---	861	---	---	---	---	---	---	---
nitro-	123.1	1.199 ²	412 ²	142 ¹⁶	---	0.0324	0.1429	---	---	900 ¹²	---	---	---	---	---	---	---
propyl-	120.2	0.867	319	137	17,887	0.0171	0.0727	---	---	853	---	---	---	---	---	---	---
1,2,3-trimethyl- (hemimellitene)	120.2	0.899	349	143	17,825	0.0171	0.0727	---	---	895	---	---	---	---	---	---	---
1,2,4-trimethyl- (pseudocumene)	120.2	0.880	337	140	17,809	0.0171	0.0727	---	---	970	109	f 84 ¹³	4180	---	---	---	---
1,3,5-trimethyl- (mesitylene)	120.2	0.870	328	140	17,802	0.0171	0.0727	---	---	1039	---	---	---	---	---	---	---
vinyl- (styrene)	104.1	0.911	293	---	17,598	0.0205	0.0755	---	---	914 ¹²	---	---	---	---	---	---	---
Benzyl alcohol	108.1	1.050 ²	401 ²	---	---	0.0240	0.0923	---	---	802 ¹²	---	---	---	---	---	---	---
Biphenyl	154.2	1.180 ²	490 ²	---	---	0.0141	0.0772	---	---	1071	---	---	---	---	---	---	---
2-butyl-	210.3	---	---	---	---	0.0101	0.0745	---	---	811	---	---	---	---	---	---	---
2-ethyl-	182.3	---	---	---	---	0.0118	0.0755	---	---	840	---	---	---	---	---	---	---
2-methyl-	168.2	1.010 ²	500 ²	---	---	0.0129	0.0763	---	---	936	---	---	---	---	---	---	---
2-propyl-	196.3	---	---	---	---	0.0109	0.0750	---	---	845	---	---	---	---	---	---	---
1,2-Butadiene (methylallene)	54.1	e 658	52	---	19,567	0.0366	0.0714	a 53 ¹¹	a 340 ¹¹	784 ¹²	117	149 ¹³	4355	e 23.5	12.5	.07	.05
1,3-Butadiene (divinyl, vinylacetylene)	54.1	e 627	24	---	19,153	0.0366	0.0714	---	---	119	119	140 ¹³	4275	---	---	---	---
2,3-dimethyl-	82.1	0.731	156	---	---	0.0240	0.0701	---	---	119	119	112 ¹³	4170	---	---	---	---
2-methyl- (isoprene)	68.1	0.686	93	---	19,003	0.0290	0.0706	---	---	824 ¹²	118	119 ¹³	4220	---	---	---	---
<i>n</i> -Butane	58.1	e 584	31	166	19,655	0.0312	0.0648	54 ¹⁹	330 ¹⁹	807	113	97	4060	76 ⁹	26 ⁹	.12	.07
2-cyclopropyl-	98.2	---	---	---	---	0.0195	0.0678	---	---	129	102	102	4055	164	d 25 ¹⁵	.18	.07
2,2-dimethyl-	86.2	0.654	122	131	19,299	0.0216	0.0659	55 ¹⁹	351 ¹⁹	824	113	92	4055	---	---	---	---
2,3-dimethyl-	86.2	0.666	136	136	19,338	0.0216	0.0659	55 ¹⁹	372 ¹⁹	790	113	93	4055	---	---	---	---
1,1-diphenyl-	210.3	---	---	---	---	0.0101	0.0745	---	---	863	---	---	---	---	---	---	---
2-methyl- (isopentane)	72.1	0.625	82	146	19,451	0.0255	0.0654	50 ¹⁹	359 ¹⁹	800	114	94	4055	e 96	d 21 ¹⁵	.14	.07
2,2,3-trimethyl-	100.2	0.695	178	124	19,241	0.0187	0.0661	58 ¹⁹	358 ¹⁹	849	116	92	4035	100	---	.14	---
Butanone (methyl ethyl ketone)	72.1	0.805 ²	175 ²	191 ²	---	0.0366	0.0951	---	---	100	100	92 ¹⁴	---	---	---	---	---
1-Butene	56.1	e 601	21	168	19,475	0.0337	0.0678	53 ¹⁹	353 ¹⁹	830 ¹²	116	111	4175	53	28	.10	.08
2-cyclopropyl-	96.2	---	---	---	---	0.0205	0.0698	---	---	115	109 ¹³	4215	---	---	---	---	---
2,3-dimethyl-	84.2	0.683	132	---	19,159	0.0227	0.0678	---	---	697	131	101 ¹³	3970	---	---	---	---
2-ethyl-	84.2	0.694	148	---	19,198	0.0227	0.0678	---	---	615	117	101	4110	---	---	---	---
2-methyl-	70.1	0.656	88	---	19,252	0.0271	0.0678	---	---	706	115	100	4135	---	---	---	---
3-methyl- (α -isoamylene)	70.1	0.633	68	---	19,297	0.0271	0.0678	---	---	706	115	106	4150	---	---	---	---
2,3,3-trimethyl-	98.2	0.710	172	---	19,092	0.0195	0.0678	---	---	721	---	---	---	---	---	---	---
<i>trans</i> -2-Butene	56.1	e 610	34	174	19,389	0.0337	0.0678	a 52 ¹¹	a 307 ¹¹	---	---	---	---	---	---	---	---
2,3-dimethyl-2-butene	84.2	0.713	164	---	19,135	0.0227	0.0678	---	---	764	115	95 ¹³	4115	---	---	---	---
2-methyl-2-butene	70.1	0.668	101	---	19,214	0.0271	0.0678	---	---	---	---	---	---	---	---	---	---
3-Buten-1-yne (vinylacetylene)	52.1	0.687 ²	41 ²	---	---	0.0402	0.0755	---	---	---	109	193 ¹³	4520	8.22	---	.04	---
<i>n</i> -Butyl chloride	92.6	0.884 ²	172 ²	---	---	0.0324	0.1075	---	---	---	---	---	---	e 124	---	.15	---
1-Butyne	54.1	e 650	47	---	19,590	0.0366	0.0714	---	---	---	120	149 ¹³	4345	---	---	---	---
3,3-dimethyl-	82.1	---	---	---	---	0.0240	0.0701	---	---	---	121	122 ¹³	4210	---	---	---	---
2-Butyne	54.1	0.697	81	---	19,440	0.0366	0.0										

TABLE XXXII.—PHYSICAL AND COMBUSTION PROPERTIES OF FUELS—Concluded

[Numbered superscripts indicate references.]

Fuel	Molecular weight	Specific gravity	Boiling point, °F	Δ <i>H</i> _v , Btu/lb	Δ <i>H</i> _B , gas-gas, Btu/lb	Stoichiometric mixture		Flammability limit, % stoichiometric		Spontaneous ignition temp., °F	<i>C</i> for <i>U</i> _{<i>F</i>, max} , % stoichiometric	Relative <i>U</i> _{<i>F</i>, max}	<i>T</i> _{<i>F</i>} at <i>U</i> _{<i>F</i>, max} , °R	Min. ignition energy, 10 ⁻³ joule		Quenching distance, in.	
						% by volume	<i>f</i>	Lean	Rich					Stoich.	Abs. min.	Stoich.	Abs. min.
Furan	68.1	0.936 ²	90 ²	172 ²	---	0.0444	0.1098	---	---	---	---	---	---	22.5	---	0.07	---
tetrahydro-	72.1	---	149 ²	---	---	0.0366	0.0951	---	---	---	---	---	---	54	---	---	---
thio- (thiophene)	84.1	1.064 ²	183 ²	---	---	0.0337	0.1017	---	---	---	---	---	---	60	---	---	---
n-Heptane	100.2	0.688	209	136	19,314	0.187	0.661	53	450	477	122	99	3985	115	24 ¹⁵	15	0.07
3,3-dimethyl-	128.3	0.730	279	118	---	0.147	0.665	---	---	626	---	---	---	---	---	---	---
1-Heptene	98.2	0.702	201	---	19,202	0.195	0.678	---	---	505	---	---	---	93.1	---	13	---
1-Heptyne	96.2	0.738	212	---	19,262	0.205	0.698	---	---	---	108	95 ¹³	4115	---	---	---	---
Hexadecane	226.4	0.777	548	98	19,052	0.085	0.671	---	---	446	---	---	---	---	---	---	---
1-Hexadecene	224.4	0.785	544	---	19,000	0.086	0.679	---	---	464	---	---	---	---	---	---	---
1,5-Hexadiene	82.1	0.697	139	---	---	0.240	0.701	---	---	---	118	113	---	---	---	---	---
n-Hexane	86.2	0.664	156	144	19,391	0.216	0.659	51	400	501	117	99	4030	95 ⁹	23 ⁹	14	0.07
2,3-dimethyl-	114.2	0.717	240	126	19,236	0.165	0.663	---	---	820 ¹²	---	---	---	---	---	---	---
1-Hexene	84.2	0.678	146	---	19,262	0.227	0.679	52	393	521	118	108	4115	---	---	---	---
1-Hexyne	82.1	0.721	161	---	19,334	0.240	0.701	---	---	---	124	124	4200	---	---	---	---
3-Hexyne	82.1	0.726 ²	---	---	---	0.240	0.701	---	---	---	---	116 ¹³	4150	---	---	---	---
Hydrogen	2.0	---	423 ²	194 ²	51,571	0.2950	0.0290	---	---	1060-12	≈ 170	679 ¹⁴	---	2.0	1.8	0.025 ¹⁰	0.024 ¹⁰
Hydrogen sulfide	34.1	---	79 ²	237 ²	---	0.1224	0.1650	---	---	554 ¹²	---	---	---	65	---	0.04	---
Isopropyl alcohol	60.1	0.785 ²	180 ²	286 ²	---	0.0444	0.0969	---	---	852 ²⁰	100	89 ¹⁴	4030	65	---	0.11	---
Isopropylamine	59.1	0.690 ²	93 ²	---	---	0.0383	0.0817	---	---	---	114	68 ¹³	4030	200 ²²	---	0.19	---
Isopropyl chloride	78.5	0.859 ²	96 ²	---	---	0.0422	0.1199	---	---	---	---	---	---	155 ²²	---	0.17	---
Isopropyl mercaptan	76.2	0.836 ²	154 ²	---	---	0.0337	0.0922	---	---	---	---	---	---	87	---	0.13	---
dl-Limonene	136.2	0.842 ²	351 ²	125 ¹⁶	---	0.147	0.706	---	---	505	---	---	---	---	---	---	---
Methane	16.0	---	259	219	21,502	0.0947	0.0581	46 ¹⁹	164 ¹⁹	1170-12	106	87	4025	33 ⁹	29 ⁹	10 ⁹	0.08 ⁹
diphenyl-	168.2	1.001 ²	503 ²	---	---	0.129	0.763	---	---	962	107	77 ¹³	4280	---	---	---	---
Methyl alcohol	32.0	0.793 ²	148 ²	473 ²	---	0.1224	0.1548	48	408	878 ²⁰	≈ 101	122 ¹⁴	---	21.5	14 ¹⁵	0.07	0.06
Methyl formate	60.1	0.975 ²	89 ²	203 ²	---	0.0947	0.2181	---	---	---	---	---	---	62	---	---	---
Naphthalene, 1-ethyl-	156.2	1.012	498	---	---	0.138	0.755	---	---	898	---	---	---	---	---	---	---
1-methyl-	142.2	1.025	472	---	---	0.153	0.764	---	---	1017	---	---	---	---	---	---	---
n-Nonane	128.3	0.722	303	124	19,211	0.147	0.665	47	434	453	---	---	---	---	---	---	---
2-methyl-	142.3	0.732	332	---	---	0.133	0.666	---	---	418	---	---	---	---	---	---	---
n-Octane	114.2	0.707	258	129	19,256	0.165	0.663	51	425	464	---	---	---	---	---	---	---
2,3-dimethyl-	142.3	0.742	327	---	---	0.133	0.666	---	---	447	---	---	---	---	---	---	---
4-ethyl-	142.3	0.744	334	---	---	0.133	0.666	---	---	458	---	---	---	---	---	---	---
2-methyl-	128.3	0.718	290	123	---	0.147	0.665	---	---	440	---	---	---	---	---	---	---
3-methyl-	128.3	0.725	292	123	---	0.147	0.665	---	---	442	---	---	---	---	---	---	---
4-methyl-	128.3	0.724	288	123	---	0.147	0.665	---	---	450	---	---	---	---	---	---	---
1-Octene	112.2	0.719	250	---	19,157	0.171	0.678	46	384	493	---	---	---	---	---	---	---
1,2-Pentadiene (ethylallene)	68.1	0.698	113	---	19,444	0.290	0.706	---	---	---	119	133 ¹³	4285	---	---	---	---
cis-1,3-Pentadiene	68.1	0.696	111	---	19,018	0.290	0.706	---	---	---	120	119 ¹³	4205	---	---	---	---
trans-1,3-Pentadiene (piperylene)	68.1	0.681	108	---	19,016	0.290	0.706	---	---	---	119	117 ¹³	4230	---	---	---	---
2-methyl-(cis or trans)	82.1	0.724	169	---	---	0.240	0.701	---	---	---	115	100 ¹³	4220	---	---	---	---
1,4-Pentadiene	68.1	0.666	79	---	19,190	0.290	0.706	---	---	---	115	119 ¹³	4270	---	---	---	---
2,3-Pentadiene	68.1	0.700	119	---	19,399	0.290	0.706	---	---	---	119	130 ¹³	4280	---	---	---	---
n-Pentane	72.1	0.631	97	154	19,499	0.255	0.654	54	359	544	115	99	4050	82	22 ¹⁵	13	0.07
2,2-dimethyl-	100.2	0.678	175	125	19,235	0.187	0.661	---	---	---	119	89 ¹³	4040	---	---	---	---
2,3-dimethyl-	100.2	0.699	194	130	19,265	0.187	0.661	69	437	640	119	94 ¹³	3995	---	---	---	---
2,4-dimethyl-	100.2	0.677	177	127	19,253	0.187	0.661	---	---	---	117	92	4025	---	---	---	---
n-Pentane, 2,4-dimethyl-3-ethyl-	128.3	0.742	278	119	---	0.147	0.665	---	---	734	---	---	---	---	---	---	---
3,3-dimethyl-	100.2	0.698	187	127	19,255	0.187	0.661	---	---	---	---	---	---	---	---	---	---
2-methyl-	86.2	0.658	140	139	19,356	0.216	0.659	60 ¹⁹	372 ¹⁹	585	115	94	4050	---	---	---	---
3-methyl-	86.2	0.669	146	140	19,369	0.216	0.659	---	---	580	116	94	4040	---	---	---	---
2,2,3,3-tetramethyl-	128.3	0.761	284	118	---	0.147	0.665	54 ¹¹	344 ¹¹	845	---	---	---	---	---	---	---
2,3,3,4-tetramethyl-	128.3	0.759	287	117	---	0.147	0.665	---	---	818	---	---	---	---	---	---	---
2,2,3-trimethyl-	114.2	0.720	230	121	19,212	0.165	0.663	---	---	816	---	---	---	---	---	---	---
2,2,4-trimethyl- (isooctane)	114.2	0.696	211	117	19,197	0.165	0.663	48	360	837	117	89 ¹³	4020	175	28 ¹⁷	0.08	0.07
2,3,3-trimethyl-	114.2	0.730	239	123	19,226	0.165	0.663	---	---	806	---	---	---	82	18 ¹⁵	0.13	0.06
1-Pentene	70.1	0.646	86	---	19,346	0.271	0.678	47	370	569	114	109	4165	---	---	---	---
2-methyl-	84.2	0.687	141	---	19,185	0.227	0.678	---	---	582	124	102	4025	---	---	---	---
4-methyl-	84.2	0.669	129	---	19,225	0.227	0.678	---	---	580	117	104	4130	---	---	---	---
2,3,4-trimethyl-	112.2	0.733	226	---	---	0.171	0.678	---	---	495	---	---	---	---	---	---	---
2,4,4-trimethyl- (diisobutylene)	112.2	0.719	215	---	---	0.171	0.678	---	---	788	---	---	---	---	---	---	---
cis-2-Pentene	70.1	0.661	99	---	19,308	0.271	0.678	49	345	---	124	111 ¹³	4035	175	18 ¹⁵	0.18	0.06
2,4,4-trimethyl-	112.2	0.726	221	---	---	0.171	0.678	---	---	587	---	---	---	---	---	---	---
3,4,4-trimethyl-(cis or trans)	112.2	0.743	234	---	---	0.171	0.678	---	---	626	---	---	---	---	---	---	---
trans-2-Pentene	70.1	0.653	97	---	19,280	0.271	0.678	---	---	---	---	---	---	---	---	---	---
1-Pentyne	68.1	0.695	104	---	19,436	0.290	0.706	---	---	---	122	136	4265				

APPENDIX REFERENCES

1. Rossini, Frederick D., et al.: Selected Values of Physical and Thermodynamic Properties of Hydrocarbons and Related Compounds. Carnegie Press (Pittsburgh), 1953.
2. Hodgman, Charles D., ed.: Handbook of Chemistry and Physics. Thirty-fifth ed., Chem. Rubber Pub. Co., 1953-1954.
3. Spakowski, Adolph E.: Pressure Limits of Flame Propagation of Pure Hydrocarbon-Air Mixtures at Reduced Pressure. NACA RM E52H15, 1952.
4. Jackson, Joseph L.: Spontaneous Ignition Temperatures—Commercial Fluids and Pure Hydrocarbons. Ind. and Eng. Chem., vol. 43, no. 12, Dec. 1951, pp. 2869-2870.
5. Simon, Dorothy Martin: Flame Propagation. III. Theoretical Considerations of the Burning Velocities of Hydrocarbons. Jour. Am. Chem. Soc., vol. 73, no. 1, Jan. 1951, pp. 422-425.
6. Levine, Oscar, and Gerstein, Melvin: Fundamental Flame Velocities of Pure Hydrocarbons. III—Extension of Tube Method to High Flame Velocities—Acetylene-Air Mixtures. NACA RM E51J05, 1951.
7. Huff, Vearl N., Gordon, Sanford, and Morrell, Virginia E.: General Method and Thermodynamic Tables for Computation of Equilibrium Composition and Temperature of Chemical Reactions. NACA Rep. 1037, 1951. (Supersedes NACA TN's 2113 and 2161.)
8. Calcote, H. F., Gregory, C. A., Jr., Barnett, C. M., and Gilmer, Ruth B.: Spark Ignition—Effects of Molecular Structure. Ind. and Eng. Chem., vol. 44, no. 11, Nov. 1952, pp. 2656-2660; discussion, pp. 2660-2662.
9. Blanc, M. V., Guest, P. G., von Elbe, Guenther, and Lewis, Bernard: Ignition of Explosive Gas Mixtures by Electric Sparks. III. Minimum Ignition Energies and Quenching Distances of Mixtures of Hydrocarbons and Ether with Oxygen and Inert Gases. Third Symposium on Combustion and Flame and Explosion Phenomena, The Williams & Wilkins Co., 1949, pp. 363-367.
10. Lewis, Bernard, and von Elbe, Guenther: Combustion, Flames and Explosions of Gases. Academic Press, Inc., 1951, pp. 408-414.
11. Coward, H. F., and Jones, G. W.: Limits of Flammability of Gases and Vapors. Bull. 503, Bur. Mines, 1952.
12. Scott, G. S., Jones, G. W., and Scott, F. E.: Determination of Ignition Temperatures of Combustible Liquids and Gases. Anal. Chem., vol. 20, no. 3, Mar. 1948, pp. 238-241.
13. Wagner, Paul, and Dugger, Gordon L.: Flame Propagation. V. Structural Influences on Burning Velocity. Comparisons of Measured and Calculated Burning Velocity. Jour. Am. Chem. Soc., vol. 77, no. 1, Jan. 5, 1955, pp. 227-231.
14. Calcote, Hartwell F., Barnett, Charles M., and Irby, Moreland R.: The Burning Velocity of Various Compounds by the Bunsen Burner Method. Paper presented at meeting Am. Chem. Soc., Atlantic City (N. J.), Sept. 18-23, 1949.
15. Metzler, Allen J.: Minimum Spark-Ignition Energies of 12 Pure Fuels at Atmospheric and Reduced Pressure. NACA RM E53H31, 1953.
16. Perry, John H., ed.: Chemical Engineers' Handbook. Third ed., McGraw-Hill Book Co., Inc., 1950, p. 216.
17. Metzler, Allen J.: Minimum Ignition Energies of Six Pure Hydrocarbon Fuels of the C₂ and C₆ Series. NACA RM E52F27, 1952.
18. Simon, Dorothy Martin: Flame Propagation—Active Particle Diffusion Theory. Ind. and Eng. Chem., vol. 43, no. 12, Dec. 1951, pp. 2718-2721.
19. DiPiazza, James T., Gerstein, Melvin, and Weast, Robert C.: Flammability Limits of Hydrocarbon-Air Mixtures. Reduced Pressures. Ind. and Eng. Chem., vol. 43, no. 12, Dec. 1951, pp. 2721-2725.
20. The Associated Factory Mutual Fire Insurance Cos.: Properties of Flammable Liquids, Gases, and Solids. Ind. and Eng. Chem. (Ind. ed.), vol. 32, no. 6, June 1940, pp. 880-884.
21. Jost, Wilhelm: Explosion and Combustion Processes in Gases. McGraw-Hill Book Co., Inc., 1946.
22. Fenn, John B.: Lean Flammability Limit and Minimum Spark Ignition Energy. Ind. and Eng. Chem., vol. 43, no. 12, Dec. 1951, pp. 2865-2868.
23. Gerstein, Melvin, Levine, Oscar, and Wong, Edgar L.: Flame Propagation. II. The Determination of Fundamental Burning Velocities of Hydrocarbons by a Revised Tube Method. Jour. Am. Chem. Soc., vol. 73, no. 1, Jan. 1951, pp. 418-422.
24. Dugger, Gordon L., and Grabb, Dorothy D.: Flame Velocities of Propane- and Ethylene-Oxygen-Nitrogen Mixtures. NACA RM E52J24, 1953.